

AD-A158 658

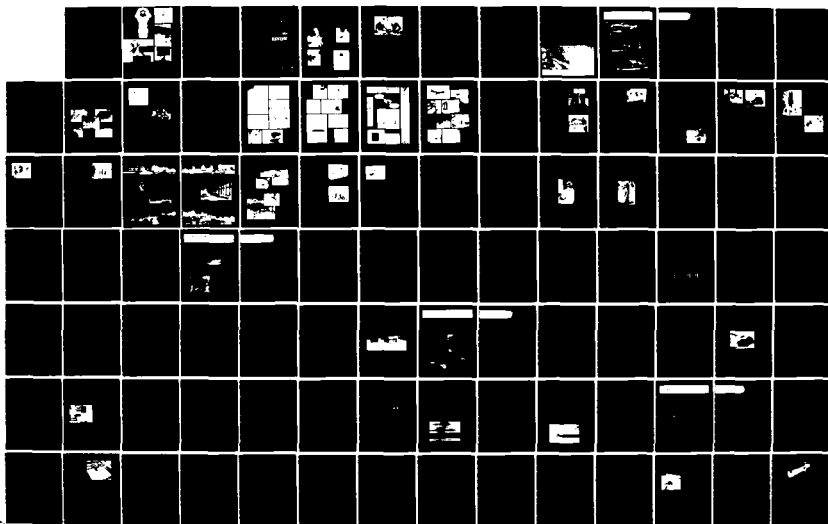
NAVAL RESEARCH LABORATORY 1983 REVIEW(U) NAVAL RESEARCH
LAB WASHINGTON DC 1983

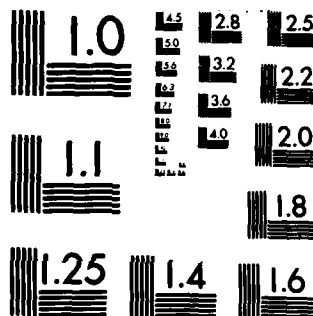
1/4

UNCLASSIFIED

F/G 5/1

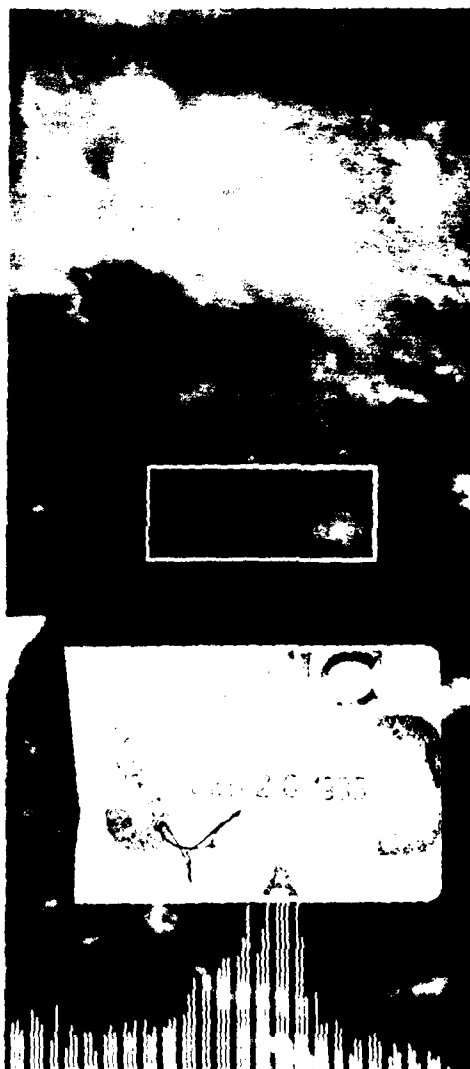
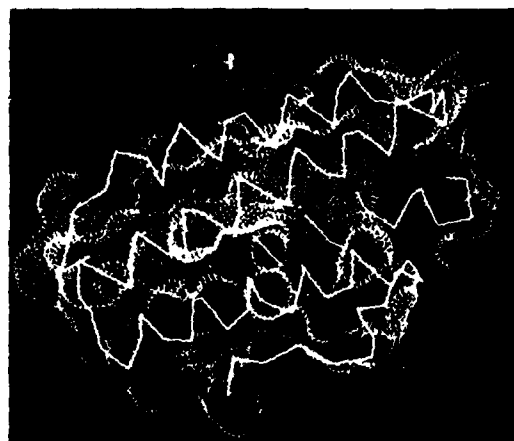
NL



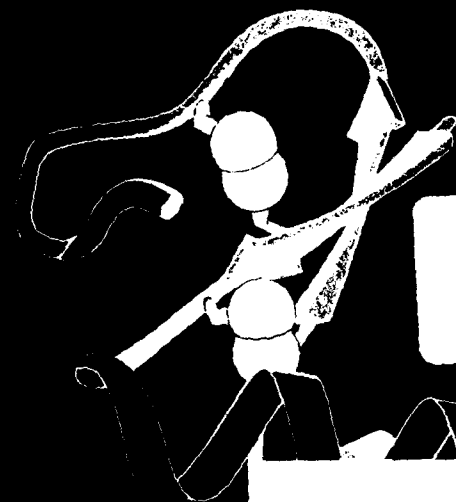


MICROCOPY RESOLUTION TEST CHART
NATIONAL BUREAU OF STANDARDS-1963-A

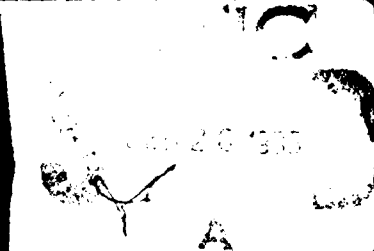
AD-A150 650



Approved for public release; distribution unlimited.



OTIC FILE COPY



Naval Research Laboratory
Washington, D. C.

6-1 10 21 333

The graphics on the covers are representative of today's research as NRL prepares for tomorrow's Navy.

Front cover, clockwise from upper left:

Computer simulation of the interaction of the magnetized solar wind and the earth's magnetosphere. Magnetic field lines are white. Plasma flow speed is color-coded from highest (red, 400 km/s) to lowest (black, < 20 km/s) (P. Palmadesso).

Computer representation of the oxygen-transport protein hemerythrin whose atomic structure was determined at NRL. The dot matrix showing the surface of the molecule is drawn over the wire-model backbone, and color is used to show relative mobility of the surface with the more mobile surfaces shown in red (W. Hendrickson).

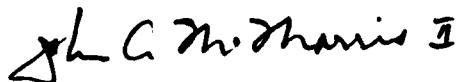
Infrared view of warm (bright) mountain ridges showing through a layer of cold (dark) patchy clouds, taken by a scanning sensor looking down from a high-altitude aircraft. The histogram shows part of the distribution of radiance values in the scene (H. Stone).

A schematic drawing of the backbone of the plant-seed protein crambin. This representation of crambin (drawn by Jane Richardson of Duke University) was derived from computer maps of the atomic model as determined at NRL.

Back cover:

Color-coded isophotal contour map of a far-ultraviolet (UV) image of the North America Nebula in the constellation of Cygnus. The far UV intensity increases from red to violet, and white is the most intense. The astronomical observation was made from a rocket by using a wide-field electrographic camera which is scheduled for reflight on the space shuttle as the Spartan-3 payload (H. Heckathorn).

REVIEWED AND APPROVED
25 August 1983



JOHN A. McMORRIS II, Captain, USN
Commanding Officer

NRL-2600-0041-11/84-5000

Available from: National Technical Information Service • U.S. Department of Commerce
5285 Port Royal Road • Springfield, VA 22161

Naval Research Laboratory



1983

REVIEW

RE: NRL 1983 Review
DTIC has permission to furnish microfiche of this report. Hard copies are available National Technical Information Service.
Per Mr. Ken Thoenes, NRL/Code 2627

Research For Tomorrow's Navy

The Naval Research Laboratory (NRL) is the Navy's corporate experimental laboratory whose mission is to conduct a broadly based multidisciplinary program of technological research and development for the Navy of the future. Celebrating 60 years of major scientific accomplishments, NRL presents in this Review highlights of the unclassified research and development programs for calendar year 1983. With contributions felt at every corner of the world, NRL is committed to pursue the high quality of performance that has made the Laboratory a respected institution conducting "research for tomorrow's Navy."

Accession For		
NTIS GRA&I	<input checked="" type="checkbox"/>	
DTIC TAB	<input type="checkbox"/>	
Unannounced	<input type="checkbox"/>	
Justification		
\$25.50		
Distribution NTIS		
Availability Codes		
Dist	Avail and/or	Special
A1	21	21



Washington, D.C. 20375-5000

**DTIC
ELECTE**
S FEB 26 1985 D
A

THE 1983 NRL REVIEW

is dedicated to the men and women
— past and present —
of the

Naval Research Laboratory

Sixty Years of Discovery and Development Through Research for the Navy and the Nation



NRL's early discoveries based on the reflection of radio frequency observed in 1922 led to radar which reached the prototype stage when the XAF Search Radar (antenna circled) was installed on the battleship USS NEW YORK in December 1938.



Dr. A. Hoyt Taylor, a pioneering radio scientist who joined NRL at its inception in 1923, was responsible for the early discoveries of radio reflection from ships

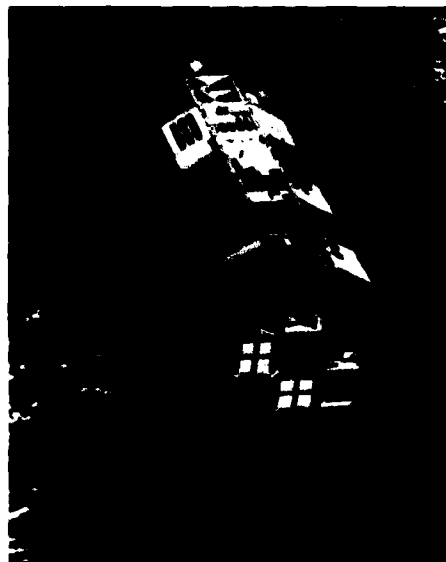
From
Radar
to



Dr. Dianne Prinz of the Space Science Division has been selected as an alternate space shuttle crew member to operate the Solar Ultraviolet Spectral Irradiance Monitor

Rocketry

The Heavy Ions in Space Experiment (circled), developed at NRL during 1983, is shown aboard NASA's Long Duration Exposure Facility (LDEF) spacecraft. This photo was taken from the space shuttle after LDEF was deployed on April 6, 1984. LDEF (14 ft in diameter and 30 ft long) will return to earth via another shuttle in 1985.



PREFACE



Dr. Timothy Coffey, Director of Research, with
Capt. John A. McMorris II, Commanding Officer

This *NRL Review* reports 11 major categories of unclassified work performed during calendar year 1983 at the Naval Research Laboratory (NRL). Although not comprehensive in scope, the selected projects highlighted here demonstrate the broad technological base of research conducted at NRL.

This *Review* has been published in its present form since 1967. One of its purposes is to provide an exchange of information among scientists, engineers, and scholars—both inside and outside of the Navy. We hope that this *Review* communicates the essential technical features of our work and thereby fosters increased scientific interaction.

The theme of this year's *Review* is "research for tomorrow's Navy." This theme reflects a part of NRL's mission—to devote its resources to a broad-spectrum approach to the basic scientific research of technologies that will improve the overall effectiveness of the Navy. This *Review* clearly shows that the multidisciplinary expertise available at NRL allows the Laboratory to fulfill its mission comprehensively.

Research and development at NRL encompass nearly all areas of science and engineering. Such a program is necessary to meet the everchanging needs of the Navy. Sponsors of NRL's work reflect this multidisciplinary character of the Laboratory. Our primary sponsors include the Chief of Naval Research, the Chief of Naval Material, and the Naval Systems Commands. Our multidisciplinary scope, however, allows us to collaborate with others such as NASA, DOE, other U.S. military, industry, and academia.

During 1983, NRL celebrated 60 years of research. To keep pace with naval and national needs, the Laboratory has continually grown—from the original five small buildings and a dozen or so scientists to today's approximately 150 buildings and 3200 researchers and support personnel. NRL of the future will continue to evolve both physically and intellectually, so that it will fulfill its role in an evermore complex world.

NRL operates directly under the Chief of Naval Research, who reports to the Assistant Secretary of the Navy for Research, Engineering, and Systems. As the Navy's corporate research laboratory, NRL serves as a major focal point for research and development. The Laboratory's contributions have been felt at every corner of the globe, and we at NRL strive to continue this tradition.

As you read this *Review*, you will become even more aware that the Laboratory is a dynamic family working together to promote the programs, progress, and innovations that will continue to foster discoveries, inventiveness, and scientific advances for the Navy of the future.

DEDICATION	iii
PREFACE	v
Capt. John A. McMorris II, Commanding Officer, and Dr. Timothy Coffey, Director of Research	
MISSION	1
THE NAVAL RESEARCH LABORATORY	2
NRL—Our heritage, NRL today, NRL in the future	5
Research for Tomorrow's Navy: NRL in the Scientific, Technological, and Defense Community, by the Director of Research	29
Highlights of NRL Research in 1983	33
SCIENTIFIC ARTICLES	38
EXCELLENCE IN RESEARCH FOR TOMORROW'S NAVY	212
Special Awards and Recognition	215
Individual Honors	221
Alan Berman Research Publication Awards	228
PROGRAMS FOR PROFESSIONAL DEVELOPMENT	232
Programs for NRL People—University education and scholarships, continuing education, professional development, and other activities	235
Programs for Non-NRL People—Fellowships, exchange programs, and cooperative employment	240
NRL CONTRIBUTIONS TO SCIENCE AND TECHNOLOGY	246
Papers in Journals, Books, and Proceedings of Meetings	249
Formal Reports	278
Patents Granted	280
GENERAL INFORMATION	282
Funding Profile, Organizational Charts, Key Personnel, and Map	282

SCIENTIFIC ARTICLES

38-211

→ Partial Contents:

- Artificial Intelligence, Information Processing, and Signal Transmission -38→ - -
*Speech analysis, propagation, network management, equipment
diagnosis, and radar* ;

- Electromagnetic Sensing and Systems for the Navy Environment -56→ - -
Radar, environment simulator, and shipwakes ;

- Acoustic Systems and Technology -74→ - -
*Sound field properties, noise and testing, propagation,
and sonar dome testing* ;

- Optical Research and Systems Technology -92→ - -
Lasers, laser propagation, and atmospheric transmission ;

- Atmospheric and Ionospheric Research and Military Applications -102→ - -
Nuclear blasts, hurricanes, and aerosols ;

- Aerospace Science and Technology -114→ - -
*X rays, spacecraft design and theory, timing, space radiation effects,
and fluid mechanics* ;

- High-Powered Radiation Sources and Pulsed-Power Technology -136→ - -
Laser fusion, high-current laser emission, and fast opening switch

- Materials Modification and Behavior -148→ - -
*Hyperfine layer growth, sensors, composites, corrosion inhibition,
and deck coatings* ;

- Materials Analysis and Properties -168→ - -
*Semiconductor behavior, molecular structures, ultrafine particles,
and materials behavior* ;

- Component Technology and Specialized Devices -186→ - -
*Chemical detection, electronic devices, microprocessors,
and ultrafine chip manufacture* ;

- Numerical Modeling and Simulation with Physical Applications -198→ - -
Fluid mechanics, auroral plasma, radar, and lasers ;

MISSION ...

To conduct a broadly based multidisciplinary program of scientific research and advanced technological development directed toward new and improved materials, equipment, techniques, systems, and related operational procedures for the Navy. In fulfillment of this mission, the Naval Research Laboratory:

Initiates and conducts scientific research of a basic and long-range nature in scientific areas of special interest to the Navy.

Conducts exploratory and advanced technological development deriving from or appropriate to the scientific program areas.

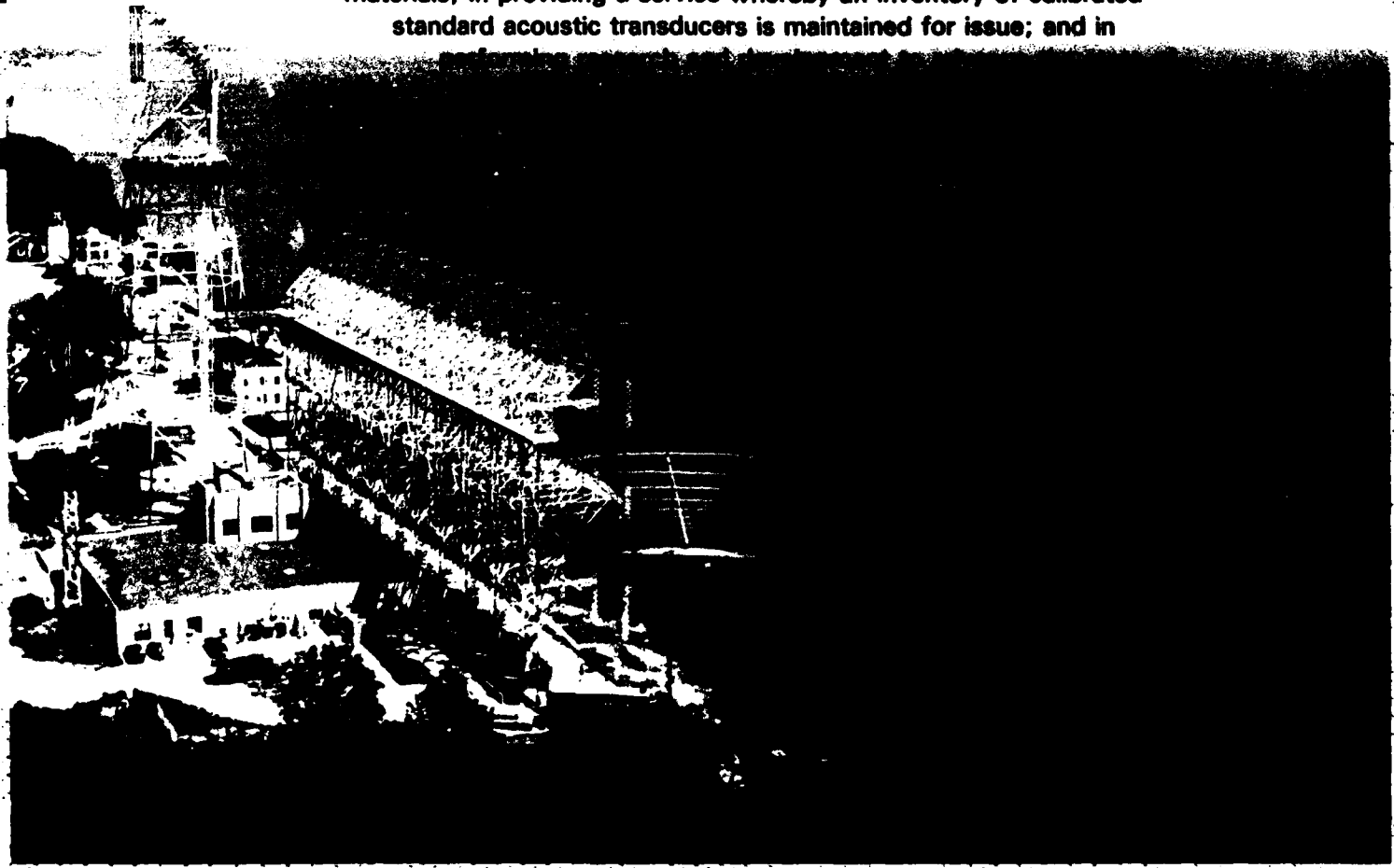
Within areas of technological expertise, develops prototype systems applicable to specific projects.

Performs scientific research and development for other naval commands and, where specially qualified, for other agencies of the Department of Defense and, in defense-related efforts, for other Government agencies.

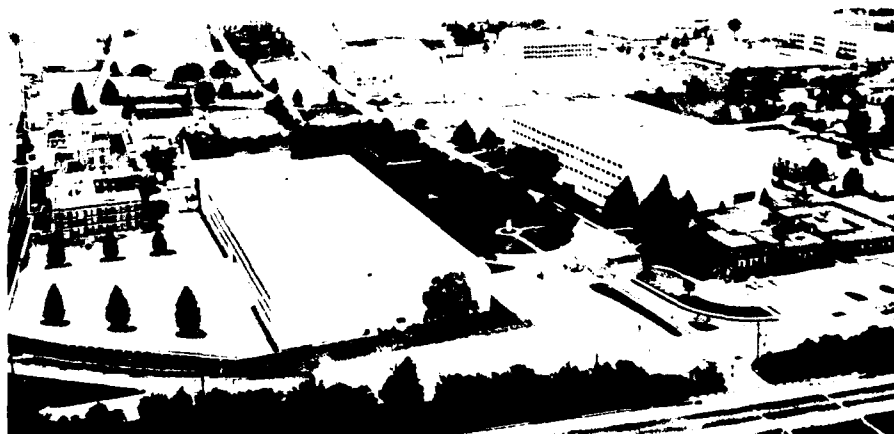
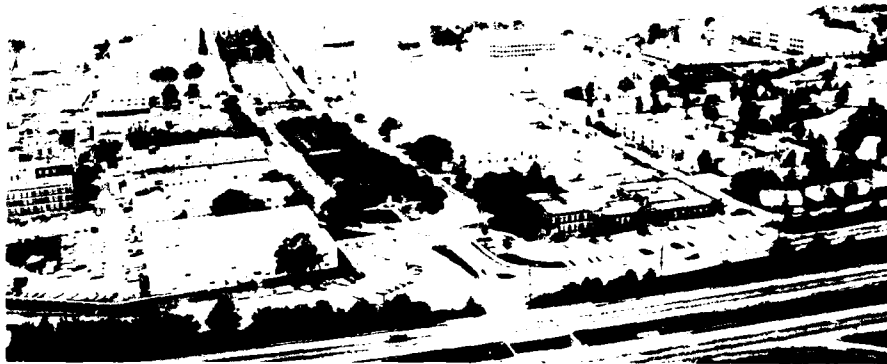
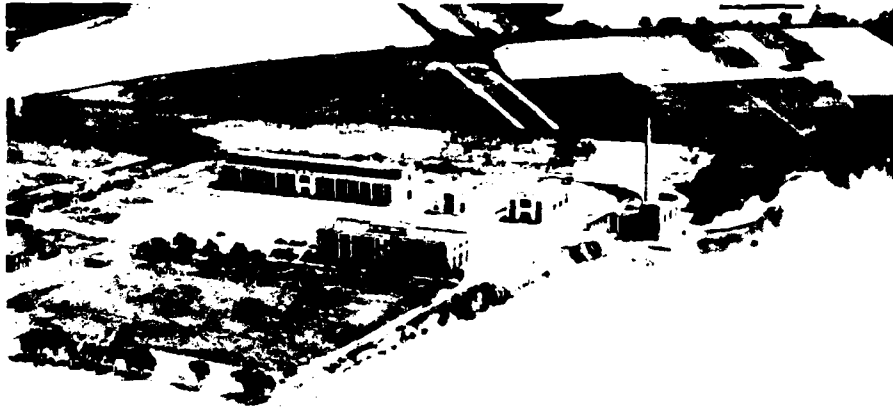
Upon request from appropriate naval commands, assumes responsibility as the Navy's principal R&D center in areas of unique professional competence.

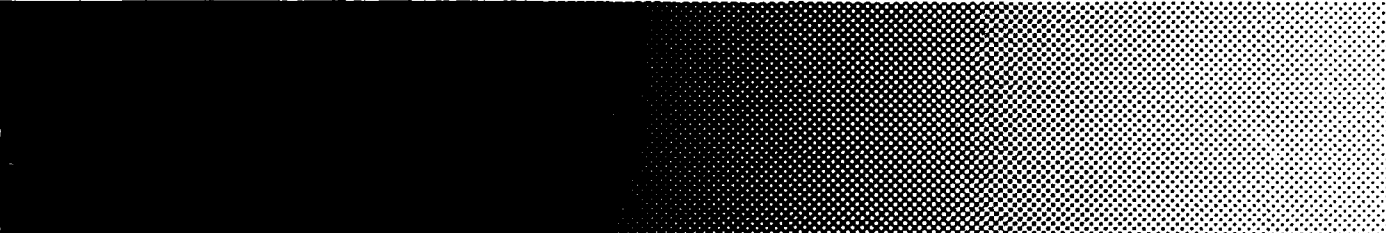

Serves as the principal activity for the Navy and its contractors in providing accurate calibration, test, and evaluation services on acoustic transducers and materials; in providing a service whereby an inventory of calibrated standard acoustic transducers is maintained for issue; and in

performing research and development in the field of



The Naval Research Laboratory



- 
- 
- 5 NRL—Our heritage, NRL today, NRL in the future**
- 29 Research for Tomorrow's Navy: NRL in the Scientific, Technological,
and Defense Community, by the Director of Research**
- 33 Highlights of NRL Research in 1983**

THE NAVAL RESEARCH LABORATORY

"I believe [that] the Government should maintain a great research laboratory, jointly under military and naval and civilian control. In this could be developed the continually increasing possibilities of ... all the technique of naval progression

"When the time came, if it ever did, we could take advantage of the knowledge gained through this research work and quickly produce the very latest and most efficient instruments"

Thomas A. Edison
The New York Times Magazine
May 30, 1915

Page 2, top to bottom:

The original Naval Research Laboratory in 1923 as viewed from the Potomac River among the farmlands of Blue Plains

NRL today, looking toward the Potomac River

THE NAVAL RESEARCH LABORATORY

Our Heritage

Today, when government and science seem inextricably linked, when virtually no one questions the dependence of national defense on the excellence of national technical capabilities, it is noteworthy that in-house defense research is relatively new in our Nation's history. The Naval Research Laboratory (NRL), the first modern research institution created within the United States Navy, began operations in 1923, just 60 years ago.

Thomas Edison's Vision: The first step came in May 1915, a time when Americans were deeply worried about the great European war. Thomas Edison, asked by a *New York Times* correspondent to comment on the conflict, argued that the Nation should look to science. "The Government," he proposed in a published interview, "should maintain a great research laboratory In this could be developed . . . all the technique of military and naval progression without any vast expense." Secretary of the Navy Josephus Daniels seized the opportunity created by Edison's public comments to enlist Edison's support. He agreed to serve as the head of a new body of civilian experts—the Naval Consulting Board—to advise the Navy on science and technology. The Board's most ambitious plan was the creation of a modern research facility for the Navy. Congress allocated \$1.5 million for the institution in 1916, but wartime delays and disagreements within the Naval Consulting Board postponed construction until 1920.

The Laboratory's two original divisions, Radio and Sound, pioneered in the fields of high-frequency radio and underwater sound propagation. They produced communications equipment, direction-finding devices, sonar sets, and, perhaps most significant of all, the first practical radar equipment built in this country. They also performed basic research, participating, for example, in the discovery and early exploration of the ionosphere. In addition, the Laboratory was able to work gradually toward its goal of becoming a

broad-based research facility. By the beginning of World War II, five new divisions had been added: Physical Optics, Chemistry, Metallurgy, Mechanics and Electricity, and Internal Communications.

The War Years and Growth: Total employment at the Laboratory jumped from 396 in 1941 to 4400 in 1946, expenditures from \$1.7 million to \$13.7 million, the number of buildings from 23 to 67, and the number of projects from 200 to about 900. During the war, scientific activities necessarily were concentrated almost entirely on applied research. New electronics equipment—radio, radar, sonar—was developed. Countermeasures were devised. New lubricants were produced, as were antifouling paints, luminous identification tapes, and a sea marker to help save survivors of disasters at sea. A thermal diffusion process was conceived and used to supply some of the ^{235}U isotope needed for one of the first atomic bombs. Also, a host of new devices that developed from booming wartime industry were type-tested and then certified as reliable for the Fleet.

NRL Reorganizes for Peace: After the war, scientific research was widely recognized as a vital national resource, and the Laboratory had a major and continuing role to play in providing such research. When the Office of Naval Research was created in 1946, NRL was transferred to this office; NRL thus became the *corporate research laboratory* of the Navy.

The demands of this new position required substantial reorganization. Rapid expansion had met wartime demands but had left NRL improperly structured to address long-term Navy requirements. One major task—neither easily nor rapidly accomplished—was that of reshaping research. This was accomplished by transforming a group of largely autonomous scientific divisions into a unified institution with a clear mission and a fully coordinated research program. The first attempt at reorganization vested power

in an executive committee composed of all the division superintendents. This committee was impracticably large, so in 1949 a civilian director of research was named and given full authority over the program. Positions for associate directors were added in 1954.

The Breadth of NRL: During the 38 years since the war, the areas of study at the Laboratory have included basic research concerning the Navy's environment of sea, sky, and space. Investigations have ranged widely from monitoring the sun's behavior, to analyzing marine atmospheric conditions, to measuring parameters of the deep oceans. Detection and communications capabilities have benefited by research that has exploited new portions of the electromagnetic spectrum, extended ranges to outer space, and provided means of transferring information reliably and securely even through massive jamming. Submarine habitability, lubricants, shipbuilding materials, fire fighting, along with the study of sound in the sea, have also been steadfast concerns.

The Laboratory has pioneered naval research into space, from atmospheric probes with captured V-2 rockets, through direction of the Vanguard project—America's first satellite program—up to involvement in such projects as the Navy Global Positioning System. Today, NRL is the Navy's lead laboratory in space research, fire research, tactical electronic warfare, microelectric devices, and artificial intelligence. NRL has also evaluated new issues, such as the effects of intense radiation and various forms of shock and vibration on aircraft, ships, and satellites. In 1977, NRL studied and identified the source of the mysterious sonic boom heard along the east coast of the United States. And in 1983, NRL helped identify the reason for the failure of Barney Clark's mechanical heart and then improved its design. NRL has made and continues to make important nonmilitary contributions to science and technology: development of better composite materials, new numerical techniques, new and improved microelectronic devices, and high-energy sources.

One goal has guided NRL's diverse activities through the years—to conduct pioneering scientific research and development that will provide improved materials, equipment, techniques, systems, and operations for the Navy, for the Department of Defense, and for the U.S. Government.

NRL Today

ORGANIZATION AND ADMINISTRATION

The position of NRL within the Navy, illustrated on the organization chart that appears on page 283 of this *Review*, is that of a field command under the Chief of Naval Research.

Heading the Laboratory with joint responsibilities are the naval commanding officer, Capt. John A. McMorris II, and the civilian director of research, Dr. Timothy Coffey. Staff functions such as security and personnel management fall within their administration. Line authority passes from the commanding officer and the director of research to five associate directors of research in the following areas:

- Technical services
- General science and technology
- Systems research and technology
- Material science and component technology
- Space and communications technology

The first of these provides centralized technical support; the other four are the research directorates responsible for executing NRL's research and development program. Further details of the organization of the Laboratory are given on the organization chart that appears on page 284 of this *Review*.

Financially, NRL operates under the naval industrial fund system, which requires that all costs, including overhead costs, be charged to various research projects. Funding for scientific projects in 1983 came from the Chief of Naval Research, the Naval Systems Commands, the Naval Material Command, and other government agencies, such as the Defense Advanced Research Projects Agency, the Department of Energy, and the National Aeronautics and Space Administration. NRL's relationship to its sponsoring agencies, both inside and outside the Department of Defense, is defined by a comprehensive policy on interagency support agreements.

Besides funding for scientific work, NRL received Navy monies for general construction, maintenance, and operations. In fiscal year 1983, the Laboratory's budget totaled \$325 million.

PERSONNEL DEVELOPMENT

At the end of 1983, NRL's military staff comprised 132 military personnel—33 officers and 99 enlisted—and 3060 civilian employees. The research staff of 1498 employees consists of 667 with doctorates, 330 with master's degrees, and 491 with bachelor's degrees. The 1529-person support staff provides administrative, computer-aided designing, machining, fabrication, electronic construction, publication, personnel development, information retrieval, and large mainframe computer services to the research staff.

Opportunities for higher education and other professional training for NRL employees are available through several programs offered by

the Employee Development Branch. These programs provide for graduate work leading to advanced degrees, advanced training, college course work, short courses, continuing education, and career counseling. Graduate students, in certain cases, may use their NRL research for thesis work.

For non-NRL employees, several postdoctoral research programs exist. There are also cooperative education agreements with several universities, summer and part-time employment programs, and various summer and interchange programs for college faculty members, professional consultants, and employees of other Government agencies.

NRL has active chapters of Women In Science and Engineering, Sigma Xi, Toastmaster's



NRL celebrated 60 years of naval research in 1983. Some of the events that occurred on the actual celebration day of October 19 are shown above. In the center photo, Dr. Robert Frosch, vice president in charge of research laboratories for General Motors Corporation, speaks. Listening are, left to right, NRL's Director of Research, Dr. Timothy Coffey; Navy Secretary, John Lehman; NRL's Commanding Officer, Captain John A. McMorris II; and Chief of Naval Research, Admiral Leiland S. Kollmorgen. Other photos are: upper left—the Navy band, upper right—the reception cake, lower left—the unveiling of one of the three streets named for NRL pioneer researchers, and lower right—some of the 800 Laboratory employees and guests who attended the celebration.



P-1982(6)

1977 Nobel prize winner, Dr. Ilya Prigogine, speaks on irreversible statistical mechanisms at a recent NRL Sigma Xi lecture

International, and the Federal Executive and Professional Association. Three personal computer clubs meet regularly—Edison Atari, NRL IBM-PC, and Edison Commodore. An amateur radio club, a wives' club, a musical drama group—the Showboaters, and several sports clubs are also active. NRL has a recreation club which provides swimming, sauna, whirlpool bath, gymnasium, and weight room facilities. The recreation club also offers classes in karate, aerobics, swimming, and cardiopulmonary resuscitation.

A community outreach program at NRL provides tutoring for local students, science fair judging, participation in high school and college career day programs, career counseling, an art and essay contest during Black History Month, and a Christmas party with donated gifts for disadvantaged children.

NRL has an active, growing Credit Union with assets of \$55 million. A day care center is located near one of the gates to NRL, and public transportation to NRL is provided by Metrobus.

More information on these programs can be found in the *Review* chapter entitled "Programs for Professional Development," page 232.

SCIENTIFIC FACILITIES

In addition to its main campus of about 130 acres and 152 buildings, NRL maintains 12 other research sites and a Flight Support Detachment. The many diverse scientific and technological

research and research support facilities are described in the following paragraphs. Some of NRL's major facilities are shown on page 13.

Research Facilities

• Space

NRL has been a major center for space research and technology since the late 1940's. For nearly 40 years it has provided technical expertise and guidance for the nation's civilian and military space programs. NRL's facilities supporting the Laboratory's efforts in space science include the E.O. Hulburt Center for Space Research, the 26-m (85 ft), high-precision radio telescope at Maryland Point, and antennas for radio astronomy.



P-2039(8)

Dr. Herbert Friedman (left), chief scientist emeritus, Space Science Division, and Fellow, National Academy of Sciences, discusses the implications of X-ray emission from regions near black holes and neutron stars with Dr. Herbert Gursky (right), superintendent, Space Science Division

In its role as the Navy's lead laboratory for space research, NRL establishes and supports the development of spacecraft and systems that use these spacecraft. NRL facilities that support this role include large electromagnetic anechoic chambers, clean rooms, shock and vibration facilities, an acoustic reverberation chamber, a spin balance facility, large and small thermal-vacuum test chambers, and large static load and modal analysis test facilities. These facilities provide NRL with the capability of testing and space qualifying spacecraft up to and including the space transportation system size and weight payloads. NRL's Blossom Point Satellite Tracking and Command Facility provides spacecraft command, control, and data collection. NRL also has a

(Continued on page 15)

Many varied and interesting facets of science and engineering are illustrated on pages 10 to 12.

Page 10, clockwise from upper left:

U.S. Coast Guard firefighter using infrared camera during shipboard tests conducted by NRL. These devices, which allow firefighters to see through smoke, are being evaluated for use on Navy vessels.

The Optical Sciences Division is in the process of developing infrared models of ships. This is an example of a false-color ship image in the 8- to 12- μ m wavelength band (J. Kershenstein).

A numerical simulation of a series of 6-Mton nuclear blasts spaced 3 km apart. Each blast is separated by 24 s. The contours represent atmospheric density increasing from red to blue, green, yellow, pink, and white and then repeating that sequence (D. Fyfe, M. Fry, and D. Book).

Fibers are coated with energetic metal ions and atoms from a magnetron-sputtered vapor source. Basic phenomena at the metal/fiber interface are studied to improve properties of metal matrix composite materials. See article on p. 162.

Interior of an RF sputtering system showing argon plasma discharge and 1000°C substrate table. The argon plasma provides high-energy ions that "knock" atoms from a niobium target to a heated substrate. See article on p. 176.

Computer-aided design images of a charge-coupled device (CCD) optical detector array having 32 by 32 pixels. The total chip (represented on the left-hand side) is about 2.2 mm square. The device contains nine distinct layers, each of which is represented by a separate color. Each separate color image is used as a mask to manufacture that layer. On the right-hand side is an enlargement of the region about one quarter of the way down from the top and about one third of the way over from the right-hand edge of the device (G. Miller).

Page 11, upper left to lower right:

A Landsat-D nighttime infrared (10 μ m) image of eastern Maryland and Chesapeake Bay. The image has been differentially stretched in two colors to make the bay show warm (yellow) beneath the dark (green) clouds. Because of the time of day (9:30 pm) the water is warmer than the land. This illustrates one technique to enhance satellite imagery (N. Stone).

A technician in the Microelectronics Facility loads silicon wafers into a diffusion furnace—one step in the production of sophisticated electronic devices

Optical arrays may be used to synthesize extremely large telescopes at moderate cost. This is a false-color image of the function used to produce the white-light diffraction pattern from the single-color diffraction pattern for a 15-element optical array (J. Spencer and R. Simon).

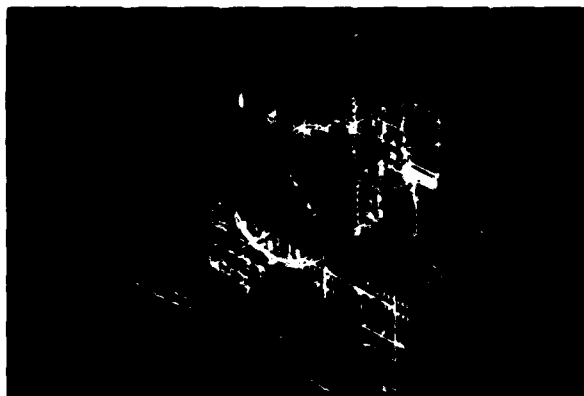
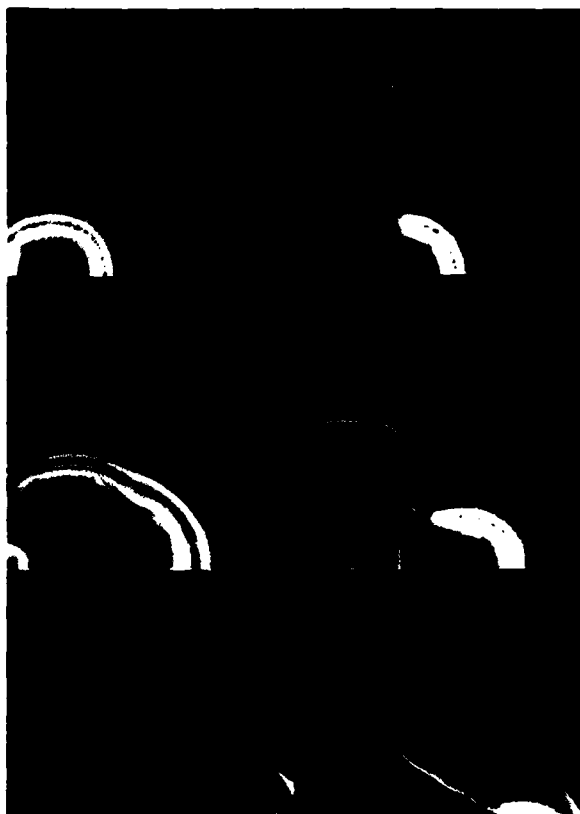
Pyrotechnic generation of a hygroscopic aerosol cloud at sea on the fantail of the USNS *Lynch*. Measurements of the electromagnetic (EM) properties of such clouds will increase our understanding of EM propagation in the lower atmosphere at sea. (See article on p. 110).

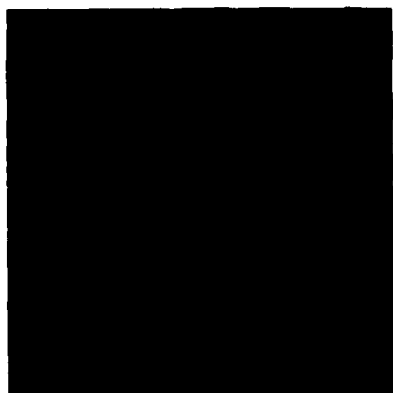
The 15-cm-wide plasma which is generated in an X-ray, preionized discharge-pumped laser. This emission is from a gaseous mixture of neon, xenon, and hydrochloric acid. This discharge gives rise to a 180-ns-long, 60-J laser pulse at a wavelength of 308 nm. The single pulse energies in this device are four times greater than in any other device of this kind (L. Champagne).

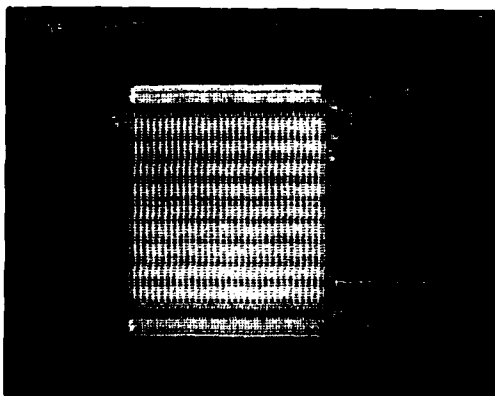
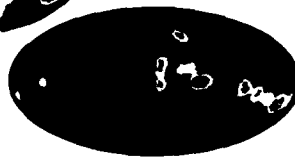
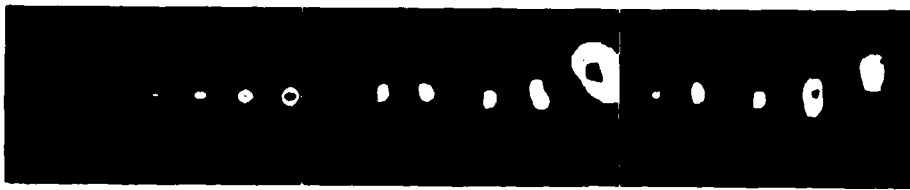
Laser photolysis with an argon-ion laser to produce 1-nitroadamantane

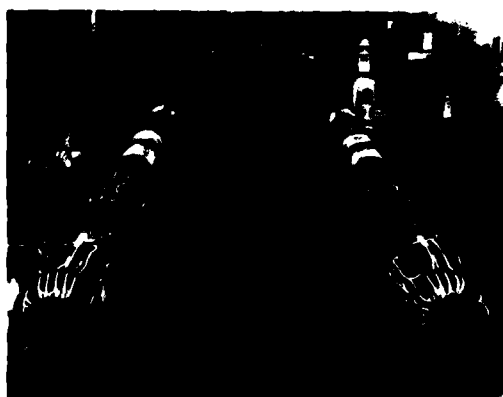
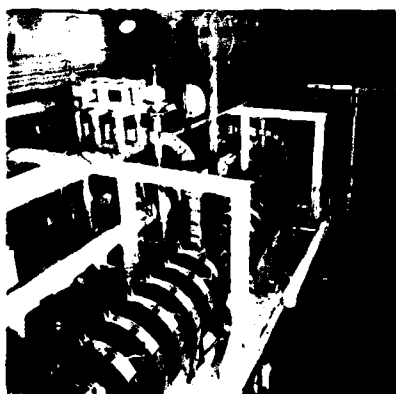
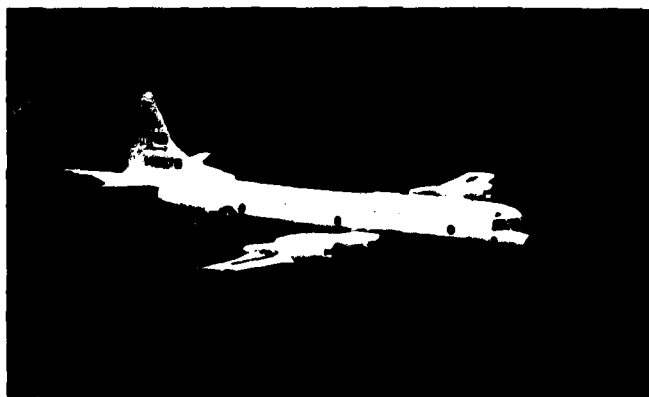
Computer simulation of diffusion-limited growth of a fractal cluster. The colors refer to the stage of growth; magenta is the earliest, yellow is intermediate, and red is the last. Films grown at NRL by a unique sputter deposition process show nearly identical cluster growth (T. Elam).

Captions continued on p. 14.









Page 12, across top:

The vertical velocity field (reds are up, blues and greens are down) at three stages in the development of a Kelvin-Helmholtz instability. Fluid having a vertical increase of density and a vertical change in its horizontal velocity can form these unstable cells (J. Boris, E. Oran, and J. Tutsworth).

Down left side:

A numerical simulation of the oscillatory motion of a flat plate that is sinusoidally driven at its center. Different driving frequencies produce different modal patterns. These are patterns of energy flux (W/m^2). Energy is radiated away from the plate in green areas, and the plate acts as an energy sink in red areas (E. Williams).

Down right side:

A computer-generated, false-color image of the thermal surface wake generated by the twin-hulled, oceanographic research vessel, the USNS Hayes, as it moves through the water at 9 knots. The length of the wake shown is nearly 3 km (R. Peltzer).

Upper center:

Images of the sky in the very far ultraviolet (975 \AA) are shown in the three ovals. Sky brightness increases from black to red through the spectrum to white. From left to right: calculated from the Jaschek Star Catalog of spectral types, measured with the STP-72-1 extreme ultraviolet photometer, and determined from the TD-1 satellite observations at 1500 \AA extrapolated to 975 \AA (C. Opal).

Lower center:

High-power lasers are used to compress tiny ($\sim 0.02\text{-cm}$) argon-filled glass microballoons to extreme densities and temperatures to study fusion processes. This X-ray emission spectrum of argon at peak compression as a function of radius in the microballoon was calculated by using the Plasma Physics Division's radiation hydrodynamics model (J. Apruzese).

Bottom:

Computer-aided design/computer-aided manufacture (CAD/CAM) drawing of a microship developed at NRL's Microelectronics Facility. The entire ship is about 2 mm square. To the right is shown an enlarged portion of the CAD/CAM image (D. Cheville).

A selection of NRL's major research facilities

Page 13, upper left to lower right:

One of NRL's fleet of four P-3 Orion aircraft. These have been modified for various projects from in situ atmospheric research to remote sensing of the ocean and the seafloor.

The 5-MV Van de Graaff (left-hand side of photo) is used to generate intense ion beams for various studies. The beams pass through an analyzing magnet (center) and then into an experimental chamber. Here the effects of ionized radiation on microelectronic circuits are being studied. See article on p. 127.

Sections of the 65-MeV, 6-m-long electron linear accelerator (Linac) showing the waveguides and klystrons. The Linac is used to study radiation effects on microelectronic devices and circuits as well as energetic materials.

The Space Science Division Thermal Vacuum Chamber, 5 m in diameter and 9 m long, is capable of simulating outer space environments. It presently contains the world's largest Gyrodynamic Motion Simulator used to study the dynamics of liquid propellants in spacecraft. See related article on p. 122.

The Fire I Test Chamber is a 324-m^3 pressurizable test facility equipped for research on combustion and energy transfer mechanics and continuous spectroscopic monitoring of certain gases. The chamber is ideally suited for fire simulation and testing fire suppression systems aboard submarines.

Scientists studying air-sea interaction processes with NRL's wave tank. The tank, 30 m long, 1 m wide, and 2 m deep, can accommodate varied studies of wind and mechanically generated waves, wave forces, breaking waves, and heat transfer through air-water interfaces.

Interior view of a shielded anechoic chamber, showing the microwave absorber lining and matrix array of antennas to generate the radio frequency environment of radar targets and electronic countermeasures signals. The Central Target Simulator is used to conduct real-time test and evaluation of electronic warfare systems and techniques under simulated tactical conditions. The chamber is approximately 40 m wide and 25 m deep. See related article on p. 63.

Pharos II is an 800-J neodymium glass laser. It is 24 m long with a 10-cm output aperture. It is used for high-altitude nuclear explosion (HANE) simulations and laser fusion research. See article on p. 105.

(Continued from page 8)

dedicated digital image processing laboratory to process satellite imagery such as synthetic aperture radar images and LANDSAT infrared images. Moreover, NRL uses the Patuxent Naval River Command P-3s to perform experiments in surveillance that may have satellite applications and NRL maintains experimental ground facilities, to perform communications experiments that may have space implications. Finally, the space divisions of NRL possess many specialized computer facilities of the most recent designs to perform numerous functions required for space research programs.

- Electronic Warfare

The field of electronic warfare has been a growing concern at NRL since the 1940's, and NRL is the Navy's lead laboratory for in-house exploratory development in electronic warfare. A major area of expansion is simulation studies, which not only eliminate many costly field measurements, but also permit rigorous and repeatable analyses in controlled environments. As research tools, NRL has a mobile infrared signature measurement and simulation facility and a hybrid RF/IR missile seeker simulation facility. A complex, computer-supported central target simulator is now operating with good results, and its capabilities are being expanded to accommodate a broader range of electronic warfare problems. A number of antenna measurement chambers, a radar cross section measurement facility, and other advanced research facilities are also available.

- Information Technology

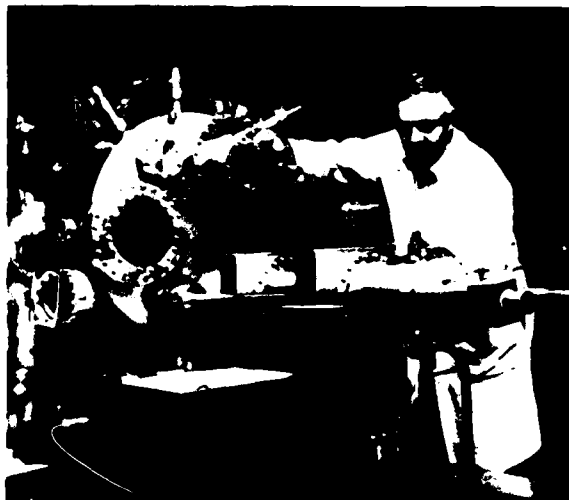
In recent years, NRL has become the Navy's lead laboratory in information science and technology. Much of this effort supports Navy requirements in space systems and in communications and navigations. Major information technology facilities include a microwave space research facility, a voice processing and analysis facility, the Navy Center for Applied Research in Artificial Intelligence, a computer architecture and evaluation facility, and facilities for high frequency (HF) and signal intelligence (SIGINT) analysis.

- Electronic Sciences

NRL's contribution to electronics science and technology is enhanced by many specialized



Dr. John Montgomery, Tactical Electronic Warfare Division, discusses systems testing in NRL's Advanced Electronic Warfare Simulator. See article on page 63.



Dr. James Comas of the Electronics Technology Division mounts gallium arsenide substrates in the molecular beam epitaxy facility. See article on page 151.

facilities and equipment. These include: a full range of crystal-growing equipment used to grow compound semiconductors and other materials of military interest; a molecular beam epitaxy (MBE) system used to grow GaAs-Ga_xAl_{1-x}As superlattice and quantum well heterostructures; an organometallic chemical vapor deposition

(OMCVD) system used to grow various heterostructures; radiation sources for activities in radiation effects and hardening; state-of-the-art microelectronics facilities, including a processing facility in which microelectronics devices with very large scale integrated (VLSI) circuit complexity are designed and fabricated with feature sizes of less than $1\ \mu\text{m}$; several scanning electron microscopes and a scanning transmission electron microscope (STEM); an ion implantation facility; a high magnetic field (>17 tesla) facility to study how variable magnetic fields affect semiconductor materials and heterostructures; a wide range of lasers to characterize materials, interfaces, and heterostructures, and to use in optical biasing applications; ultrahigh vacuum systems used primarily to study interfaces; and a tube fabrication facility to support activities in microwave and millimeter wave tube technology.

• Chemistry

NRL has been a major center for chemical research in support of Navy operational requirements since the late 1920's. The Chemistry Division continues its tradition with a broad spectrum of basic and applied research programs concerned with fuels and combustion (NRL is the Navy's lead laboratory in fire research), corrosion, advanced polymeric materials, ultrasensitive detection methods for chemical agents, and special materials for electronic warfare applications. Modern facilities for research include a wide range of the most modern optical, magnetic, and ion-based spectroscopic instruments, lasers, computers, electrochemical devices, a $10,000\ \text{ft}^3$ fire research chamber (Fire I), multiple facilities for materials synthesis and physical/chemical characterization, high- and low-temperature equipment, and extensive surface-analytical instrumentation.

• Optics

Fabrication of Optical Fibers (Oxide/Fluoride)—During the past year, NRL has established a unique state-of-the-art facility to purify and synthesize both silica and fluoride glass waveguide materials and has established dedicated fiber drawing laboratories for each class of materials. Fiber-optic materials and preforms can now be prepared by either chemical vapor desposition methods or conventional crucible melting. In addition, NRL has developed a comprehensive



Members of the Chemistry Division operate the Secondary Ion Mass Spectrometer. This device is used to study secondary ion emission processes from, and diagnosis of, material surfaces.

capability to characterize the optical, mechanical, structural, chemical, and compositional properties of fiber-optic waveguides for both communication and sensor applications.

Focal Plane Evaluation Facility—This is used to evaluate infrared focal plane arrays being developed for advanced Navy sensors. The facility includes clocking and drive electronics to operate the arrays, calibrated continuous wave (CW) and pulsed infrared sources and electronics for video signal processing and digitization, and computer data reduction for the large volumes of data required to obtain statistical information on each detector in the array. The arrays that have been evaluated include monolithic and hybrid structures which use charge coupled device (CCD), charge injection device (CID), and charge imaging matrix (C/M) technologies.

IR Missile Seeker Evaluation Facility—This facility performs open loop measurements of the susceptibilities of infrared tracking sensors to optical countermeasures. The facility includes rate tables to simulate target motion, infrared sources with optics and modulators, and electronic instrumentation and data recording capabilities. The operation of the sources and rate table, as well as the data acquisition and reduction, is computer controlled.

Large-Optic, High-Precision Tracker—NRL has developed a tracker system with an 80-cm primary and an 8-mrad field of view designed to measure atmospheric transmittance on the open sea. The unique optical design sends incoming radiation down through the yoke of the tracker

mount and presents it at an optical port inside the trailer. Conversely, radiation can be sent out through this port if desired. The optical bench in the trailer holds a high-resolution Fourier transform spectrometer to use in the receiving mode and several lasers to use in the transmitting mode. The tracking system control is through joystick, track ball, digital switches, or error input. By using a silicon quad cell detector, the servo system has been able to produce a 12- μ rad tracking accuracy while locked onto a signal. An optical correlation tracking system is being added to facilitate automatic tracking of moving objects without the requirement of a beacon.

High-Energy Excimer Laser—An X-ray pre-ionized discharge excimer laser has been constructed which has reliably produced 40 J of laser radiation at 308 nm in a 200-ns-long pulse, representing the highest output energy achieved to date in any discharged pumped excimer laser device. In addition to numerous research activities requiring these energy levels in the ultraviolet portion of the spectrum, studies are also in progress to extend these lasers to high repetition rate operation with projected average power levels of 10 to 100 kW. This facility will be used to study high-energy laser-beam properties, optical damage, and laser resonator configurations.

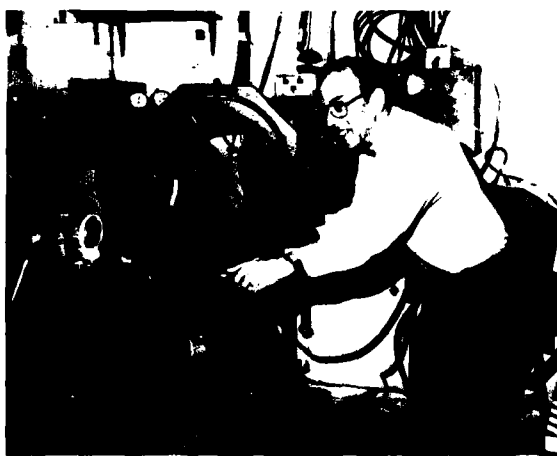
Fiber Sensor Facility—The development and characterization with acoustic, magnetic, gyroscopic, and temperature optical fiber sensors are carried on in the advanced fiber sensor facility. This facility includes equipment to fabricate diode laser drivers for the sensors, fiber sensing elements, and fiber telemetry links, and to evaluate the various sensor concepts. It also includes rate tables, low magnetic field chambers, and acoustic test facilities. This facility has also developed the world's most sensitive fiber-optic acoustic, magnetic, and gyro sensors.

Digital Processing Facility—This facility is used to collect, process, analyze, and manipulate infrared data and imagery from several sources. A Digital Equipment Corporation VAX 11/780 Computer system aids the facility digital image and signal processing. This central processing unit (CPU) accesses 2 megabytes of memory, a storage disk of 512 megabytes, a floating point systems AP-120B array processor with its own disk storage, and a Gould Deanza three-color cathode ray tube (CRT) image display. In addition, the facility operates a video system consisting of visible and infrared television cameras, a high-quality video cassette recorder and display,

and a digitizer to convert television raster images into digital image data.

• Plasma Physics

For studies in plasma physics, NRL has high-power pulsed sources to generate intense electron and ion beams, powerful discharges, and various types of radiation which span the spectrum from X rays to microwaves. The largest of these pulsers is Gamble II, used to study the production of megampere ion beams and their use for producing very hot, high-density plasmas. It is also used to develop inductive switching to allow its input to increase from 2 terawatts (TW) to substantially higher levels needed for new generation weapon effects simulators. Smaller electron-beam pulsers are used to study the propagation of the electron beams through the atmosphere and to investigate beam interaction with magnetic fields or structures so that microwave pulses sufficiently powerful to break down air at atmospheric pressure may be generated; related research involves lasers. NRL's PHAROS II neodymium glass laser can generate powerful beams to examine laser-matter interactions; applications presently include inertial fusion research and high-altitude nuclear explosion effects. Lasers are equally important in other parts of the research program. They are used in the atmosphere to guide long discharges that are being studied to find better propagation modes for electron beams, as instantaneous antennas that radiate RF signals, and for possible other military applications.



Dr. Barrett Ripin aligns the disc amplifier in the Pharos II laser. See article on page 105.



Dr. Robert Meger of the Plasma Physics Division adjusts the vacuum valves for plasma sources to be used for research on a high-power, ultrafast, plasma opening switch. See article on page 144.

• Computational Physics

The Laboratory for Computational Physics has been developing a stand-alone Reactive Flow Modelling Facility on its VAX 11/780 computer. The host VAX system has been installed, and a virtual memory system (VMS) driven, general purpose reactive flow model (RFM) has been written, debugged, and applied to a number of fluid dynamics problems in the Laboratory. A Fortran vector version of this two-dimensional fluid dynamics model was used to benchmark several modest array processors and array processor combinations. This system also serves as a centralized high-speed communications link to the DNA CRAY 1 supercomputer system at the Los Alamos National Laboratory.

• Radar

NRL has gained worldwide renown as the "birthplace of radar," and the Laboratory has maintained its reputation as a leading center for radar-related research and development for a half-century. An impressive array of facilities managed by NRL's Radar Division continues to contribute to this reputation. These include an antenna measurement laboratory, a radar area measurement system, a radar research and development activity (at the Chesapeake Bay Detachment, Chesapeake Beach, Maryland), an identification, friend or foe (IFF) ground station, and six separate facilities relating to specific types of radar systems.



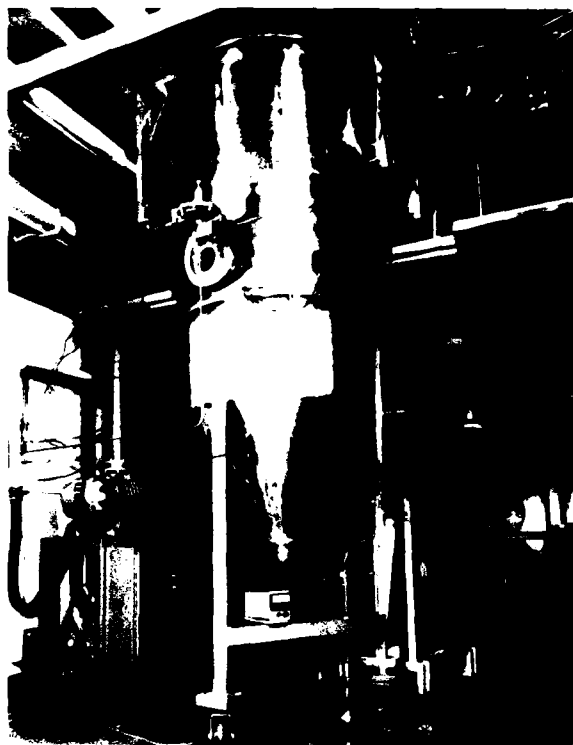
Dr. Jay Boris, head, Laboratory for Computational Physics, reviews results of numerical simulations of instabilities observed in laser fusion experiments. See article on page 139.

• Acoustics

NRL's facilities in support of acoustical investigations are located at the main Laboratory site and in Orlando, Florida—at the Underwater Sound Reference Detachment (USRD). At the main Laboratory site, there are three research tanks instrumented to study echo characteristics and to develop devices; the largest tank is 9 m deep, 12 m long, and 8 m wide. There is also an underwater acoustic holography facility for research in acoustic fields; and a water tunnel having a large blow-down channel with a 15-m test section used for acoustic and flow-induced vibration studies of towed line arrays and flexible cables. For acoustic surveillance array processing and acoustic data processing, researchers have access to the multichannel, programmable, digital data processing system—a system of DEC computers, high-speed array processors, and peripherals for up to 256 channels. The USRD facilities are described with NRL's Field Stations.

• Materials

The characteristics of materials also can be examined with a number of instruments. NRL has capabilities for X-ray analysis, and electron and Auger spectroscopy. It has a high-performance secondary ion mass spectrometer that represents a standard for surface analysis and



Ultrasonic gas atomizer used in the Material Science and Technology Division to produce ultrafine (less than 20 μm) spherical metal powders. The gas nozzle described in the article on page 178 is mounted within the chamber.

significantly extends the diagnostic capability of the technique. A high-resolution, high-performance, reverse-geometry mass spectrometer is used for probing reactions between ions and molecules. The Laboratory has a variety of machines with capacity up to 272,000 kg to test fatigue and fracture of new materials.

NRL facilities for rapid solidification processing were expanded significantly when the ultrasonic gas atomization (UGA) system was completed. This atomizer includes a UGA nozzle, a molten alloy capacity of 1 to 5 kg, a gas inlet pressure capacity of up to 27.6 MPa, and a process controller for programmable actuation of the system components.

The Laser-Materials Application Center provides laser irradiation services in support of a wide range of laser material interaction and effects studies, and material processing development. A high-energy continuous wave (CW) CO_2 electrical discharge laser operating at 10.6 μm can provide 12 kW or more of optical power at a workpiece. Both highly focusable (unstable

resonator) and spatially uniform (multimodal resonator) optics are available along with associated workpiece optics and fixtures. Laser output characteristic and workpiece transducer data-recording capabilities are also available.

• Condensed Matter and Radiation

To support studies in condensed matter and radiation technology, NRL has a 60-MeV linear electronic accelerator, a 75-MeV sector-focusing cyclotron, a 5-MV positive-ion Van de Graaff accelerator, a 2-MV electron Van de Graaff accelerator, a high-current 200-kV ion implantation system, a cobalt-60 radiation source, and a helium-3 dilution refrigerator. Taken together, these versatile facilities are unique in the Department of Defense. They are used for a variety of experiments, including the modification of materials by means of ion implantation and experiments on the radiation vulnerability and hardening of earth satellite components.



Dr. Alvin Knudson of the Condensed Matter and Radiation Sciences Division uses a microscope to position a micro-circuit before measuring charge upsets due to an incident ion beam. See article on page 127.

• Marine Technology

The Marine Technology Division has several facilities for experimental studies in fluid dynamics. These include a 30-m-long wind/wave tank to study wave forces on ocean structures and the interaction of ship wakes with ambient waves;



Dr. Kenneth Grabowski of the Condensed Matter and Radiation Division implants ball bearings with chromium ions. The implantation process greatly improves the corrosion resistance of the bearings which are used in Navy F-4 aircraft.

a 20-m dual-carriage tow channel capable of vertical stratification to study geophysical flows and wakes; and a large blow-down water tunnel with a 15-m-long test section to study noise associated with turbulent boundary layer flows around towed arrays. These facilities are equipped with state-of-the-art data acquisition and analysis systems. Other facilities include towed sensor arrays and related processors to acquire field information on upper ocean dynamic processes, a computer-controlled experimental stress analysis capability, and extensive equipment for shock and vibration measurement.

With these and other research facilities, NRL scientists are able to undertake advanced research in the 11 broad fields highlighted in this *Review*. The high-quality instrumentation required to support such a diversity of research represents a capital investment of over \$100 million.

Research Support Facilities

- Central Computing Services

NRL uses over 300 mainframe and mini-computer systems to provide high-speed data processing and numerical computation. The largest and most powerful, a Texas Instruments Advanced Scientific Computer located in the Research Computation Division, has a central processor, a high-speed bipolar central memory with a million-word capacity, and a disk storage

capacity of over 450 million words. It is a two-pipeline machine and is capable of 50 million floating point operations per second. The TI computer system is particularly well-suited to scientific usage, including vector calculations. It has an optimizing Fortran compiler and other scientific, statistical, and mathematical libraries. The Research Computation Division also has a DEC-10 and a Vax 11/780 that provide time-share services to the Laboratory.

A DICOMED System located in the Technical Information Division provides off-line graphics capability. It uses computer-generated data tapes to produce either color or black and white images on 16-mm movies, 35-mm slides, 8 by 10 in. viewgraphs, or microfiche. Some of the figures on pages 10 and 12 of this *Review* were generated on the DICOMED.

- Technical Information Services

The Ruth H. Hooker Memorial Library contains more than one million volumes, reports, and microfiche reports, along with 1700 current journal subscriptions. The library has access to 5 on-line computer search services accessing well over 100 databases. These can search mos. of the open literature, classified and unclassified DoD publications, other technical report material, and chemical substances by structure and substructure. The library also provides interlibrary loans, Library of Congress stack passes, translation services, foreign language tapes, college catalogs, published technical society standards, telephone books from major U.S. cities, and a map collection.

Publication services are offered by technical and nontechnical editors who arrange and format communications from author to audience into quality publications such as formal reports, brochures, handbooks, manuals, proceedings, or monographs. Illustrators and visual information specialists prepare camera-ready artwork, proceedings, journals, bulletins, certificates, and plaques for composition and printing. These specialists also prepare interpretive art, brochures, flyers, and displays, and cartoons and caricatures for special projects. The computerized technical composition (CTC) section prepares material which may contain difficult formulas or mathematical equations. Typewritten copy (in machine-readable typeface) can also be read by the optical character recognition (OCR) scanner. This OCR scanner

then generates double-spaced typescript and camera-ready copy. The motion picture and still camera section provides skills in the areas of microphotography, aerial and high-speed photography, and other experienced data documentation for the R&D community at NRL, as well as in the field.

Information Services specialists help researchers prepare visually effective material for exhibits and for presentations at professional meetings and seminars. They help scientists plan meeting agendas as well as help set up their visual equipment. These specialists also arrange for the use of NRL conference rooms and auditoriums and assist in the planning of videotaped programs.

• Engineering Services

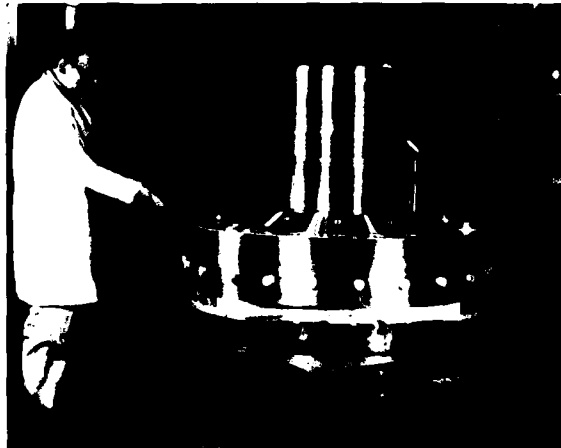
The Engineering Services Division (ESD) provides NRL and other Navy laboratories with engineers and highly skilled mechanics in support of research projects. The work is normally accomplished in one main building and several small shops located throughout the Laboratory.

The engineers and mechanics work with researchers on state-of-the-art needs from briefings, freehand sketches, detailed drawings according to MIL-STD requirements, NASA standards, or specifications generated by the scientists. ESD's extensive shop facilities and personnel perform a broad spectrum of tasks from engineering analysis in support of space research, fabricating heavy structures, and producing dense printed circuit boards by means of computers/computer graphics, to conventional/numerically controlled machines.

ESD also has extensive shop capabilities for sheet metal fabrication and assembly, metal finishing, electroforming, and electroplating. ESD operates a foundry in which heat treating of metals, limiting castings, and sand blasting jobs are performed. A plastics shop has extensive capability in machining, fabricating, molding, and forming various devices and forms from laminates, polymers, fiber-glass, and plastics.

FIELD STATIONS

NRL has acquired or made arrangements over the years to use a number of field sites or auxiliary facilities for research that cannot be conducted in Washington, D.C. They are locat-



P-1825(4)

The Engineering Services Division supports researchers in many ways. A machinist in the main shop adjusts a large assembly prior to final machining.

ed in Maryland, Virginia, California, and Florida. The two largest facilities are the Chesapeake Bay Detachment (CBD) and the Underwater Sound Reference Detachment (USRD).

• CBD

CBD, which occupies 68.1 hectares near Chesapeake Beach, Maryland, provides facilities and services for research in radar, fire-control equipment, optical devices, materials, communications, and other subjects. Because of its location on the west shore of Chesapeake Bay, unique experiments can be performed. Radar antennas 50 to 60 m above the water overlook the bay. Another site, Tilghman Island, is 16 km across the bay from CBD and in a direct line of sight from CBD. This creates a unique environment for low clutter and generally low background radar measurements. Experiments involving chaff dispensing overwater and radar target characterizations of aircraft and ships are examples of military-oriented research. Basic research in radar antenna properties, testing of radar remote sensing concepts, use of radar to sense ocean waves, and laser propagation is also conducted.

• USRD

Located at Orlando, Florida, USRD functions in many ways like a standards bureau of



Across top:

Panorama (eastward) of building 210 (on the left-hand side), which houses the Tactical Electronic Warfare Division, and building 222, home of the Technical Information, Public Works, and Financial Management Divisions

Far left:

Bust of Thomas A. Edison facing the Laboratory's main entrance. The Naval Research Laboratory originated from his suggestion for a national laboratory for defense-related research.

(Continued on next page)





Center left:

Navy Center for Applied Research in Artificial Intelligence, located near the south gate of Bolling Air Force Base, Washington, D.C. This building houses some of the members of the Information Technology Division.

Center right:

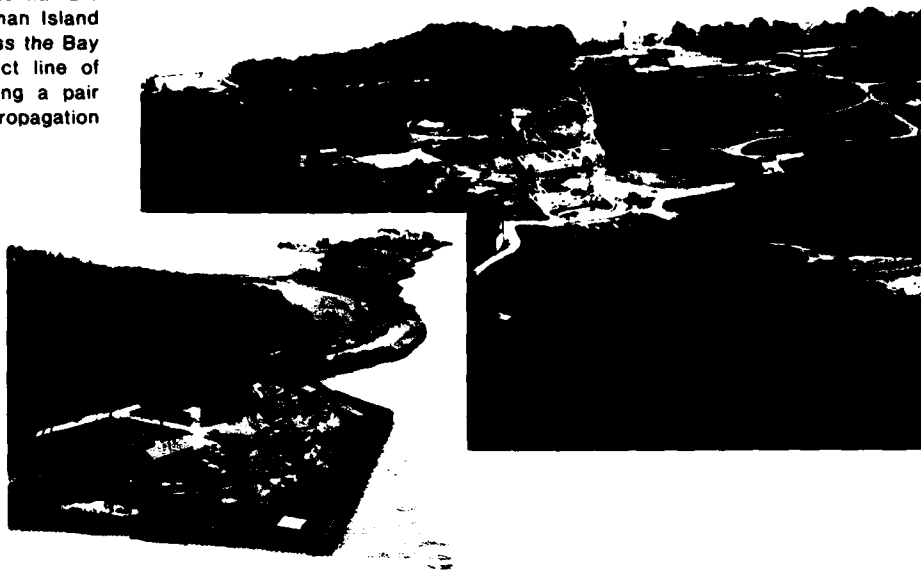
North side of the mall looking west toward the Potomac River. Shown from left to right are buildings 1 (part of the original NRL), 12, and 30.

Across bottom:

Panorama (westward) of building 207, which houses the Chemistry Division; building 208, home of the Electronics Technology Division; building 226, a secure auditorium; and building 209, which houses the Space Science Division



The Chesapeake Bay Detachment (CBD) facility overlooks the Chesapeake Bay from 50-m cliff. An over-the-horizon radar and a 46-m steerable microwave antenna are located there. The Tilghman Island site (*inset*) is 16 km across the Bay from CBD and in a direct line of sight from it, thus creating a pair of facilities for unique propagation studies.



NRL is the principal Navy activity for acoustic calibration, tests, and evaluation. The Underwater Sound Reference Detachment, located near Orlando, Florida, carries out the majority of these tasks. The nearly circular 50-m diameter lake is ideal for these purposes. *Inset:* the Leesburg (Florida) Facility provides an extremely quiet, natural underwater anechoic environment for calibration.

underwater sound. Its semitropical climate and two clear, quiet lakes (the larger is 50 m across, 11 m deep and nearly circular) are distinct assets to its research and development on sonar transducers and underwater reference standards and to its improvement of techniques to calibrate, test, and evaluate underwater acoustic devices. USRD has an anechoic tank for simulating ocean depths to 700 m and smaller pressure tanks for simulating depths to 7000 m. A spring located in a remote area about 40 miles north of USRD, at the Leesburg Facility, provides a natural anechoic tank for water depths to 52 m with ambient noise level 10 dB below that for sea state zero; larger objects can be calibrated here. The detachment has provided acoustic equipment and calibration services not only to hundreds of Navy activities and their contractors but also to allied governments.

• Marine Test Facilities

Located on Fleming Key at Key West, Florida, these facilities contain piers in an average water depth of 3 m and several flowing seawater test facilities capable of flow speeds to 70 knots (36 m/s). The site offers a clear, unpolluted seawater and atmospheric environment to study salt atmosphere weathering, stress corrosion, fouling resistance of coatings, cathodic protection, and electrochemical corrosion.

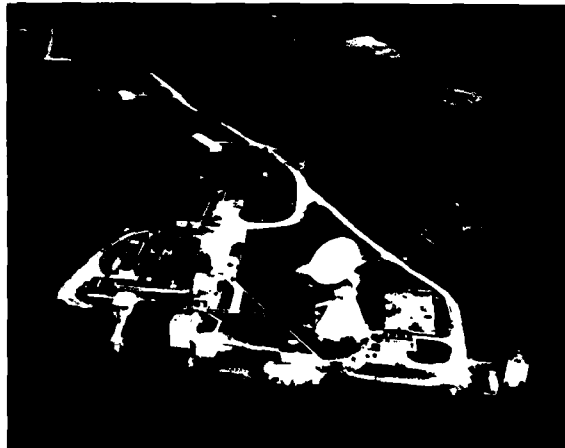
• Other Sites

Some field sites have been chosen primarily because they provide favorable conditions to operate specific antennas and electronic subsystems. Maryland Point, Maryland, 80 miles south of NRL, operates two radio telescopes with antennas measuring 25.6 and 26 m in diameter for radio astronomy research; NRL's Waldorf facility, 40 miles south of NRL, operates an 18.3-m X-band antenna and an S-band antenna of the same size for space and communications research. Pomonkey, a third field site in Maryland, 40 miles south of NRL, has a free-space antenna range to develop and test a variety of antennas. Another facility used in improving communications is the antenna model measurement range in Brandywine, Maryland, 40 miles southeast of NRL. Here, scaled model ships can be set up and rotated in the center of a range 305 m in diameter to provide data to aid in theoretical and experimental antenna design. NRL has



77425(1)

Radio telescope site, Maryland Point, Maryland. Each telescope, about 25 m in diameter, is used for high-precision radio astronomy measurements.



77425(7)

The Satellite Communication Facility, Waldorf, Maryland, is used as a transmit/receive site in the 2 to 20 GHz range

installations for satellite tracking in Blossom Point, Maryland, and at Vandenberg Air Force Base, California.

• Research Platforms

NRL uses ships and aircraft to conduct some of its research. Oceangoing research ships are obtained from a pool of vessels maintained by the Naval Oceanographic Office, Mississippi. For airborne research, NRL uses three four-engine



78383(2)

The satellite tracking station, Blossom Point, Maryland, is mainly used by the Space Systems Division

turboprop P-3A Orions and one four-engine turboprop P-3B Orion. These airplanes annually log about 1300 hours of flying time on projects ranging from magnetic bathymetry and electronic countermeasure research to studies of radar signal reflections.

NRL in the Future

To continue its growth and provide preeminent research for tomorrow's Navy, NRL must maintain and upgrade its scientific and technological facilities at the forefront. Its physical plant to house these facilities must also be adequate. NRL recently embarked on a Corporate Facilities Investment Plan (CFIP) to renew its physical plant. This plan and future facility plans are described below.

THE CFIP — NEW SCIENTIFIC FACILITIES

In 1983 NRL celebrated its 60th anniversary; some of its buildings date back to its beginning, 1923. With today's rapid growth and tomorrow's acceleration of science and technology, NRL is none too soon with its modernization plan (CFIP). It calls for the expenditure of nearly \$250 million to provide 46,500 m² of either new or renovated floor space by 1995. The plans call for the construction of 5 new buildings or facilities, major rehabilitation of 8 buildings,

limited rehabilitation of 25 buildings, and demolition of 34 very old or temporary buildings. The title page of this chapter (page 2) depicts NRL's campus after the completion of the CFIP. Present and future research require, in addition to sound structures, more precise environmental (temperature, humidity, and dust) control and more reliable power sources. Collocated, secure laboratory, computation, and office space is needed for future involvement in highly sensitive research. Buildings must be easily adaptable to presently unknown future needs, and greater overhead space will be needed for the larger pieces of equipment that will be required.

The five new facilities to be constructed will contain specialized laboratories. These are:

• Electro-Optics Laboratory

This 3359-m² facility will provide critically needed, highly specialized laboratories for research in ultrapure materials for low-loss, long-distance communication and surveillance links; fiber-optic sensors for undersea applications and for weapons fusing; infrared technology for detection and surveillance schemes; and laser weaponry and related technologies for space applications. Construction, scheduled to begin in 1985, will include special soil preparation and development techniques to minimize building vibration and settling; structurally isolated laboratory rooms in the ground bays, where the laboratory floors will hang free from the building structure and thereby be "vibration-free"; "isolated" foundation blocks for a centralized mechanical space and specialized mountings for mechanical equipment, piping, and ducts installed in the mechanical runways in the laboratory bays; class 100 clean suites; a 7.32-m, class 100 fiber draw tower; vaulted and specially shielded laboratory rooms and computer facility; and 24-hour temperature, humidity, pressure control, and stabilization.

• Plasma Physics Facility

Two separate laboratories will be constructed (in an existing building with a high overhead) to provide facilities for advances associated with the generation and propagation of very high-energy density plasmas and charged particle beams.

One of the laboratories will house an inductive energy storage and switch development facil-

ity. This facility will develop opening switches and power flow techniques to generate output pulses at levels exceeding 10^{13} W. It will also provide intense sources of X-ray radiation to simulate nuclear weapon effects on military systems.

The other laboratory will be established to study the propagation of very intense charged particle beams. A 5-MW generator will inject short pulses of electron current into the atmosphere or into other simulated environments. An optional laser beam will be available to preionize the propagating channel, and the properties and effects of such beams will be studied. The characteristics of more energetic beams should provide information for future military applications.

- Tactical Electronic Warfare (TEW) Laboratory

When this project is completed, NRL will augment its present TEW test facilities and coordinate them into a centrally managed system capable of assessing and improving the coordinated use of a variety of EW responses to various challenges. The proposed addition of 13,935 m² will about double the size of the current EW facility. This addition will contain a radar cross section model measurements facility, an off-board (remote) countermeasures facility—principally a subsonic wind tunnel, an EW-pod development laboratory, and an optical integration laboratory. These new facilities and the present EW test facility will be integrated with a broadband cable TV network. The total integrated EW complex will permit quicker and more effective response to Navy EW needs. Variations in operational conditions can be explored under completely controlled conditions leading to less expensive and quicker development of better EW systems. These variations can also lead to a scale-down in the number of the very expensive at-sea and in-air tests and evaluations now required to quantify system effectiveness and to optimize utilization.

- Secure Laboratory Facility

This facility will address the continuing and expanding need for secure computational and laboratory spaces. The building will house more than 70% of the highly classified work now in progress at NRL.

- General Purpose Laboratory

This will be an environmentally controlled facility to provide stringently clean laboratories with carefully controllable temperature, humidity, ambient dust, and power for investigations in the rapidly evolving fields of electronic technology and composite materials synthesis and exploitation.

REHABILITATION OF SCIENTIFIC FACILITIES

Several of the research facilities at NRL will be upgraded in the near future. These are highlighted below.

- Central Computing Facilities

A replacement for the Advanced Scientific Computer (ASC) is presently being procured. It will be replaced with a current generation Class VI supercomputer to perform at least 20 million floating point operations per second on a combination of vector and scalar code. Overall performance of at least 2.5 times the ASC on a set of benchmark programs is required. The Class VI machine will have front-end processors providing interactive access, some timesharing services, and access from local area networks and the military network (MILNET).

An NRL integrated communications network (NICENET) is planned that will provide access to the central site facilities from both terminals and other computers at NRL; other potential NICENET uses (e.g., video conferencing) are also under consideration. The ultimate goal of this network is to provide universal access to common-shared computer resources, gateways to other networks and graphics peripherals, and other noncomputer communications services.

- Other Facilities

Specialized facilities are being installed or upgraded in several of the research and support divisions.

Information Services—The Artificial Intelligence (AI) Center will continue installation of the local area network for its eight computers. Additional computers planned are the Symbolics 3500 listing processing (LISP) machines to

complete accessibility to all LISP and AI developments, plus SUN Microsystems, Inc. SUN workstations for the multisensor integration project also will be installed.

Plasma Physics—Facilities (combining the established technology with new concepts) are being constructed to study methods of accelerating electrons to high energy at very high current levels. Such facilities will provide the technology needed to develop very compact (and economical) accelerators for advanced military systems. A large inductive store is being designed to provide a driver for an advanced plasma implosion facility to serve in a variety of applications, including X-ray laser development.

Electronic Warfare—The electronic warfare program includes plans to develop, as part of the CFIP, a major simulation capability—the coordinated electronic warfare simulation laboratory (CEWSL)—to explore electronic countermeasure applications in all stages of naval combat.

Computational Physics—Work is continuing on the Reactive Flow Modeling Facility, which the Laboratory for Computational Physics is developing on its VAX 11/780 computer. This facility couples multiple inexpensive array processors working asynchronously in parallel. It is now being installed and, when complete, will provide near-supercomputer performance for the cost of a minicomputer installation. This facility can be used for applied research on nuclear and environmental airblast effects; turbulence modeling for jets, wakes, and reactive flows; and for atmospheric turbulence predictions.

Materials—In 1985 a repetitively pulsed high-energy, CO₂ laser operating at 10.6 μm will join the existing Laser-Materials Application Center's 12-kW continuous-wave (CW) CO₂ laser. Pulse energies up to 500 J will be available as 20 to 100 μs during pulses at repetition rates to 100 Hz. New test cells and optics will permit CW, repetitively pulsed, or combined simulta-

neous irradiation of samples. The extension of state-of-the-art molecular beam epitaxy (MBE) technology to silicon and related materials is planned with the addition of new equipment.

Marine Technology—The addition of a recirculating flow capability to the blow-down water metal-mixture fabrications, ion implantations, base metal claddings, boron and graphite fiber-reinforced plastics, and laser-activated machining of ceramics. An advanced technology and fabrication facility is being planned to pursue investigations leading to fabrication techniques using these new and/or unusual materials, processes, and techniques developed by NRL research divisions or other Navy Laboratories. Longer range plans call for new machines, both computer and human controlled with enhanced precision capability using new and unusual material fabrication. Coupled with this modernization will be structural and thermal analysis capabilities, plus electronic engineering, design, analysis, and printed-circuit board layouts.

Further Information: The *NRL Fact Book* gives more details about the Laboratory and its operations. It lists major equipment, current fields of research, field sites, and outlying facilities, and it also presents information about the responsibilities, organization, key personnel, and funding of the divisions, detachments, and other major organization units.

Information on the research described in this *Review* may be obtained by contacting Mr. Richard Fulper, Jr., Head, Technology Transfer and Special Programs, Code 1005.4, at the above address. He may be reached at (202) 767-3744. General information about NRL may be obtained from the Public Affairs Office, Code 2630, at the above address or by phone (202) 767-2541. The sources of information on the various non-research programs at NRL are listed in the *Review* Chapter entitled "Programs for Professional Development."

NRL IN THE SCIENTIFIC, TECHNOLOGICAL, AND DEFENSE COMMUNITY

The NRL Review

This *Review* contains highlights of the unclassified research and development program of the Naval Research Laboratory (NRL) for the 1983 calendar year. As such, it sets in perspective a portion of the accomplishments of over 3000 people and expenditures in excess of \$350 million. A detailed report of a program of this magnitude cannot be accomplished within the pages available to this publication. Rather, the document attempts, through articles in 11 selected topics, to illustrate the nature of the NRL undertaking for 1983, the impact of this undertaking on the national and international scene, and the proficiency with which the undertaking was accomplished. Although these 11 selected areas of research exhibit the broad base of expertise in the unclassified research program at NRL, the 64 scientific articles represent but a small fraction of the total effort of the Laboratory personnel.

The State of NRL

The scientific and technological efforts reported in this *Review* indicate that NRL's performance during the past year has continued the Laboratory's tradition of excellence. NRL has always faced the interesting situation of having near-term sponsor requirements to satisfy and "turning to" for special high-priority projects,



Dr. Timothy Coffey
Director of Research

while at the same time maintaining its role as the Navy's corporate laboratory with responsibility for conducting long-term research in areas of potential significance to naval warfare. The objective of these long-term programs is to ensure that our military posture will not become unstable by unanticipated advances in the technology of other nations. At any time, these two requirements are likely to be at odds with one another. To be successful, therefore, we must continue to demand an orderly prosecution of a substantive research program supplemented by a rapid response to perceived Navy needs.

A review of the past several years indicates that NRL's programs are continuing to expand at a healthy rate. Our sponsoring community has a continuing and growing interest in our products. Their sponsorship will continue to grow because the Laboratory will continue to advance its technology activities to meet their needs. This past year, for example, we had major new initiatives in the fields of fiber optics, advanced radar concepts, and biotechnology.

NRL Today

Today NRL's programs encompass most areas of the physical and chemical sciences including plasma physics, electronics and electronic warfare, materials, optical and radiation sciences, acoustics, atmospheric and aerospace

sciences, component technology, numerical modeling, and artificial intelligence. The multidisciplinary nature of NRL, during 1983, was demonstrated by contributions in very diverse areas. For example,

- we helped to identify the mechanical factors that contributed to the failure of Dr. Barney Clark's mechanical heart;
- we developed the Space Ultraviolet Radiation Experiment instrument which will measure the natural radiation field in the upper atmosphere during future space shuttle flights; and
- we produced, evaluated, and tested an improved Central Air Monitoring System that will detect hazardous gases in nuclear submarines.

The breadth and depth of NRL, which make it unique among Navy research laboratories, allow us to pursue a varied research and development program, but more importantly, allow solutions to any single problem to come from the many diverse scientific and technical fields that NRL personnel represent.

It is necessary that the Laboratory retain state-of-the-art facilities to accomplish its scientific and technical program. Over the past year, the Laboratory has made several significant additions or improvements to its already extensive portfolio of facilities. Significant improvements to the Central Target Simulator Facility have continued. This facility is used for electronic warfare simulation activities; it is unique in the Western world. The Laboratory has developed a facility for drawing fluoride glass fibers. This unique facility is an important component of our fiber-optics program. A major

investment has been made in upgrading the Laboratory's Spacecraft Payload Checkout Facility, and when this extensive facility is completed, it will represent a major national asset. NRL has also been making significant investments in upgrading the computing capabilities across the Laboratory.

But NRL is more than programs, projects, and facilities. NRL is *people* engaged in creative enterprise. Our success begins with a single scientist or a small group of researchers with ideas and goals fostered by the diverse scientific interactions which occur among our divisions, as well as the backing of a well-managed scientific

and support organization whose personnel put a premium on excellence and create a climate for inventiveness. And even though this *Review* emphasizes the scientific programs of NRL, these programs comprise people who are often involved in other programs and activities of a less scientific nature, but nevertheless very important to the success of the Laboratory. These are described in more detail in the section, "NRL—Our heritage, NRL today, NRL in the future" and the chapter, "Programs for Professional Development."



The Future of NRL

Within the next few years, NRL will see significant new capabilities and facilities developed in its electronic warfare programs, in its superpower plasma physics programs, in fiber-optic sensors and systems, and in naval applications of molecular engineering. We will also see major new initiatives in our space science and technology programs.

Predicting the future is always difficult. This is especially true in high-technology areas. Nevertheless, I think it is clear that NRL can

anticipate significant future programs in the areas of

- biotechnology for naval application,
- ultraviolet sensing of the upper atmosphere,
- advanced accelerators for charged particle beams,
- advanced multilayer electronic components,
- active undersea surveillance,
- inverse synthetic aperture radar,
- offboard countermeasures, and
- applications of artificial intelligence to Navy problems.

These programs will assist in maintaining the intellectual vitality of the Laboratory and promise major advances in Navy technology.

Looking downstream beyond the next several years, I see a clear need for a major renovation program at the Laboratory. We are setting such a program into motion which permits us to enter the 21st century with vintage 1980 and 1990 facilities. Formulating and selling such a plan will require substantial work on the part of Laboratory management and significant support from our patrons. It is, however, a program which must be undertaken. This program is described in the section entitled "NRL—Our heritage, NRL today, NRL in the future."

One of the observations I have made during the past year, in spite of the apparent turmoil of the moment, is that the Laboratory in retrospect has been rock solid in its level of programs, in its mix of programs, and in its ability to contribute to the Navy and the national science and technology enterprise on both a short- and long-term basis. I predict that this situation will continue to prevail—both the turmoil and the ultimate stability of the program. Across the board, the Laboratory will continue its excellent tradition of "research for tomorrow's Navy."

HIGHLIGHTS OF NRL RESEARCH IN 1983

- A more complete model for the hydrodynamic wake of a ship has been developed that allows scientists to simultaneously predict, for the first time, the ship-generated Kelvin wave and turbulent wake with their mutual interactions. See article on page 71.

* * *

- Damage susceptibility of composite structures can be predicted and experimentally verified without testing the full-scale structure. The cost saving is significant, and the technique provides data for a material selection program where damage susceptibility is a factor.

* * *

- A practical method of making ceramic-coated fiber composites has been demonstrated. The composites are tough and have very useful strengths (nearly 50,000 psi flexural strength). These advances can help meet a variety of Navy needs from improved radomes to improved armor. See article on page 160.

* * *

- A universal law of solids, which relates twin density with grain size and temperature, has received significant developmental contributions from NRL. The use of these formulations in the study of transformation kinetics under nonisothermal conditions may lead to metallurgical processes necessary to reduce or eliminate planar defects in advanced materials.

* * *

- The characteristics of turbulent boundary-layer-imposed wall-pressure fluctuations have been correctly predicted by a numerical solution of the full Navier-Stokes equations. This work should help eliminate hydrodynamics noise and structural vibrations which limit the detection capability of many Navy sonar systems. See article on page 202.

* * *

- Structural information can now be obtained up to 10,000 times faster from a high-pressure, variable temperature environment by using energy-dispersive X-ray diffraction techniques and heterochromatic synchrotron radiation. This permits the study of much faster pressure-induced phase transitions which occur in a number of new solid lubricants for use in the cruise missile engine as well as the thermal barrier coatings for turbine blades.

* * *

- NRL has produced bolometers that are much faster, more rugged and reliable, and operate over a much wider temperature range. These superconducting devices are fabricated of ultrathin niobium nitride on single crystal insulating or semiconducting substrates. They are used to study the basic properties of semiconducting materials.

* * *

- Spacecraft hydrogen maser frequency standards for the NAVSTAR Global Positioning System (GPS) were significantly improved. The GPS requirements on frequency stability can now be fulfilled with a laboratory prototype hydrogen maser. This frequency stability will maintain satellite synchronization for more than one day, which may be necessary in wartime. The technology is currently being used in a hydrogen maser GPS program. See article on page 129.

* * *

- The development of a future Identification, Friend or Foe system has been significantly advanced at NRL. This system not only provides security against deception by an enemy appearing as a friend (as is already done by the Mark XII IFF system), but it also provides protection against enemy exploitation and jamming. The system will be acceptable to NATO and meet anticipated requirements.

* * *

- The Ocean Surveillance Tracker Correlator (OSTC) test-bed software specification and development was partially done at NRL. The OSTC should provide the test bed needed to test alternate tracker/correlators—there are nearly 300 at present—and should result in more effective algorithms and an elimination in redundant development efforts.

* * *

- The true vulnerability of submarine hull insulation to fire has been demonstrated, resulting in an ambitious hull insulation program. The full feasibility of the fire-suppression technique—nitrogen pressurization—for immediate extinguishment of fires in submarines has been realized by using NRL's Fire I, a 10,000 ft³ fire test chamber.

* * *

- Radar communication can provide surveillance information needed for effective task force operation inexpensively and without significant degradation of radar operation. The first data test patterns were successfully transmitted through an NRL radar and were correctly received. See article on page 59.

* * *

- A burnthrough range contour about a radar target that is being screened by a number of noise jammers of various types and dispositions has been digitally modeled. The model can evaluate systems and tactics for screening a high-value radar target by

means of noise jamming, will have continuing application to countertargeting and counter C³ studies, and has been used for the Outer Air Battle Study.

* * *

• The crystal structures of dye synthesis intermediates have been determined and are to be used at the Lawrence Livermore National Laboratory in the Laser Isotope Separation Program. NRL's work indicates that large-scale, low-cost industrial systems of enough of the dyes are possible so that dye-laser isotope separation can be accomplished on the scale of the Oak Ridge process. An ultimate application is an enhanced source of nuclear fuel for the Navy.

* * *

• NRL has determined the cause of sonar dome rubber window (SDRW) failure in U.S. Navy surface combatants. Techniques for correcting deficiencies in existing SDRWs are being developed, and new SDRW construction is being modified to eliminate the corrosion fatigue failure mechanism. This will save the Navy considerable cost and loss of operational readiness. SDRWs with incipient corrosion fatigue failures are identified by X-ray nondestructive evaluation in drydock and are repaired or replaced. Pierside inspection is being extended to all ships with SDRWs, independent of location or drydock schedules.

* * *

• Ocean temperature fluctuations on horizontal scales of 1 cm to 2000 km have been estimated with a variety of observations. Towed thermistor array observations have been used to characterize the horizontal/vertical structure of the smaller scale fluctuations. These estimates potentially permit the optimization of sensors for submarine detection.

* * *

• NRL has estimated the force-time histories associated with the impact of MK48 Mod. 1, AD CAP, and ALWT exercise torpedoes against 637-class submarines. These estimates are used by Navy agencies and contractors to calculate the damage that might be sustained by a submarine struck by an exercise torpedo. The estimates also help to develop protective measures and/or operational constraints which must be used to permit torpedo exercises with submarines.

* * *

• A picture data compression system has been developed to increase the information throughput rate of the Advanced Unmanned Search System (AUSS) vehicle by a factor of two to four. This will greatly increase vehicle search rate and significantly advance Navy capabilities in the area of deep ocean search.

* * *

• NRL scientists have invented a procedure for electrodepositing tough, dense, adherent coatings of tantalum carbide and tungsten carbide on metals from a eutectic

fluoride melt. Electrodeposition promises better control of coating thickness, structure, and perhaps composition, with the ability to coat inside valve bodies and cooling holes. These coatings can be used for rub and wear surfaces operating up to 600°C in Navy engines and machinery.

* * *

• A technique to correct underwater acoustic tests was discovered at NRL. This technique analytically removes the acoustic effects of both the support plate used in a panel test of an underwater acoustical material and the water medium in which the test is conducted. With this technique, panel tests can now provide results that are more useful to the designer of Navy systems that use underwater acoustical materials. Also, this technique can now be used as a benchmark for other test methods.

* * *

• A hydrophone incorporating PVDF piezopolymer in tubular form has been designed at NRL-USRD with very good results. The hydrophone has a flat receiving response to 6 kHz and a smooth usable response to over 50 kHz. It has survived explosive shock greater than that specified for Navy use.

* * *

• A fast vacuum-opening switch called a plasma erosion opening switch has been developed to use with pulsed-power generators. This switch can conduct several megamperes for 100 ns and can open to a high impedance in less than 20 ns. In the open state, the switch can hold off megavolt potential differences without shorting. See article on page 144.

* * *

• Very uniform illumination of laser targets is produced by a new technique that imposes controlled spatial incoherence on a laser beam. This uniform illumination may be a step forward in achieving direct illumination laser fusion and may be applicable to optical microlithography.

* * *

• An acoustically transparent test chamber for pressure cycling underwater electroacoustic transducers constructed of rubber hose eliminates chamber boundary effects and nearly approximates free-field conditions. The test chamber allows the undistorted measurement of acoustic and electrical transients that may be produced by hydrostatic pressure changes. See article on page 89.

* * *

• A standard neoprene formulation, designated as Neoprene 5109, has been developed for NAVSEA. For the first time, the Navy is now able to designate the neoprene rubber to be used in sonar transducer design and fabrication. This will greatly improve the reliability of Fleet transducers and consequently the operation of sonar systems.

* * *

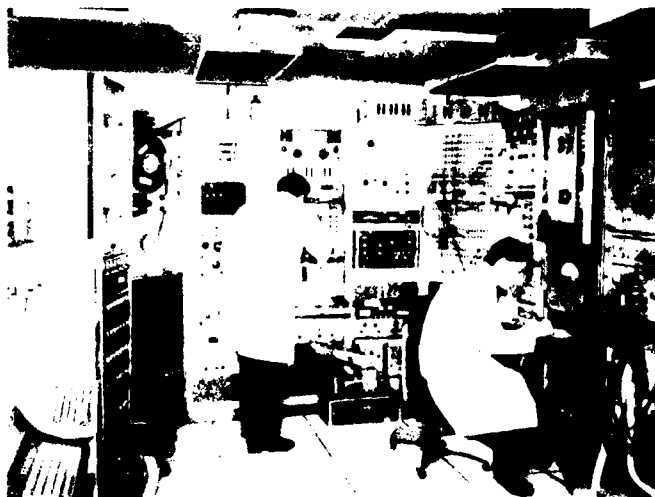
- Accurate measurements of very small aerosols at low concentrations can be made by instruments developed at NRL. These measurements will allow evaluation and prediction of C³I system performance under various meteorological conditions. See article on page 110.

- A team including NRL scientists identified the reason for the failure of Dr. Barney Clark's mechanical heart valve. They recommended improvements to the design and assembly of the heart valves.

- The Space Ultraviolet Radiation Experiment (SURE) is an extreme ultraviolet spectrograph developed by NRL to obtain moderate resolution spectra of the earth's extreme ultraviolet dayglow and nightglow. The SURE experiment was flown successfully on the space shuttle (STS 7) in June 1983. It was also the first experiment to use the newly developed Get Away Special (GAS) cannister opening lid. The experiment recorded over 5 h of airglow data and measured the diurnal variation of the intensities of the He 584 Å and O⁺ 834 Å emissions.

- Elastic body resonances have been identified both experimentally and theoretically for various solid bodies and shells. These resonances result in identifiable patterns in both the time and frequency domains. The major application for the Navy is the development of accurate classification algorithms.

*Artificial intelligence, information
processing, and signal transmission*



41 An AI Expert System for Radar Target Recognition

David W. Kerr

AI can improve an operator's ability to identify targets.

43 Applying Information Theory to Speech Recognition

David K. Burton

A new technique produces high recognition rates.

45 Improving the Narrowband Voice Processor

George S. Kang and Stephanie S. Everett

Voice quality is greatly improved in narrowband transmission.

48 Improving Fault Isolation in Complex Systems

Kenneth DeJong

Can AI-aided medical techniques find a faulty component?

49 Ground Wave Propagation over Multilayered Earth

Edward J. Kennedy

A realistic earth model improves radio wave propagation theory.

50 Design of High-Frequency Networks for Tactical Communication

*Dennis J. Baker, Jeffrey E. Wieselthier, Anthony Ephremides,
and Dennis N. McGregor*

More efficient network management provides higher survivability.

53 Model for Moving Platform Multipath

David E. Corman

Moving sea and ships distort radar returns.

ARTIFICIAL INTELLIGENCE

Certain knowledge can only be obtained by combining data from sensor suites—either collocated and/or dispersed, and either from the same or different sensors. Such integrated systems (or even a single sensor) can produce extremely high data rates; thus, automated processing and analysis and adequate signal transmission—in both data rate or bandwidth and distance—are crucial to maximize the use of the information received. Rapid advances in processing information are made by interactively combining the human mind with artificial intelligence (AI) techniques. Many simple tasks can be successfully accomplished with AI alone, freeing a human operator for higher level tasks. The first three articles describe such applications of AI, and the last four articles discuss transmission techniques.

The divisions involved in the work described in this section are Radar (Code 5300), Tactical Electronic Warfare (Code 5700), and Information Technology (Code 7500).

NRL has many research projects in artificial intelligence, information processing, and signal transmission. These include

- Navy telecommunications networking and broadband architects,
- combat management information systems,
- decoys and offboard countermeasures, and
- improving radars through adaptive techniques, clutter-reduction signal processing, and waveform designs.

Page 38, clockwise from upper left:

To extend the Navy's program in satellite communications, this 60-ft antenna, located at the Waldorf microwave research facility, provides a transmit and receive capability to various communications satellites in a range of frequencies from 2 to 4 GHz.

Prototype long duration expendable decoy (LODED) ready to take off from a pneumatic catapult prior to a test flight (R. Foch)

Time sequence of smoothed power spectra of the acoustic energy in the "VE" of the word "SEVEN." See article on p. 43 by D. Burton.

Centralized facility for playback, duplication, and analysis of analog tape. Tailored analysis of electromagnetic signals is performed through various spectral analysis techniques and universal demodulator and media outputs (J. Davis).

An AI Expert System for Radar Target Recognition

D.W. Kerr
Radar Division

An artificial intelligence (AI) "expert system" was developed and demonstrated which recognizes classes of targets based on their radar images. Until now, radar image recognition has been performed only by skilled human interpreters. The human expert's interpretation procedure may be divided into two stages: visually analyzing a radar image into patterns and features; then deciding on the target class by comparison of the image features with those of possible targets (target recognition). Human judgment is required in the decision process because only some of the possible features are available in a given image frame, and even those may have a considerable degree of uncertainty. In some applications hundreds of different possible target classes must be distinguished, and human training and memory impose significant limitations. The computer-based AI radar image classifier automated the second, target recognition, portion of the human interpreter's task. As an operator viewed a radar image, the computer questioned him about features which distinguish possible targets. After a short sequence of questions, it announced the target's classification with a confidence estimate. It was tested on many examples from 10 similar target classes, and high classification rates were attained.

Microwave radar is usually thought of as a sensor only for the detection and location of targets at long ranges—typically tens to hundreds of miles away. NRL engineers have found methods which use coherent processing of wide-bandwidth radar signals to provide detailed images of small regions at long ranges—a radar zoom mode. Radar imaging of targets has the usual advantages of microwave radar itself: availability at long stand-off ranges in all weather, day or night. Radar imagery has lower resolution than high-quality optical photography, and it often provides unusual apparent viewing aspects. Human operators can classify targets from their radar images when they are properly trained. Human operators, however, are subject to fatigue, and

can only remember the details of a quite limited number of possible targets.

The Basic System: The idea of using digital computers to aid or replace human operators for classifying radar imagery is attractive. Until recently, however, computers have been used mainly to perform straightforward calculations rather than to do reasoning from uncertain evidence as is done by human interpreters. Using AI techniques, the expert system developed by NRL scientists allows a computer to use the same rules of reasoning used by a human expert. If the human expert's inference rules can be formulated clearly, the AI expert system can reason from uncertain information to arrive at reliable conclusions.

In this project the knowledge used by radar image interpreters was formulated into inference rules which were encoded into an existing AI expert-system program. The existing program was originally designed to advise a U.S. Marine Corps artillery battery on which target to fire for maximum effect. It was changed to embody the new domain of knowledge of radar image classification. A small but very difficult portion of the target classification problem was chosen for the test: distinguishing among 10 similar targets.

In the operation of the system a human interpreter observes a radar image. The expert-system program, via a computer terminal, asks the operator questions about fine details in the image, the operator responds to each question with a number between -5 and +5: -5 is "definite no," 0 is "don't know," and +5 is "definite yes." Intermediate numbers represent varying degrees of uncertainty. The program continues to ask questions until it has built up a desired degree of confidence in its classification decision. Then it produces a list of the 10 classes of targets in descending order of likelihood. The program uses a unique criterion called "merit" to select the question to be asked next to make the greatest step toward the final classification.

Design of Expert System: Figure 1 shows the expert system design for this project. The human operator interacts with the EXECUTIVE portion of the system. When a classification sequence is initiated, the user has the option of

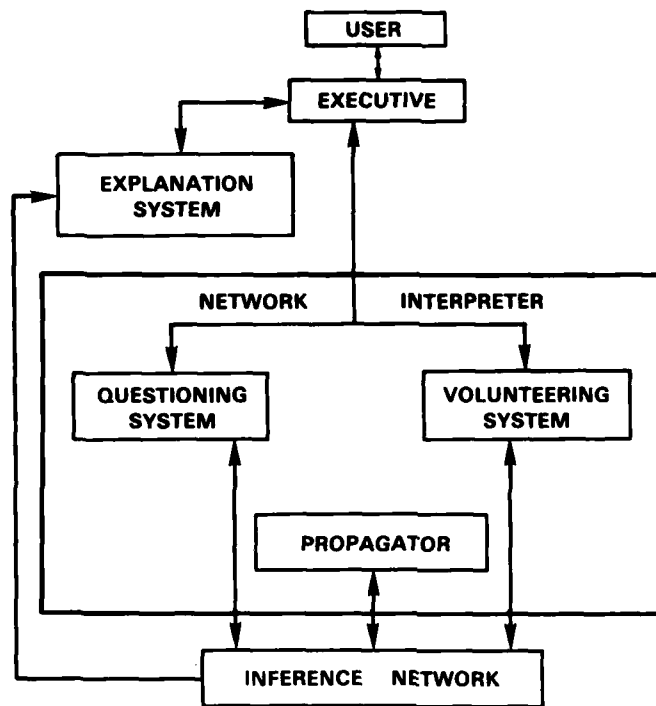


Fig. 1 - Expert-system architecture

volunteering information he sees in the image or allowing the system to select questions. The **INFERENCE NETWORK** contains the expert knowledge of the radar classification problem. The **NETWORK INTERPRETER** accepts radar image feature information, calculates the confidence factors for all possible target classes, and selects the next question with the highest "merit." The outputs of the **NETWORK INTERPRETER** are passed back to the operator via the **EXECUTIVE**. At any time the user can use the **EXPLANATION SYSTEM** to determine the logic behind either classification results or the last question asked. The **NETWORK INTERPRETER** terminates a classification sequence when either a confidence threshold has been achieved or the possible questions have all been asked.

Testing of System: The expert-system classifier was tested against more than 100 samples of radar target imagery of all qualities. In general, the quality of the image determined the confidence the operator expressed in his -5 to +5 responses. The greater the operator's

confidence, the greater the confidence expressed by the program in its results, and the greater the accuracy of the classifications. Even when the operator had to answer most of the questions with +3 or -3 ("think so" or "think not") the classifier provided the correct classification in 84% of the tests as is indicated in Fig. 2.

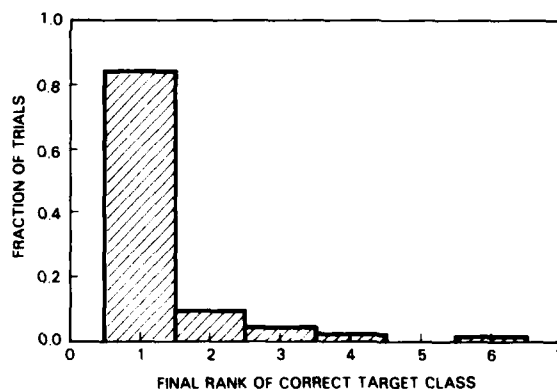


Fig. 2 - Histogram of rank of the correct target. Rank is the location on the list of the order of likelihood that the actual target occupies.

The highly promising results of this work suggest at least two possible applications. Such an expert-system, essentially in its present form, could be used as an online advisor to a human interpreter on board any Navy aircraft or ship with an imaging radar. In the future, the addition of a machine image-understanding front-end could produce a fully automatic target classifier.

This work was performed in a cooperative project between David L. Drake of the Radar Division who provided the radar imagery and the human expertise in target classification, and Dr. Lashon Booker of the Navy Center for Applied Research in Artificial Intelligence who modified the existing expert-system program to the target classification task.

[Sponsored by ONR, NAVELEX] ■

Applying Information Theory to Speech Recognition

D. Burton

Information Technology Division

Recognition and translation of human speech by a computer is becoming an important requirement in modern information processing systems. To meet this requirement, scientists at NRL have studied new information theory methods of speech recognition. When trained for a particular speaker, these speech recognition methods achieve 99% correct recognition of isolated words (words spoken out of context), and they do this without using any information about the time ordering of individual speech sounds within the word.

A computer speech-recognition capability is important because it would increase the speed of data handling. It is especially important to the Navy because it would improve the performance of personnel in hands-busy, eyes-busy situations such as those frequently encountered by fighter or helicopter pilots. It would certainly benefit the hearing impaired and the physically handicapped, and it would increase office (word processing) and factory (inventory control) productivity.

In the next section, we briefly describe the fundamental concepts that led to our speech

recognition methods. This is followed by descriptions of two new speech recognition methods and results using these methods. Finally, we conclude with a discussion on the significance of these results.

Fundamental Concepts: These new speech recognition methods are the result of research done at NRL on the inference properties of an information measure known as *relative entropy*. Entropy is a measure of the information or uncertainty in a signal that can be described by a probability distribution; and the relative entropy between two probability distributions is a measure of the similarity of information contained in the two distributions. For example, if the probability of occurrence of an event is one, then there is no uncertainty in its occurrence, and its entropy is zero. If a large relative entropy exists between two distributions, however, the information content of the two distributions is very different; a small value indicates that the two distributions are similar. In earlier work, NRL provided an axiomatic foundation for an existing method of inference based on relative entropy called the *principle of minimum relative entropy* and recently, together with Stanford University, developed a new pattern recognition technique based on this inference principle [1].

Our speech recognition work [2,3] is an application of this new pattern recognition technique, which we call minimum-relative-entropy pattern classification and cluster analysis (MRECCA) [1]. MRECCA is a very general procedure for classifying an input vector (set of scalars) of measurements as one of a prestored set of vectors that characterizes a stochastic source. The first step in the application of MRECCA to speech recognition is to obtain a set of typical vectors (lagged autocorrelation values) from a source; we call this set of measurements the training data. The typical source vectors are obtained from repetitions of a speech unit (word, syllable, phoneme, etc.) produced by either a single or several different speakers. The set of training vectors is then grouped into clusters with similar properties using the smallness of their relative entropies as a measure of their similarity. The cluster centroids define the characteristic vectors for that source. We call this set of

vectors a *codebook*. Using this codebook, an unknown input vector is classified according to the codebook vector that is closest in the relative entropy sense.

Approaches and Results: There are two categories of isolated-word recognition techniques: speaker-dependent and speaker-independent. In speaker-dependent recognition, the speaker whose speech is to be recognized provides training samples of each word. The training samples in speaker-independent recognition, however, come from many different speakers, and new speech from additional speakers is recognized. Because MRECCA is a general procedure for representing an information source, it can be used in both speaker-dependent and speaker-independent recognition.

NRL has developed and evaluated two new isolated-word recognition approaches that use MRECCA. In one approach we design a single codebook for each word in the recognition vocabulary—a *single-section* codebook. Each vector in a single section codebook has no time information associated with it. The second approach uses MRECCA to design a separate, time-ordered sequence of codebooks for each vocabulary word—a *multisection* codebook.

A single-section codebook is designed from training data consisting of several repetitions of a word. This is done for each word to be recognized. An unknown input word is identified by representing it as a set of measured autocorrelation vectors and finding the codebook that represents the input vector set with the smallest average relative entropy. Since a codebook contains no time-sequence information, none is used in classifying an input utterance. Using the single-section approach [2], NRL achieved a speaker-dependent recognition accuracy of 99% on a standard 20-word-vocabulary data base that is distributed by the National Bureau of Standards [4].

A multisection codebook is also designed from multiple repetitions of a word. After designing the codebooks, an input word is recognized by first temporally dividing it into sections that are the same size as those used in making each of the components of this codebook. Each input section of vectors is then compared with

the appropriate multisection codebook component. The unknown input is classified according to the multisection codebook that represents the input word with the smallest relative entropy averaged over the word. For speaker-independent recognition, this approach achieved a recognition accuracy of 97% on the standard 20-word vocabulary, and a recognition accuracy of 99% when the words were just digits (zero through nine) [3].

Discussion: Traditionally, successful approaches to isolated word recognition use information about the time sequence of speech sounds. This is intuitively attractive because it seems obvious that accurate recognition requires the use of such information. Our results show, however, that time-sequence information is less important than was previously assumed. Without using it, the single-section approach achieved speaker-dependent recognition accuracy greater than 99% [2]! Thus, NRL has shown that, for certain vocabularies, single-section codebooks alone contain enough information to recognize isolated words, and MRECCA does an excellent job of finding such vectors.

The present method requires large amounts of speech data from a source, many times inconvenient to obtain. We are studying methods to minimize this inconvenience and improve the computational efficiency of our isolated-word recognition method. We are also studying methods to achieve recognition of acoustically similar words and of connected speech.

[Sponsored by ONR]

References

1. J.E. Shore and R.M. Gray, "Minimum Cross-Entropy Pattern Classification and Cluster Analysis," *IEEE Trans. Pattern Anal. Mach. Intel.*, PAMI-4, 11-17 (Jan. 1983).
2. J.E. Shore and D.K. Burton, "Discrete Utterance Speech Recognition Without Time Alignment," *IEEE Trans. Inform. Theory*, IT-29, 473-491 (July 1983).
3. D.K. Burton, J.T. Buck, and J.E. Shore, "Parameter Selection for Isolated Word Recognition Using Vector Quantization," *Proceed-*

ings 1984 IEEE Intl. Conf. Acous., Speech, and Signal Proc., 9.4.1-9.4.4 (Mar. 1984).

4. G.R. Doddington and T.B. Schalk, "Speech Recognition: Turning Theory to Practice," *IEEE Spectrum*, 26-32 (Sept. 1981). ■

Improving the Narrowband Voice Processor

G.S. Kang and S.S. Everett
Information Technology Division

High quality voice transmission requires data rates of about 64,000 b/s, but intelligible speech can be transmitted at 2400 b/s using a special encoder—the narrowband linear predictive coder (LPC). Unfortunately, the resulting speech is unnatural and of poor quality because the LPC removes some of the critical features present in the original voice. Researchers at NRL have successfully improved the quality of narrowband LPC speech by reintroducing some of these missing features into the LPC process. Since the Navy relies heavily on narrowband channels (having approximately a 3 kHz bandwidth) such as high frequency (HF) channels and public telephone lines, the techniques developed at NRL will provide important improvements to existing communication systems.

The LPC *analyzes* the speech waveform at the transmitter into a limited number of speech

parameters (or descriptors); only these are transmitted. The analysis involves representing each speech sample in terms of a weighted sum of past speech samples. (The weighting factors are known as filter parameters.) At the receiver, the speech waveform is *synthesized* using the descriptors.

Improvements: Figure 3 shows a simplified description of the speech production mechanism and the electrical analog used by the narrowband voice processor. In the electrical analog, the vocal tract is represented by an all-pole filter having only resonant frequencies. Filter weights are generated by the LPC analysis. Voiced speech is synthesized by applying periodic pulses at the filter input, and unvoiced speech is synthesized by applying random noise at the filter input. To generate continuous speech, the following parameters are updated once every 22.5 ms: 10 filter weights, the pitch period with the voicing decision, and root-mean-square speech amplitude value. The conventional narrowband LPC synthesizer generates speech by using an overly simplified form of excitation signal. This signal is a pulse train if the speech is voiced (vowel sounds) or random noise if the speech is unvoiced (consonant sounds). While such an excitation signal can be characterized by using only 500 b/s, it does not produce very natural sounding speech. In the LPC analysis/synthesis system, the difference between the original and

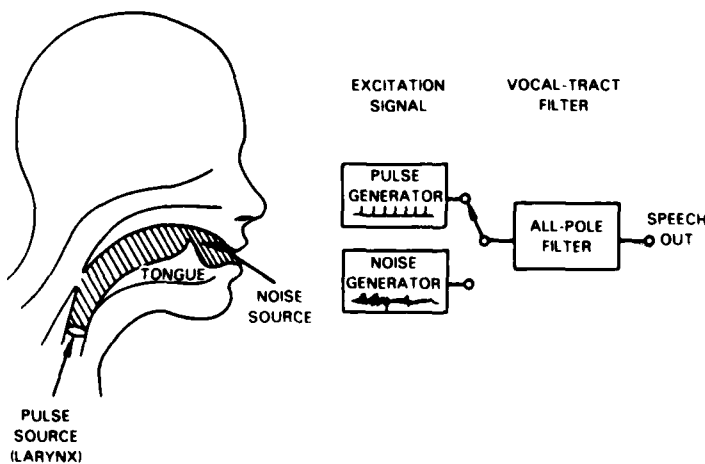


Fig. 3 — The speech production mechanism and the narrowband voice processor electrical analog

the predicted waveforms, called the prediction residual (PR), represents the ideal excitation signal. There are numerous features present in the PR that are lacking in the conventional LPC excitation signal. To improve the synthesized speech quality, some of these residual features may be introduced into the excitation signal without requiring additional data. Three of these features are described below.

1. *Resonant Frequencies in the Voiced Excitation Signal*—The amplitude spectral envelope of the PR is much flatter than that of the original speech, but it still contains a considerable number of resonant frequency components, as shown in Fig. 4 (at 400 Hz, 1 kHz changing to 2 kHz, 2.5 kHz, and 3.5 kHz). This is caused by limitations inherent in the linear predictive analysis, such as all-pole modeling and the use of a limited number of filter weights. Therefore, to generate more natural sounding speech, the narrowband LPC excitation signal should contain resonant frequencies similar to those in the PR. Since the resonant frequencies of the PR track closely with those of the original speech, they may be approximated at the synthesizer by using the filter weights calculated to describe the speech spectrum.

In NRL's investigation, the use of such a modified voiced excitation signal produced a 5.2-point improvement in LPC speech quality as evaluated by the Diagnostic Acceptability Measure (DAM)—a standard test for speech quality. This indicates that the resulting speech quality is comparable to that of some voice processors operating at 9600 b/s, or four times the data rate of the narrowband LPC.

2. *Period-to-Period Waveform Variations in the Voiced Excitation Signal*—The individual waveform of the conventional voiced excitation signal repeats exactly from one pitch cycle to the next; in contrast, the PR rarely repeats exactly see (Fig. 5). This variation is due to irregularities in vocal cord movement and the turbulent airflow from the lungs during the glottis-open period of each pitch cycle. The extreme uniformity of the LPC excitation signal causes the synthesized speech to sound tense and machine-like. To reduce this effect, randomness was introduced into the phase spectrum of the voiced excitation signal. The frequency dependency and magnitude of the randomness are similar to that of the actual prediction residual of a normal voice. The use of the modified phase spectrum in the voiced

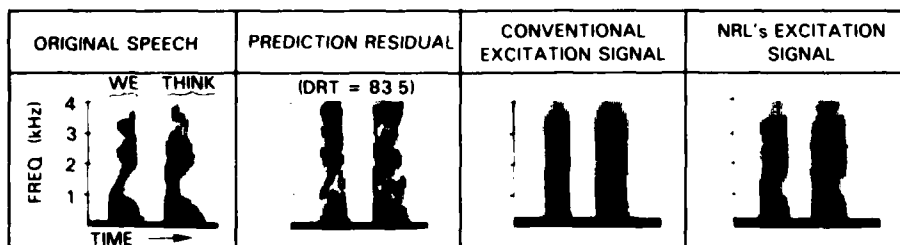


Fig. 4 — Various components of LPC speech. Each box represents a time history of the rms speech amplitude spectrum (higher power is darker) for the words "we think." The resonant frequency components in the prediction residual are at about 400 Hz, 1 kHz changing to 2 kHz, 2.5 kHz, and 3.5 kHz.

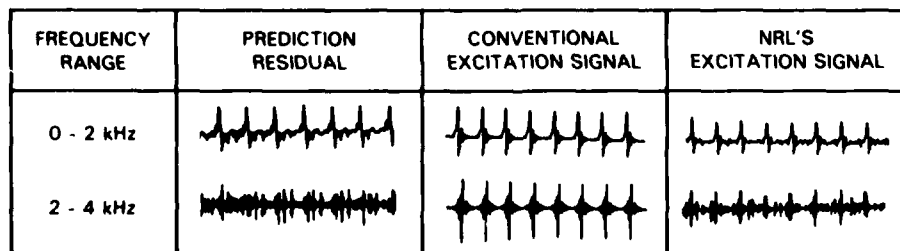


Fig. 5 — Time-waveform of the prediction residual, the conventional, and improved voiced excitation signals

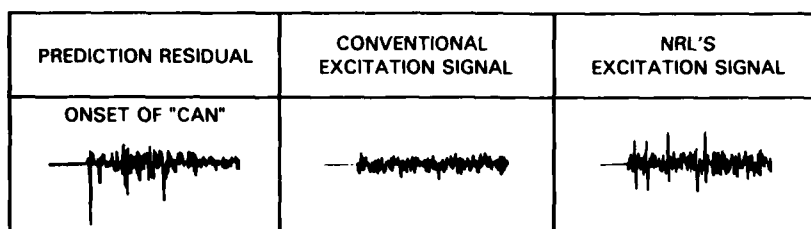


Fig. 6 — Onset time-waveforms of the prediction residual, the conventional, and improved unvoiced excitation signals

excitation increased overall DAM quality scores by 4.7 points for male speakers and 5.0 points for female speakers.

3. *Modified Unvoiced Excitation Signal*—The conventional narrowband LPC uses flat random noise as the excitation signal for all unvoiced sounds. This produces satisfactory nonabrupt unvoiced sounds such as /f/, /th/, /s/, and /sh/ because the PRs of these sounds are essentially random. However, the PRs for abrupt consonants such as /k/, /t/, /ch/, and the like are quite spiky and irregular, especially at the beginning of the sound (see Fig. 6). This is because the rapidly changing speech waveform at the onset is not well modeled by a linear combination of past speech samples. The satisfactory production of abrupt sounds therefore requires an excitation signal that includes spikes at the onset. Without these spikes, synthesized stop consonants usually sound more like continuants (i.e., CAT sounds like HAT).

The abruptness of a consonant is easily measured at the LPC receiver by observing the change in the root-mean-square (RMS) speech amplitudes between two adjacent unvoiced frames. Modifying the unvoiced excitation signal to include spikes produced a 3.6-point improvement in the overall speech intelligibility as evaluated by the Diagnostic Rhyme Test (DRT), a standard test for speech intelligibility. Significantly, the partial score for the discrimination of abrupt vs nonabrupt unvoiced sounds was improved by 14.4 points. This indicates that a major weakness in the unvoiced excitation has been properly identified and corrected.

Implementation: NRL's improvement of narrowband LPC speech was effected within the

confines of the interoperability requirements established by the Department of Defense (DoD). In this way the standard speech sampling rate, frame rate, and parameter encoding formats were maintained. This allowed NRL's analysis and synthesis improvements [1,2] to be incorporated into the DoD advanced narrowband digital voiced terminal (ANDVT) currently under development.

The Navy relies heavily on high-frequency and other narrowband channels for voice communications. Because this capability is vital to the Navy, NRL has played a significant role in the research and development of the narrowband LPC. In 1973, NRL developed one of the first narrowband LPCs capable of operating in real time. Since 1978, NRL has been a technical agent for the development of LPCs intended for tri-service tactical use. In 1981, NRL produced a narrowband LPC terminal that is only slightly larger than a conventional desk telephone. These improvements in the narrowband LPC speech are part of a continuing effort by NRL to make the narrowband LPC more practical for military voice communications.

[Sponsored by ONR]

References

1. G.S. Kang and S.S. Everett, "Improvement of the Narrowband Linear Predictive Coder, Part 1: Analysis Improvements," NRL Report 8645, Dec. 1982.
2. G.S. Kang and S.S. Everett, "Improvement of the Narrowband Linear Predictive Coder, Part 2: Synthesis Improvements," NRL Report 8799, July 1984.

Improving Fault Isolation in Complex Systems

K. DeJong

Information Technology Division

Artificial intelligence (AI) techniques have been used successfully to develop expert decision aids in a variety of areas, including the diagnosis of diseases in the medical domain. In a parallel situation with military significance, the Navy Center for Applied Research in AI at NRL is using AI techniques to diagnose failures in complex man-made systems.

The rapid increase in the sophistication of military weapon systems has created a corresponding need for improved methods of maintaining their readiness. There are many complementary strategies for improving readiness, including better mechanisms for built-in-test (BIT) procedures, more sophisticated external diagnostic systems (both stand-alone and operator-controlled), and improved methods for training personnel in the required maintenance and troubleshooting skills. We have been focusing on the use of AI techniques to improve the performance and reduce the cost of acquiring the software which drives computer-controlled automatic test equipment (ATE). However, we are planning joint-service activities in the areas of job aids and training as well.

The current approach to developing ATE is to design a computer-controlled test station which, when coupled to a unit under test (UUT), generates an appropriate sequence of stimulus-response procedures capable of isolating any faults present to a small set of replaceable components. To keep down the cost of such stations, they are frequently designed to serve a reasonably general class of systems; for example, analog electronics gear with certain frequency ranges. What remains then is to design an interface from these generic test stations to a new piece of gear and write the software (test program sets) to generate the fault isolation sequences. Unfortunately, these test program sets are expensive to acquire (typically a multimillion dollar contract), and the quality of the resulting software varies widely.

NRL'S Approach: NRL has been exploring the possibility of using AI technology to reduce the cost and improve the performance of these test program sets. The motivation for looking at the AI field comes from the advances in expert system technology, particularly in the area of medical diagnosis. The open question is whether this new technology can be successfully applied as well to the problem of fault diagnosis in complex man-made systems. To answer this, our experience with expert system technology suggested focusing on two key technical issues. The first, and most obvious, is the extent to which the diagnostic skills of an expert technician can be captured using AI techniques. The second, more subtle but equally important, is the ability in this domain to avoid the knowledge acquisition bottleneck that has plagued most of the first generation expert systems. (In most existing AI expert systems, the process of identifying, collecting, and building an appropriate knowledge base has been difficult and time-consuming.)

Diagnostic Skills: An expert technician uses three major sources of knowledge during fault isolation: general domain knowledge (e.g., electronics), detailed knowledge of the UUT (e.g., schematics), and a set of empirical "rules of thumb" built up over time from experience. The fault isolation process can be viewed as a knowledge-based strategy for selecting the next best test, given constraints on the costs and availability of tests. Using this point of view, we have built and are continuing to refine a prototype system that combines several AI knowledge representation techniques as a knowledge base which supports the selection of "optimal" test sequences for fault isolation.

Knowledge Acquisition: Building such a knowledge base by hand for each type of UUT can be a lengthy and error-prone activity which would detract from the usefulness of such an approach. Hence we have been simultaneously developing a knowledge base compiler that automates the process considerably by accepting as input a reasonably high-level description of a UUT and producing as output the knowledge base format required by the diagnostic system. The design of the compiler is considerably simplified

by the high-level data structuring facilities available in most AI programming environments. These facilitate the description of collections of components with default properties, hierarchical subcomponents, and inherited features.

Results: We have built and demonstrated a system that uses block diagrams, *a priori* component failure rates, and test and replacement costs to generate "optimal" fault isolation sequences. We are currently expanding this system to include knowledge about electronics. We plan to demonstrate the new system on UUTs taken from a class of naval avionics communications gear. In addition, we are participating in a triservice program through the Joint Directors of Laboratories where these same ideas will be applied to fault isolation in other types of complex systems.

[Sponsored by ONR and NAVAIR] ■

Ground Wave Propagation over Multilayered Earth

E. J. Kennedy

Information Technology Division

Ground wave propagation over the earth's surface has been extensively studied and reported by numerous authors. In general, these previous analyses have addressed propagation over a smooth spherical earth where the earth's electrical parameters can be considered constant to any depth. We have studied a more general problem in which the ground parameters may vary with depth such as when the communication path traverses sea ice or an estuary in which fresh water overrides a deeper seawater layer. The attenuation function in these cases may be markedly different from the usual smooth variation with range.

The Ground Wave: The ground wave is that portion of the total radiation field from an antenna which reaches a distant receiver by traveling along the earth's surface. When the receiving antenna is within sight of the transmitting antenna the propagation mechanism is simple and straightforward; however, at greater distances a ground wave persists and is of great value for communications. This extended range charac-

teristic of the ground wave was first realized early in this century, and later works have treated a variety of cases which are of practical interest. For example, the ground wave serves the primary coverage area of AM broadcast stations. For the Navy, intratask force communication between surface platforms can be accomplished using the ground wave. In general, this mode possesses the advantages of predictability, reliability, and freedom from the temporal variations which afflict skywave and other propagation modes. An additional advantage is that the ground wave supports very wide bandwidths for communication signaling.

The attenuation function describing the ground wave path loss between two antennas situated at the earth's surface is well known and available for a variety of ground types including smooth and rough sea and land. From time to time, anomalous ground wave behavior has been reported for cases in which, upon close examination, a definite layer is found to exist near the surface having properties distinct from the underlying medium. Practical examples of this situation include an ice-covered sea and a river mouth or estuary in which fresh water runoff overrides a lower layer of high-conductivity seawater.

Propagation Studies and Results: The problem of ground wave propagation over layered earth has been studied theoretically by Wait [1] who, with Hill [2], has given an example of propagation loss over sea ice at 10 MHz. This work was extended at NRL during 1983 to include the frequency region from 0.1 to 15 MHz. The attenuation function was found as the summation of a series of residues resulting from integration in the complex plane, the term of which are functions of frequency, layer parameters, and layer depths. An example showing the ground wave attenuation as a function of range is given in Fig. 7 which presents four cases, all at 3 MHz.

Curve 1 shows the normal ground wave loss over seawater alone. Similarly, curve 4 shows the loss associated with propagation over a surface consisting of sea ice to great depth. Curves 2 and 3 show the effect of a layer of ice over seawater of thicknesses of 1 m and 3 m respectively. There are three regions of interest in the layered

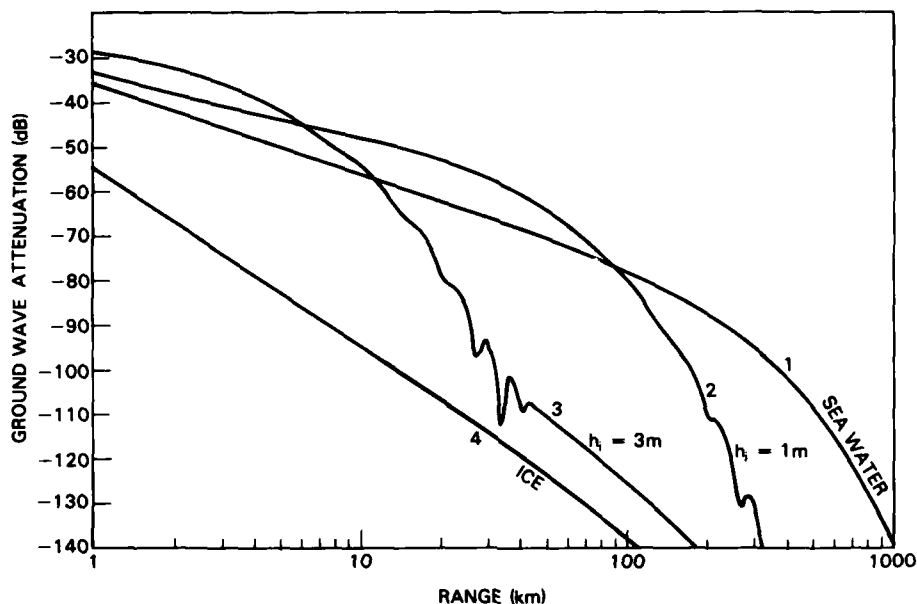


Fig. 7 — Ground wave attenuation as a function of range over spherical earth for 3 MHz. Curve 1 is for seawater only ($\epsilon_R = 81$, $\sigma = 4$ Siemens). Curves 2 and 3 are for ice thicknesses of 1 m and 3 m respectively over seawater. Curve 4 is for ice only ($\epsilon_R = 6$, $\sigma = 3.3 \times 10^{-4}$ Siemens).

cases: (a) a region at short ranges in which propagation is enhanced over the seawater only case, (b) an intermediate region in which the loss increases rapidly and nonmonotonically with range and, (c) a region in which the loss function resumes a smooth variation but at a much greater attenuation than for seawater alone. It was found that the boundaries between these regions are strongly dependent on frequency and layer thickness. For an ice thickness of approximately 3 m, which is frequently used as a common value in the Arctic, the ground wave loss over most of the lower HF band (3 to 15 MHz) is so severe as to limit the usefulness of the ground wave at these frequencies to ranges typically much shorter than is normally expected in this mode over seawater.

In future work all of these theoretical results will be subjected to experimental verification.

[Sponsored by NAVELEX]

References

1. J.R. Wait, "Radiation from a Vertical Antenna over a Curved Stratified Ground," *Journal of Research of the National Bureau of Standards*, **56**, 237-244 (1956).
2. D.A. Hill, and J.R. Wait, "HF Ground Wave Propagation over Sea Ice for a Spherical Earth Model," *IEEE Transactions on Antennas and Propagation*, AP-29(3) (May 1981). ■

Design of High-Frequency Networks for Tactical Communication

D.J. Baker, J.E. Wieselthier, A. Ephremides,
and D.N. McGregor
Information Technology Division

Communication is essential during tactical warfare. For example, it permits a naval task force, which consists of a group of diverse platforms (surface ships, aircraft, and submarines), to respond in a coordinated way to hostile enemy action. These platforms are normally not all within communication range of each other, and so a networking structure is needed to facilitate the relaying of messages. A military communication network must be able to withstand physical attacks, which can result in loss of platforms, as well as jamming attacks, which in turn causes loss of the radio communication links that connect these platforms—a military communication network must be survivable. To meet this need

NRL has developed a design concept for a high frequency (HF) intratask force (ITF) communication network. This concept relies on two techniques: flexible network organization and spread spectrum signaling.

Network Organization: To reduce system vulnerability it is necessary to spread the responsibility for controlling the network among several, if not all, of the network platforms. NRL has developed a fully distributed linked cluster algorithm (LCA) for the organization of the HF ITF network that is based on the exchange of information among the network platforms [1]. Each platform first determines who its neighbors are; i.e., those platforms with which it can communicate bidirectionally without the aid of an intermediate relay. It then broadcasts this list of neighbors so that all platforms will know not only their own neighbors, but also their neighbors' neighbors. This connectivity information permits the network to structure itself into collections of platforms known as node clusters, as schematically illustrated in Fig. 8. The execution of the LCA designates one member of the cluster, which is within communication range of all cluster members, as a clusterhead (square). These clusterheads can act as local controllers and can

quickly and reliably broadcast messages to all cluster members. Clusterheads are linked by relay gateway nodes (triangles), which are also designated during the execution of the LCA. Ordinary nodes are shown by dots in Fig. 8. The entire network organization is accomplished without the use of a central controller. The set of clusterheads and gateways and the links that connect them together form a backbone network that can be used for actual communication or for the exchange of control information throughout the task force.

The maximum range for which communication is possible varies considerably with frequency in the HF (2 to 30 MHz) band. To exploit this dependence, separate simultaneously functioning linked cluster networks are formed in several subbands over each of which the communication range remains relatively constant. The organizational structure may vary considerably in the different subbands.

Resistance to Jamming and Platform Loss: The connectivity of the network can vary because of jamming, platform motion, or platform loss. As a result, the links needed to maintain a previously established network structure may no longer exist. Each of the networks in the

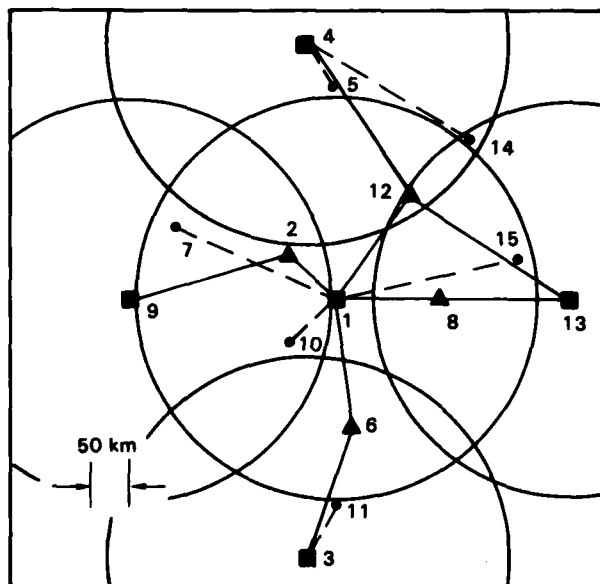


Fig. 8 — Example of linked cluster organization of a mobile radio network. A fixed communication range is assumed, as indicated by the circular coverage area around each clusterhead. Clusterheads are linked via the backbone network (solid lines), and every ordinary node is two-way connected to a clusterhead (dashed lines). Other links may also exist that are not shown.

individual subbands adapts to such topological changes by periodically reorganizing itself using the LCA. The proposed use of several networks in different subbands enhances jamming resistance because it would be difficult for a jammer to disrupt all of them simultaneously. Figure 9 shows how the network of Fig. 8 has reorganized itself in response to both jamming and the loss of a clusterhead—new clusterheads are designated and a new network structure is formed that connects all of the remaining platforms, despite the loss of several links [2]. Frequency hopping, a form of spread spectrum signaling, provides further resistance against jamming because the jammer does not know in which part of the frequency band the signal is being transmitted.

Code Division Multiple Access Techniques: The use of spread spectrum signaling leads naturally to the use of code division multiple access (CDMA) techniques that permit the successful simultaneous transmission over a wide-band channel by a number of users. The most

important networking questions that arise from the use of CDMA signaling are: how many signals can share the channel simultaneously while maintaining acceptable performance levels and how can channel access techniques be designed to take advantage of spread spectrum signal properties while satisfying the constraints imposed by their use? New network control schemes that make use of CDMA techniques have been developed to coordinate the transmissions of the various platforms in the network.

These studies provide a firm basis for the design of efficient, survivable, mobile communication networks. They represent the use of novel networking techniques combined with robust antijamming signal design. Ultimately, such approaches will result in fundamental changes in the way military communication networks are implemented. Research is continuing to develop improved network control schemes that are even more responsive to changing user demands and to a wider variety of threats.

[Sponsored by ONR]

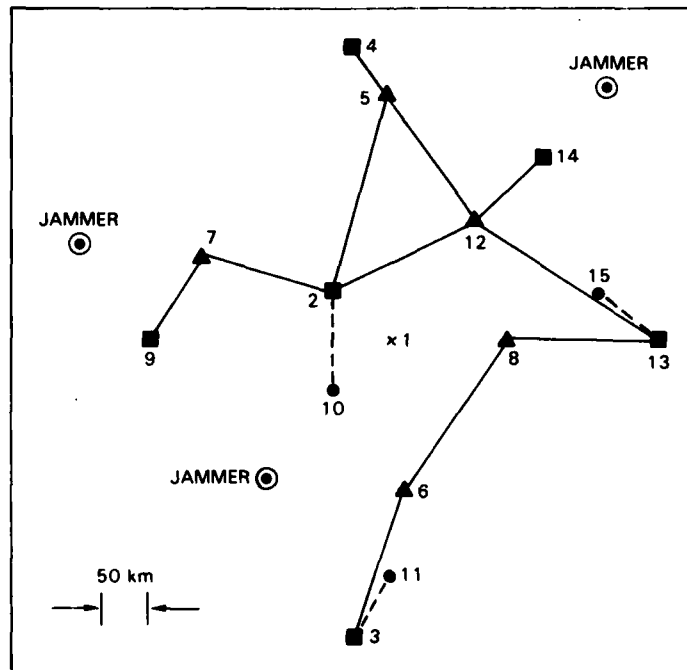


Fig. 9 — In the presence of three jammers and with the loss of a clusterhead (platform 1), the network of Fig. 8 has reorganized as shown above

References

1. D.J. Baker, A. Ephremides, and J.E. Wieselthier, "An Architecture for the High-Frequency Intratask Force (ITF) Communication Network," NRL Report 8638, Dec. 1982.
2. D.J. Baker, J.E. Wieselthier, A. Ephremides, and D.N. McGregor, "Resistance to HF Jamming Interference in Mobile Radio Networks by an Adaptive Distributed Reconfiguration Technique," NRL Report 8834, Aug. 1984. ■

Model for Moving Platform Multipath

D.E. Corman

*Tactical Electronic Warfare Division/
University of Maryland*

In radar engagements involving moving platforms near a sea surface, multipath strongly affects the received signal. The multipath effects are due to secondary signal paths which are reflected by the sea surface and reinforce or cancel the primary, direct path of transmission. This applies to both bistatic, point-to-point transmission, as shown in Fig. 10, as well as to round trip transmission from a monostatic radar to a target and back again. The multipath fluctuations are random and severe, and the consequent signal distortion induced by the multipath can have a major impact on the effectiveness of electronic countermeasure (ECM) techniques. To model this impact, we determined the statistical behavior of the received signal and investigated the dependence of these statistics on relative transmitter-receiver, sea-surface motion and on environmental parameters, especially wind speed and direction. The approach has been to develop a scattering model that is sufficiently detailed to yield the desired statistics, but also simple enough to allow for rapid digital simulation.

Multipath Model Structure: Figure 11 illustrates the overall multipath model structure. The model has three modules. The first specifies the scenario geometry and environmental data input. The second is an ocean surface wave height model. This model is described in Ref. 1

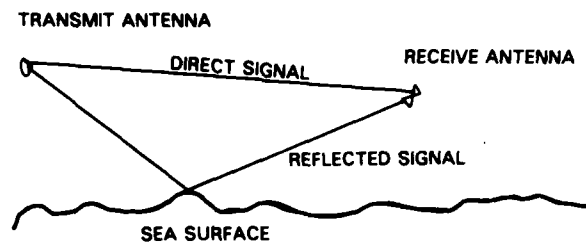


Fig. 10 — Paths of direct and reflected signals

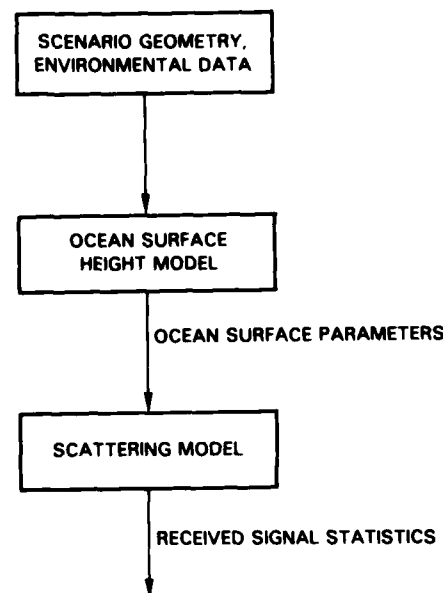


Fig. 11 — Moving platform multipath model

and provides a statistical characterization of sea surface fluctuations in both spatial and time coordinates. The third module is the scattering model; it is here that the statistics of the received signal are computed.

Ocean Wave Model: In the research described here, the ocean is modeled as a Gaussian process with a spectrum as given in Ref. 1. The spectrum provides the frequency distribution of ocean wave energy. A digital simulation has been developed to generate a three-dimensional ocean surface according to the spectrum.

waves with higher regimes. This decomposition is performed by selecting an appropriate separative frequency based on the requirement that the energy contained in the high-frequency wave band be a prescribed constant. Given this decomposition, three important parameters are defined. These are the root-mean-square (rms) waveheight, surface correlation length, and surface slope. The first parameter describes the intensity of the random surface fluctuations, the second measures the linear dimension of the surface irregularities, and the third estimates the surface smoothness. The magnitude of these parameters determines the nature of the scattering model needed.

In scenarios of current tactical electronic warfare interest, both gravity and gravity-capillary waves are characterized by smooth slopes with radius of curvature greater than the wavelength of incident radiation (≈ 3 cm). The received signal can then be computed as a power series in surface slopes modulated by a doppler frequency shift induced by relative receiver-transmitter motion. The statistics of the received signal are then expressed in terms of the first- and second-order slope statistics. From the surface wave decomposition described previously, these slope statistics are then easily computed from the sea spectrum.

This work extends previous scattering models by specifically considering the effect of relative receiver-transmitter motion on the second-order statistical properties of the forward scattered signal. Specifically we have modeled the following:

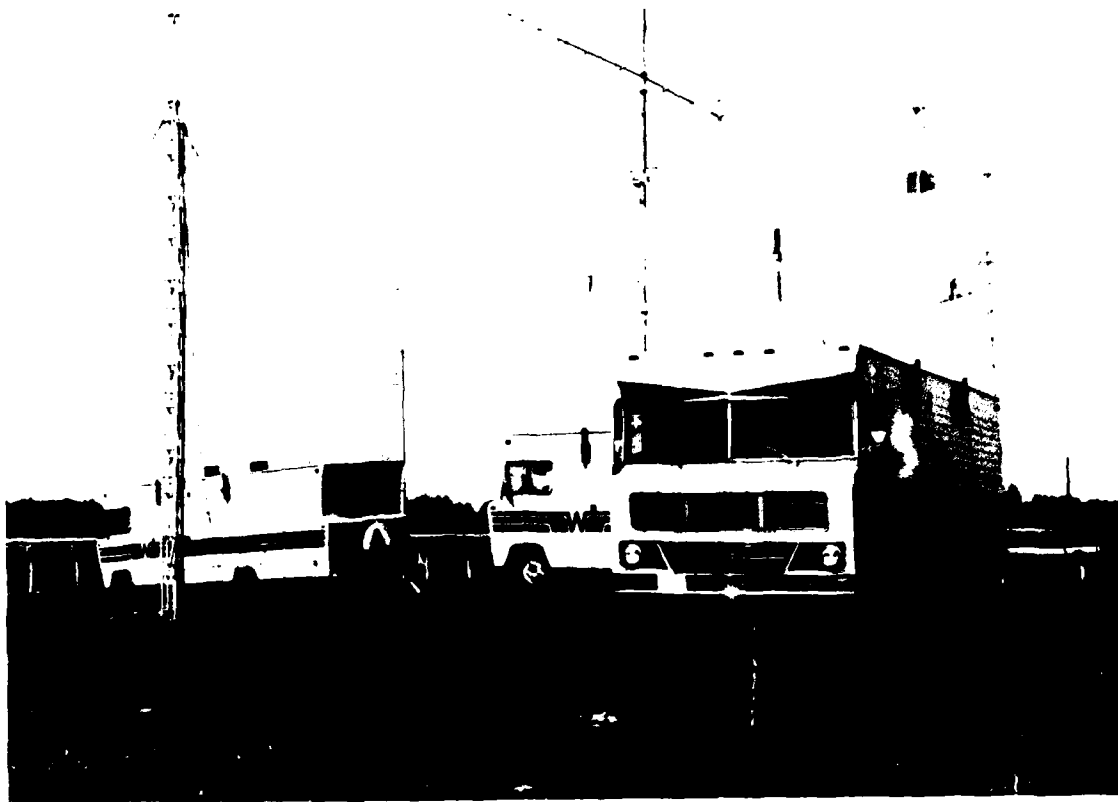
- (a) doppler shift within the received pulse caused by platform motion,
- (b) depolarization of the incident field caused by reflection from sea swell, and
- (c) signal fluctuation caused by interaction with high-frequency gravity-capillary wave.

The scattering model has been used to calculate the first-order reflection coefficients for horizontally polarized incident fields with good agreement for the case of static receiver-transmitter geometry.

[Sponsored by NAVELEX]

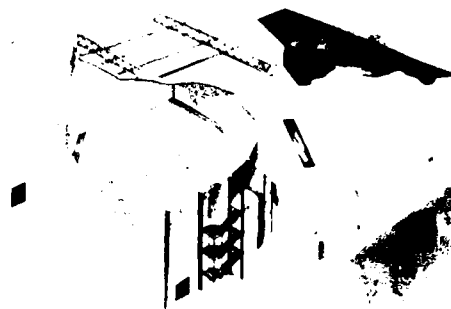
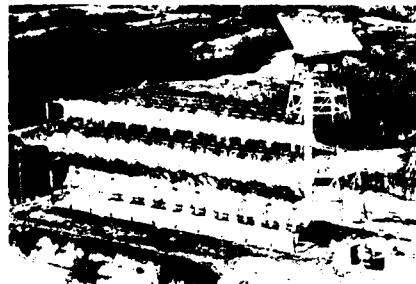
Reference

1. D.E. Corman, "Ocean Surface Model for Over-Water Multipath Scattering," Univ. of Md. Technical Research Report CSR 82-9, June 1982. ■



Mobile communication and vulnerability assessment laboratories
used by the Information Technology Division

*Electromagnetic sensing and
systems for the Navy environment*



59 Communication Through a Radar

Jeffrey O. Coleman

Combining and communicating radar data produces more useful information.

60 Directed Mirror Antenna Radar

Dean D. Howard, David C. Cross, and James W. Titus

A lightweight mirror rapidly changes beam direction.

61 High-Resolution S-Band Surveillance Radar

Seth K. Meads

Clutter and susceptibility to countermeasures are reduced.

63 Advanced Tactical Electronic Warfare Environment Simulator

Richard L. Robinson

A computer-based system improves evaluating system performance.

65 Three-Frequency Scatterometer Concept

Dale L. Schuler, William J. Plant, and Wah P. Eng

Three frequencies eliminate sea clutter noise and improve resolution.

68 Radar Backscatter from Splashing Raindrops

James P. Hansen

Measurements and a model help understand sea clutter.

69 Thermal Infrared Imagery of Ship Wakes

William D. Garrett

Surfactants make the wake more persistent.

71 The White-Water Wake of a Surface Ship

Rodney D. Peltzer

Ship operating conditions determine the wake length.

ELECTROMAGNETIC SENSING

Continuing in a long tradition of radar research and development, NRL scientists are generating various techniques to improve radar performance and its use in integrated Fleet systems. Much of this work is very closely connected with the artificial intelligence program here; this is evident in the article by Coleman. Radars are also designed and tested for very special uses such as the three-frequency scatterometer (see article by Schuler, Plant, and Eng).

Radars must also be effective in noisy environments. The environmental simulator allows evaluation of radars in complex environments. The last three articles deal with electromagnetic sensing of the naval environment with radar, infrared, and visible radiation. While environmental studies are necessary in their own right, understanding the environment and how it is related to naval implications is crucial for evaluating the noise backgrounds in which sensing systems must operate.

The Divisions involved in this research are Radar (Code 5300), Tactical Electronic Warfare (Code 5700), Marine Technology (Code 5800), and Aerospace Systems (Code 7900).

NRL has many other radar projects. Some of these studies concern

- shipboard air surveillance in hostile environments and against new threats,
- investigation of target characteristics,
- large space-based radars,
- frequency agility and diversity,
- coherent sidelobe cancellation,
- low sidelobe antennas,
- adaptive antennas,
- superresolution, and
- multiple-frequency tracking radar.

Page 56, left:

Experimental wideband transmission-line loaded monopole transmitting antenna having potential application in frequency-agile shipboard HF communication systems

Center:

Antennas come in various configurations. *Lower left to upper right:* Senrad air-surveillance radar antenna which can operate over a wide frequency band; an artist's concept of the directed mirror radar antenna (DMAR) in shipboard configuration. See article on p. 60 by D. Howard (illustration by T. Phillips); and the MADRE over-the-horizon (OTH) radar antenna located on a cliff at the Chesapeake Bay Detachment overlooking the Chesapeake Bay.

Lower right:

The central target simulation facility includes a centrally located modern computer complex and a radio-frequency physical effects simulator. The facility is instrumented for testing and evaluating electronic warfare systems and electronic countermeasure-hardened missile seekers under simulated tactical conditions using hardware in the loop. See article on p. 63 by R. Robinson.

Communication Through a Radar

J.O. Coleman
Radar Division

The NRL Radar Division is building a system to demonstrate computer-to-computer communication using the powerful transmitter and large rotating antenna of a conventional surveillance radar. This communication capability is being added to the radar without significantly impairing its radar function. The demonstration system, now nearly complete, illustrates ideas on which an operational radar-communication system could be built for a naval task force.

Radar communication would typically be used to transmit surveillance data among task-force members. Navy radars themselves, for example, generate large amounts of data that are more useful when shared between the task force's various ships and aircraft.

Basic Design: The earliest work on this project consisted of evaluating several basic concepts for radar communication [1]. The demonstration system is based on the concept that showed the most promise for Fleet use: The radar's transmitter and antenna are used for data transmission, but incoming data are received with a separate receiver and antenna. The transmit (radar) antenna is highly directional and, as part of the radar's normal operation, is rotating at a constant rate of one rotation every 4 to 10 s. To communicate with a particular receive site by using this directional antenna, it is necessary to wait until the antenna is pointing toward that receive site. Data can then be transmitted for a brief interval. The receive antenna must be omnidirectional, because data may arrive from any direction at any time if this technique is being used throughout the task force. By using high data rates during the short intervals in which data are actually being transmitted, data may be transmitted at an average data rate of several thousand bits per second.

It is clear that the normal radar operation need not be impaired when the radar antenna is not pointing toward a receive site. When the radar antenna is pointing toward a receive site, the degradation in radar performance can be

minimized by using part of the transmitted energy for the radar function.

The Demonstration System: NRL's two-way demonstration radar-communication link was designed around an experimental surveillance radar located at NRL's Chesapeake Bay Detachment (CBD). NRL's Tilghman Island field station, located about 8 miles to the east of CBD across the Chesapeake Bay, was chosen as the second site for the demonstration. Because there is no radar at Tilghman suitable for the radar-communication function, a simple "radar emulator" was built as a substitute for a real radar at that site. The emulator cannot function as an actual radar, but it can transmit the communication waveforms.

For the demonstration, messages can be typed into a small computer at either site for transmission to the other as the antenna position allows. In addition to preparing and formatting messages, the computer monitors various transmitter functions and the radar's antenna position. With this information, it controls the switching between radar and communication functions. To transmit the data, the computer passes the data to a modem (modulator/demodulator), where it is converted to a waveform suitable for transmission and passed to the radar transmitter. Incoming communication signals from the other site are converted by the modem back into data and passed into the computer for decoding and display. At CBD, it will be possible to observe the radar's performance in detecting aircraft while it is transmitting data to Tilghman.

During 1983, the focus of the project was on programming the demonstration-system computers and designing and building the hardware necessary to allow them to interact with the modems. The system will be completed in early 1984.

[Sponsored by NAVSEA]

Reference

1. B.H. Cantrell, J.O. Coleman, and G.V. Trunk, "Radar Communications," NRL Report 8515, Aug. 1981.

Directed Mirror Antenna Radar

D.D. Howard, D.C. Cross, and J.W. Titus
Radar Division

The Directed Mirror Antenna Radar (DMAR) is a novel combined surveillance and weapon control radar system for potential Fleet anti-air warfare applications. It is based on new implementations of the mirror antenna technology that allow a radar beam to be scanned by movement of only one lightweight, radio-frequency (rf) mirror. This technology is being exploited for two major applications. In the first, high data rate three-dimensional (3-D) surveillance and multitarget precision tracking can be achieved by combining the rapid scanning capability of mirror antenna systems with dual-band monopulse techniques. In the second application, improved one-on-one tracking radars and target illuminators are developed by using the mirror antenna's potential for light weight, low cost, and high survivability.

DMAR Description: The basic mirror-antenna system is constructed with a conventional paraboloid and feed that may remain in a fixed position while the mirror is tilted about one or two angle coordinates to effect beam scanning. With a paraboloid constructed of a set of near-parallel wires and with a mirror capable of rotating the beam's polarization, a compact antenna has been designed so that the paraboloid does not block energy reflected from the mirror.

Figure 1 illustrates a mirror antenna in a simplified one-axis-scan system, showing a fixed feed and radome-supported paraboloid subreflector to collimate the radar beam. The beam propagates toward a mirror which may be tilted by an angle θ to obtain 2θ displacement of the beam. The factor of 2 aids in accomplishing wide angle coverage and the necessary rapid changes in beam direction. The paraboloid is a grid of conductors parallel to the feed polarization and acts as a solid reflector to the feed energy; but the paraboloid becomes essentially transparent to the energy after reflection from the mirror, which rotates (twists) the polarization by 90° . This is a low-loss technique used for many years in the Nike Hercules precision tracking radar. Losses

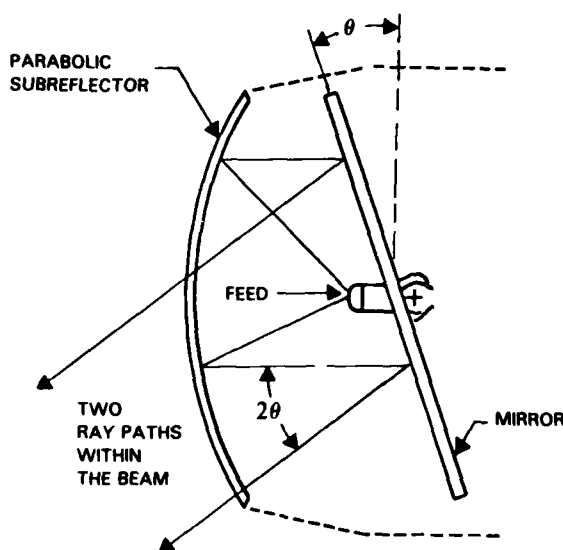


Fig. 1 — Basic two-axis mirror antenna technique

due to polarization and reflections in the DMAR are about 0.15 dB. Figure 2 illustrates the novel two-axis gimbaling, high-speed linear actuator mirror drive, and dual-band feed used for DMAR. The ultimate goal of DMAR is to attain antenna accelerations about 300 times greater than conventional radars of equivalent size.

The Prototype System: An experimental DMAR system was constructed with dual S- and X-band monopulse operation. The design of the novel dual-band mirror is described in detail in Ref. 1. The high angular velocity and acceleration mirror drive system was first demonstrated and tested at NRL. The full dual-band monopulse radar system was assembled and is presently installed on the roof of a radar building at the NRL Chesapeake Bay Detachment (CBD), overlooking the Chesapeake Bay. Figure 3 shows the DMAR tilted radome in the foreground.

Initial experiments have been performed at S-band, demonstrating both rapid surveillance and closed-loop monopulse tracking of ship and aircraft targets. Major parts of the X-band system have been tested, but the full X-band monopulse operation is awaiting delivery of receiver parts.

The current plan is to evaluate the full DMAR system to demonstrate its potential as a high-performance, cost and weight effective, anti-

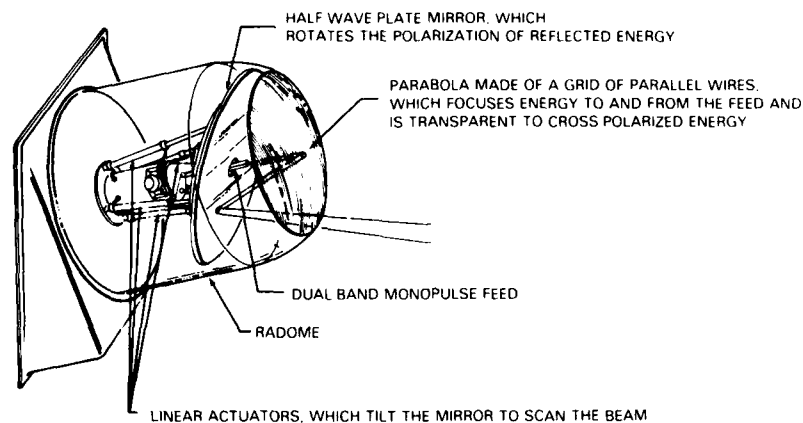


Fig. 2 — Two-axis mirror antenna with linear actuators

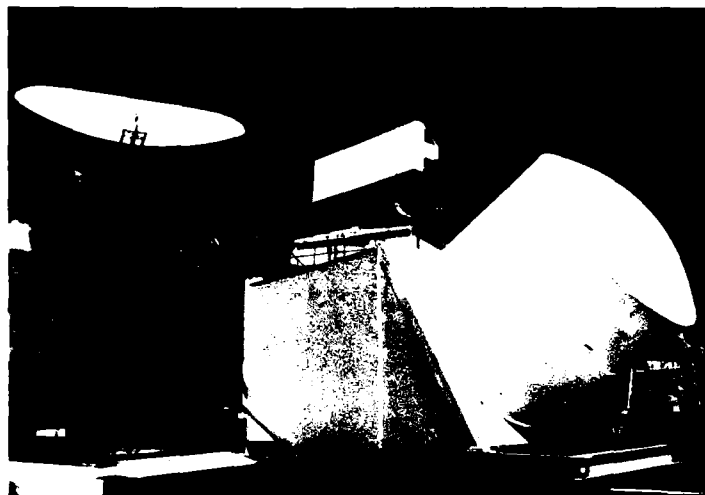


Fig. 3 — Experimental DMAR antenna in the foreground overlooking the Chesapeake Bay

80743(6)

air warfare radar system. Other potential mirror antenna applications, one-on-one tracking and target illumination, will also be demonstrated.

The authors acknowledge the valuable assistance of Mr. Billy Wright and Mr. Paris Coleman of the Radar Division in the development and construction of the microwave portions of DMAR.

[Sponsored by NAVSEA]

References

1. D.D. Howard and D.C. Cross, "Mirror Antenna Dual-Band Lightweight Mirror Design," NRL Report 8765, December 12, 1983. ■

High-Resolution S-Band Surveillance Radar

S.K. Meads
Radar Division

Currently deployed shipboard S-band (10 cm) air surveillance radars have some recognized performance limitations, among which is an inability to detect and track small targets at long ranges in volume-distributed clutter. The Radar Division of NRL has investigated several new concepts to meet currently perceived performance requirements of main air-battle-support surveillance radars. A concept study was completed in 1983 for an S-band radar employing high range resolution for suppression of volume clutter.

Background: Radars operating in S-band (2 to 4 GHz) have been used for a number of years as principal shipboard sensors performing the function of airborne target surveillance. These radars typically locate targets in three coordinates: range, and azimuth and elevation angles. It is highly desirable to operate at S-band or higher microwave frequencies if three-coordinate information is desired, because it is difficult, for shipboard installation, to provide the antenna aperture required to make accurate elevation angle measurements at lower frequencies. On the other hand, the microwave radars suffer major disadvantages, compared to lower frequency radars, in suppressing returns from rain and chaff so that targets of interest can be detected in those environments. These disadvantages stem from two effects. One is the fact that the amplitude of backscattered energy from rain drops increases approximately as the fourth power of the radar's frequency; the second effect is due to the doppler shifting of the returned signal by rain or chaff. Rain and chaff move about with a range of velocities. Both the higher radar frequency and this velocity range increase the frequency spread of the returned signal. Because of this spread, suppression of the clutter by means of velocity filtering is more difficult at microwave frequencies; and perhaps it is impossible if other system constraints preclude the transmission of a long train of closely spaced, constant-frequency pulses. These considerations motivate the radar designer to attempt to counter clutter by other techniques. One such technique is to reduce the resolution cell size. If the target is approximately contained in the reduced cell size, then its return will not be diminished, but the clutter signal will be reduced approximately as the volume of the smaller cell size.

Conceptual Radar: A radar system concept has been developed which has as its primary new feature the use of a 100 MHz signal bandwidth, providing a compressed pulse width of 10 ns. This compressed pulse reduces the resolution cell size significantly over present S-band radars. A rotating array antenna is employed which combines electronic scan in elevation and multiple simultaneous beams to achieve the desired elevation coverage and data intervals. This way,

unambiguous range coverage is simultaneously provided to 200 nmi with a 12-s data interval and to 100 nmi with a 4-s interval. The way in which this dual-rate coverage is obtained with a rotating antenna is illustrated in Figs. 4 through 6, which depict the calculated range height detection coverage on a 1-m² target obtained in each of a set of three sequential antenna scans. Radar coverage on a 1-m² target is provided in each 4 s to a range of about 100 nmi and to an altitude of about 100,000 ft. A pair of high sensitivity beams provide detection capability to about 200 nmi in a different elevation sector on each of the three scans in the sequence. The first scan covers 0° to 2.5° (Fig. 4), the second scan, 2.5° to 5.5°

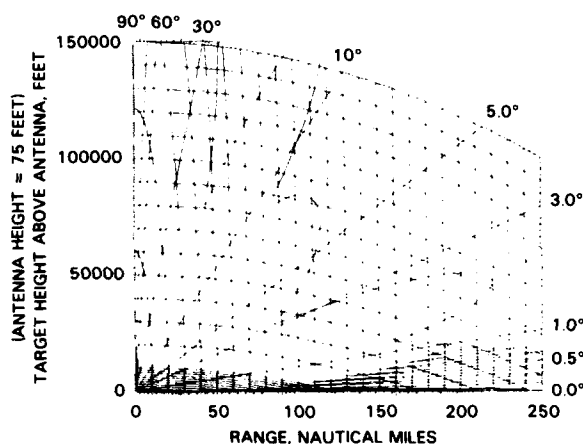


Fig. 4 — Range-height coverage diagram for the first of three sequential antenna azimuth scans

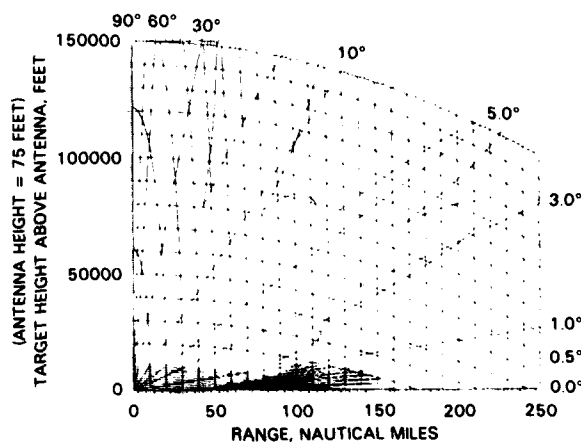


Fig. 5 — Range-height coverage diagram for the second of three sequential antenna azimuth scans

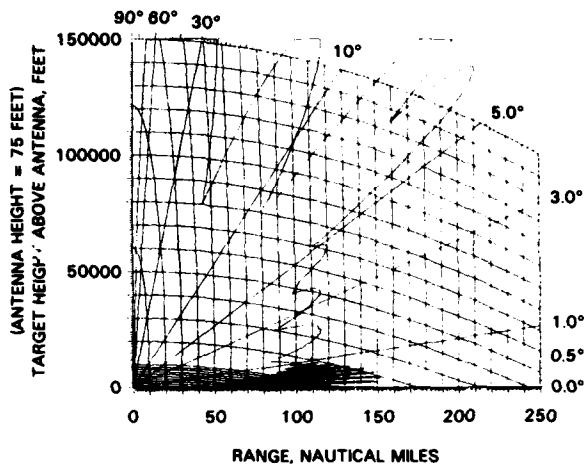


Fig. 6 — Range-height coverage diagram for the third of three sequential antenna azimuth scans

(Fig. 5), and the third scan, 5.5° to 8.5° (Fig. 6), thus covering the range to 200 nmi and 8.5° elevation once every 12 s.

The required pulse compression system is within the current state of the art using reflective-array, pulse-compressor technology. A dispersion of 50 μ s and a bandwidth of 100 MHz are necessary to provide the required pulse energy together with range resolution of 10 ns.

The absence of velocity filtering processing provides several advantages:

- Pulse-to-pulse frequency agility is available as an electronic counter-countermeasure.
- Targets of all radial velocities can be detected; the blind speeds due to filtering are absent.
- Performance against volume clutter (rain and chaff) is independent of the wind-blown characteristics of the clutter.

Performance calculations indicate that detection ranges on a 1-m² or larger target will not be limited by rainfall rates of 4 mm/h and that detection of these targets will be achieved in an 8-mm/h rainfall to ranges of 60 nmi. This is a significant improvement over the predicted performance of current systems.

[Sponsored by NAVSEA]

Advanced Tactical Electronic Warfare Environment Simulator

R.L. Robinson

Tactical Electronic Warfare Division

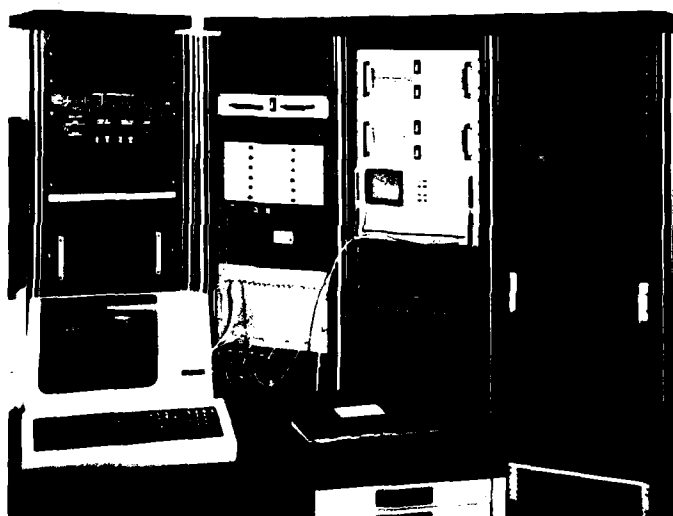
A unique and versatile simulation system can now better prepare military receiving systems for operation in the real-world "electronic battlefield." An ongoing NRL program has provided a variety of simulators capable of generating dense, complex, and dynamic, electromagnetic signal environments and of evaluating receiving system responses to these situations. The Advanced Tactical Electronic Warfare Environment Simulator, developed under joint Air Force and Navy sponsorship, represents a significant advancement in a realistic signal environment simulation capability that is applicable to a wide range of existing and developing receiving systems.

Military electronic systems that receive, analyze, and identify electromagnetic signals have become indispensable to any tactical operation because of their ability to assess enemy force strength, mix, and intent. A major problem is to identify the primary signals of interest in the midst of a dense and complex electromagnetic background, and to do so in a timely fashion. While receiving systems have been specified to operate in these situations, realistic testing in a controlled fashion has been quite limited. The accelerated trend toward increasing density and complexity of the background and of signals of interest in real-world situations faces all military services. This trend prompted the development of a simulator structured for general purpose applicability. The advanced version of the simulator, developed for operational support of electronic equipment on the EF-111A fighter aircraft, has recently demonstrated substantially increased capabilities.

Simulator Characteristics: The single most significant aspect of the advanced simulator is its ability to generate a dynamic electromagnetic environment consisting of up to a thousand simultaneous signals with a total pulse density of one million pulses per second. The combination of signal characteristics and modulations for

Table 1 — ATEWES System Characteristics

Scenarios	4 + h	SIGNAL PARAMETERS	RANGE RESOLUTION
Platforms	250	Frequency	500-18,000/0.125 MHz
Signals	1000	Amplitude	120/1 dB
Pulse Density	1 Megapulse/s, Average 4 Megapulse/s, Peak	Angle of Arrival	360/0.36°
		Pulse Interval	0.050 to 32,760/0.05 μ s
		Scan Rate	1 to 12,000/1 rpm
PRI ^a Modulations	Stable, Stagger, Switching, Continuous/Discrete Jitter, Continuous/Discrete Patterns, Synchronization	RF Modulations	Stable, Sequence, Switching, Continuous/Discrete Agility, Continuous/Discrete Patterns, Multiple Coincident Beams, Chirp, Continuous Wave
Scan Types	Circular, Sector, Raster, Conical, Helical, Spiral, Palmer, Steady, Omni, Tracking		

^aPulse repetition interval

80784(6)

Fig. 7 — The Advanced Tactical Electronic Warfare Environment Simulator (ATEWES) showing the scenario control computer, digital and RF generation units, and specialized interfaces

frequency, pulse interval, and scans, as shown in Table 1, provides features previously unavailable. This capability is achieved by a relatively compact system, as shown in Fig. 7, that consists of a scenario control computer, digital and radio-frequency (RF) generation units, and specialized interfaces. In operation, the simulator allows the definition of realistic tactical situations, the generation of complex signal environments, and the evaluation of responses of electronic warfare (EW) systems under test.

Simulator Operation: The power of the simulator approach is extended by the combination of the flexibility of operator control, the variety of available signal modulation characteris-

tics, the efficiency of signal generation, and the realism of real-time platform motion. A highly interactive approach to operation provides complete and rapid control of creating scenarios, altering signal characteristics, running the simulation, displaying simulation status, and evaluating EW system responses. The variety and flexible use of modulations available for each of the thousand signals within any scenario is achieved with the high-speed pipeline processing of the digital generation architecture. Signal generation efficiency derives from centralized pulse scheduling; pipeline processing; and ultrahigh speed, time-multiplexed, RF signal synthesis. Superimposed on each signal are the dynamically updated angle and range effects of the simultaneous

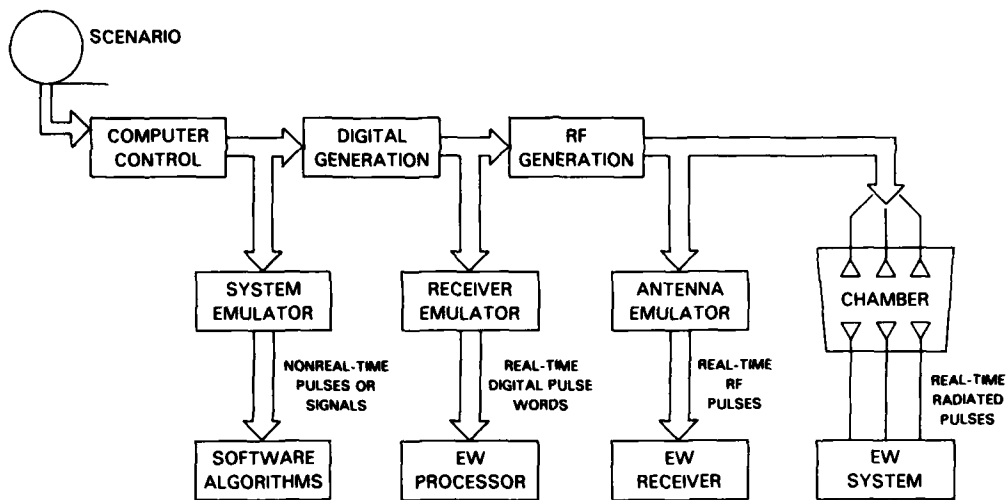


Fig. 8 — Various interfaces and emulators that can be used to test a complete system or various portions of it. A complete system is tested in the TEW Division one choice chamber (on right). To test only software algorithms, a system emulator is employed (on left).

motion of both the observer platform and up to 250 emitter platforms. Antenna and scan pattern effects are updated on a pulse-by-pulse basis for each emitter.

All simulator versions have been widely used because of their versatility for interfacing to systems under test and for their independence of signal generation and system interfacing functions. The basic components of an EW system include the antenna that collects RF pulses, the receiver that converts RF to digital pulse form, and the processor that executes analysis algorithms. The NRL simulator can test a complete system or any of these components separately, as illustrated in Fig. 8. For example, a complete system could be tested in the TEW Division anechoic chamber. For receiver tests an antenna emulator would be required, while processor tests would require a receiver emulator. Evaluations can thus be made of algorithms, processors, receivers, and complete EW systems by using software, digital, directly coupled RF, or radiated stimulation, respectively. The elements shown at the top, middle, and lower rows of Fig. 8 illustrate the simulator's general purpose generation units, specialized interfaces, and candidates for systems under test, respectively. Depending upon the method used to stimulate the systems under test, the special interface is the only unit unique to each application.

The advanced simulator is now being adapted for use with the EA-6B Prowler ADVCAP (advanced capability) equipment, high-speed signal sorters, AN/SLQ32 electronic warfare system, and acousto-optical receivers. Further signal generation enhancements are being incorporated within the original simulator's basic architecture.

[Sponsored by AFSC and NAVAIR]

Reference

1. R.L. Robinson, "Tactical Electronic Warfare Environment Simulator," *NRL Annual Review*, 1976. ■

Three-Frequency Scatterometer Concept

D.L. Schuler, W.J. Plant, and W.P. Eng
Aerospace Systems Division

There is considerable interest within the Navy, as well as within the oceanographic and remote sensing communities, in building an instrument which can measure directional sea surface wave spectra. An ideal instrument should be sensitive enough to allow accurate measurements of virtually the entire ocean wave spectrum and wavelengths from several hundred meters

down to one meter. In addition, the directivity of such a system should far exceed that obtainable from single buoy measurements and should be comparable with the directivity of currently available *in-situ* buoy/pressure sensor arrays. Finally, the system should be compatible with airborne and spaceborne platforms for large-scale remote sensing of the seas.

Genesis of the New Technique: The three-frequency scatterometer is a recently conceived microwave remote sensing technique which theoretically has the ability to meet these performance criteria. This technique was developed through a reexamination of the theory behind the related dual-frequency scatterometer. Both techniques involve scattering areas which are so large that wave features are not resolved. Instead, wave properties are studied by spatially resonating with selected waves over the entire area. A non-resonant, clutter background return forms a significant and undesirable part of the dual-frequency scatterometer output. This unwanted contribution severely limits the minimum signal detectability. The new three-frequency technique actually converts this background return into a part of the wave modulated signal, thus creating a system whose detectable signal range is limited only by system thermal noise. The most obvious benefit from the improved signal quality and dynamic range is that accurate measurements can be made on the weaker, low-amplitude wave systems that occur at both ends of the spectrum. Previously, most surface wave measuring techniques were only able to detect one or two predominant peaks in a surface wave spectrum. The higher sensitivity of the three-frequency radar will allow measurements of the detailed structure of the wave spectrum over a wide wavenumber range. At large wavenumbers, more

detailed studies will be possible of the early stages of growth of wind-wave systems, i.e., the input of kinetic energy into the ocean from the atmosphere and nonlinear energy transfer from higher to lower wavenumbers.

Theory of the Technique: The three-frequency scatterometer concept is most easily understood by visualizing a microwave system transmitting four carrier frequencies (Fig. 9(a)) either simultaneously or in rapid time sequence. Each of the pairs of signals separated by Δf could be processed to obtain a conventional dual-frequency scatterometer output. If, however, we allow the separation δf between these two pairs to become equal to Δf , then f_2 would equal f_3 and high signal quality three-frequency scatterometer measurements can be made using the new processing technique shown in (Fig. 9(b)). Each frequency is transmitted sequentially, and the back-scattered signals are $E_1(t)$, $E_2(t)$, and $E_3(t)$. The processed signals $P_n(t)$ and $P_i(t)$ are equal to the complex products $E_1 E_2^*$ and $E_2 E_3^*$. The second multiplication

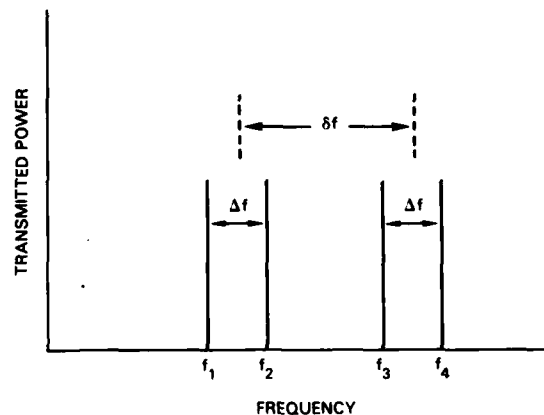


Fig. 9(a) — Frequencies of transmitted signals for a three-frequency scatterometer

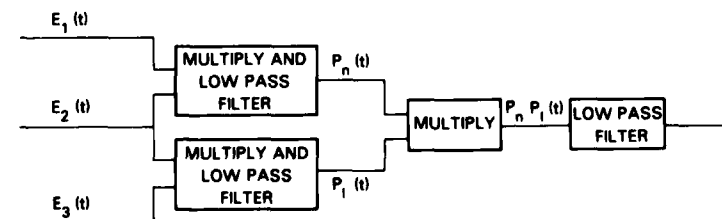


Fig. 9(b) — Output processing of returns E_1 , E_2 and E_3 due to individual frequencies

and filtering produces an output which is the mean of the product of P_n and P_l . The output signal P_{nl} from the processing may be normalized and represented by

$$\frac{P_{nl}}{P} = \frac{2\pi^2 |m(\Delta k)|^2 S(\Delta k) \coth^2(\Delta kd)}{A}, \quad (1)$$

where $\Delta k = \frac{2\pi \Delta f}{c}$ (c is the speed of light),

$m(\Delta k)$ = modulation transfer function,

$S(\Delta k)$ = wave slope spectral density,

A = scattering cell area,

d = water depth,

P = system output when $\delta f = \Delta f = 0$.

Equation (1) indicates that the system output is related to the wave slope. Wave slope and wave height spectra $F(\Delta k)$ are, however, related by

$$S(\Delta k) = (\Delta k)^2 \cdot F(\Delta k). \quad (2)$$

By combining Eqs. (1) and (2) we may solve for the ocean wave height spectrum $F(\Delta k)$,

$$F(\Delta k) = \frac{A}{2\pi^2 (\Delta k)^2 |m(\Delta k)|^2 \coth^2(\Delta kd)} \frac{P_{nl}}{P}. \quad (3)$$

The value of $m(\Delta k)$ is, in reality, a complicated function of both geophysical and microwave parameters. Its value, however, has been experimentally determined for many cases, and Eq. (3) may then be used to determine $F(\Delta k)$ from the three-frequency scatterometer outputs. To actually obtain the spectrum, Δk is varied over a desired range of wavenumbers by varying Δf . This is usually done in discrete steps.

Experimental Verification of the Concept:

A prototype version of the three-frequency scatterometer has been built and experimentally tested at the Army Coastal Engineering Research Center (CERC) pier facility at Duck, N.C. Measurements of wave spectra were carried out during the period 5 to 9 December 1983 from a site at the end of the pier, 1840 ft out in the Atlantic ocean. Wave spectra measured by this new instrument are consistent with simultaneous (nondirectional) Baylor-Gauge wave measurements carried out by CERC personnel. A wave

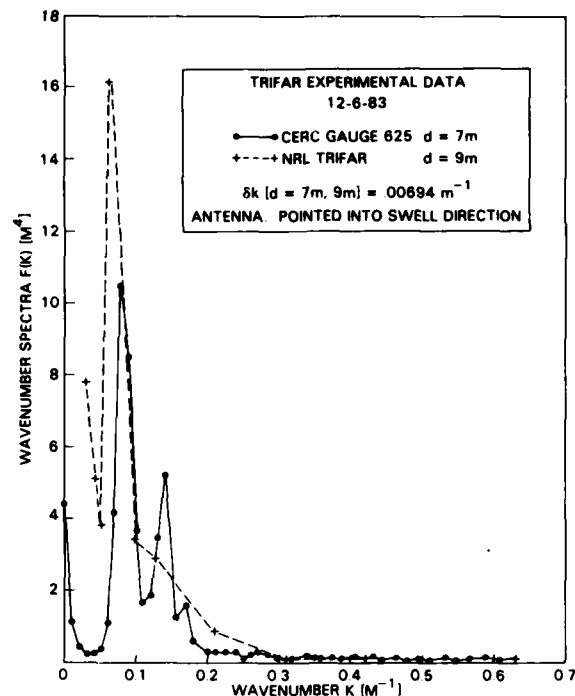


Fig. 10 — Comparison of scatterometer and buoy-derived wave-height spectra (vs wave number) for 6 December

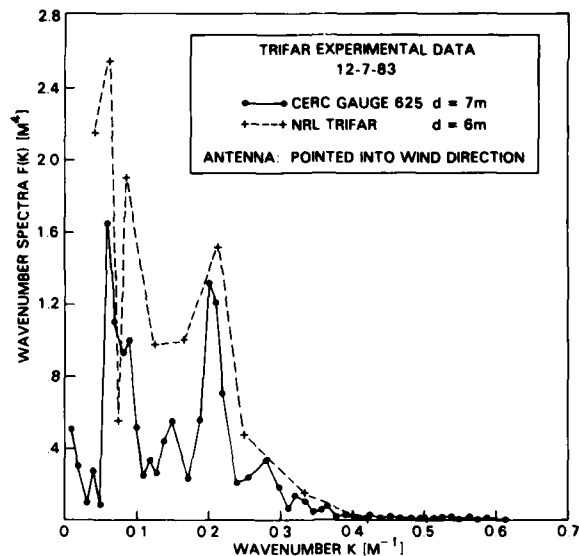


Fig. 11 — Comparison of scatterometer and buoy-derived wave height spectra for 7 December

height spectrum of a 79-m swell system ($k = 0.08 \text{ m}^{-1}$) propagating toward shore from the NE on 6 December is given in Fig. 10. Figure 11 shows similarly obtained data on

7 December which contains the superposition of the swell system and a developing wind-wave system ($k = 0.2 \text{ m}^{-1}$).

Future Instrument Development: Future plans include the development of a compact scanning Ku -band version of the three-frequency scatterometer which will be mounted and used in an NRL RP-3A aircraft.

[Sponsored by ONR]

Reference

1. D.L. Schuler, W.J. Plant, A.B. Reeves, and W.P. Eng, "Removal of Clutter Background Limitations in Dual-Frequency Scattering from the Ocean: The Three-Frequency Scatterometer," *Int. Journal of Remote Sensing* (in press). ■

Radar Backscatter from Splashing Raindrops

J.P. Hansen
Radar Division

An understanding of the basic radar scattering mechanisms from the sea surface is useful both for remotely sensing physical conditions of wind and sea and for detection of target signals against the backscattering surface (sea) clutter. While it is well recognized that surface features such as wind blown ripples, breaking waves, swells, wedge-like wave crests, and specular facets all contribute to sea clutter, little work has been focused on the disturbing influence of rain. Results from a recent NRL experimental measurement program now indicate that splashing raindrops also produce unique surface features which can strongly influence sea clutter.

Experiments: These NRL experiments were conducted from a cliff overlooking the Chesapeake Bay. A 3.2-cm wavelength, pulsed radar was used to observe low grazing angle radar backscatter with both horizontal and vertical linear polarizations. Temporal records of received backscatter were made for regions which spanned the space above and on the water surface. Measurements were conducted before, during, and after

several rainstorms and for a variety of wind and sea conditions.

Results: Analysis of the data has indicated that, with initially calm sea conditions, the splashing of raindrops on the water surface can greatly increase the radar scattering. The time records of received power and rainfall rate shown in Fig. 12 illustrate this effect. For this 60-s example, an initially calm water surface ($19 \times 30 \text{ m}$) was observed by the radar system as rain, with virtually no winds, started to fall (the rainfall rate increased from 0 to 4 mm/h). During this period of increasing rainfall, median backscatter power from the surface increased by more than 15 dB. In effect, the backscatter level for this relatively calm surface increased to that normally expected from a much rougher sea (sea state 2 to 3) with its higher winds and an established wave structure.

The backscatter was also observed to be very rain rate dependent, and it quickly reached a saturation value in only moderate rainfall rates for both radar polarizations. In higher rainfall rates, backscatter from vertical polarization remained near the saturation value while that for horizontal polarization actually decreased. This effect, due to rain splash, was not as dramatic for rougher initial sea conditions, with two notable exceptions: high rainfall rates actually tended to quiet surface backscatter for horizontal polarization below the values without rain, and the fluctuation rates were observed to occur over a wide frequency band in light rainfall for both polarizations.

Interpretation: These experimental results have led us to start examining the types of surface features which a splashing raindrop can produce and how these features might cause some of the scattering phenomena. Consider the simplified diagram of one phase of a raindrop splash depicted in Fig. 13. Initial photographic measurements in a typical rainstorm have shown that the solid water spout reaches heights similar to those of our observing radar wavelength. In addition, the characteristic outwardly propagating circular ripples are of the same physical size as windblown capillary waves which have been

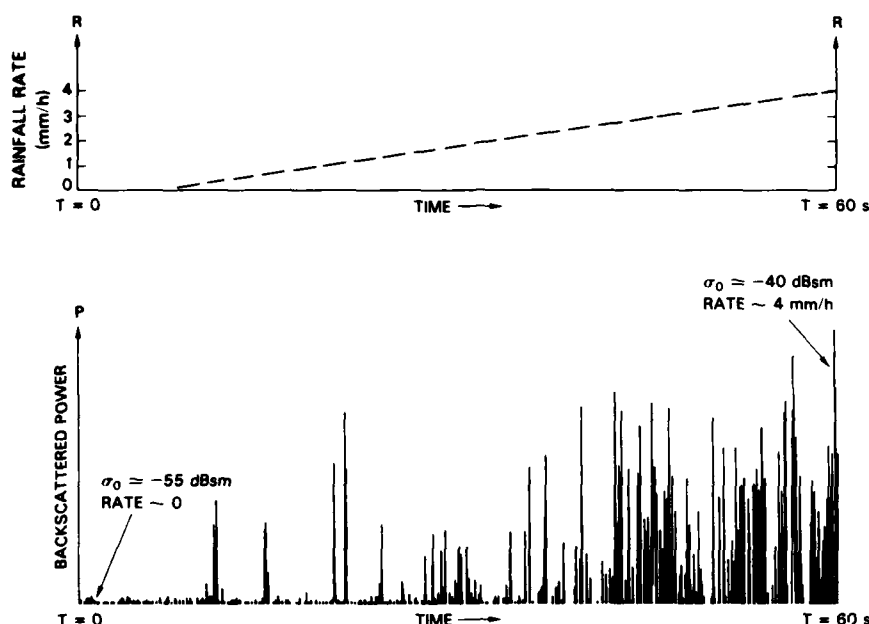


Fig. 12 — Time records of received backscatter and rainfall rate

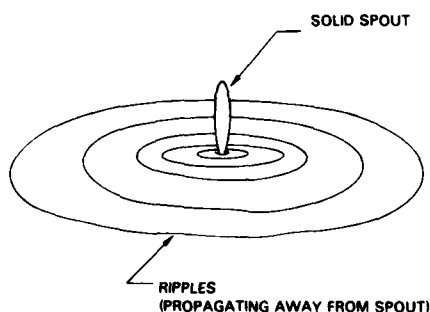


Fig. 13 — Splashing raindrop (one phase)

previously cited as being dominant contributors to sea surface backscatter.

We are currently developing an analytical model which is intended to relate the characteristics of these unique rain splash structures to the observed backscatter phenomena. The understanding gained from this model is expected to lead to both improved interpretation of remote sensing information from a rain-influenced environment and a better recognition of the potential sea clutter problems against which our target detecting radar systems must operate.

[Sponsored by ONR]

Thermal Infrared Imagery of Ship Wakes

W.D. Garrett
Aerospace Systems Division

Active and passive remote sensing systems are being increasingly utilized to characterize the marine environment and to determine man's modifications of it. Surface ships produce remotely sensible wakes which are influenced by natural environmental parameters and may be altered by ship effluents such as bilge and galley discharges. An airborne thermal infrared scanner was flown over the USNS *Hayes* in the southeast portion of Nantucket Shoals to image and evaluate the temperature of the surface water in its turbulent wake. During the overflights the average wind speed was 10 kts, the ship speed was 9 kts, and the seas were light, 0.3 to 0.6 m (1 to 2 ft). Computer profiles of wake temperature derived from digitized infrared (IR) imagery were analyzed to explain the influence of wake hydrodynamics and organic surface film effluents on the surface temperature characteristics of the ship wakes.

Measurements: Thermal IR images of a natural wake of the USNS *Hayes* and one treated

with an ultrathin (one molecule thick) organic surface film are displayed in Fig. 14. The wake treated with the simulated organic ship effluent (top) is marked with an arrow to indicate the point where treatment was initiated. The lower thermal image is an untreated wake generated at the same ship speed under similar environmental conditions. The imagery was produced by a thermal infrared scanner flown over the wake at an altitude of 457 m (1500 ft). Data recorded on magnetic tape in analog form were subsequently digitized and analyzed on a digital imaging computer system. Imagery from 305 m (1000 ft) of the *Hayes'* wake treated with the organic film over a longer distance (5450 m) is displayed in Fig. 15. The imagery in Figs. 14 and 15 show warm temperatures (ship) as darker and cool temperatures (wake) as lighter tones relative to that of the ambient sea surface. Visual examination of the two wake segments in Fig. 14 indicates that the cool ship wake treated with the organic film is more persistent and clearly defined than the natural, untreated turbulent wake produced under similar conditions.

Results: Thermal surface characteristics were quantified by determining temperature

profiles across the wakes using a computer program applied to the digitized wake images. Temperature profiling was performed on the treated and untreated wake signatures depicted in Fig. 14 at various distances behind the stern of the ship, and temperature values were calculated for points of interest on the profiles (Fig. 16). Widths of the thermal wake signatures can be determined from the scales at the bottom of the figure. The wind direction was from right to left in this data display.

Several significant aspects of the thermal wake signatures can be seen in the temperature profiles in Fig. 16. The cool surface water shows a temperature minimum for both treated and untreated wakes which is nearly the same as the water temperature measured at the 7-m keel depth of the ship. This suggests that upwelling of the subsurface water is responsible for the signal. In the case of the wake treated with the organic surface film, this temperature difference (undisturbed ocean surface to coldest portion of surface wake signature) is too large to be attributed to the film's influence on the evaporative-cooled surface boundary layer, an effect which is normally on the order of a few tenths of a degree. However, it is apparent that the wake treated with



Fig. 14 — Thermal IR image of the turbulent wake of USNS *Hayes*. Top wake treated for 13 min with a monomolecular film of oleyl alcohol; length of treated wake, 3530 meters (1.91 nautical miles). Lower image is the thermal signature of a natural, untreated wake.



Fig. 15 — Thermal IR wake image of USNS *Hayes*. Wake treated for 20 min with a monomolecular film of oleyl alcohol; length of treated wake, 5450 meters (2.94 nautical miles).

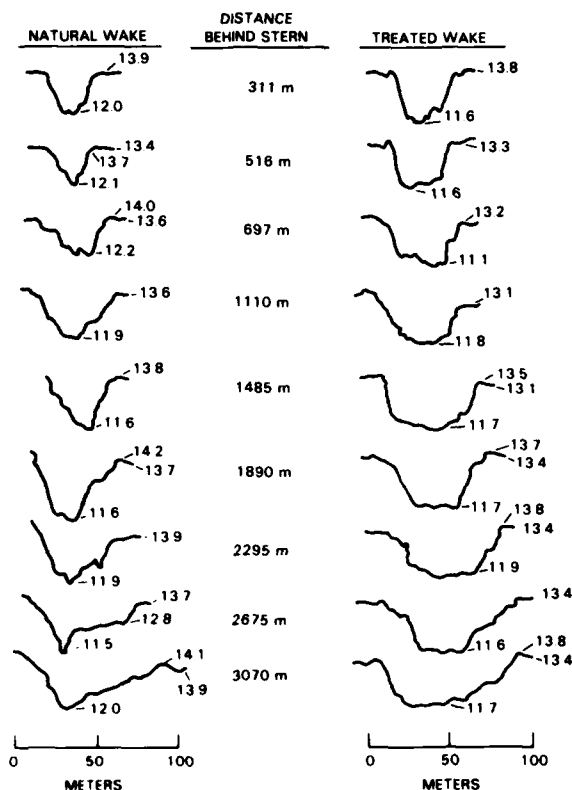


Fig. 16 — Thermal IR temperature profiles across natural and organic surface-film treated turbulent wakes

the monomolecular organic film maintains its cool surface temperature over a broader cross section of the wake. This indicates that the immobilized surface layer due to the organic film inhibits the reintroduction of warm ambient surface water from the windward direction. It is also evident from Fig. 16 that the thermal wake signature broadens with age, an effect which is more pronounced in the case of the wake treated with the surface film.

The wake temperature characteristics are explained on the basis of wake hydrodynamics, wind-stress considerations, and surface film physics. It is concluded that organic ship effluents can increase the persistence of a thermal wake signature by inhibiting the reentry of warmer ambient surface water, or modifying the thermal signatures by the organic discharge.

This research was performed in collaboration with Peter M. Smith, NORDA. Hydrographic and meteorological data were collected

from the ship under the supervision of J. A. C. Kaiser, NRL Code 5810.

[Sponsored by ONR]

The White-Water Wake of a Surface Ship

R.D. Peltzer
Marine Technology Division

The highly visible turbulent wake generated by a ship as it moves across the surface of a body of water is easily detected by radar, photography, infrared and microwave radiometry, as well as the naked eye.

An ongoing NRL research program in free-surface hydrodynamics addresses the behavior of the foamy white-water component of the turbulent ship wake that extends several ship lengths downstream (aft of the ship). The foamy white water has a high relative volumetric content of air to water and is confined to a thin layer (less than 1 ft thick) at the surface in the wake. Most of the major research on the structure and physical constitution of white-water wakes was conducted during World War II, and the results were presented in a National Defense Research Committee Report which has been republished more recently by the Navy [1].

Wake Structure: The three major sources contributing to the foamy white-water wake of a displacement ship are: (1) breaking or folding over of the bow wave; (2) entrainment of air into the ship's turbulent boundary layer at the surface; (3) entrainment and violent mixing of air at and below the water surface by the rotating propeller(s).

Figure 17 illustrates these three sources. When enough energy has been input into the bow wave by the ship's movement through the water, the bow wave breaks, creating highly aerated, foamy water at the surface. The propeller wake can be divided into two regions, an initial region of high divergence angle directly behind the stern, called the initial spreading region, and the far wake where the white water spreads at a small angle of about 1° or slightly more. Adjacent to the ship's hull is the turbulent, air-entraining

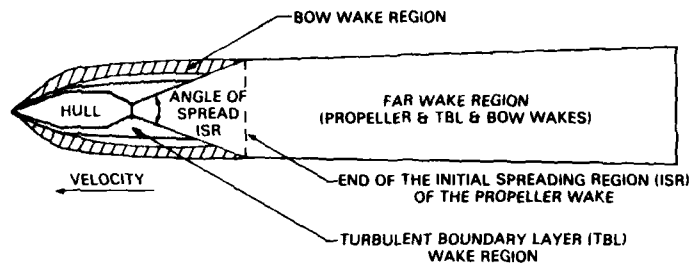


Fig. 17 — Three major sources of white water production from displacement ships

boundary layer. The width of the boundary layer region just aft of the stern is on the order of one and one half times the ship's beam. Both the boundary layer and bow wave white water merge with the propeller wake in the initial spreading region. The relative contributions from each of these sources depend on the type of ship and its speed. Figure 18 is a photograph of the destroyer USS *Moale* moving at 33 knots. The bow wake, boundary layer wake, and propeller wake are fully developed and highly visible.

Wake Length Parameterization: An empirical relation that will estimate the downstream extent of this highly agitated, aerated region in the wake is required as an integral part of any computational model of the surface ship wake. There are many variables that influence the production and persistence of the foamy white water.

An attempt was made to find a dimensionless relationship, involving these variables, that would collapse onto a single curve the white-water wake length data gathered from a collection of aerial photographs.

This dimensional analysis applied to a sample of 15 different displacement ships showed that the maximum length of the foamy region (L_{ww}) of the wake was proportional to the ratio of some power of the ship's speed (V_s) divided by a different power of the ship's propeller revolutions per second (n). Sixty seven numbered data points, where the numbers represent the individual ship wakes studied, are shown in Fig. 19. The data cover ships ranging in displacement from 95 tons (subchaser) to 39,150 tons (aircraft carrier). The empirical relation, derived from a linear fit to these data points, is

$$L_{ww} = 138.7 (V_s^5 / ng^2)^{1/3} = (13.7) V_s^{5/3} / n^{1/3}$$

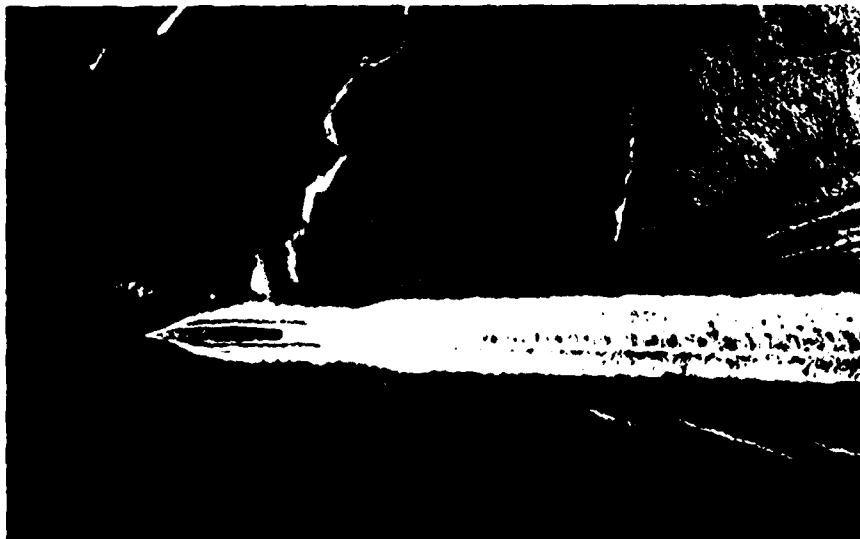


Fig. 18 — White-water wake of the destroyer USS *Moale*

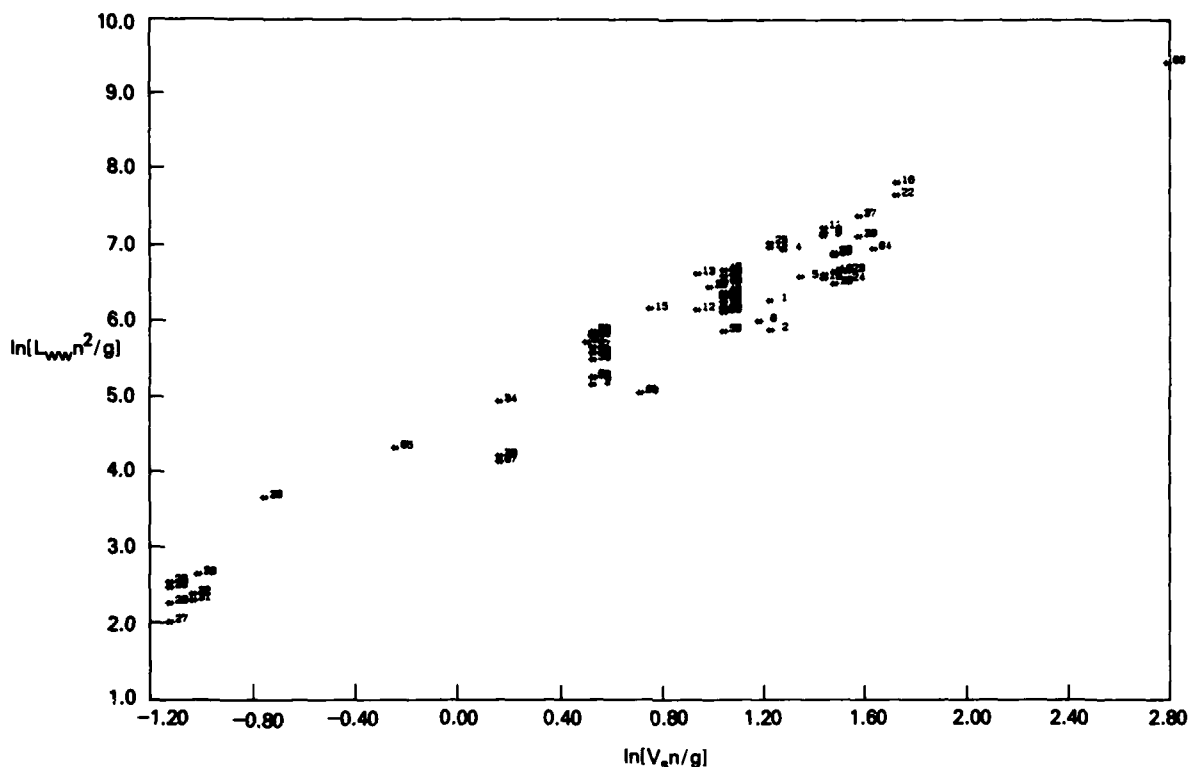


Fig. 19 — Dimensionless relationship that collapsed the white-water length data onto a single curve

with L_{ww} in ft, V_s in ft/s, n in rps, and $g = 32.2$ ft/s². For a given combination of speed and propeller rotation rate, one can be fairly confident that this estimate of the length of the foamy region gives an upper bound for the downstream extent of the visible wake independent of vessel displacements and other ship parameters.

Future research efforts at NRL will include development and verification of models for tur-

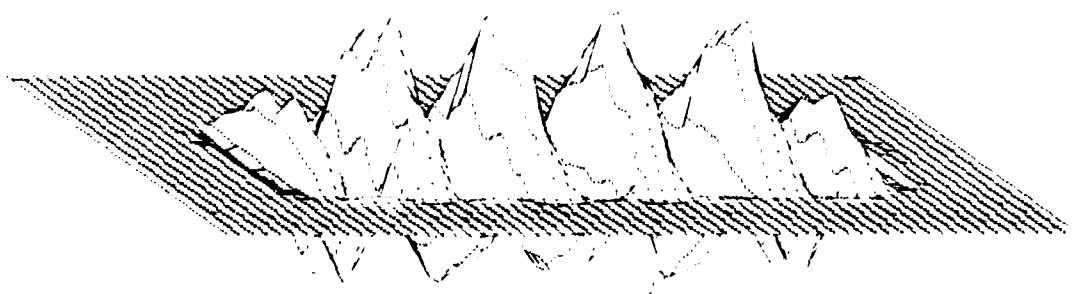
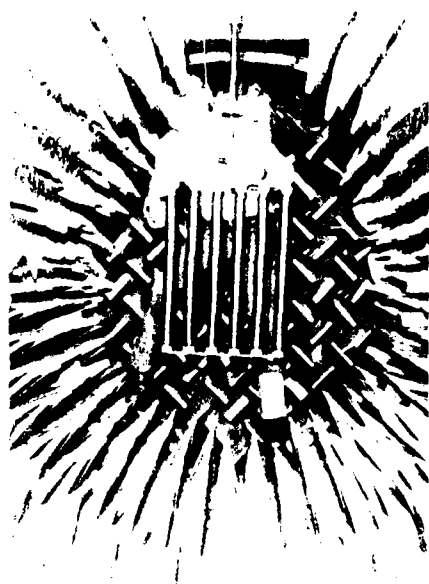
bulent wake spreading and decay, and foam formation and decay.

[Sponsored by ONR]

Reference

1. "Physics of Sound in the Sea," Naval Material Command Report P-9675, 1969; originally published as Summary Technical Report of Division 6, National Defense Research Committee, 1946. ■

Acoustic systems and technology



- 77 Underwater Nearfield Acoustical Holography**
Earl G. Williams, Henry D. Dardy, and Richard G. Fink
Measurements around a body can define sources and the far field.
- 79 Source Localization in Complex Acoustic Environments**
Richard G. Fizell
The structure of realistic ocean acoustic fields is exploited.
- 82 Measurement of Hydroacoustic Particle Motion by Hot-Film Anemometry**
Pieter S. Dubbelday
A mean fluid velocity increases measurement sensitivity.
- 84 A New Acoustic Method of Measuring Properties of the Ocean Bottom**
Tsih C. Yang
The properties of ocean sediments or sea ice can be determined remotely.
- 85 Acoustic Propagation and Ambient Noise in a Wedge-Shaped Ocean**
Michael J. Buckingham
Noise in a continental margin model is plane-wave and isotropic.
- 87 Failure Analysis and Nondestructive Testing of Sonar Dome Rubber Windows**
Robert D. Corsaro, Joel Covey, Rosanna Falabella, William B. Moniz, and Cedric D. Beachem
Early flaw detection and repair can save the Navy significant costs.
- 89 Acoustically Transparent Pressure Chamber**
Joseph F. Zalesak and Lynn B. Poché
Pressure-cycled underwater noise tests are simplified.

ACOUSTIC SYSTEMS

Sonar has long been the principal means of detecting and locating underwater objects. In addition, properties of these objects, the water mass, and boundaries of the ocean can likewise be obtained by specialized analysis of acoustic fields. The first four articles describe work in these areas. Test procedures and acoustic properties of materials are being exploited in a sonar dome program to save the Navy considerable cost in its production and repair of faulty domes. NRL is also involved in acoustic testing and calibration of many devices. The work described in this section was performed in the Acoustics Division (Code 5100) and at the Underwater Sound Reference Detachment, Orlando, Fla. (Code 5900).

Many other basic and applied research projects in acoustics are being performed by the Laboratory. A few of these concern

- basic propagation theory,
- higher order coherence,
- estimation theory for signal processing,
- high-resolution beamforming,
- specialized transducers,
- tow-powered, low-frequency sources, and
- environmental assessments of large ocean areas and of the Arctic.

Page 74, clockwise from upper left:

Checking out an array in the Underwater Sound Reference Detachment's anechoic chambers

Perspective view of a seamount drawn to scale with a 5 to 1 vertical exaggeration. This view was derived from a data set generated by a multibeam bathymetric mapping system. These systems reveal small topographic details not normally resolved by conventional single-beam echo sounders (I. Jewett)

Normal velocity in a plane containing a vibrating, fluid-loaded rectangular plate derived by using nearfield acoustic holography, from a measurement of the acoustic pressure. See article on p. 77 by E. Williams.

Underwater Nearfield Acoustical Holography

E.G. Williams, H.D. Dardy, and R.G. Fink
Acoustics Division

The Physical Acoustics Branch at NRL has undertaken a program to extend the principles of nearfield acoustical holography to the study of complex underwater acoustic fields. Many techniques are available to the experimenter in acoustics to study the sound radiation from complicated sources. Each technique, however, usually illuminates a particular quantity of interest, such as the directivity pattern, the motion on the surface of the source, the acoustic power output, or the on-axis pressure. Often the results lead to misconceptions about the sources under study. A few years ago, however, Williams and Maynard [1] demonstrated a technique to analyze sound sources. This technique, called nearfield acoustical holography (NAH), is based on Green's theorem and was used to verify experimentally that the measurement of the acoustic pressure on a closed, two-dimensional (2-D) surface containing an acoustic source is sufficient to determine the complete (3-D) sound field from the surface of the source out to infinity. The major difference between this technique and conventional acoustical holography is that it is not wavelength limited in its resolution of the sound field—there is no intrinsic limit to its resolving power. As a result, it can be applied to low-frequency radiation problems, where the wavelength of the radiating structure is often much smaller than the acoustic wavelength, as we will demonstrate in the results presented below.

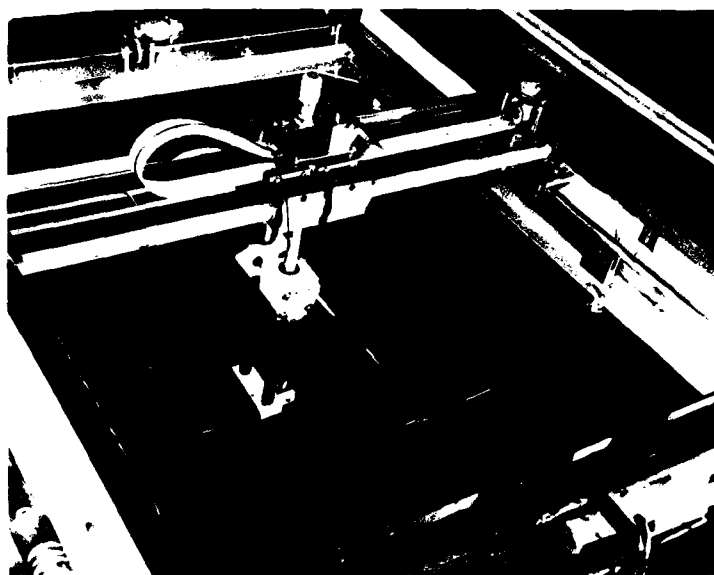
This ability to reconstruct the 3-D sound field from a 2-D pressure measurement allows the experimenter to explore some very meaningful quantities. One in particular, a quantity which has eluded the experimentalist for some 40 years, is the energy flux vector. The energy flux (the power per unit area) pinpoints the areas of a source which give off (or absorb) energy in the sound field; it thus has the potential for source identification and ranking according to strength. With a knowledge of the location and strengths of sources, for example on a naval vessel, one can methodically proceed to provide quieting techniques.

Measurement System: To make this 2-D measurement, a mechanical system must be developed so that a hydrophone can be accurately scanned along some predescribed 2-D surface. Thus the initial thrust of the work has been on building a sophisticated, computer-controlled, robotic scanner which can position a hydrophone anywhere in a 6-m³ meter volume with an accuracy of 30 mils. The completed working scanner is illustrated in Fig. 1. Three motors control linear translation along the X , Y , and Z axes, oriented as shown in the figure insert, under computer command. A dual hydrophone probe can be seen at the end of the boom in the lower right-hand side of the figure. The on-site computer (PDP11) will be optically linked to the Physical Acoustics Branch VAX computer where most of the computations are done.

Experiments and Results: The first underwater experiments using NAH were performed by scanning in a planar 2-D contour. The acoustic source was a point-driven, 36-cm² clamped plate held vertically in the plane $Y = 0$ at the lower right-hand side of Fig. 1 plate not shown in photograph. The radiated pressure (at 3 kHz) was measured for 4000 points in a vertical plane ($Y = \text{const.}$) located 1.0 cm away from the plate using the scanner. As described above, the complete 3-D sound field was computed from the surface of the plate out to infinity (in the positive Y direction). Figure 2 shows the resulting computation of the radiated pressure field in one particular vertical plane ($X = 0$). The dashed line in the figure represents the end view of the actual measurement plane (located at $Y = 1.0$ cm). The contours represent lines of constant pressure normalized to a maximum of one. The rapid decay of the sound field, as it travels away from the plate because of the exponential decay of the evanescent wave components, is evident. It is very interesting to note that the variation of the sound field follows the wavelength (13 cm) characteristic of the flexural wave on the plate as opposed to the actual wavelength (49 cm) in the water.

Figure 3 shows the energy flux vectors in a plane perpendicular to the plate as well as the location of the plate driver (5) and clamping mass (6); the clamping mass is just a driver which is

Fig. 1 — Computer-controlled, robotic scanner. Three motors, using a chain-link drive, control translations along the X, Y, and Z axes (directions shown in the insert). The dual hydrophone probe is shown in the lower right-hand side of the photograph at the end of the boom.



81097(2)

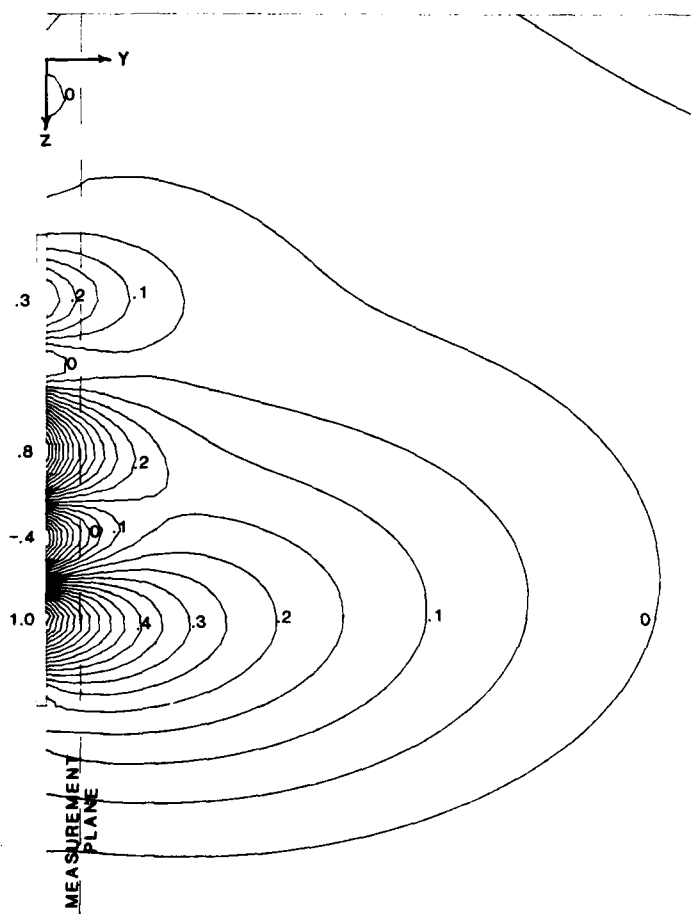


Fig. 2 — Contours of equal pressure normalized to a maximum of 1.0 show the acoustic field at one instant in time in a vertical plane through the centerline of the plate source and perpendicular to it. The dashed line represents an end view of the measurement plane. The data on this plane were used to reconstruct the contours shown using the NAH technique. The rapid decay of the field from the surface of the plate is due to the exponential decay of the evanescent waves produced by the subsonic plate waves.

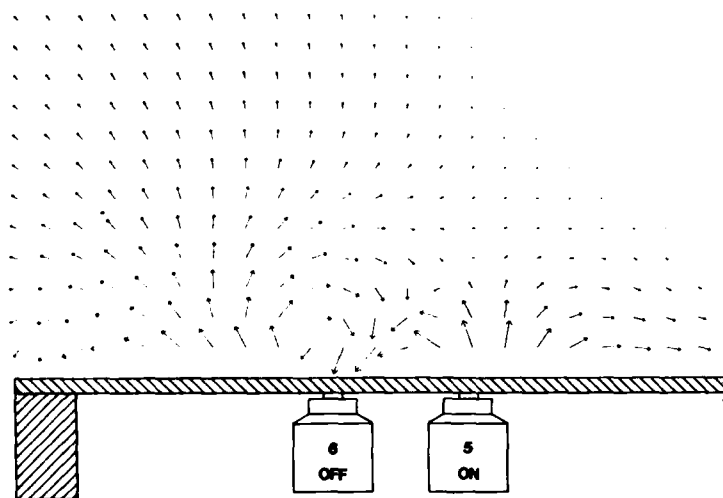


Fig. 3 — Energy flux (vector acoustic intensity) in a plane perpendicular to the plate through the exciting driver (5) and clamping mass (6). The vectors are reconstructed by using the NAH technique from the pressure measured in a plane. The absorption of energy by the plate over the clamping mass is evident.

turned off. The energy flux, often called the vector intensity, is shown to circulate in the nearfield with the region above the driver acting as an energy source and the drone acting as a sink—an absorber of energy. One can additionally see that the plate support at the left-hand side of the figure is also absorbing energy from the sound field.

The ability to measure the energy flux, as illustrated here, along with the ability to completely reconstruct the radiated sound field, including the normal vibrations of the surface of the source, has the potential for great utility in a number of Navy programs, most notable of which is quieting of U.S. boats.

Presently, we are developing dual-surface methods (measurement of the pressure of two congruent surfaces) so that nearfield acoustical holography can be applied to a number of Fleet-relevant scattering problems as well as radiation problems.

[Sponsored by ONR]

Reference

1. E.G. Williams and J.D. Maynard, "Holographic Imaging Without the Wavelength Resolution Limit," *Phys. Rev. Lett.* **45**, 554 (1980). ■

Source Localization in Complex Acoustic Environments

R.G. Fizell
Acoustics Division

Conventional beamforming methods for localizing acoustic sources in various ocean environments usually involve correlating the field received on an array of hydrophones with the plane-wave fields which would be expected if the source were at a given location. A horizontal array can thus determine the relative bearing of the source, or a vertical array can determine the vertical arrival angles of bottom- and surface-bounce paths and then, in principle, can determine the source range and depth by ray-tracing methods (Fig. 4). However, the acoustic environment often supports fields with far more complex structures than this simple plane-wave model. For example, either cylindrical spreading, vertical structure induced by multipaths in the deep ocean, or normal-mode propagation in a shallow channel can cause the fields to depart considerably from the simple plane-wave model. This can cause a severe degradation in the ability of the vertical and (to some extent) horizontal beamformers both to detect and to localize the target.

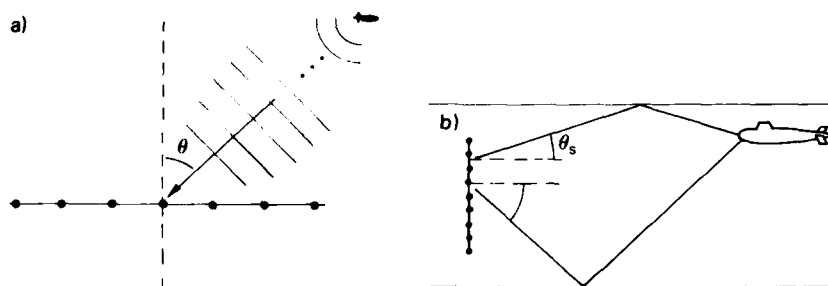


Fig. 4 — (a) Aerial view of horizontal array used to determine bearing to a distant source by observing (nearly) plane waves impinging on array. Closer to the source, the waves are more curved; (b) Vertical array used to determine vertical angles of arrival of surface-bounce path (θ_s) and bottom-bounce path (θ_b). Rays then can be traced to determine position of target.

Recently, however, we have been investigating a method which actually utilizes this complexity of the acoustic field to improve rather than degrade the localization of a target, if certain characteristics of the acoustic medium are understood well enough [1].

Technique: The field in such a complex environment is in general a function of range, depth, and azimuth relative to the array, and it contains a great deal of information which can be used to detect and localize the target. If we can characterize the medium well enough to know the functional form of the fields it supports, we can predict what field would be produced by a source at a given hypothetical position P_s' . This "replica" field is then correlated with the actual received field caused by a source at the (as yet unknown) position P_s to produce an "ambiguity function," which is a measure of the closeness of the match between the true and replica fields. The ambiguity function can be shown analytically to be a maximum if both of the following conditions are

satisfied: the functional form of the replica functions is identical to the structure of the true field supported by the environment, and the hypothetical position P_s' is the same as the true source position P_s . If we assume that we know this field structure, therefore, we can perform the correlation for all possible hypothetical positions P_s' , and the maximum of the ambiguity function will localize the target. The ambiguity function is in principle the optimum detector (gives the highest probability of detection with the least number of false alarms) of low-level signals as well.

Simulation of a Channel: This method has been applied in computer simulations to an assumed shallow-water environment which supports normal modes. That is, the field is a superposition of modes, each of which is represented by a pair of (upward- and downward-going) waves which are spreading cylindrically from the source and moving between surface and bottom at a definite angle to the vertical. This rich vertical structure is illustrated in Fig. 5, which shows ray

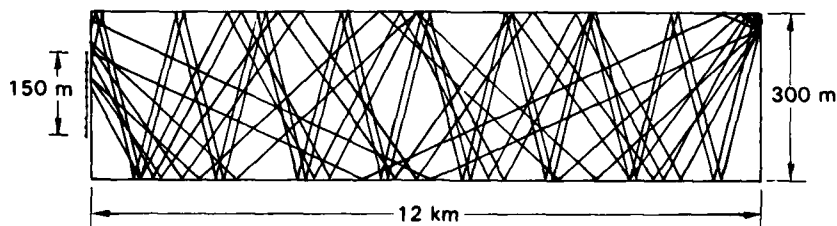


Fig. 5 — Ray trace showing most of the modes for the particular Pekeris channel used for the simulations in Fig. 3. Note that the vertical scale is expanded by a factor of ten. The vertical array spans half the channel depth and is vertically centered.

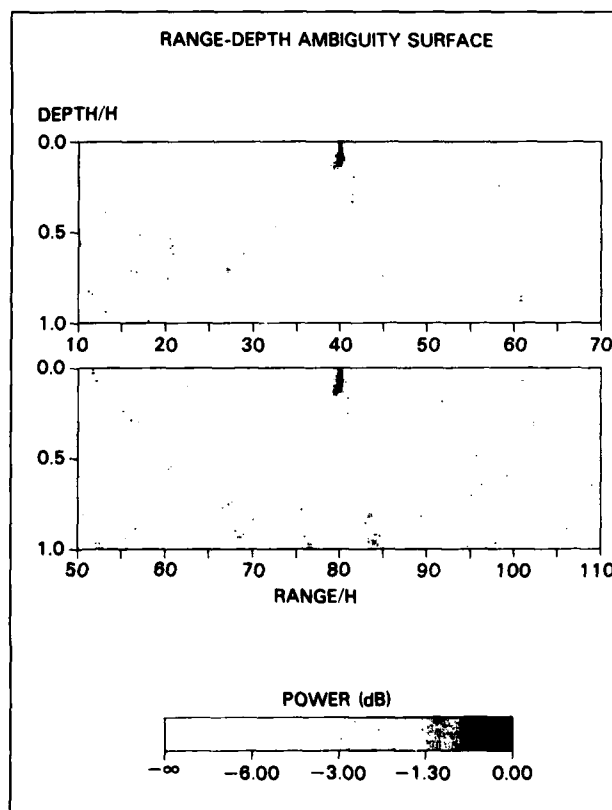
traces for a few of the eight modes which are supported by this channel. It can be shown that a plane-wave beamformer in a typical channel cannot resolve the vertical arrival angles, and hence it is impossible to determine the source range and depth by ray tracing. We will restrict our attention to determining range and depth for now, because it is a more interesting problem scientifically, and a more important problem operationally, than azimuth determination.

Figure 6 shows plots of the ambiguity function for one source at two different ranges ($\text{range}/H = 40$ and 80) using a vertical array in the simulated environment: a Pekeris channel, which is a water channel of constant depth above a semi-infinite bottom, both with uniform, but distinct, densities and sound velocities. The vertical array was assumed to span half the water column and to be centered at middepth. The plots show the source, which has signal-to-noise ratios (SNR) of 0 dB, to be localized accurately by a narrow main peak (dark spot); although

sidelobes (grey spots) which are within 3 dB of the main peaks appear at other positions, they are not so strong as to be confused with the true source positions. In simulations of fairly weak targets, however, it has been found that these sidelobes can become comparable to the main peak. Note that the target is resolved nearly equally well at the two ranges. Thus, performance does not seem to be overly sensitive to source range.

Future Considerations: Several important questions about the method must be answered before it can be useful for realistic acoustic environments and target levels. Among the most critical are (1) its susceptibility to nonuniform noise fields, (2) the problem of excessive sidelobes, and (3) its sensitivity to mismatches between the replica- and actual field structures (i.e., errors in our understanding of the environment). In recent years, high-resolution beamforming techniques have been developed for the

Fig. 6 — Ambiguity surfaces for a target at a depth of one-tenth the channel depth, and two ranges of 40 and 80 channel depths, respectively. The grey scale indicates power.



plane-wave-bearing-estimation problem which can significantly improve the discrimination between source peak and sidelobes and can regularize noise fields in various ways [2]. We are currently investigating whether these techniques can be adapted to ambiguity function processing to help solve the first two problems and under what environmental circumstances the third problem is amenable to solution. If these questions can be answered positively, the ambiguity function method should provide a significant improvement over conventional methods in localizing even moderately weak targets in richly structured environments.

[Sponsored by ONR]

References

1. R.M. Heitmeyer, W.B. Moseley, and R.G. Fizell, "Full-Field Ambiguity Function Processing in a Complex Shallow-Water Environment," Proceedings of the Workshop on High-Resolution Spatial Processing in Underwater Acoustics, sponsored by NORDA, NSTL Station, Miss., Oct. 1983.
2. *Modern Spectrum Analysis*, D.G. Childers, ed., (IEEE Press, New York, 1978). ■

Measurement of Hydroacoustic Particle Motion by Hot-Film Anemometry

P.S. Dubbelday

Underwater Sound Reference Detachment

Most hydroacoustic transducers are sensitive to pressure fluctuations. For a more complete description of an acoustic field, it is also desirable to know the concomitant fluid-particle velocity. The latter has been determined by means of a neutrally buoyant body that follows the fluid motion [1]. An alternative method was developed at NRL.

Hot-Film Anemometry in Hydroacoustics:

This technique relies on the measurement of the heat transfer from an electrically heated film (or wire) to the surrounding medium. This heat

transfer is a function of the strength of the fluid flow. The small size of the sensor (Fig. 7) and its fast time response make hot-film anemometry the method of choice in the study of turbulence. In hydroacoustics it will be especially useful for measurements inside small spaces, at low frequency.

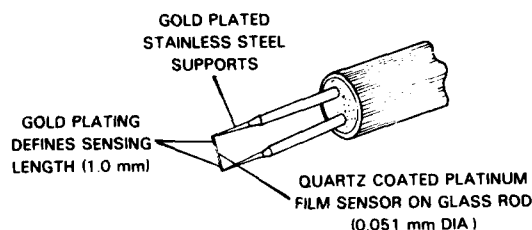


Fig. 7 — Cylindrical hot-film sensor at end of probe

The temperature of the sensor is kept constant by holding its resistance constant in a bridge circuit (Fig. 8). To accomplish this, the bridge voltage must be varied to match the heating of the film to the cooling by the fluid flow, and this bridge voltage is the output of the instrument. Since the sensor is warmer than the fluid, heat is transferred from the sensor by heat conduction and by free convection from the sensor even in a quiescent medium.

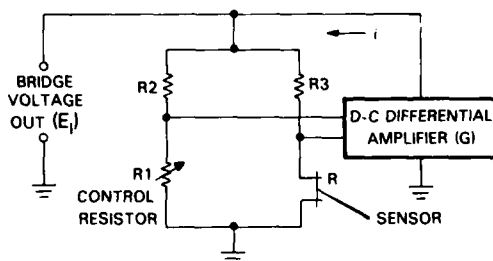


Fig. 8 — Constant temperature system

Modes of Operation: The presence of free convection results in two modes of operation, depending on the direction of the acoustic particle motion relative to the direction of gravity. When the particle motion is horizontal, it will cool the sensor going either to the right or to the left. Therefore, the frequency of the fluctuating heat

transfer is twice that of the acoustic field, and the output voltage is proportional to the square of the particle motion. In vertical particle motion, the free convection acts as a bias. Compared with the constant cooling due to the bias flow, an upward motion will augment the cooling of the sensor, but a downward motion will reduce the cooling and is equivalent to heating. Therefore, the output voltage has the same frequency as the acoustic field and is proportional to the particle motion. There is directional sensitivity in both modes of operation.

Accomplishments in 1983: The calibration of the hot-film anemometer for hydroacoustics was performed in an NRL-USRD-type G40 calibrator (using a piston, to vertically oscillate a water column) for the vertical particle motion and in a specially designed trough-and-shaker arrangement for the horizontal motion. In addition to the amplitude and frequency of the acoustic field, the experimenter has other parameters at his disposal: temperature difference between sensor and medium, diameter of the sensor (in this study, 25, 50, and 150 μm), and different fluids (here water and ethylene glycol).

Obviously the variation of these experimental parameters leads to a large quantity of data. Table 1 gives some sample results to demonstrate the order of magnitude of input and output parameters. Reference 2 gives a more complete description.

Table 1 — Sample Results

Frequency (Hz)	Particle Velocity (mm/s)	Relative Displacement	Voltage Output (mV)
a. Anemometer Output for Horizontal Motion in Water			
20	5.2	0.83	43
48	2.5	0.17	2.4
120	0.90	0.024	0.095
b. Anemometer Output for Vertical Motion in Water			
100	4.3	0.14	32
200	2.3	0.036	9.1
300	1.6	0.017	4.4

Temperature difference between sensor and medium is 30°C.
Length of sensor is 1 mm; diameter is 50 μm .

The dependence of this experiment on the various parameters can be considerably simplified by the introduction of dimensionless groups or

parameters. Dimensional analysis shows that four parameters can describe the experiment. The dependent variable (which is the output voltage) is cast in the form of a dimensionless heat transfer, namely the Nusselt number, which compares the actual heat transfer to that of pure conduction. The fluid motion is expressed by the particle displacement relative to the diameter of the sensor. The other relevant independent groups are the Grashof number, which may be considered as a Reynolds number for free convection in the sense that it compares the magnitude of inertia with that of viscosity; and the Fourier number, which represents the relative importance of heat conduction and local heating rate.

The introduction of dimensionless groups not only reduces the number of independent variables to a manageable size, but also describes the functional dependence in terms of variables that have a direct physical interpretation, as the previous descriptions clearly show. This is particularly useful to give a picture of the relative importance of the physical processes involved, especially since the theoretical description by means of the hydrodynamic equations of continuity, motion, and heat leads to formidable mathematical problems.

Future Work: The role of free convection as a bias flow prompted the introduction of an imposed jet flow that considerably improves the sensitivity and, moreover, liberates the device from the limitations set by the natural direction of gravity. Preliminary measurements were performed, but more experiments are needed. The phase of the output signal also displays a structure in accordance with the dimensionless numbers pertinent to the situation. This deserves further study. More extensive calibration of the device would be in order and could be used for a deeper theoretical understanding and description of the processes.

The connection between the acoustic field and free convection suggests that this application of hot-film anemometry is not only a useful tool in hydroacoustics but that the imposition of an acoustic field also might conversely serve as a means of studying free convection itself.

[Supported by ONR]

References

1. T.A. Henriquez, "A Standard Pressure Gradient Hydrophone," *J. Acous. Soc. Am. Supp.* 11, 70, S100, 1981.
2. P.S. Dubbelday, "Measurement of Hydro-acoustic Particle Velocity by Hot-Film Anemometry," NRL Memorandum Report 5223, Feb. 1984. ■

A New Acoustic Method of Measuring Properties of the Ocean Bottom

T.C. Yang
Acoustics Division

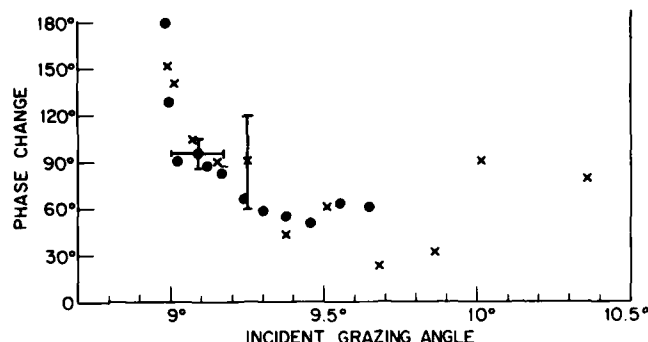
The properties of the ocean bottom influence sound propagation and hence affect naval operations, especially in the shallow water (continental shelf) areas. The Navy has programs to predict and improve the detection capability in these areas. At present, the methods of surveying the bottom involve either taking samples from the ocean sediment or using air guns, high-powered electrical sparkers, or explosives with a towed array system to deduce the sound velocities in the bottom. These methods are expensive and limited in the area they can cover at a time. Since one cannot possibly cover the whole ocean with these methods, an inexpensive remote sensing method for surveying the bottom types would be of great value to the Navy.

Almost all of the bottom interaction research has been concerned with the magnitude of the coefficient of sound reflection from the bottom boundary. Theoretically, the phase portion of the reflection coefficient also carries information about the reflection media, but the reflection phase change is very difficult to measure directly. The method developed here is the first one which has measured the phase change experimentally. It shows promise of being a convenient means of finding more information about the physical properties of the ocean sediments or even the sea ice cover of the Arctic Ocean than is available by measuring only the magnitude of the reflection coefficient.

Overview of Method: This method uses the broadband energy of a distant explosion to measure group velocities of sound waves and extract from that information the phase change introduced at each boundary reflection. This is a remote sensing method which will provide information about the different bottom types. The method is inexpensive and easy to carry out. A set of single sensor (one hydrophone) data at different ranges from the explosive sources provide information about the bottom variability along the path. Using explosives to measure broadband propagation is a well-developed method in underwater acoustic research. To measure the phase change, certain criteria for selecting the charge depth and receiver depth should be followed, according to the frequency range of interest. The method can be implemented by a microcomputer. This allows a real-time analysis of the explosive data, thus providing real-time information about the ocean bottom for naval applications.

Basis of Method: This method uses normal mode theory. Normal modes exist in a waveguide, such as a shallow ocean, when the major portion of the energy associated with the mode remain trapped inside the waveguide. How the normal modes are formed and propagate depends on the boundary conditions, in particular the phase change of the sound waves reflected at each boundary. In a medium in which all waves have the same velocity of propagation, a signal of any form would travel without distortion. On the other hand, in an acoustic dispersive medium (sound velocity varies with depth and the group velocity is a function of frequency), such as the ocean, all propagation is accompanied by a change in the form of the signal (except for an infinitely long sinusoidal wave). A way to characterize the normal modes is to measure the group velocity of each mode, which is the propagation velocity of the sound energy at the mode frequency. Since the formation of the mode is related to the phase change at the boundary, we have theoretically determined a relation between the phase change at the boundary, the group velocity, and the mode frequencies. To adequately measure the phase change, we need a measurement of the mode frequency to a precision of 0.5 Hz or

Fig. 9 — Phase change of the bottom reflection coefficient as the incident angle is changed



better. The sonogram method (a standard acoustic technique) which has been used heretofore to measure the group velocity has an uncertainty of 2 to 3 Hz. To achieve the required frequency resolution of 0.5 Hz, a new method was developed at NRL [1] which expresses the normal mode spectrum in terms of mode frequencies. This prior knowledge of mode structure is then used as a precision interpolation tool. This allows a high-resolution measurement of the mode frequency when certain bounds on the processing parameters are met.

With this new method, we have deduced the phase change of reflection at the ocean bottom from explosive data collected on the continental shelf east of the United States. Figure 9 shows some measurements of the phase change of the reflection coefficient as the incident angle is changed. This data will be useful to analyze the structure and characteristics of the bottom. We have also applied the same method to deduce the phase change of reflection from the sea ice cover in the Arctic Ocean.

In summary, we have presented a new remote sensing method which shows promise of being a convenient, inexpensive means of finding the physical properties of ocean sediments or sea ice in a shallow water region. Further testing is planned to examine the effectiveness of this new method and to improve and simplify the algorithm for Navy use.

[Sponsored by ONR and NAVELEX]

Reference

1. T.C. Yang, "A Method for Measuring the Frequency Dispersion for Broadband Pulses Propagated to Long Ranges," *J. Acous. Soc. of America*, in press.

Acoustic Propagation and Ambient Noise in a Wedge-Shaped Ocean

M.J. Buckingham*
Acoustics Division

A depth-varying ocean such as that occurring over the continental slope may be approximated as a wedge-shaped domain with the shore line coinciding with the apex of the wedge. Acoustic propagation in this type of region is of particular interest in connection with submarine detection just off the continental shelf. An interesting feature of propagation over a sloping bottom is that the rays out of the plane normal to the apex of the wedge undergo horizontal refraction; i.e., they follow curved paths in the horizontal plane because of the reflection of the rays off the surface and the bottom. Thus, a ray traveling upslope is turned around before it reaches the apex of the wedge and then proceeds to propagate back downslope. Any satisfactory propagation or ambient noise model of a depth-varying environment must take this mechanism into account; the model must be *truly* three-dimensional in character. Many of the available numerical propagation models are either intrinsically two-dimensional or, with some of the more recent models, are 2-1/2-dimensional in the sense that they give a three-dimensional field but neglect the effects of horizontal refraction. These models are not adequate for this problem.

An alternative approach is to seek an analytical solution to the propagation problem. This article describes two related analytical models developed at NRL. The first, a propagation

*On exchange from the Royal Aircraft Establishment, Farnborough, Hampshire, England.

model, gives the acoustic field (magnitude and phase) because of a point source in a wedge-shaped ocean [1]. The second model gives the spatial statistics of the ambient noise because of a random distribution of surface sources in the same type of ocean environment [2]. In both models the boundaries are assumed to be perfectly reflecting, which, as far as the bottom is concerned, is a crude but tractable representation.

Propagation Model: The propagation model derives from a solution of a Helmholtz equation for a point source in a wedge of angle θ_0 . A cylindrical coordinate system is used, in which the z -axis runs along the apex of the wedge, range r is measured perpendicular to the apex (see Fig. 10), and the angular coordinate θ is measured about the apex down into the ocean, with $\theta = 0$ and $\theta = \theta_0$ representing the surface and the bottom, respectively.

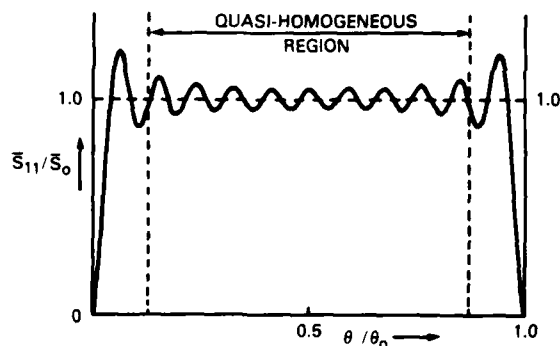


Fig. 10 — The first-mode beam of radiation (broken line) and a few of the first-mode rays (solid lines) in a 10° wedge

This solution is a sum of normal modes, with eigenfunctions which are oscillatory functions of θ . The mode amplitudes are given by a complicated integral containing the entire (r, z) dependence. This integral has been evaluated using approximation techniques, yielding a result which is valid for most frequencies and source/receiver configurations of practical interest.

Each mode in the (r, z) plane takes the form of a beam of radiation, as illustrated by the

broken line in Fig. 10 for the first mode. The sound intensity is high within the beam, and outside it there is a shadow zone where there is essentially no energy in the mode. As the mode number rises, the width of the associated beam becomes progressively smaller. Thus the overall extent of the sonified region is determined by the lowest order mode.

The modal beams of radiation can be interpreted in terms of rays and the mechanism of horizontal refraction. Rays are launched in all directions from the source, and those travelling up-slope follow curved horizontal paths, as illustrated by the solid lines in Fig. 10. It is apparent that these rays are constrained to fall within the sonified region (broken line in figure) determined from the Helmholtz equation. The ray and mode approaches are thus seen to give complementary and mutually consistent descriptions of the field in the wedge. Notice that a point receiver placed in the beam, say at point A in Fig. 10 will have two rays per mode incident upon it (as indicated by the double headed arrows in the figure). One implication of this is that a directional receiver located over a sloping bottom may show severe bearing errors as well as a degraded detection performance due to signal rejection.

Ambient Noise Model: The ambient noise model gives the noise field in the wedge due to a (statistically) uniform distribution of independent sound sources at the surface such as might be produced by waves or rain. It incorporates the same three-dimensional propagation features described above. The model provides analytical expressions for the power spectral density and the directionality of the noise. Figure 11 shows an example of the normalized power spectral density at one frequency, S_{11}/S_0 , as a function of the angular depth, θ , normalized to the wedge angle, θ_0 . (The receiver is at a range where a total of eleven modes are supported by the water column.) Note that the intensity of the noise field is approximately independent of depth (i.e., the noise is quasi-homogeneous). The analysis also shows that the noise is very closely isotropic; i.e., the noise power incident at a point in the field is the same from all directions.

In the real ocean the bottom is not usually perfectly reflecting, but is penetrable in that it

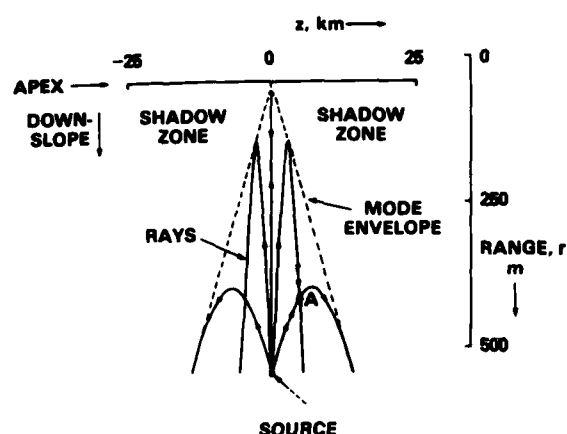


Fig. 11 — The (normalized) power spectral density of the ambient noise as a function of the angular depth normalized to the wedge angle, θ_0

shows a critical angle. The solution for the field in this case is extremely difficult to achieve. However, the analysis of propagation in the "perfect" wedge provides an essential background for understanding the peculiarities of the more difficult environment; modal beams, for example, may still be expected.

In September 1984 an international sea trial involving NRL is to be conducted off the east coast of Australia. The aim is to investigate acoustic propagation in a depth-varying ocean, and several of the experiments have been planned on the basis of the theoretical models described above. Thus, the trial constitutes perhaps the first systematic attempt to measure (three-dimensional) modal effects in a wedge-shaped ocean.

[Sponsored by NRL]

References

1. M.J. Buckingham, "Acoustic Propagation in a Wedge-shaped Ocean with Perfectly Reflecting Boundaries," Proc. NATO Advanced Research Workshop on Hybrid Formulation of Wave Propagation and Scattering, held in Rome, August 1983.
2. M.J. Buckingham, "A Theoretical Model of Surface-generated Noise in a Wedge-shaped Ocean with Pressure-release Boundaries," to be submitted to *J. Acoust. Soc. Am.*

Failure Analysis and Nondestructive Testing of Sonar Dome Rubber Windows

R.D. Corsaro and J. Covey

Acoustics Division

R. Falabella and W.B. Moniz

Chemistry Division

C.D. Beachem

Material Science and Technology Division

The main sonar transducers used on many Navy surface ships are located on the lowest part of the bow and are covered by a large rubber dome. This sonar dome is transparent to underwater sound, and hence it has been dubbed a "window." It is the size of a large room, weighs 19,000 lb, and is the largest rubber part ever molded. It is constructed much like a steel-belted automobile tire, in that it is composed predominately of rubber reinforced with steel wire cords. While the use of this window construction has substantially improved the acoustic performance of the sonar system, it suffers from one drawback—in a few instances it has catastrophically ruptured in service for no apparent reason. One such rupture is shown in Fig. 12.

In a multidisciplinary study, NRL scientists have been studying this problem with three goals: determining the failure mechanism involved, eliminating the potential for this type of failure in new windows, and developing techniques for monitoring existing windows so that repairs can be implemented before catastrophic failure occurs. Substantial progress has recently been made in each of these areas.

Failure Mechanism: NRL fractologists (fracture and failure analysis scientists) have determined that corrosion fatigue failure of the steel cords is the cause of such failures. The failure process begins with water seepage into the dome through small breaks or tears in the bead cable region. This bead cable runs along the entire periphery of the window and is used to clamp the window to the ship. Once a water entrance path occurs, salt water will then wick through internal voids in the rubber and the steel wire reinforcement cable and will begin corroding these structurally important wires. While these wires are unlikely to rust through, the presence



Fig. 12 — Rupture of a rubber sonar dome window on the USS O'Brien, DD 975

of a corrosive agent causes a second failure contributor to take on new importance. Some areas of the dome are much stiffer than others, giving rise to local stress concentrations. If corrosion occurs at these locations of high stress, wire breakage is considerably accelerated. This phenomenon is called corrosion fatigue. As each wire breaks, stress on neighboring wires is increased and an internal crack develops, spanning many wires. Eventually the internal crack propagates to the surface and a rupture occurs.

Flaw Detection Schemes: NRL polymer scientists have verified the importance of this failure mode by using stress simulation experiments and failure analysis techniques. This work led to recommendations for changes in the factory fabrication procedures which should greatly reduce the likelihood of failure by this mechanism in new windows. These scientists are also exploring techniques to locate flaws before cata-

strophic failure can occur. One technique which has been particularly successful in locating broken wires is x-ray radiography. Radiography is now being used to detect internal cracks prior to rupture of the window and to monitor the growth of cracks for convenience in scheduling repairs. Radiography, however, cannot detect flaws in the rubber portions of the dome.

In a parallel program, NRL acousticians have been developing nondestructive ultrasonic techniques which can detect voids or channels in the rubber portions of the dome. Such flaws may serve as sites for rubber crack growth leading to water intrusion. Typical voids located in the bead cable region are tubular channels 1 to 5 in. long and 0.05 to 0.15 in. in diameter. The specialized diagnostic apparatus which has been developed at NRL to locate such voids is now in use at the factory where these flaws can easily be repaired prior to shipboard installation. Other ultrasonic apparatus is under development for use on existing domes either for drydock inspection or for underwater testing by Navy divers.

Ultrasound Detection: The use of ultrasound (0.5 to 1 MHz) in this structure is complicated by the layered construction, which gives rise to multiple echoes, and the high sound absorption of the rubber at this frequency, which limits the resolution and depths available. Figure 13 shows the types of signals typically obtained from this structure. In some areas strong echoes are obtained near the outside surface of the window (depth of 0.25 cm); these tend to obscure deeper detail and generally correspond to regions in which a patch has been applied in the shipyard to smooth or streamline the window contour. In a flawless region, the next echo observed is then the outermost wire ply. The depth of this ply varies considerably, particularly in the region where wire cord layers are overlapped or spliced. Any echo observed before this wire layer indicates the presence of a flaw in the rubber. The figure shows a particularly interesting case where a flaw is detected directly in front of the first wire cord layer. The feature which distinguishes this signal as a flaw rather than a wire is that the echo is seen to be phase reversed (appears upside down). This behavior indicates a reflection from a very soft region (an air-filled void) rather than

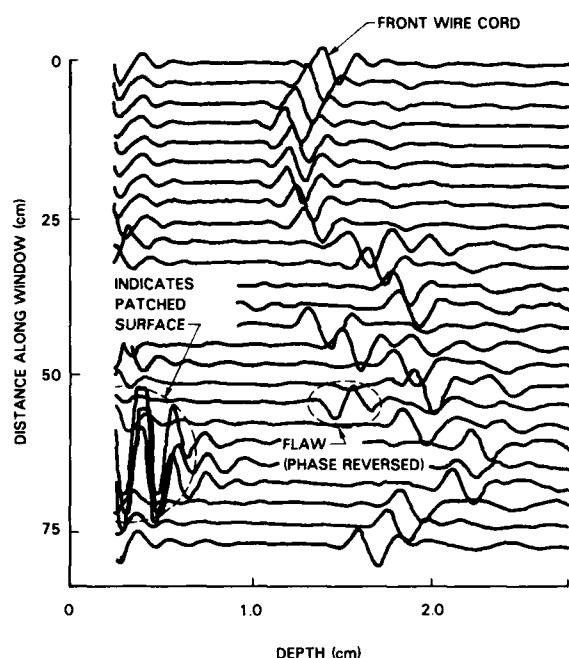


Fig. 13 — Ultrasonic echo signatures collected during inspection of a sonar dome rubber window, showing the ability of this technique to detect small flaws even in this highly complex composite

a very hard region (such as a steel wire). Subsequent dissection of this dome revealed the flaw to be a 0.05 in. delamination and serves to illustrate the sensitivity of this technique.

Other techniques now being studied for nondestructive testing include the optical techniques of holography and shearography. Additionally, new material choices and construction techniques are being evaluated by fatigue simulations at NRL.

[Sponsored by NAVSEA] ■

Acoustically Transparent Pressure Chamber

J.F. Zalesak and L.B. Poché
Underwater Sound Reference Detachment

Much of the Navy's undersea equipment is operated at various ocean depths. When equipment is changing depth in the ocean, sounds are sometimes emitted spontaneously; such sounds

from Navy equipment are undesirable. Sometimes the emission of sound is an indication of a failure of the device emitting the sound, and accurate characterization of the sounds can pinpoint the failure modes of that device. Hydrophones that are changing depth can be sources of these sounds as well as sources of electrical noise. In some cases an electrical impulse is generated, and in other cases sound is emitted and an electrical impulse is generated. This electrical impulse degrades the performance of the sonar apparatus and in extreme cases can damage components of the apparatus. To eliminate these problems in electroacoustic devices (hydrophones and transducers), it is first necessary to accurately characterize the sound from these devices.

The Test Chamber: An acoustically transparent pressure chamber allows transducers to be operated in a pressurizable environment while physically located in a shallow body of water. The pressure within the chamber is quietly cycled, and the sound from the device is recorded in the conventional manner outside the pressure chamber; therefore, a costly pressure chamber large enough to contain the entire experiment is not needed. In the past, acoustically transparent pressure chambers have been used successfully for evaluating transducers. However, when the pressure within these chambers is varied, they themselves emit sound, thus "confusing" the test of the transducer. NRL scientists have shown that a specially designed high-pressure hose used as the pressure chamber eliminates this problem. The hose itself does not emit sound while the pressure is being changed, and the sound transmitted through its walls is only slightly attenuated.

A significant development in connection with the use of the transparent pressure chamber was the fabrication of a quiet, pressure cycling apparatus. This apparatus was designed to vary the pressure within the chamber in a controlled manner while introducing minimal noise (flow noise, valve noise, pump noise, etc.) into the chamber. This apparatus has applications in other NRL calibration facilities for quietly changing the pressure in pressure chambers.

A 3-m section of a 25-cm diameter, AramidTM fiber reinforced, commercially available

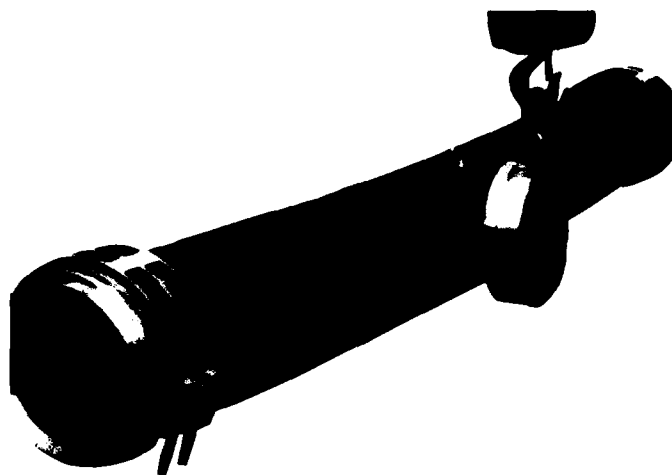


Fig. 14 — Acoustically transparent pressure chamber with stainless-steel end closures

pressure hose, shown in Fig. 14, was fitted with end closures to serve as a prototype pressure chamber. The end closures of the hose have fittings to allow water to enter for filling and pressurization and to allow for water circulation to remove air from the chamber. The end closures also have an electrical connection to allow the sound within the chamber to be monitored.

The Experiment: This hose was tested at NRL's Leesburg Facility. No sound was emitted either inside or outside of the hose when it was pressure cycled within its rated pressure range. The magnitude of the acoustic transmission loss either perpendicular to or parallel to the axis of the hose was no greater than 3 dB for frequencies up to 7 kHz and was essentially independent of the pressure within the hose. When the hose was

pressure cycled to pressures up to three times its rated pressure, sounds within the hose could be detected but none without. At these pressures the hose was permanently deformed, indicating that it had been significantly weakened. Although this off-the-shelf hose will not operate at the maximum desired pressure, a hose specifically designed would have the desired pressure capability. The hose could also be provided with a closed end instead of the metal end closures to minimize transmission loss along the axis of the hose.

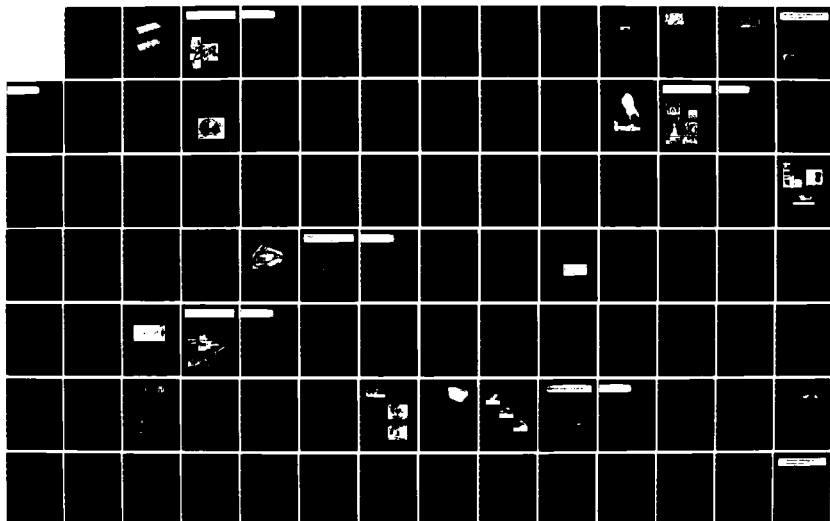
Thus NRL scientists have shown that a specially designed high-pressure hose is suitable for an acoustically transparent pressure-cycling chamber for testing Navy equipment.

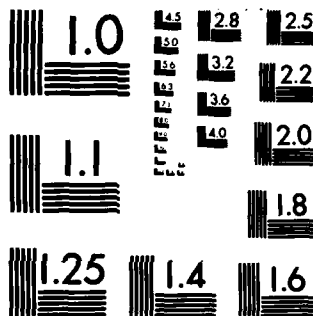
[Sponsored by NAVSEA] ■

UNCLASSIFIED

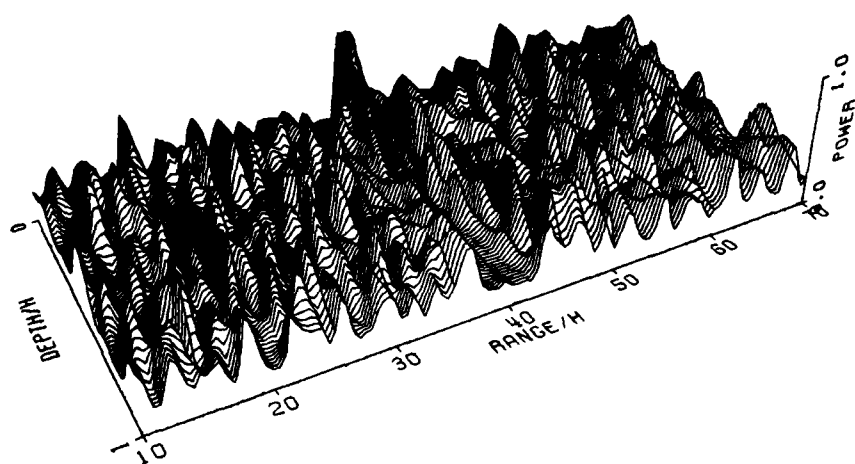
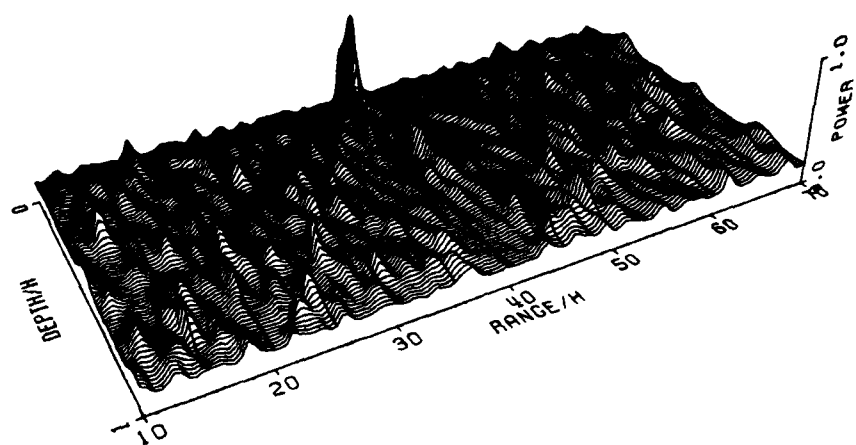
F/G 5/1

NL



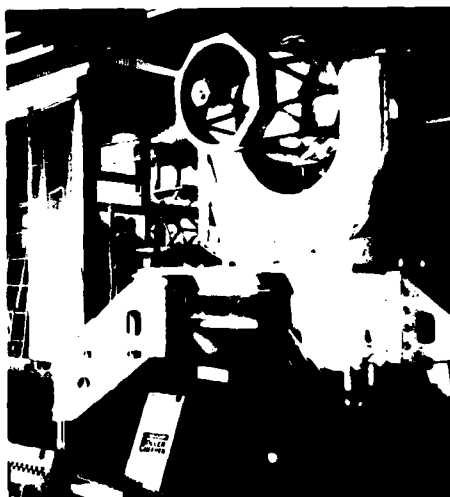


MICROCOPY RESOLUTION TEST CHART
NATIONAL BUREAU OF STANDARDS-1963-A



Ambiguity surfaces for a case where the location of an acoustic source is highly certain and one for a case of less certainty (more ambiguity). See article on p. 79.

Optical research and systems technology



95 Microwave Pumping of Excimer Lasers

Ronald W. Waynant

Longer pulse lengths and elimination of gas-metal reactions result.

96 Laser Diagnostics of Solid Propellant Flames

James W. Fleming and Andrew P. Baronavski

Researchers nonintrusively measure the temperature and composition of rocket flames.

98 Laser Generation and Probing of Multi-Kbar Compressional Shock Waves

Anthony J. Campillo, Paul E. Schoen, and Joel M. Schnur

A simpler, nondestructive technique studies shocks.

100 Optical Tracker for Atmospheric Transmission Studies

Gary L. Trusty, Thomas H. Cosden, and Paul S. Lebow

Accurate tracking is needed for shipboard measurements.

OPTICAL RESEARCH

Lasers have found widespread use in science and technology, and they are continually evolving in output power, pulse length, and applications. The first four articles give examples of this evolution. A more theoretical study of the fundamental nature of electromagnetic radiation is described in the last article.

The Divisions involved in this research are Chemistry (Code 6100), Optical Sciences (Code 6500), and Space Systems (Code 7700).

These articles present a small portion of the optics research at NRL. Some of the other areas of research are

- fiber-optic sensors and communications,
- infrared focal plane arrays and surveillance,
- optical target recognition, and
- laser development for communications, weaponry, and optical countermeasures.

Page 92, clockwise from upper left:

Dr. Danh Tran of the Optical Sciences Division drawing a rod of high-transparency fluoride glass for use in low-loss, fiber-optic waveguide fabrication

The NRL optical tracker. This land-based tracker is a prototype for at-sea applications. Its large optics coupled with an angular tracking accuracy of $12 \mu\text{rad}$ provides unique tracking capabilities. See article on p. 100 by G. Trusty.

A single hair-thin glass optical fiber (held in hand) has sufficient capacity to replace the three large heavy coaxial copper cables used in a bandwidth communications link

Microwave Pumping of Excimer Lasers

R.W. Waynant
Optical Sciences Division

Excimer molecules are attractive for lasers because this type of molecule only exists in an excited state. When an excimer molecule emits a photon either spontaneously or to amplify the laser wave, the molecule immediately dissociates into two atoms, leaving no lower laser level population to bottleneck and shut off amplification. The excimers easiest to use and the most promising for high power are the rare gas-halogen molecules (e.g., XeF, XeCl, KrF, ArF). The problem with these lasing gases is that they react corrosively with everything they touch—especially metals such as the discharge electrodes within the laser volume that contains the gases.

At NRL experiments are in progress to excite halogen gases and produce excimer molecules using radio-frequency (rf) fields rather than dc discharges between metal electrodes. Since the rf fields pass through the containing vessel and excite the gas, there is no need for electrodes; hence the gas stays cleaner and needs less halogen replacement. Other problems in using rf excitation do exist, however, and must be solved. One problem is coupling the rf energy

into the gas. Early lasers used coils or antenna-like devices which radiated rf noise in all directions. At NRL, frequencies in the microwave region (1 to 10 GHz) are used for the excitation or pumping. The rf energy is contained within a metal waveguide cavity having only small windows to extract the laser emission, greatly reducing stray rf radiation. The gas laser tube is actually contained within the microwave cavity (Fig. 1). A flat metal plate—the "stripline coupler"—lies just above the laser tube and capacitively couples the rf field in the cavity to the laser tube. The rf noise emission from this pump source is very small, and coupling to the gas approaches 80 to 90%.

Small Tubes Improve Coupling: Another problem is that rf plasmas sometimes collapse and exhibit strong excitation within a fraction of a millimeter from the walls of the tube. This collapse to the walls makes it difficult to couple the excited plasmas to normal cavity modes. To circumvent this, tubes with small cross sections can be used. This then requires careful alignment of the optical system to extract the most laser energy. Recent advances at NRL have employed a 1.6 GHz stripline coupler (Fig. 1) to excite a glass tube 0.5 mm × 5 mm × 40 cm containing a XeCl gas mixture (1% Xe: 0.1% HCl: 98.9% He). Using a cavity which allows 50% of the

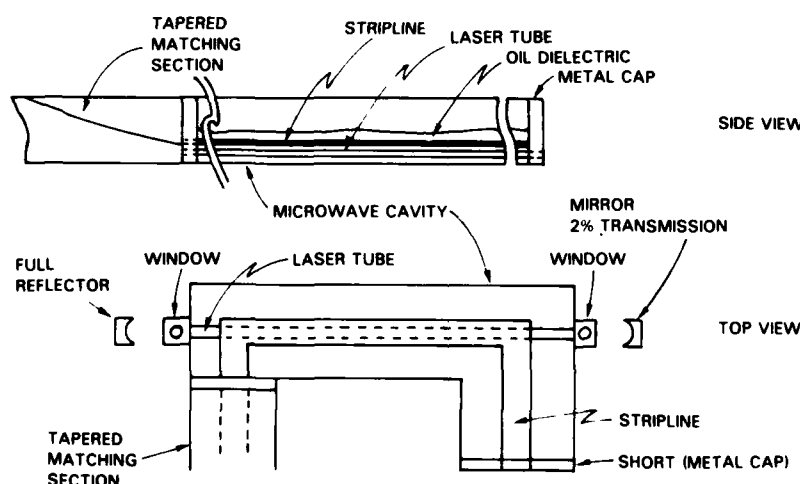


Fig. 1 — Side and top view of the partially oil-filled microwave cavity containing the laser tube and stripline coupler. The rf energy from a waveguide enters the cavity through a tapered matching section. The laser tube output is coupled to two mirrors through two windows in the cavity; the mirror on the right is partially transmitting.

laser output to be emitted, and with careful attention to cavity alignment and mirror positioning, an output of 0.2 mJ (0.2 J/l) was obtained with a 1% energy efficiency. On a per-unit-volume basis, this output shows that rf-pumped lasers are about as efficient as conventionally pumped lasers.

Record Pulsewidth: Discharge-pumped rare gas halide lasers tend to have a short laser pulsewidth, presumably due to depletion of the halogen gas. RF-pumped lasers can be optimized to avoid halogen depletion and maximize pulsewidth. Figure 2 shows the rf pulse, sidelight fluorescence (a measure of the excimer life), and laser output pulse for maximum pulsewidth. To date, rf-pumped lasers have been kept lasing for a record pulsewidth of 320 ns—much longer than any dc discharge pulse. Why the rf-pumped laser pulse is still not nearly as long as the rf pulse exciting it, is unclear; however, not all of the intricate kinetic processes involved in rare-gas halide molecule formation, nor all of the rf discharge phenomena associated with laser excitation are yet understood.

RF-pumped excimer lasers, when fully understood and developed, might be expected to offer long pulsewidth, long operational life, and

efficient operation. Such systems would have little or no rf leakage, no electrode erosion, and operate at much lower voltages than do their dc counterpart.

[Sponsored by ONR]

Laser Diagnostics of Solid Propellant Flames

J.W. Fleming and A.P. Baronavski
Chemistry Division

The combustion processes occurring when double-based (two main components) missile propellants burn at high pressure, and in particular their burning rates, are questions which have concerned researchers in the propellant field for many years. However, accurate diagnostics of flames, including identification of transient chemical species which exist in them, are difficult to perform. One technique, coherent anti-Stokes Raman spectroscopy (CARS) shows particular promise as a diagnostic technique for analyzing the chemical species and events which occur in high-pressure solid rocket propellant combustion. CARS has already been successfully applied to a variety of atmospheric and lower pressure studies. We have adapted the CARS technique for use with a high-pressure combustion chamber to study double-base propellant combustion at pressures up to 100 atm (1500 psi). This is a collaborative effort with the Naval Surface Weapons Center, Indian Head, Maryland, which is responsible for construction and operation of the high-pressure combustion chamber.

CARS: CARS is a laser Raman technique, and, like conventional or nonlaser Raman spectroscopy, it provides information concerning the rotational and vibrational energy levels of chemical entities present in a system, thus providing a means to identify these entities. Fortunately, the intense signals and coherent directional properties associated with CARS reduce the severity of interferences from fluorescence and particle emissions which limit the effectiveness of conventional Raman spectroscopy. "Gating" the CARS signal detector (1- μ gate) eliminates most of the continuous portion of the flame emission. An

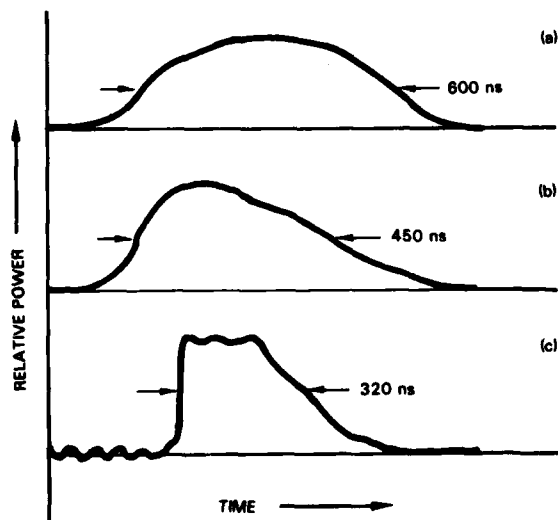


Fig. 2 — Waveforms of (a) rf pumping power (70 to 80 kW peak), (b) sidelight fluorescence, and (c) extended laser pulsewidth.

arrangement of three crossed beams provides good spatial resolution and eliminates certain problems associated with the flame boundaries. Since the propellant and laser beams are stationary during a burn of propellant, each successive laser shot probes a position progressively more distant from the burning propellant surface as it erodes. Two of the laser beams have narrow bandwidths and the same frequency, but the third has a lower frequency and a wide bandwidth. The frequency (i.e., energy) difference in the laser beams is chosen to correspond to the vibrational energy level separation in the molecules to be probed. Because one of the laser beams is broadband, we can probe several rotational-vibrational energy levels during each laser shot.

CARS Apparatus: The experimental arrangement is shown in Fig. 3. The frequency-doubled output of a Nd:YAG laser and a broadband dye laser are configured to give two sets of three parent beams. A CARS signal is generated when a set of the three beams is crossed and focused at a common point. One beam set generates a reference signal outside the combustion chamber (Ref. B); the other set generates one signal inside the chamber and a second signal

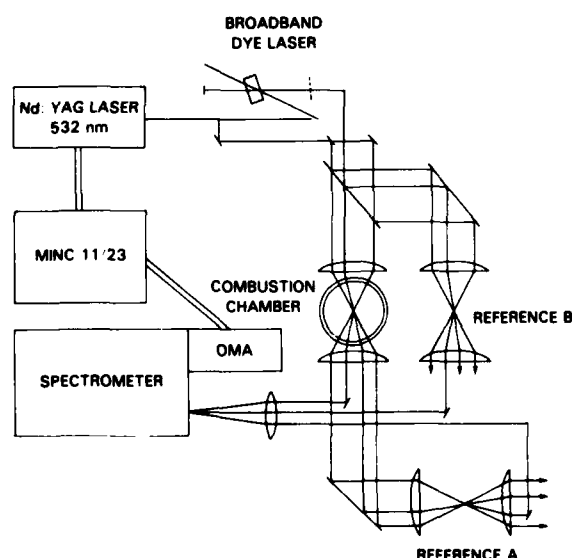


Fig. 3 — Configuration for generating coherent anti-Stokes Raman spectroscopy (CARS) signals in high-pressure solid propellant flames. References A and B produce CARS signals in the air.

after the beam has passed through the chamber (Ref. A). All three CARS signals are made parallel and focused ahead of the front slit of a spectrometer. This separates the signals generated by Refs. A and B and the test chamber from each other. An optical multichannel analyzer (OMA) records the signal intensities and permits acquisition of an entire spectral waveform in a signal scan. Our initial CARS measurements were made on nitrogen produced from the propellant burn. Since N_2 is the major component in air, reference signals were conveniently generated outside the chamber. Figure 4 shows the OMA output from both reference signals and the signal generated from a mixture of 0.5 atm of N_2 and 29.5 atm of helium inside the chamber.

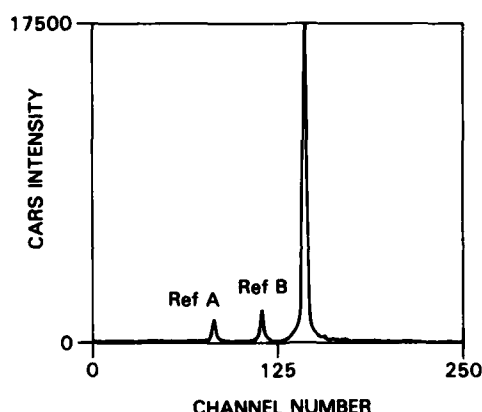


Fig. 4 — Plot of the CARS signal intensity generated by Refs. A and B as well as the signal from a mixture of 0.5 atm of N_2 in helium at a total chamber pressure of 30 atm as a function of channel number on the optical multichannel analyzer. All three signals are at the same frequency but have been displaced from each other; thus, channel number does not convert directly to frequency in this figure.

Sample Data: Reference signal A provides critical information about the quality of the flame probe site, because the parent beams generating Ref. A are the same beams that generate the flame signal. Soot particles, turbulence, or laser-induced breakdown inside the chamber are indicated by the degradation of the signal from Ref. A. Reference B serves as a good monitor for laser intensity fluctuations and provides a means of estimating concentrations of the species being

examined. Figure 5 displays the OMA output for a sample burning at 30 atm total pressure enclosed in a flowing helium shroud. References A and B, and the background signal from the flame gases are shown. These gases generate a CARS signal which follows the gain profile of the broadband dye laser. Superimposed on this structure are the signals from individual N_2 molecules produced from the burning propellant. A reference dye profile is used to obtain quantitative information, i.e., flame temperature and species concentration.

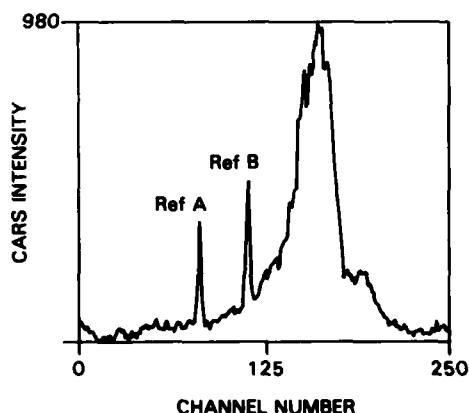


Fig. 5 — Display of the optical multichannel analyzer output indicating the CARS intensity vs channel number of Refs. A and B in air, and the CARS signal in the flame of a burning solid propellant at 30 atm total pressure. Note that the signals have been displaced from each other as in Fig. 2.

This study shows that CARS is a good nonintrusive technique for diagnosing the combustion of propellants at high pressures. The use of reference signals for monitoring laser intensities and flame probe sites are fundamental in the interpretation of data. Future work will center on the generation of appropriate references for quantitative temperature and concentration measurements for N_2 as well as other flame species. Such measurements will give valuable insight into the nature of the combustion reactions taking place and yield information concerning the action of catalysts and additives on the propellants.

Laser Generation and Probing of Multi-Kbar Compressional Shock Waves

A.J. Campillo, P.E. Schoen, and J.M. Schnur
Optical Sciences Division

Many research problems of interest to the Navy hinge upon a deeper understanding of the interaction of shock waves with molecules in the liquid or solid phase. One example is the detonation of explosives where it has been suggested that there are chemical reaction pathways unique to shock initiation (as opposed to thermal initiation) that affect the intrinsic sensitivity of energetic materials (rocket propellants and explosives) to impact. Unfortunately, conventional shock wave experiments are inherently single shot in nature as well as destructive to apparatus. Low repetition rates and lack of suitable molecular probes have made systematic investigations difficult and time-resolved chemical diagnostics almost impossible. To bypass the single shot limitations of conventional shock generation schemes such as the gas gun or explosive detonation, NRL scientists have been studying the properties of laser-driven compressional shocks to assess the feasibility of simultaneously probing the state of shock-loaded matter by using a second laser beam. Driving shocks with a laser is favored because it requires relatively modest table-top setups and affords higher experimental repetition rates, permitting rapid material surveys. The experimental progress described below encourages us to believe that this approach will indeed be productive.

Shock Generation and Characterization:

Figure 6 illustrates in schematic form how lasers may be utilized to both drive and measure the magnitude of the shock. Multi-kbar (1 bar = 1 atm) shocks are produced in thin (20 to 200 μm) confined foils of copper by heating with a 10 ps duration 1.054 μm laser pulse (1 to 10 J/cm²), thereby generating plasmas in the region between the front surface of the foil and an overlaying glass window. As the trapped plasma/metal vapor attempts to expand, an intense compressional wave is launched into and through the foil, which then penetrates into the glass "witness plate" (see

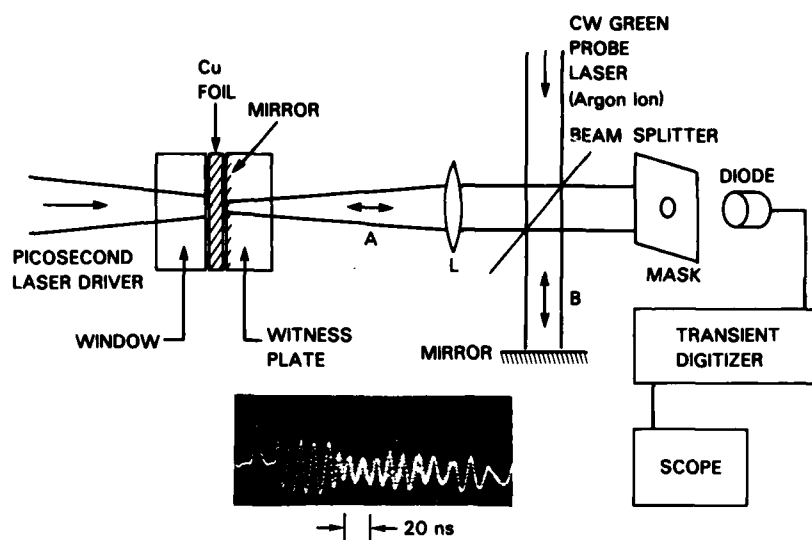


Fig. 6 — Schematic of laser interferometer measurement of particle velocity histories of laser-driven shocks. Insert shows interferogram of 20 kbar shock.

Fig. 6). The mirrored side of the witness plate forms one mirror of a Michelson interferometer, illuminated by a single frequency argon ion laser. The interferometer compares the optical path length A to B. Any changes in A show up as movement of interference fringes at the photodiode detector. As the shock moves from the foil into the witness plate, the mirror surface begins to move. The interferometer fringes produced at the diode generate an oscillatory signal (see insert of Fig. 6) with a frequency proportional to the mirror velocity. From this particle motion history, the shock pressures are estimated by using the known equation of state of the metal. Depending on laser energy, rear surface motions in the range 10^{-2} to 10^{-1} $\mu\text{m}/\text{ns}$ ($1 \mu\text{m}/\text{ns} = 1 \text{ km/s}$) are measured, corresponding to pressures of 2 to 20 kbar. Both the magnitude and temporal characteristics of measured pressure profiles are consistent with a simple model we have developed to describe the shock generation process. In this model, the hot plasma/metal vapor is approximated by an ideal gas.

Condensed Phase Shock Chemistry: The initial phase of the laser shock program emphasized shock generation and characterization. We recently began to use this technique to understand condensed phase shock chemistry.

We hope to answer the following questions: (1) What are the initial chemical reactions produced by the shock wave in various organic materials? (2) Are shock-induced reactions different from those occurring during pure heating at the same pressure? (3) Immediately after shock front passage, what is the degree of intramolecular vibrational excitation (i.e., effective temperature), and is it in equilibrium? (Are the energy states of the material in a normal distribution for thermal equilibrium—i.e., is the material thermalized?) In this phase of the program two laser facilities are used; a 10 J, long-duration pulse (20 to 150 ns) system (see Fig. 7), and a low energy ($\sim 30 \text{ mJ}$) ultrafast (10 ps) system. The long-pulse laser can drive shocks to 300 kbar and is currently employed to consider the first two questions which concern chemical species. Ultraviolet transmission spectroscopy and spontaneous Raman scattering are used as probes in shocked liquid benzene. The ultrafast system is used to answer question 3 by addressing the physics of energy transfer from macroscopic shock to intramolecular modes. Picosecond-resolving probes are necessary because the energy transfer takes place on this time scale.

We have conducted an experiment in which coumarin dye is used as a molecular thermometer to measure the effective shock temperature. The



Fig. 7 — Dr. Richard Griffin, an NRL/NRC research associate, working with the long-pulse laser shock facility

shock-induced intermolecular vibrational changes are monitored with a green laser probe pulse that is time delayed from the shock generation pulse. The green pulse induces fluorescence in the shock-heated dye. The green probe pulse photons are energetically able to excite only molecules that are in an excited vibrational state. The percentage of these excited molecules increases with the temperature of the probed region, and the corresponding fluorescence also increases. Typically 20 kbar shocks raise the temperature 100°C, which increases the fluorescence by a factor of two. At present, 1 μm thick samples limit our time resolution to about 1 ns and our ability to observe early nonthermal effects, but we are able to estimate the thermalized temperature. Future experiments will involve the use of samples only a few molecular layers ($\sim 1 \mu\text{m}$) thick, for which the early time information should be observable.

This line of experiments should lead to a better fundamental understanding of the sensitivity of energetic materials to shock.

[Sponsored by ONR]

Optical Tracker for Atmospheric Transmission Studies

G.L. Trusty, T.H. Cosden, and P.S. Lebow
Optical Sciences Division

In the past, NRL scientists performed several outdoor, long-path, overwater optical transmittance measurements with a 36-in. (91.4-cm) beam-launching telescope and a 48-in.

(121.9-cm) collecting mirror. Both optical systems were in large tractor-trailers that were fixed on land at each end of the overwater path. Subsequently, measurements were needed over the open sea between ship-mounted platforms. To maintain the necessary pointing accuracy for the experiments, servo systems had to replace the stability previously provided by dry land and the large mass of the equipment. The need for large-scale optics remained. The result of responding to this rather challenging combination of requirements is an optical system that will not only perform well for this special project but may be a valuable tool for other types of atmospheric studies.

Land-Based Tracker: Figure 8 shows the tracker with its associated trailer. The tracker base is a Nike/Hercules radar mount that we modified for optical use. In the overwater experiment the tracker can operate in two modes. For absolute transmittance measurements at a single wavelength, the tracker operates as a transmitter that sends a laser beam to a receiver at the other end of the path. In the second mode, the tracker is used for broadband relative transmittance measurements. Now the tracker operates as the receiver of blackbody radiation that originates at the other end of the path.

The optical design in Fig. 9 incorporates a Coude-configured Cassegrainian telescope into a unique optical system that allows incoming radiation to pass unimpeded down through the yoke of the mount to an optical port inside the trailer. Conversely, radiation can be sent out through this port when in the transmitting mode. The mount size allows the use of an 80-cm primary mirror, and the optical design results in an 8-mrad field of view.

Inside the trailer is an optical bench which, although housed in the trailer, is mounted to the tracker base to avoid optical misalignment from movements in the trailer. One side of the bench is configured for laser source devices, and the other side is designated for receivers. Currently, for use in the receiving mode, the bench holds a high-resolution Fourier transform spectrometer. Additional imagers or radiometers could also look out through the optical port. For use in the

Fig. 8 — Land-based tracker and its instrument trailer. The tracker is a modified Nike/Hercules radar mount.

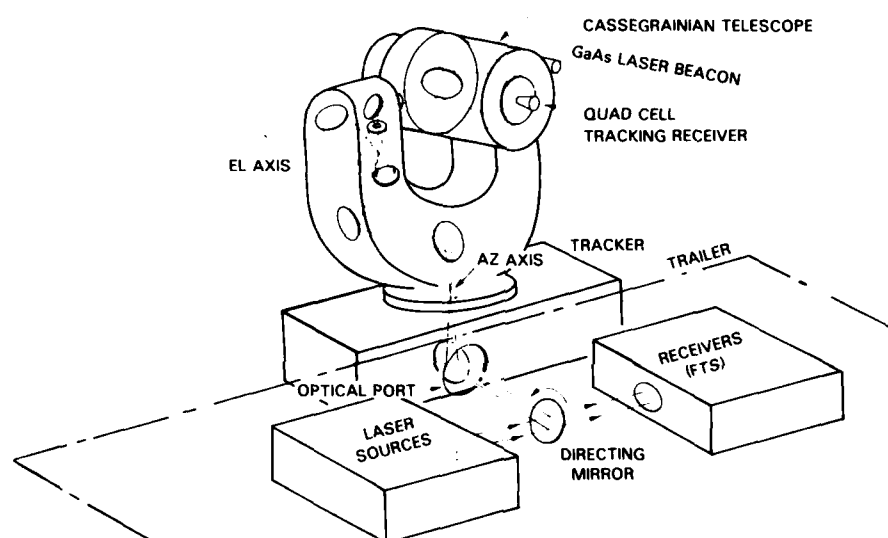


Fig. 9 — The tracker, showing the optical system that transmits incoming radiation through the optical port into the trailer

transmitting mode, helium-neon and deuterium-fluoride lasers now occupy the output side of the bench. Other laser sources could readily replace, or be added to, this set.

Adaptations for Automatic Tracking: For the at-sea experiment, the receiver for the laser transmittance measurement is a modified "60-in. searchlight" (152 cm diam) of World War II vintage. To keep the 80-cm beam from the tracker on the 60-in. searchlight mirror over a 5-km path requires a tracking accuracy of $75 \mu\text{rad}$. By use of a standard silicon quadcell detector, the modified servo system (designed and built by Massachusetts Manufacturing Corporation) has been able to achieve a $12\text{-}\mu\text{rad}$ tracking accuracy

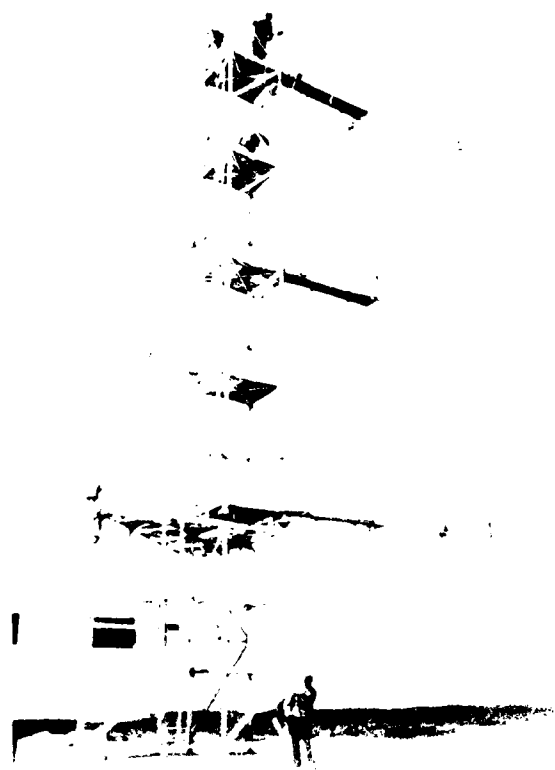
while locked on to a GaAs laser beacon, which is more than adequate.

The tracking system is also manually controllable through joystick, track ball, or digital switches. Optical correlation tracking electronics will be used in the future to automatically track moving objects without a beacon. To track jet or rocket plumes for infrared signature measurements, the silicon quadcell can be replaced with one appropriate for the plume-radiation spectrum.

Thus, although specifically designed for a particular experiment this optical tracker will not only satisfy the needs of that experiment, but will also be invaluable for various other transmission studies.

[Sponsored by NAVSEA]

*Atmospheric and ionospheric research
and military applications*



105 Laser-Plasma HANE Simulation Experiment

Barrett H. Ripin

Collisionless interactions and strong nonuniformities may develop in a high-altitude nuclear explosion.

107 Intensification of Tropical Disturbances

Simon W. Chang and Rangarao V. Madala

Numerical simulations identify factors favoring tropical disturbance growth.

110 Marine Particle Size Distributions

William A. Hoppel, James W. Fitzgerald, and Reginald E. Larson

Submicron particles which affect C³I systems are measured.

ATMOSPHERE AND IONOSPHERE

Atmospheric behavior is critical to many naval systems from the effects of weather on Fleet operations and sensors to the effects of the ionosphere on C³I. NRL has active research programs which study these aspects of atmospheric behavior, and the articles in this section describe some of these efforts.

The Space Science Division (Code 4100) and Plasma Physics Division (Code 4700) are performing the research reported in this section. Some of the other research efforts at NRL concentrating on the atmosphere and ionosphere include

- atmospheric electricity,
- aircraft icing,
- relativistic electron beam propagation in the atmosphere, and
- high-energy blasts in the atmosphere.

Page 102, clockwise from upper left:

Free energy surface for formation of sulfuric acid droplet in atmospheric environment of 95% RH and 10^{-6} ppm sulfuric acid used to calculate formation of sulfate aerosol in the atmosphere. See article on p. 110 by W. Hoppel.

Research tower on San Nicolas Island, California, used to probe the atmosphere in a marine environment. Sensors measure turbulence, wind, temperature, humidity, aerosols, and optical properties at three levels. The data are used to deduce electro-optical properties of the atmosphere.

Energetic laser-produced plasma expanding into a low-density gas emulated the effects of a nuclear detonation in the ionosphere. This dualtime shadowgraph shows several features of this phenomenon, such as high-velocity shocks (blast waves), turbulent plasma (*top section*), and peculiar jets called aneurisms (*lower right*). The laser beam from below strikes a thin target, held by a stalk. See article on p. 105 by B. Ripin.

Laser-Plasma HANE Simulation Experiment

B.H. Ripin
Plasma Physics Division

Within the Department of Defense, there is concern over the possible disruption of communication and detection systems as well as electromagnetic pulse (EMP) effects following a high-altitude nuclear explosion (HANE). A laser-plasma interaction experiment has recently been initiated at NRL to simulate HANEs and to examine the physics involved in the interaction between the weapon debris and the surrounding ionosphere [1,2]. The mechanisms that are responsible for the interaction depend on the altitude that is being simulated in the experiment. The experimental results also have applicability to inertial fusion reactors, to natural ionospheric disturbances, to some astrophysical problems such as supernovae, and to the basic physics of high Mach-number magnetic shocks and plasma-beam instabilities.

Experiment and Diagnostics: The basic experimental arrangement used in this study is sketched in Fig. 1. An intense, focused pulse from the NRL Pharos II Neodymium glass laser strikes a target, typically aluminum, and creates a target-debris plasma with an energy density comparable to nuclear-burst debris. A background gas surrounds the target; the pressure of this gas is varied to simulate various ionospheric altitudes. The laser-produced plasma streams through the low-density ambient plasma that is formed as the background gas is photoionized by radiation from the laser-target interaction. A magnetic field B_0

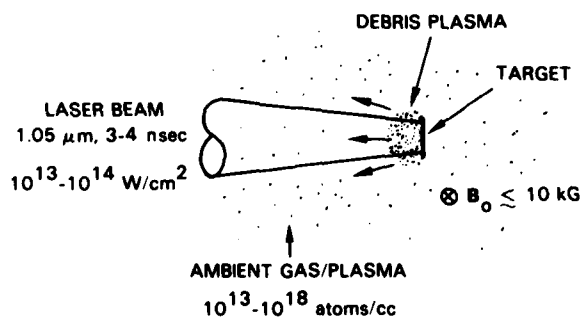


Fig. 1 — Laser-plasma HANE simulation experimental configuration

is often applied across the region to simulate the ionospheric magnetic field.

Many diagnostics are employed in these experiments to gain a good understanding of the phenomena and to compare with predictions of hydrodynamic and plasma computer models. For example, temperatures and densities are determined through spectrally resolved measurements of electromagnetic radiation from the visible into the soft X-ray region. Magnetic probes monitor the formation of self-generated magnetic fields and magnetic bubbles in the coupling region; probes are also used to measure local electric fields and microwave emission. Optical techniques such as shadowgraphy, laser scattering, photography, and interferometry are employed to make two-dimensional images of the coupling regions and to make measurements of the plasma density and structure. Ion detectors directly measure the debris properties.

Some Results: Although the laser-produced plasma initially streams rapidly (up to 1000 km/s) away from the target, it eventually stops as its energy is transferred to the ambient plasma through collisions or plasma effects. Several questions arise concerning the process; these have been answered in part by the experiments.

When the ambient plasma is tenuous and collisions are weak, are there collective plasma effects, such as beam-plasma instabilities, that can still stop the debris ions? What are the responsible mechanisms?

Indications of a "collisionless" interaction between the debris ions and low-density ambient plasmas (lower background gas pressures) were seen in the experiment in the presence of a magnetic field. This corresponds to high-altitude (above 400 km) bursts where collisions are not sufficient to stop the debris. Debris-ion velocity distributions were broadened and reduced in speed after passing through the ambient plasma; in some cases a group of very fast ions was observed. These features are similar to those of the magnetized ion-ion, beam-plasma instability—a collisionless coupling mechanism that is

predicted to be operative in this regime. The coupling mechanism has a large impact on the nature of the disturbance in the ionosphere subsequent to a detonation. Communications over areas of thousands of square kilometers can be affected.

What happens after good coupling occurs between the energetic plasma and the ambient plasma? The plasma conditions in such a system, especially at the high Mach numbers encountered in this regime, are not well established.

A high-density front is formed at the interface between the debris and ambient plasmas after good coupling occurs between them. An example of this coupling front is seen in Fig. 2. This dark-field shadowgram shows that a very thin, rapidly decelerating shock-front, or blast-wave (bright ring), has formed around the target. This high-density shell has strong electric and magnetic fields associated with it and can be an intense source of infrared emission that can interfere with detection systems.

What structure or turbulence occurs in this disturbed debris-ambient plasma? How is it generated and how does it evolve with time? What are the practical consequences in the full-scale system?

Plasma structure does develop on the blast wave both in front of the target (left-hand side of Fig. 2) and behind the target (right-hand side of Fig. 2). The aneurism-like feature on the left and the very turbulent phenomena on the rear are not yet well understood. Hence, current experimental and theoretical work is concentrating on these features. It is vital to know the sources and power spectrum of these fluctuations as a function of time because this plasma turbulence can disrupt propagation of microwaves for communications and detection systems.

Altitude Effects: The nature of the interaction between the laser-produced plasma and the background gas is found to be sensitive to the gas pressure. A collisionless beam-plasma instability appears to play a role in the interaction with low-density gas (simulating high altitudes). At higher

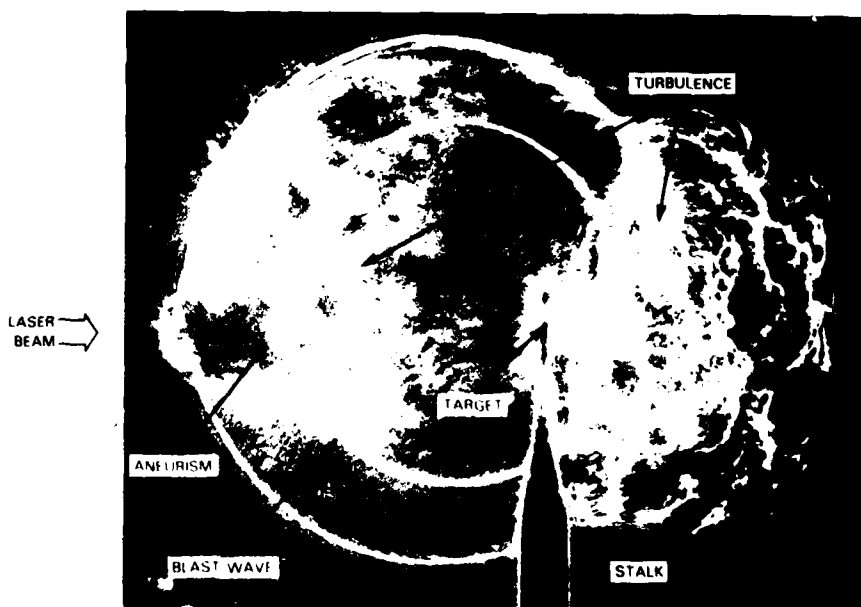


Fig. 2 — Dual-time dark-field shadowgrams of the blast wave and associated structure in the coupling region of a high-pressure shot (5 Torr nitrogen). The small laser-irradiated aluminum target sits atop a thin stalk. Bright regions indicate large density gradients. One can note the blast wave, aneurism, and turbulence formed 55 and 155 ns after the laser pulse. (This photograph was taken by Dr. J.A. Stamper.)

ambient gas pressure (simulating lower altitudes), well-formed blast waves are observed, confirming many of the theoretical predictions of such strong shocks. However, striking and unexpected nonuniformities form on these shock fronts. Moreover, the dense target material itself has been seen to develop nonuniformities due to Rayleigh-Taylor instability.

Future: The experimental facility is presently being upgraded to enable us to better address the higher altitude regimes and to follow the interactions to later time. This upgrade consists of increasing the laser energy to over 1 kJ, constructing a larger target chamber and magnetic field coil, and improving diagnostic facilities.

[Supported by the Defense Nuclear Agency]

References

1. B.H. Ripin, J. Grun, S. Kacenjar, E.A. McLean, and J.A. Stamper, NRL Memorandum Report 5268 (1984).
2. B.H. Ripin, J.A. Stamper, and E.A. McLean, NRL Memorandum Report 5279 (1984). ■

Intensification of Tropical Disturbances

S.W. Chang and R.V. Madala
Space Science Division

Introduction: Early warnings of cyclones over tropical oceans, which cover about one-half of the earth's surface, are of extreme concern to the Navy. Tropical cyclones carry with them severe weather that often compromises Navy operations, hinders weapon system performance, and causes loss of life and material. A three-dimensional, finite-difference numerical model has been successfully used to simulate and study the intensifications of weak tropical disturbances into weather-producing tropical depressions. The intensity of the tropical storm that develops depends on the surrounding large-scale wind pattern as well as on the characteristics of the initial disturbance. As a result of this study, we have extended the capability to forecast incipient tropi-

cal cyclones from the present capability of 2 days to 3 to 4 days.

Numerical models have been successful in simulating the growth of moderate vortices into mature tropical cyclones with wind speeds of 30 m/s. These early simulations almost uniformly began with initial perturbations of considerable strength and size, comparable to tropical depressions with maximum wind speeds near 10 m/s. The development of the initial disturbances in these simulations normally takes place isolated from the influence of large-scale environments. In 1983, we have succeeded in simulating the early transformation of weak disturbances with maximum wind speeds near 1 m/s into tropical disturbances and ultimately into tropical cyclones. Moreover, the effect of the surrounding large-scale wind pattern has now been included, and the initial disturbances are embedded in tropical trade winds (easterlies) with horizontal and vertical wind shear. (A horizontal shear has different wind velocities at different locations; a vertical shear has different wind velocities at different altitudes.)

The Numerical Model: We solve an initial value problem by using the three-dimensional hydrodynamic equations. These equations conserve mass, momentum, and energy and retain only the horizontal wind components with temperature and pressure as dependent variables. We assume that the pressure is hydrostatic, which eliminates the need for solving the vertical equation of motion. The model does account for effects of the major physical processes that regulate the tropical circulations; these include the condensation heating from cumulus clouds and the air-sea exchanges of momentum, heat, and water vapor. It is believed that the growth of tropical disturbances is caused by an instability which arises when friction between the air and the ocean generates convergent air flow near the air-sea interface. The convergent flow increases condensation, which in turn creates more convergence. The proper representation of these surface friction and condensation processes in the model is crucial to an accurate calculation of the growth of any initial disturbance. Because the equations are nonlinear, the system is solved in a computer by a finite-difference method. A more

detailed description of the model can be found in Ref. 1.

Results: In studying the intensification of tropical disturbances, we perform three types of calculations. Observations have shown that the tropical easterlies contain various horizontal and vertical wind shears. Therefore, the first two types of calculations address the effects of these two large-scale wind shears. For these simulations, the initial disturbances are the same and are characterized by a weak counterclockwise (cyclonic) circulation with maximum wind speed near 1 m/s. The third type of calculation has a fixed wind shear and addresses the effect of the character of the initial disturbance. Horizontal wind shears can be cyclonic (stronger easterly winds at higher latitudes) or anticyclonic (stronger easterly winds at lower altitudes). The horizontal wind shear $-\bar{u}_y$ is positive with cyclonic shear and negative with anticyclonic shear.

First, we study the effect of various horizontal wind shears. Figure 3 shows the temporal evolutions in terms of the central pressure of the

disturbances in different horizontal wind shears. It is evident that the wind shear has a significant influence on the behavior of the weak initial disturbance. The disturbance intensifies most when it is embedded in an easterly flow with cyclonic shear at lower altitudes and anticyclonic shear at higher altitudes. In this case (the lowest curve), the central pressure drops from 1011 mbar to 996 mbar in 24 h. In contrast, anticyclonic shear throughout the atmosphere effectively prevents any development of the initial disturbance (uppermost curve). The three curves in the middle show that the initial disturbance tends to intensify more as the large-scale horizontal wind shear becomes progressively more cyclonic.

Next, we study the effect of vertical shear \bar{u}_z . If $\bar{u}_z > 0$ the shear is westerly (the easterlies decrease with altitude) and if $\bar{u}_z < 0$ the shear is easterly (the easterlies increase with altitude). Figure 4 shows the central pressure of the initial disturbances under various large-scale vertical wind shears. The disturbance seems to intensify most when the vertical shear is easterly (10 m/s between pressure levels of 200 and 900 mbar—

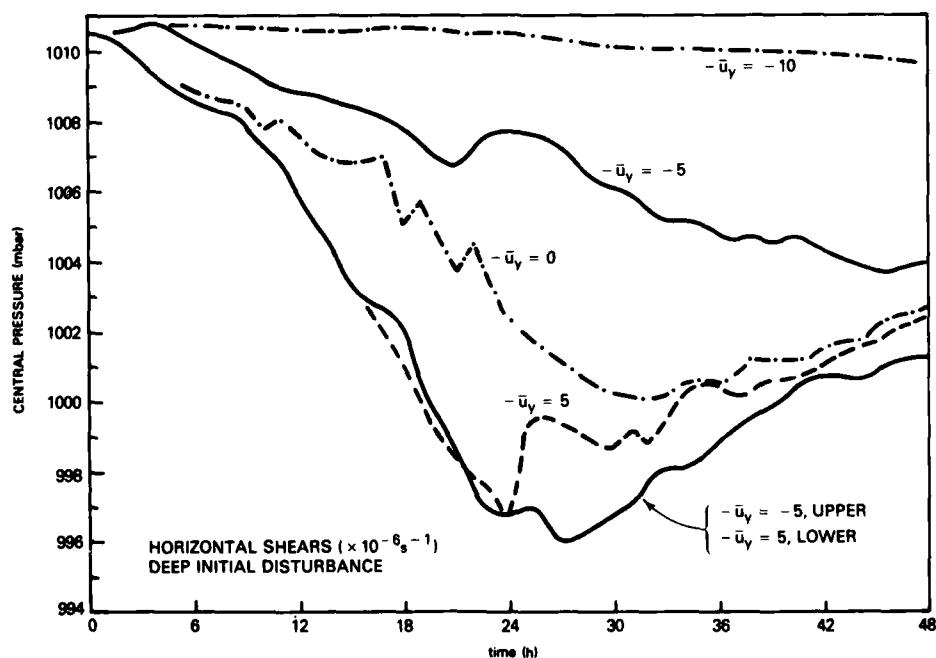


Fig. 3 — The temporal variation of intensities of tropical disturbances in terms of pressures in mbar at centers of the disturbances under various large-scale horizontal wind shears $-\bar{u}_y$. Positive values denote cyclonic shears, and negative values denote anticyclonic shears.

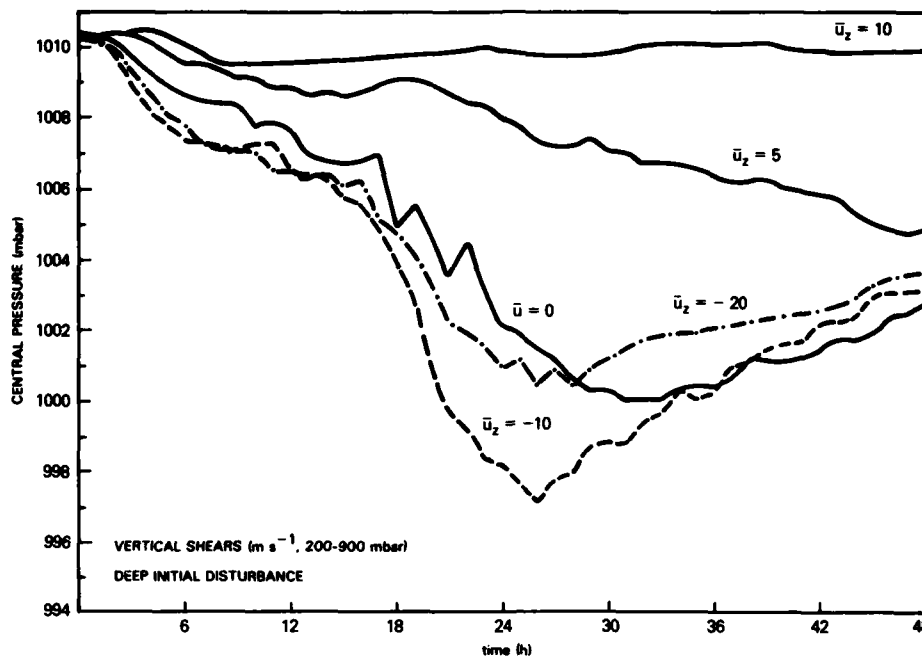


Fig. 4 — The temporal variation of intensities of tropical disturbances in terms of pressures in mbar at centers of the disturbances under various large-scale vertical wind shears \bar{u}_z . Positive values denote westerly shears, and negative values denote easterly shears.

approximately corresponding to altitudes between 12,000 and 1000 m). However, the development of the disturbance is hampered when the easterly shear is too strong (20 m/s between 200 and 900 mbar). There is also less intensification with westerly vertical shear than with no shear.

We also tested the dependence of the growth on the depth and size of the initial disturbance. A deep disturbance has cyclonic winds from 200 mbar (approximately corresponding to an altitude of 12,000 m) to the surface, while a shallow one is confined below 700 mbar (or 3000 m). Large and small disturbances have radii of 440 km and 220 km, respectively. In both cases, the maximum wind speeds are initially near 1 m/s. As shown by Fig. 5, large and deep initial disturbances have more rapid developments than small and shallow ones. This is because the large disturbances contain more angular momentum for spinning up. Also, deep disturbances have well-defined convergences at lower altitudes and divergences at higher altitudes; this increases the condensation in tall cumulus clouds.

In the above experiments, all of the disturbances, except for those under very unfavorable wind shear conditions, seem to approach some constant strength after 2 days. This is because the ocean surface temperature (28°C) is held constant and a mean tropical static stability is used initially in each numerical experiment. If the ocean surface temperatures were allowed to rise, or if a lower initial static stability were used, the initial disturbances might develop further. In fact, meteorological conditions *are* transient in the real atmosphere; therefore, the calculation accurately represents only the initial development of the disturbance into a depression. The further growth of tropical depressions into larger storms depends on several characteristics of the tropical depression, such as central pressure and wind speed. These characteristics are shown here to depend on the shears that are seen by the initial disturbance; thus, the initial development of the disturbance is a decisive factor for growth at times greater than 48 h (past the depression stage). Our numerical experiments show that the

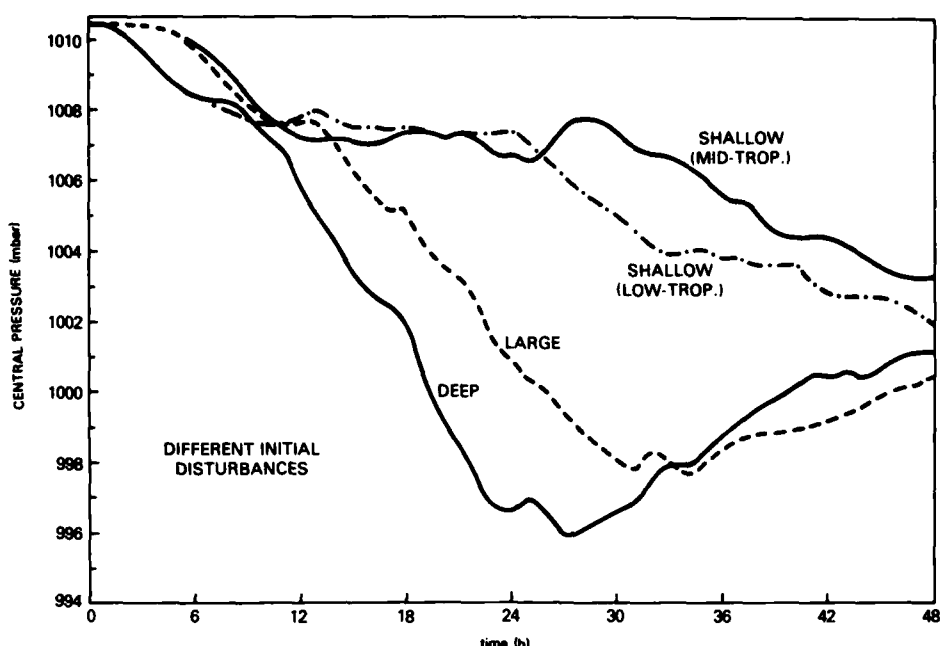


Fig. 5 — The temporal variation of intensities of tropical disturbances in terms of central pressures in mbar developed from initial perturbations of different sizes and vertical extent. The large-scale shears are $-\bar{u}_y = 5$ for the lower troposphere, $-\bar{u}_y = -5$ for the upper troposphere, and $\bar{u}_z = 0$.

most favorable large-scale conditions for growth are moderate easterly vertical shears and cyclonic horizontal shears in the lower troposphere. Deep and large initial disturbances are the most likely to develop under these conditions.

[Sponsored by ONR]

Reference

1. S.W. Chang, "A Numerical Study of the Interactions Between Two Tropical Cyclones," *Monthly Weather Review*, **111**(9), 1806-1817 (1983). ■

Marine Particle Size Distributions

W.A. Hoppel, J.W. Fitzgerald, and R.E. Larson
Space Science Division

Particles suspended in the atmosphere are important in the study of extinction of electromagnetic waves, the transfer of solar radiation through the atmosphere and its effect on climate,

acid-rain chemistry, and cloud formation. Of particular importance to the Navy is the role that aerosol particles play in extinction of electromagnetic signals that are used in communications and intelligence gathering. For Navy systems that operate at near infrared and visible wavelengths, the attenuation of the signals is mainly due to particles with radii less than one micron. New instruments have been developed at NRL to make accurate measurements of these very small particles even at low concentrations. Using this apparatus, particle size distributions have been measured over the ocean at various distances from the eastern coast of the U.S. and in the remote Atlantic [1]. More accurate calculations of signal extinction at various operating wavelengths are made possible by these measurements. This has improved the Navy's capability to predict system effectiveness in the marine environment.

Background: In the past, measurements of the size distribution were made with optical particle counters and impactors and were confined to

particles larger than about $0.3 \mu\text{m}$. Very little data were available on particles smaller than about $0.3 \mu\text{m}$, the most important size range for extinction at visible wavelengths, and little was known about the source and sinks of these small particles. NRL has developed the differential mobility size spectrometer and a continuous flow, single-particle counting cloud chamber. Working together, these two instruments have made it possible to make accurate measurements of very small particles even at low concentrations.

Measurements: With the NRL-developed instrumentation, data were taken in 1980 from the USNS *Hayes* in air masses advecting off the east coast of the U.S. A rapid decrease in the number of small particles (smaller than $0.04 \mu\text{m}$) was observed on the time scale of 12 h. An example of this decay is shown in Fig. 6 where curve 1 is the size distribution taken in the Chesapeake Bay and curves 2, 3 and 4 are average size distributions taken at about 25, 75, and

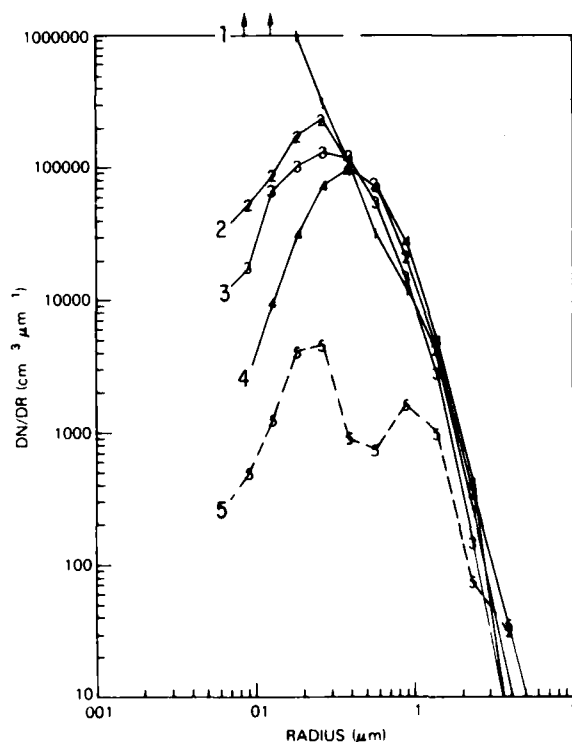


Fig. 6 — Curves 1 to 4 illustrate the change in the size distribution in the Chesapeake Bay and in an air mass advecting off the east coast of the U.S. at 25, 75, and 130 nmi. Curve 5 is the size distribution measured in the remote Atlantic.

130 nmi off the coast. Analysis of the trajectory of the air mass indicates that the air for curves 2, 3, and 4 had spent about 2, 5, and 10 h over the water before arriving at the ship. The decrease in the number of small particles is due primarily to coagulation of these particles with larger particles. In contrast, the size distribution in the region between 0.08 and $0.5 \mu\text{m}$ radius shows little change since coagulation and gravitational fallout of particles in this size range is negligible. Particles in this size range are removed primarily by precipitation which did not occur during the period of these observations. This stable region of the particle size distribution (between 0.08 and $0.5 \mu\text{m}$) is called the accumulation zone.

During a cruise of the USNS *Lynch* in 1983, particle size distributions were measured over areas of the tropical Atlantic which were remote from continental influences. These size distributions exhibited greatly reduced numbers of particles in the small radius portion of the accumulation zone. A distribution typical of the remote Atlantic is shown by the dotted curve in Fig. 6. The depletion of particles in the accumulation zone is believed to be a result of the removal of particles by cloud droplets and precipitation. A more precise characterization of the physical mechanisms responsible for shaping the marine particle size distribution, and their relative importance in relation to the meteorological history of the air, is the subject of continuing study. Together with proposed computer modeling, these new measurements should result in a much better understanding of the role of the various physical mechanisms.

Extinction Coefficients: The data are currently being used to evaluate and predict the extinction effects of aerosol particles on backscatter signals from lidar and on various other Navy systems. The upper curve of Fig. 7 shows the total extinction due to all particle sizes as a function of wavelength; this is calculated for a typical size distribution measured off the east coast of the U.S. (using curve 4 of Fig. 6). Also shown are the contributions to the total extinction that are made by particles in various size ranges. Particles in the 0.1 to $0.3 \mu\text{m}$ size range contribute most to the extinction at visible wavelengths, whereas the larger particles are

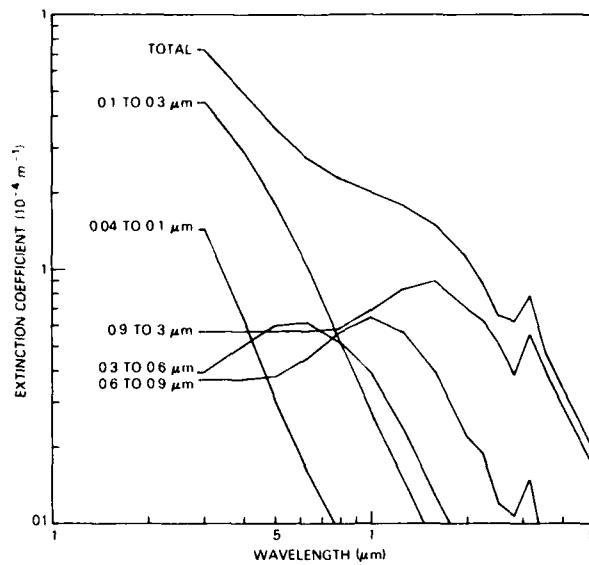


Fig. 7 — Upper curve gives the total extinction coefficient calculated from the size distribution given by curve 4 of Fig. 6. Remaining curves give the contributions to the total extinction coefficient due to particles in the indicated size ranges.

primarily responsible for extinction in the infrared. The extinction as a function of wavelength is strongly dependent on the size distribution; Fig. 7 would be radically different if the extinction computed for curve 5 of Fig. 6 had been plotted instead of that computed for curve 4.

[Sponsored by ONR and NAVAIR]

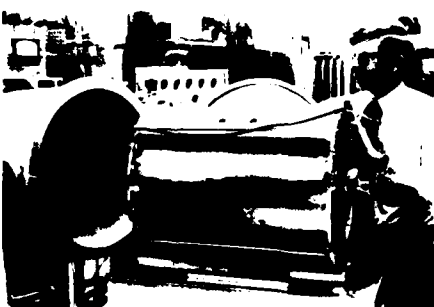
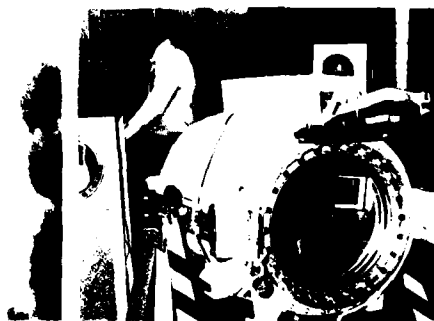
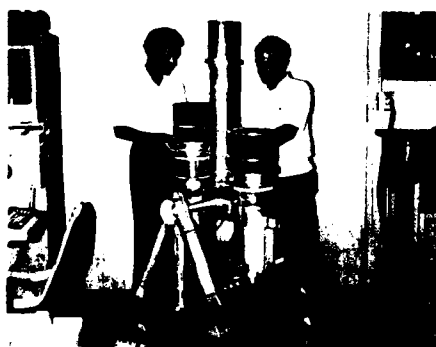
Reference

1. W.A. Hoppel, J.W. Fitzgerald, and R.E. Larson, "Measurement of Atmospheric Aerosols: Experimental Methods and Results of Measurements off the East Coast of the United States," NRL Report 8703, 1983. ■



Various instrument packages can be suspended from a captive balloon which is used to probe the lower 1000 feet of the atmosphere from a research ship

Aerospace science and technology



117 Spectra of Cosmic Gamma-Ray Bursts

Gerald H. Share and Pat L. Nolan

High- and low-energy bursts observed by the Solar Maximum Mission satellite differ fundamentally.

119 Semianalytic Satellite Theory

Bernard N. Kaufman and William H. Harr

An orbit calculation algorithm is sixfold more efficient.

122 Propellant Slosh Investigations in Spinning Spacecraft

Michael F. Zedd

Measurements map fluid modes that can destabilize spacecraft.

124 Radiation Effects on Microelectronic Components in the Upper Atmosphere

Chen H. Tsao and Rein Silberberg

The upper atmosphere partially shields devices from malfunction-causing cosmic radiation.

127 Charge Collection in Multilayer Structures

Alvin R. Knudson, Arthur B. Campbell, and Eligius A. Wolicki

Measurements using energetic ions may improve the models of these complex structures.

129 Clock Technology

James A. Murray

More accurate clocks improve the NAVSTAR Global Positioning System precision.

131 Effects of a Free Surface on the Wake of a Flat Plate

Thomas F. Swean, Jr.

The wake decays slower than in an infinite fluid.

133 Low-Reynolds-Number Airfoil Testing

Richard J. Foch

Sub- and transonic measurements aid in high-performance design.

AEROSPACE SCIENCE

NRL has been a pioneer in X-ray astronomy and the space program and continues to contribute to the national space program in several different capacities. This major area of research is highly multidisciplinary, with six separate divisions contributing to the eight articles in this section. These articles deal with measurements of space radiation (with the Solar Maximum Mission satellite) and its effects on solid-state devices, satellite motion and stability, clock technology, and fluid dynamics applied to airfoils and moving plates.

The six NRL divisions contributing to this section are Space Science (Code 4100), Tactical Electronic Warfare (Code 5700), Marine Technology (Code 5800), Condensed Matter and Radiation Sciences (Code 6600), Space Systems (Code 7700), and Aerospace Systems (Code 7900).

Some of the other projects at NRL in aerospace science and technology include

- Combined Release and Radiation Effects Satellite (CRRES) Microelectronics Experiment,
- Navy Remote Ocean Sensing Satellite (NROSS),
- Oriented Scintillation Spectrometer Experiment (OSSE) on NASA's Gamma-Ray Observatory (GRO),
- High Resolution Telescope and Spectrograph (HRTS) on Spacelab II,
- SPARTAN I & II—small space experiments to be thrown overboard from the shuttle for 40 hours and then retrieved,
- Atmospheric and Ionospheric Remote Sensing (AIRS) Program,
- large structure control theory,
- advanced tethered Vehicle Control System, and
- Synthetic Aperture Radar (SAR) image processing and analysis.

Many of NRL's space research projects are involved with experiments on the shuttle.

Page 114, clockwise from upper left:

The NRL Solar Ultraviolet Spectral Irradiance Monitor (SUSIM), to fly repeatedly aboard the shuttle (next flight 1985), is designed to measure the varying ultraviolet emissions from the sun for a precise assessment of the sun's influence on the earth's ionosphere and atmosphere.

George Carruthers and Darrell King with the far ultraviolet cameras for Air Force P6-75 to be flown on the shuttle

The Space Ultraviolet Radiation Environment (SURE) experiment, in its Get Away Special (GAS) canister, flies attached to the outside of the shuttle bay. SURE observes extreme and far ultraviolet spectroscopic emissions from constituents in the earth's ionosphere.

The imaging ultraviolet camera that will be launched from the shuttle aboard the SPARTAN III free-flying satellite. The SPARTAN will be picked up from space by the shuttle for return to earth.

The High Resolution Telescope and Spectrograph (HRTS) will observe the solar atmosphere from shuttle with maximum spatial and ultraviolet spectral resolution to discover the fundamental physics of the sun's behavior

Spectra of Cosmic Gamma-Ray Bursts

G.H. Share and P.L. Nolan

Space Science Division

Puzzling bursts of high-energy electromagnetic radiation were detected in the 1960's by gamma-ray instruments on the Vela satellites that were designed to monitor nuclear explosions from space. Vela's directional measurements demonstrated that the bursts were neither of terrestrial nor of solar origin. Although several hundred bursts have subsequently been observed, their origin is still largely a mystery. NRL scientists have previously studied these bursts using a variety of instruments flown from balloons and aboard satellites such as NASA's Orbiting Solar Observatory and High Energy Astronomy Observatory, NRL's SOLRAD satellites, and the Air Force's STP satellites. However, our most detailed information has recently come from measurements made with NASA's Solar Maximum Mission (SMM) satellite. Spectral measurements with SMM provide new information concerning the mechanism which produces the bursts. Understanding the nature of the bursts will further our knowledge of astronomical phenomena. It will also aid in the design of improved systems for detecting artificial sources of radiation in space and may aid in the development of terrestrial sources of energy.

Observations: SMM was launched in February 1980 with a complement of instruments designed primarily to study solar flares. The gamma-ray spectrometer experiment on SMM is a collaborative effort by NRL, the University of New Hampshire (the lead institution) and the Max Planck Institute for Physics and Astrophysics in Munich. In its four years of operation, over 70 cosmic gamma-ray bursts and more than 100 solar flares have been detected [1]. The instrument's large field of view and broad spectral coverage (10 keV to 100 MeV) make it a unique tool for studying cosmic gamma-ray bursts.

These cosmic bursts exhibit a range of temporal variations. They are identified in the satellite data by a computer algorithm which searches for significant fluctuations in the intensity of the background gamma radiation. Visual inspection

of microfilm summaries of the data enable the cosmic bursts to be distinguished from solar flares, geomagnetic events, or telemetry errors. Figure 1 illustrates time histories of three bursts that were detected by SMM at an energy near 300 KeV with a time resolution of 1 s. Cosmic bursts are known to last from tenths of seconds to hundreds of seconds, and to have temporal structures on time scales as short as a few milliseconds. A few bursts even exhibit periodic variations. The variety and complexity of temporal histories is difficult to explain by any simple model for the origin of the bursts.

Sources of Bursts: The most plausible sources for the gamma-ray bursts are highly compact objects known as neutron stars. These are the remains of stars, with masses somewhat larger than that of the sun, which have undergone a catastrophic explosion known as a supernova. In the process, the radius of the star shrinks to about 10 km, at which point its stability is determined by the repulsion of densely packed nucleons. Some of these neutron stars are predicted to have magnetic fields with strengths of 10^{12} G (for comparison, the earth's field is about 0.5 G). The observed gamma-ray bursts can be produced when matter falling onto the surface of the neutron star triggers a thermonuclear explosion, but the details of the emission mechanism are not well understood.

Until the launch of SMM it was widely assumed that the radiation from the bursts came from very hot electrons (10^9 °K or 100 keV) produced in the thermonuclear explosion. These electrons radiate gamma rays by a process known as thermal bremsstrahlung when they collide with some other material. However, measurements from the SMM spectrometer indicate that the observed spectra extend to too high an energy to be explained solely by thermal bremsstrahlung. The spectra of more than 60% of the bursts were observed by SMM to extend to energies in excess of 1 MeV and 15% of the bursts even exhibited emission above 10 MeV. Spectral measurements are shown in Fig. 2 for the three bursts plotted in Fig. 1. With isotropic radiation mechanisms, such as thermal bremsstrahlung, significant emission above 1 MeV would not be expected for sources that are more distant from Earth than a

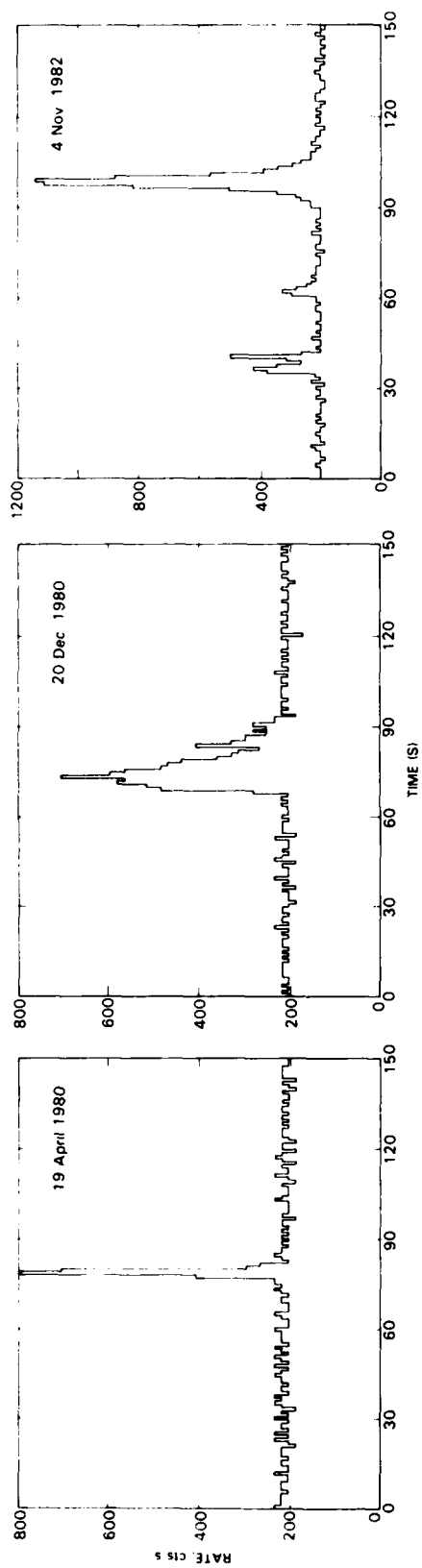


Fig. 1 — Time histories of three cosmic bursts measured near 300 keV by SMM

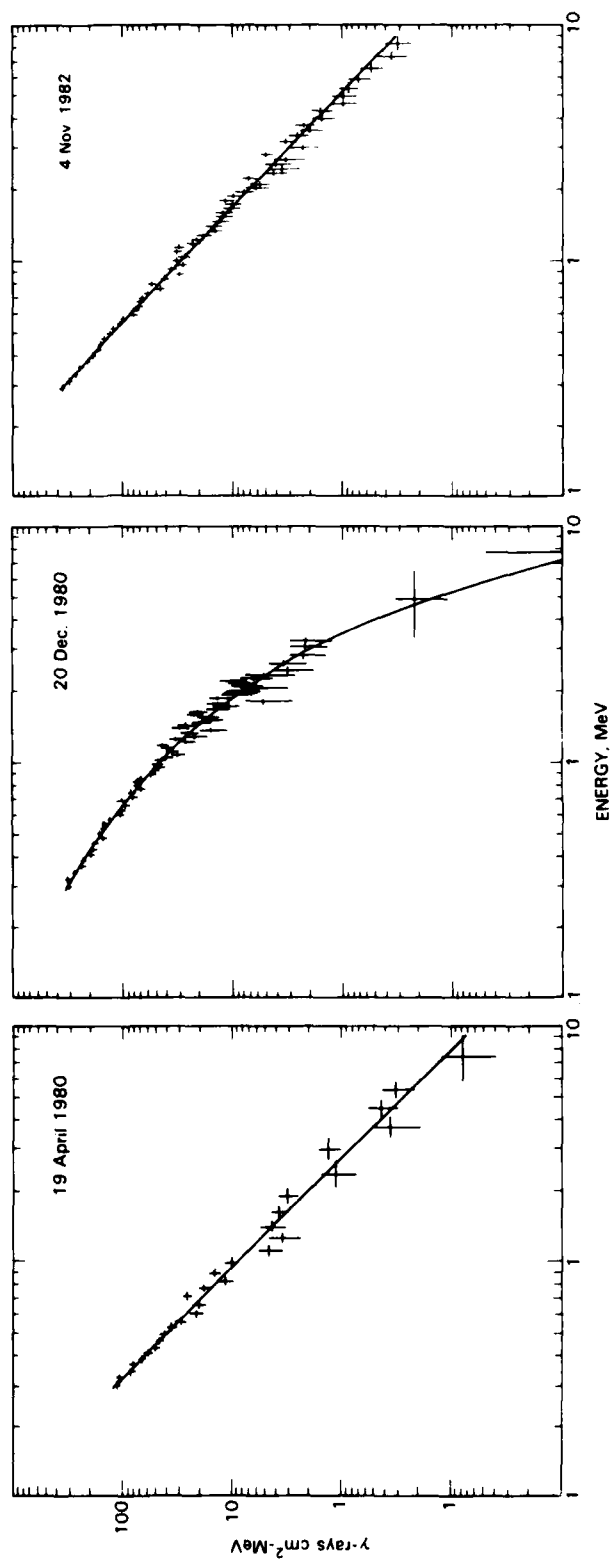


Fig. 2 — Integrated photon spectra for the three bursts. The curves show the best fits to the data.

few hundred light years. Therefore, the SMM observations indicate either that the sources are relatively close to Earth or that the gamma-ray emission is directional rather than isotropic. One way in which directional radiation can be produced is by beams of high-energy electrons.

Comparison with Soviet Data: The SMM measurements do not confirm spectral features reported by the Soviets using data from their Venera spacecraft. Spectra in about 5% of the bursts detected by Venera appear to contain broadened lines in the vicinity of 500 keV. The Soviets believe these features are due to gamma rays produced when positrons and electrons annihilate near the surface of a neutron star. The SMM spectrometer detected one of the bursts for which such a feature was reported. Our measurement does not show this emission feature, and we therefore question the significance of similar features reported by the Soviets in other bursts.

Future Work: Spectral data obtained thus far from SMM have set constraints on the mechanisms that can be responsible for the production of the gamma-ray bursts. However, more observations are required if we are to identify the origin of the bursts. The SMM satellite was recently repaired in orbit by astronauts on the Shuttle. The satellite is now functioning normally and is expected to return data for at least 2 to 3 years. This will allow SMM to make detailed observations of gamma-ray bursts until the launch of NASA's more sensitive Gamma-Ray Observatory in 1988.

[Supported by NASA]

Reference

1. G.H. Share, 1981 *NRL Review*, p. 106. ■

Semianalytic Satellite Theory

B.N. Kaufman and W.H. Harr
Aerospace Systems Division

Numerical integration methods traditionally used for orbit determination and prediction are very accurate but require the calculation of many points on the trajectory. Most of these points are

of no interest; however, they are necessary for the numerical integration. As a result, extensive amounts of computer time are needed. Within the last decade, machine automated algebra has facilitated the use of semianalytic methods in this area. By using these methods, substantial computer savings are realized; however, to develop the equations of motion, complex algebraic manipulation is required.

Theory: At NRL, research is in progress on a semianalytic method to obtain accurate estimates of satellite position and velocity at specific times of interest without calculating unwanted positions and velocities. This is accomplished by using analytical methods to average out short-period effects (those with periods on the order of the satellite's orbital period). These "averaged" equations of motion can then be numerically integrated by using very large time steps. The resulting averaged ephemeris is very useful for predicting long-term behavior. The averaged equations of motion include accurate representations of perturbations caused by the sun and the moon, and of specific contributions caused by the nonspherical shape of the earth. The accurate position and velocity is obtained by analytically applying the short-period perturbative contributions only when desired.

Recovery of the short-period contributions caused by the sun, the moon, and a portion of the earth's nonsphericity is obtained by developing the appropriate equations using low-order expansions. This is possible because short-period perturbations have small amplitude compared to those of long-period effects. The short-period terms are separated from the equations by perturbation techniques, and analytically integrated to obtain a short-period "generating function." Short-period contributions to the coordinates are computed analytically from partial derivatives of the generating function only at the times of interest, and they are added to the averaged coordinates yielding the accurate position and velocity. (Reference 1 contains a technical description of the mechanics involved.)

Implementation of the Method: Development of the equations of motion for both the 119

averaged and the short-period contributions consisted of manipulating thousands of terms in the form of Poisson series [2]. These can be represented as a sum of terms consisting of products of numeric ratios (α/β), algebraic factors ($x^l y^m$), and trigonometric factors (Eq. 1).

$$\sum \frac{\alpha}{\beta} (x^l y^m \dots) \frac{\sin}{\cos} (j \Pi p + k \Psi + \dots) \quad (1)$$

For numerical evaluation, however, this form can be very inefficient. In most Poisson series, many of the factors contain elements which are repeated in various terms (that is, they are not unique). The duplication increases storage space and computation time. However, the terms can be grouped in various ways, and common elements can be factored out. A judi-

cious choice of algorithms to group the terms can drastically reduce the computational effort needed.

Figure 3 schematically shows the various factoring algorithms that are used for optimization. The terms of the original series, symbolically shown as $a_i b_i c_i$, can be represented in step one as products of either numeric-algebraic terms d_i with trigonometric terms c_i or as products of numeric-trigonometric terms d'_i with algebraic terms b_i . In either case, the resulting series is a sum of products of two factors. If each factor d_i or d'_i is not unique, we can use the distributive law to remove common factors from the d_i or the d'_i in step 1, thus producing the unique factors c_i or b_i in step two. Alternatively, we can apply the same procedure to the b_i and c_i factors of step 1 to obtain the unique factors d_i and d'_i of step 2.

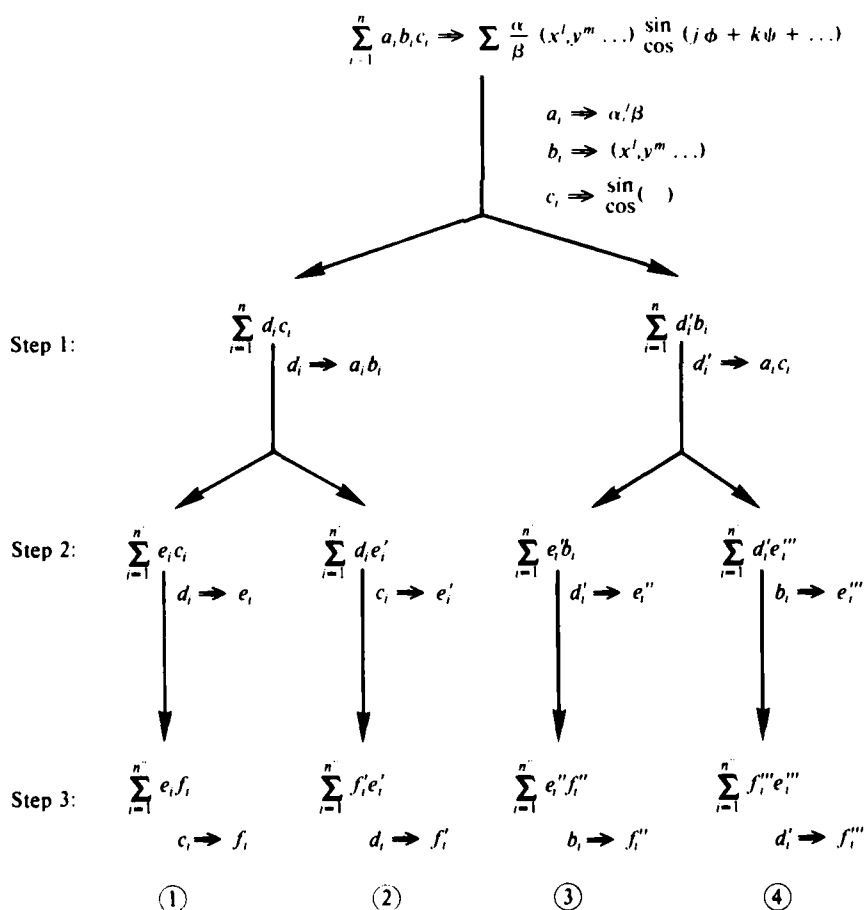


Fig. 3 — Technique of series compression showing four possible routes

The series is now composed of sums of pairs consisting of the two factors, one of which is unique. The other factors e_i , e_i' , e_i'' , e_i''' are not necessarily unique, so by using the distribution law again we can combine nonunique terms producing the corresponding series in step 3.

The series are now composed of terms of two factors, each unique in the series. It is very important to note that there are four possible routes to do the sum that results in the forms of step 3 as shown Fig. 3. Which route to use depends upon the particular series being optimized, and it cannot be determined a priori. The method also depends upon the goal of the optimization. Normally, the order of compression would be chosen to minimize the computation time (not necessarily minimizing the series length). Further optimization is obtained by using trigonometric identities to eliminate sine and cosine calls.

Comparison with Numerical Integration:

For this theory, the original short-period series for the sun and moon contained 24,481 terms, requiring 24,481 additions, 48,962 multiplications, and 6,050 sine and cosine calls. After optimization using the above procedure, the series consisted of only 1,742 unique terms, requiring 10,946 additions, 4,364 multiplications, and 4,520 sine and cosine calls. Substituting trigonometric identities reduced the sine and cosine calls to only 12, but increased the number of multiplications and additions. The final form of the series can be evaluated over 8-times faster than the initial form and requires much less computer memory.

Figure 4 shows an example of the accuracy that can be obtained with this semianalytic theory. This test case used an accurate numerical orbit predictor to produce a time history of the orbit. Points from this history are used as "truth" data, representing the real world, and they are fit in a least squares sense with an orbit determination program that uses this semianalytic theory. To produce a meaningful comparison, the truth model included only those forces (sun, moon, and portions of earth's nonsphericity) modeled in the semianalytic theory. The position residuals (truth minus semianalytic) shown in Fig. 4 are due to the approximations made in the development of this theory.

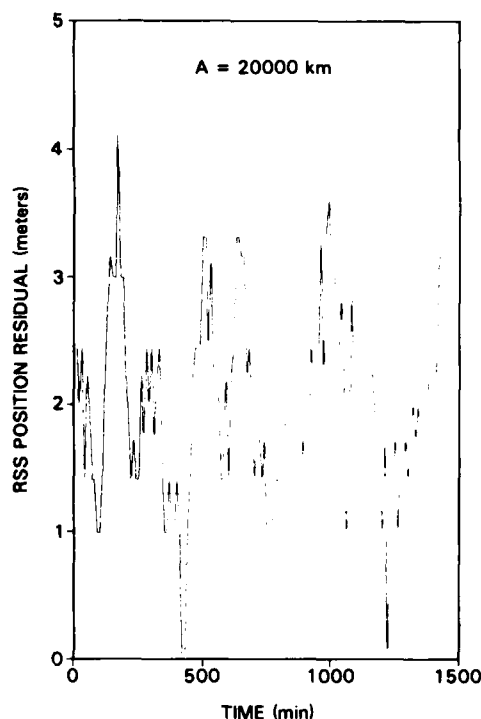


Fig. 4 — The RSS (root-sum-square) position residuals (truth minus semianalytic) for a satellite in a nearly circular 20,000 km orbit

Discussion: The theory is developed in coordinates that contain no singularities for circular or equatorial orbits, and it is applicable from medium to high orbits. Future work will concentrate on the inclusion of other perturbative forces such as drag to make this technique applicable to lower orbits.

For practical use, the theory would be tailored to the specific type of orbit desired. The program would then contain only the terms necessary, further minimizing computational requirements and allowing on-board processing for autonomous navigation. A detailed discussion of this work may be found in Ref. 1.

[Sponsored by ONR]

References

1. B. Kaufman and W.H. Harr, "Implementation of a Semianalytic Satellite Theory With Recovery of Short Period Terms," *ACTA Astronautical*, (publication pending, 1984).
2. R.R. Dasenbrock, "A FORTRAN-Based Program for Computerized Algebraic Manipulation," NRL Report 8611, 1982.

Propellant Slosh Investigations in Spinning Spacecraft

M.F. Zedd
Space Systems Division

Background: Successful spacecraft designs require that the user be able to maintain long-term control of vehicle orientation. A simple and cost-effective method of attitude control is spin stabilization. Normally, power consumption or external control is not needed for this method. During spin stabilization, the entire spacecraft rotates so that its angular momentum vector remains approximately fixed in inertial space—the same principle which governs a gyroscope.

If the spacecraft is spin stabilized about its axis of minimum moment of inertia (MOI), then it is called a prolate spinner. The axis of minimum MOI in a cylindrically shaped spacecraft is located through the ends of the spacecraft. This configuration requires energy to maintain this prolate spin state. The sloshing liquid propellant in a prolate spinner results in energy dissipation that causes a coning motion (the spin vector describes a cone in time). This coning motion (nutation), if not controlled, eventually results in a flat spin. A flat spin, or spin about the axis of maximum MOI (an oblate spinner), is the minimum spin energy state. In a cylindrical spacecraft, the axis of maximum MOI is transverse to the axis of the cylinder. This description of motion is analogous to that of a toy top as it wobbles from the maximum to the minimum spin energy state.

A free spacecraft in orbit must conserve angular momentum; the result is that

$$\text{nutation rate} = (N - 1) \times \text{spin rate}, \quad (1)$$

where N is (MOI about spin axis)/(MOI about transverse axis). For a particular spin rate, only one nutation rate is possible, since N is fixed for a rigid, cylindrical spacecraft. However, to accomplish our investigations, we wanted to simulate different values of N ; we did this by varying the nutation rate independently of the spin rate by forcing different nutation rates with a special turntable. The necessity to vary N arose because liquid propellant consumption, within

spacecraft, causes N to change during the mission, and differently shaped spacecraft have different values of N . For a combination of spin and nutation rates, N can be regarded as a dependent variable in a forced motion experiment.

Recognizing the usefulness of a prolate spinning configuration for future shuttle-launched spacecraft, we at NRL have conducted an extensive investigation of the effects of sloshing liquids on spacecraft dynamics. The most significant contribution to both the Navy and the larger space community will be the demonstration of long-term controllability of a prolate spinner that has a large liquid mass fraction.

Test Objectives: At NRL we performed tests to determine the energy dissipation rates in a nutating smooth-walled spherical propellant tank by using model tanks mounted on a forced-motion table. While performing these tests, we also identified liquid resonant frequencies, measured liquid forces and moments, and, in general, we identified and quantified other liquid phenomena that might adversely affect prolate spacecraft under the control of spin stabilization. In addition, we found it necessary to determine the location of resonant frequencies to eliminate possible interaction with vehicle control frequencies. The test results were used to derive equivalent mechanical models that were in turn used to (1) scale test results to full-size tanks and (2) compensate for the presence of the gravitational field.

Forced-Motion Spin Facility: Figure 5 shows model propellant tanks mounted on a forced-motion table. The table rotates the tanks about a fixed point in a manner which simulates spin and nutation motions of spacecraft. Referring to Fig. 5, the basic spin motion is about the z-axis driven by the spin turntable. The nutation is produced by tilting the table with the linear actuator to the desired nutation angle and then rotating the inner (nutation) table at the nutation rate. For a particular spacecraft configuration, values of N were established by separate control of the spin and nutation drive motors (Eq. (1)). In this experiment, we independently varied spin rate, nutation rate, nutation angle, fill fraction, and liquid viscosity. We measured, with strain

DESIGN PARAMETERS

- 1 SPIN RATE 0 - 107 RPM
- 2 NUTATION RATE 10 - 100 RPM
- 3 NUTATION ANGLE 0 - 3°

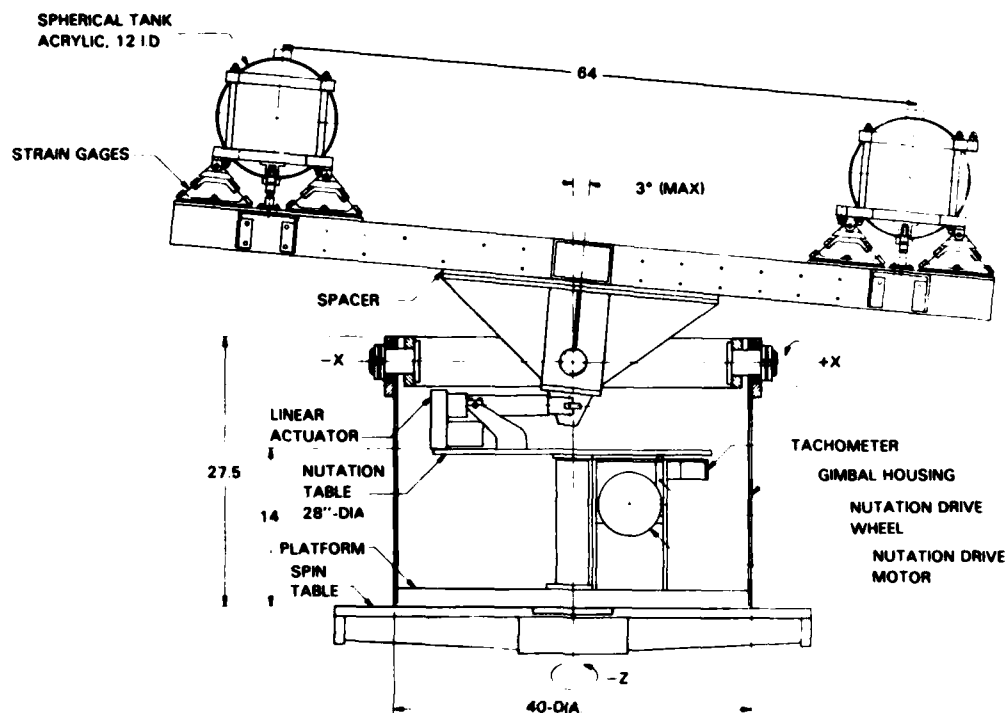


Fig. 5 — Forced-motion, spin-facility. Gimbal housing rotates at constant speed in vertical direction. Nutation table rotates the linear actuator in opposite direction. The linear actuator holds the lower cone off center to form nutation angle.

gauge instrumentation, forces and moments produced on the tank by the liquid motions.

Results: Figure 6 shows operating regions of the forced-motion table, and it identifies where prolate (between $N = 0$ and $N = 1$) and oblate (between $N = 1$ and $N = 2$) spinners lie. Operating conditions outside the "V" correspond to unrealizable inertia ratios for unforced bodies; that is, no free, rigid, physical objects exist with inertia ratios less than 0 or greater than 2. The horizontal lines on the left show the eight different constant rotation speeds of the spin table. For each of these speeds, the nutation table rate increased from 10 to 100 rpm in the opposite direction to the fixed spin table rotation. These rotations simulated prolate spinning spacecraft. Resonance conditions were evident when the measured forces and moments first increased; then they decreased as the nutation rate

increased. Results show that slosh wave resonances in the tanks are readily excited by nutation frequencies that can be predicted by fluid dynamics theories. These frequencies were found to be the same as those for the nonspinning, shaking tanks. The resonances occur at nutation rates that correspond to unrealizable values of realistic spacecraft inertia ratios—this shows that spacecraft in orbit, with spherical tanks, would not be subject to these oscillations under spin stabilization.

An equivalent mechanical model of the liquid motion, with parameters chosen to duplicate the observed forces and moments, is used to interpret the test data in terms of energy dissipation rates. The results clarify the effects of liquid motion on the stability of spinning spacecraft by providing, for the first time, a "map" of the liquid resonant frequencies and modes over a wide range of parameters.

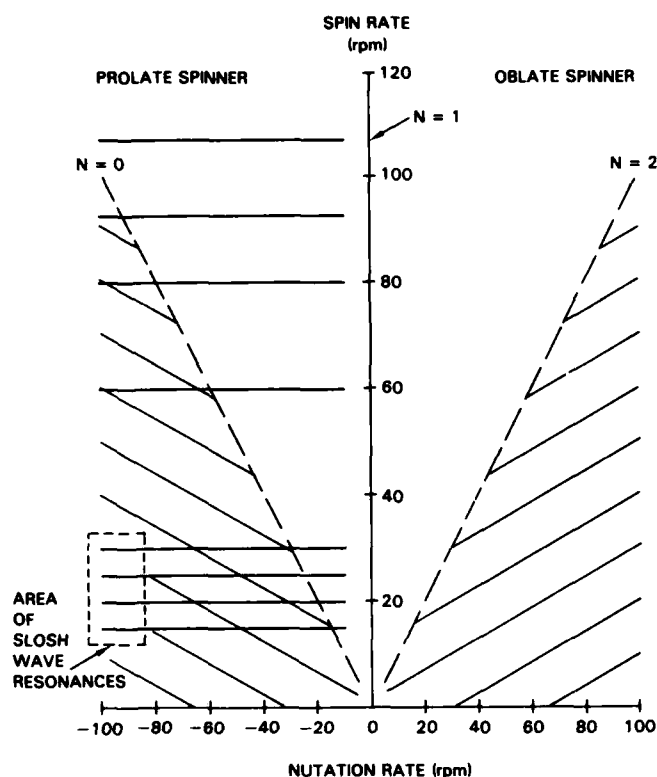


Fig. 6 — Forced-motion table operating regions. Slosh wave resonances excited outside physically realizable inertia ratios.

Acknowledgments: Tom Dilello, Daniel Clark, and Russ Barnes and his technical staff within NRL's Mechanical Systems Branch, designed, built, and maintained the test hardware. Dr. Franklin T. Dodge, a fluid dynamics specialist from Southwest Research Institute, translated the results of the tests into a working model of energy dissipation for actual spacecraft.

[Sponsored by ONR]

References

- H.N. Abramson, ed., *The Dynamic Behavior of Liquids in Moving Containers* NASA SP-106, 1966.
- M.F. Zedd and F.T. Dodge, "Energy Dissipation of Liquids in Nutating Spherical Tanks Measured by a Forced-Motion Spin Table." AIAA Guidance and Control Conference, Paper 84-1842-CP, 1984. ■

Radiation Effects on Microelectronic Components in the Upper Atmosphere

C.H. Tsao and R. Silberberg

*E.O. Hulburt Center for Space Research
Space Science Division*

Due to advances in integrated-circuit technology, logic chips and other microelectronic components have been reduced in size to dimensions of a few microns. Signals can be registered in these miniaturized devices by smaller amounts of electrical charge than were required in older, larger components. Therefore, the new circuits are more susceptible to single-event upsets, in which spurious signals are produced by unwanted sources of electrical charge. The traversal of highly ionizing, cosmic-ray particles through a device can produce sufficient charge to cause

these malfunctions. For space vehicles or military aircraft that fly at high altitudes, the flux of cosmic rays is high enough for this to be a significant problem. At NRL, we determined the magnitude of this effect theoretically by first calculating the flux and energy spectrum of cosmic rays as a function of altitude, then computing the energy deposition, and finally calculating the associated upset rate in typical microelectronic components at several altitudes. This yields a more accurate determination of the radiation effects than previously used measurements of the total radiation dose.

Cosmic rays are high-energy atomic nuclei that sweep toward earth from extraterrestrial sources such as the solar wind. As these particles penetrate the earth's atmosphere, they collide with air molecules. Some of these collisions are elastic, and the cosmic-ray nuclei simply give up momentum and energy. Other collisions are inelastic. For example, cosmic-ray energy may be lost to ionization of air molecules. Also, the primary flux of cosmic rays can generate secondary particles through the breakup of the atomic nuclei of the air; neutrons produced in this way can penetrate much deeper into the atmosphere. Finally, the cosmic ray ions can break up into lighter nuclear fragments (ions of lesser atomic number).

To properly calculate the changes in the ionic species and energies of the cosmic rays as a function of the altitude to which they have

penetrated, the transport equation in our three-dimensional computer model includes these various collisional processes. The rates of secondary particle generation depend critically on collision probabilities or cross sections; these are calculated from empirical relations developed at NRL [1]. As the initial condition at high altitude, the calculation uses the cosmic-ray composition and intensity that is observed above the earth's atmosphere; these are described in an NRL report [2]. In addition to collisional effects, the model must account for effects of the earth's magnetic field. The geomagnetic field deflects slower particles and causes the particle flux to be directional rather than isotropic. Moreover, there is a reduction in this vertical flux that depends on the geomagnetic latitude.

Figure 7 illustrates the reduction in the number of cosmic-ray ions as they reach lower altitudes. This is shown for three groups of charged particles: *L* for low atomic numbers $Z = 3 - 5$; *M* for medium $Z = 6 - 9$; and *H* for high $Z = 10 - 26$. This figure applies to locations where vertically incident particles with a magnetic rigidity of 1 GV or higher can enter the atmosphere without being deflected by the geomagnetic field. (Rigidity is defined as momentum per unit charge, the energy in GeV divided by the particle charge q and the speed of light c .) These locations include the northern fringe of the United States and that of the USSR. The reduction of the fluxes of the primary cosmic

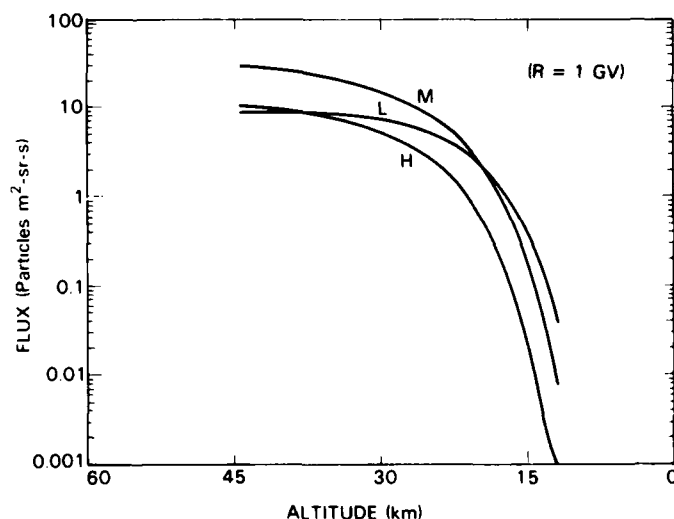


Fig. 7 — Variation of total cosmic-ray ion fluxes (with rigidity higher than 1 GV) as a function of altitude (km). *L* denotes nuclei of low atomic number $Z = 3 - 5$, *M* that of medium $Z = 6 - 9$, and *H* that of high $Z = 10 - 26$.

rays is seen to be very pronounced at altitudes below 22.5 km (75,000 ft). Therefore, the effects of radiation on microelectronic components at lower altitudes will be mostly due to secondary particles, such as slow protons and neutrons.

The flux of particles alone does not adequately describe the effects of the radiation. These effects are critically related to the linear energy transfer (LET), which is the energy that a charged particle of a given energy will deposit per unit distance within a device. We have summed the LET values over the various types of nuclei in cosmic rays, and summed or integrated over their energy spectra. The resulting LET-distributions, which will be used to calculate upset rates, are shown in Fig. 8 at altitudes of 45 km (150,000 ft), 22.5 km (75,000 ft), and 15 km (50,000 ft). The figure shows the number of particles that contribute to energy deposition in the silicon material above a given threshold value of LET.

The single event upset rate is highly dependent on the size of the particular device and the threshold charge (also known as critical charge) for registering an upset. (A moving charged particle strips electrons from atoms; if the combined charge of these electrons exceeds the critical charge of the device, the stored information will be altered or upset.) The charge that is generated in the device can be directly related to energy loss

rate or LET of the cosmic ray particles. Figure 9 shows the rate of upsets per day in a thousand microelectronic data bits (assuming a rectangular device of $5 \times 10 \times 10 \mu\text{m}$ in size) as a function of the critical charge of a device. The various curves show the upset rates due to cosmic-ray ions at various altitudes and the rates due to low-energy secondary protons and neutrons. The latter two are calculated for an altitude of 16.5 km (55,000 ft).

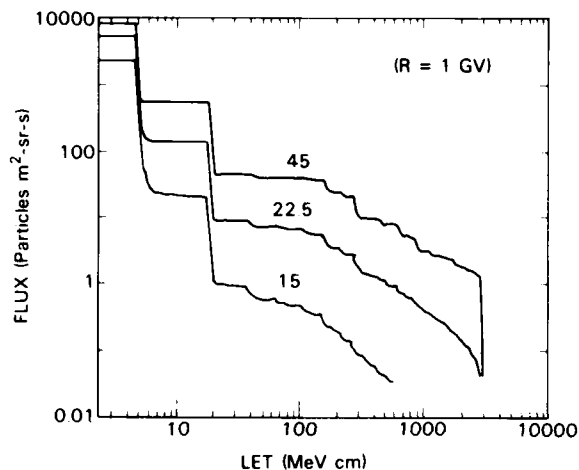
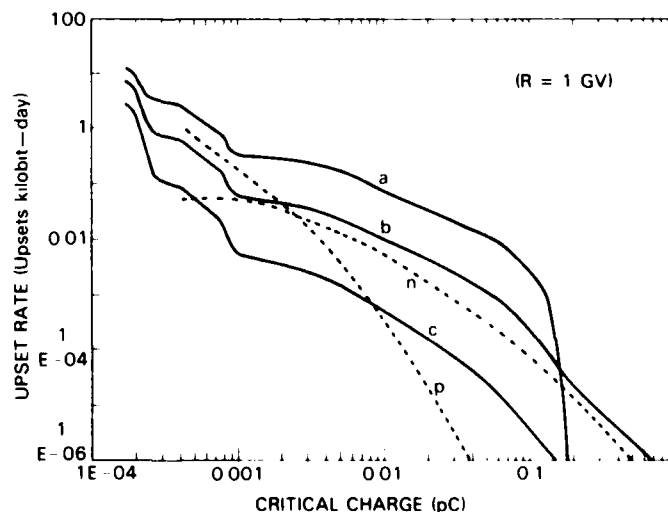


Fig. 8 — Integral LET-distributions of the atmospheric cosmic-ray ions in silicon at 45, 22.5, and 15 km with rigidity greater than 1 GV. The step-like increases of fluxes at the left are due to the contributions from high-energy primary protons and alpha particles.

Fig. 9 — Upset rates from: (a) cosmic-ray ions of rigidity greater than 1 GV at an altitude of 45 km, (b) the same at 22.5 km, (c) the same at 15 km, (p) low-energy secondary protons (generated when cosmic ray nuclei cause the breakup of atomic nuclei in the atmosphere), and (n) collisions of secondary neutrons with atomic nuclei of the device, both at 16.5 km. The critical charge for the device is expressed in pico-coulombs. The rates were evaluated for a rectangular device of $5 \times 10 \times 10 \mu\text{m}$.



The single event upset rate at 22.5 km (curve b) is about 10% of that above the atmosphere and is dominated by the cosmic-ray ions. Below 22.5 km, it is mainly due to collisions of secondary neutrons with the atomic nuclei of the device. When struck by the neutrons, these nuclei recoil, and they are highly ionizing. The upset rates of Fig. 9 are appropriate for periods of normal solar activity. At the time of very large solar flares, the rate of computer malfunctions may be larger by a factor of 1000. These results are important to the Navy and to other military planners that select design criteria for computer components for space vehicles and high altitude military aircraft.

[This work is supported by the DNA/DARPA Single Event Effects Program.]

References

1. R. Silberberg and C.H. Tsao, "Partial Cross-Sections in High-Energy Nuclear Reactions; and Astrophysical Applications," *Ap. J. Suppl.* 25, 315 (1973).
2. J.H. Adams, R. Silberberg, and C.H. Tsao, "Cosmic Ray Effects on Microelectronics, Part I: The Near Earth Environment," NRL Memorandum Report 4506, Aug. 1981. ■

Charge Collection in Multilayer Structures

A.R. Knudson, A.B. Campbell, and E.A. Wolicki
Radiation Sciences Division

Microelectronic circuits in space applications are subject to errors produced by the passage of cosmic rays and protons through device elements. These errors, often referred to as soft errors or single event upsets, result from collection of the charge—produced by these incident ions—on sensitive circuit electrodes or nodes. These electrodes can be the drains of field-effect transistors in static random access memories (RAMs) or the metal-oxide-semiconductor (MOS) capacitors used to store information in dynamic RAMs. Single-event upsets have already caused malfunctions of satellites. The problem is expected to become more severe as these circuits are scaled

down in size with concomitant reductions in the amount of stored charge which represents a bit of information.

Mechanism: To find solutions to the single-event upset problem, one must understand the basic charge collection process. The charge collection process involves both the motion of charge in an electric field (drift) and the random motion (diffusion) of electrons and holes in the semiconductor. Because the internal fields are considerably altered by the dense charge produced in the ion track, numerical modeling is extremely difficult. Therefore, experimental measurements are necessary to check the validity of the modeling approximations which are required to make the problem tractable.

Measurement Technique: Charge collection has been measured for simple MOS capacitor and diode structures. However, no measurements were available for more complex multilayer structures. The present measurements provide information on the sharing of the charge when two electrodes are competing for the charge produced by the incident ion. The structures used for these studies represent standardized microelectronic structures—the (Sandia National Laboratories) bulk CMOS (complementary MOS) and bulk CMOS-on-epi (epitaxial substrate) technologies. They consist of layers of $n+$, p , n , and, in the case of the epi structures, an $n+$ substrate. Figure 10 provides a cross section of a CMOS-on-epi structure. The $n+$, p , and bottom layers can be connected to external circuitry by pins 1, 2, and 3, respectively. Measurements have been performed with the p -layer grounded (pin 2) and with bias voltages applied to and charge collection signals obtained from the top $n+$ and the bottom layers. Energetic ions (1 to 60 MeV) of helium, oxygen, and copper were used to produce the charge in the affected layers. In this work, 2.5- and 25- μm diameter pinhole apertures restricted the incident ions to the central portion of the structure.

Results: The charge collection depends on the bias voltages, the angle of incidence of the ion, the ion type, and the ion energy. Substantial differences in charge collection by the upper $n+$

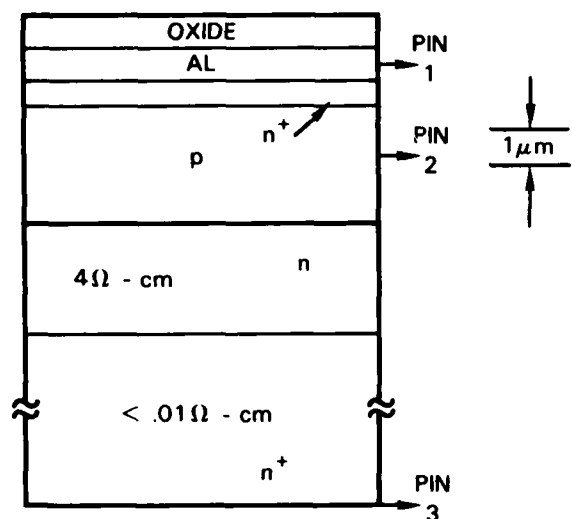


Fig. 10 — Cross section of bulk CMOS-on EPI (Sandia) test structure. The top $n+$, p , and bottom $n+$ layers can be connected to external circuitry by pins 1, 2, and 3.

contact are observed as the biases on the upper $n+$ contact and the substrate are changed. These differences become larger as the ionization density of the ion track is increased by using ions of greater atomic weight (i.e. helium < oxygen < copper ions). For the heavier ions under some bias conditions, almost all of the charge is collected on the $n+$ substrate as long as the range of the ion is sufficiently great to penetrate into the $n+$ substrate. Figure 11 shows data obtained

using a 19.2-MeV oxygen ion beam on a bulk CMOS-on-epi test structure for two bias conditions. It shows the charge collection efficiency, i.e., the fraction of the charge produced by the ion that is collected on a particular electrode, as a function of angle of incidence of the ion beam. Data are given for both the $n+$ substrate (pin 3) and the top $n+$ element (pin 1). Increasing the angle of incidence decreases the depth of penetration of the ion track. For the case of 0 V on pin 1 and 10 V on pin 3, no charge is collected on the upper $n+$ contact until the angle of incidence exceeds about 50 degrees. This corresponds to the ions just reaching the $n+$ substrate in this epi structure (Fig. 10). Note that the charge collected in the substrate drops off at large angles because the ion passes through increasingly greater depths of material above the substrate. If the ion track does not penetrate the $p-n$ depletion region (the region about the interface), all of the charge is collected on the top $n+$ electrode independently of bias voltages.

While the results of these experiments apply to the analysis of the single-event upset sensitivity of Sandia devices of this type, these results can also be extended to provide a foundation for the analysis of other devices considered for use in the space environment.

[Sponsored by ONR/DARPA and NAV-ELEX]

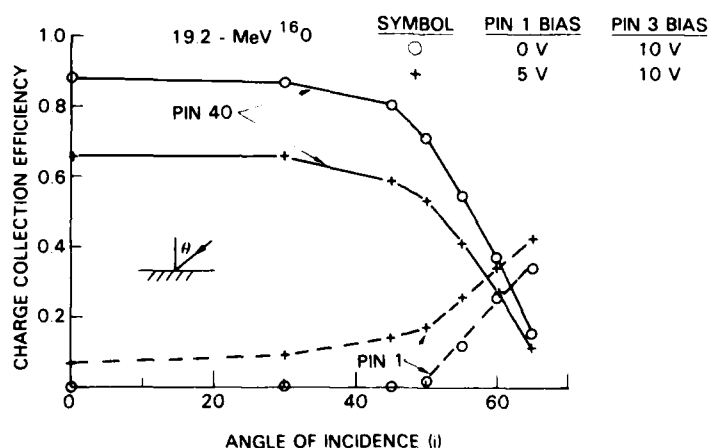


Fig. 11 — Measurements of the charge collection efficiency as a function of the angle of incidence of 19.2-MeV oxygen ions are shown here for two different bias conditions. Pin 1 is connected to the upper $n+$ layer, and pin 3 is connected to the $n+$ substrate.

Clock Technology

J.A. Murray
Aerospace Systems Division

Clock technology has played an important role in naval progress. Originally, determining longitude at sea depended directly on the precision of the ship's chronometer. In the modern Navy, each advance in accurate timing has been immediately adopted by designers of new systems for navigation, surveillance, weapon delivery, and enhanced military communications. As part of its continuing research in timing technology, NRL is developing atomic clocks to meet the demanding requirements of the NAVSTAR Global Positioning System (GPS).

GPS is based on precise timing. A user accurately determines his position in three dimensions by measuring the differences in arrival times of radio signals received from several NAVSTAR satellites. In addition, GPS also disseminates the Naval Observatory's Master Clock time to Fleet units for their sophisticated command, control, communications and intelligence (C^3I) systems. Therefore, the satellites must be coordinated to billionths of a second in time. Clocks based on the highly stable resonances of rubidium, cesium, and hydrogen are potential candidates for the spacecraft and the ground stations that periodically check and correct them.

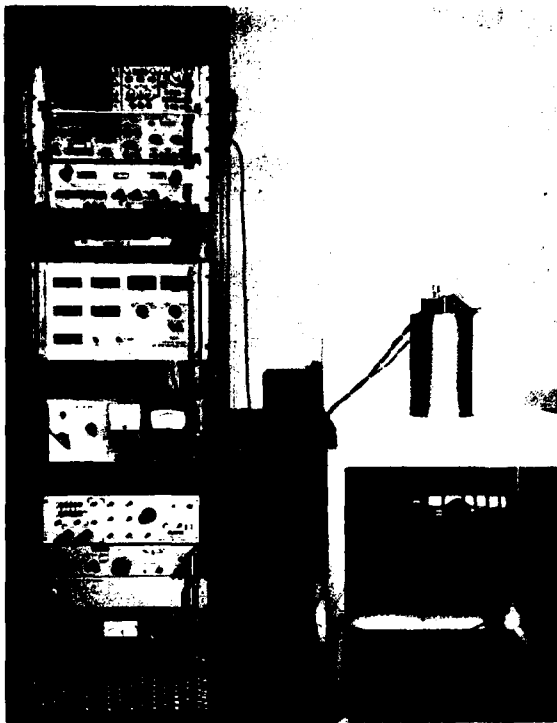
Cesium Beam Program: NRL has been engaged in the development of atomic frequency standards for GPS since the formation of the program in 1973. Two NRL Navigation Technology Satellites (NTS) with experimental atomic clocks have been launched and their performance evaluated. Based on the results of the cesium-beam standards contained in NTS-2, NRL has contracted with three vendors to produce space-qualified cesium clocks with enhanced performance and reliability. A test facility has been built at NRL to evaluate the performance and longevity of the resulting products; this facility is now being expanded. It contains a highly stable ensemble of cesium and hydrogen clocks that serve as a timing reference; thermal-vacuum chambers simulate the thermal environment of space.

On-Orbit Analysis: To evaluate the rubidium and cesium clocks aboard the developmental NAVSTARs now in operation, NRL conducts on-orbit performance analyses. These analyses use reference orbits determined by the Naval Surface Weapons Center and other data from the GPS control stations; they are intended to separate actual clock performance from measurement uncertainties caused by orbit and atmospheric propagation effects.

Hydrogen Maser Program: For years, the potential of the hydrogen maser as a superior GPS clock has been recognized. However, several factors have made its use impractical. Its weight and size greatly exceeded those of cesium standards. Its longevity was impaired by uncertain lifetimes for the pumps that disposed of spent hydrogen. Sensitivity of the massive, tuned cavity (in which the maser action takes place) to temperature variations and mechanical instability made temperature and tuning control of the cavity necessary. Sensitivity of the hydrogen resonance to magnetic fields also required very effective magnetic shielding.

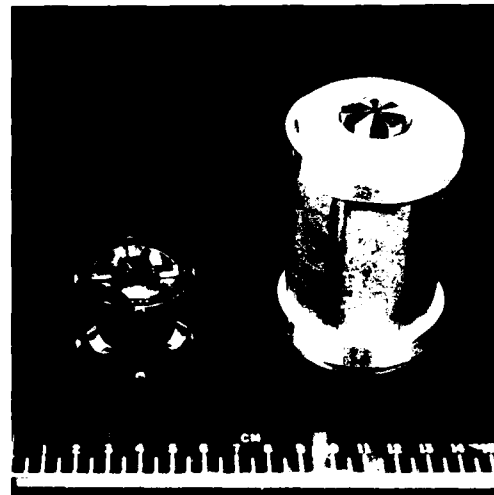
Size, weight, temperature control, and magnetic shielding problems are significantly reduced simply by making the cavity smaller. This has been the subject of much recent research and development at NRL. Cooperative studies are taking place at the National Bureau of Standards (NBS), Hughes Research Laboratories (HRL), and the Smithsonian Astrophysical Observatory (SAO), among others. Small cavities have been developed, some using dielectric (sapphire) loading (Fig. 12) to produce the effect of a larger cavity and others using different resonant structures, for "passive" masers which do not oscillate on their own. These masers are used as frequency references to control externally generated signals. Sigma Tau Standards, however, has also developed a small-cavity oscillating maser under an NRL contract, and HRL and NRL have applied a "Q-multiplier" approach. With this approach, the inherently higher signal losses in small cavities are offset by external amplification to produce an oscillating maser.

Besides the small-cavity development for the maser, NRL is conducting research on specific issues in maser technology, such as



79388(2)

Fig. 12 — NRL small hydrogen maser cavity using single-crystal sapphire loading, mounted on test stand



79476(2)

Fig. 13 — NRL quadrupole state-selector magnet (left) compared with its predecessor hexapole state-selector



80604(2)

Fig. 14 — Zirconium-graphite sorption pump designed cooperatively by NRL and SAES Getters

unwanted resonances in loaded cavities, coupling techniques for passive masers, automatic cavity tuning, magnetic shielding, atomic state selection (Fig. 13), and sorption-pump technology (Fig. 14). Other laboratories are also working on various aspects of these and other issues, including the use of metal hydrides for hydrogen storage.

participants in the NRL program has formed a basis for producing two engineering development models of hydrogen-maser clocks by Hughes Aircraft Corporation. One clock is intended for GPS spacecraft use; the other is designed for use in the GPS ground stations and would also be a candidate for shipboard applications.

[Sponsored by NAVELEX]

Effects of a Free Surface on the Wake of a Flat Plate

T.F. Swean, Jr.

Marine Technology Division

For several decades it has been realized that the presence of a free surface above the wake of an object influences the evolution of mean velocity and turbulence, but the mechanisms have not been completely described. Recent studies have suggested that the turbulent eddy viscosity is significantly attenuated near a free surface [1]. There is also evidence that the velocity fluctuations normal to the surface are diminished while the fluctuations in the plane of the surface are increased, suggesting an overall kinetic energy preservation in that region.

The interaction between turbulent currents and the free surface is of both practical and theoretical interest. Such interactions are believed to influence several phenomena observed in the wakes of surface ships including foam formation and dissipation, wave breaking, and the damping of capillary waves. These problems have been the subject of recent study as part of continuing research programs on wake hydrodynamics at NRL. Experiments have been designed to study the evolution of a turbulent wake in the vicinity of a free water surface, and numerical models have been constructed to interpret the laboratory data.

Experiment: The simplest turbulent flow which can be realized in the laboratory is perhaps in the wake of a flat plate. The study of such a flow near a free surface has the added advantage that the results can be compared with data and calculations readily available in the literature for wakes in an unbounded fluid. An experimental program was carried out in the towing channel of the Marine Technology Division. The towing system consists of an instrument carriage mounted on rails atop the channel sidewalls and a submerged model support carriage mounted on the channel floor. Both carriages are driven by a variable speed DC motor via a cable/pulley arrangement. The model used in the experiments was a $1 \times 0.91 \times 0.006$ -m aluminum flat plate horizontally mounted on the submerged

carriage. Turbulence measurements were obtained in the wake of the plate by using constant temperature anemometers with cross-fiber-film sensors. The towing speed in all instances was 0.59 ms^{-1} corresponding to a Reynolds number of 5.81×10^5 based on plate length. The model was towed at a depth of 5 cm from the free surface. Additional measurements were obtained at a tow depth of 25 cm to approximate a fluid of infinite depth and provide a means of comparing the near surface data.

The mean flow velocity distributions in the wake for a tow depth of 5 cm (finite fluid) are shown in Fig. 15. In this figure, the dimensionless longitudinal coordinate x/θ_0 is measured downstream from the plate trailing edge, while the dimensionless vertical coordinate y/θ_0 is measured from the plate centerline and is positive in the direction toward the free surface. Since U is measured in coordinates moving with the plate, U_∞ is the plate velocity. The trailing edge momentum thickness θ_0 is 2.53 mm. For purposes of comparison, the infinite fluid data are

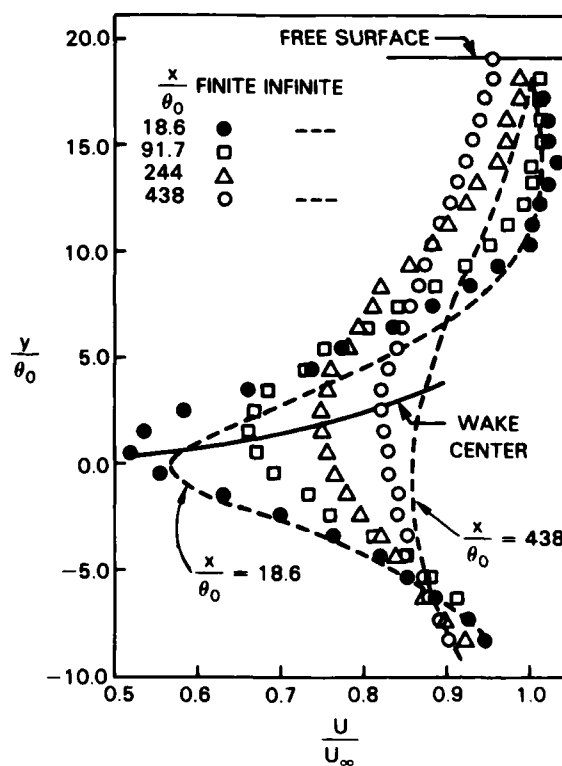


Fig. 15 — Measured mean velocity profiles in the wake of a flat plate near a free surface

also shown on this figure (the dashed lines at $x/\theta_0 = 18.6$ and 438). The contrast between the two flows is evident even at the first station ($x/\theta_0 = 18.6$). The minimum velocity is about 10% less than in the infinite wake, and its location has already moved a small distance (~ 2.1 mm) above the plate center. A greater velocity defect (the average velocity deficit) is observed in the entire upper half-wake, and finally there is a region of velocity overshoot which is not so evident in the infinite fluid. At the final station ($x/\theta_0 = 438$), the results show a drag wake ($U/U_\infty < 1$) of approximately 5% existing at the surface. At this distance behind the plate, the minimum velocity is 4% less than for the infinite fluid. The estimated trajectory of the point of maximum velocity defect is shown by the solid line in Fig. 15. At the final station, the maximum defect has migrated to a position nearly 7 mm ($\sim 2.5 \theta_0$) above the plate. In the lower half-wake, there appears to be only a very gradually evolving difference between the two flows. At $x/\theta_0 = 18.6$ the profiles are essentially identical below $y/\theta_0 = -2$, whereas at $x/\theta_0 = 438$ there are significant differences until approximately $y/\theta_0 = -6$.

Numerical Model and Conclusions: As described in detail in Ref. 2, the two-dimensional inviscid free shear layer equations coupled with a two-equation k, ϵ -turbulence model were solved numerically to simulate the laboratory flow. The experimental and calculated velocity profiles are shown in Fig. 16. Starting with the measured curve at $x/\theta_0 = 18.6$, the curves at 91.7 and 438 were calculated. The major features observed in the data are exhibited by the calculation, with the differences between calculation and experiment tending to be smaller in the lower half-wake.

These results suggest that there is less turbulent diffusion in the longitudinal direction for a wake near the free surface when contrasted with a similar wake existing far from the surface. In a region near the surface, there is evidence that the vertical diffusion is greater than that predicted by commonly accepted turbulence models developed from the observation of relatively simple flows.

It is anticipated that additional experiments will be planned using laser anemometry which will allow the exploration of the very near surface

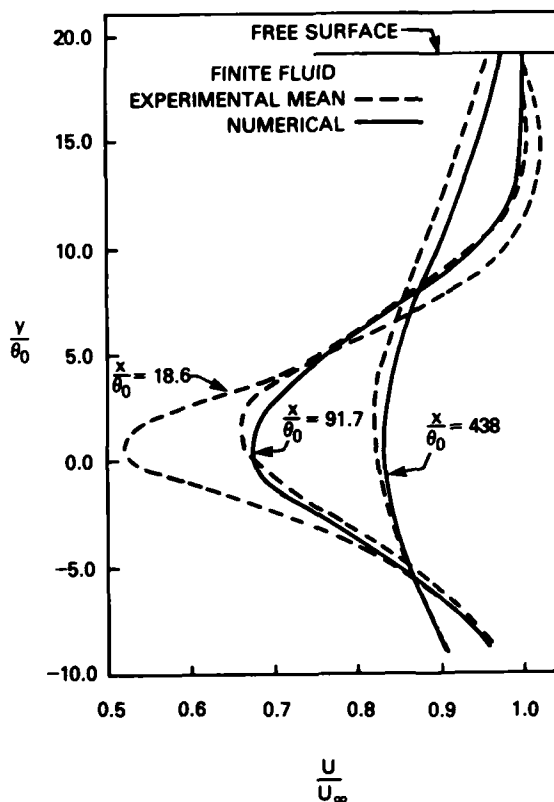


Fig. 16 — Measured and predicted mean velocity profiles in the wake of a flat plate near a free surface

region. The knowledge gained and the computational methods developed in this research program will lead to the numerical simulation and experimental verification of more complex interactions between free surfaces and turbulent flow fields including the effects of free surface waves.

[Sponsored by the ONR]

References

1. D. Noat and W. Rodi, "Calculation of Secondary Currents in Channel Flow," *ASCE*, 108 (HY8), 948-968 (1982).
2. T.F. Swann, Jr. and G.A. Keramidas, "The Turbulent Wake of A Flat Plate Near a Free Surface," *Computational Methods and Experimental Measurements*, Proc. of the Second Int. Conference, June 1984. ■

Low-Reynolds-Number Airfoil Testing

R.J. Foch

Tactical Electronic Warfare Division

Airfoil models representing wing profiles for use on small unmanned aircraft have been tested in wind tunnels to accurately measure their aerodynamic qualities. These tests were conducted at low, subsonic, and transonic speeds, and focused on flight conditions in which the effect of air viscosity degrades the airfoil's aerodynamic performance.

When significant viscous effects are present in the airflow surrounding a wing, the airfoil is said to be operating at a low Reynolds number (Re). $Re = \text{velocity} \times \text{airfoil width} / \text{kinematic air viscosity}$. Low Reynolds number occurs when the numerical value of the airfoil's Reynolds number is less than about one million.

Large manned aircraft designs, by virtue of sheer size and speed, avoid viscous-related aerodynamic difficulties by operating at an Re on the order of 10^7 or greater. It is, however, operationally desirable for unmanned Navy aircraft to be sized and flown at speeds in which low-Reynolds-number effects significantly influence their flight performance. Aerodynamically, low-Reynolds-number airfoil characteristics are often unsteady and unpredictable. Operation at low Re is further complicated by the fact that good high-Reynolds-number airfoils developed for manned aircraft are not necessarily good low-Reynolds-number airfoils and vice versa. To improve the aerodynamic characteristics of small aircraft, the Vehicle Research Section of the Offboard Countermeasures Branch has found it necessary to conduct wind tunnel testing of low-Reynolds-number airfoils to provide low Re airfoil performance data and identify and understand the predominant aerodynamic phenomena involved.

The testing of the NRL-selected airfoils for this study was conducted in the University of Notre Dame's subsonic and transonic low turbulence wind tunnels. The use of low turbulence wind tunnels for studying low-Reynolds-number flow assured that viscosity effects were not masked by the turbulence of the wind tunnel.

Subsonic Airfoil Testing: A German sailplane airfoil (Wortmann FX-63-137) was selected

for the low-speed tests. Previous experience with this airfoil has shown it to be unique among low-Reynolds-number airfoils because its performance is actually optimized at certain low-Reynolds-number flow regions and it exhibits predictable characteristics.

The wind tunnel model consisted of a wing having a uniform cross section with no twist or taper. In planar view, the wing was rectangular. Additionally, the model was sealed to the walls of the wind tunnel to avoid wing tip effects. Smoke injection during the wind tunnel tests was used to observe the airflow patterns and to identify particularly interesting regions of flow instabilities such as separation or reattachment of the air boundary layer.

Lift and drag force measurements were also taken to provide quantitative data for future design use. The effects of variations in surface finishes and surface contour were studied. All tests were conducted at Reynolds numbers from 80,000 to 800,000 corresponding to a 6-in. chord wing flying at speeds of 17 to 170 mph. These air speeds are typical for low-speed, low-altitude small aircraft launched from ships.

Transonic Airfoil Tests: The candidate airfoil was a biconvex, circular arc airfoil. This is a symmetrical arc shape in which the upper and lower convex surfaces of the airfoil are identical. The depth of the airfoil was one-tenth its length.

This model was extremely delicate to handle since the airfoil must be quite tiny (model wing's dimensions were $0.1 \times 1.0 \times 4.0$ in.) to obtain low Reynolds numbers at transonic speeds. Smoke was injected into the wind tunnel test section to visualize the airflow direction, and a Schlieren optical diffraction technique was used to make the shock waves visible. Still photographs and high-speed motion picture data were taken.

The tests were conducted at Reynolds numbers of 400,000 to 700,000, which correspond to an unmanned aircraft with a 1-in.-wide wing flying at speeds of 510 to 900 mph (0.7 to 1.2 Mach). Such speeds and dimensions are typical of small, high-speed aircraft being studied.

Observations: Despite the large difference in velocities, both the subsonic and transonic testing were related by similar values of Reynolds number. This research disclosed many factors

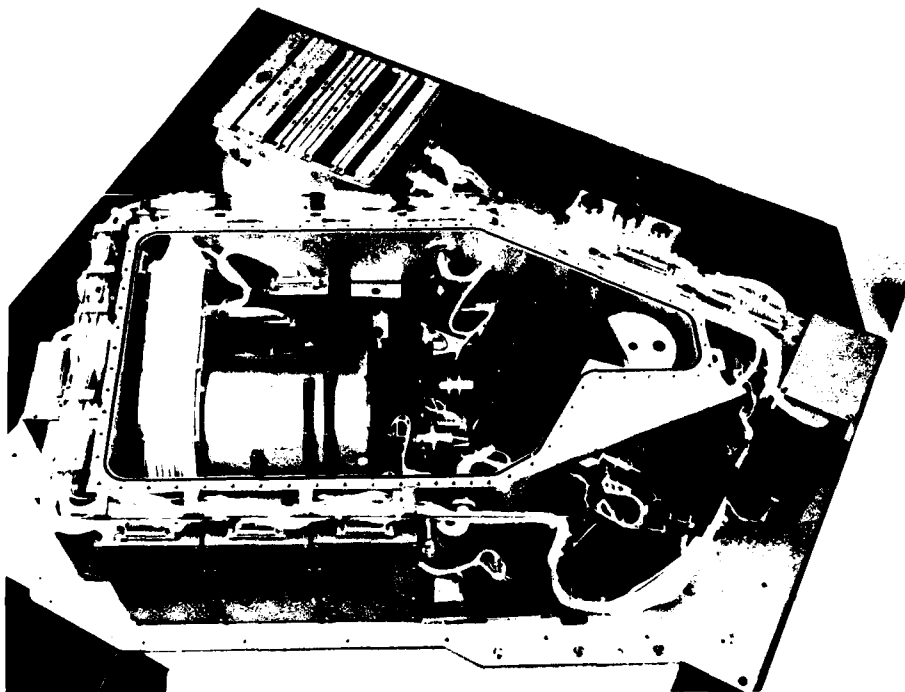
significant to the development of small aircraft airfoils such as:

- The quality of the flow region near the surface of the wing (the boundary layer) which determines the critical aerodynamic characteristics is much more sensitive than previously realized to small changes in surface contour, surface finish (roughness), vibration, and acoustic levels.
- In view of their small total forces and sensitivity to probes placed within the wind tunnel, testing of small wings often requires innovative new techniques such as micro-strain gauge force balances in conjunction with laser doppler velocimeter (LDV) measurements to obtain high accuracy.
- Detrimental aerodynamic performance characteristics for one airfoil often appear in certain Reynolds numbers ranges (100,000 to 400,000 typical), where mixed laminar and turbulent flow occur, but are never seen at higher speed or with increased size on that particular airfoil.

- Additional work using higher resolution measurements is required to determine how much effect the wind tunnel itself has on the airfoil's performance.
- By careful design of airfoils, maintenance of precise contours, and accurate alignment with rigid structures, the performance of these low-Reynolds-number airfoils can actually be much better than expected when traditional predictions are used.

Critical factors affecting the aerodynamic performance of airfoils for small unmanned aircraft have been identified in this series of wind tunnel tests. The traditional theory that low-Reynolds-number airfoils are physically limited to poor performance is gradually being supplanted with accurate, reliable airfoil test data which indicate otherwise. This new data may help form the basis for the technology to develop very efficient small aircraft for use in important and vital Navy missions.

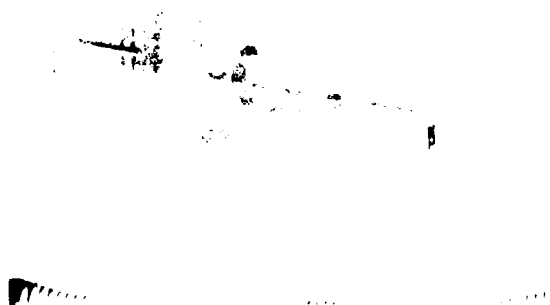
[Sponsored by the ONR]



Interior of the NRL Solar Ultraviolet Spectral Irradiance Monitor (SUSIM) which is to fly aboard Spacelab 2 in 1985. It will measure the variability of the solar ultraviolet spectrum in the 1100- to 4000-Å region with a 1-1/2 Å and a 50 Å resolution. Light enters through a slit on the left, is refracted off two rotatable gratings and then impinges on one of seven selectable detectors (in the cylinder at the lower left). The cubical structure at the top left is a sophisticated microprocessor to control the instrument.

Dr. John Bartoe has been selected to fly aboard Spacelab 2 to operate SUSIM, and Dr. Dianne Prinz has been selected as an alternate. They are both members of NRL's Space Science Division.

*High-powered radiation sources and
pulsed-power technology*





- 139 Stability in Laser Fusion**
Mark H. Emery and John H. Gardner
Symmetry and thermal transport strongly affect laser-heated plasmas
- 142 Long-Pulse, Free-Electron Laser with No External Focusing**
John A. Pasour, Christos A. Kapetanakis, Phillip A. Sprangle, and Cha-Mei Tang
High-current laser emission may be important for communications
- 144 Fast Opening Switch for Pulsed-Power Applications**
Robert A. Meger
Megamperes can be switched in 10 ns without shorting megavolts

HIGH-POWER TECHNOLOGY

Future defense systems will probably rely on devices that can produce extreme power levels. As a result, production, conversion, and use of large amounts and intense concentrations of energy may well become the number one problem of tomorrow. Several high-technology approaches to the production and concentration of high power levels are described in the articles in this section. They range from laser research to high-power switching.

This research was done in the Laboratory for Computational Physics (Code 4040) and the Plasma Physics Division (Code 4700).

Several other research projects in high-power technology in progress at NRL concern

- inertial confinement fusion with lasers and light ion beams,
- modified betatron,
- dense Z-pinch, and
- gyrotrons as high-power radiation sources.

Page 136, clockwise from upper left:

Capacitor bank for the Gamble II Marx generator. Energy is accumulated in this bank for several minutes, then switched to the pulse-forming transmission line in $1 \mu\text{s}$ to produce a high-power electrical pulse.

Gamble II—a high-voltage, pulsed-power generator, can produce 1-MA, 2-MV, 50-ns ion- or electron-beam pulses. Gamble II is used for studying plasma confinement, nuclear blast simulations for fast-opening switch development, and other work requiring intense beams. See article on p. 144 by R. Meger.

Wiggler magnet for millimeter-wave free-electron laser (FEL) on NRL's Versatile Electron Beam Accelerator (VEBA). Bifilar magnet windings provide 3-cm-period helically symmetric transverse "pump" magnetic field. Ends are flared at constant pitch to provide adiabatic entry and exit conditions. See article on p. 142 by J. Pasour.

Stability in Laser Fusion

M.H. Emery and J.H. Gardner
Laboratory for Computational Physics

Using two-dimensional hydrodynamic simulations, we have developed a fairly self-consistent picture for the evolution of the interchange instability on the surface of a laser-irradiated, hollow, spherical shell (pellet). Strong vortex structures (miniature whirlpools) are generated in the fluid flow at the surface of the pellet, and this vorticity is found to be the controlling element in the evolution of the instability. We are able to explain why the growth rate in the laser-pellet case is smaller than that predicted by simple theory and why the predicted variation with perturbation wavelength is different. These results have important implications for laser fusion.

In the laser-fusion process, powerful laser beams are used to compress pellets filled with the heavy hydrogen isotopes deuterium and tritium (DT). As the laser energy is absorbed, hot pellet material blows off the pellet surface, creating high pressures that drive the pellet inward in a rocket-like process. If the remaining shell stays cool and converges inward (implodes) with sufficient symmetry and kinetic energy, the DT nuclear fuel is compressed to a very high density and temperature. This allows the DT nuclei to fuse into helium and release large amounts of energy.

Comparison to Classical Instability: There are many obstacles that must be overcome before laser fusion can be achieved. One of the most critical problems is that of stability. In the implosion process, the cold, dense shell is being accelerated inward by the hot, low-density plasma on the outside, and this arrangement is hydrodynamically unstable (inward acceleration is equivalent to gravity acting outward). This instability is one form of the Rayleigh-Taylor or interchange instability, so called because the more dense fluid will attempt to interchange positions with the less dense fluid to reach a more stable configuration. This instability is a potential obstacle to laser fusion since it can cause the DT fuel to mix with the shell material or the shell to fracture thus destroying the fuel containment. Even in its mildest form, it can cause a nonuni-

form implosion and severely reduce the amount of energy released by the fusion process.

The classical inviscid, incompressible problem of the Rayleigh-Taylor instability is much simpler than the laser-fusion problem. The classical calculation assumes a fluid of fixed density suspended over a second fluid of lower density. If the interface between the two fluids is perturbed, then the heavy fluid will fall through the light fluid in finger-like projections called spikes, and the light fluid will rise like a bubble through the heavy fluid. The rate at which this proceeds is proportional to $(g/\lambda)^{1/2}$, where g is the gravitational acceleration and λ is the wavelength of the periodic perturbation. The laser-fusion case is far more complex than the classical case because (a) density varies continuously with distance from the pellet surface, (b) there are high rates of energy deposition with associated gradients in temperature and velocity, and (c) there are high rates of mass flow due to material being blown off the pellet surface.

Although the result has not been explained previously, numerical simulations of the laser-fusion Rayleigh-Taylor instability have consistently shown that the growth rate is reduced from the classical growth rate. Numerical simulations performed at NRL (using our FAST2D code) and elsewhere show that the laser-fusion instability growth rate is about one-half of that predicted by the classical theory. Also, the predicted variation of the growth rate with perturbation wavelength (λ) is different from the classical model. The classical theory predicts that the growth rate will increase without limit as λ decreases. In contrast, laser-fusion simulations show that there is a maximum growth rate at some perturbation wavelength, with decreasing growth rates at both larger and smaller wavelengths. Up to now, there has not been a satisfactory explanation for the smaller growth rate in the laser-fusion case or for the decrease in the growth rate at smaller perturbation wavelengths.

Laser-Fusion Instability Mechanisms:

Fluid flows observed in the two-dimensional hydrodynamic simulations of the laser-pellet case exhibit vortex structures that are analogous to those observed in fluid flow past a bluff body. In

Fig. 1, for example, we show a classical photograph of fluid flowing past a cylinder. Vortices are clearly seen in the flow downstream from the cylinder; these are generated as the fluid passes the body and are convected downstream or shed with the flow. Also shown in Fig. 1 is a flow pattern from our numerical simulation, showing the vorticity being generated and shed from the surface of a target struck with a high-intensity laser. Imperfections on the pellet surface or nonuniformities in the laser illumination cause the density of the shell and the pressure on the shell to reach their maximum values at different locations. This misalignment generates strong vortex structures on the pellet surface. As the outer portion of the shell heats up and blows away, it carries part of this vorticity away with it.

This shedding of vorticity is responsible for the reduced Rayleigh-Taylor growth rate in the laser-fusion case. The vorticity that is generated on the pellet surface is the driving force for the

instability. The vorticity interchanges the heavy and light fluids; the heavy shell material flows into the region which will become the spike, and the light blowoff material flows into the region which will become the bubble. A schematic illustration of this process is given in Fig. 2. The important difference between this case and the classical case of two fixed-density fluids is that some of the vorticity in this problem is being convected downstream by the blowoff process. This reduces the amount of vorticity that is available at the pellet surface to cause the interchange of the heavy and light fluids, thereby reducing the instability growth rate.

The vortex-shedding mechanism can also account for the reduced growth rate at smaller perturbation wavelengths. As the wavelength λ of the perturbation becomes smaller, the vortices on the target surface become closer together. This causes them to interact more strongly and to shed vorticity more rapidly. Therefore, the

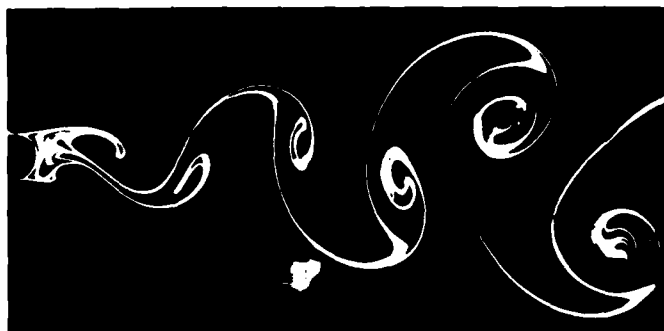
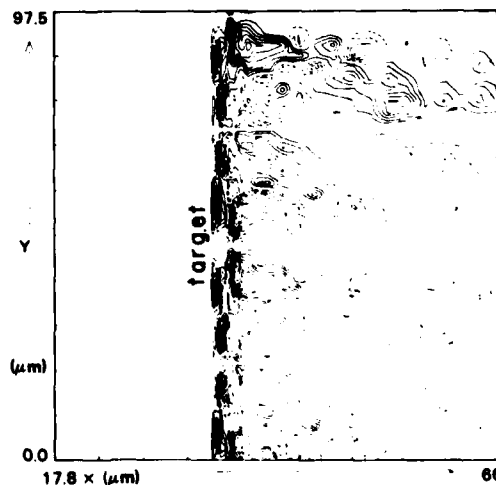


Fig. 1 — (Top) Classic photograph showing vortex structures being shed from a cylinder as fluid flows from left to right. (S. Taneda, *J. Phys. Soc. Jpn.* **11**, 302 (1956)). (Bottom) Computer-generated vorticity contours showing the generation and shedding of vorticity from the surface of a flat target struck with a laser that is incident from the right. Dotted lines are clockwise rotation, solid lines are counter-clockwise rotation. Note that the scale-factors for the horizontal and vertical axes are different.



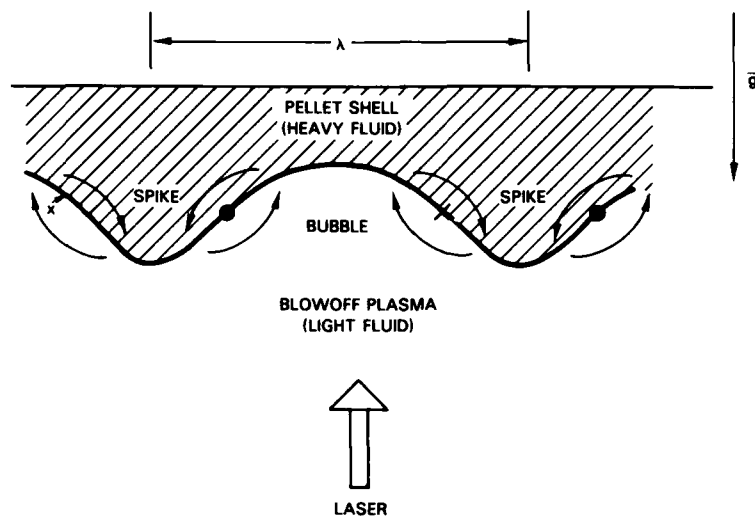
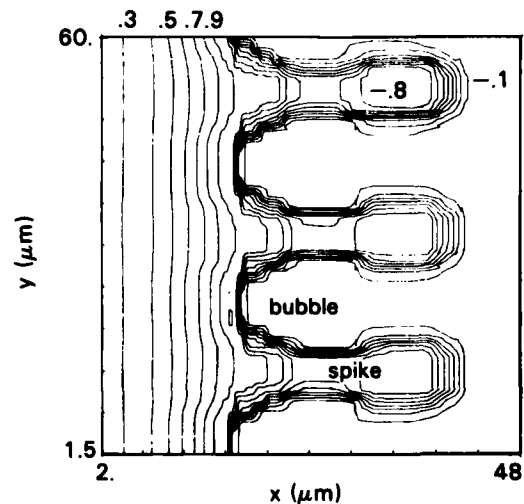


Fig. 2 — Simplified schematic of the Rayleigh-Taylor process for a laser-fusion pellet. The laser strikes the target from below and, as a result of the acceleration process, the system feels a gravitational field, g , directed downward. The heavy pellet shell is being supported by the light blowoff plasma, and any perturbation of the target surface (one of wavelength λ is shown) is unstable. The vorticity generated on the target surface attempts to interchange the two fluids; $x(\cdot)$ represents clockwise (counterclockwise) flow. The vorticity feeds the heavy shell material into the spike which falls and the light blowoff plasma into the bubble which rises.

Fig. 3 — Isodensity contours showing late-time development of the interchange instability on a flat target. The contours are labeled with the ratios of the densities to the solid density of the target material. Note that the scale factors for the horizontal and vertical axes are different. The laser is incident from the right.



reduction in growth rate is even larger at smaller λ , explaining the observed decrease of growth rate in that case. A simple analytical model, based on the analogy with the flow past a bluff body, gives quantitative agreement with the growth rates obtained from the two-dimensional simulations [1].

Finally, the dynamics of the vorticity can also explain the widening of the tips of the spikes that is observed in the simulations. As the spike grows in size, part of the vorticity rolls down the side of the spike and collects there. This rotational flow causes the head of the spike to widen (see Fig. 3). This increases the drag on the spike and reduces its rate of fall through the hot, blowoff plasma. In some cases, this can even saturate the instability. This widening of the spike tip has recently been observed experimentally [2].

We now have a fairly self-consistent picture, based on the dynamics of the vorticity, for the evolution of the interchange instability on the surface of a laser pellet. We are using this new information to find ways to control this instability, either dynamically or by the proper selection of physical parameters.

[Sponsored by DOE and ONR]

References

1. M.H. Emery, J.H. Gardner, J.P. Boris, and A.L. Cooper, "Vortex Shedding Due to Laser Ablation," NRL Memorandum Report 5989, Sept. 1983; *Phys. Fluids*, **27**, 1338 (1984).
2. R.R. Whitlock, M.H. Emery, J.A. Stamper, E.A. McLean, S.P. Obenshain, and M.C. Peckerar, "Observation of Rayleigh-Taylor-like-Structures in a Laser-Accelerated Foil," *Phys. Rev. Lett.* **52**, 819 (1984). ■

Long-Pulse, Free-Electron Laser with No External Focusing

J.A. Pasour, C.A. Kapetanakis, P.A. Sprangle,
and C. Tang
Plasma Physics Division

The Navy is interested in high-power radiation sources in the infrared-to-millimeter wavelength region of the electromagnetic spectrum. Important applications include advanced radar, communications, countermeasures, and directed-energy weapons. A relatively new device, the free electron laser (FEL), has several unique features which make it very attractive for these applications; these features include broad tunability, high power, and high efficiency. We have built an FEL that produces up to 4 MW of 9-mm radiation with a duration of 1 to 2 μ s. This device is the longest duration, high-power FEL yet operated in the millimeter wavelength band. In addition, it is simpler than previous FELs in this regime because no focusing field (other than that provided by the wiggler) is used in the interaction region to confine the electron beam.

Conventional Devices vs FELs: Other devices produce radiation in the desired spectral region, but they each have some fundamental limitations. Conventional microwave tubes have been extrapolated to millimeter wavelengths, but they are limited in power by the small size of the waveguides and radio frequency (rf) structures that must be used. A newer high-power tube, the gyrotron, has produced megawatt radiation at wavelengths λ as short as a few millimeters.

However, gyrotrons also are ultimately limited at shorter wavelengths because the output frequency f is proportional to the applied magnetic field. For example, a clearly impractical field of 1 MG would be necessary to achieve $\lambda = 0.1$ mm. Of course, conventional infrared lasers are available, but they operate only at specific frequencies corresponding to transitions between particular energy levels in the lasing medium. Also, pumping the laser to the proper excited state is inherently inefficient at longer wavelengths because the energy levels of the lasing transition are closely spaced and far above the ground state of the atom or molecule.

To see why the FEL is not constrained by these limitations, it is necessary to understand the basic FEL mechanism. The FEL consists of a relativistic electron beam together with a periodic magnetic field or "wiggler." When the beam is passed through the wiggler, the electrons oscillate in the periodic magnetic field and therefore begin to radiate. The combination of the radiation field and the wiggler field bunches the beam electrons so that they radiate coherently. The radiation wavelength λ is related to the spatial period l of the wiggler, the electron energy γmc^2 , and the wiggler field amplitude B_w by

$$\lambda = \frac{l}{2\gamma^2} [1 + a^2], \quad (1)$$

where $a = 0.093 B_w l$ for B_w in kilogauss and l in centimeters. Consequently, the FEL can be tuned over a wide range of wavelengths by varying the electron-beam energy or the wiggler field amplitude. Furthermore, very short wavelengths can be achieved by increasing the electron-beam energy rather than by scaling any mechanical dimensions to correspondingly small values, as would be required in conventional microwave devices. The efficiency of an FEL can also be quite high. Simple FELs have typical efficiencies of 5 to 10%, but this can be increased to 30 to 50% by various techniques, such as tapering the wiggler period or amplitude.

The NRL Long-Pulse FEL: The FEL interaction region is shown schematically in Fig. 4. Our device [1] employs a linear induction accelerator which produces a 700 keV, 600 A electron beam. This beam is focused through a

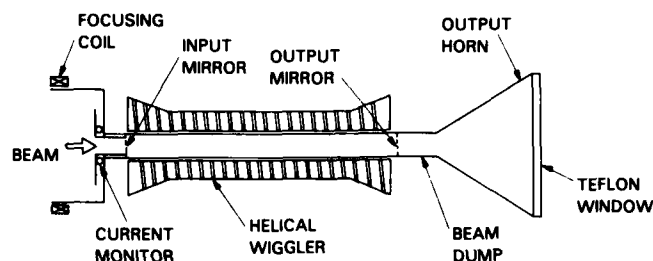


Fig. 4 — Schematic diagram of FEL experiment. The electron beam from the accelerator is focused into the helical wiggler by the final accelerator focusing coil. Only the wiggler field is used to confine the beam in the interaction region.

2.5-cm-diameter aperture into a 3-cm-diameter beam tube which passes through the 128-cm-long wiggler. The wiggler consists of a continuous double-helix winding having a 4-cm period. A current I_w flows through the first helix from one end of the wiggler to the other. The current returns in the second helix, whose turns are located midway between those of the first. The opposing current flow causes cancellation of the axial field component and produces a spiralling wiggler field ($B_w = 1$ kG for $I_w = 8$ kA) which is perpendicular to the axis of the device. In the present experiments, the input and output mirrors have not been used, so the output radiation is amplified from noise during a single transit.

Two properties of our experiment make it a particularly good test bed for FEL development. The electron-beam accelerator used in our device produces pulses of $2\text{-}\mu\text{s}$ duration. Previous high-current FEL experiments have had pulse durations of approximately 50 ns, a factor of 20

shorter than our experiment. The longer pulse allows many bounces of the radiation through the interaction region during the pulse (if the mirrors are used), so that nonlinear effects and saturation mechanisms are more easily studied. The other important difference between this experiment and previous ones is the absence of an axial magnetic field in our device. In addition to simplifying the apparatus, this feature allows an unambiguous identification and analysis of FEL modes. Whenever an axial field is present, there is a strong possibility that cyclotron radiation will be generated; this emission can detract from the FEL process and interfere with the interpretation of the experiment.

FEL Performance: The variation of transported electron-beam current and output radiation with wiggler field amplitude B_w is shown in Fig. 5. It is obvious that there is an optimum field, $B_w \approx 500$ to 800 G, for both current

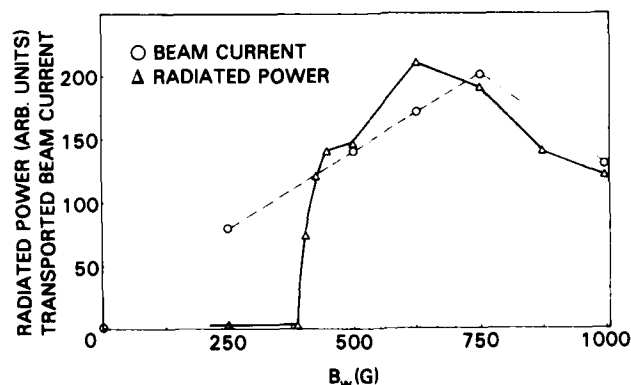


Fig. 5 — Variation of radiated power and transported beam current with wiggler field

transport and radiation production. The optimum field depends on the beam current and the inherent angular beam divergence, both of which produce a radially outward pressure on the beam. The helical wiggler provides a radial focusing force proportional to B_w , and beam transport is maximized when B_w is chosen such that these opposing forces are properly balanced. Also, it is apparent from the figure that there is a sharp threshold at $B_w = 400$ G for the generation of significant radiation. This behavior is often observed in FEL experiments because the growth rate of the radiation increases with both B_w and the beam current. Until the growth rate is large enough to overcome the inherent losses in the system, little output is produced.

The output radiation has been analyzed with various diagnostics. Our group has developed a gas breakdown spectrometer [2] which measures both the dominant wavelength and the power at that wavelength. In addition, we have measured the total energy of the radiation with a calorimeter, and we have obtained power spectra with a Fabry-Perot interferometer and with calibrated detectors and high-pass filters. A maximum power of 4 MW is achieved at $B_w = 625$ G, in which case the frequency is 30 GHz. The output frequency is tunable with beam energy as predicted by Eq. (1). The width between half-power points of the output spectrum is less than 20% of the central frequency, as measured by time-integrating detectors. The 4 MW output power is 3% of the electron beam power in the interaction region. This efficiency is only a factor of 2 or 3 less than the maximum theoretical efficiency for this experiment, which assumes a negligible spread of energies in the electron beam.

Currently, we are using the novel features of this experiment to expand our study of the FEL. With no axial magnetic guide field, there is no cyclotron emission to complicate the spectrum; therefore, a quantitative study of fundamental issues such as nonlinear and saturation effects is possible. Also, the long pulse duration enables us to operate the device as an oscillator by placing mirrors at the ends of the interaction region. Experiments to address these issues are in progress.

[Sponsored by ONR]

References

1. J.A. Pasour, R.F. Lucey, and C.W. Roberson, "Long Pulse Free Electron Laser Driven by a Linear Induction Accelerator," in *Free Electron Generators of Coherent Radiation*, C.A. Brau, S.F. Jacobs, and M.O. Scully, eds. (SPIE Publishing Co., Bellingham, Wash., 1984), Vol. 354, pp 328-335.
2. F. Mako, J.A. Pasour, C.W. Roberson, and R. Lucey, "A Broadband, High-Power Millimeter-to-Centimeter Spectrometer," *Rev. Sci. Instrum.* **55**, 712 (1984). ■

Fast Opening Switch for Pulsed-Power Applications

R.A. Meger

Plasma Physics Division

A new device to switch large electrical currents very rapidly is under development at the NRL. This switch represents a significant advance in switching technology because it can conduct megamperes while closed, then open on a very short (10 ns) timescale. When open, the switch can withstand voltages of several megavolts without shorting. Conventional opening switches operate on longer timescales (> 100 ns) and can withstand much lower voltages (< 1 MV) after opening. The system is simple and relatively inexpensive to build. Its applications include nuclear weapons effects simulation, production of electron or ion beams for directed-energy weapons or inertial confinement fusion, pumping of high-power lasers, and any other areas which require very fast risetime pulses of high-power electrical energy.

The primary application of this type of switch is in the field of pulsed power. In conventional pulsed-power generators, energy is first stored capacitively over a period of seconds then released to a load through a series of closing switches on a 100-ns or longer timescale. The time compression of the stored energy results in the high-power pulse delivered to the load. Present machines can produce voltage pulses of several megavolts and currents of several

megamperes lasting up to 200 ns with risetimes of about 50 ns. Although these generators produce very high power bursts of electrical energy, the peak power is not high enough and the risetime of the load current is not fast enough for certain applications. By using a fast opening switch in conjunction with such generators, higher power and shorter risetime pulses can be obtained.

Switch Operation: The switch under investigation at NRL is called the Plasma Erosion Opening Switch (PEOS). Unlike conventional opening switches, such as circuit breakers or fuses, this switch uses a low-density carbon plasma injected into a vacuum region near the load to switch the current [1]. When the plasma is in the switch it allows the generator to charge an inductor (L_1 in Fig. 6). As the current through the switch increases, it eventually begins to erode the low-density plasma near the cathode. This erosion starts to open the switch. After enough of the plasma has been eroded, the switch can no longer carry the current driven by the generator and the current switches to the load (R_L in Fig. 6). The risetime of the current through the load now depends on the opening time of the switch, which can be much faster than the generator current risetime into a load without the switch. Thus, higher output power is obtained because the energy can be removed from the system on a shorter timescale than allowed by conventional switches.

Switch Experiments: Several experiments have been performed at NRL and other laboratories by NRL personnel using PEOS systems. Figure 7 shows a schematic of NRL's Gamble II experiment. The generator drives current through the coaxial inductor section which is shorted at the downstream end by the injected plasma in the switch. The length of time which the switch conducts current is determined by the switch geometry and by the amount of plasma injected in the switch region. Downstream of the switch is the load, represented in this case by an electron beam diode.

Figure 8 shows a typical experimental result from the switch operation. The solid line is the

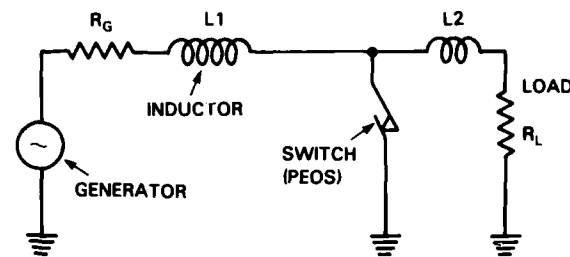


Fig. 6 — Generator with its characteristic output impedance R_G charges the inductor L_1 through the closed PEOS. When the switch opens, the current stored in L_1 discharges through the output inductance L_2 into the load impedance R_L .

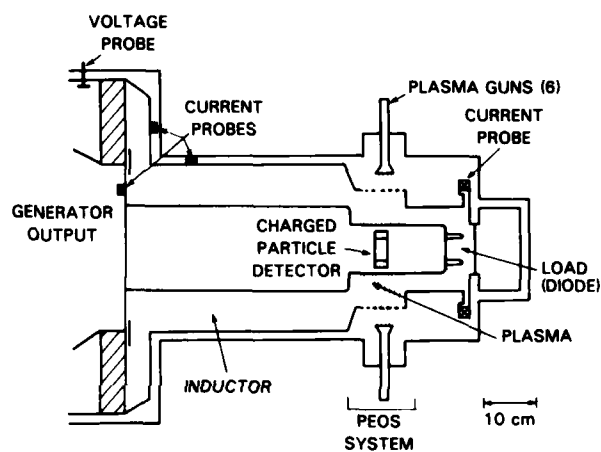


Fig. 7 — Gamble II switch system with the generator output, inductor, switch, and load regions. Timing for the generator and PEOS is provided by the Faraday-cup charged-particle detector located inside the inner conductor.

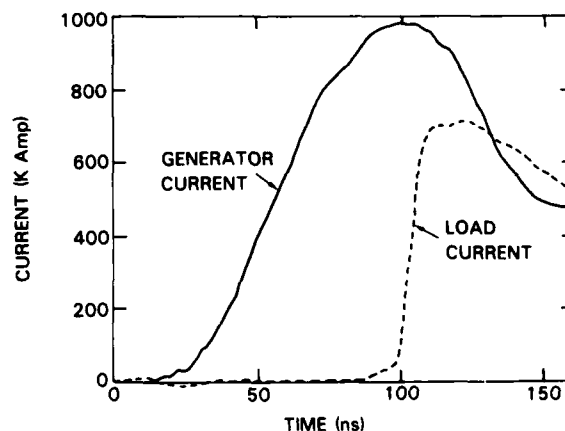


Fig. 8 — Current measured by probes on the generator side of the switch (solid) and on the load side of the switch (dashed) for the Gamble II experiment

current in the inductor driven by the Gamble II generator, and the dashed line is the load current. Note that the generator current is diverted through the switch for the first 100 ns; then the switch opens in about 10 ns, and the current is redirected through the load. The rate of current rise in the load is nearly 0.1 MA/ns which is significantly faster than comparable high-power generators. These experiments have demonstrated 50% increases in output power over similar experiments without the switch.

Other experiments by NRL personnel using PEOS systems have been performed on the Gamble I generator at NRL [2], on the Aurora generator at Harry Diamond Laboratories in Adelphi, Md., and on the PBFA 1 generator at Sandia National Laboratories in Albuquerque, N.M. These experiments have demonstrated fast switching of currents in excess of 5 MA and for a variety of different loads for various applications of the switch. Similar experiments have been performed by laboratories in Germany, France, and Japan.

This work represents the first successful demonstration of fast switching and output power gain by a vacuum opening switch at terrawatt power levels. Future work is aimed at further understanding and improving the present PEOS operation, decreasing the switch opening time by another order of magnitude to 1 ns, and applying the technology to a host of different pulsed-power applications. This work may lead to a new generation of higher power and more compact pulsed-power machines based on opening switches.

[Sponsored by ONR, DOE, and DNA]

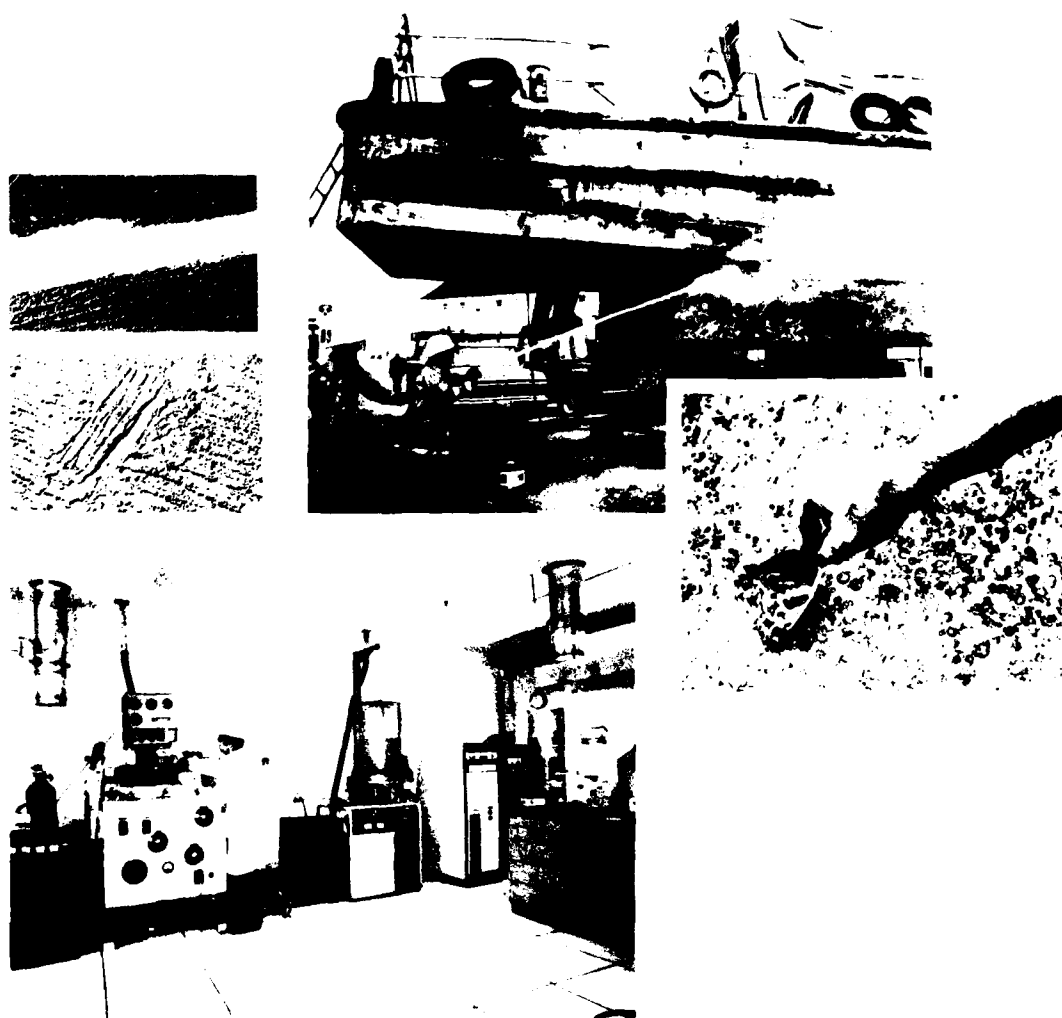
References

1. P.F. Ottinger, S.A. Goldstein, and R.A. Meger, NRL Memorandum Report 5205, Oct. 1983; also accepted for publication in *J. Appl. Phys.*, 1984.
2. R.A. Meger, R.J. Commisso, G. Cooperstein, and S.A. Goldstein, *Appl. Phys. Lett.* **42**, 943 (1983). ■



A time-integrated photograph of microwave breakdown in nitrogen at 25 Torr. The microwaves are produced by a free electron laser. The bright spots result from the standing-wave interference pattern generated when the microwaves are reflected from a copper plate located at the right of the photograph. The spacing between spots is one half the wavelength of the case, about 2 cm (J. Pasour).

Materials modification and behavior



151 Novel Device Structure Grown by Molecular Beam Epitaxy

Steven W. Kirchoefer and James Comas

Hyperfine interfaces and layers produce devices with new properties.

154 Orientation-Dependent Etching of Silicon

Edward D. Palik, Victor M. Bermudez, and Orest J. Glembocki

A new study determines the physics and chemistry of etching.

156 Photochemical Separation of Noble Gases

Terence Donohue

Radioactive krypton emissions, such as at Three Mile Island, could be drastically reduced.

158 Chemically Suppressing Intermodulation Interference

John C. Cooper and Rm. Panayappan

Corrosion inhibitors reduce radio-frequency noise fields on ships.

160 Coated Ceramic Fiber-Ceramic Matrix Composites

Dave I. Lewis and Roy W. Rice

A fiber-coating technique can dramatically improve ceramic composites.

162 Metal Matrix Composites by Physical Vapor Deposition

S. Carlos Sanday

Coating matrix fibers improves strength and quality of composites.

164 Performance of Nonskid Deck Coatings

Larry W. Kraft and Robert F. Brady, Jr.

NRL methods improve testing of abrasion and impact-resistant deck coating.

MATERIALS MODIFICATION

The properties of materials are fundamental to the performance of all devices, machines, and structures. Modification of existing materials by diverse techniques produces a host of new materials having enhanced or new properties. Sometimes these new properties form the basis for whole new technologies, such as the transistor. NRL conducts a broad spectrum of research in these fields, from solid-state devices, to chemical processes, to the development and use of fiber composites for enhanced strength and safety.

The work in this section was performed in four NRL Divisions in the Material Science and Component Technology Directorate; they are Chemistry (Code 6100), Material Science and Technology (Code 6300), Optical Sciences (Code 6500), and Electronics Technology (Code 6800).

A few of the many research projects at NRL in materials modification and behavior, other than those described in this chapter, are

- energetic materials,
- advanced joining science,
- rapid solidification techniques,
- advanced marine alloy development,
- development of high toughness and wear-resistant ceramics, and
- antimalarial drugs (with Walter Reed Hospital).

Page 148, clockwise from upper left:

Two samples of nonskid deck coatings. The coarse texture of the deck coatings protects people, aircraft, and machinery from slippage while operating on aircraft carrier flight decks. See article on p. 164 by L. Kraft.

The Seamule, a Navy tugboat, had a special NRL-developed polymer coating applied to the hull in 1977. This polymer still provides excellent protection to the hull and, as the inset shows, the fouling is easily removed after 7 years.

Metalization area of the NRL microelectronics facility. This equipment is used to precisely sputter metal surfaces onto microelectronic devices designed and constructed at the Laboratory.

Novel Device Structure Grown by Molecular Beam Epitaxy

S.W. Kirchoefer and J. Comas
Electronics Technology Division

The ability to deposit ultrathin epitaxial (having the same crystalline orientation as the substrate) layers to form compound semiconductors has led to the recent emergence of fundamentally new and novel materials and device concepts. At NRL, one technique used to fabricate thin epitaxial layers is molecular beam epitaxy (MBE). The MBE growth of a compound semiconductor film involves the reaction of thermally produced beam fluxes of the semiconductor constituents with a substrate under ultrahigh vacuum conditions.

MBE Technique: Beam fluxes of gallium (Ga) and arsenic (As) from individually controlled (Knudsen-type) evaporation cells impinge

and combine on a GaAs substrate held at 580°C to form a GaAs layer. In this case, the growth rate would be controlled by the Ga beam flux and the stoichiometry (the proportion of the components) by the As beam flux. Doping of *n*-type (negative charge carriers) and *p*-type (positive charge carriers) layers are achieved by use of silicon (Si) and beryllium (Be) beam fluxes respectively. $\text{Al}_x\text{Ga}_{1-x}\text{As}$ layers are also grown with the addition of a controlled beam of aluminum (Al). Growth rates are relatively slow under most MBE growth conditions, usually about 16 nm/min, but the beam fluxes are well-controlled. Figure 1 shows the MBE growth system configuration. An important factor is that the very close lattice matching of GaAs and $\text{Al}_x\text{Ga}_{1-x}\text{As}$ enables well-matched multilayer structures to be readily grown. Layered structures, with each layer of different composition, and with well-defined thicknesses, are called superlattice (SL) structures. A typical layer structure might be GaAs/AlGaAs/GaAs, etc. The MBE technique has grown superlattices with layer

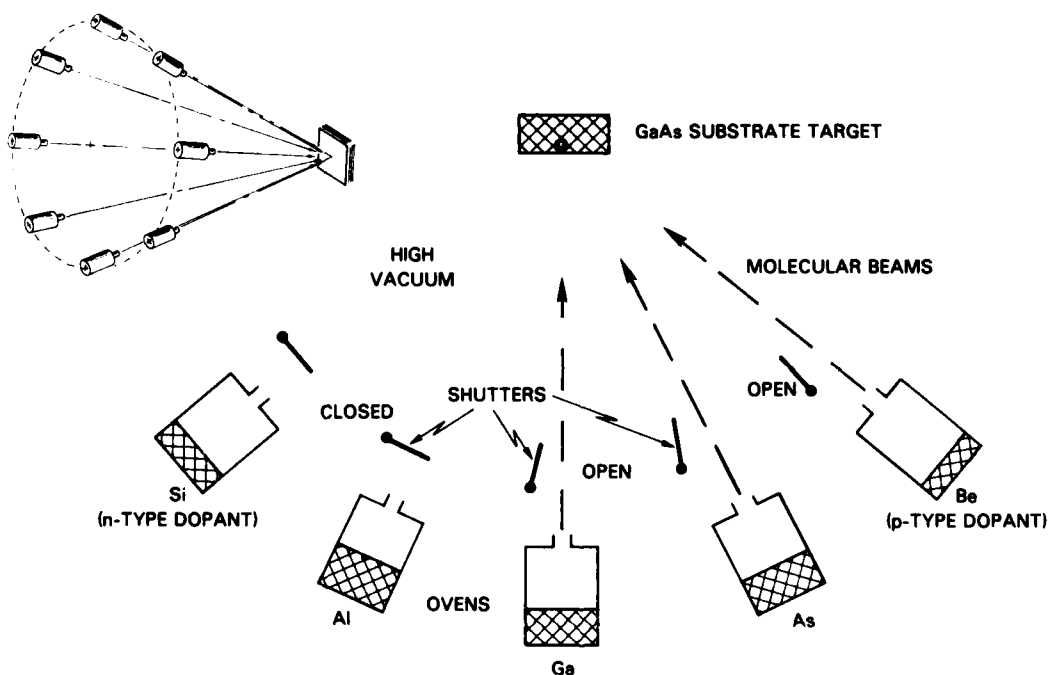


Fig. 1 — MBE system. The substrate, which is heated during growth, is located at the focal point of an 8-oven array located on a circle (inset). This configuration allows all beams to impinge on the target at the same angle. High purity, elemental charges such as As, Ga, Al, Be, Si, are placed in the ovens for evaporation. The ovens operate at fixed, elevated temperatures (e.g., As at 350°C, Ga at 1070°C), so that the ratio of the flux densities of the beams impinging on substrate can be controlled for GaAs growth. Layer thicknesses are controlled, and hyperabrupt interfaces are formed, by precisely opening and closing the shutters.

thicknesses approaching interatomic spacing (~ 1 nm). In addition to producing novel devices, layer thicknesses of about 10 nm or less allow study of some fundamental quantum mechanical properties of electrons. This is because these thin layers cause electrons to exhibit nearly two-dimensional behavior rather than their normal behavior in a three-dimensional crystal lattice.

The MBE growth process can provide hyperabrupt interfaces and control of layer thicknesses, alloy compositions, and doping levels. At NRL, the principal focus of the MBE effort is on the growth, characterization, and applications of III-V compound (composed of elements from the 3rd and 5th columns of the periodic table) semiconductors. The precise growth control has been fundamental to a variety of research programs on novel electronic devices

and materials. This work is centered around doped GaAs layers and GaAs/ $\text{Al}_x\text{Ga}_{1-x}\text{As}$ quantum well (heterojunction) structures.

NDR Device: The result of one program is a novel negative differential resistance (NDR) device which actually has a negative resistance at high enough applied voltage. Such devices may be used in electronic amplifiers and oscillators. NDR properties are based on unique transport properties of electrons in superlattice structures with two quantum levels. The devices fabricated from structures having these unique properties are called quantum-state transfer (QST) devices and are described below.

The NDR devices were fabricated from samples grown by MBE on semi-insulating GaAs substrates (Fig. 2). The superlattice portion of the original QST device consists of about 120

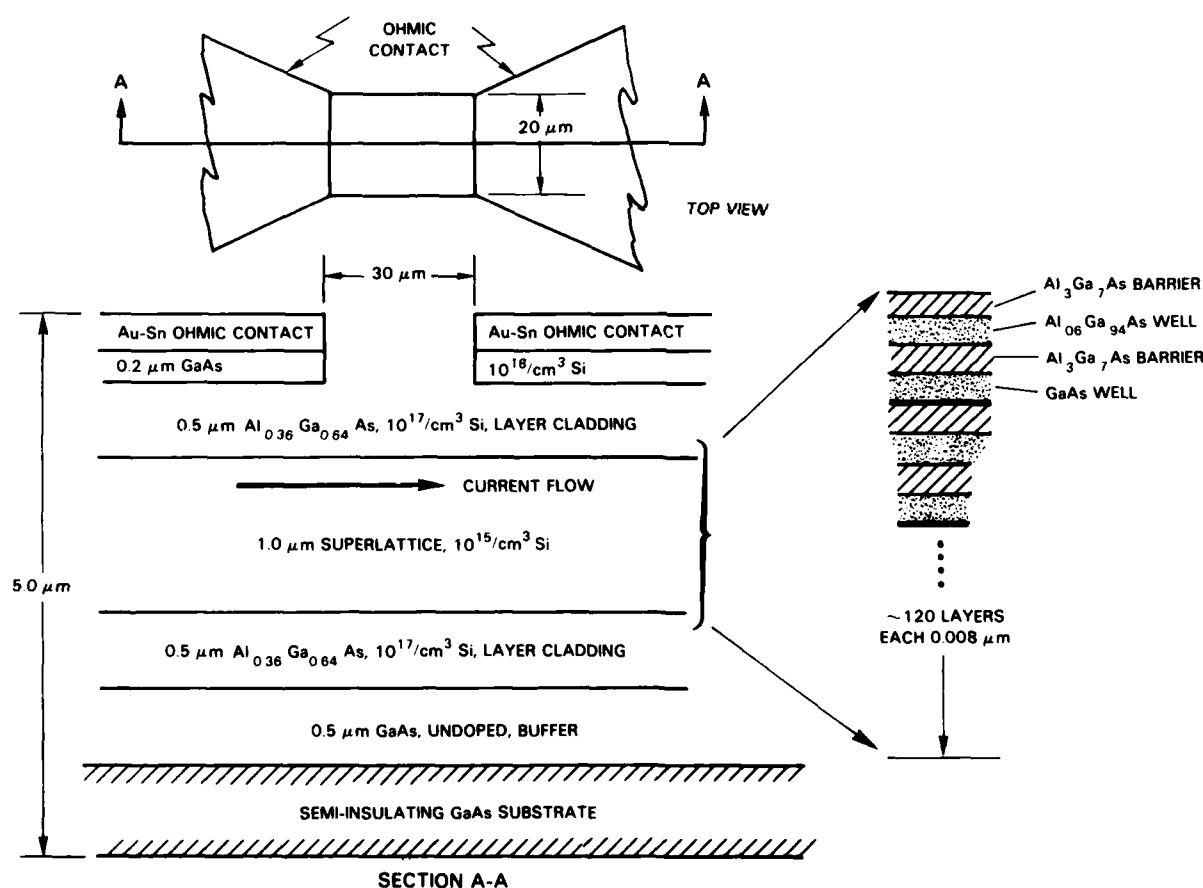


Fig. 2 — Top view and cross section A-A of the quantum-state transfer structure. The bilevel (barrier-well) structures on the right are repeated many times to obtain a superlattice region which is 1 μm thick. The resulting device is 5 μm high (the section is not to scale). Current flows mainly along the superlattice layer since its resistance is lower than the cladding layers and other layers.

8 nm-thick layers. Each unit cell of four layers is sequentially repeated in the superlattice. The sequence consists of an $\text{Al}_{0.3}\text{Ga}_{0.7}\text{As}$ barrier, an $\text{Al}_{0.06}\text{Ga}_{0.94}\text{As}$ well, an $\text{Al}_{0.3}\text{Ga}_{0.7}\text{As}$ barrier, and a GaAs well. These quantum well structures can be varied in thickness to produce devices with many different characteristics. GaAs buffer and Si-doped ($10^{18}/\text{cm}^3$) layers were grown at 580°C , the superlattice at 648°C , and the $\text{Al}_{0.36}\text{Ga}_{0.64}\text{As}$ cladding layers at 680°C . Layers grown under similar conditions were used for calibration and material characterization. The device shown in Fig. 2 was produced by using photoresist techniques (masking and etching) to define two ohmic contacts separated by $30\text{ }\mu\text{m}$. The contacts were made by alloying evaporated gold-antimony (Au-Sn) at 450°C for $\sim 15\text{ s}$. A second photoresist step was used to define a bar $20\text{ }\mu\text{m}$ wide between the ohmic contacts (Fig. 2). The resulting device was a $5\text{ }\mu\text{m}$ high structure through which the current flows mainly along the superlattice layers. Although the superlattice region is lightly doped ($10^{15}/\text{cm}^3$), electron depletion from the $\text{Al}_{0.36}\text{Ga}_{0.64}\text{As}$ cladding layers

increases the electron density in the superlattice region by an order of magnitude.

Negative differential resistance has been observed at room temperatures in QST devices fabricated from the above superlattice structures. The basic operating principle of the QST device relies on the difference in conduction of high-mobility, low-energy electrons (at low voltage) in the GaAs wells and low-mobility, high-energy electrons (at high voltage) in the $\text{Al}_{0.06}\text{Ga}_{0.94}\text{As}$ wells. As the voltage across the device increases, the electrons make a transition from the high-conduction GaAs to the low conduction $\text{Al}_{0.06}\text{Ga}_{0.94}\text{As}$ producing the NDR effect prominent in Fig. 3(a). (Reference 1 has a more detailed explanation of the phenomenon.)

NDR Performance: Current-voltage data obtained at room temperature for devices constructed with superlattices having multiple and single potential well depth superlattices are shown in Fig. 3. The NDR is observed in multiple well depth samples (Fig. 3 (a and b)) with a largest observed maximum-to-minimum current ratio

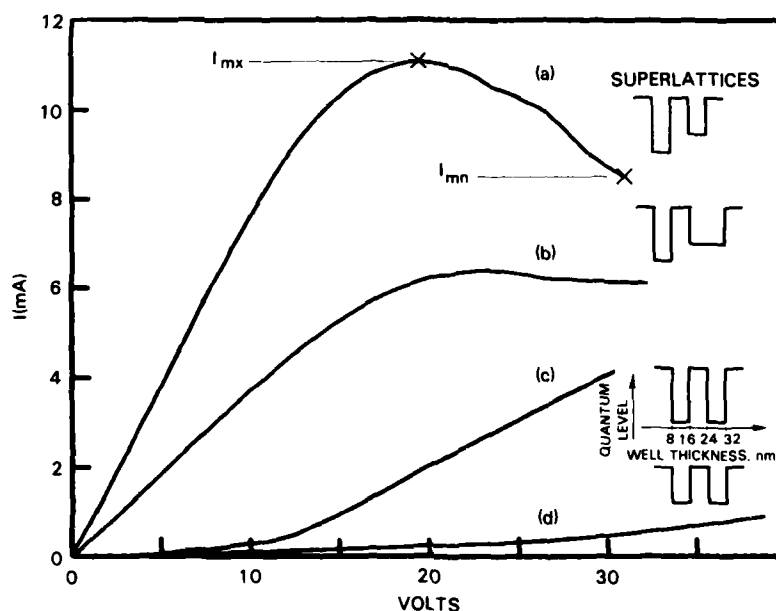


Fig. 3. — Current voltage data at room temperature for quantum-state transfer devices and the corresponding quantum well structures shown to scale: (a) 8 nm-wide GaAs and $\text{Al}_{0.06}\text{Ga}_{0.94}\text{As}$ wells; (b) 8 nm GaAs well and 16 nm $\text{Al}_{0.06}\text{Ga}_{0.94}\text{As}$ well; (c) only 8 nm GaAs well; (d) only 8 nm $\text{Al}_{0.06}\text{Ga}_{0.94}\text{As}$ wells. Negative differential resistance is observed only in the structures (a) and (b) where there are bilevel superlattices. The largest observed maximum-to-minimum current ratio (I_{mx}/I_{mn}) is ~ 1.4 observed in (a).

(I_{mx}/I_{mn} , Fig. 3(a)) of ~ 1.4 . Single well depth samples (Fig. 3 (c and d)) exhibit no negative differential resistance under the same processing and testing conditions. This allows the identification of quantum state transfer effects as distinct from competing Gunn or bulk-layer real space effects. These results were obtained by applying a sequence of voltage pulses with increasing amplitude to the device to avoid distorting the data through heating effects.

Quantum State Transfer devices, with their ultrathin epitaxial layer structure are valuable for studying certain basic physics of electrons. They may also be used as infrared detectors and at microwave frequencies, since their molecule-like dimensions can allow extremely high-frequency response.

[Sponsored by ONR]

Reference

1. S.W. Kirchoefer, R. Magno, and J. Comas, "Negative Differential Resistance at 300K in a Superlattice Quantum State Transfer Device," *Appl. Phys. Lett.*, **44**, 1054 (1984). ■

Orientation-Dependent Etching of Silicon

E.D. Palik, V.M. Bermudez, and O.J. Glembocki
Electronics Technology Division

An important step in the processing of silicon wafers to obtain integrated-circuit electronics components and other microstructures is gaseous and liquid etching. For the continued microminaturization of such microstructures, knowledge of the detailed etching mechanisms is required so that dimensional accuracy, material selectivity, and crystal-orientation dependence can be better controlled.

Liquid Etching: Orientation-dependent etching is invariably done with liquid etches. Liquid etching is accomplished by first masking the silicon wafer with the desired pattern using a non-etchable material and then chemically removing the unprotected silicon (Si). Generally, the {100} and {110} crystal planes etch one-to-two orders of magnitude faster than the {111} plane. (Figure 4 illustrates these planes for the cubic Si

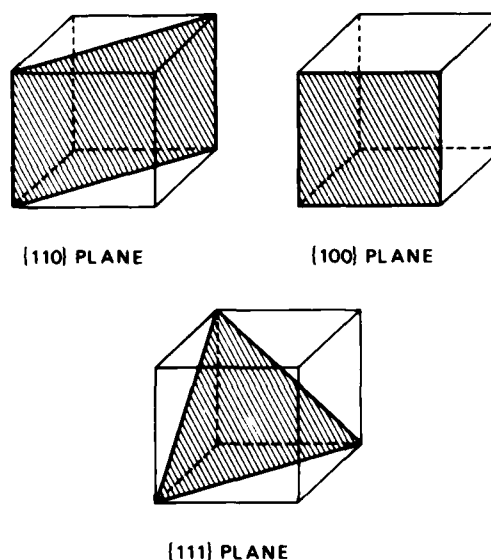


Fig. 4 — Crystalline Si has a cubic structure. The various planes in the cube are identified by a set of three indexes as shown above. The etch rate for each of these planes is very different.

structure.) It is these etching rates which are exploited in the fabrication of microstructures. Above a doping density of 10^{19} cm^{-3} for both n -type (electron-conducting) and p -type (hole-conducting) Si, the etching virtually stops for all crystal planes.

An NRL study of orientation-dependent etching of Si in aqueous potassium hydroxide (KOH) is in progress. These experiments are performed in an electrochemical cell. The cell contains the Si wafer, a reference electrode, and the platinum counter electrode. The "open-circuit" potential appears across the Si and the reference electrode when no current flows in the cell. To gain further knowledge about the etching process, current-voltage, etch-rate, ellipsometry, and electroreflectance measurements (optical techniques to measure electromagnetic properties of the Si/electrolyte interface) have been carried out as the sample etches at open-circuit potential and at anodic (positive) and cathodic (negative) bias.

Results: Figure 5 shows results for the bias-dependent etch rates for {100}, {111} n , p surfaces at room temperature. Generally, the

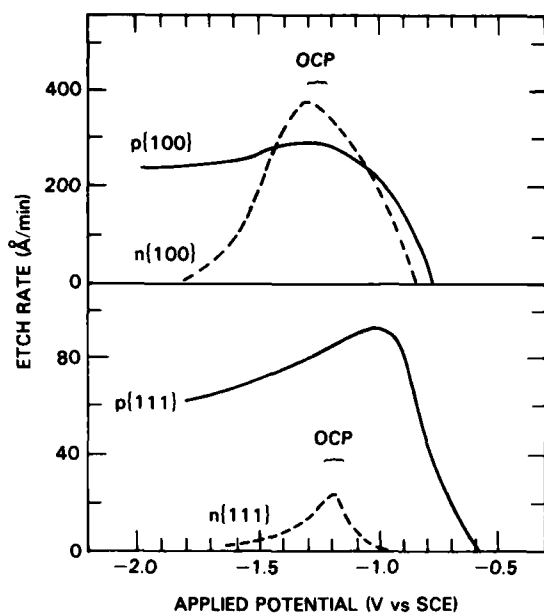


Fig. 5 — Etch rates as a function of applied potential for {100}, {111}, *n*, *p* surfaces of Si. The open-circuit potentials for each sample lie in the voltage range indicated.

This promotes electrolysis of the aqueous KOH rather than etching of the Si.

Figure 5 suggests that by proper biasing (≤ 1.7 V) of an appropriately masked Si wafer, it is possible to stop the etching of an *n*-type surface with respect to a *p*-type surface and to slow down an *n* or *p* {111} surface even more with respect to a {100} surface than can be done at open-circuit potential. A further study of how planes, edges, corners, and grooves etch under bias is under way.

etch rates are nearly zero on all samples for anodic potential because the anodic-oxide growth process begins to dominate the etching process near -0.9 V. The etch rate for cathodic bias remains nearly constant for *p*-type Si below -1.2 V and decreases rapidly for *n*-type Si. The decreased etch rate for *n*-type Si is due to the accumulation of electrons in the space-charge region near the surface of Si for cathodic bias.

Layer Growth: For anodic potential, the ellipsometry measurements reveal the growth of a graded connective or transition layer of SiO_x ($x \leq 0.4$) first, followed by the growth of SiO_2 on top of this (see Fig. 6). During growth, the connective layer evolves out of the crystal Si (c-Si) while the amorphous SiO_2 evolves out of the connective layer.

For cathodic potential, the ellipsometry measurements reveal growth of another layer of different SiO_x ($x \approx 0.8$). This growth is rapid on the *n*-type Si surface and slow on the *p*-type Si

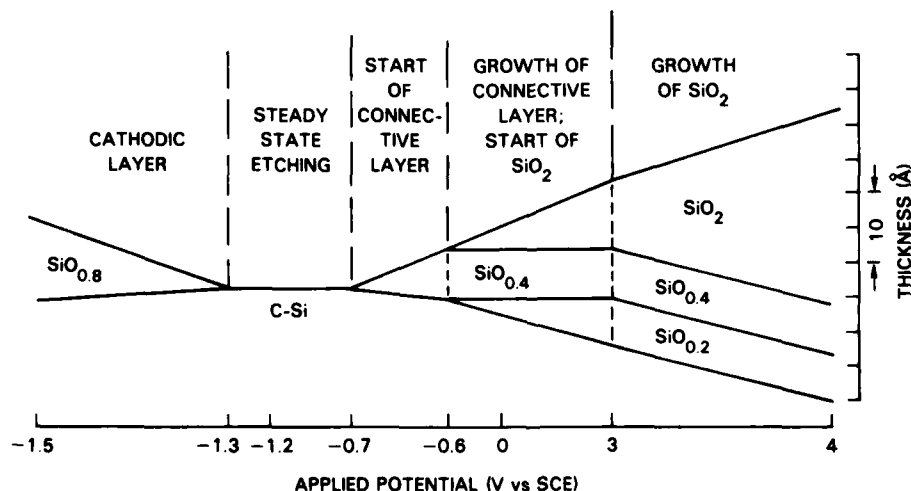


Fig. 6 — Model for growth of anodic and cathodic layers on Si as a function of applied potential. Layers of the thicknesses indicated account for the ellipsometric data.

surface. This layer is the accumulation of incomplete silicates adhering to the surface rather than dissolving. The layer builds up from the incomplete etching which slowly continues on the n -type Si surface at a rate of a few angstroms/min. In the case of the p -type Si, the layer builds up much more slowly because most of the etch products are completed silicates of the soluble form $\text{Si}(\text{OH})_2(\text{O}^-)_2$. Figure 6, a schematic diagram of the layers formed in the anodic and cathodic potential directions, is based on a model using the appropriate optical constants for the different SiO_x layers.

Doping with boron (p -type) to above 10^{19} cm^{-3} causes the open-circuit potential (-1.2 V) to shift slightly anodic to -0.7 V (because of a downward shift of the Fermi level). This induces spontaneous growth of the connective layer which passivates (protects) the surface and stops the etching. Doping with phosphorous (n -type) to above 10^{19} cm^{-3} causes the open-circuit potential to shift slightly cathodic to -1.3 V (the Fermi level shifts upward). This shift causes the cathodic layer to grow spontaneously thereby leading to a stopping of the cathodic etch of n -type Si.

Etching Mechanisms: Other measurements show that there are two H_2 molecules released for every Si dissolved, and there is an overall conservation of OH. These results indicate that etching is a sequential attack of Si-Si bonds by first H_2O and then OH^- to form the soluble silicate $\text{Si}(\text{OH})_2(\text{O}^-)_2$.

The orientation-dependence of etching then appears to be due to the ease with which H_2O and OH^- can attack the bonds between the first two molecular layers of Si on the $\{100\}$ surface. These bonds are less shielded by the outer molecular layer of Si than the corresponding bonds just below the $\{111\}$ surface, leading to a faster etch rate for the $\{100\}$ surface.

These studies give insight into the microscopic etching process and its control with applied bias, which may lead to the fabrication of sharper edges and smoother planes. At NRL, these ideas will be applied to orientation-dependent etching of the III-V compound semiconductors GaAs and InP in aqueous Cl^- and Br^- ion solutions.

Photochemical Separation of Noble Gases

T. Donohue

Optical Sciences Division

Most of the elements formed in the fissioning of uranium are radioactive, but only a small fraction of these are in the gaseous state (Fig. 7). However, these gases would be a major danger to the environment because of their widespread dispersal in the event of an accident. Gases are the most difficult of the fission products to isolate from the environment.

The majority of gases released in fission are the noble gases, xenon (Xe) and krypton (Kr). These noble gases are extremely nonreactive chemically, and the first compounds incorporating them were not synthesized until about 20 years ago. They constitute less than 0.002% of the atmosphere and hence are quite valuable, due both to their scarcity and utility. A new technique for removing the radioactive fraction in

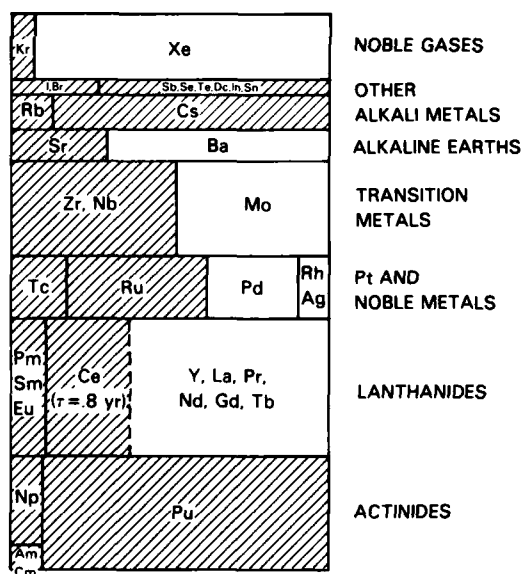


Fig. 7 — Elements formed during the fission process in a light water uranium reactor. The area of each group indicates relative amounts by mass. Shading shows those elements with one or more radioactive isotopes which require isolation from the environment. Note that only a small fraction of the gases formed are radioactive. (Adapted from a figure published by J.G. Eden, R. Burnham, L.F. Champagne, T. Donohue, and N. Djeu in *IEEE Spectrum* 16, 50 (1979).

noble gases has been developed at NRL. This process is a major improvement over current methods used in rare gas separation of fission products. Furthermore, the technique can be used to purify and concentrate these gases from the atmosphere for industrial and research applications. Therefore costs for Xe and Kr can be reduced, and our supply of these limited resources can be expanded. This research represents the first gas-phase photochemical separation of any elemental mixture.

Photochemical Method: The method we have developed uses a selective reaction for forming certain noble gas fluorides. While this process has been demonstrated chemically before, we have shown that it can be initiated photochemically. Use of photons in a separation process has significant advantages over conventional methods since photons are clean and massless. Thus such a system is simple and produces no undesirable chemicals requiring further waste disposal.

In our reaction scheme, the mixture of the rare gases is combined with fluorine (F_2) gas. Ultraviolet light from a mercury lamp, or from a rare gas-halide excimer laser, is used to photodissociate the F_2 molecules into atoms. The result-

ing F atoms then react with Xe, eventually forming XeF_2 , which precipitates as a white solid. Near room temperatures, Kr will not undergo this reaction and remains in its noble, gas-phase form. Figure 8 presents mass spectrometric data from one separation experiment in a reaction cell; this demonstrates the high efficiency of our technique. In our best results, 99.99% pure Xe has been obtained with yields exceeding 99.8% in other runs. The separation process is also effective in the presence of normally occurring atmospheric impurities, including air, water, and the nitrogen oxides.

We have also performed similar experiments in a flowing system, where the mixture of noble gases and F_2 flows past a mercury lamp with a special ultraviolet transmitting, fluorine-inert window. While yields and purities were not as favorable in experiments in this configuration, scaling up to practical size systems appears feasible. For example, a facility using a 10-kW mercury lamp could process the offgases from a typical nuclear reprocessing plant. Such a lamp is commercially available today.

Advantages: This noble gas separation method is superior to those previously considered or currently in use because it works well at near-ambient conditions; thus cryogenic temperatures and high pressures are avoided. Cryogenic temperatures increase ozone explosion and radiation hazards while high pressures tend to increase leakage problems of radioactive materials.

Application of this technique at Three Mile Island (TMI) could have reduced or eliminated the major radioactive emission, ^{85}Kr . To remove the radioactive gases from the TMI reactor, the entire gas volume was vented to the atmosphere. Since about 93% of the fission-produced gases in the reactor vessel was Xe (Fig. 7), the gas could have been run through this process which would have reduced it to about 7% of its original volume. Then it would have been feasible to package the 7% residual and safely dispose of it; this would not have been feasible for the original volume of gas.

While the photochemical process developed here can remove radioactive noble gas isotopes from the gaseous discharges of nuclear reactors or reprocessing plants, the concentration of ^{85}Kr

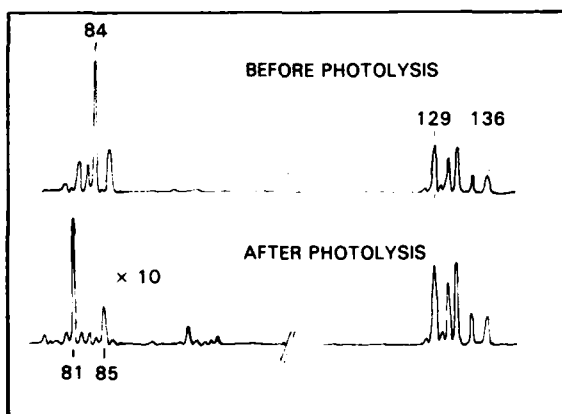


Fig. 8 — Mass spectrometric analysis of noble gas mixtures before photolysis and of the precipitate product after a photochemical separation run. The peaks in the high end (128 to 136) are from Xe, and those at the lower end (80 to 86) from Kr. The peaks at 81 and 85 in the "after photolysis" scan are from background impurities, indicating that virtually no Kr is found with the desired product Xe.

(which accounts for 7% of fission product gases) would allow less costly use of this isotope in such diverse applications as remote lighting for aircraft landing strips and crack detection in turbine blades.

We have investigated a molecular laser isotope separation (LIS) method for enriching this isotope for such applications. Thus, photochemical elemental separation combined with LIS can produce and purify elements or isotopes of both Xe and Kr in any enrichment, for both environmental considerations and commercial applications.

[Sponsored by DOE] ■

Chemically Suppressing Intermodulation Interference

J.C. Cooper and Rm. Panayappan
Chemistry Division

When high-frequency transmitters and receivers are placed in close proximity, as on ships or aircraft, nonlinear diode-like conduction [1] through metal-oxide-metal junctions (e.g., rusty bolts) in various structures generates intermodulation interference that seriously degrades or even obscures received signals. Offending structures on ships typically include lifelines, points of attachment of ladders and flagpoles, and other nonwelded metal-to-metal joints. The clamping or welding of ground straps across rusty-bolt junctions, or the replacement with nonconductive materials, can short out or remove the nonlinear junctions and thus eliminate the interference. However, these traditional solutions are structurally limited and are costly. To overcome these problems, NRL scientists have developed an inexpensive, easily applied, effective chemical approach which uses chemical bonding agents to eliminate rusty-bolt interferences.

A rusty-bolt simulator was developed by NRL and LOCUS, Inc. [2] to allow easy, reliable, laboratory measurements of the reduction of interference when candidate chemical formulations are applied to rusty-bolt junctions. This simulator accurately reproduces the shipboard

power levels, frequencies, and materials in the rusty-bolt junctions, while providing a stable and reproducible test method that permits quantitative measurements of interference suppression as a function of frequency.

Interference Reduction Techniques: The level of interference from a rusty-bolt junction can be reduced by creating a low-resistance path (or, for high frequencies, a low-reactance path) that reduces the current flow through the nonlinear junction. To provide a low-resistance or low-reactance path, several chemical formulations were developed with a polymer base to provide flexibility and environmental stability. Typical polymers include an adiprene prepolymer that polymerizes upon exposure to air (the adiprenes are commonly used flexible polymers), and polyvinylpyrrolidone (PVP), that polymerizes further by contact with metal oxides. This approach generates easily applied, low-viscosity materials that set after application to an environmentally stable material.

Interference Reduction Compounds: Conductivity is achieved by (1) chemical transformation of the metal oxide to free metal by PVP or by an added chemical reducing agent such as erythorbic acid, or by (2) incorporation of finely divided copper, silver, or other metal into the polymer. In the first method, the chemical reduction of some of the metal oxide to free metal, accompanied by the chemical bonding or chelation of polymer molecules to the remaining metal oxide, efficiently removes the metal oxide from the surfaces and incorporates it into the polymer as a conductive metal fill. This method provides a clean metal surface for bonding of the polymer. In the second method, which involves metal-filled polymers, it was found that by forming the conducting metal particles in place from metal salts rather than adding powdered metal, materials with considerably higher conductivity could be produced with lower metal contents than the commercially available materials. In the presence of chelating agents, this produces very finely divided metal with very little oxide coating, thus decreasing the net resistance of the material. The savings in materials and labor achieved by using this approach could be significant for the Navy.

Low reactance polymers for high-frequency applications were prepared by incorporating compounds with high dielectric constants. Since the formulations are homogeneous, the overall dielectric constant of the material is the weighted average of the constituents. The most successful formulations were those using adiprene-L with ethylene glycol, which, when combined with low-resistance materials, provided a combination of low resistivity and low reactance.

Some flexibility of the polymer is necessary to avoid breaking the contact during the slight flexing and bending motions common to some rusty bolts. This was achieved by adding small amounts of a plasticizer or by using a flexible polymer base such as adiprene. The effectiveness of the chelating agents depended on the type of metal oxide to be removed; therefore, the selection was based on known rates of bonding and stabilities of the chelating agent-metal complexes. The PVP itself and ethylenediaminetetraacetic acid (EDTA) were the most effective.

Laboratory Tests: Laboratory tests of the chemical bonding agents showed that intermodulation interference was reduced by more than 40 dB. Aboard ship, it is desirable to reduce the level of interference to that of normal atmospheric background noise. Figure 9 shows the typ-

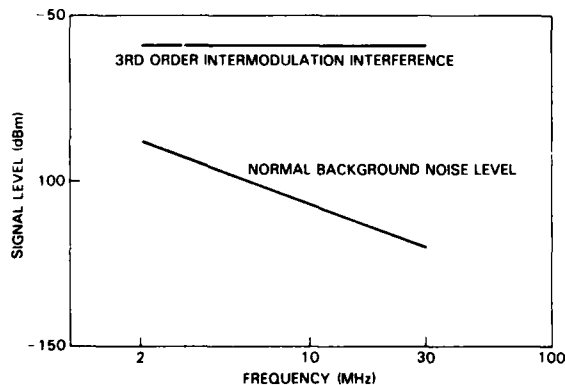


Fig. 9 — Typical shipboard third-order intermodulation interference and background noise vs frequency dependence. The excess intermodulation noise is caused by proximity of high-frequency transmitters and receivers to such common shipboard structural components as rusty bolts and other metal-oxide-metal junctions. NRL has developed techniques using chemical bonding agents to reduce this interference to background noise levels.

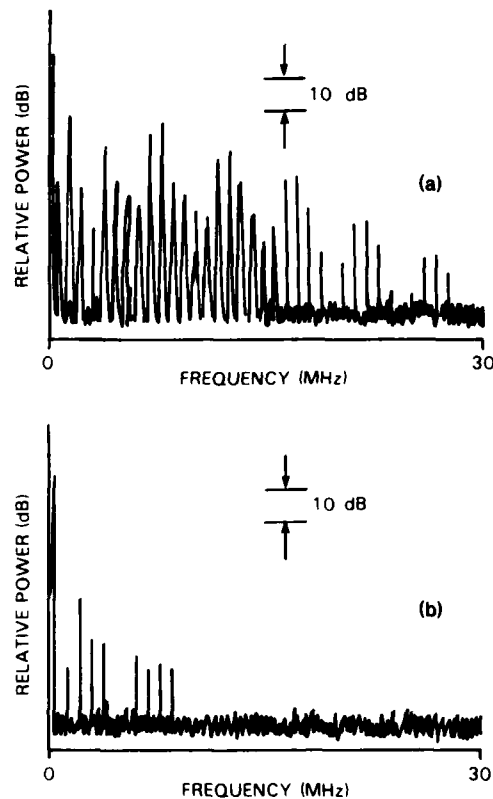


Fig. 10 — Typical results of laboratory tests of chemical bonding agents used to reduce the interference levels of a laboratory rusty bolt for 0-30 MHz. (a) shows the intensity of interference before treatment and (b) shows the reduced (by 40 dB) intensity after treatment.

ical third-order (the highest intensity) intermodulation interference and the frequency dependence of the background noise. Typical laboratory measurements of interference levels between 0 and 30 MHz for an untreated rusty bolt are shown in Fig. 10(a); and measurements for the same rusty bolt treated with a chemical bonding agent are shown in Fig. 10(b). Intermodulation interference is normally reduced by more than 40 dB.

Shipboard Tests: Shipboard tests on an untreated laboratory rusty bolt coupled to a receiving antenna under the ship's transmitting fan antenna showed power levels coupled into the rusty bolt to be close to the +25 dBm value that is used in the laboratory simulations. These results validated the laboratory measurements and

demonstrated that the chemical bonding agents could handle the power levels of 1-kW transmitters (typical of most ships). Intermodulation interference from this rusty bolt was reduced by more than 27 dB with one chemical bonding agent. Tests on shipboard rusty bolts with a standard portable receiver and its associated loop antenna showed reduction of interference for all rusty bolts identified to barely audible or below audible levels. Generally, when chemical bonding agents were tested, reduction in intermodulation interference immediately followed the application, and it remained low.

[Sponsored by NAVSEA, NAVELEX, and NOSC]

References

1. C.D. Bond, C.S. Guenzer, and C.A. Carosella, "Intermodulation Generation by Electron Tunneling through Aluminum-Oxide Films," *Proc. IEEE*, 67, (12) 1643, Dec. 1979.
2. J.C. Cooper, Rm. Panayappan, and R.C. Steele, "Chemically Suppressing Rusty-Bolt Intermodulation Interference," *IEEE Symp. EMC*, CH2035-4/84/0000-0233, Apr. 1984. ■

Coated Ceramic Fiber-Ceramic Matrix Composites

D.I. Lewis and R.W. Rice
Material Science and Technology Division

Recently, significant advances have been made in ceramic fiber-ceramic matrix composites. These composites contain ceramic fibers, typically graphite, silicon carbide, or aluminum oxide in a ceramic matrix. The successful matrix materials include glass (Pyrex and silica), glass-ceramics such as Corning Code 9608 (the material used in bakeware), and polycrystalline ceramics such as zirconium oxide. The potential for wide application of these composites is great because they offer a high temperature performance similar to that of the more common glass fiber reinforced plastics. In addition, they can combine high strength, high toughness, and fatigue resistance approaching that of the aluminum alloys at tem-

peratures as high as 1300 to 1800K. (Most polymer and metal matrix composites are usable at temperatures up to approximately 400K and 800K respectively.) However, the ceramic-ceramic composites are currently limited by processing problems such as deleterious matrix fiber reactions, strong matrix-fiber bonding, and susceptibility of the fibers to deterioration in aggressive environments as, for example, oxidation of graphite fibers. These problems are exacerbated by the high processing temperatures (up to 1800K) required to consolidate the composites and by the anticipated high service temperatures (1300 to 1800K).

Performance of Coated Fiber Composites:

Research at NRL has shown that a proprietary fiber coating technique can be used to alleviate these problems. Figures 11 and 12 compare results from experiments on two composite systems and indicate that coatings dramatically improve both strength and toughness. Coated aluminum oxide (Al_2O_3) fibers have more than twice the strength (maximum stress) and four times the fracture resistance (area under the curve) compared to uncoated fibers (Fig. 11). More dramatically, coated silicon carbide (SiC) fibers in a silica glass matrix have nearly four times the strength and 400 times the fracture resistance as uncoated fibers (Fig. 12).

Bonding and Oxidation Control: The technique used to coat the fibers prior to incorporating them into composites and similar techniques under development at NRL should permit the combination of a variety of ceramic matrix materials with a variety of ceramic fibers that have formerly been precluded by fiber-matrix reaction problems. The coating technique also permits the independent control of the degree of interfacial bonding (between fiber and matrix) in ceramic-ceramic composites. The control of interfacial bonding is critical to attain optimum combination of strength and toughness in these composites. Coating techniques may provide the only means for controlling the degree of bonding independently of the choice of matrix, fiber, and processing conditions. Also, the coating can potentially increase the oxidation resistance of the ceramic fibers, thus alleviating one of the more

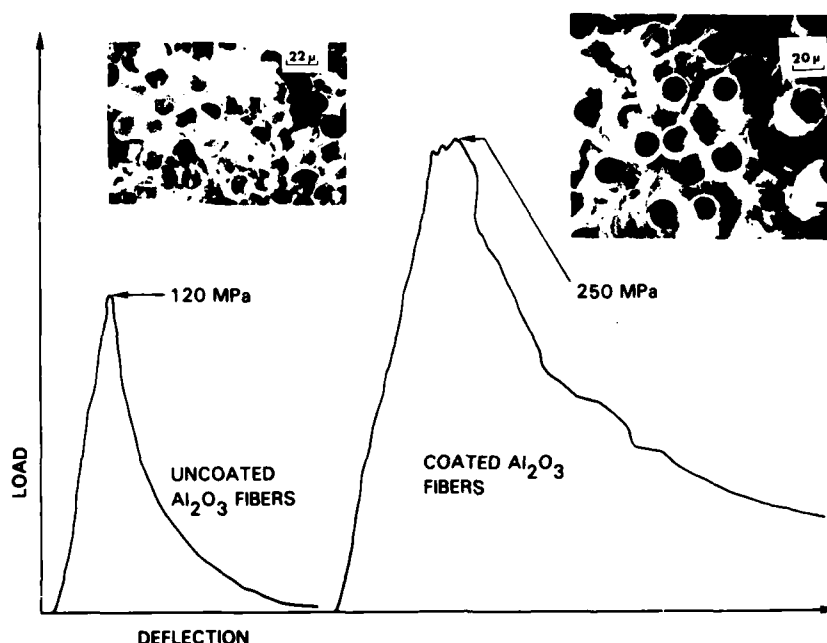


Fig. 11 — Composites prepared with coated aluminum oxide (Al_2O_3) fibers in a silicon-oxygen-carbon matrix obtained by polymer pyrolysis show more than twice the strength (maximum load) and four times the fracture resistance (area under curve) of similar composites prepared with uncoated fibers (7 MPa = 1000 psi). Microphotographs of both coated (R) and uncoated fibers (L) are shown.

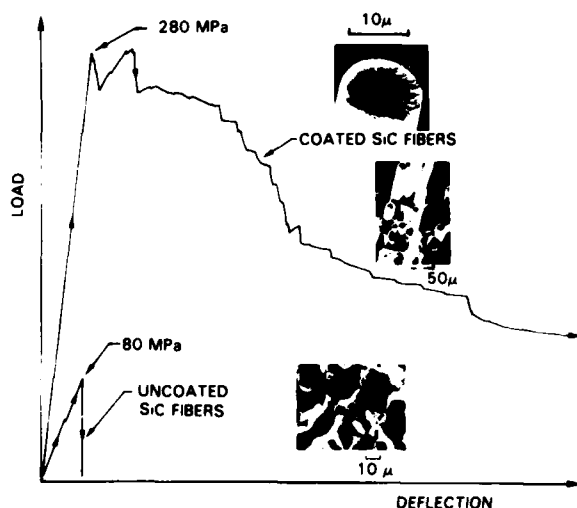


Fig. 12 — Composites made with silica glass (SiO_2) matrix and coated silicon carbide (SiC) fibers show an almost fourfold increase in strength (maximum) and a 400-fold increase in fracture resistance (area under curve) over that obtained with uncoated fibers (7 MPa = 1000 psi).

critical problems in the high temperature applications of these materials. Both the graphite and the silicon carbide fibers now widely used in composites can rapidly degrade at temperatures over 1000K because of oxidation. Because the ceramic matrices normally crack during use (not causing catastrophic failure however), the matrix materials do not provide the necessary antioxidation protection to the fibers. Coating not only increases the oxidation resistance of the fibers, but makes these composites usable in applications such as advanced heat engines. The coating technique also promises the means by which the fibers can be protected from hostile environments.

This coating technique supplies the freedom to choose among a variety of combinations of matrix and fiber materials. Moreover, the coating technique, besides adding oxidation resistance, enables us to tailor the fiber-matrix interface and

to establish a controlled degree of binding that is critical to the production of strong and tough ceramic-ceramic composites. Current research at NRL is directed toward more detailed evaluation of the results of the fiber coating technique, and the application of this technique to a wide variety of matrix-fiber combinations. Success with fiber coating will greatly increase the applicability of ceramic-ceramic composites and will accelerate and diversify the use of these very promising new materials.

[Sponsored by ONR and NAVAIR] ■

Metal Matrix Composites by Physical Vapor Deposition

S.C. Sanday

Material Science and Technology Division

Specialized materials and creative design are both necessary to improve the performance of, and indeed often to make feasible, advanced airborne and space structures. In recent years, composites consisting of fibers imbedded in a matrix material have produced remarkable new structural materials. Low mass-density metal matrix composite materials have the potential to satisfy many of the design requirements of space-age structures because of their high stiffness, strength, and dimensional stability. However, understanding how to control the factors that determine material response to complex loads and operating environments is the key to optimizing the behavior of metal matrix composite materials.

For most composites, material properties are determined by the choice of fiber and matrix materials, as well as the volume fraction, morphology, size, spatial distribution, and orientation of the fibers. Appropriate choices, though frequently limited by availability of materials, often produce composites that attain a very high percentage of their potential material properties. However, in metal matrix composites, the complex physical and chemical interactions between matrix and fibers are usually strong enough to prevent the realization of expected properties. At NRL, recent research on continuous-fiber reinforced metals has focused on developing a process to control the critical factors, such as

matrix/fiber interactions or fiber spatial distribution, that affect composite properties.

Composite Forming Process and Its Advantages: The process chosen for development of metal matrix composite materials consists of sequentially coating an array of reinforcing fibers by physical vapor deposition of several selected materials to produce composite "precursors." These precursors are then plied and subsequently pressed into the desired shape at elevated temperature. The few complexities inherent to the process are far outweighed by the benefits. The most attractive benefits of the process are its versatility and the capability it provides to control manufacturing parameters critical to composite materials properties. This precise control of most of the critical parameters involved, complemented by a combination of chemical and physical microanalyses, and mechanical and thermal response measurements, is used to understand phenomena affecting composite properties.

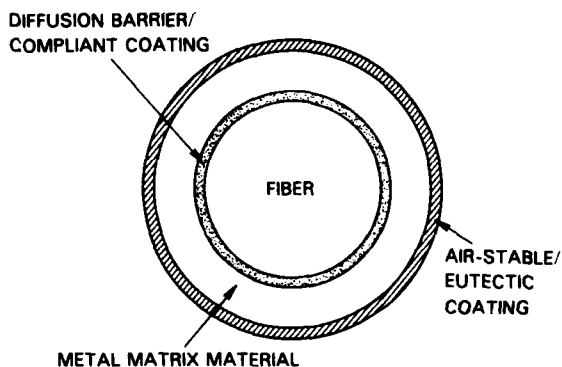
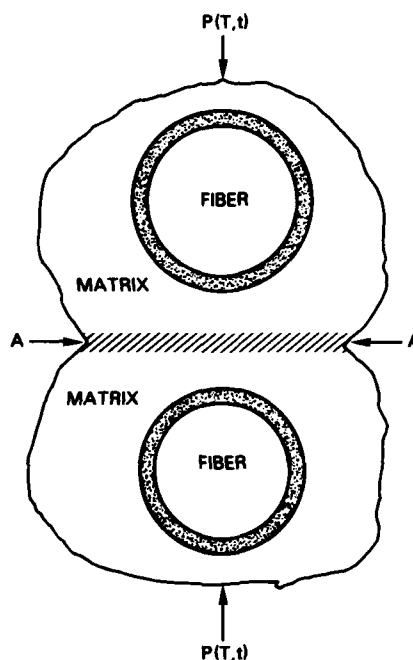


Fig. 13 — Sequential physical vapor deposition onto fibers. Diffusion barriers control reactions between fiber and matrix materials while air-stable coatings inhibit matrix oxidation.

The factors that ultimately determine the composite properties are controlled through sequential deposition of several uniform coatings of different thicknesses and materials onto the fibers, shown schematically in Fig. 13. The first coating can be chosen to produce a diffusion barrier which controls reactions between the fiber and matrix, or it may be a compliant coating

Fig. 14 — Consolidation by transient liquid phase diffusion bonding. During consolidation, the eutectic-forming coating produces a transient liquid phase and diffuses into the matrix material (A-A).



which accommodates differential thermal strains at the matrix/fiber interfacial zone; ideally both functions could be fulfilled by a single coating. The thickness of matrix material deposited on this coated fiber determines the fiber volume fraction, while the type of fiber and matrix, and the bonding strength of the interfaces between the fibers, coatings, and matrix material, partially control the mechanical and thermal properties. Further control of the mechanical and thermal properties of the composite is achieved by depositing thin air-stable or, when feasible, eutectic-forming coatings on the matrix material. The air-stable coatings prevent the formation of hard matrix oxides which inhibit good solid state diffusion bonding between matrix-matrix interfaces in the composite pressing process. This reduces the pressure needed to form the composite. The eutectic-forming coatings promote transient liquid phase diffusion bonding, schematically shown in Fig. 14, which reduces both the consolidation pressure and temperature.

Application to Graphite-Aluminum Composite: An example illustrates the versatility available in both the development and fabrication processes. For a composite reinforced with a

given volume fraction of parallel fibers, the tensile strength in the direction transverse to the fibers is determined by the transverse tensile strengths of the fiber, the matrix, the matrix/fiber interface, and the matrix/matrix interface. Fractographic studies in graphite-fiber-reinforced aluminum reveal that failure originates at the matrix/fiber interfacial zone, which is usually a hard, brittle aluminum carbide, or at the matrix/matrix interfacial zone, which is usually a hard, brittle aluminum oxide. The diffusion barrier material, to be most effective in reducing carbide formation, should diffuse as little as possible into the aluminum during the composite forming process. Niobium, vanadium, and the lanthanide series elements have been identified as good candidate diffusion barrier materials because of their short diffusion lengths into aluminum.

Figure 15 shows these elements to have very short diffusion lengths into aluminum during the 10-min exposures that are typical of the composite consolidation processes. To reduce oxide formation, which results from exposure of the aluminum matrix to air, copper coatings are used. Copper, however, as well as the other elements indicated in the upper portion of Fig. 15, is also a good eutectic-forming element with aluminum.

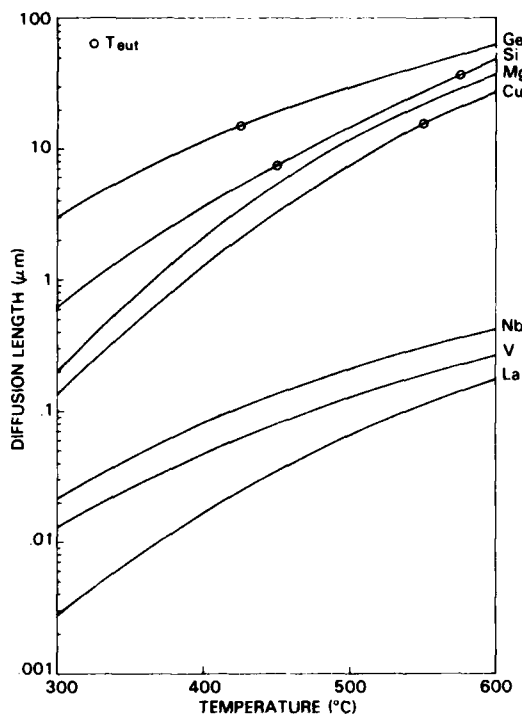


Fig. 15 — Diffusion lengths of various elements into aluminum after 10 min as function of temperature. Niobium (Nb), vanadium (V), and the lanthanide series elements (La) are candidate diffusion barriers between aluminum and graphite. Silicon (Si), copper (Cu), magnesium (Mg), and germanium (Ge) are candidate eutectic-forming elements for transient liquid phase bonding of aluminum matrices.

The large diffusion length into aluminum near the eutectic temperature (T_{eut}), which is well below the temperature needed for solid-state diffusion bonding, makes it a good candidate for matrix coatings. Indeed, transient liquid phase bonding of 6061 aluminum, using copper as the eutectic-forming element, has produced bonding shear strengths as high as 75% of the base metal strength and creep rates significantly higher than those of the base metal. Subsequently, copper-coated aluminum/graphite precursors have been fully consolidated at 560°C (1040°F) and at a pressure less than 3.5 MPa (500 psi), which is approximately an order of magnitude less pressure than that needed for solid-state diffusion bonding. Since no fiber damage has been noted, this has far-reaching implications for the consolidation process: low-pressure processes such as hot-roll bonding and hot-die strip drawing be-

come practical candidates for continuous consolidation.

Substantial progress has been made toward understanding and controlling critical property-determining factors in metal matrix composites. Understanding the complex phenomena observed during the integration of continuous graphite fibers and aluminum matrices has already resulted in substantial improvements in the mechanical properties of graphite fiber reinforced aluminum. The techniques described are generic and will have a significant impact on improving the response of many metal matrix composite systems to specific combinations of manufacturing conditions and in-service monotonic and cyclic mechanical and thermal loads.

[Sponsored by ONR]

Performance of Nonskid Deck Coatings

L.W. Kraft and R.F. Brady, Jr.
Chemistry Division

Flight and hangar decks of aircraft carriers and helicopter operating areas of air-capable ships, are covered with coarse-textured coatings which provide traction to men, aircraft, and machinery. Current Navy coatings are two-component epoxies or polyurethanes with a coarse aggregate added to impart slip resistance. Two types of aggregate are used, depending on the location of the coating. A nonabrasive aggregate (e.g. aluminum metal) is used for carrier landing areas so as not to abrade the arresting gear cables (Fig. 16). In all other applications, an abrasive aggregate (e.g. silicon carbide or aluminum oxide) is used.

Reports of unsatisfactory performance of nonskid coatings increased during the early years of this decade. Operating forces reported a short service life (less than six months) and a tendency for the coatings to detach in large (1/2-inch) chips that damaged aircraft engines internally, when sucked into the intakes. A wide variation in nonskid performance was also noted. Tasked by the Naval Sea Systems Command, NRL is developing improved nonskid coatings to be used by the Navy for a variety of purposes; NRL is also testing commercial coatings that are currently



P-2050(14)

Fig. 16 — Navy jet landing on carrier deck. The arresting gear cable used to stop the plane imparts severe wear on the nonskid coating when dragged across the deck.

in use. Complaints from the fleet that can be traced to faulty coatings have greatly decreased since this testing began.

The proper performance of a nonskid coating is critically dependent on its resistance to sliding and on its ability to withstand the external stresses of impact and wear. For safety and cost effectiveness, these properties must be retained over a significantly longer service life. The first step in developing improved coatings is to establish performance characteristics and tests for these characteristics that may be used to predict shipboard performance.

Slip-Resistance Testing: The Naval Ship Systems Engineering Station (NAVSSSES), located in Philadelphia, conceived a new test for slip resistance that the NRL investigators have used as the basis for the development of a standard test for slip resistance of nonskid coatings. With statistically designed experiments, we have determined the optimum conditions necessary for the test to provide relatively error-free, reproducible results. This test uses a $4 \times 5 \times 1$ -in. steel sled (covered on the sliding side with neoprene) that is pulled at a steady rate across the coated surface of the simulated deck (Fig. 17a). A digital force gauge measures the drag due to friction on the sled. The test is run on dry, wet, or oily nonskid surfaces. NRL standardized the NAVSSSES test concept by evaluating all important testing conditions. The factors considered include rubber hardness and angle of the leading edge (either 45° or 90°) to the surface, the type of sled surface (rubber, corrugated steel, stair tread), and the

speed and direction of pull across the coating. (Direction is important since many coatings have anisotropic friction characteristics which are due to coating application procedures.) This test is superior to others because of reduced error and the use of a larger, more realistic experimental area than was used in older tests. Based on these improvements, NRL is designing a portable, battery-operated tester for shipboard use.

Wear Testing: To predict the service life of the nonskid coating, a practical method of imparting reproducible wear was needed. NRL has developed a test apparatus (Fig. 17b) that

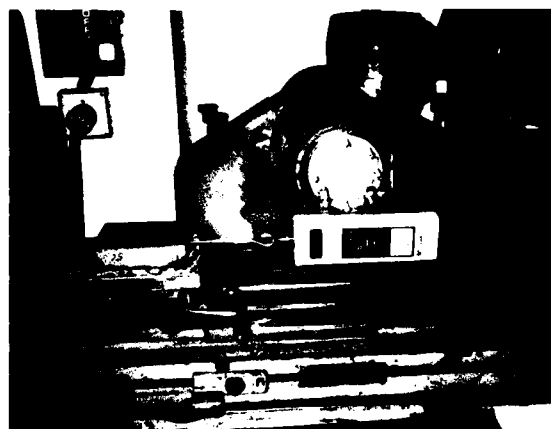


Fig. 17a — A standard rubber-covered sled is drawn across a sample of nonskid coating to measure its slip resisting properties. The coating is a light-colored, mottled surface.

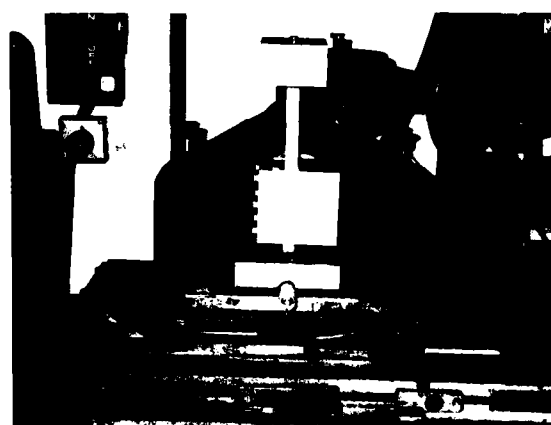


Fig. 17b — A sample nonskid coating undergoing wear testing. The sample is oscillated horizontally against a horizontal 1/8-in. diameter steel wire.

realistically and accurately evaluates the rapid wear of a nonskid coating sample under laboratory conditions. Before this test was developed, wear was evaluated on a very small sample which made it difficult to measure performance properties such as slip-resistance on worn panels. The new wear-test apparatus eliminates this problem by wearing a larger sample, and it has enabled us to characterize the slip resistance of nonskid coatings as a function of the extent of wear. This is done by interrupting the wear test in progress to evaluate the slip resistance with the new NRL-developed slip resistance tester. We have subsequently used this wear-test apparatus to evaluate the effect of the coating application method (e.g., spraying vs rolling) on wear, and we are cooperating with NAVSSES to correlate results obtained from the use of this wear tester with shipboard service life.

Impact Testing: The Navy's requirements for impact resistance of nonskid coatings are very stringent. The test is performed by dropping a 2-lb steel ball from a height of 8 ft onto a $6 \times 6 \times 1/8$ -in. well-supported panel coated with nonskid. The test requires 25 impacts, $3/4$ -in. apart, in a 5×5 pattern (Fig. 18). NRL has used statistically designed experiments to determine the optimum conditions of application and curing of the coating to improve this important property and to improve reproducibility.

Development of MILSPEC: In addition to these major performance tests, all other tests for nonskids have been evaluated and modified for

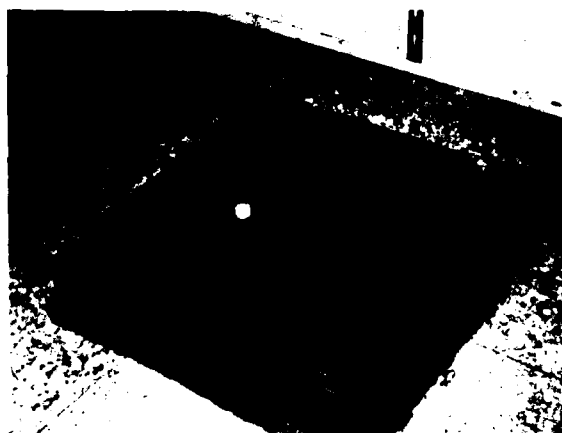
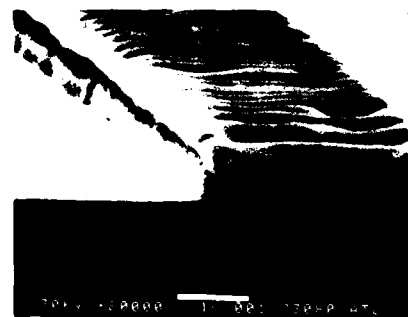
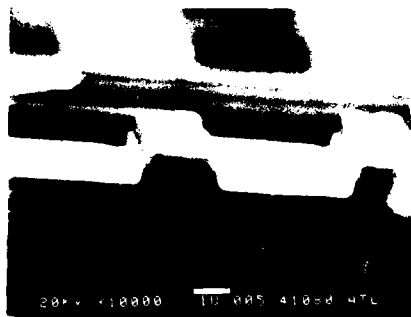


Fig. 18 — An impact sample showing the 2-lb steel ball used for the test sequence of 25 impacts. The sample is supported by a $2\frac{1}{2}$ -in. thick steel plate.

reproducibility, accuracy, and practicability. NRL has incorporated the results of this work into a Military Specification (MILSPEC) for nonskid deck coatings to be published by NAVSEA. This document fully and accurately defines the performance requirements and methods of evaluation of nonskids. It will allow the Navy to purchase more consistent, higher quality coatings, thus reducing the frequency of costly recoating and aircraft engine repairs. We are now formulating new nonskid coatings of enhanced performance and durability for the Fleet, and we are using the test methods which we have developed as a basis for evaluating these coatings.

[Sponsored by NAVSEA] ■



Microphotographs of different etches used in the production of microcircuit components. The horizontal white bar represents 1 μm . Top to bottom: parallel plate plasma etch, anisotropic etch of silicon, and a wet chemical etch. See related article on 154.

Materials analysis and properties



171 Electron Structure of Alloys

Louis M. Pecora and Alexander C. Ehrlich

Positron annihilation reveals structure of copper alloys.

173 Molecular Structure Analysis of Dense Energetic Materials

Richard D. Gilardi

X-ray and electron diffraction map three-dimensional cage structures.

174 The Phosphorus Antisite in Indium Phosphide

Neal D. Wilsey and Thomas A. Kennedy

A new native defect is identified in this important semiconductor.

176 Superconducting Molybdenum Nitride: Theory and Experiment

Larry L. Boyer, Wendy W. Fuller, Donald U. Gubser, Ken E. Kihlstrom,

Barry M. Klein, Dimitrios A. Papaconstantopoulos, Warren E. Pickett,

Syed B. Qadri, Earl F. Skelton, and Stuart A. Wolf

Molybdenum nitride in the proper structure has a critical temperature around 30 K.

178 Ultrasonic Gas Atomization for Ultrafine Metal Powders

Iver E. Anderson, Jack D. Ayers, Wayne P. Robey, and Ronald G. Hughes

New gas-flow techniques increase yields of ultrafine powders.

180 Mechanical Response of Laser-Irradiated Panels

Chine I. Chang and Fred R. Stoneseifer

Ultrarapid heating makes the panels seem stronger under fracture.

183 A Comparison of Two Theories of Acoustoelasticity

Alfred V. Clark and Richard B. Mignogna

An anisotropic theory of higher order stress results.

MATERIALS ANALYSIS

New chemicals, materials, and material composites are continually being developed. The way these products are used can only be determined after their composition and physical properties are well known. Determination of these characteristics often requires varied techniques; in some cases new techniques must be developed to make suitable measurements. Materials analysis and properties is so closely related to materials modification and behavior that most articles in these two sections could be properly included in either section.

The eight papers deal with sophisticated analysis techniques, properties of semiconductors, production of ultrafine particles, and material properties under various stresses.

The work in this section was done in five NRL Divisions: Marine Technology (Code 5800), Laboratory for Structure of Matter (Code 6030), Material Science and Technology (Code 6300), Condensed Matter and Radiation Sciences (Code 6600), and Electronics Technology (Code 6800).

Some other NRL research in materials analysis and properties not described in this section includes

- structure determination of macromolecules by using anomalous X-ray dispersion,
- nondestructive evaluation of composites,
- three-dimensional magnetic resonance imaging of solids, and
- elastoplastic fracture criteria and evaluation.

Page 168, clockwise from upper left:

Two 2-dimensional distributions of the momentum vectors for electrons in a model of pure copper (*left*) and a copper-germanium alloy ($\text{Cu}_{92}\text{Ge}_8$) (*right*). See article on p. 171 by L. Pecora.

Tin alloy powders produced by high-pressure gas atomization at NRL. The micrographs reveal the ultrafine size and spherical shape of the powder particles. See article on p. 178 by I. Anderson.

Three-dimensional molecular structure of the energetic cage compound 1, 3, 5, 7-tetranitro-adamantane. This structure was determined by analyzing the X-ray diffraction from a single crystal of the pure material. The atoms which are labelled with numbers only are the carbon atoms of the "cage" backbone of this organic molecule. See article on p. 173 by R. Gilardi.

Electron Structure of Alloys

L.M. Pecora and A.C. Ehrlich

Condensed Matter and Radiation Sciences Division

Knowledge of the motion and energy states of the electrons in a material enables one to determine many of the material's electrical, thermal, and optical properties. An understanding of the origin of the motions and energy states is thus paramount to modifying these material properties for Navy needs.

To some extent the electronic properties of pure and low concentration alloys are understood, but alloys with high concentrations (>5%) of elements are poorly understood. This poor understanding persists even though high-concentration alloys constitute the majority of metallic materials used in engineering and applied science technologies. These alloys remain the least studied of metallic materials because of the stochastic nature of the electronic motion which discourages the use of standard analysis methods, however, a few methods which do employ electronic interactions at single points in the material are suitable for studying concentrated alloys.

Positron Annihilation Technique: One such method is angular correlation of positron annihilation radiation which does *not* require long electron paths and therefore is not greatly affected by the stochastic motion. An irradiated alloy sample is used which emits positrons. The annihilation process takes place at a point: An emitted positron annihilates an electron and generally generates two gamma rays in place of the original electron-positron pair. The gamma rays separate at an angle which conserves the momentum of the original electron-positron pair. The simultaneous detection of these two emerging gamma rays and their corresponding angular distribution yields information on the momentum distribution of electrons in the solid (i.e. the number of electrons with a given value of momentum). This leads to basic knowledge of physical quantities associated with electronic momentum and electronic band structure (energy states).

The annihilation experiment is carried out by irradiating a single crystal copper (Cu) alloy

sample using the National Bureau of Standards nuclear reactor. The irradiation activates some Cu atoms which emit positrons. The sample is then returned to a rotating stage in a hot cell in NRL's High-Level Radiation Laboratory. On either side of the sample, two detectors count coincidentally emitted gamma rays as a function of emitted angle at various preset angles. This technique provides a set of count rates that are proportional to the momentum distribution of the electrons in the sample. Because the sample is a single crystal and is oriented with respect to the detectors, we probe only certain planes of momentum space variables in each experimental run. Several alloys of Cu and germanium (Ge) and Cu and zinc were studied with this method.

Results and Significance: In general, momentum distributions involve the three components p_x , p_y , and p_z . For this work, two-dimensional (2-D) distributions were obtained due to the nature of the experimental apparatus. Figure 1 shows a 2-D momentum distribution obtained from the (110) plane of pure crystalline Cu. The central *peak* is the main component of the momentum distribution of Cu which is centered at the origin. The steep falloff in this peak comes about because the electronic energy states which conduct electricity in Cu suddenly become empty at higher momentum values. The set of electronic states at which this falloff occurs generates a surface in momentum space—the well-known and often studied Fermi surface. Its shape influences the electrical and thermal properties of the material. Figure 1 yields information on the intersection of the Fermi surface with planes in momentum space; thus angular correlation positron annihilation experiments reveal important information on electronic band structure, or energy states. We used our momentum distributions to calculate the Fermi surfaces in certain crystal planes of CuGe alloys. Figure 2 shows the projection of several Fermi surfaces on the p'_x , p'_z plane for various Ge concentrations in Cu. The hatched region defines the edges of Brillouin zones. The coordinates of p'_x and p'_z , which transform into p_x and p_z , are related to electronic energy levels. Several subtle changes in the Fermi surfaces result from changes in electron

Fig. 1 — The momentum distribution of electrons in the (110) plane of Cu as determined by positron annihilation is plotted in a momentum space plane. The unnormalized probability of finding an electron with a certain value of momentum is $\rho(p)$.

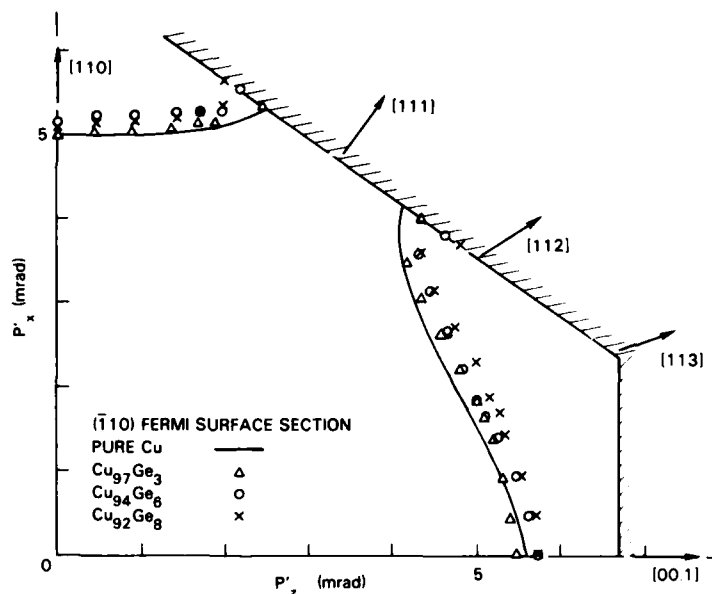
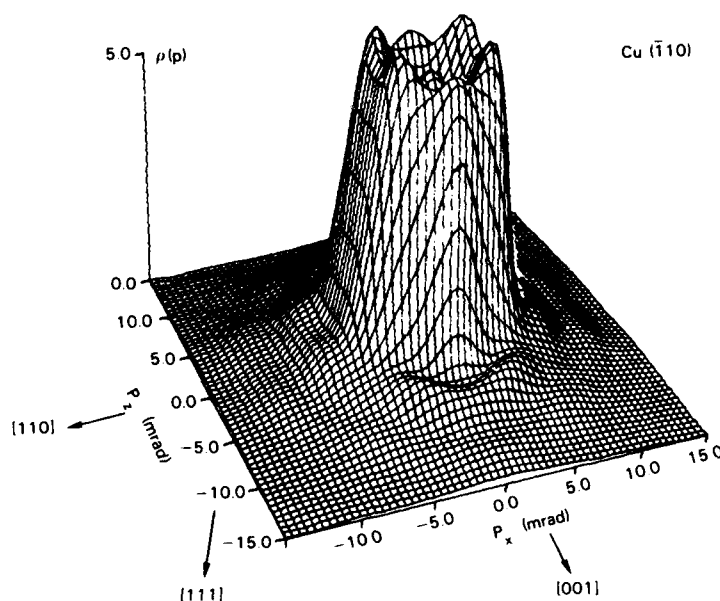


Fig. 2 — The Fermi surface for the CuGe face-centered cubic alloys in a plane is plotted to show the nonuniform growth of the surface with increasing Ge concentration. Note the change in shape of the Fermi surface near $p'_z = 5$ mrad as the Ge concentration increases from 0 to 3%. These electrons on the Fermi surface determine the electrical and the thermal properties of the alloy. The hatched region defines the edges of Brillouin zones. The coordinates p'_x and p'_z which transforms into p_x and p_z of Fig. 1, are related to energy levels.

energy states in the alloy as the Ge concentration increases.

Figure 1 shows that there is structure further out in the momentum distribution beyond the central peak (at momentum values ≥ 7 mrad). This represents processes which are higher frequency parts of the momentum distribution. We developed an analysis scheme which

can extract information from certain outlying regions of the momentum distribution and thereby delineate the actual electronic population of the energy states in these alloys. We found that in the region beyond the Fermi surface, the nature of the d-like energy states was changing as Ge was added to Cu. The "s" states were intermixing with "d" states, and the amount of this

intermixing increased monotonically with Ge concentration. This was the first time such *direct* evidence for energy state changes has been detected in alloys. These fundamental electronic structure changes must be explained by sophisticated computational methods; in particular, reproduction of these electronic effects remains a critical test for any energy state structure calculation. Since these energy states are directly related to bonding in these materials, the information on state changes gained by the positron annihilation technique relates to changes in chemical properties as alloys are fabricated.

These results demonstrate that positron annihilation is a sensitive and valuable probe for studying the electronic structure of concentrated alloys. In fact, it remains one of the few experimental tools available for studying these materials. We have also shown that much more information can be extracted from the momentum density studies than was previously realized, especially in relationship to fundamental electronic properties and structure on the atomic level.

[Sponsored by ONR] ■

Molecular Structure Analysis of Dense Energetic Materials

R. Gilardi

Laboratory for the Structure of Matter

NRL scientists are analyzing the molecular structures of a large number of new, dense, energetic compounds by using electron and X-ray diffraction experiments. These compounds have been synthesized by ONR-sponsored chemists in a program that is seeking ways to make new types of high-density propellant materials. The results of the diffraction experiments are not only being used to facilitate the synthesis of new materials by using structural information from existing substances, but they are used to "calibrate" a general molecular mechanics program that can predict the possibility of synthesizing new compounds, their structures, and their energetics.

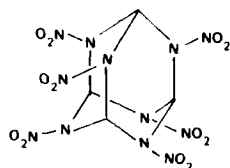
Energetic Materials: Solid propellants are often complex mixtures of several compounds.

However, the major component is usually a high-energy compound that, if pure, would be an explosive. In a propellant mixture, the other propellant components separate the explosive particles and enable a controlled or slowed release of energy. Some of the most effective high-energy compounds in use today as explosives or propellant components are organic nitro compounds. Most organic compounds have densities to 1.5 g cm^{-3} , however, high-energy compounds have significantly greater densities of 1.65 to 1.94 g cm^{-3} . Empirical evidence suggests that the detonation pressure developed by an explosive depends not only upon the number of energetic groups it contains, but also upon the square of the density of the pure material. When an actual device such as a missile is designed, additional benefits such as increased range are often derived from the use of dense materials in the propellant formulation. Thus, many researchers in this area have proposed methods for extrapolating properties of unknown compounds such as density and detonation pressure from properties of known compounds. By using these empirical structure-activity relationships, new classes of materials can be hypothesized that will be equally energetic and will also form super-dense organic solids.

Cage Compounds: One such class of compounds is formed by substituting energetic nitro NO_2 groups for the hydrogen atoms in molecules known as "cage compounds." In these molecules, rings of carbon atoms are connected to other rings so as to create a three-dimensional cage. Two highly nitrated hypothetical cages are illustrated in Fig. 3. Many nonenergetic cage compounds have been synthesized, so the unsubstituted carbon atom frameworks are well known. It is difficult to modify these frameworks, once they have been made; however, in the past five years, many new synthetic pathways have been discovered that have led to a number of new cage compounds with more and more energetic groups substituted for hydrogen atoms about the exterior of the molecule.

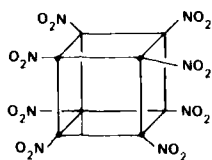
Examples of New Structures: In the course of this research, ONR-sponsored chemists have produced many new and unusual compounds. NRL's X-ray diffraction program has provided the

HEXANITROHEXA-AZA-ADAMANTANE



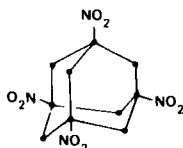
PREDICTED DENSITY =
2.1-2.2 g/cc

OCTANITROCUBANE

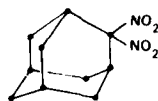


PREDICTED DENSITY =
2.0-2.1 g/cc

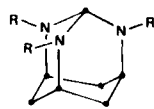
Fig. 3 — Hypothetical (proposed) target materials



1,3,5,7-TETRANITROADAMANTANE



2,2-DINITROADAMANTANE

2,8,9-TRIBENZYL-
2,8,9-TRIAZA-ADAMANTANE

TETRANITRO-BIS-HOMOCUBANE

Fig. 4 — New molecules obtained from DoD energetic synthesis programs; molecular structures were derived at NRL by X-ray diffraction analyses (● is carbon, and R is an unspecified radical).

three-dimensional (3-D) structures of more than a dozen of the new molecules that have been synthesized. Several of these molecules are schematically shown in Fig. 4. Besides corroborating the structural formulas, the study of these structures has permitted the characterization of the 3-D structures of large groups of atoms which occur repeatedly in known energetic materials and also in the proposed target materials. NRL is using this information to calibrate the parameters in a molecular mechanics computer program that can computationally synthesize candidate energetic materials and predict their molecular structures and their strain energies, (i.e., potential energies stored in a molecule in which the bonding forces cause crowding despite electrostatic repulsion). The program is currently being applied to study the structures of hypothetical (i.e., proposed, but not yet synthesized) polynitroadamantanes and polynitrocubanes (such as are shown in Fig. 3).

The calculations will improve the capability to predict molecular shape, strain, and crystal density for newly proposed compounds.

[Sponsored by ONR]

The Phosphorus Antisite in Indium Phosphide

N.D. Wilsey and T.A. Kennedy
Electronics Technology Division

Indium phosphide (InP) is an interesting compound that holds promise of important optoelectronic and microwave/mm-wave applications in future military systems. As part of an evaluation of InP for device applications at NRL, its vulnerability to radiation is being determined. Important in such a determination is an understanding of the defects that arise upon irradiation.

Defect Types: When high energy particles, such as electrons or neutrons, bombard crystals, atoms are displaced from their normal lattice sites. In elemental semiconductors, such as silicon and germanium, there are two types of intrinsic point defects which are formed by radiation. These are vacancies (atoms missing from normal lattice positions) and interstitials (atoms at nonlattice positions). Compound semiconductors offer a greater variety of intrinsic defects. The III-V semiconductors (composed of elements in the 3rd and 5th columns of the Periodic Table) can have two kinds of vacancies and two species of interstitial atoms. In addition to these, there is the possibility of two different kinds of defects (called antisites). For example, a group V atom could be on a group III lattice site, or a group III atom could be on a group V site. Figure 5 illustrates the phosphorus antisite in InP, where a phosphorus atom is in a position normally occupied by an indium atom. These antisites (or wrong site defects) can trap electrons or holes and degrade the performance of semiconductor devices.

Defects and EPR: Among the fundamental properties of defects in semiconductors are the

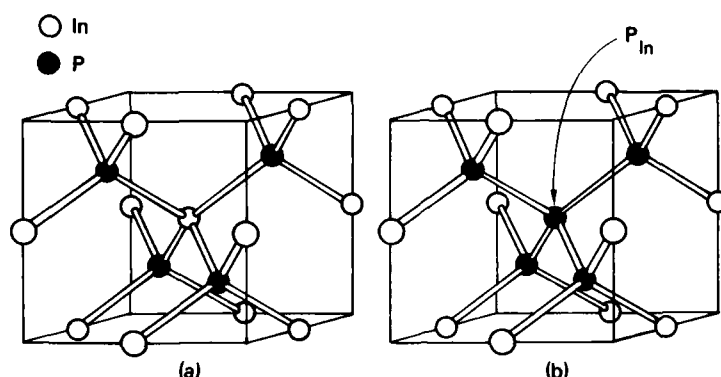


Fig. 5 — Indium phosphide perfect lattice (a) showing each indium at the center of a tetrahedron and covalently bonded to four neighboring phosphorus atoms and (b) an antisite defect in which a phosphorus atom is on an indium site

identity of the defect, the details of the lattice structure around the defect, the electronic charge associated with the defect, and the way it interacts with charge carriers. The structural information about vacancies and interstitials has been investigated in some detail for the most widely used semiconductor, silicon. Defects often have electrons which are not paired off (in electron spin) in covalent bonding as in the perfect lattice. Electron paramagnetic resonance (EPR), the resonant absorption between spin states of unpaired electrons, has been used effectively at NRL to obtain structural information. It is more difficult to use EPR to investigate III-V semiconductors, however, because the resonant lines are broad due to interactions between electron spins and high nuclear spins of the group III and group V atoms.

EPR Measurements and Interpretation: InP was irradiated at room temperature with 2 MeV electrons and measured at 12 K with an EPR spectrometer (see Fig. 6). The EPR spectrum after irradiation did not differ substantially from that of the unirradiated sample. However, when the sample was illuminated with near infrared light (1000 nm), the spectrum of Fig. 6(a) changed to that of Fig. 6(b). The difference between the two spectra (Fig. 6(c)) shows two broad resonance lines at A and B. Several conclusions can be drawn from these data. Since the two lines are not observed before infrared irradiation, the normal state of the defect does not have an unpaired electron. The illumination process

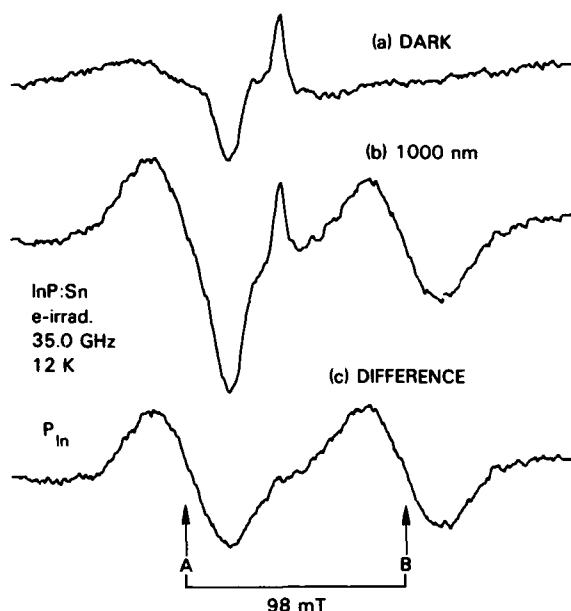


Fig. 6 — EPR derivative signal vs magnetic field for electron-irradiated InP (a) with the sample in the dark and (b) after illumination with 1000 nm light. Spectrum (c) is the difference between (b) and (a) and shows two lines A and B separated by a magnetic field of 98 mT.

changes the charge state of the defect and renders it paramagnetic. The splitting of the paramagnetic resonance into two lines is typical of the interaction of electrons with a nucleus having a spin of $1/2$. Since natural phosphorus only contains the isotope P with nuclear spin $1/2$, the defect is most likely centered on a phosphorus atom. If the phosphorus were in its normal lattice site, then all of its electrons would be

covalently bonded and hence would not produce an EPR signal. Crystal orientation experiments show that the center has tetrahedral symmetry, giving evidence that the phosphorus atom occupies either an indium site or a tetrahedral interstitial site in the lattice. The magnitude of the line splitting rules out the latter possibility. Therefore, the defect is an antisite, a P atom on an In site, surrounded by four P atoms as illustrated in Fig. 5(b).

Models for Antisite Formation: This antisite defect is observed only after irradiation. This contrasts with GaP [1] and GaAs [2] for which antisites have been observed in the material as it is grown (without irradiation). Studies of EPR signal strength as a function of fluence (number of incident particles—in this case, electrons—per unit area) indicate that the antisites are radiation-induced. Several mechanisms have been proposed to explain how irradiation can produce antisites. The most likely theory suggests that incident electrons dislodge atoms to produce In vacancies with resulting In interstitials and P vacancies with resulting P interstitials. These may recombine, leaving no defect, or diffuse and react with other species to produce secondary defects. Diffusion of a P interstitial to an In vacancy will then produce the P_{In} antisite. Other explanations for antisite formation processes, including a change in the mobility of the group V interstitials with change in its charge state have been presented [3]. Further experiments are being performed to clarify the antisite formation mechanism and to correlate the EPR data with luminescence spectroscopy studies and transient capacitance studies of InP.

This NRL work represents the first structural identification of an intrinsic defect in InP. These antisites are observed in *n*- and *p*-type material which has been irradiated to high fluences with 2 MeV electrons. The observation further demonstrates the generality and importance of antisites in III-V semiconductors.

[Sponsored by the ONR]

References

1. U. Kaufmann, J. Schneider, and A. Rauber, "ESR Detection of Antisite Lattice Defects in

GaP, CdSiP₂ and ZnGeP₂," *Appl. Phys. Lett.* **29**, 312 (1976).

2. R.J. Wagner, J.J. Krebs, G.H. Stauss, and A.M. White, "Submillimeter EPR Evidence for the As Antisite Defect in GaAs," *Solid State Commun.* **36**, 15 (1980).
3. N.K. Goswami, R.C. Newman, and J.E. Whitehouse, "The Observation of High Concentration of Arsenic Antisite Defects in Electron Irradiated *n*-Type GaAs by X-Band EPR," *Solid State Commun.* **40**, 473 (1981). ■

Superconducting MoN: Theory and Experiment

L.L. Boyer, W.W. Fuller, D.U. Gubser,
K.E. Kihlstrom, B.M. Klein,
D.A. Papaconstantopoulos,
W.E. Pickett, S.B. Qadri, E.F. Skelton,
and S.A. Wolf

Condensed Matter and Radiation Sciences Division

Refractory carbides and nitrides in the B1-structure (a cubic structure identical in form to sodium chloride) are renowned for their hardness, high melting temperatures, and in many cases, the high transition temperatures T_c to a superconducting state. Because materials with significantly higher T_c s than are currently available would have a dramatic impact on the utility of numerous superconducting devices, NRL scientists have been interested in these carbonitrides. Theoretical electronic structure studies on these materials, with particular emphasis on understanding superconductivity, have been going on at NRL for a decade. These materials have large electron-ion matrix elements and, in some cases, relatively large values of the density of electronic states at the Fermi energy $n(E_F)$. (E_F is the energy level separating occupied and unoccupied electronic states.) Both characteristics favor high T_c .

Theoretical Basis: First-principles studies of carbides and nitrides of niobium with 9 (e.g., NbC) and 10 (e.g., NbN) valence electrons per molecule indicated a monotonic increase in $n(E_F)$ as the number of valence electrons increased.

These studies suggested that a material with 11 valence electrons would have even higher $n(E_F)$, favoring a higher T_c ; molybdenum nitride (MoN) is a good candidate [1]. Detailed electronic structure calculations [1,2] verified that BI-structure MoN should indeed have a high T_c , perhaps exceeding 30 K. Because of this, NRL and other groups have undertaken efforts to stabilize MoN in this structure.

Fabricating MoN Films: At NRL, the most successful experiments to stabilize MoN in the BI-structure involved sputtering a split target of molybdenum and niobium in argon mixed with nitrogen and cyanogen [3]. The geometry inside the sputtering system, shown in Fig. 7, allows a series of different compositions of niobium, molybdenum, and nitrogen to be made in a single sputtering run. The films to the far left are very niobium-rich while the substrates to the right are molybdenum-rich.

Film Structure and Properties: The resulting films are all BI-structure (as determined by X-ray diffraction) but have increasing deficiencies of nitrogen as the molybdenum content is increased. For example, the film with the highest content of molybdenum (determined by X-ray fluorescence) was $\text{Mo}_{0.92}\text{Nb}_{0.08}\text{N}_{0.5}\text{C}_{0.1}$. This film had only about half the amount of nitrogen necessary to form the stoichiometric structure (a

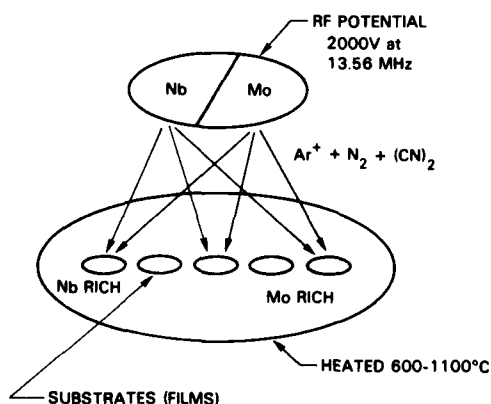


Fig. 7 — Sputtering system used to fabricate MoNbNC films. Because of the split niobium, molybdenum target, the molybdenum concentrations of the substrates increase to the right. An RF potential is across the target and substrates, and the substrate temperature is externally controlled.

structure in which all positions are properly filled).

Figure 8 shows the evidence for the increase in nitrogen deficiency as the molybdenum content is increased. It shows the lattice parameter a_0 , which is a measure of the size of the cubic structure, plotted against the niobium concentration of the film. The solid line represents the calculated value of a_0 if the material had all the positions in the lattice filled throughout the composition range. The highest Nb concentration occurs for NbN and a lattice constant of 4.39\AA . The lowest Nb concentration is for MoN ($a_0 = 4.22\text{\AA}$). Between these, the film contains a mixture of molybdenum, niobium, and nitrogen. The experimental data points are for a series of sputtering runs at different substrate temperatures. Experimental points systematically deviate from the calculated curve as the niobium content decreases (molybdenum content increases) to approach a lattice parameter of about 4.16\AA , the lattice

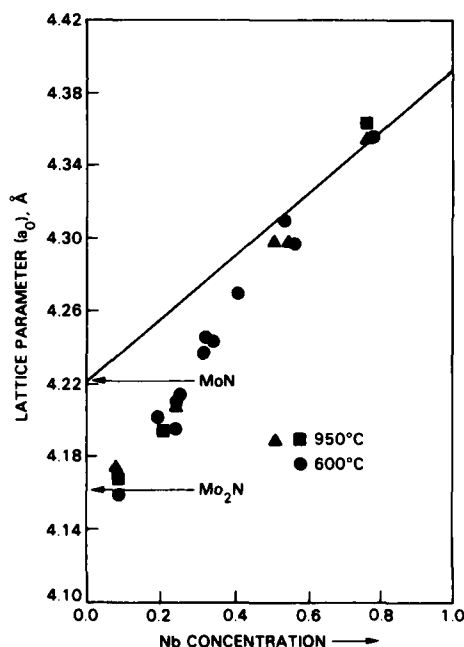


Fig. 8 — Lattice parameter vs niobium concentration for a series of sputtered films. Films were grown on substrates at two different temperatures (600° and 950°C). The solid line is the calculated variation for stoichiometric $\text{Nb}_x\text{Mo}_{1-x}\text{N}$. The insert shows the experimental geometry in the sputtering system.

parameter of pure molybdenum nitride (Mo_2N); there is one nitrogen deficiency for every two molybdenum atoms. Thus, for these films, as a_0 decreases from 4.40\AA to 4.16\AA —as the molybdenum content increases—the nitrogen deficiency in the lattice increases.

Ion Implantation and T_c : Figure 9 shows the dependence of the superconducting T_c plotted versus the lattice parameter. We attribute the deviations of the experimental data (dotted curve) from the theoretical predictions (solid curve) to the nitrogen deficiencies in the lattice. One way to increase the nitrogen content and thereby raise T_c is by nitrogen ion implantation. We therefore implanted some of the molybdenum-rich and some of the niobium-rich samples with nitrogen ions to study the effect on T_c .

It is important to realize, however, that ion implantation usually depresses the T_c of superconductors because of the radiation damage to the crystal lattice due to the energetic ions. The results of the first series of implants are shown in

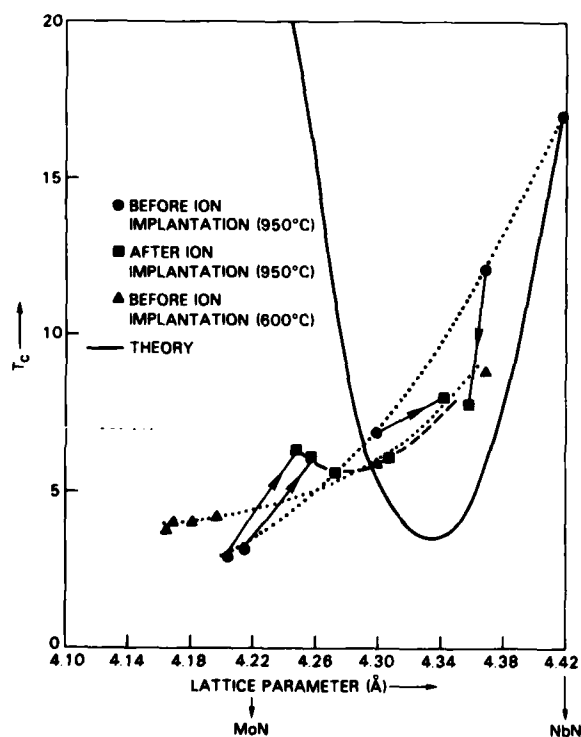


Fig. 9 — T_c vs lattice parameter for a number of films of NbMoN before and after ion implantation

Fig. 9 by the arrows and the broken curve. The implantation did not destroy the BI-structure as indicated by X-ray diffraction measurements, but did alter the lattice parameters as well as the T_c s. The T_c of the niobium-rich samples was decreased but both the T_c and the lattice parameter of the molybdenum-rich samples increased; thus, the T_c values are brought closer to theoretical predictions. This positive result indicates that additional implantation and thermal anneals to reduce the radiation damage may significantly raise T_c , quite possibly to the theoretical values.

References

1. W.E. Pickett, B.M. Klein, and D.A. Papaconstantopoulos, "Theoretical Prediction of MoN as a High T Superconductor," *Physica* **107B**, 667 (1981).
2. D.A. Papaconstantopoulos, W.E. Pickett, B.M. Klein, and L.L. Boyer, "Nitride offers 30 K Transition?" *Nature* **308**, 496 (1984).
3. W.W. Fuller, S.A. Wolf, D.U. Gubser, E.F. Skelton, and T.L. Francavilla, "Properties of a New Molybdenum Nitrogen Phase," *J. Vac. Sci. Technol. A1*, 517 (1983).

Ultrasonic Gas Atomization for Ultrafine Metal Powders

I.E. Anderson, J.D. Ayers, and W.P. Robey
Material Science and Technology Division

R.G. Hughes
Marine Technology Division

Metal powder processing is one of the most promising avenues of application for rapid solidification technology. Among the many potential applications are high coercive strength magnetic materials, corrosion-resistant coatings and high-strength, high-toughness alloys. The benefits of rapid solidification resulting from repressed microsegregation or development of novel product phases are most pronounced in power particles that are smaller than 10 to 20 μm in diameter. These ultrafine particles solidify

rapidly partly because of their small size which promotes rapid cooling. Gas atomization, an important commercial method for producing metal powders, results from the disintegration of a molten stream by impinging gas jets. Unfortunately, conventional atomizer nozzles generate relatively coarse powders, where only about 5%, by volume, of a typical yield is less than $10\text{ }\mu\text{m}$. Recent nozzle designs, including the ultrasonic gas atomization (UGA) nozzle, show promise for producing high yields of ultrafine, rapidly solidified powders. A research program was initiated at NRL with the aim of boosting the ultrafine powder yield of a high-pressure, automated atomizer that has been fitted with a UGA nozzle. The approach was an experimental analysis of UGA-nozzle gas flow effects. The analysis then led to the determination of a range of parameters at which stable, high-pressure atomization experiments were performed.

Gas Atomization System: The gas atomization system, designed and assembled at NRL, includes a UGA nozzle, a gas inlet pressure capacity of up to 27.6 MPa (4000 psig), and a process controller for programmable actuation of the system components. The UGA nozzle (Fig. 10) consists of 18 gas jets in a ring around the melt path axis. A melt guide tube tip delivers a molten metal stream close to the focus of the gas jets during atomization. A noble gas, argon (Ar), was used for the gas flow and atomization experiments.

Gas Flow Effects: Highly localized pressure effects on the melt stream, resulting from gas flow interactions, can significantly affect atomization stability. These effects were measured, in the absence of a melt, by means of a pressure transducer and static pressure probe. Melt orifice pressure was measured as a function of gas inlet pressure at several different positions in several guide tube tip designs to identify a suitable tip configuration and an inlet pressure range where stable atomization conditions were expected.

The gas flow effects also were observed visually with Schlieren photography to assess the time-averaged flow patterns in the nozzle gas stream. With this optical imaging technique, gas flow from the nozzle appears as a conventional

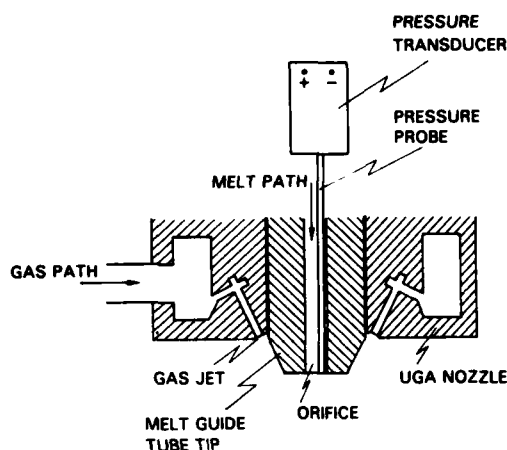


Fig. 10 — Cross section of an ultrasonic gas atomization (UGA) nozzle. The transducer and pressure probe are positioned for melt orifice pressure measurements. The nozzle consists of 18 gas jets distributed in a ring pattern around the melt path axis.

photographic image with contrast that varies with gas density. Schlieren images were recorded for a series of stable gas inlet pressures with the selected melt tube tip in place to observe flow pattern changes through the selected inlet pressure range.

Atomization Experiments: A high-tin alloy (5% lead by weight) was atomized by using process parameters and the UGA nozzle design chosen from the gas flow analysis. (The pressure probe is removed for atomization runs.) The atomization trials were conducted at three stable gas inlet pressures with the same melt guide tip. The size distribution was determined for each powder sample.

Backstreaming and catastrophic eruption of the melt from the crucible can occur when the orifice pressure is greater than 1 atm. The previous gas flow and melt orifice pressure measurements identified a range of gas inlet pressures from 8.4 MPa (1200 psig) to 19.4 MPa (2800 psig) where the orifice pressure was less than 1 atm and, hence where a melt stream would aspirate from the selected guide tube tip during atomization. In fact, a partial vacuum was measured at the orifice for a 12.5-MPa (1800 psig) gas inlet pressure, which corresponds to the minimum orifice pressure (0.6 atm) shown in

Fig. 11. Tin alloy charges were atomized at inlet pressures of 10.4 MPa (1500 psig), 12.5 MPa (1800 psig), and 17.3 MPa (2500 psig), within the aspiration region. The use of the orifice pressure is a powerful technique which can determine the range and magnitude of stable melt aspiration in advance of an atomization trial.

Particle Size Control: With the experimental latitude determined, a systematic test of the inlet pressure effect on powder particle size was performed. Many previous studies report a continuous decrease of particle size with increasing gas inlet pressure in conventional atomization

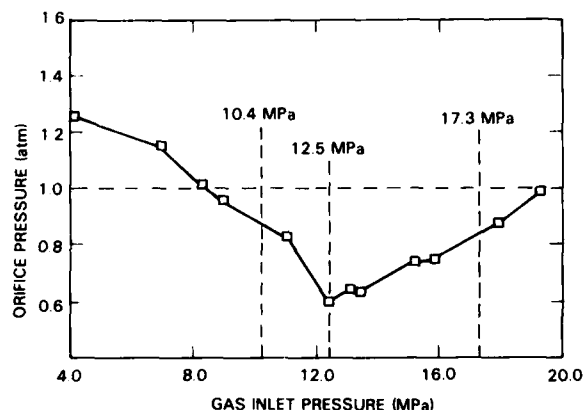


Fig. 11 — The orifice pressure measurements are summarized for the melt guide tip selected for atomization trials at the indicated inlet pressures. Aspiration occurs below and backstreaming occurs above an orifice pressure of 1 atm.

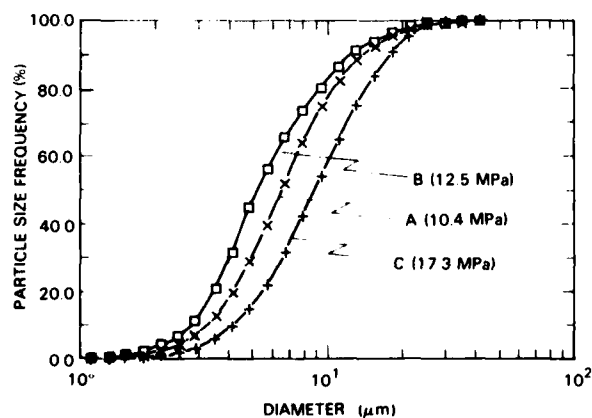


Fig. 12 — Cumulative frequency distribution of the atomized powder size, by volume

nozzle. The results of the size distribution analysis indicate that the decreasing particle size trend reverses when the inlet pressure exceeds about 12.5 MPa (Fig. 12). The minimum particle size results from atomization at a 12.5-MPa inlet pressure, which corresponds to the minimum orifice pressure. Although the atomization mechanism that produces such extreme particle size refinement has not been identified, the results demonstrate the effectiveness of this controlled high-pressure atomization process.

[Sponsored by the ONR]

Mechanical Response of Laser-Irradiated Panels

C.I. Chang and F.R. Stonesifer
Marine Technology Division

C.A. Griffis
Material Science and Technology Division

Aerospace vehicles subjected to normal flight loads may undergo catastrophic structural failure when exposed to severe thermal environments such as accidental fire or laser irradiation. The Naval Research Laboratory is currently developing an analytical methodology for assessing the structural survivability of aircraft and missile systems subjected to simultaneous mechanical loading and intense, rapid heating. This complex task requires the generation of a database of material properties at time-dependent elevated temperatures, as well as the creation and integration of nonlinear thermal and structural analysis computer codes. Although the present study is associated with the thermomechanical response of a well-known aircraft alloy, similar efforts are underway for laminated composite materials frequently employed in advanced aerospace applications.

Measurements: To establish mechanical properties suitable for characterizing behavior at extremely high temperatures, narrow aluminum test coupons were instrumented with thermocouples and then exposed to uniform high energy laser (HEL) heating while under constant tensile load. Even though the thermocouples were on the aluminum surface they were within 5°C of the temperature anywhere in the coupon; this was

verified with heat transfer calculations. By performing the tests over a range of load levels, the short-time (0.02-0.5 s) fracture strength was established over the temperature range 25-475°C. The data points in Fig. 13 show the measured variation in fracture stress with temperature for both 0.81 and 1.57 mm thick material. The solid curve illustrates the strength relationship typically employed in aircraft design and shows the mechanical strength of the material after a 30-min heat soak. The pronounced decrease in strength with increasing temperature for both heating rates is due in large part to accelerated annealing and overaging reactions. The less extensive strength degradation for the HEL test results shows that much shorter times at temperature are available for these diffusion-controlled, softening reactions to occur.

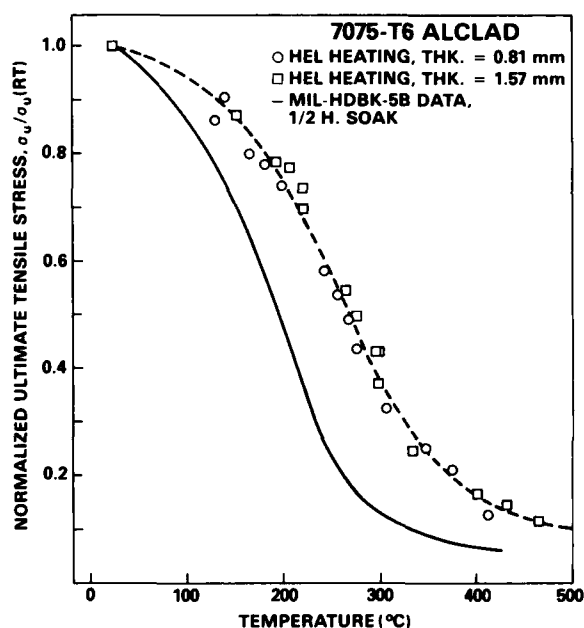


Fig. 13 — Influence of temperature on normalized fracture stress for 7075-T6 aluminum alloy. Dashed curve denotes mean of the experimental data shown. The solid curve is typically employed in aircraft design.

To assess the accuracy of a simplified thermomechanical model to predict the time to failure incorporating the above described data on material properties, 76 mm-wide tension sheets were preloaded to various fractions of their

room-temperature breaking strength and were then spot irradiated using laser beams having diameters of about 18 to 60 mm and intensities of 0.3 to 0.7 kW/cm². To simulate aerodynamic cooling effects, a Mach 0.3 airflow was passed over the irradiated surface of the panels. The results of these measurements will be compared to the simplified thermomechanical model developed below.

The Model: Prediction of the panel test results required development and integration of both thermal and stress analysis techniques. The transient thermal calculations were performed by using a lumped-mass, finite-difference procedure. To simplify the computations, an axisymmetric, rather than a rigorous three-dimensional, analysis was adopted. Typically, 400 ring-shaped elements were allocated in the thickness and radial directions. This model includes nonlinear effects such as temperature-dependent thermophysical properties, convection/radiation losses, and melting phenomena. It was assumed that all melted material is instantaneously removed and any impinging radiation is subsequently transmitted directly to an adjacent (unmelted) element in the thickness direction. Figure 14 shows the calculated surface temperature distribution along the panel half-width (center to outer radius) after selected periods of laser irradiation. In general, the temperature at each point on the cross section increases continuously with exposure time up to 2 s. After 2 s the temperature just outside the beam drops abruptly because of the removal (melting) of material throughout most of the beam impingement zone. The melting causes a much smaller area of the panel to absorb energy, thus greatly reducing the subsequent heat input to the panel.

The mechanical analysis adopted in the present study predicts failure load as a function of time by using the above thermal analysis. It assumes that at complete fracture, each point on the panel cross section simultaneously is stressed to its temperature-dependent fracture strength. This assumption produces an upper-bound estimate of the failure load for a given exposure time which is determined by integrating the fracture stress along the panel width using: (a) the measured fracture stress vs temperature relationship

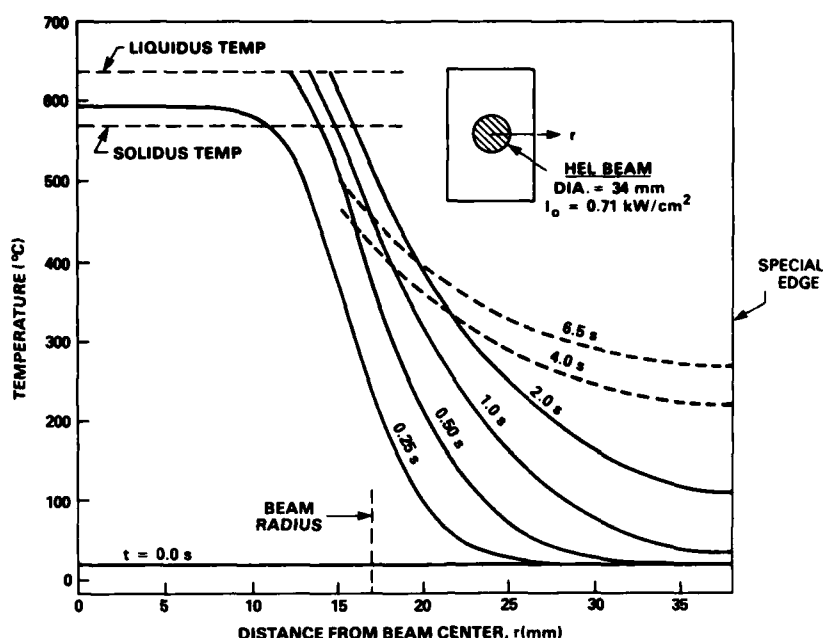


Fig. 14 — Computed (finite difference) surface temperature distributions in the width direction for spot-irradiated panel

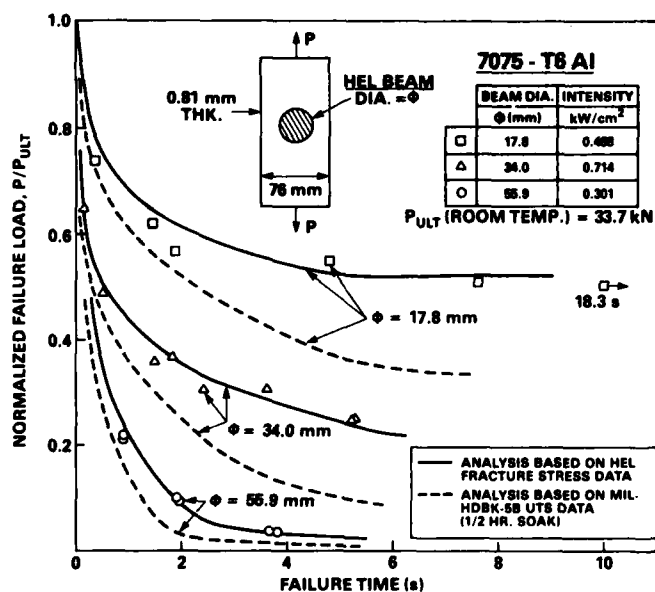


Fig. 15 — Analytical (curves) and experimental (points) fracture response of aluminum panels subjected to various load levels, laser beam intensities, and beam diameters

given in Fig. 13 and (b) the computed temperature distributions as typified by Fig. 14.

Model-Measurement Comparison: Figure 15 compares the analytical and experimental relationship between specimen fracture load and heating time for three laser-beam configurations.

For each condition an initial, rapid drop in load occurs, which is due to the rapid reduction of the cross-sectional area produced as burnthrough of the panel progresses under the laser beam. The more modest strength reductions at longer times result from the relatively slow conduction of heat into the unirradiated flanks of the panel after

burnthrough. Figure 15 further shows excellent agreement between the measured and computed fracture response provided that the short-time laser-strength data are employed in the computations (solid curve). However, as might be expected, use of the 30-min heat-soak data in the calculations (dashed curve) leads to a large disparity between the theory based on slow-heating material properties and the experiments which employed the laser as a heat source.

The present research has resulted in the definition of material properties and computational methods necessary for reliable prediction of the ductile, elevated-temperature, time-dependent fracture behavior of aluminum alloys. Future studies will focus on the brittle fracture response of these alloys, wherein mechanical and thermal stress can initiate a defect near the beam periphery which may propagate unstably at very low stress levels.

[Sponsored by NAVAIR] ■

A Comparison of Two Theories of Acoustoelasticity

A.V. Clark and R.B. Mignogna

Marine Technology Division

The presence of a stress field causes small changes in the phase velocity of acoustic waves, i.e., the acoustoelastic effect. The difference in the phase velocities of orthogonally polarized horizontal shear SH-waves (birefringence) caused by a plane stress field can be used for nondestructive stress measurement. Knowledge of the stress within a structure allows decisions to be made in regard to its structural integrity and probable service life.

The theory of acoustoelasticity, developed 20 years ago by Hughes and Kelly, considered materials as isotropic (having the same properties in all directions). The isotropic theory predicted that the acoustic birefringence would be a linear function of stress, the polarization directions of the acoustic waves would be along the stress axes, and there would be no initial birefringence. However, it was found that at zero stresses many materials exhibited a nonzero initial bire-

fringence. Attempts were made to correct for this by subtracting the initial birefringence from the total birefringence due to applied stress. In certain cases this would then give good agreement between experimental data and theory. In other cases it would not.

Many materials, such as rolled plate, are considered isotropic for engineering purposes. However, a slight amount of anisotropy exists because forming processes. Certain acoustic waves are very sensitive to material anisotropy. A slight amount of material anisotropy can affect the phase velocity of acoustic waves to the same extent as stress and has greatly hindered the development of acoustoelasticity as a viable non-destructive measurement technique.

Two Theories of Acoustoelasticity: Recently, two theories of acoustoelasticity have been developed accounting for effects of both stress and small amounts of anisotropy. We have generalized the rigorous theory of Iwashimizu and Kubomura (the IK-theory) and have shown how the Okada theory, based on optical analogies, can be made to agree with our generalized theory. Comparisons of theoretical predictions and experimental data are presented and show good agreement.

The IK-theory, using well-known acoustic and elasticity relations, treats the case of free waves propagating through the thickness of a slightly anisotropic plate exhibiting macroscopic orthotropic symmetry (having three twofold macroscopic symmetry directions). In their equations, the material is treated as a nonlinear elastic solid with the effects of orthotropy retained in the second-order elastic moduli but ignored in the third-order moduli. They derived an equation relating birefringence and stress containing the initial birefringence B_0 and a single acoustoelastic constant. However, they found that in the most general case, there was a nonlinear relationship between birefringence and stress. Another aspect of the theory indicates that the acoustic axes (where pure-mode shear waves will propagate) rotates as a function of stress relative to the axes of material symmetry.

Okada also derived a relation between birefringence and stress. He made the assumption that an index of refraction matrix exists for

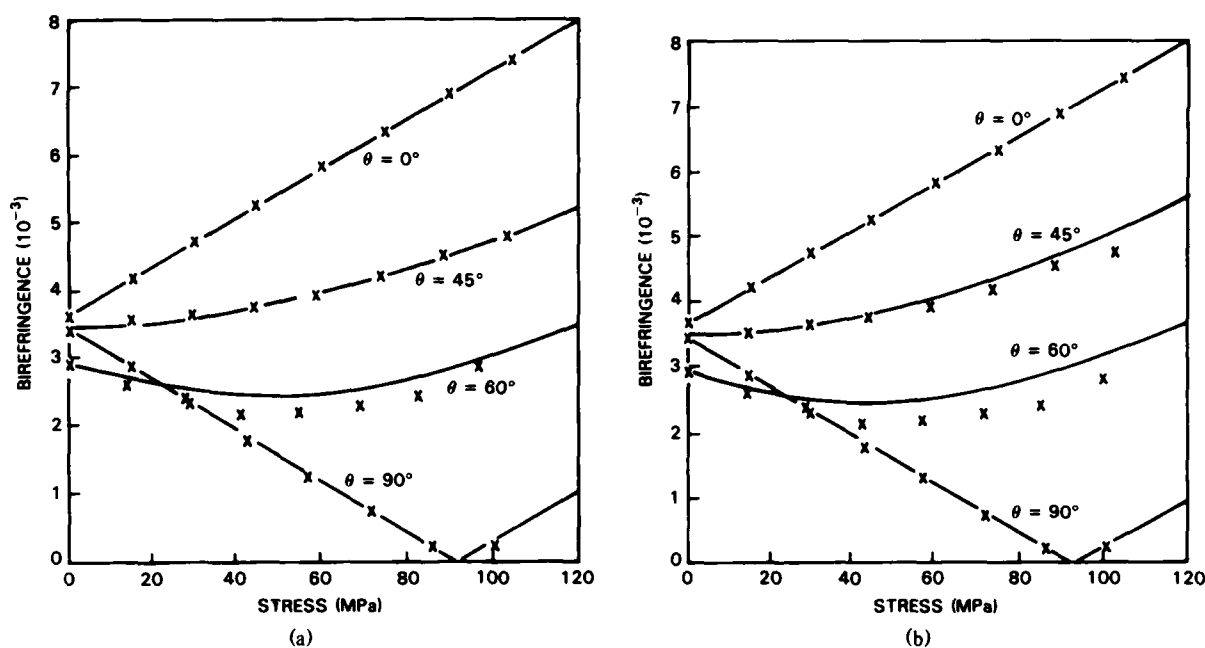


Fig. 16 — Birefringence vs stress. (a) Okada theory and (b) Iwashimizu and Kubomura theory. Theory shown as (-), data by symbols.

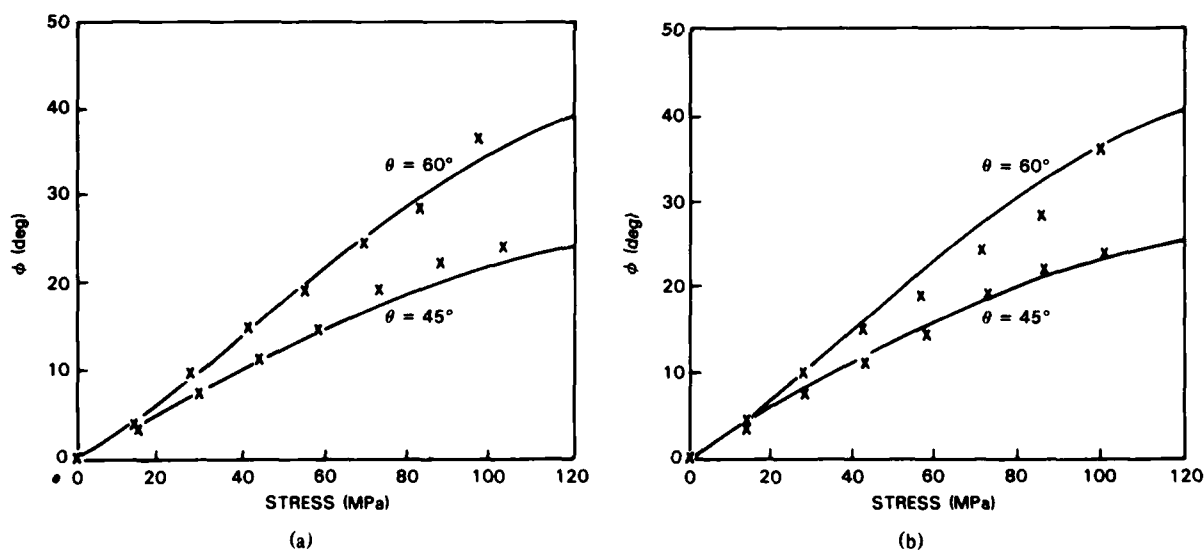


Fig. 17 — Polarization angle ϕ vs stress. (a) Okada theory and (b) Iwashimizu and Kubomura theory. Theory shown as (-), data by symbols.

the solid and that the components of the matrix are linear functions of stress. The coefficients relating the matrix components to stress were assumed to be nine in number when referenced to axes of material symmetry in the plate (parallel

and perpendicular to the rolling direction). This is analogous to the behavior of the second-order elastic moduli for an orthotropic solid. Okada assumed that the inverse velocities (slownesses) of free waves propagating in an orthotropic solid

are the eigenvalues of the index of refraction matrix. Okada then derived a nonlinear birefringence stress relation involving B_0 and three acoustoelastic constants. His theory reduces to that of Iwashimizu and Uemura if one of the constants vanishes and the other two are equal.

It is curious, however, that Okada's theory works as well as it does. Okada postulates the existence of a matrix analogous to the refraction index matrix in optics. However, using analogies between optics and acoustics requires some care, since there are obvious differences between the two fields: for example, the existence of only two optical phase velocities in anisotropic crystals, as opposed to three acoustic phase velocities.

Okada tested his theory and found that it gave good agreement with birefringence measurements for uniaxial tension specimens made of various aluminum alloys. He noted in particular that, for 5052 aluminum, his three-parameter model was able to fit the data much better than the IK-theory.

We were thus left with somewhat of a paradox, in that the Okada theory, which appears to be the less rigorous, seems to give better agreement with experiment than the IK-theory, which is based on a seemingly more rigorous theoretical foundation.

The NRL-Developed Theory: To remove this paradox, we developed a rigorous theory that gives the phase velocities, birefringence, and polarization directions for free SH waves propagating normal to the surface of a slightly orthotropic plate in a state of plane stress. The theory is an extension of the IK-theory. In our derivation, we retained anisotropy in second- and third-order moduli, whereas they ignored anisotropy in third-order moduli. Our theory gave rise to a birefringence equation involving three acoustoelastic constants, m_1 , m_2 , and m_3 , where the

IK-theory involves only one. Our theory reduces to the IK-theory if $m_1 = 0$ and $m_2 = m_3$.

Our theory formally gives the same results as that developed by Okada. He assumed that the inverse phase velocities (slownesses) can be calculated as the eigenvalues of an index of refraction matrix, whose elements are assumed linearly related to stress.

The phase velocities in our theory are proportional to the squares of the eigenvalues of the (second-order) acoustical tensor. By formally relating the acoustical tensor to the Okada index of refraction, we found that our theory and the Okada theory give the same results, provided that the relationships between the Okada stress-acoustic constants and the acoustoelastic constants (of our theory) are satisfied.

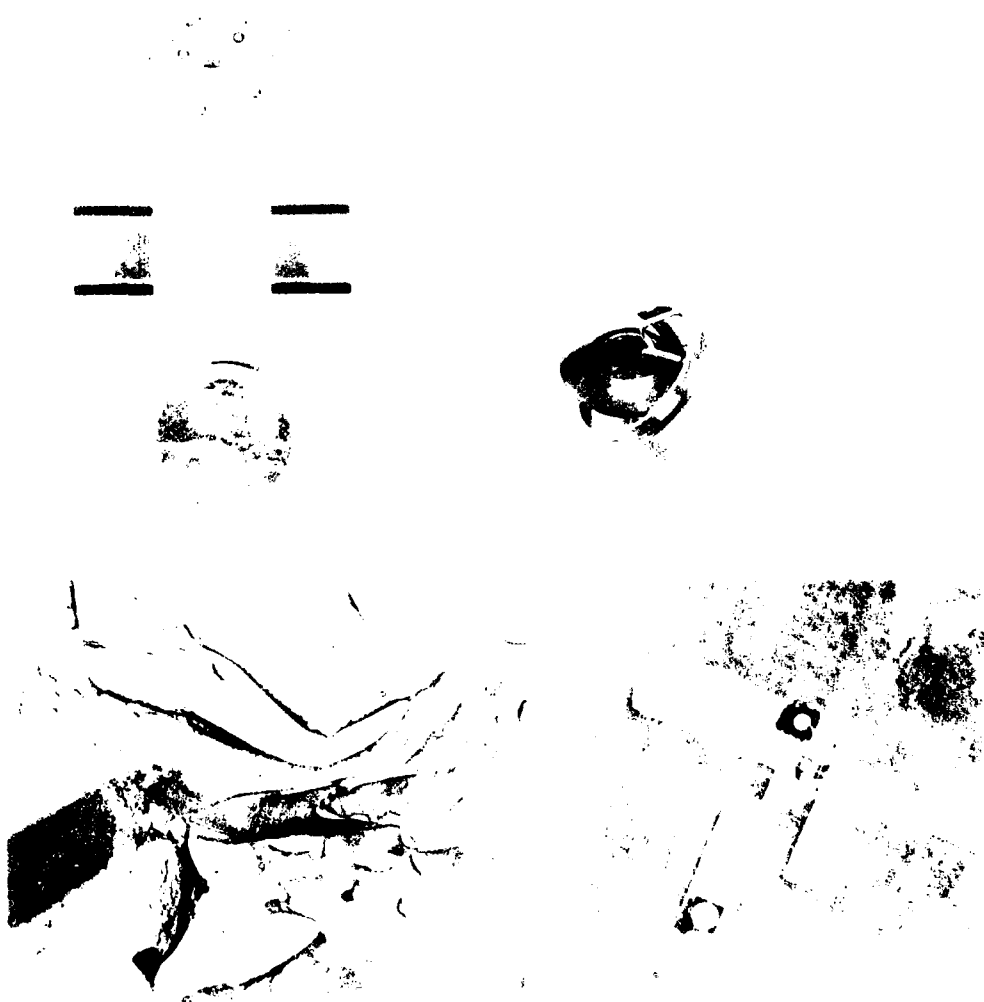
Experimental Comparison: We compared the agreement between experimentally obtained values of birefringence B and polarization angle ϕ with the predictions of the theory of Okada for uniaxial tension specimens made from 2024-T351 aluminum plate, shown in Figs. 16(a) and 17(a). The agreement was excellent. We also compared the same data to the predictions of the IK-theory, shown in Figs. 16(b) and 17(b). The agreement was quite good. In fact, we found that for our specimens $m_1 \approx 0$ and $m_2 \approx m_3$, which are very nearly the conditions under which our generalized theory (and hence the Okada theory) reduces to the IK-theory for this case. For more detailed information, please refer to Refs. 1 and 2.

[Sponsored by ONR]

References

1. "Acoustoelastic Measurement of Stress and Stress Intensity Factors Around Crack Tips," *Ultrasonics* **21**, 57-64 (1983).
2. "A Comparison of Two Theories of Acoustoelasticity," *Ultrasonics* **21**, 217-225 (1983). ■

*Component technology and
specialized devices*



AD-A150 650

NAVAL RESEARCH LABORATORY 1983 REVIEW(U) NAVAL RESEARCH
LAB WASHINGTON DC 1983

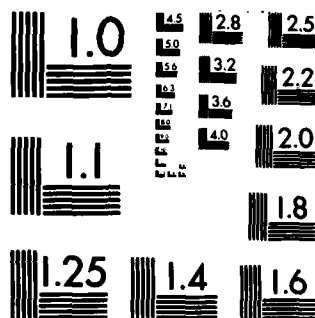
3/4

UNCLASSIFIED

F/G 5/1

NL

[illegible]



MICROCOPY RESOLUTION TEST CHART
NATIONAL BUREAU OF STANDARDS-1963-A

- 189 Immunologically Based Chemical and Biological Detection**
Bruce P. Gaber, Anne Plant, James P. Sheridan, and Eddie L. Chang
An ultrasensitive detector of chemical and biological warfare agents may result.
- 190 Chemical Microsensors**
Henry Wohltjen, Neldon L. Jarvis, and Arthur Snow
Microelectronic devices married to chemical films can produce very sensitive detectors
- 191 A Regenerative 16 GHz Frequency Divider**
Christen Rauscher
A simple frequency divider is demonstrated.
- 194 Planar, Fully Ion Implanted Indium Phosphide Junction Field Effect Transistors**
John B. Boos, and Steve C. Binari
A successful technology for indium phosphide GHz transistors results.
- 196 Electronic Warfare Microprocessor**
Ross M. Christiansen
High performance and low cost signal processing are achieved

COMPONENT TECHNOLOGY

Specialized devices based on modern technology have provided new ways of performing old tasks as well as the means to achieve new capabilities. Such devices are characterized by increased precision and high cost effectiveness. The articles in this section describe NRL's development of new devices and new techniques for their production and military applications. These articles also discuss the development of extremely sensitive techniques to detect about 100 molecules of various chemical agents.

The work is being carried out in five divisions: Tactical Electronic Warfare (Code 5700), Chemistry (Code 6100), Optical Sciences (Code 6500), Condensed Matter and Radiation Sciences (Code 6600), and Electronics Technology (Code 6800).

In addition to the work described in these articles, NRL has many other projects in component technology and specialized devices. A few of these are

- suppression of smoke in fire environments,
- submarine atmosphere analyzer,
- improved radar antennas,
- lightweight, solid-state transmitters,
- fiber-optic sensors, and
- optoelectronic devices.

Page 186, clockwise from upper left:

Typical surface acoustic wave chemical microsensors can be fabricated in a variety of configurations and sizes. Shown is a single 31-MHz device and a smaller dual 70-MHz device. See article on p. 190 by H. Wohltjen.

Regenerative 16-GHz frequency divider. Close-up view of field-effect transistor surrounded by input and output impedance matching circuitry, with regenerative feedback provided through miniature air coil. See article on p. 191 by C. Rauscher.

Electron micrograph of freeze-fracture replica of monomeric lipid tubules. Note the wrapped bilayers and the open water-filled channel (41,000X) (P. Yeager).

Heart valve similar to the one implanted in Dr. Barney Clark. NRL scientists participated in a team which discovered why it failed and modified its design to prevent future failures.

Immunologically Based Chemical and Biological Detection

B.P. Gaber, A. Plant, J.P. Sheridan,
and E.L. Chang
Optical Sciences Division

The detection and identification of minute (less than a few hundred molecules) chemical and biological substances has major military application in chemical and biological warfare defense, disease control, and drug abuse programs. If we impose the requirement that the detection scheme be capable of very high selectivity, the problem poses a formidable challenge. To meet this challenge we are developing a hybrid detector that exploits the inherent selectivity of antigen-antibody interactions, coupled with fluorescence-based optical amplification to achieve the required sensitivity. The carrier for the detector relies on model biomembrane technology, an area of intense research at NRL.

Principle of Detector: The detection system consists of a $0.4\ \mu\text{m}$ diameter spherical vesicle (Fig. 1) formed from a synthetic biomembrane $0.004\ \mu\text{m}$ thick. The vesicle is loaded internally with fluorescent dye molecules. At the high concentration of dye within the vesicle, the

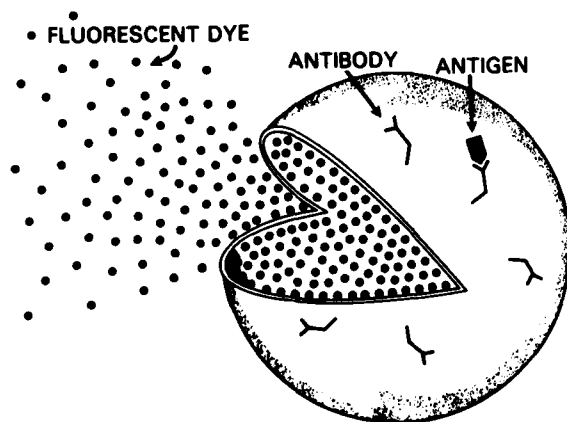


Fig. 1 — Schematic representation of the vesicle immunolysis detector concept. A phospholipid vesicle ($0.4\ \mu\text{m}$) contains fluorescent dye at a concentration sufficient to inhibit emission. Chemically coupled to the vesicle's skin ($0.004\ \mu\text{m}$ thick) are antibodies which serve as receptors. Interaction of a receptor with a molecule of the substance to be detected initiates attack (lysis) of the vesicle and dye release. Diluted in the external solution, the dye exhibits an intense green fluorescence.

molecules are fluorescently inactive. Monoclonal antibodies, serving as highly specific receptors for the chemical or biological antigens to be detected, are chemically coupled to the vesicle surface. Interaction of antigens and antibodies then triggers a series of biochemical events which results in the dissolution or lysis of the vesicle's skin by forming holes. As a consequence, dye molecules escape and become diluted in the external solution. The released dye molecules, no longer inactive, appear green because of intense fluorescence. In principle, a single antigen molecule can activate the release of the tens of thousands of dye molecules contained in a single vesicle. Using laser-induced fluorescence methods, it should be possible to detect lysis of a few tens or hundreds of vesicles and thereby detect the presence of a like number of target molecules.

Detector Configurations: This basic vesicle immunolysis system composed of carrier, receptor, and reporter can be configured in several ways depending on the particular substance we wish to detect. For example, in one experiment we have chosen to detect antibody in solution rather than antigen (see Fig. 2). To accomplish this, the antigen itself is coupled to the vesicle surface and serves as receptor for the antibody.

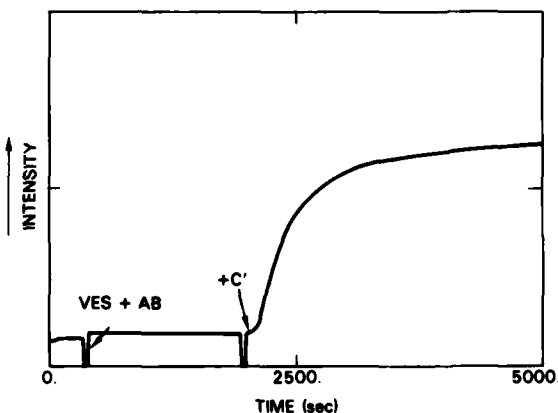


Fig. 2 — Time course for the release of fluorescent dye from vesicles containing the antigen dinitrophenol (DNP) on their surface. Antibody to DNP is added at the point marked "VES + AB." After 30 min incubation, the biochemical reagent "complement" (C') is added. Complement recognizes the antibodies bound on the vesicle surface and causes lysis and dye release.

The antigen used in this experiment is the organic compound dinitrophenol (DNP); however, biological antigens can be used as the basis of clinical assays for the presence of small amounts of antibody which may signal the onset of disease.

Another modification of the vesicle immunolysis scheme is called the "sandwich" technique and holds the promise of very high selectivity. The name derives from the use of two antibodies "sandwiching" the antigen to be detected. One antibody is the vesicle-bound receptor, and the second antibody binds to a different location on the antigen and stimulates the complement reagent (a complex of proteins which when activated perforate cell membranes) which causes vesicle lysis. Development of sandwich vesicle immunolysis assays for the early detection of typhus and bacterial meningitis are currently being pursued at NRL in collaboration with the Naval Medical Research Institute, the Naval Biosciences Laboratory, and Georgetown University School of Medicine.

By taking advantage of the emerging technology for production of highly purified and chemically defined monoclonal antibodies, we anticipate the development of a variety of chemical/biological detectors and clinical assays derived from NRL's vesicle immunolysis research.

[Sponsored by DARPA]

Chemical Microsensors

H. Wohltjen, N.L. Jarvis, and A. Snow
Chemistry Division

The detection and monitoring of hazardous vapors is an important Navy problem. Numerous situations exist in which hazardous vapors (e.g., from fuels, fire, chemical warfare (CW) agents, refrigerant leaks) must be detected quickly at low concentration levels. Traditional solutions to the vapor monitoring problem have used sensor systems which are large, relatively complex, and very expensive (e.g., infrared spectrophotometry, gas chromatography/mass spectrometry). Thus, the cost of information regarding vapor concentrations has been very high. The high cost of the

traditional sensors has seriously impeded the development of systems which could otherwise exploit the benefits of ever cheaper microcomputer technology for process control and environmental monitoring. Chemical microsensors can reduce this high cost and also provide much enhanced sensitivity in monitoring and detecting harmful vapors.

In their most general form, chemical microsensors consist of at least two elements: a microfabricated physical probe device and a chemically selective coating. The coating is chosen so it changes properties in the presence of the vapors to be detected. The probe device contacts the coating and provides an electrical signal with characteristics that reflect the changed properties of the coating. Variations in the coating properties, caused by chemical and physical interactions, control the transport of matter or energy through the probe device. Work at NRL has focused on probe devices in which the transport of acoustic waves, electrons, or electromagnetic waves is modulated by chemical interactions.

Acoustic Probes: In probes which use acoustic waves (surface acoustic wave (SAW) probes), sorption of the vapor into the selective coating increases the mass of the coating and reduces the velocity of the surface acoustic wave moving across it (Fig. 3). This is detected as a reduction of the resonant frequency of the probe. Rapid and reversible detection of many vapors at the ppm concentration level and below has been demonstrated. Figure 4 shows a typical response of a 31 MHz SAW water vapor sensor to consecutive pulses of 5 ppm water vapor in air.

Chemiresistors: In probes which depend on the modulation of electronic charge transport through thin organic semiconductor films, the effect is observed with a device called a chemiresistor. The device consists of closely spaced "fingers" of two electrodes (e.g., an interdigital microelectrode array, usually gold) fabricated on an insulating substrate (usually quartz) as shown in Fig. 3. These microelectrodes are then coated with a thin organic semiconductor film. Good devices are obtained with phthalocyanine films. NRL researchers have obtained

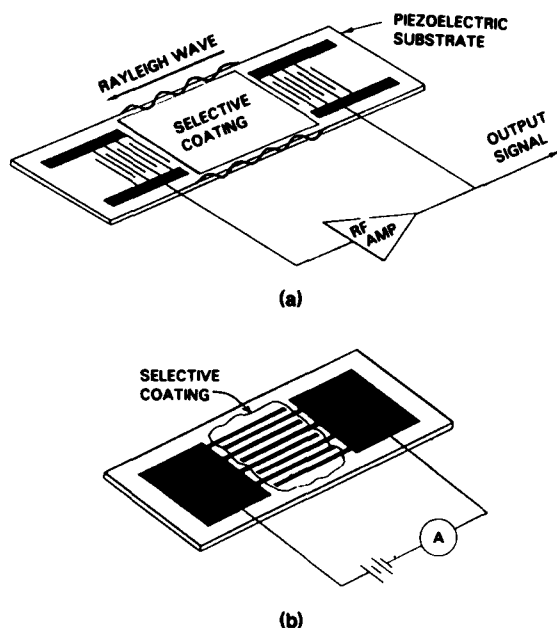


Fig. 3 — Surface acoustic wave vapor sensor (a) and chemiresistor (b). The SAW device is sensitive to nanogram mass changes of the selective coating. The chemiresistor measures changes in electronic conduction in organic semiconductors which are affected by ambient vapors. Both devices are fabricated lithographically.

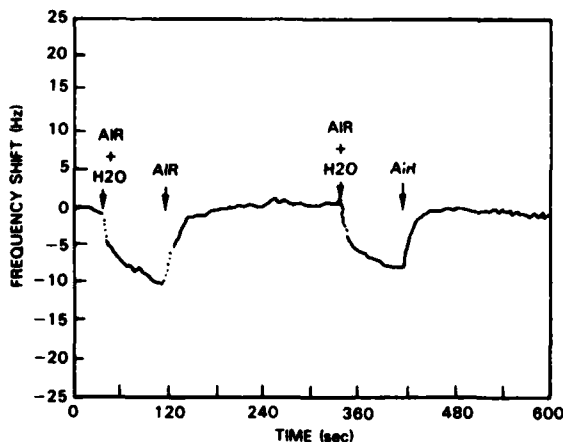


Fig. 4 — Typical response of a polymer-coated 31 MHz SAW device exposed to consecutive pulses of 5 ppm water vapor in dry air.

exciting results from ordered, multilayer films prepared by the Langmuir-Blodgett technique, which coats a substrate with a succession of films, each one-molecule thick. Rapid, sensitive, and reversible responses to electron donor gases such as ammonia, amines, ethers, and alcohols, are common. Figure 5 shows a typical response of a

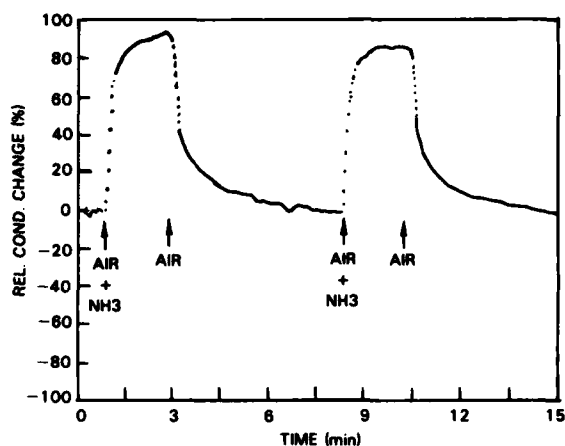


Fig. 5 — Response of a derived copper phthalocyanine multilayer film chemiresistor exposed to consecutive pulses of 2 ppm ammonia in dry air (starting conductance $\approx 9 \times 10^{-13}$ ohms $^{-1}$).

copper phthalocyanine Langmuir-Blodgett film to 2 ppm pulses of ammonia.

The key technical challenge is to improve sensor selectivity. Efforts at NRL have emphasized chemical design, synthesis, and characterization of selective coatings, along with precise film deposition methods. The use of pattern recognition techniques to analyze the simultaneous responses of arrays of different sensors may ultimately result in an inexpensive system comparable to the human nose in its ability to detect and identify vapors. Such systems will find many naval applications for monitoring breathing atmospheres; detecting chemical threats such as fires, explosives, fuel leaks, and CW agents; and providing sensory input for automated systems (e.g. robots) designed to take corrective action.

[Sponsored by ONR, NAVSEA, and U.S. Army CRDC]

A Regenerative 16 GHz Frequency Divider

C. Rauscher
Electronics Technology Division

Frequency dividers, which operate on inputs over a frequency band, are important to a variety of microwave systems in areas such as instrumentation, communication links, and signal processing. A number of different microwave frequency

divider concepts have been described in the literature, with each concept fitting into either of two basic categories. The first category comprises circuits that function like digital frequency counters and provide instantaneous frequency division of a given signal on essentially a cycle-by-cycle basis. The other major category contains the regenerative divider circuits which operate by inducing oscillation at the subharmonic of the incident signal frequency. The object of this NRL investigation was to study the use of single-gate gallium arsenide (GaAs) field-effect transistors (FET) to achieve regenerative frequency division with incident signal frequencies around 16 GHz.

Principle of Operation: The regenerative frequency divider concept in its classical discrete component implementation is illustrated in Fig. 6. Its main ingredients include amplification, mixing capability, subharmonic feedback, and filtering. Basically, we take advantage of low-level quasi-white noise present in the circuit. The noise contains a frequency component at the subharmonic ($f_{in}/2$) of the incident frequency. This signal is mixed with the incident signal to produce an upper and lower sideband at $f_{in} \pm f_{out}$. The lower sideband is subsequently passed by the filter, is amplified, and is then fed back to the mixer. To avoid spurious oscillations, the loop gain is chosen to be less than unity in the absence of an injected input signal. Because of mixer action, the overall loop gain increases with rising input signal level, subsequently leading to the buildup of a subharmonic oscillation as the loop gain exceeds unity. This yields an accurate

frequency-divided counterpart to the input signal. However, regenerative frequency dividers are afflicted with various inherent peculiarities. These include a turn-on threshold to be overcome by the input signal, partial loss of amplitude information caused by the threshold and saturation effects, and leading edge delay for pulsed signals (to be illustrated below). Moreover, the divider response may exhibit confusion if the input signal contains more than one prominent frequency component.

The particular implementation of the basic regenerative approach studied at NRL uses a 0.5 μm -gate GaAs field-effect transistor in grounded source configuration. Biasing the transistor slightly above pinch-off still produces some gain and yields a pronounced quadratic-type nonlinearity for efficient mixing, so that both the mixing and the subharmonic amplification are accomplished by the one transistor. The transistor merely needs to be augmented by appropriate embedding circuitry to accommodate the remaining feedback and filtering functions.

The Device: The actual 16-to-8 GHz divider circuit, implemented in microstrip on a 0.25-mm-thick fiberglass reinforced teflon substrate, is depicted in Fig. 7 (the entire device is 3 cm wide). The transistor used in this experiment is one cell of an Avantek M110 device and is flanked by coupling networks at input and output. The coupling networks provide the required impedance matching and filtering functions at the incident signal frequency and its subharmonic. Feedback at the subharmonic frequency is primarily controlled by a miniature air coil inductor

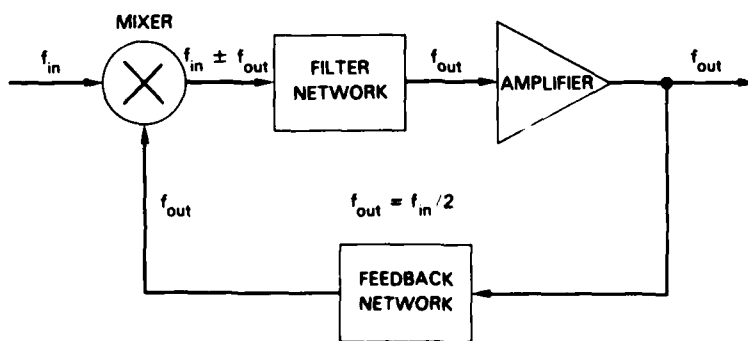


Fig. 6 — Concept of regenerative frequency division

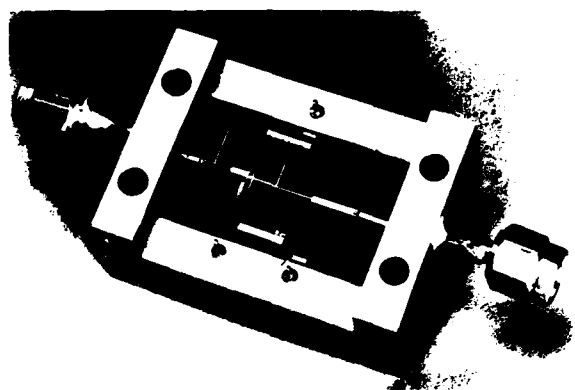


Fig. 7 — The 16 GHz GaAs FET frequency divider.
The overall width of the device is 3 cm.

and a silicon nitride blocking capacitor connected in series between the drain and gate terminals of the transistor. The amount of feedback, in conjunction with transistor gain, determines the divider turnon threshold to be overcome before the regenerative process can begin.

Pulsed Performance: To obtain conclusive information on the divider performance, a variety of different excitations were used. One of the test cases involved applying a pulsed 16 GHz signal of 200-ns pulse duration to the input of the

circuit and then observing the pulsed 8 GHz output response on a sampling oscilloscope. The results which illustrate the inherent peculiarities of regenerative frequency dividers, are illustrated next. Figure 8(a) depicts the shape of an incident 16 GHz pulse while Figs. 8(b-e) represent the associated frequency-divided 8 GHz output signals for increasing incident drive levels. The output level increases nonlinearly with drive level because the dynamic range is restricted by the inherent turnon threshold and saturation effects. The pulse-leading, edge-delay phenomenon in the output response is also quite evident. It represents the time it takes the subharmonic signal to build up from noise and is influenced by factors such as circuit-Q (resonance characteristics) and overall loop gain. The effective loop gain increases with drive level, and this reduces the leading edge delay as is evident in Fig. 8.

In this pulse test, as in all other test cases investigated, the transistor divider proved to be predictable and well-behaved. Obviously, the circuit remains subject to the various behavioral peculiarities mentioned earlier which are inherent in regenerative dividers in general. Despite these factors, regenerative frequency division can play a

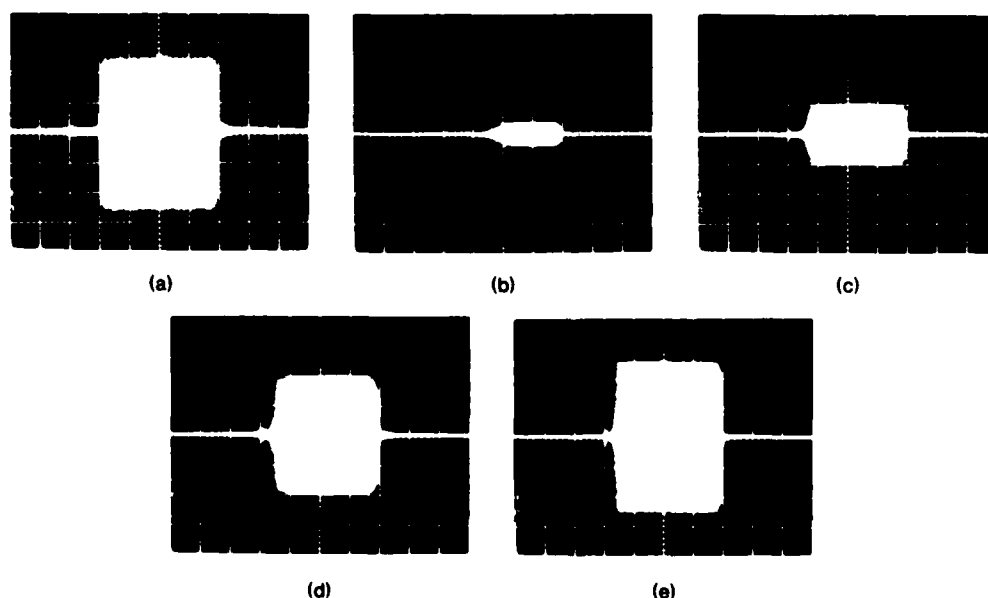


Fig. 8 — (a) Incident 16 GHz pulse of 200-ns duration; (b) 8 GHz pulsed output response of the GaAs FET frequency divider for 16 GHz input peak power level of + 7 dBm, (c) + 10 dBm, (d) + 13 dBm, and (e) + 16 dBm. Time scale: 50 ns per division.

valuable role in a variety of microwave systems applications such as instrumentation, communication links, and signal processing. The divider circuit described here represents an attractive option for such applications based on its conceptual simplicity, ease of design, and well-disposed performance characteristics.

[Sponsored by NAVELEX]

Planar, Fully Ion Implanted Indium Phosphide Junction Field Effect Transistors

J.B. Boos and S.C. Binari
Electronics Technology Division

In recent years, indium phosphide (InP) has received considerable attention due to its potential application in the fields of microwave power amplification and optoelectronics. InP is of interest for microwave power amplification because it possesses a high peak electron drift velocity, which yields high-frequency performance, and low ionization coefficients which correspond to high breakdown fields. For optoelectronics applications, InP field effect transistors (FETs) can be monolithically integrated with InP-based lasers and detectors for use in low-loss, low-dispersion, fiber-optic communication systems.

Possible InP FET structures include metal-semiconductor FETs (MESFETs), metal-insulator-semiconductor FETs (MISFETs), and junction FETs (JFETs). The InP MESFET tech-

nology is hindered by excessive gate leakage current. The MISFET approach has shown a susceptibility to transient and total dose radiation. This low radiation tolerance, which probably arises from the poor quality of the insulator-semiconductor interface, may limit the application of MISFETs in a military or space environment. The InP junction FET, however, circumvents the insulator technology problems associated with the InP MISFET approach and the gate leakage problem of InP MESFETs; for these reasons, it is being emphasized at NRL.

Structure and Key Design Features: Figure 9 illustrates the cross section of the InP junction FET. Electron current flowing from the source to the drain through the n -channel is controlled by varying the depth of the p/n junction depletion region beneath the gate. The p -region contains charge carriers that are predominantly holes (positive charges); the n -regions contains charge carriers that are predominantly electrons (negative charges). The regions denoted with a plus (n^+ and p^+) contain very high charge concentrations. Under normal DC bias conditions, an input signal applied to the gate and source terminals generates an amplified output signal at the drain and source terminals.

We have made significant improvements in the device technology by incorporating three key features in the JFET design. First, the gate metal resistance plays a major role in determining the ultimate performance characteristics of microwave FETs. The metal resistance of a gold zinc-gold

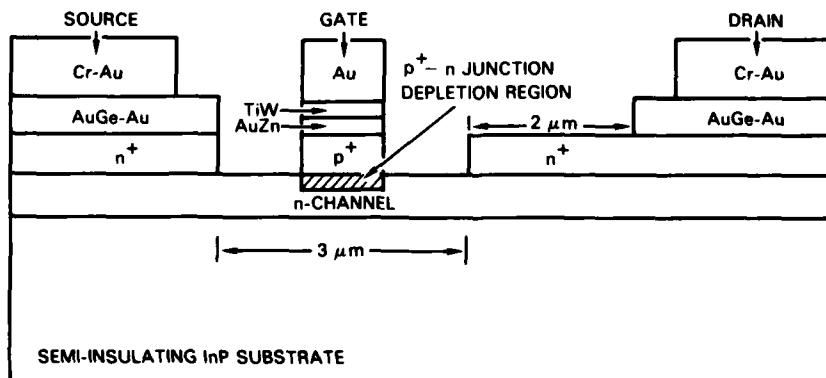


Fig. 9 — The channel cross section of an InP junction field-effect transistor. Electron current from the source to the drain (through the n -channel) is controlled by varying the depth of the p/n junction depletion region (hatched). The n , n^+ , and p^+ regions are formed by ion implantation.

(AuZn-Au) gate contact in earlier studies was found to increase substantially as a result of Zn migration into the outer Au film after alloying. A sputtered titanium tungsten (TiW) layer deposited between the AuZn and the Au films acts as a barrier to the Zn out-diffusion. Increasing the Au overlay thickness then effectively reduces the gate metal resistance.

A second key feature is the use of n^+ ion implantation in the source and drain regions. The benefits of n^+ implantation include the reduction of the source-drain channel resistance and ohmic contact resistance as well as the increase of the drain-to-source voltage tolerance to catastrophic burnout. These improvements in the device provide higher power output capability.

The third key feature is the nature of selective ion implantation, the process which can produce planar structures. This planar process is more technologically attractive since it eliminates step coverage problems and improves lithographic yield.

Fabrication: The n - and p -type regions of the planar InP JFETs were fabricated by sequential, selective ion implantation into iron (Fe)-doped, semi-insulating InP substrates. Silicon (Si) implantation was used to form the n -channel region with a carrier concentration of approximately $2 \times 10^{17} \text{ cm}^{-3}$. Beryllium (Be) implantation was used to form the p^+ -region with a surface carrier concentration of approximately $2 \times 10^{18} \text{ cm}^{-3}$. The contacts to the source-drain and gate were gold germanium-gold (AuGe-Au) overlaid with chromium-gold (Cr-Au) and gold zinc-titanium tungsten-gold (AuZn-TiW-Au), respectively.

JFET Characterization: The typical DC current-voltage (I-V) characteristic for the completed devices is shown in Fig. 10. Here the drain current is displayed as a function of drain voltage (measured with respect to the source). For this measurement the source voltage is maintained at zero volts. With zero gate voltage applied (top curve), the p/n junction depletion region depth is near a minimum, and the source to drain current is at its maximum saturated value. Increasing the negative gate voltage extends the depletion region further into the channel (see Fig. 9), resulting in lowered saturated drain current, indicated by the lower curves in Fig. 10.

The power and small signal microwave performance of the implanted JFETs were also evaluated. The ratio of the output power to the input power is the power gain of the JFET. Maximum power gains as high as 13.1 dB and 9.4 dB were measured at 4.5 and 8.0 GHz, respectively. The typical bias setting for small signal operation was a gate voltage of -4 V and a drain voltage of 8 V . To evaluate power performance, the devices were tested for their maximum power output with 3.0 dB gain. With a 14.5 V drain bias, maximum output powers of 300 mW were measured at 4.5 GHz corresponding to a scaled maximum output power of 1 W/mm gate width. At 8.0 GHz, scaled output powers as high as 0.66 W/mm were obtained. These microwave power results at NRL are a factor of two higher than the best laboratory performance previously reported for InP junction FETs.

[Sponsored by NAVAIR and NAVELEX] ■

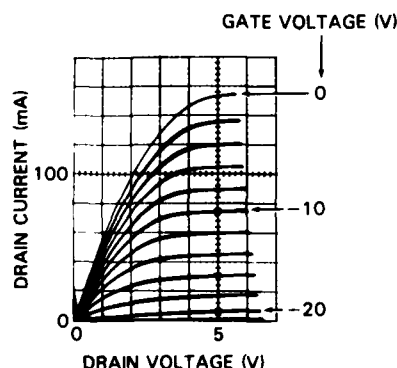


Fig 10. — The current voltage (I-V) characteristic of a typical InP junction field effect transistor. The drain voltage is shown on the horizontal axis (1 V/division), and the drain current is shown on the vertical axis (1 mA/division). The top curve corresponds to zero applied gate voltage. The lower curves show the reduction in drain current achieved by increasing the gate voltage in -2 V intervals.

Electronic Warfare Microprocessor

R.M. Christiansen
Tactical Electronic Warfare Division

NRL is developing a new microprocessor design, for electronic warfare (EW) application, that will provide greatly improved signal processing performance at a significantly reduced cost. A breadboard model demonstrating feasibility of such a microprocessor has been completed and is being tested. This breadboard can operate at speeds four times greater than the top speed of the best currently available standard Navy computer. A second-generation production model will be designed employing a special set of chip devices using state-of-the-art technology.

Experience over the useful life of many computer/processor designs has shown that the cost of software development and maintenance will be many times more than cost of the hardware. These relative costs of software decrease as the quantity of computers and their related software increase. Significant potential life-cycle cost savings can be achieved by basing new designs on familiar computer characteristics rather than creating new unfamiliar characteristics. These characteristics are reflected primarily in the instructions executed by the processor.

Characteristics: This new processor is designed to operate with instructions used in current standard Navy computers. This permits the use of standard Navy support software to write programs in popular or standard Navy higher order language, or in assembly language. This new processor also has new instructions added to achieve improved performance. Some of these new instructions permit operations directly to the processor memory to improve general usefulness of the design. EW applications largely use small number values and simple instructions. Many of these types of instructions have been added to improve performance in EW applications. In addition, several special compare-between-limits instructions have been added to accommodate popular EW signal processing operations.

Processor operating speed has been improved by the incorporation of several speed-

up techniques in the hardware design. These techniques include instruction pipelining, split memory, and path length minimization. Three level instruction pipelining has been applied in a straightforward manner to permit overlapped fetch, decode, and execution cycles. Memory has been organized into separate interleaved instruction and data memories. Instruction memory has been further divided into odd and even sections, resulting in a threefold improvement in the rate at which stored files can be retrieved. This permits use of less expensive memory without limiting performance. Overall operating speed is optimized by minimizing the worst-case execution paths for the most commonly used instructions. Operating speed is further increased by individually timing instructions to a minimum number of high-speed clock cycles.

Prototype Performance: A breadboard demonstrating these design features has been constructed with currently available integrated circuit components. To measure processor speed, a benchmark program consisting of a representative mix of EW application instructions has been established. In this program, the most used 12 instruction types account for 98% of all instructions used in typical EW applications. The processor breadboard has demonstrated its capability of executing this instruction test program at a rate of 3 million instructions per second, which is more than four times the rate achievable in the best current standard Navy computer. Additional representative application programs have been written and executed; these demonstrate the ease of programming and speed of the breadboard. These programs have been written and executed in multiple formats to compare the effects of other characteristics of language use and support software on processor operation. These characteristics include the quantity of code generated by programs and execution speed when assembly code and higher order languages are used. Effects of data impact on performance and use of the new instructions have also been evaluated.

A follow-up production processor will implement the proven design by using advanced integrated circuit technology. This technology employs dense gate array structures containing 6000 logic gates, which will be customized to the

processor design. Five devices will be designed, including an arithmetic logic unit, a memory controller, and a microsequencer. The resultant processor will have a minimum two-card configuration consisting of a central processing unit (CPU) and 128K word memory, with a total power dissipation of 40 W. Operating speed for this new configuration will be 4 million instructions per second on the EW benchmark program. An unusual feature of this new design is that it can be used in hardware designs capable of exe-

cuting a number of different instruction sets in addition to the original standard Navy instruction set.

[Sponsored by NAVAIR]

Reference

1. R.M. Christiansen, "A Low Life-Cycle Cost EW Microprocesor," Proceedings of the Government Microcircuit Applications Conference, Orlando, Fla., Nov. 1982. ■

*Numerical modeling and simulation
with physical applications*

201 Fast Three-Dimensional Airblast Calculations

David L. Book, David E. Fyfe, and John H. Gardner

Very large codes can run faster out of core memory.

202 Navier-Stokes Calculations of Turbulent Wall-Pressure Fluctuations

Robert A. Handler

The spectral properties of channel flow agree with measurements.

204 Anomalous Resistivity in the Auroral Plasma

Peter J. Palmadesso

Turbulent waves account for the observed "spikey" nature of the auroral plasma.

206 X-Ray Gain Enhancement Using Suprathermal Electrons

John P. Apruzese and Jack N. Davis

Hot electrons can enhance amplification in X-ray lasing media.

208 Bandwidth Extension for Shipboard Twin-Fan Antenna

Richard K. Royce

Resistively loading the fan wires can triple bandwidth.

NUMERICAL MODELING

Advances in numerical techniques and computer hardware are providing new tools for scientists and engineers to study more complex systems. These studies can be used for fundamental science research, or for design and optimization studies. The first article describes a new numerical technique with an application to nuclear airblasts. The other articles describe numerical simulations which produced new fundamental knowledge or were engineering design studies. Several of the articles in other sections could equally have been included here since numerical modeling is a universal tool of science and engineering.

This work was done in the following divisions: Laboratory for Computational Physics (Code 4040), Plasma Physics (Code 4700), Marine Technology (Code 5800), and Information Technology (Code 7500).

Many other numerical modeling research projects are under way at NRL. Other than those in this *Review*, a few study

- droplet combustion,
- jets,
- shear-flow instabilities, and
- detonation chemistry.

Page 198, upper left down to lower right:

Time sequence of a numerical simulation of the first second of a ground blast of 600 tons of explosives to simulate an atomic detonation. Each box shows the horizontal structures of a constant pressure surface.

A full-scale shipboard test facility at NRL's Pomonkey, Maryland field site. This facility simulates the electromagnetic environment encountered by HF communication systems aboard actual ships and is patterned after the physical characteristics of the USS *AINSWORTH* (FF 1090). Data from this facility have been used to develop and test numerical models of shipboard antennas. See article on p. 208 by R. Royce.

Fast Three-Dimensional Airblast Calculations

D.L. Book, D.E. Fyfe, and J.H. Gardner
Laboratory for Computational Physics

During an attack on closely spaced, hardened missile silos, incoming reentry vehicles may be disabled through erosion by the dust clouds resulting from detonation of preceding missiles. To study these dust "fratricide" effects, a new three-dimensional computer model simulates the progressive detonation of a linear array of megaton-sized weapons (the "slow walk" attack scenario). The calculated flow fields that result from the interacting bursts are used to predict wind velocities, dust sweepup and lofting, and cloud rise. The eroding effects of the dust clouds depend in a complicated way on the timing and spacing between successive bursts.

The Numerical Technique: These calculations were made possible by the development of FAST3D, a code for solving the three-dimensional hydrodynamic equations using a new Flux-Corrected Transport (FCT) algorithm. The flux-correction algorithm minimizes numerical errors arising from the finite-difference approximations in the hydrodynamic equations. This algorithm, previously used in two-dimensional models [1], allows highly accurate treatments of shock phenomena. FAST3D is the first three-dimensional code to use FCT.

FAST3D also uses a new design that provides higher computational speed. To get adequate resolution in a problem as complicated as that of multiple interacting explosions, a large number of zones—up to one and a half million—are needed in the computational mesh. Five fluid variables are stored for each zone. Since the computer used for the calculations, a Cray-1 located at Los Alamos National Laboratory, has less than a million words of useable core memory, most of the stored information must be kept on disk. Only the arrays from that part of the mesh which is actively being updated are in core at any time (Fig. 1). Hence, the FAST3D code has been designed to allow data to move into and out of core quickly; this makes optimum use of the computer's high speed in parallel processing (vectorization) of arithmetic operations.

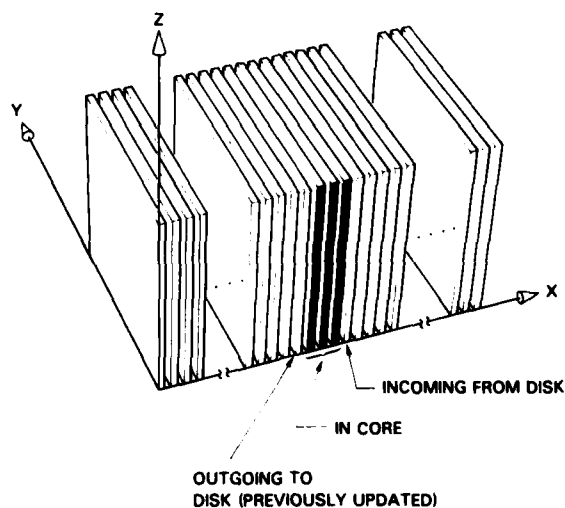


Fig. 1 — Data structure in FAST3D. Each of the slices shown is a two-dimensional array of computational cells or zones. To advance the physical variables in a particular zone by one timestep, information is needed from the nearest zones. At any time, three y - z slices of data from the preceding timestep are in core, a fourth slice is coming from disk, and a fifth slice is returning to disk. This permits the program to sweep through the individual zones of the central slice, updating all variables. After the updated slice is returned to disk, the leftmost slice in core is discarded, the other three slices are incremented to the left, and a new slice is added from disk on the right. The arithmetic and input/output functions overlap and occur simultaneously.

The solution is found by numerically solving the equations for the conservation of mass, momentum, and energy of an ideal, compressible fluid in Cartesian geometry on a rectangular, variably spaced mesh. The main region of the calculation employs equally spaced zones to maintain high accuracy. The grid may be stretched in regions of little activity to reduce running time or near the edges of the mesh to minimize the influence of boundary approximations. A number of different boundary conditions can be applied, and a variable time step is chosen to ensure numerical stability over the whole mesh. The momentum equation contains a gravity term and the model uses a real-gas, equation-of-state routine to obtain the pressure.

Airblast Calculations: After testing the numerical model with a variety of simple idealized calculations, we calculate the effects of a linear array of 6-Mton nuclear weapons exploding

at intervals of 24 s. Four cases were studied. In the first case, the bursts were collocated. In the second case, each successive burst was displaced along the x-axis by 1 km with respect to the preceding one. In the third and fourth problems, successive bursts were 3 km and 8 km apart.

The rate of generation of dust clouds is sensitive to the spacing between bursts. As the shocks produced by interacting fireballs reflect from one another and the ground, complicated wind fields with maximum speeds of several hundred m/s led to enhanced dust entrainment. After 60 s, the top of the dust cloud rises faster in the collocated case than in the other cases, causing dust and debris to be lifted higher from the ground. If the bursts continue for several minutes, the successive shocks punch a hole through to the upper atmosphere. With bursts separated by 1 and 3 km, the fireballs from successive bursts merge to form an elongated slanting "chimney" about 50-75 km high which acts as a duct for the vertical updrafts. However, the dust still does not rise as fast as in the case of collocated bursts. Because of the larger displacement between the energy sources for 8 km separation, shock strengths in the interaction region are considerably smaller and the bursts evolve almost as though they were isolated.

These flow fields are used as inputs for codes that calculate damage to incoming reentry vehicles. This information is essential for determining the vulnerability of various silo configurations to possible attack scenarios.

[Sponsored by the Defense Nuclear Agency]

Reference

1. D.L. Book, 1981 *NRL Review*, p. 97. ■

Navier-Stokes Calculations of Turbulent Wall-Pressure Fluctuations

R.A. Handler
Marine Technology Division

Turbulent flows over solid bodies generate local pressure fluctuations which may cause unwanted structural vibration and may directly contaminate the signals obtained by hydrophones

and sonar systems. Therefore, turbulent boundary layer flows which generate these fluctuations are of great interest to the Navy. This paper describes a joint NRL/MIT effort to apply recently developed numerical methods to simulate fully developed turbulence directly from the highly nonlinear Navier-Stokes equations. The NRL contribution focused on the analysis and interpretation of the results of a 3-D turbulence code developed at MIT and executed on a Cray-I computer located at Los Alamos National Laboratory.

One advantage of the present approach is that the experimental acquisition of equivalent information about turbulent flows would be very difficult and costly. The simulation described in this paper provides the required details of the flow at a large number of spatial locations and thereby permits the assessment of the spatial and temporal structure of the sources of wall-pressure fluctuations. It should be emphasized that the present approach is significantly different from traditional methods used in the computation of turbulent flows in that, while standard methods rely heavily on empirical data to model the nonlinearities in the Navier-Stokes equations, the present methods rely on no empirical input. Thus, turbulent flows can now be computed directly from the governing equations of fluid dynamics.

The Calculations: Recently, pseudospectral techniques, in which Fourier series and Chebyshev polynomials are used in the spatial domain and traditional time differencing is used in the temporal domain, have been shown to accurately represent many of the features of real turbulent flows [1]. These methods have been employed here to compute the wall-pressure field at a low Reynolds number (5000 based on channel half-width) in a turbulent channel flow from the full three-dimensional Navier-Stokes equations using $(32)^3$ grid points [2]. In Fig. 2, the computed spectral density ϕ of the pressure fluctuations at a point on the surface is normalized with respect to the wall shear stress τ_w , the channel centerline velocity U_{cl} , and the channel half-width h , and is plotted against the normalized frequency fh/U_{cl} , and compared with experimental results. The agreement with experiment

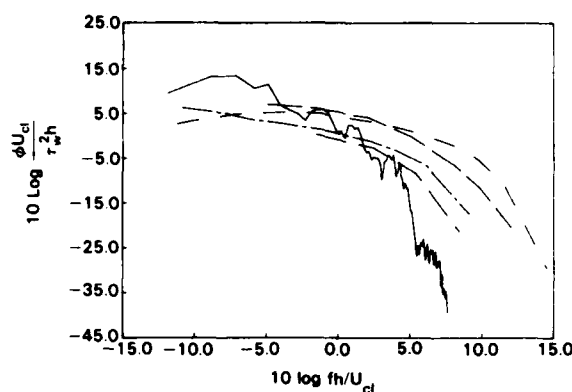


Fig. 2 — Comparison of computed and experimental pressure spectral densities: (solid line—computed; dashed lines—experiments).

is good for $0.4 \leq fh/U_{cl} \leq 2.0$ (-4.0 to 3.0 on the logarithmic scale of Fig. 2). At a nondimensional frequency of about 2.5 (4.0 on the scale of Fig. 2), we observe a sharp drop in the computed spectral level. This is due to the finite spatial resolution of the calculation (i.e. the smallest scales of turbulence may not be adequately resolved). However, the root mean square pressure level normalized with respect to τ_w is in excellent agreement with experimental results in the range.

In addition, the two-point spectral properties of the pressure field have been computed. These calculations clearly demonstrate that the field has a wave-like pattern that is being convected by the mean flow, and their streamwise length is about the width of the channel. The computed broadband and narrow band convection speeds of the pres-

sure field (phase velocities of the wave-like patterns) given by \bar{U}_c and U_p respectively, are compared with experiment in Fig. 3. The broadband convection speed shown in Fig. 3(a) is plotted against $\Delta x/h$, where Δx is the distance separating two computational points in the streamwise direction. (The minimum computational grid spacing in this calculation is $\Delta x/h = 0.162$). Figure 3(b) shows the narrowband convection speed as a function of nondimensional frequency. Both representations of the convection speed indicate that the pressure pattern travels at about 65% of U_{cl} . As shown in Fig. 3, this is in excellent agreement with experiment.

The results obtained thus far are encouraging in that the dominant features of the wall-pressure field in a complex, inhomogeneous, anisotropic turbulent flow have been exhibited by

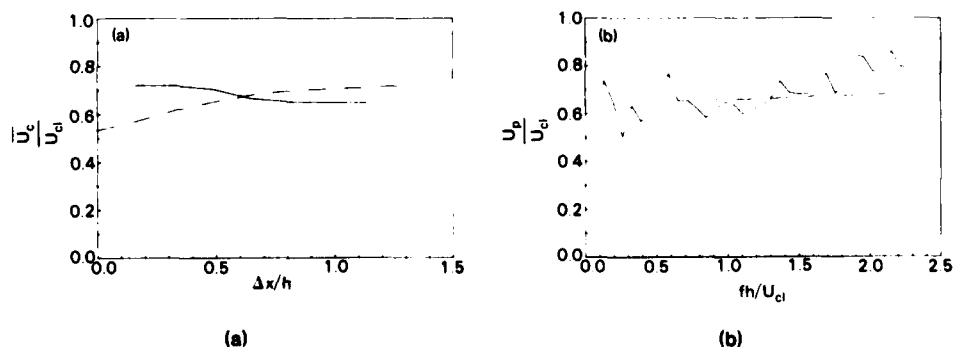


Fig. 3 — Comparison of computed and experimental convection velocities (a) broadband velocities (solid line—computed; dashed line—experiment); (b) Narrowband velocities (solid line—computed; dashed line—experiment).

the computation. In future work, the number of grid points in the calculation will be increased to $(64)^3$, enabling the resolution of finer scales of turbulent motion. The success of these preliminary findings suggests that a detailed investigation of the sources of the pressure field is warranted. To this end, conditional sampling techniques will be employed to determine the relationship between events in the velocity field and events in the pressure field.

[Sponsored by ONR]

References

1. S.A. Orszag and A.T. Patera, *Phys. Rev. Lett.* **47**, 832 (1981).
2. R.A. Handler, R.J. Hansen, L. Sakell, S.A. Orszag, and E. Bullister, *Phys. of Fluids* **27**, 579-582 (1984). ■

Anomalous Resistivity in the Auroral Plasma

P.J. Palmadesso
Plasma Physics Division

The auroral displays that are observed at higher latitudes are produced in the ionosphere by energetic electrons that stream downward along the earth's magnetic field lines. Several mechanisms have been proposed to explain the generation of these electrons, including a model based on plasma instabilities that was developed jointly by NRL and University of Maryland scientists in 1981. Experimental data obtained from satellites in 1982 provided new opportunities for testing the theoretical explanations and stimulated a new series of theoretical calculations by the NRL/Maryland group. We now find that the NRL model agrees well with these new observations, explaining features that other models do not.

The impact on Navy systems depends on the mechanisms by which the energetic electrons are produced. The electrons, along with electric fields and currents involved in the process, play a major role in the generation of local environmental disturbances which can disrupt Navy com-

mand, control, communications, and intelligence (C³I) systems operating in the high-latitude regions. Electric fields parallel to the earth's magnetic field lines ($E_{||}$) accelerate the plasma particles, which can in turn degrade satellite systems via spacecraft charging, radiation damage, and increased atmospheric drag associated with atmospheric heating. Plasma instabilities driven by the currents involved in the process can cause strong irregularities in the refractive index of the ionosphere at transmission frequencies of C³I systems. This leads to random fluctuations in signal amplitude, phase, and polarization of received signals. These irregularities in refractive index can also be caused by spatially nonuniform energy deposition by the energetic particles or by the fluctuating electric fields that are involved in the acceleration of the particles. To have a predictive capability for the effects on Navy systems, it is essential that we understand the basic physical processes underlying these phenomena.

Earlier Models: A notion arose during the early 1970's that the precipitating auroral electrons gained most of their energy by falling through a potential drop that was aligned along the earth's magnetic field. However, the existence of such $E_{||}$ fields at these high altitudes was paradoxical; the low particle densities implied negligibly small collision rates between particles (or high mobility for electric charges) and very low classical values for the electrical resistivity. If charges could move freely along the magnetic field lines, they would "short out" the $E_{||}$ field!

In 1981, the NRL/Maryland group proposed a mechanism for sustaining electrical resistivity on auroral field lines despite these negligibly small particle collision rates [1]. Large-amplitude ion waves are driven by a collisionless plasma instability, and some of the ionospheric electrons are trapped in the potential troughs of these waves. The electrons that carry the current along the magnetic field lines lose momentum to these trapped electrons by a collisionless electron-electron streaming instability, which has much the same effect as high collision rates. The anomalous electrical resistivity caused by this enhanced rate of momentum transfer is much higher than the classical resistivity and, therefore, an electric field can be maintained along the field

line. In the auroral plasma, the collisionless instability that drives the large-amplitude ion waves may either be the electrostatic ion cyclotron (EIC) instability, the oscillating two stream instability, or the ion acoustic instability. The first of these instabilities (EIC) is the most easily excited and is thus expected to be the dominant mechanism.

Explanations of Newer Data: The original computer simulations of this anomalous resistivity mechanism were successful in reproducing the shapes of the electron velocity distributions that were experimentally observed on auroral field lines (Fig. 4). However, because experimental data on the E-fields were not available, these earlier calculations did not address the characteristic spatial shapes of the resulting electric field fluctuations. This is an important issue. Satellite electric-field sensors provided high-resolution records of the E_{\parallel} fields in 1982 [2]. These showed a series of well separated spikes, similar in appearance to the discrete electric field

spikes called "double layers" which have been seen in some laboratory discharge experiments. A number of researchers have identified the auroral E_{\parallel} spikes as multiple weak double layers as a result of these and similar observations.

Older models of anomalous resistivity were based on weak turbulence theory and could only predict a relatively uniform parallel electric field. In the NRL/Maryland model, the ion waves can reach sufficient amplitude to become strongly turbulent. Then, a significant fraction of the electrons can be trapped between the ion-wave cavities. These trapped electrons can short out the spatially uniform electric field between the ion-wave cavities, leaving localized spikes within the cavities. New simulations of this mechanism include higher harmonics of the ion-wave turbulence, as observed in space, and they exhibit E_{\parallel} signatures strikingly similar to those in the experimental data (Fig. 5).

Other features of the experimental data are also explained by the model. Satellite records of E_{\perp} , the electric field component perpendicular to the geomagnetic field, were taken simultaneously with the E_{\parallel} measurements; these exhibit strong EIC waves, as predicted by the NRL/Maryland theory. Also, the average spacing between the experimentally observed E_{\parallel} spikes in the satellite data is approximately ten times the observed transverse EIC wavelength. This feature is consistent with the NRL/Maryland model because the effective wavelength of EIC waves in the parallel direction is typically ten times the transverse wavelength. This close association with EIC waves is not a feature of the double layer theory. These results, taken in combination with other features of the observational data, support the conclusion that the fields that are responsible for the auroral electrons are due to an anomalous resistivity that accompanies the electrostatic ion-cyclotron instability.

[Sponsored by ONR and NASA]

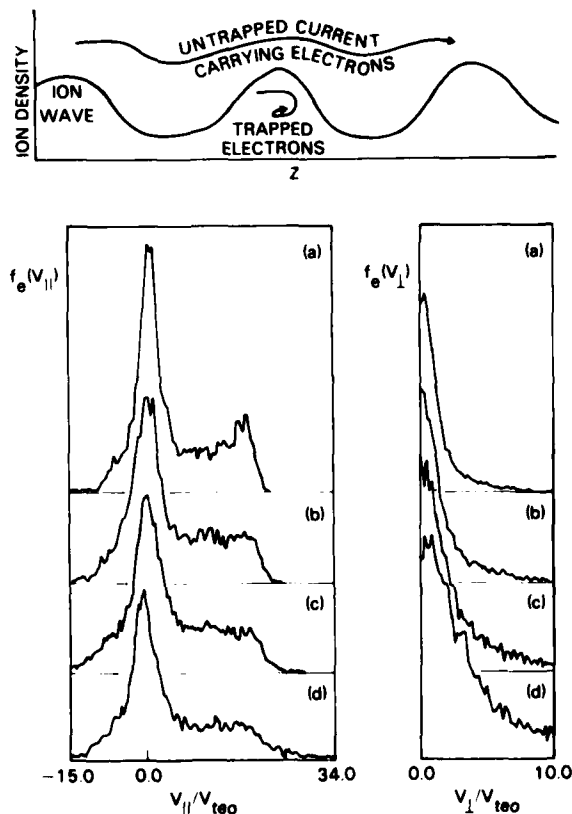


Fig. 4 — Upper panel shows a schematic illustration of the resistivity mechanism. The lower panels show the characteristic features of the electron velocity distribution functions for parallel and transverse velocities, obtained in a computer simulation of the resistive interaction. Subpanels a through d represent successively later times. v_{te0} is the initial electron thermal speed.

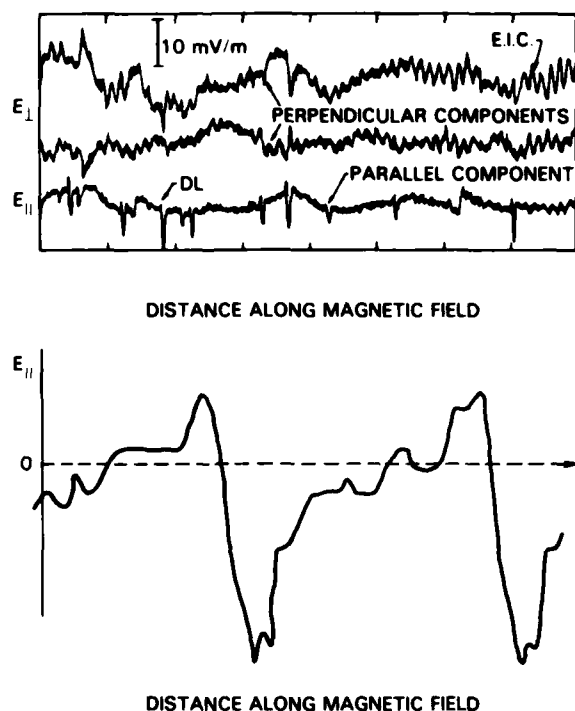


Fig. 5. — Upper panel shows experimentally observed auroral electric field signatures ("Observations of Double Layers and Solitary Waves in the Auroral Plasma," by M. Temerin, K. Cerny, W. Lotko and F.S. Mozer, *Phys. Rev. Lett.*, **48**, (17) 1175 (1982) The American Physical Society, used by permission). DL indicates an E_{\parallel} spike, identified as a double-layer by the authors. EIC indicates an electrostatic ion-cyclotron oscillation in E_{\perp} . Lower panel shows a computer-generated E_{\parallel} spike characteristic of the NRL resistivity model (enlarged relative to data traces).

References

1. H.L. Rowland, P.J. Palmadesso, and K. Papadopoulos, *Geophys. Res. Lett.*, **8**, 1257 (1981).
2. M. Temerin, K. Cerny, W. Lotko, and F.S. Mozer, *Phys. Rev. Lett.*, **48**, 1175 (1982). ■

X-Ray Gain Enhancement Using Suprathermal Electrons

J.P. Apruzese and J.N. Davis
Plasma Physics Division

For years, lasers have existed which produce coherent, highly amplified, monochromatic

radiation in the ultraviolet and longer wavelength regions of the electromagnetic spectrum. A major challenge to current high-power radiation technology which remains elusive is the generation of similarly coherent radiation in the X-ray region of the spectrum. Such an X-ray laser would find applications in condensed matter physics and structural deformation studies, in radiation damage assessments, X-ray microscopy, and diagnosis of hot plasmas. We have found through computational study that the suprathermal or "hot" electrons produced in laser-plasma interactions may be used to increase the X-ray gain in neon-like ions. Experimental realization of this effect would significantly advance the effort to produce an X-ray laser.

Because X-ray photons have high energies, any successful X-ray amplifying medium is likely to be so hot as to create a plasma. This introduces some problems: maintaining the appropriate plasma densities and temperatures, shaping the plasma properly, and obtaining enough power at the correct electron or photon energies to "pump" the medium and maintain its amplifying properties. It is this latter problem of pumping that our work has addressed.

Hot Electron Generation and Use: For a decade or longer, the interaction of plasmas with longer wavelength ($\lambda > 1 \mu\text{m}$), high-power lasers has been studied in connection with the problem of achieving laser-driven fusion. In these studies, the intense laser radiation has produced populations of high-energy or suprathermal electrons quite distinct from the normal thermal or "cold" electrons which characterize the usually defined plasma temperature. For a variety of reasons, these hot electrons have rendered the achievement of laser fusion considerably more difficult than anticipated. In a given experiment, the physical parameter which principally controls the hot electron production is $I \lambda^2$ where I is the driving laser's intensity and λ its wavelength. As $I \lambda^2$ increases, both the amount and the temperature of the hot electrons increase.

We have discovered through detailed and extensive calculations that these hot electrons may be used for populating or pumping excited states of certain ions, thereby greatly enhancing their X-ray amplifying gain. A particularly

appropriate candidate for demonstration of these effects is neon-like iron, an iron ion with 16 of the normal 26 electrons stripped from the nucleus, leaving 10 electrons and an atomic structure similar to neutral neon. This ionic transition used yields X rays of wavelength 254.9 Å. However, virtually any ion of atomic number higher than iron would also be amenable to enhanced pumping. For instance, tin, of atomic number 50, would produce X rays at 118 Å. The key concept is to match the energy of the suprathermal electrons to the excitation energy of the upper state of the lasing transition. The laser intensity and wavelength would be chosen to produce the correct hot-electron energies and cold-electron temperature for the plasma element used. For specificity, the calculations reported below have used a detailed atomic physics model for ionized iron. Our principal goal was to determine the relevant ionic species and level populations and the resulting gain under various plasma conditions.

Calculated Gain Enhancements: Figure 6 presents some typical results. In this figure, the X-ray gain coefficient g (per cm) for 254.9 Å X rays is plotted as a function of the ratio of the number of hot electrons to the number of cold electrons. (The X rays would be amplified by a

factor of e^g after passing through 1 cm of this plasma.) In addition to the gain coefficient, the fraction of the iron ions that are in the 10-electron (neon-like) ionization state is shown. The hot-electron energy is 800 eV, the cold-electron temperature is 70 eV, and the cold-electron density is $4 \times 10^{20} \text{ cm}^{-3}$. As is evident, the X-ray gain peaks at 40 cm^{-1} when 25% of the electrons are hot. The gain is much smaller with no hot electrons present. In the absence of hot electrons, when sufficient thermal electrons are available to pump the upper lasing state, those same thermal electrons tend to ionize the iron past the neon-like stage. The two-component electron distribution enhances gain by providing hot electrons that are precisely tailored to pump the upper level and cold thermal electrons that maintain the neon-like stage through recombination.

A major advantage of this technique for plasma pumping is that large gains are obtainable over a wide range of plasma densities. Figure 7 presents the calculated gain coefficient as a function of thermal electron density. Note that the gain exceeds 10/cm for the wide range of electron densities between $8 \times 10^{19} \text{ cm}^{-3}$ and $3 \times 10^{21} \text{ cm}^{-3}$. The requirement for thermal electron temperature (30 to 130 eV) is not very exacting, either. Thus, the constraints on plasma

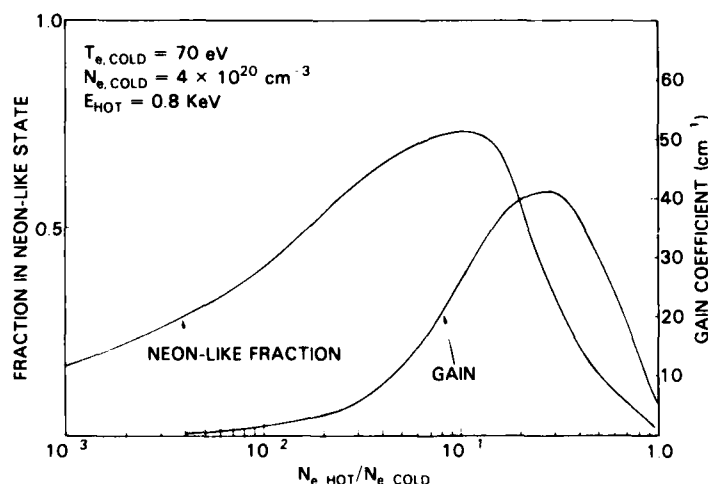
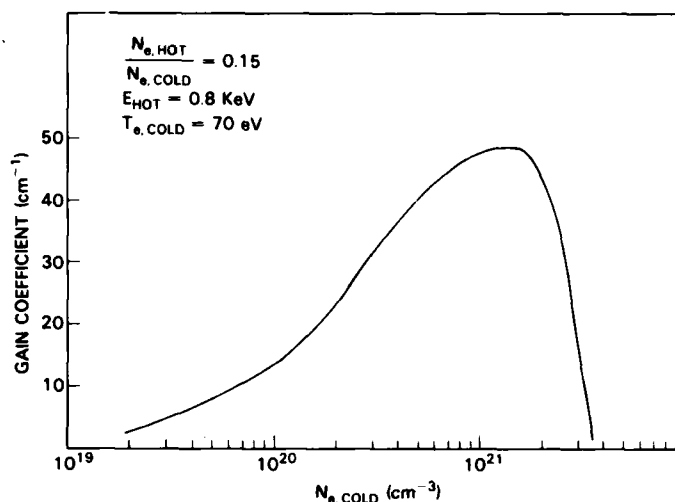


Fig. 6 — The X-ray amplifying gain coefficient at a wavelength of 254.9 Å in an iron plasma is plotted as a function of hot-electron fraction. Also shown is the fraction of all ions in the neon-like (10 bound electrons) stage.

Fig. 7 — The X-ray amplifying gain coefficient at a wavelength of 254.9 Å in an iron plasma is plotted as a function of thermal electron density. The number of hot electrons is 0.15 that of the thermal electrons in this calculation.



conditions are generally not as severe as in other proposed X-ray amplification schemes.

Future work in this area will concentrate on two objectives. First, we will perform calculations to determine which plasma elements other than iron would be most suitable for similar X-ray amplification with presently available laboratory lasers. Some preliminary results suggest that tin would be even more promising. Second, we intend to pursue a laboratory demonstration of these concepts using laser-heated plasmas.

[Sponsored by Los Alamos National Laboratory and ONR]

Reference

1. J.P. Apruzese and J. Davis, "Enhancement of X-Ray Gain in Neon-Like Ions by Direct Collisional Pumping with Suprathermal Electrons," *Phys. Rev. A* 28, 3686 (1983). ■

Bandwidth Extension for Shipboard Twin-Fan Antenna

R.K. Royce
Information Technology Division

Introduction: A new high-frequency communication system is being developed under the Navy's High Frequency Improvement Program

(HFIP). One feature of this new system is the ability to rapidly shift operating frequency. Realization of this feature requires that system components have broadband characteristics. Since existing shipboard transmitting antennas typically provide efficient radiation over a bandwidth having a ratio of only about 3 to 1 between the upper and lower frequencies, there is a need to develop antennas having much greater broadband characteristics. An antenna used on most Navy combat ships today is the twin-fan type transmitting antenna [1]. Figure 8 shows this antenna, which typically exhibits a useful band from 2 to 6 MHz, installed on a ship model. The fan wires of this twin-fan antenna were resistively loaded in an attempt to extend the operating bandwidth. The resistive loading has resulted in a potentially useful operating range from 2 to 14.5 MHz for the twin-fan antenna, thus extending its bandwidth to greater than 7 to 1.

Extended Bandwidth Design: Altshuler [2] has shown that the effect of loading a monopole (whip type) antenna with a resistor equal to the antenna's characteristic impedance at a point along its length is to establish a traveling-wave current distribution on the antenna at a frequency which defines the distance between the resistor and the top end of the antenna to be 1/4 wavelength. The traveling-wave current distribution (one with no standing waves on the antenna) is achieved at only one frequency, but the effect

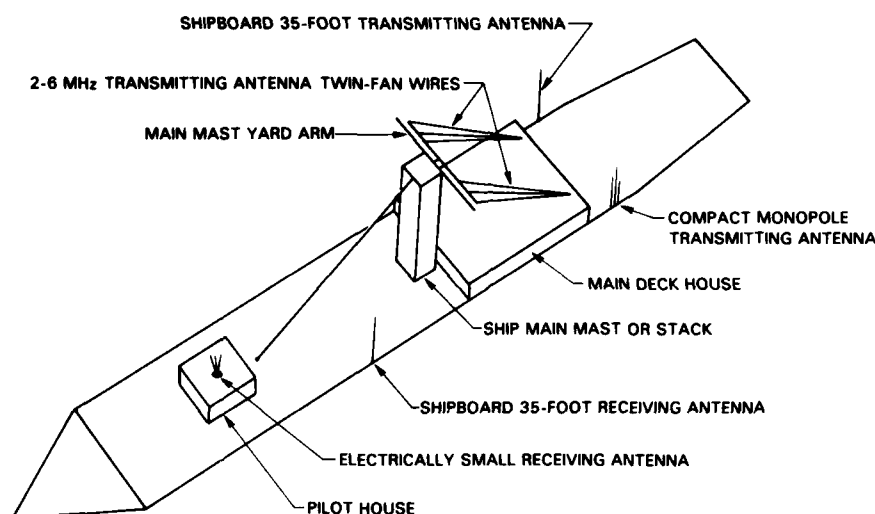


Fig. 8 — USS *Pomonkey*, a shipboard electromagnetic environment simulation

degrades slowly over a broad bandwidth. Thus a relatively constant antenna input impedance is provided to the transmitter. It was believed that a similar effect might occur on the twin-fan antenna even though it bears little resemblance to a monopole. The design challenge is to determine an optimum resistance value and location for the loads in the fan wires. The current distribution on an arbitrary structure, such as the twin-fan antenna in the shipboard environment, can be determined by a general numerical antenna simulator primarily developed by NRL. Since the antenna impedance can be determined from the current distribution, it is only necessary to vary the loading resistance values and locations by trial and error until the impedance is uniform within a given voltage standing wave ratio (VSWR) tolerance over the broadest possible band, thus significantly reducing impedance mismatch losses to the transmitters.

The impedance of the twin-fan antenna without resistive loading as shown on the ship model in Fig. 8 was first calculated numerically. The calculated data compared favorably with measured data obtained on actual ships, indicating that the computer model was a realistic representation of typical shipboard twin-fan antennas. Next, to extend the bandwidth, a resistance value and location for loading the fan wires were estimated by using Altshuler's theory as a starting point. The resistance value and location

then were varied around the initial estimate in an iterative procedure by using the numerical model to determine a resistance value and location providing acceptable feedpoint impedance VSWR over the greatest frequency range.

Results: Figure 9 shows the twin-fan antenna feedpoint impedance VSWR both before and after resistive loading has been applied to the fan wires. Since a VSWR of 4 or less has been defined as an acceptable goal for the new HFIP broadband system, the data indicate the useful operating band for the twin-fan antenna is 2.5 to 6.5 MHz before resistive loading, and 2.0 to 14.5 MHz after the calculated loading is applied.

Figure 10 shows the resistively loaded antenna radiation efficiency. It has a minimum value of 37% at 2 MHz, and the average efficiency is better than 60% over the useful band. Without resistive loading, the radiation efficiency of the twin-fan antenna is assumed to be nearly 100%. However, present use of the twin-fan antenna without resistive loading requires a tunable coupling network (called a multicoupler) with a nominal efficiency of about 70% to permit the simultaneous operation of several transmitters. Thus, the overall efficiency for the resistively loaded twin-fan antenna is only slightly decreased while the bandwidth is increased to more than twice the original bandwidth.

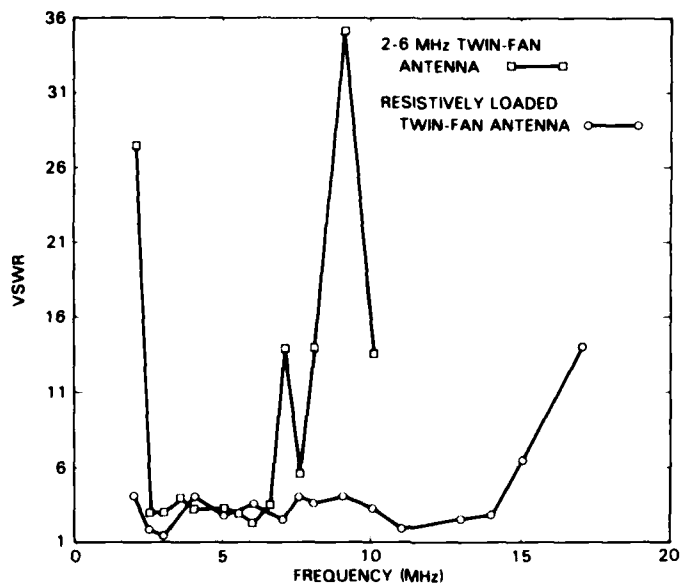


Fig. 9 — Feedpoint VSWR for the twin-fan antenna, before and after resistive loading

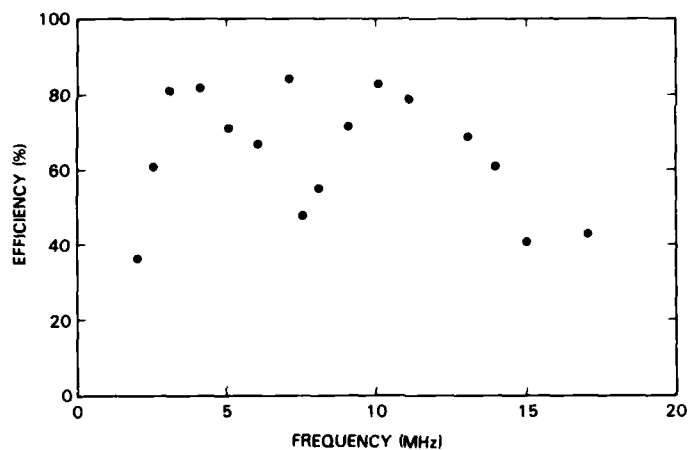


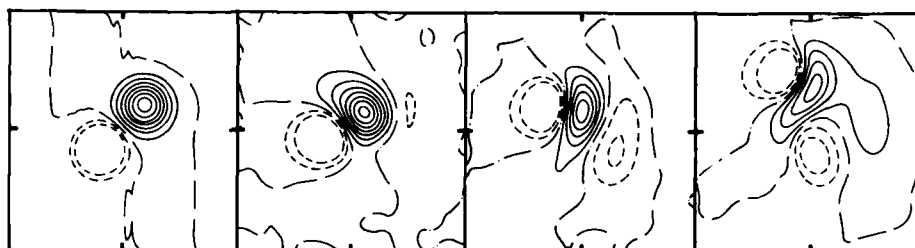
Fig. 10 — Radiation efficiency for the resistively loaded twin-fan antenna

Future Plans: The ship model shown in Fig. 8 has been fabricated on a full-scale basis at the NRL Pomonkey Test Range, Pomonkey, Maryland. The model, named the USS *Pomonkey*, is being used to evaluate new broadband components as system development progresses. Plans are being formulated to resistively load the twin-fan antenna on the USS *Pomonkey* and to evaluate its performance characteristics for the new HFIP broadband system.

[Sponsored by NAVELEX]

References

1. D.W. DuBrul and L.M. Peters, "Shipboard Antenna and Topside Arrangement Guidance," NELC TD 356, pp. 4.4-9 through 4.4-12, 1 Sep. 1974.
2. E.C. Altshuler, "The Traveling-Wave Linear Antenna," IRE Trans. Antennas and Propag. AP-9, 324-329 (1961). ■



Numerical simulation showing the interaction of the cyclonic (counterclockwise rotating-dashed) and an anticyclonic (clockwise rotating-solid) velocity fields of two ocean eddies. Each frame is 10 days apart. In this simulation the ocean is treated as two vertically homogeneous layers; the upper layer occupies 20% of the total depth. Such eddy interactions are observed southeast of the Gulf Stream (R. Mied).

*Excellence in research for
tomorrow's Navy*



215 Special Awards and Recognition

221 Individual Honors

228 Alan Berman Research Publication Awards

AWARDS AND RECOGNITION

"We should ask ourselves, 'Are we, as an in-house laboratory, performing our job as Mr. Edison thought we should?' I believe the answer is that we are doing considerably better than he ever imagined we would. We have been responsive to Navy problems, we have maintained sustained technical competence over the many fields of Navy interest, and we have managed to maintain our intellectual independence.

"In the final analysis, [these awards recognize exceptional] commitment to continued productivity, intellectual integrity, and forefront work in science and technology."

Dr. Alan Berman, former Director of Research
10th Annual Research Publication Awards Presentation

Page 212, from upper left to lower right:

Richard P. Mied, Kazhikathr Kailasanath, Gloria J. Lindemann

Patricia A. Tatem, John Baras, Joseph M. Bologna

Dennis McGregor, Harold G. Eaton, Clifford F. George, Jr.

Richard D. Gilardi, Philip R. Schwartz, William J. Plant

Donald Y. Northam, Frederick W. Williams, Captain John A. McMorris II, USN

SPECIAL AWARDS AND RECOGNITION

NRL is proud of its many distinguished scientists and engineers. A few of these have received exceptional honor for their achievements.



Thomas C. Giallorenzi
Optical Sciences Division

RANK OF MERITORIOUS EXECUTIVE

"The President of the United States of America has conferred on

THOMAS C. GIALLORENZI

the rank of Meritorious Executive in the Senior Executive Service for sustained superior accomplishment in management of programs of the United States Government and for noteworthy achievement of quality and efficiency in the public service."



Peter G. Wilhelm
Space Systems Division

1983 E. O. HULBURT ANNUAL SCIENCE AND ENGINEERING AWARD

"Mr. Wilhelm's keen appreciation of the complex interrelationships among various functions and systems within single and multiple satellites has resulted in an enviable record for the Navy Space Program. He has continuously served as the key technical architect and focus for a space system that today provides a unique and significant operational capability to the Navy and the Nation."



Robert E. Gardner
Radar Division

DEPT. OF THE NAVY SUPERIOR CIVILIAN SERVICE AWARD

"For his superior technical contributions to the advancement of U.S. Naval Surveillance and Non-Cooperative Target Recognition (NCTR) Radar Systems while serving as an Electronic Engineer in the Target Characteristics Branch, Radar Division, Naval Research Laboratory during the period 1965 through the present. ... He has served his country and the Navy in an exceptionally outstanding manner as a recognized innovator, engineer, and leader in his profession and has achieved a position of national prominence."



Frederick V. Hellrich
Space Systems Division

**DEPT. OF THE NAVY
SUPERIOR CIVILIAN SERVICE AWARD**

"For his superior performance and exceptional accomplishments throughout his career at the Naval Research Laboratory and as Associate Superintendent of the Space Systems Division from October 1981 to present. Mr. Hellrich's distinguished contributions to the Navy Space Program include design, development, deployment, and logistic support of an advanced satellite ground station. These achievements have resulted in major technological advancements and have provided a superior improvement to a critical Navy activity."



Albert I. Schindler
Material Science and Component
Technology Directorate

**DEPT. OF THE NAVY
SUPERIOR CIVILIAN SERVICE AWARD**

"For exceptionally outstanding service while serving as the Acting Director of Research for the Naval Research Laboratory from 22 June 1982 to 28 November 1982. ... His exemplary performance during this critical transitional period provided vigorous personal leadership and sustained the momentum and morale of the Laboratory's senior managers. As a direct result of his dedication, perception, sensitivity, and hard work, operational disruptions were minimized, and the transition process was greatly facilitated."



Donald J. Michels
Space Science Division

**NRL - SIGMA XI
PURE SCIENCE AWARD FOR 1983**

"For the conception, promotion, development and use of continuous imaging of the solar corona, especially from the NRL space coronagraph, a unique, continuing solar monitor which has yielded discovery of dramatically rapid changes in the corona. ... Further, for the unexpected observations from the P78-1 coronagraph of unusual 'sungrazer' comets, a class of comet rarely observed through the centuries."



Gary A. Prinz
Electronics Technology Division

**NRL - SIGMA XI
APPLIED SCIENCE AWARD FOR 1983**

"For his pioneering work in establishing molecular beam epitaxy as a viable technique for single-crystal thin film growth of magnetic materials onto semiconductor substrates, thus opening the way for the wedding of these two important fields of solid state physics into a common materials technology."



Conrad H. Cheek
Environmental Sciences Division

**DEPT. OF THE NAVY
MERITORIOUS CIVILIAN SERVICE AWARD**

"This award is presented to Dr. Conrad H. Cheek for services to NRL, the Navy, and the scientific community. The excellence of his technical efforts in chemical oceanography has contributed substantially to the direction and quality of NRL and Navy research; has encouraged high standards of scientific professionalism, responsibility, and integrity; and has fostered production of research results of substantial interest and value to the Navy. He has been an effective advocate of NRL and Navy programs and richly deserves this recognition."



Robert J. Goode
Material Science and
Technology Division

**DEPT. OF THE NAVY
MERITORIOUS CIVILIAN SERVICE AWARD**

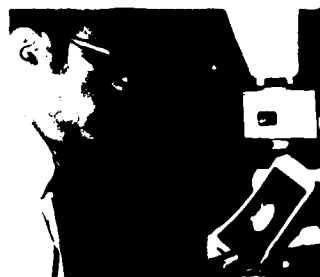
"For his significant contributions as Technical Coordinator to the HY-130 Steel Certification Program for material and weldment research at the Naval Research Laboratory. Mr. Goode coordinated all tasks for developing fracture toughness and stress corrosion testing methods and criteria, resolving the weld hydrogen embrittlement program, and examining metallographic fatigue and stress corrosion fractures."



Donald U. Gubser
Condensed Matter and
Radiation Sciences Division

**DEPT. OF THE NAVY
MERITORIOUS CIVILIAN SERVICE AWARD**

"For his outstanding leadership and significant contributions in the field of superconductivity, both in enhancing our basic understanding of the phenomena and in recognizing and vigorously pursuing development of those aspects of superconductivity which have important Navy and technology impact. His professionalism and his dedication are in keeping with the finest traditions of naval research."



Howard Lessoff
Electronics Technology Division

**DEPT. OF THE NAVY
MERITORIOUS CIVILIAN SERVICE AWARD**

"Mr. Lessoff is being recognized for his outstanding contributions to the numerous programs that he has led which recognize the importance of GaAs-based devices to improve naval microwave capabilities for his vigorous and very successful attack on the problems which were limiting GaAs use. ... His professionalism and his dedication are in keeping with the finest traditions of naval research."



Edward A. Metzbower
Material Science and
Technology Division



Jimmie R. McDonald
Chemistry Division



Merrill I. Skolnik
Radar Division



Jerome Karle
Laboratory for Structure of Matter

**DEPT. OF THE NAVY
MERITORIOUS CIVILIAN SERVICE AWARD**

"... in recognition of his significant contributions to the HY-130 Steel Certification Program through failure analysis research and development at the Naval Research Laboratory. Dr. Metzbower assisted in defining stress corrosion cracking mechanisms in HY-130 base material and weldments and in defining these findings to the failure analysis of laboratory specimens, structural elements, and models. ... These efforts resulted in improvements in structural design and fabrication of HY-130 structures for future deeper diving submarines."

THE HILLEBRAND PRIZE

"The Chemical Society of Washington, in recognition of his research contributions in the fields of Molecular Excited State Dynamics and Photo Chemistry, has awarded the Hillebrand Prize for 1982 to JIMMIE R. McDONALD in Washington, D.C. the third day of March, 1983."

HARRY DIAMOND MEMORIAL AWARD

"For fundamental contributions to radar system engineering including antennas, propagation, clutter, accuracy, and biostatic techniques"

**ELECTED PRESIDENT
INTERNATIONAL UNION OF CRYSTALLOGRAPHY**

The International Union of Crystallography comprises national academies from 34 nations and publishes four research journals, volumes of abstracted structure reports, and international tables. The Union supports and sponsors schools on special topics and a variety of international meetings. Scientists at its main congress, held every 3 years, discuss topics such as diffraction physics, geosciences, materials science, chemistry, and biomedical topics such as physiologically active materials and macromolecular and genetic engineering.



Homer W. Carhart
Chemistry Division

**ELECTED CHAIRMAN,
NATIONAL ACADEMY OF SCIENCES/NATIONAL RESEARCH COUNCIL
ON STUDIES OF HAZARDOUS SUBSTANCES**

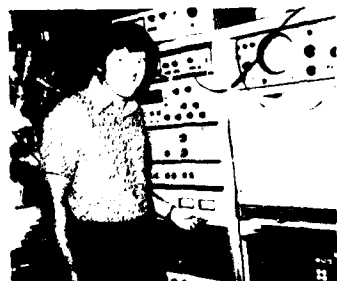
Sponsored by the Occupational Safety and Health Administration, the committee assesses hazards associated with combustible gases, vapors, and dusts found in industrial work places, particularly as related to the use of electrical equipment.



Joel M. Schnur
Optical Sciences Division

**PROFESSOR INVITEE, UNIVERSITY OF PARIS (INSTITUTE
DE MADAME CURIE), PARIS, FRANCE**

The position of Professor Invitee was established at the University of Paris to promote collaboration and interaction between scientists at the University of Paris and scientists of other countries. Dr. Schnur was selected on the basis of his research contributions in the area of liquid crystals, molecular spectroscopy, and fast energetic reactions.



Bruce D. Sartwell
Condensed Matter and
Radiation Sciences Division

AMERICAN VACUUM SOCIETY AWARD

"For outstanding contributions to the International Conference on Metallurgical Coatings"



Anthony J. Campillo
Optical Sciences Division

ELECTED FELLOW, AMERICAN PHYSICAL SOCIETY

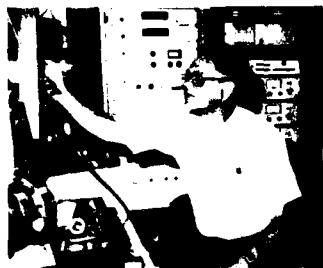
"For his contributions toward understanding the propagation and spatial breakup of high-power laser beams and for his extensive application of novel picosecond techniques toward understanding molecular energy transfer processes"



Owen M. Griffin
Marine Technology Division

**ELECTED FELLOW, AMERICAN SOCIETY
OF MECHANICAL ENGINEERS**

For significant contributions to the field of engineering for research in fluid mechanics and marine hydrodynamics



James J. Krebs
Condensed Matter and
Radiation Sciences Division

ELECTED FELLOW, AMERICAN PHYSICAL SOCIETY

"For important original contributions in the field of magnetic resonance in semiconductor materials, and particularly for studies of deep level centers in GaAs and InP"



Fred A. Smidt, Jr.
Condensed Matter and
Radiation Sciences Division

ELECTED FELLOW, AMERICAN SOCIETY FOR METALS

"In recognition of major accomplishments in the application of metallurgical principles to development of alloys for advanced nuclear application"

INDIVIDUAL HONORS

During 1983 NRL staff members earned 2435 awards under the Federal Incentive Awards program. These awards are summarized in the following table.

Distribution of
Federal Incentive Awards During 1983

Rank of Meritorious Executive	1
SES Bonuses	5
NRL E.O. Hulburt Annual Science Award	1
Navy Superior Civilian Service Award	3
Navy Meritorious Civilian Service Award	5
Commanding Officer's Award for Achievement	4
Outstanding Performance Ratings	522
Special Achievement Awards	90
Quality Step Increases	192
Research Publication Awards	88
Invention and Patent Awards	168
Merit Pay Performance Awards	346
Sustained Superior Performance Awards	221
Employee Suggestions	18
Length of Service	662
Safety Certificates	100
Blood Donor Certificates	9
TOTAL	2435

In addition, Laboratory employees received numerous scientific medals, military service awards, academic honors, and other forms of recognition, including election and appointment to offices in technical societies. The following is an alphabetical list of the persons receiving such recognition in 1983.

August, L.S., *Distinguished Poster Paper Award, 1983 IEEE Conference on Nuclear and Space Radiation Effects*
 Ayers, J.D., *Member, Solidification Committee, AIME; Member, Powder Metallurgy Committee, AIME*

Bishop, S.G., *Member, Organizing Committee, 3rd Conference on Semi-Insulating III-V Materials; Member, Organizing Committee, Topical Conference on Optical Effects in Amorphous Semiconductors; Member, Navy Technical Review Committee, Joint Services Electronics Program*

Bleach, R.D., *Member, Investigations and Surveys Committee, U.S. House of Representatives; Member, Department of Energy Instrumentation Development Review Panel; Treasurer, Organizing Committee for International Astronomical Union Meeting on Laboratory and Astrophysical Plasma Spectroscopy*

Book, D.L., *Translation Editor of Soviet Journal of Plasma Physics; Translation Editor of Soviet Physics—Technical Physics*

Boris, J.P., *Member, NAS/NRC Review Panel of the NASA Numerical Aerodynamic Simulator (NAS)*

Brady, R.F., *Associate Member, Membership Affairs Committee, American Chemical Society; Member, Executive Board, University of Virginia Chemists*

Brueckner, G.E., *Member, COSPAR (Committee on Space Research), Task Group on Transfer of Energy in the Solar System (TESS); Member, COSPAR Sub-Commission E.2 on Solar Physics*

Campbell, F.J., *Member, Program Committee, IEEE International Symposium on Electrical Insulation*

Campillo, A.J., *Fellow, American Physical Society*
 Carhart, H.W., *Chairman, National Academy of Sciences/National Research Council Committee on Studies of Hazardous Substances; Member, NAVSEA Survivability Review Group and Fire Protection Subgroup*

Carruthers, G., *Member, Technical Committee on Space Sciences and Astronomy, American Institute of Aeronautics and Astronautics; Chairman, Editorial Review Committee, National Technical Association*

Chang, C.I., *Chairman, Structural Hardening Subgroup, Tri-Service Laser Hardening Materials and Structural Group; Editor, Theoretical and Applied Fracture Mechanics; Advisor, Laser Countermeasure Materials Development Program; Advisor, Strategic Defense Initiative Lethality and Target Hardness Project*



Dr. Conrad Cheek, Head of the Environmental Sciences Division, is pinned with the Navy Meritorious Civilian Service Award by his wife Billie

Christou, A., *Chairman, IEEE Workshop on GaAs Device Reliability; Member, IEEE Reliability Physics Symposium publication committee; Member, DOD-Industry GaAs Reliability Advisory Group; Member, organizing committee NATO Workshop on Semiconductor Devices and Circuit Reliability*

Colton, R.J., *Chairman, Secondary Ion Mass Spectrometry (SIMS) Subcommittee, American Society for Testing and Materials (ASTM); Chairman, Solids and Surface Analysis Committee, American Society for Mass Spectrometry; Chairman, Fifth International Conference on Secondary Ion Mass Spectrometry; Member, Editorial Board, International Journal of Mass Spectrometry and Ion Processes*

Comas, J., *Co-Chairman, Workshop on Dielectric Systems for III-V Compounds; Secretary/Treasurer, IEEE Electron Devices Society, Washington, DC Chapter*

Compton, R.T., *Fellow, IEEE; Barry Carlton Best Paper of the Year Award (Aerospace Electronics Systems Transactions); Senior Research Award, Ohio State University Engineering College*

Crooker, T.W., *Member, Technical Advisory Committee of the Metal Properties Council; Co-Editor, American Society for Testing and Materials Special Technical Publication No. 801 on Corrosion Fatigue: Mechanics, Metallurgy, Chemistry and Engineering*

Cruddace, R.G., *Member, NASA Shuttle Science Working Group*

Del Balzo, D.R., *Member, Airborne ASW Assessment Committee*

Diachok, O.I., *Member, Acoustical Society of America Committee on Underwater Acoustics; Member, ONR Marginal Ice Zone Experiment (MIZEX) Planning Committee*

Dicus, R.L., *Member, ONR Marginal Ice Zone Experiment (MIZEX) Planning Committee*

Doolittle, R.D., *Member, Panel on SURTASS Array*

Doschek, G.A., *Member, Solar Physics Division of the American Astronomical Society*

Ephremides, A., *Elected to Fellow, IEEE; Member, Board of Governors of the Information Theory Group, IEEE*

Fox, R.B., *Member, Board of Directors, American Chemical Society; Member, ACS Board Committee on Public Affairs and Public Relations; Member ACS Board Committees on Grants and Awards and on Planning; Secretary, Interdivisional Committee on Nomenclature and Symbols, Intl. Union of Pure and Applied Chemistry*

Gabriel, W.F., *Guest Editor, 3rd Special Issue, IEEE AP-S Transactions on Adaptive Arrays; Feature Article AP-S Newsletter*

Garrett, W.D., *Chairman, Working Group on Interchange of Pollutants Between the Atmosphere and the Oceans (World Meteorological Organization); Member, Joint Group of Experts on the Scientific Aspects of Marine Pollution (United Nations)*

Gerber, H., *Co-Editor, World Climate Program Report 55, Experts Meeting on Aerosols and Their Climatic Effects, World Meteorological Organization*

Giallorenzi, T.G., *SES Presidential Rank; Fellow, IEEE; Chairman IEEE/OSA Optical Fiber Sensor Conference; Technical Committees: European Optical Fiber Sensor Conference and IEEE Conference on Lasers and Applications; Editor, IEEE/OSA Journal of Light Wave Technology; IEEE Quantum Electronics Society Administrative Board*

Goode, R.J., *Navy Meritorious Civilian Service Award*

Greene, R.F., *Member, Editorial Board, Applications of Surface Science*
 Griffin, O.M., *Fellow, American Society of Mechanical Engineers*
 Grindlay, A., *Chairman, Software Sub-Panel, Anti-submarine Warfare Signal Processing Study for ASN RE&S*
 Gubser, D.U., *Navy Meritorious Civilian Service Award*



Dr. Don Gubser (left) and Dr. Stu Wolf assemble NRL-designed magnetic shields used for atomic clocks and superconducting magnetic sensor applications

Gursky, H., *Member, Executive Committee, Astrophysics Division, The American Physical Society; Member, Ad Hoc Working Group, Solar Optical Telescope (SOT), NASA*
 Haas, G.A., *Invited Speaker, International Meeting on "Surface Imaging and Analysis with High Spatial Resolution," Arizona State University*
 Hansen, R.J., *Chairman, Flow-Induced Noise and Vibration Technical Committee, ASME; Licensed Professional Engineer, District of Columbia*
 Hazlett, R.N., *U.S. Coordinator, Conference on Long Term Storage Stabilities of Liquid Fuels, Tel Aviv, Israel*
 Hendrickson, W.A., *Delegate to the 13th Congress of the International Union of Crystallography; Member, Proposal Review Panel of the Stanford Synchrotron Radiation Laboratory;*



Fred V. Hellrich shows his Navy Superior Civilian Service Award to his wife Mary

Member, Molecular Biology Advisory Panel of the National Science Foundation
 Hubler, G.K., *Symposium Chairman, "Ion Implantation and Ion Beam Processing of Materials," Materials Research Society Annual Meeting and Co-Editor of Proceedings*
 Hurdle, B.G., *Member, ASW Signal Processing Study for Principal Deputy ASW (RE&S)*
 Jolles, M.I., *Chairman, ASTM Task Group on Surface Crack Testing*
 Jordan, A.K., *Co-Editor, Proceedings of NATO Advanced Research Workshop on Inverse Methods in Electromagnetic Imaging (Bad Windsheim, West Germany); Group Leader and Reporter, Working Discussion Group on Mathematical Inverse Methods, Co-Author of Lead Overview Article for Proceedings and Speaker*
 Kabler, M.N., *Member, Domestic Advisory Committee, 1984 International Conference on Defects in Insulating Crystals; Member, Solid State Sciences Panel of the National Research Council*
 Kaplan, D., *Member, ASW Signal Processing Study for ASW RE&S*
 Karle, I.L., *Biographical sketch in "Chemistry, Experimental Foundations," by R.W. Parry et al., Prentice-Hall, 3rd Edition (1982), p. 345; Who's Who in America, 43rd Ed.; Who's Who of American Women, 14th Ed.; Who's Who in the World; Who's Who in the East*
 Karle, J., *President, International Union of Crystallography; Biotechnology Advisory Panel, Stanford Synchrotron Radiation Laboratory; Chair-*

man, Auditing Committee, National Academy of Sciences, Committee on Publications and Communications, International Council of Scientific Unions

Keramidas, G.A., Vice President, International Society for Computational Methods in Engineering (ISCME); Member, Editorial Board, International Journal of Engineering Analysis

Kim, C., Executive Director, Korean Scientists and Engineers Association in America

Klein, B.M., Member, Steering Committee, Greater Washington Solid State Physics Colloquium Committee

Klein, P.H., Member, Associate Editorial Board of Materials Letters

Knudson, Alvin R., Member, Program Committees, 1984 IEEE Conference on the Application of Accelerators in Research and Industry and International Conference on Atomic Collisions in Solids

Koon, N.C., Editor, Conference on Magnetism and Magnetic Materials, Pittsburgh, Pa., November 8-12, 1983

Krebs, J.J., Fellow, American Physical Society

Krowne, C.M., Chairman, Field Theory Session, IEEE International Microwave Theory and Techniques Symposium; Chairman, Microstrip Antennas Session, IEEE International Antennas and Propagation Symposium; Member, Technical Program Committee, IEEE International Microwave Theory and Techniques Symposium; Member, Technical Program Committee, IEEE International Antennas and Propagation Symposium

Krutar, R., Member, DoD Ada Language Environment Interface Team

Kurfess, J.D., Executive Member, COSPAR Panel on Technical Problems Related to Scientific Ballooning

Landwehr, C.E., Member, Program Committee, IEEE Symposium on Security and Privacy; Invited Speaker, 6th DoD/NBS Computer Security Conference

Leonard, J.T., Guest Lecturer, Course on Fire Safety Engineering, University College, Dublin Ireland; Member, Editorial Advisory Board, Journal of Fire Sciences

Lessoft, H., Navy Meritorious Civilian Service Award; Chairperson, TTG-H Round II Negotiations; Session Chairman, Committee and Technical Program, Electronic Materials Conference; Member, Editorial Board, Journal of Electronic Materials; Member, Organizing



Howard Lessoft is pinned with the Meritorious Civilian Service Award by his wife Vera

Committee, III International MO-VPE Conference; Secretary, Electronic Materials Committee, The Metallurgical Society of AIME

Lewis, D., Chairman-Elect, Baltimore-Washington Section, The American Ceramic Society

McCafferty, E., Secretary, Treasurer, Corrosion Division of the Electrochemical Society; Co-Chairman, "Symposium on Fundamental Aspects of Corrosion Protection by Surface Modification"; Divisional Editor, Journal of the Electrochemical Society; Member, Honors and Awards Committee, The Electrochemical Society

McDonald, J.R., Officer-at-Large, Sigma Xi, National Research Society

McLean, E.A., Vice President, IEEE Nuclear and Plasma Sciences Society

Metzbowser, E.A., Chairman, Laser Beam Welding Subcommittee, American Welding Society C-7; Chairman, Electron Beam Welding Committee and Laser Beam Welding Committee, Metals Handbook, Vol. 6, Welding, Brazing and Soldering, ASM; Chairman, Materials Processing Sessions of International Congress on the Applications of Lasers and Electro-Optics; Member, Board of Directors, Laser Institute of America; Co-Chairman, Organizing Committee for Applications of Lasers in Materials Processing II, ASM; Member, Joining Division Council, ASM

Michel, D.J., Member, Task Force on Crack Propagation Technology, American Society of Mechanical Engineers & Metals Properties Council; Professorial Lecturer, The George Washington University; Co-Editor, Proceedings of Topical Conference on Ferritic Alloys for use



Sigma Xi pure science award to
Dr. Donald J. Michels, (on right)

in Nuclear Energy Technologies, The Metallurgical Society of AIME

Mignogna, R.B., *Vice Chairman, American Society for Metals, Baltimore Chapter*

Mount, G., *NASA Achievement Award for Solar Mesosphere Explorer Program*

Munson, J.C., *Member, Technical Assessment Panel for ASW Systems Project Office*

Murday, J.S., *Chairman, Scholarships and Awards Committee, American Vacuum Society; Co-Chairman, Applied Surface Analysis Symposium; Member-at-large, Division of Colloid and Surface Chemistry Executive Committee, American Chemical Society*

Nagel, D.J., *Member, National Synchrotron Light Source Users Committee; Member, Department of Energy Advanced Planning Study for Synchrotron Radiation; Member, Optical Society Objectives and Policy Committee*

Nisenoff, M., *Member, International Board of Advisory Editors, Cryogenics Journal; Member, Organizing Committee Workshop on Josephson Digital Devices, Circuits and Systems 1983; Member, Organizing Committee, 1984 International Conference on Refrigeration for Cryogenic Sensors and Electronic Systems*

Oran, E.S., *Chairman, American Geophysical Union Committee on Electronic Publishing; Member, Program Committee of 20th Symposium (International) on Combustion; Guest Professor, Heidelberg University*

Ossakow, S.L., *Member, Program Committee, American Geophysical Union Chapman Conference on Ion Acceleration in the Ionosphere and Magnetosphere*

Ozimina, C.D., *Member, Northern Virginia Chapter of IEEE Control System Society*

Pande, C.S., *Member, New York Academy of Sciences; Session Chairman, Non-Ferrous Metals, EMSA; Chairman, Electrical, Magnetic and Optical Phenomena Committee, ASM; Member, Physical Metallurgy Committee, AIME; Member, Board of Review, Metallurgical Transactions; Member, Mechanical Metallurgy Committee, AIME*

Pattnaik, A., *Member, AIME Composite Committee; 'Key Reader' for Met. Trans. (A)*

Petersen, E.L., *Principal Investigator, DNA/DARPA Single Event Program; Program Chairman, DNA Single Event Symposium; Invited Speaker, IEEE Nuclear and Space Radiation Effects Short Course*

Rath, B.B., *Chairman, Surfaces and Interfaces Committee of ASM; Chairman, Electrical Magnetic and Optical Phenomena Committee of ASM; Director at Large, TMS Board of Directors of AIME; Member, Joint Commission of the Metallurgical Transaction of ASM and AIME; Member, Board of Directors of Maryland Institute for Metals; Advisory Board of the Materials Science Department of Carnegie-Mellon University; Member, National Materials Advisory Board of NAS on Science and Technology Implications for Processing of Strategic Materials; Steering Committee, Rapid Solidification Processing Principles and Technology Conference; Editor, Novel NDE for Materials, AIME Publication*

Reinecke, T.L., *Secretary, Steering Committee of the Greater Washington Solid State Physics Colloquia*

Resing, H.A., *Member, Editorial Board, Journal of Magnetic Resonance; Member, Organizing Committees, III International Symposium on Magnetic Resonance in Colloid and Interface Science, Torun, Poland*

Reuss, M.L., Jr., *Member, IEEE/MTT-S Standard Committee P1004 (IEEE Standard Definition of Forms for Planar Transmission Lines)*

Ripin, B.H., *Member, IEEE Nuclear and Plasma Society ADCOM; Associate Editor of Phys. Rev. Lett. and Trans. on Plasma Science*

Ritter, J.C., *Chairman, Panel to Write Chapter for DNA EM-1 Handbook; Member, Program* 225

Committee for 3rd Annual Space Electronics Conference (Albuquerque, 1985)

Sadananda, K., *Member, Flow and Fracture Committee, American Society for Metals; Member, Mechanical Metallurgy Committee, Structural Materials Committee, American Institute of Mining and Metallurgy; Keynote Speaker, Inelastic Analysis and Life Prediction in High Temperature Environment, American Society for Testing and Materials*

Sartwell, B.D., *Member, Program Committee of International Conference on Metallurgical Coatings; Award for Outstanding Contributions to that Conference; Member, Executive Committee of Washington, D.C. Chapter of American Society for Metals*

Schindler, A.I., *Navy Superior Civilian Service Award*



Dr. Albert I. Schindler is pinned
by his wife Phyllis

Schnur, J.M., *Adjunct Professor, University of Paris VI*

Schriempf, J.T., *Member, Steering Committee for the Laser Countermeasure Materials Development Program*

Shapiro, P., *Distinguished Poster Paper Award, 1983 IEEE Conference on Nuclear and Space Radiation Effects*

Sheinson, R.S., *Treasurer, Eastern States Section of the Combustion Institute*

Shore, J.E., *Member, 1983 IEEE Delegation to China—Oct. 18-Nov. 10*

Silberberg, R., *Outstanding Handicapped Employee of the Navy*

Skelton, E.F., *Member, Stanford Synchrotron Radiation Laboratory Users Organization Executive Committee*

Skolnik, M.I., *Harry Diamond Memorial Award*

Sleger, K., *Member, DARPA GaAs Pilot Line Program; Associate Member, AGED Working Group A; Publications Chairman, 1984 GaAs IC Symposium*

Smardzewski, R.R., *Member, ONR Historically Black College Council; Member, Awards Committee, The Coblenz Society*

Smidt, F.A., *Fellow, American Society for Metals*

Speilman, B.E., *Steering Committee, IEEE Microwave and Millimeter-Wave Monolithic Circuit Symposium; Session Chairman, IEEE Monolithic Circuits Symposium; Member, IEEE MTT-S Administrative Committee; Member, Technical Program Committee, IEEE International Microwave Symposium; Member, Program Committee, IEEE Microwave and Millimeter-Wave Monolithic Symposium; Member, DoD MM-Wave Fact-Finding Committee to Japan; Associate Member, AGED*

Sprangle, P., *Chairman, Basic Plasma Physics Session, American Physical Society, Los Angeles, Calif.; Member, Executive Session of the Novel Sources of Electromagnetic Radiation Panel, DOE; Member, Executive Panel, National Research Council Survey Committee Report on the Physics of Plasmas and Fluids; Invited Speaker, American Physical Society, Los Angeles, Calif.*

Statler, R.L., *Chairman, Solar Photovoltaic Panel of the Interagency Advanced Power Group; Member, IEEE 17th Photovoltaic Specialists Conference Committee*

Steele, L.E., *President, Federation of Materials Societies; First Vice Chairman, ASTM Board of Directors; Member, ASTM Executive Committee; Editor-Author, two books published by ASTM and one by Applied Science Publishers, LTD, London*

Stern, K.H., *Contributing Editor, Phase Diagrams for Ceramicists*

Stonesifer, F.R., *Member, Structures Committee, JTCG/AS Technology R and D Subgroup; Who's Who in the East*

Treado, P.A., *Member, Board of Trustees, Southeastern University Research Association*

Trunk, G.V., *U.S. National Leader KTP-2 Technical Panel, Subgroup K, TTCP*

Trzaskoma, P.P., *Chairman, National Capital Section, Electrochemical Society; Member, Individual Membership Committee, Electrochemical Society*

Tsao, C.H., *Treasurer, Sigma Xi, NRL Chapter*

Turner, N.H., *President-Elect (for 1984), Chemical Society of Washington (Washington Section of the American Chemical Society); Member, Chemical Society of Washington Centennial Symposium Steering Committee; Membership Secretary, Division of Colloid and Surface Chemistry, American Chemical Society*

Valenzuela, G.R., *Member, Review Panel of European Space Agency (ESA) for Remote Sensing of Laboratoire de Telecommunications et d'Hyperfréquences, Université Catholique de Louvain, Louvain-La-Neuve, Belgium; Member, Technical Program Committee, International Union of Radio Science Symposium on Wave Propagation and Remote Sensing, Louvain-La-Neuve, Belgium*

Venezky, D.L., *Secretary, American Chemical Society (ACS) Council Committee on Committees; Liaison to the ACS Council Committees on Science and Public Relations; Assistant Secretary, American Society for Testing and Materials (ASTM) Committee D-19 on Water*

Vittoria, C., *Senior Member, Institute of Electrical and Electronics Engineering*

Votaw, C.W., *Member, ONR Marginal Ice Zone Experiment (MIZEX) Planning Committee*

Wales, S.C., *Member, ONR Marginal Ice Zone Experiment (MIZEX) Planning Committee*

Webb, D.C., *Member, IEEE Magnetics Society Technical Committee for High Frequency Properties of Magnetic Materials; Member, IEEE Microwave Theory and Techniques Society for Microwave Acoustics; Member, Technical Committee for 1984 IEEE Ultrasonics Symposium*

Wieting, T.J., *Member, DoD Microwave Effects Panel, Office of Directed Energy Weapons (OUSD)*

Williams, C.M., *Member, U.S. National Commission for UNESCO (United Nations Educational, Scientific, and Cultural Organization)*

Williams, F.W., *Vice President, Eastern Section of Combustion Institute 1984-1985*



Linda Greenway attaches the E.O. Hulburt Award on the lapel of Peter G. Wilhelm

Wilsey, N.D., *Member, Finance Committee, 13th International Conference on Defects in Semiconductors*

Wolf, S.A., *Director, NATO Advanced Study Institute on Percolation Localization and Superconductivity Les Arcs France; Session Chairman, March 1983 APS Meeting*

Wolicki, E.A., *Chairman, DNA-DARPA Symposium on Single Event Effects, Los Angeles, Calif.*

Wolock, I., *Chairman, Organic Composites Working Group, Technology Initiative Panel for Advanced Materials, Joint Directors of Laboratories; Session Organizer and Chairman, 28th National Symposium, Society for the Advancement of Materials and Process Engineering; Session Chairman, Conference on Aerospace Transparent Materials and Enclosures; Member, Ad Hoc Meeting of Filament Wound Solid Rocket Cases for the Space Shuttle, National Research Council*

Young, F.C., *Member, Plasma Sciences and Applications Executive Committee of the IEEE Nuclear and Plasma Science Society*

ALAN BERMAN RESEARCH PUBLICATION AWARDS

The Annual Research Publication Awards Program was established in 1968 to recognize the authors of the best NRL publications each year. These awards not only honor individuals for superior scientific accomplishments in the field of naval research, but also seek to promote continued excellence in research and in its documentation. In 1982, the name of this program was changed to the Alan Berman Research Publication Awards in honor of its founder.

There were 164 separate publications in 1983 that were considered for recognition. Of those considered, 30 were selected. These selected publications represented 88 authors, who received awards. Each of the divisions was permitted \$1000, which was shared by varying numbers of authors. On March 9, 1984, the awards were presented to the authors at the Alan Berman Annual Research Publication Awards Dinner held at the Bolling Air Force Base Officers' Club. Each winner received a certificate, a bronze paperweight, and a booklet of the publications receiving special recognition.

The unclassified winning papers with their respective authors are listed below by their research units. Non-Laboratory coauthors are indicated by an asterisk.

Laboratory for Structure of Matter

*Crystal Structure of 2-Bromo-2-nitroadamantane (I), $C_{10}H_{14}BrNO_2$,
and 2,2-Dinitroadamantane (II), $C_{10}H_{14}N_2O_4$*
Clifford F. George, Jr. and Richard O. Gilardi

Laboratory for Computational Physics

*Ignition of Flamelets Behind Incident Shock Waves and the Transition
to Detonation*
K. Kailasanath* and Elaine S. Oran

Space Science Division

*Observations of High-Energy Jets in the Corona Above the Quiet Sun, the Heating of the Corona,
and the Acceleration of the Solar Wind*
Guenter E. Brueckner and John-David F. Bartoe

*An Observational Study of Water Vapor in the Mid-Latitude Mesosphere
Using Ground-Based Microwave Techniques*
Richard M. Bevilacqua, Philip R. Schartz, Joseph M. Bologna,
Dorsey L. Thacker, John J. Olivero,* and Chris J. Gibbins*

Plasma Physics Division

*Use of Induced Spatial Incoherence for Uniform Illumination of
Laser Fusion Targets*
Robert H. Lehmborg and Stephen P. Obenschain

*Numerical Simulation of the Axisymmetric Hollowing Instability
of a Propagation Beam*

Glenn R. Joyce and Martin Lampe

Radar Division

On the Design of an Advanced System for Carrier Air Traffic Control (CATC)

William M. Waters, George J. Linde, Raymond P. Meixner,
Bobby R. Jarrett, and William L. Thrift

Radar Cross-Section Analysis—USS Estocin FFG-15

David L. Drake, David W. Kerr, Benjamin Y. Koo,
and Rene Miroy*

Tactical Electronic Warfare Division

*Analysis and Evaluation of an Advanced Electronic Warfare System:
Deterministic Formulation*

John S. Baras* and Allen J. Goldberg

Low-Grazing-Angle, Forward-Scatter, Over-Water Multipath Measurements

Armondo D. Elia, Richard D. Gurney, and Donald Y. Northam

Marine Technology Division

Azimuthal Structure of a Cyclonic Gulf Stream Ring

Richard P. Mied and Gloria J. Lindemann

Analytical HEL Vulnerability Assessment of a Flight-Loaded Aircraft Structure

Chine I. Chang, Kuang M. Wu, and Christopher A. Griffis

Underwater Sound Reference Detachment

Experimental Constant Beamwidth Transducer

Arnie L. Van Buren, L. Dwight Luker, Michael D. Jevnager,
and Allan C. Tims

Magnetic Boundary Conditions for Metallic-Glass Piezomagnetic Transducers

Steven W. Meeks and Joseph C. Hill

Chemistry Division

Local-Density-Functional Approach to All-trans-Polyacetylene

John W. Mintmire and Carter T. White

Submarine Hull Insulation Fire Test IV — 7 December 1981

John I. Alexander, Denis J. Bogan, Homer W. Carhart, Harold G. Eaton,
Jr., Carolyn R. Kaplan, Ronald S. Sheinson, Thomas T. Street,
Patricia A. Tatem, Frederick W. Williams, Harry J. St. Aubin,
Jack P. Stone,* and Tina M. White*

Material Science and Technology Division

A Critical Analysis of Grain-Size and Yield-Strength Dependence of Near-Threshold Fatigue Crack Growth in Steels

George R. Yoder, Laurence A. Cooley, and Thomas W. Crooker

Detection of Several ω -Phase Morphologies in β -III Ti by Small-Angle Neutron Scattering and Transmission Electron Microscopy

Mohammad Fatemi, Chandra S. Pande, and Harry R. Child*

Optical Sciences Division

Encapsulation of Hemoglobin in Phospholipid Vesicles

Bruce P. Gaber, Paul Yager, James P. Sheridan,
and Eddie L. Chang

The Cesium Atomic Resonance Filter

Bernard L. Wexler, Ralph L. Burnham,
and William Nikolai*

**Condensed Matter and Radiation
Sciences Division**

Dose Dependence of Single Event Upset Rate in MOS dRAMS

Alvin R. Knudson, Arthur B. Campbell III,
and Ernest C. Hammond*

Density-Functional Theory of Excitation Spectra of Semiconductors: Application to Si
Ching-ping S. Wang and Warren E. Pickett

Electronics Technology Division

Surface Plasmon Studies of Oxidized Ba Films

John W. Gibson and Richard E. Thomas

High-Frequency Doubler Operation of GaAs Field-Effect Transistors

Christen Rauscher

Information Technology Division

Preliminary System Concept for an HF Intra-Task Force Communication Network

Jeffrey E. Wieselthier, Dennis J. Baker, Anthony Ephremides,
and Dennis N. McGregor

Space Systems Division

Statistical Radiometry

William H. Carter

Aerospace Systems Division

The Two-Scale Radar Wave Probe and SAR Imagery of the Ocean
William J. Plant and William C. Keller

Actuator-Placement Considerations for the Control of Large Structures
Robert E. Lindberg, Jr.

Special Publication Award

A History of the Chemistry Division, Naval Research Laboratory, Washington, D.C.
1927-1982
Bettye C. Gibbs

Programs for professional development



- 
- 
- 235** Programs for NRL People—University education and scholarships, continuing education, professional development, and other activities
- 240** Programs for Non-NRL People—Fellowships, exchange programs, and cooperative employment

PROFESSIONAL DEVELOPMENT

NRL has established many programs for the professional and personal development of its employees so that they may better serve the needs of the Navy. These programs develop and retain talented people and keep them abreast of advanced technology and management skills. Graduate assistantships, fellowships, sabbatical study programs, cooperative education programs, individual college courses, and short courses for personal improvement contribute to professional development.

Programs also exist for non-NRL employees. These enhance the Laboratory research program by providing a means for non-NRL professionals to work at the Laboratory and thus improve the interchange of ideas, meet critical short-term technical requirements, and provide a source of new, dynamic scientists and engineers. The programs range from two-year graduate fellowships, faculty and professional interchanges, and undergraduate work to an introduction of gifted and talented high school students to the world of technology.

Page 232, clockwise from upper left:

Dr. Herbert Nelson of the Chemistry Division lectures faculty members from the University of the District of Columbia

Captain (now Commodore) Grace Hopper, a pioneer in computer sciences, delivers a Sigma Xi lecture to a packed house at NRL

Junior Naval Reserve Officer Training Corps members from Seneca High School, Germantown, Maryland, tour the Laboratory

PROGRAMS FOR NRL PEOPLE

During 1983, NRL employees participated in about 3500 individual training events. Many of these were presented as either video taped or on-site instructed courses on diverse, technical subjects, management techniques, and enhancement of personal skills (efficient use of time, memory improvement, interpersonal communications, speed reading, etc.).

One common study procedure is for employees to work full time at the Laboratory and take job-related scientific courses at universities and schools in the Washington area. The training ranges from individual courses to full graduate and postgraduate programs. Tuition for training is paid by NRL. A description of the formal programs offered by NRL and a listing of the 1983 participants of some of the larger programs follow.

GRADUATE PROGRAMS

- **The Advanced Graduate Research Program** (formerly the Sabbatical Study Program) enables selected professional employees to devote full time to research or course work in their own or a related field for one academic year at an institution of their choice without the loss of regular salary, leave, or fringe benefits. NRL pays all education, travel, and moving expenses for the individual and dependents. Since the program began in 1964, 147 employees have participated. Criteria for eligibility include professional stature consistent with the applicant's opportunities and experience, a satisfactory program of study, and acceptance by the institution selected by the applicant. The program is open to paraprofessional (and above) employees who have completed six years of federal service, including four years at NRL.

NRL staff members who began their programs in 1983 are listed below with their respec-

tive divisions and the institutions where they studied.

Allen N. Garroway (Chemistry), University of California (Berkeley)

John M. Goodman (Space Science), SHAPE Technical Center, The Hague, Netherlands

Alfred H. Lowery (Laboratory for Structure of Matter), Picatinny Arsenal, Dover, New Jersey; and The Bureau of Standards, Gaithersburg, Maryland

Dimitrios A. Papaconstantopoulos (Condensed Matter and Radiation Sciences), University of Crete, Department of Physics, Iraklion, Greece

Warren E. Pickett (Condensed Matter and Radiation Sciences), Darebury Laboratory, Warrington; and University of Bristol, England

Angelo J. Skalafuris (Aerospace Systems), University of Pennsylvania (Philadelphia)

John E. Stannard (Electronics Technology), Santa Barbara Research Center, Goleta, California

James N. Talley (Tactical Electronic Warfare), Catholic University of America, Washington, D.C.

Joel M. Schnur (Optical Sciences), University of Paris

Chung-Chun Yang (Aerospace Systems), Illinois Institute of Technology

- **The Edison Memorial Graduate Training Program** enables employees to pursue advanced studies in their fields at local universities. Eligible employees who are selected for participation in this program normally spend 24 hours of every work week in their studies. The criteria for eligibility include a minimum of one year of service at NRL, a bachelor's or master's

degree in an appropriate field, and professional standing in keeping with the candidate's opportunities and experience.

From 1963 through 1983, 147 employees studied under the Edison Program. In 1983, only one employee began work as an Edison scholar: Carolyn R. Kaplan (Chemistry), University of Maryland.

- To be eligible for the **Select Graduate Student Program**, employees must have a college degree in an appropriate field and must have maintained at least a B average in undergraduate study. Accepted students devote a full academic year to graduate study. While attending school, they receive one half of their salary, and NRL pays for tuition, books, and laboratory expenses. During the summer, they work at the Laboratory and receive normal pay and fringe benefits. Thirty-four staff members have enrolled in the program since it began in 1967.

- Research conducted at NRL may be used as **thesis material for an advanced degree**. This original research is supervised by a qualified employee of NRL who is approved by the graduate school. The candidate should have completed the required course work and should have satisfied the language, residence, and other requirements of the graduate school from which the degree is sought. NRL provides space, research facilities, and supervision but leaves decisions on academic policy to the cooperating schools.

- The **Alfred P. Sloan Fellows Program** is designed for competent young executives whose job performance indicates senior management potential. The Sloan Fellows spend one year with the Massachusetts Institute of Technology faculty and with policymakers in industry and government. They study the theory and practice of effective and responsible management in a rapidly changing society.

- The **Education for Public Management Program** serves the training needs of individuals who are at midcareer and who have the talent to assume increasing responsibilities to direct agency programs and policies.

- The **Education Program for Federal Officials** exists for a small group of Federal employees who have demonstrated high competence and unusual promise. The Woodrow Wilson School of Princeton University has developed this program to enable selected mid-career officials to enlarge their knowledge in particular disciplines, to relate their fields of specialization to the broader concerns of government, and to sharpen their capacity for objective analysis of governmental problems.

- Federal Executive fellowships are available each year for employees to study in the **Brookings Institute Advanced Study Program**. In this program, the fellow is exposed to and participates in planning, developing, and conducting educational conferences on public policy issues for leaders in public and private life.

- The **Fellowship in Congressional Operations for Executives** provides an opportunity for some of the most promising young, technically oriented Federal executives to participate in a variety of assignments designed to develop their knowledge and understanding of Congressional operations. These fellows share activities with other members of the Congressional Fellowship Program who come mainly from journalism, law, and college teaching.

- The **Maxwell Midcareer Development Program** of the Maxwell Graduate School of Citizenship and Public Affairs, Syracuse, New York, increases the managerial knowledge, ability, and skills of experienced Government officials who have been identified by their agencies as having potential for advancement to positions demanding progressively greater managerial and executive responsibilities.

- The **Practicing Engineer Advanced Study Program** of the M.I.T. Center for Advanced Engineering, Cambridge, Massachusetts, enables experienced engineers and applied scientists to work in-depth in technological areas pertinent to their professions, preparing for continued leadership in an age of unparalleled technological change.

- **The Science and Technology Fellowship Program**, a subsidiary of the Commerce Science Program, includes a variety of special events, lectures, seminars, visits, conferences, field trips, and interactions with key people from both the public and private sectors. Participants spend one week on Capitol Hill in an intensive, congressional orientation; they spend one week with the Brookings Institute, Science Policy Conference; and they take two week-long field trips for on-site inspection of scientific institutions and industrial complexes.

- **The Stanford-Sloan Program of the Graduate School of Business**, Stanford, California, gives exceptional young executives an opportunity to make an intensive study of new concepts and developments in business, to develop a top management perspective, and to broaden their intellectual horizons.

- **The Naval Postgraduate School (NPS)** in Monterey, California, provides advanced graduate study for selected Federal civilian employees who meet NPS academic requirements for the program in which they are interested, and whose employing agency is willing to act as sponsor.

CONTINUING EDUCATION

- Local colleges and universities offer **undergraduate courses** at NRL for employees to improve their skills and keep abreast of current developments in their fields. These courses are also available at many other DoD installations in the Washington, D.C. area.

- The Employee Development Branch at NRL offers to all employees **short courses** in certain program areas which are not available at local schools; laboratory employees may attend these courses at nongovernment facilities as well. Interagency courses in management, personnel, finance, supervisory development, clerical skills, and other areas are also available.

For further information on any of the above programs, contact the Employee Development Branch (202) 767-2956.

TECHNOLOGY TRANSFER

- **The Navy Science Assistance Program** establishes an information loop between the Fleet and the R&D shore establishments to expedite technology transfer to the user. The program addresses operational problems, focuses resources to solve specific technical problems, and develops a nucleus of senior scientific personnel familiar with the impact of current research and system performance on military operations.

- **The Office of Research and Technology Applications Program** ensures the full use of the results of the Nation's Federal investment in research and development by transferring federally owned or originated technology to state and local governments and the private sector. Inquiries concerning technical information on NRL programs are invited; they should be made through the contact below.

For these last two programs, Mr. Richard Fulper at (202) 767-3744 is the point of contact.

PROFESSIONAL DEVELOPMENT

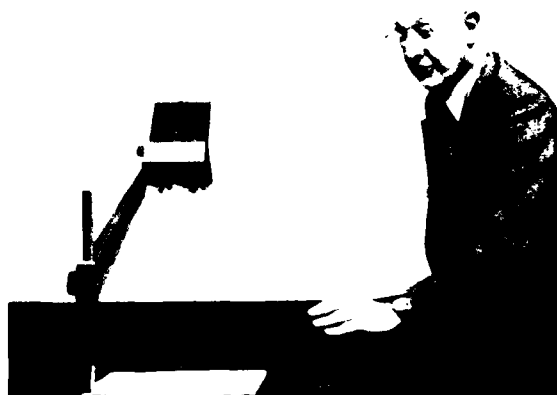
NRL has several programs, professional society chapters, and informal clubs that enhance the professional growth of employees. Some of these are listed below.

- **The Career Counseling Center** helps employees to define short- and long-range career goals, to improve their job-seeking skills, and to deal with issues affecting job productivity. (Contact Dr. Diane Koslow at (202) 767-2956.)

- A chartered chapter of **Women in Science and Engineering (WISE)** has recently been established at NRL. Informal monthly luncheons and seminars are held to inform scientists and engineers of women's research at NRL and to provide an informal environment for practicing their presentations. Most recently WISE initiated a quarterly colloquium series to feature outstanding women scientists. (Contact Dr. Marty Farmer at (202) 767-4301 or Dr. Cha-mei Tang Hui at (202) 767-4148.)



Dr. Isabella Karle, member of the National Academy of Sciences, speaks at one of the recent WISE colloquium series on X-ray crystallography as a tool for determining molecular structures



P-2013(8)

Dr. Machta of the National Oceanic and Atmospheric Administration discusses "Acid Rain" at a recent Sigma Xi lecture

- **Sigma Xi**, the Scientific Research Society, encourages original investigation in pure and applied science. The NRL chapter of approximately 450 active members meets nine times each year (from October to June) and sponsors a series of lectures on a wide range of pure and applied scientific topics of interest to both scientific and government communities. Each spring it sponsors an Edison Day at which a distinguished scientist, usually a Nobel Laureate, speaks on his or her research. During the 1983/84 season, Dr. Ilya Prigogine, 1977 Nobel Prize winner, spoke on irreversible statistical mechanisms, and Professor Istvan Hargittai, from the Hungarian Academy of Sciences, spoke on "Symmetry in Art and Science." The chapter also presents annual awards in pure and applied science. (Contact Dr. John Reintjes at (202) 767-2175.)

- Any employee who is interested in developing effective self expression, listening, thinking, and leadership potential is invited to join either of the two NRL chapters of **Toastmasters International**. Members of these clubs, who possess diverse career backgrounds and talents, meet three times a month where they learn to communicate not by rules but by doing in an atmosphere of understanding and helpful fellowship. (Contact Mrs. Kathleen Parrish at (202) 767-2782.)

- The **Federal Executive Professional Association (FEPA)** provides testimony, recommendations, and constructive criticism of the policies of the Executive Branch on existing proposed legislation and on regulatory actions. It also assists various advisory boards and commissions concerned with professional employee relations and benefits. The FEPA meets monthly for seminars given by NRL management. (Contact Dr. Louis Beach at (202) 767-5692.)

EQUAL EMPLOYMENT OPPORTUNITY (EEO) PROGRAMS

- The EEO Office at NRL prepares and develops guidelines for Affirmative Action Programs, provides advice and guidance to management on EEO policy, administers the complaint process, provides EEO training for all employees, and reaches out to the community. The Community Outreach Program provides judges for science fairs and career counselors at local schools; the Program also participates in Black History month and gives a Christmas party for local school children.

- The **Federal Women's Program (FWP)** improves employment and advancement opportunities for women in the Federal service. Special events include a three-day observance of Federal Women's Week usually held in March.



Dr. Brenda Holmes and Captain John McMorris II admire a prize-winning entry in the Black History Month art and essay contest

P-2101(5)

Dr. Herbert Nelson leads a tour of the Chemistry Division's laser laboratory for a group of teachers from the University of the District of Columbia



The highlight of the 1983 program was a talk given by Renee Pouissant, anchorwoman for WJLA-TV News, who spoke on "A Woman's Journey Through the World of Broadcast Journalism." In addition, a monthly lunchtime discussion series is held at which various topics concerning working women are discussed.

- EEO also provides the **Handicap Program** which gives technical assistance on recruitment resources, training programs, removal of architectural barriers, and accommodations for

disabled employees and applicants. The **Hispanic Employment Program**, which ensures equal employment opportunity to Hispanic Americans, is another EEO effort at NRL. (Contact Ms. Sol Eaton at (202) 767-2486 for all EEO programs.)

- Other programs that enhance the development of NRL employees include computer clubs (Edison, Atari, Edison Commodore, and the NRL-IBM PC) and the Amateur Radio Club. The Recreation Club offers many facilities such as a 25-yard, 6-lane indoor swimming pool;



Renee Pouissant, anchorwoman for WJLA-TV News (a Washington, D.C. network station), speaks on "A Woman's Journey Through the World of Broadcast Journalism," at the Federal Women's Program held in March



P-1947(30)

Dr. James Slagle of the Navy Center for Applied Research in Artificial Intelligence uses a special braille printer for his research and development of expert systems

a gymnasium with basketball, volleyball, and badminton courts; a weight room and exercise area; ping pong; meeting rooms; softball and basketball leagues; jacuzzi whirlpool; sauna; classes in karate, aerobics exercise, swimming, and swim-nastics; and specialized sports clubs (running, skiing, biking, golfing). The Showboaters, a nonprofit drama group which presents live theater

for the enjoyment of NRL and the community, performs in two major productions each year, in addition to occasional performances at Laboratory functions and benefits for local charities. Past productions have included "Fiddler on the Roof," "Brigadoon," and "Arsenic and Old Lace." Though based at NRL, membership in Showboaters is not limited to NRL employees.

PROGRAMS FOR NON-NRL PEOPLE

Several programs also exist for non-NRL employees. These programs encourage and support the participation of visiting scientists and engineers in research of interest to the Laboratory. Some of the programs may serve as stepping stones to federal careers in science and technology. Their objective is to enhance the quality of Laboratory research activities through working associations and interchanges with highly capable scientists and engineers and to provide opportunities for outside scientists and engineers to work in the Navy Laboratory environment. Along with enhancing Laboratory research, these programs acquaint participants with Navy capabilities and concerns.

RECENT PhD., FACULTY MEMBER, AND COLLEGE GRADUATE PROGRAMS

• The National Research Council (NRC)/NRL Cooperative Research Associateship Program selects associates who conduct

research at NRL in their chosen fields in collaboration with NRL scientists and engineers. The tenure period is two years, and following their tenure, the Office of Naval Research offers the associate posttenure research grants tenable at an academic institution. The associates appointed in 1983 are listed below, along with their NRL divisions and degree-granting institutions.

- David A. Baldwin (Chemistry), University of Texas
- John M. Burke (Plasma Physics), University of California (San Diego)
- John W. Cox (Chemistry), Johns Hopkins University
- Bruce J. Dalrymple (Condensed Matter and Radiation Sciences), Yale University
- David R. Foster (Optical Sciences), University of Virginia
- Mark E. Fraser (Chemistry), University of Michigan



P-2030(1)
Dr. J. Chester McKees, Director of Associateship Programs of the National Research Council (NRC), addresses the 1983 NRC postdoctoral associates. Seated in the background are Dr. Agda Cohen, Dr. Timothy Coffey, and Captain John McMorris II.

Elaine K. Fukuda (Chemistry), University of California (Irvine)

Richard D. Griffin (Optical Sciences), Purdue University

Berend T. Jonker (Condensed Matter and Radiation Sciences), University of Maryland

Brian L. Justus (Optical Sciences), University of California (Riverside)

Alfred M. Krizan (Electronics Technology), Princeton University

Frank W. Kutzler (Chemistry), Stanford University

M. Daniel Morrison (Space Science), University of Texas

Andrew N. Mostovich (Plasma Physics), University of Maryland

Paul M. Natishan (Material Sciences and Technology), University of Virginia

Susan G. Neff (Space Science), University of Virginia

Jay P. Norris (Space Science), University of Maryland

Larry J. Paxton (Space Science), University of Colorado

Andrew J. Schmitt (Plasma Physics), University of Michigan

Frederick E. Simon (Chemistry), State University of New York (Stony Brook)

John M. Tyson (Condensed Matter and Radiation Sciences), Johns Hopkins University

Deborah VanVechten (Condensed Matter and Radiation Sciences), University of Maryland

Gregory E. Vink (Acoustics), Princeton University

David F. Voss (Optical Sciences), University of Michigan

Frank R. Vozzo (Condensed Matter and Radiation Sciences), State University of New York (Albany)

- The American Society for Engineering Education (ASEE) administers the **Office of Naval Technology (ONT) Postdoctoral Fellowship Program** to increase the involvement of highly trained scientists and engineers in disciplines to meet the evolving needs of naval technology. Appointments are for one year (renewable for a second and sometimes a third year). The appointments are competitive and are made jointly by ONT and ASEE.

- The American Society for Engineering Education also administers the **Navy/ASEE Summer Faculty Research Program** for university faculty members to work for 10 weeks with professional peers in participating Navy laboratories

on research of mutual interest. NRL hosted 29 of these faculty participants in 1983; they are listed below, along with the participating NRL divisions and their home institutions.

Nagappan K. Annamalai (Electronics Technology), Clarkson College of Technology, New York
 Louis M. Brock (Material Science and Technology), University of Kentucky
 Carl L. Bumgardner (Chemistry), North Carolina State University
 George R. Cross (Information Technology), Louisiana State University
 William G. Culbreth (Marine Technology), Naval Postgraduate School, Monterey, California
 Jane A. Cyran (Optical Sciences), County College of Morris, New Jersey
 Charles H. Douglass (Chemistry), Trinity College, Washington, D.C.
 Irene M. Engle (Space Science), U.S. Naval Academy, Maryland
 Tepper L. Gill (Condensed Matter and Radiation Sciences), Howard University, Washington, D.C.
 Myron P. Hagelberg (Acoustics), Wittenberg University, Ohio
 Rodney Heisler (Acoustics), Walla Walla College, Washington
 Donald J. Hutter (Space Science), Rose-Hulman Institute of Technology, Indiana
 Robert G. Landolt (Chemistry), Texas Wesleyan College,
 Millard A. Lee (Condensed Matter and Radiation Sciences), Dickinson State College, North Dakota
 John H. Lilly (Aerospace Systems), State University of New York, (Stony Brook)
 Eugenie V. Mielczarek (Optical Sciences), George Mason University, Virginia
 Richard M. Neumann (Condensed Matter and Radiation Sciences), University of Massachusetts
 Alan H. Nye (Space Science), Rochester Institute of Technology, New York
 Vincent J. Parks (Marine Technology), Catholic University of America, Washington, D.C.

Clarence E. Pfluger (Laboratory for Structure of Matter), Syracuse University, New York
 Gary F. Riley (Chemistry), Cumberland College, Kentucky
 D. Paul Rillema (Chemistry), University of North Carolina (Charlotte)
 E. Larry Robinson (Optical Sciences), Austin College, Texas
 Walter E. Rudzinski (Chemistry), Southwest Texas State University
 William A. Sanders (Chemistry), Catholic University of America, Washington, D.C.
 John R. Schott (Optical Sciences), Rochester Institute of Technology, New York
 Charles W. Sink (Chemistry), Edinboro State College, Pennsylvania
 Margaret A. Wechter (Chemistry), Southeastern Massachusetts University
 Albert A. Wolf (Optical Sciences), Davidson College, North Carolina

• **The NRL/United States Naval Academy (USNA) Cooperative Program for Scientific Interchange** allows faculty members of the U.S. Naval Academy to participate in NRL research. This collaboration benefits the Academy by providing the opportunity for USNA faculty members to work on research of a more practical or applied nature. In turn, NRL's research program is strengthened by the available scientific and engineering expertise of the USNA faculty. Faculty members who participated in the 1983 program are listed below, along with the cooperating NRL divisions.

C. Elise Albert, Space Science
 Gerald P. Calame, Optical Sciences
 Graham T. Cheek, Chemistry
 Francis D. Correll, Condensed Matter and Radiation Sciences
 Mark L. Elert, Chemistry
 Murray S. Korman, Acoustics
 Tian S. Lim, Electronics Technology
 Richard L. Martin, Electronics Technology
 Anthony F. Norcio, Information Technology
 Robert N. Shelby, Electronics Technology
 L.L. Tankersley, Optical Sciences
 Donald J. Treacy, Electronics Technology
 Boyd A. Waite, Chemistry

- **The Office of Naval Research Graduate Fellowship Program** helps U.S. citizens obtain advanced training in disciplines of science and engineering critical to the U.S. Navy. The three-year program awards fellowships to recent outstanding graduates to support their study and research leading to doctoral degrees in specified disciplines such as electrical engineering, computer sciences, material sciences, applied physics, and ocean engineering. Award recipients are encouraged to continue their study and research in a Navy laboratory during the summer. Five ONR graduate Fellows appointed in the 1982/83 program chose NRL for their summer work. They are listed below, along with the participating NRL divisions and their home institutions.

Christopher P.J. Barty (Optical Sciences),
Stanford University, California
Brian Damkroger (Material Science and
Technology), Colorado School of Mines
John B. Deaton, Jr. (Material Science and
Technology), Johns Hopkins University,
Maryland
Karl S. Keller (Optical Sciences), University
of Virginia
Ellice Y. Luh (Material Science and Technology),
University of California
(Berkeley)

For further information about the above five programs, please contact Dr. Agda Cohen at (202) 767-2432.

- **The United States Naval Academy Ensign Program** assigns Naval Academy graduates to NRL to work in areas of their own choosing and commensurate with their academic qualifications. These graduates provide a fruitful summer of research assistance, while gaining valuable experience in the Navy's R&D program. (Contact Lt. David Gates at (202) 767-2103.)

PROFESSIONAL APPOINTMENTS

- **Faculty Member Appointments** use the special skills and abilities of faculty members for periods of short duration to fill positions of a scientific, engineering, professional, or analytical nature.

- **Consultants and experts** are employed because they are outstanding in their fields of specialization or because they possess an ability of a rare nature and could not normally be employed as regular civil servants.

- **Intergovernmental Personnel Act Appointments** temporarily assign personnel from the state or local government or educational institution to the Federal Government (or vice versa) to improve public services rendered by all levels of government.

UNDERGRADUATE COLLEGE STUDENT PROGRAMS

Several programs are tailored to the undergraduate which provide employment and work experience in naval research. These are designed to attract applicants for student and full professional employment in the Laboratory's shortage category positions such as engineers, physicists, mathematicians, and computer scientists. The student employment programs build an understanding of NRL job opportunities among students and educational personnel so that educators can provide students who will meet NRL's occupational needs. The employment programs for college students include the following.

- **The Cooperative Education Program** alternates periods of work and study for students pursuing bachelor degrees in engineering, computer science, or the physical sciences. Several universities participate in this program.

- **The Federal Junior Fellowship Program** hires students entering college to be assistants to scientific, professional, or technical employees.

- **The Summer Employment Program** employs students for the summer in paraprofessional and technician positions in engineering, physical sciences, and computer sciences.

- **The Student Volunteer Program** helps students gain valuable experience by allowing them to voluntarily perform educationally related work at NRL.



P-1757(17)

◀ Louis Kovacs of the Acoustics Division and Bonnie Heron, Summer Research Apprentice Program employee, digitize ocean bathymetric data charts

- The **1040-Hour Appointment** employs students on a halftime basis to assist in scientific work which is related to their academic program.

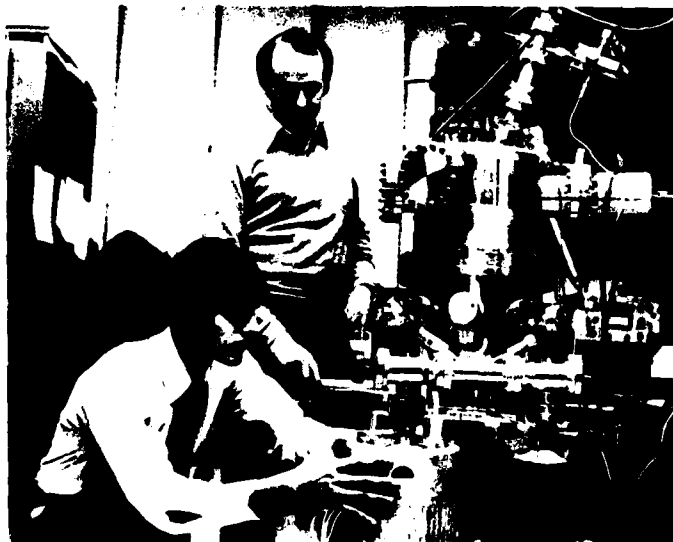
For additional information, contact Mrs. Betty Duffield at (202) 767-3030.

HIGH SCHOOL PROGRAMS

- The **Gifted and Talented Internship Program** provides a meaningful part-time employ-

ment experience for high school graduates who plan to pursue a bachelor's degree in engineering, computer science, or the physical sciences.

- The **Summer Research Apprentice Program** employs high school juniors and seniors to serve for eight weeks as junior research associates. Under the direction of a mentor, students gain a better understanding of research, its opportunities, and challenges through participa-



P-1757(9)

Dr. Richard Colton of the Chemistry Division works with Summer Research Apprentice Program employee, Cliff Hendricks, as they use the Secondary Ion Mass Spectrometer

tion in scientific programs. Criteria for eligibility are based on science and mathematics courses completed and grades achieved; scientific motivation, curiosity, and capacity for sustained hard work; a desire for a technical career; teacher recommendations; and ability and achievement

test scores.

For additional information on the professional appointments or college or high school student programs, please contact Mrs. Betty Duffield at (202) 767-3030 or the Employee Development Branch at (202) 767-2956.

Papers, reports, and patents



United States Patent Lewis et al

4,373,190
Feb. 9, 1981

EXPANDABLE PRE-COMPRESSION RANDOM-ORIENTED POLYMER FILM EXPANDER COMPRESSOR

Robert L. Lewis, et al., Lewis
F. Lewis et al.

The United States of America as
represented by the Secretary of the
State

Pat. No. 4,373,190

Filed Feb. 22, 1980

Int. Cl. 2 B29D 11/00

U.S. Cl. 264-1.1

Field of Search 264-1.1

References Cited

U.S. Pat. 3,800,000

U.S. Pat. 3,800,000

U.S. Pat. 3,800,000

U.S. Pat. 3,800,000

U.S. Pat. 3,800,000

U.S. Pat. 3,800,000

U.S. Pat. 3,800,000

U.S. Pat. 3,800,000

U.S. Pat. 3,800,000

U.S. Pat. 3,800,000

U.S. Pat. 3,800,000

U.S. Pat. 3,800,000

U.S. Pat. 3,800,000

U.S. Pat. 3,800,000

U.S. Pat. 3,800,000

U.S. Pat. 3,800,000

U.S. Pat. 3,800,000

U.S. Pat. 3,800,000

U.S. Pat. 3,800,000

U.S. Pat. 3,800,000

U.S. Pat. 3,800,000

U.S. Pat. 3,800,000

U.S. Pat. 3,800,000

U.S. Pat. 3,800,000

U.S. Pat. 3,800,000

U.S. Pat. 3,800,000

U.S. Pat. 3,800,000

U.S. Pat. 3,800,000

U.S. Pat. 3,800,000

U.S. Pat. 3,800,000

U.S. Pat. 3,800,000

U.S. Pat. 3,800,000

U.S. Pat. 3,800,000

U.S. Pat. 3,800,000

U.S. Pat. 3,800,000

U.S. Pat. 3,800,000

U.S. Pat. 3,800,000

U.S. Pat. 3,800,000

U.S. Pat. 3,800,000

U.S. Pat. 3,800,000

U.S. Pat. 3,800,000

U.S. Patent 4,373,190

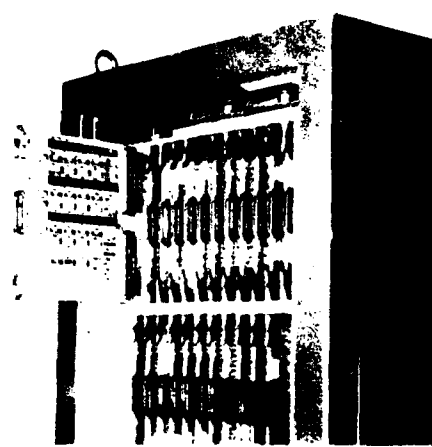


FIG. 2

249 *Papers in Journals, Books, and Proceedings of Meetings*

278 *Formal Reports*

280 *Patents*

PAPERS, REPORTS, AND PATENTS

"From the beginning of the twentieth century, the Navy has been a pioneer in initiating new developments ... and a leader in their utilization in military operations. An objective of this document is to identify NRL's numerous scientific reports ... so that the detailed information these reports contain may be made readily accessible to those who may be involved with the subject matter in the future."

Louis A. Gebhard
*Evolution of Naval Radio-Electronics
and Contributions of
The Naval Research Laboratory
1979*

Page 246, upper left:

Some of the many books, journals, and reports published at NRL

Upper right to lower left:

248

A new idea becomes patented and is manifest in the final electronic apparatus

PAPERS IN JOURNALS, BOOKS, AND PROCEEDINGS OF MEETINGS

In several respects, NRL is like a factory—the input ingredients are the talents and ideas of the people and research funds, and the output product is information. This product is packaged in the form of reports; articles in science journals and books; papers presented to scientific societies and topical conferences; and patents.

This section lists a portion of NRL's output for 1983. The omitted parts are oral presenta-

tions (about 1320), memorandum reports, reports that carry a military security classification, and letter reports to sponsors. In the following bibliography, an asterisk identifies a coauthor who is not a member of the NRL staff, and a dagger (†) identifies a prize-winning publication. In 60 years, NRL's pioneering research has led to 3003 patents. The table below summarizes the 1983 technical output.

<u>Type of Contribution</u>	<u>Unclass.</u>	<u>Class.</u>	<u>Total</u>
Papers in periodicals, books, and proceedings of meetings	691	0	691
NRL Reports	69	30	99
NRL Memorandum Reports	231	38	269
Patents granted			49

ACOUSTICS

- A Comparison of Parabolic Wave Theories for Linearly Elastic Solids**, by S.C. Wales and J.J. McCoy, *Wave Motion* 5:99-113
- A Comparison of Two Theories of Acoustoelasticity**, by A.V. Clark and R.B. Mignogna, *Ultrasonics* 21:217-225
- A Series Expansion of the Acoustic Power Radiated from Planar Sources**, by E.G. Williams, *Journal of the Acoustical Society of America* 73:1520-1524
- Acoustic Dispersion in a Deep Ocean Channel**, by A.A. Gerlach, K.D. Flowers, and R.B. Johnson, *Journal of the Acoustical Society of America* 74:196-203

Acousto-elastic Measurement of Stress and Stress Intensity Factors Around Crack Tips, by A.V. Clark, R.B. Mignogna, and R.J. Sanford,* *Ultrasonics* 21:57-64

Acousto-Optic All-Fiber Modulator, by R.P. DePaula,* J. Jarzynski, C.C. Ku,* J.A. Bucaro, and J.H. Cole, in *Single Mode Optical Fibers*, SPIE, Bellingham, Washington, SPIE Vol. 425, pp. 111-113

An Analysis of Pulsed Ultrasonic Fields as Measured by PVDF Spot-Poled Membrane Hydrophones, by G.R. Harris,* E.F. Carome,* and H.D. Dardy, *IEEE Transaction on Sonics and Ultrasonics* SU-30:295-303

Application of a New Complex Root-Finding Technique to the Dispersion-Relations for 249

- Elastic Waves in a Fluid-Loaded Plate**, by P.S. Dubbelday, *SIAM Journal of Applied Mathematics* 43:1127-1139
- Application of Tubular PVDF to Shock Resistant Hydrophones**, by T.A. Henriquez, *Ferroelectrics* 50:39-44
- Broad-Band Ultrasonic Sensor Based on Induced Optical Phase Shifts in Single-Mode Fibers**, by R.P. DePaula,* J.H. Cole, and J.A. Bucaro, *Journal of Lightwave Technology* LT-1:390-393
- Characteristics of a Hydro-Acoustic Ferrofluid Projector**, by P.S. Dubbelday and M.S. Ptak,* *Proceedings of the Third International Conference on Magnetic Fluids*, in: *Journal of Magnetism and Magnetic Materials* 39:159-161
- Determination of Stresses in Slightly Orthotropic Plates Using Off-Axis Horizontally Polarized Ultrasonic Shear Waves**, by A.V. Clark, *Ultrasonics* 21:249-255
- Effects of Eddy Currents on the Magnetomechanical Coupling of Conducting Piezomagnetic Methods**, by J.C. Hill* and S.W. Meeks, *Journal of the Acoustical Society of America* 74:348-350
- Effects of Static and Dynamic Stress on the Piezoelectric and Dielectric Properties of PVF₂**, by S.W. Meeks and R.Y. Ting, *Journal of the Acoustical Society of America* 74:1681-1686
- Experimental Constant Beamwidth Transducer**, by A.L. VanBuren, L.D. Luken, M.D. Jevnager, and A.C. Tims, *Journal of the Acoustical Society of America* 73:2200-2209
- Geometric Dispersion of Acoustic Signals Propagated in a Deep Ocean Channel**, by K.D. Flowers, *Journal of the Acoustical Society of America* 73:806-809
- High-Resolution Beamforming with Oversampled Arrays**, by C.L. Byrne and R.M. Fitzgerald, *Journal of the Acoustical Society of America* 74:1224-1227
- Imaging Techniques for Analysis of Long Range Acoustic Backscatter Data from Ocean Basin Regions**, by F.T. Erskine, G. Bernstein, and E.R. Franchi, in *1983 IEEE Proceedings of the Third Working Symposium on Oceanographic Data Systems*, IEEE Computer Society, Silver Spring, Maryland, pp. 160-164
- Interaction of Acoustic Waves and Ferroelastic Domain Walls**, by S.W. Meeks, B.A. Auld,* P. Maccagno,* and A. Miller,* *June 1983 IEEE International Symposium of Ferroelectrics ISAF*, in *Ferroelectrics* 50:245-250
- †Magnetic Boundary Conditions for Metallic-Glass Piezomagnetic Transducers**, by S.W. Meeks and J.C. Hill,* *Journal of the Acoustical Society of America* 74:1623-1626
- Modal Dispersion Effects on Coherent Signal Processing Parameters**, by K.D. Flowers, *IEEE International Conference on Acoustics, Speech and Signal Processing*, IEEE, New York, Vol. 3, pp. 973-976
- Model Validation of the Geometric Dispersion of Acoustic Signals Propagated in a Deep Ocean Channel**, by K.D. Flowers and A.A. Gerlach, *Journal of the Acoustical Society of America* 74:204-209
- Normal Mode Scaling and Phase Change at the Boundary**, by T.C. Yang, *Journal of the Acoustical Society of America* 74:232-240
- Numerical Evaluation of the Radiation from Unbaffled Finite Plates Using the FFT**, by E.G. Williams, *Journal of the Acoustical Society of America* 74:343-347
- Scattering of Forward Ultrasound by Spherical Microparticles**, by P.L. Edwards* and J. Jarzynski, *Journal of the Acoustical Society of America* 74:1006-1012
- The Piezoelectric Properties of Some PZT Composites**, by R.Y. Ting, *Ferroelectrics* 49:251-256
- Ultrasonic Sensing from 100 kHz to 50 MHz Using Single Mode Optical Fiber**, by R.P. DePaula,* J.H. Cole, and J.A. Bucaro, *Fiber Optic and Laser Sensors*, SPIE, Bellingham, Washington, SPIE Vol. 412, pp. 130-134
- Ultrasonic Sensitivity of Coated Fibers**, by N. Lagakos, J.H. Cole, and J.A. Bucaro, *Journal of Lightwave Technology* LT-1:495-498

ATMOSPHERIC SCIENCES

- A Mechanistic Model of Eulerian, Lagrangian Mean and Lagrangian Ozone Transport by Steady Planetary Waves**, by R.B. Rood* and M.R. Schoeberl, *Journal of Geophysical Research* 88:5208-5218
- A Numerical Model of Gravity Wave Breaking and Stress in the Mesosphere**, by M.R.

- Schoeberl, D.F. Strobel, and J.P. Apruzese, *Journal of Geophysical Research* 88:5249-5259
- A Practical Approach to Flux Measurements of Long Duration in the Marine Atmospheric Surface Layers**, by T.V. Blanc, *Journal of Applied Meteorology* 22:1093-1110
- A Study of Stratospheric Vacillations and Sudden Warnings on a β -Plane. Part I: Single Wave-Mean Flow Interaction**, by M.R. Schoeberl, *Journal of the Atmospheric Sciences* 40:769-787
- †An Observational Study of Water Vapor in the Mid-Latitude Mesosphere Using Ground-Based Microwave Techniques**, by R.M. Bevilacqua, P.R. Schwartz, J.M. Bologna, D.L. Thacker, J.J. Olivero,* and C.L. Gibbons,* *Journal of Geophysical Research* 88:8523-8534
- Enhancement of Heavy Ozone in the Earth's Atmosphere**, by J.A. Kaye and D.F. Strobel, *Journal of Geophysical Research* 88:8447-8452
- On the Accuracy of IR Extinction Predictions Made by the Navy Aerosol Model**, by S. Gathman and B. Ulfers, in *Ninth Conference on Aerospace and Aeronautical Meteorology*, American Meteorological Society, Boston, Massachusetts, Extended Abstracts, pp. 194-198
- Optical Properties of the Marine Aerosol as Predicted by the Navy Aerosol Model**, by S.G. Gathman, *Optical Engineering* 22:57-62
- Ozone Transport by Diabatic and Planetary Wave Circulations on a β -Plane**, by R.B. Rood* and M.R. Schoeberl, *Journal of Geophysical Research* 88:8491-8504
- Small-Scale Structure in the Earth's Ionosphere: Theory and Numerical Simulation**, by S.T. Zalesak, in *Solar-Terrestrial Physics, Principles and Theoretical Foundations*, D. Reidel Publishing Company, Boston, Massachusetts, pp. 781-804

BIOSCIENCES

- An Investigation of the Natural Resistance of *Melaleuca quinquenervia* to Tropical Marine and Terrestrial Wood-Destroying Organisms**, by J.D. Bultman, R.H. Beal,* J.B. Huffman,* and K.K. Parrish, *Forest Products Journal*, 33:39-43
- Destabilization of a Lipid Non-Bilayer Phase by High Pressure**, by P. Yager, E.L. Chang, *Biochimica et Biophysica Acta* 731:491-494
- Effect of High Pressure on a Lipid Non-Bilayer Phase**, by E.L. Chang and P. Yager, *Molecular Crystals and Liquid Crystals* 8:125-129
- †Encapsulation of Hemoglobin in Phospholipid Vesicles**, by B.P. Gaber, P. Yager, J.P. Sheridan, and E.L. Chang, *FEBS Letters* 153:285-288
- Inhibitory Effect of Solar Radiation on Amino Acid Uptake in Chesapeake Bay Bacteria**, by C.A. Bailey, R.A. Neihof, and P.S. Tabor, *Applied and Environmental Microbiology* 46:44-49
- Microbial and Particulate Contamination in Fuel Tanks on Naval Ships**, by R. Neihof and M. May, *International Biodeterioration Bulletin* 19:59-68
- Temperature Dependence of Laser-Induced Bioluminescence in *Pyrocystis unula***, by G.D. Hickman,* J.A. Edmonds,* R.D. Pike,* N. Antonoff,* and R.V. Lynch, in *Proceedings of Los Alamos Conference on Optics '83*, SPIE, Bellingham, Washington, SPIE Vol. 380
- Worker Injuries: The Effects of Workers' Compensation and OSHA Inspections**, by L.S. Robertson* and J.P. Keeve, *Journal of Health Politics, Policy and Law* 8:581-597

CERAMICS, GLASSES, AND PLASTICS

- A Material Opportunity: Ceramic Composites**, by R.W. Rice, *Chemtech* 13:230-239
- An Application of the NRL Relaxation Model to the Aging of Polystyrene Below its Glass Temperature**, by K.L. Ngai, D.J. Plazek,* and R.W. Rendell,* in *Proceedings of the 12th Annual North American Thermal Analysis Society Conference*, pp. 129-133
- Ceramics from Polymer Pyrolysis Opportunities and Needs—A Materials Perspective**, by R.W. Rice, *American Ceramic Society Bulletin* 62:889-892
- Data Acquisition Methodologies of Delayed Failure in Ceramics**, by K.R. McKinney and C.C. Wu, in *Time-Dependent Failure Mechanisms and Assessment Methodologies*, Cambridge University Press, New York, pp. 111-123
- Fundamental Defect Centers in Glass: Electron Spin Resonance and Optical Glass and Optical Fibers Absorption Studies of Irradiated Phosphorus-Doped Silica**, by D.L. Griscom, E.J. Friebele, K.J. Long,* and J.W.

Fleming,* *Journal of Applied Physics* 54:3743-3762

Mismatch Stress Effects on Microstructure-Flow Size Dependence of, by R.W. Rice, in *Science of Hard Materials*, Plenum Press, New York, pp. 631-648

Physical Aging Effects in Enthalpy Relaxation of Glassy Polymers, by K.L. Ngai, R.W. Rendell,* and T.K. Lee,* in *Proceedings of the 12th Annual North American Thermal Analysis Society Conference*, pp. 124-128

Piezomagnetic and Elastic Properties of Metallic Glass Alloys $\text{Fe}_{67}\text{Co}_{18}\text{B}_{14}\text{Si}_1$ and $\text{Fe}_{81}\text{B}_{13.5}\text{Si}_{3.5}\text{C}_2$, by S.W. Meeks and J.C. Hill,* *Journal of Applied Physics* 54:6584-6593

Preparation and Properties of Monolithic and Composite Ceramics Produced by Polymer Pyrolysis, by B.E. Walker, R.W. Rice, P.F. Becker, B.A. Bender, and W.S. Coblenz, *American Ceramic Society Bulletin* 62:916-923

Radiation-Induced Defects in Glasses with High Water Content, by A.A. Wolf, J. Acocella, E.J. Friebele, D.L. Griscom, and M.Z. Tomozowa, *International and VIIth University Conference on Glass Science*, in *Journal of Non-Crystalline Solids* 56:349-354

Thermal Shock and Thermal Shock Fatigue Testing of Ceramics with the Water Quench Test, by D. Lewis, *Fracture Mechanics of Ceramics*, Plenum Press, New York, Vol 6. Measurements, Transformations, and High-Temperature Fracture, pp. 487-496

CHEMISTRY

^{13}C NMR Chemical Shifts of Oriented Cesium-Graphite Intercalation Compounds, by D.D. Dominguez, H.A. Resing, E.F. Barbano, C.F. Poranski, and J.S. Murday, *Intercalated Graphite, Materials Research Society Symposia Proceedings*, North-Holland Publishing Co., New York, Vol. 20, pp. 363-368

A Comment on "Numerical Hartree-Fock-Slater Calculations on Diatomic Molecules" by A.D. Becke and B.I. Dunlap, *Journal of Chemical Physics* 78:4787

A Model of Freely Burning Pool Fires, by C.C. Ndubizu,* D.E. Ramaker,* P.A. Tatem, and F.W. Williams, *Combustion Science and Technology* 31:233-247

A New Method for the Determination of the Kinetics of T_g , by P. Peyser, *Journal of Macromolecular Science—Physics* 22:185-196

A Raman Study of Etching of Silicon in Aqueous KOH, by E.D. Palik, H.F. Gray, and P.B. Klein, *Journal of the Electrochemical Society* 30:956-959

A Study of the Electrical and Mechanical Properties of Alkali Metal Intercalated Graphite Fibers, by D.D. Dominguez, J.L. Lakshmanan, E.F. Barbano, and J.S. Murday, *Intercalated Graphite, Materials Research Society Symposia Proceedings*, North-Holland Publishing Co., New York, Vol. 20, p. 63

Absorption of Carbon from Residual Gases During Ti Implantation of Alloys, by I.L. Singer and T.M. Barlak,* *Applied Physics Letters* 43:457-459

Aerosolization of JP-5 Jet Fuel, by R.C. Little, R. Pratt, and J.B. Romans, *Fire Safety Journal* 5:145

Analysis of Upgraded SRC-II and H-Coal Liquid Products, by L.S. Young,* N.C. Li,* and D. Hardy, *Fuel* 62:718-723

Basis Set Effects on Spectroscopic Constants for C_2 and Si_2 and the Symmetric Dilemma in the $X\alpha$ Model, by B.I. Dunlap and W.N. Mei,* *Journal of Chemical Physics* 78:4997-5003

Carbon as a Sample Substrate in Secondary Ion Mass Spectrometry, by M.M. Ross and R.J. Colton, *Analytical Chemistry* 55:150-153

Carburization of Steel Surfaces During Implantation of Carbide-Forming Ions, by I.L. Singer, *29th National Symposium of the American Vacuum Society*, in *Journal of Vacuum Science and Technology A* 1:419-422

Catalytic Oxidation of NH_3 on a Polycrystalline Pt Surface Studied by Laser Induced Fluorescence, by G.S. Selwyn* and M.C. Lin, *Surface Studies with Lasers, Proceedings of the International Conference*, Springer-Verlag, New York, pp. 115-121

Chemical Lasers, by M.C. Lin, M.E. Umstead, and N. Djeu, *Annual Review of Physical Chemistry* 34:557-591

Coherent Anti-Stokes Raman Scattering as a Probe in Reactive Media, by J.W. Fleming, *Optical Engineering* 22:317-321

Comment on "Observation of Resonant Photoemission in an Adsorbed Molecule", by J.A.D. Matthew,* D.E. Ramaker, E. Bertel,* and M.A. Chesters,* *Physical Review Letters* 51:521

Comments on Fast Atom Bombardment Mass Spectrometry Studies, by J.E. Campana, *International Journal of Mass Spectrometry and*

- Ion Physics* 51:133-134
- Cross-Links in Polyacetylene**, by C.T. White, P. Brant,* and M.L. Elert,* *Conference Internationale sur la Physique et la Chimie des Polymeres Conducteurs*, in *Journal de Physique Colloque* C3:C-443
- Detection of CH₂ OH Radicals by Resonance-Enhanced Multiphoton Ionization Spectroscopy**, by C.S. Dulcey and J.W. Hudgens, *Journal of Physical Chemistry* 87:2296-2298
- Detection of Triplet States in a Laser Dye from Linear and Circular Polarization Studies**, by T.W. Barrett and J.F. Giuliani, *Applied Optics* 22:2522-2525
- Effects of Implantation Energy and Carbon Concentration on the Friction and Wear of Titanium-Implanted Steel**, by I.L. Singer and R.A. Jeffries,* *Applied Physics Letters* 43:925-927
- Effects of Off-Diagonal Disorder on Soliton- and Polaron-Like States in Trans-Polyacetylene**, by C.T. White, M.L. Elert, and J.W. Mintmire, *Conference Internationale sur la Physique et la Chimie des Polymeres Conducteurs*, in *Journal de Physique Colloque* C3:C-481
- Electrical Conductivity and Film Morphology of TCNQ Salt Dispersion in Polymer Matrix**, by O.K. Kim, *Journal of Polymer Science, Polymer Physics Letters Edition* 21:575-581
- Electrical Conductivity in Phthalocyanines Modulated by Circularly Polarized Light**, by T.W. Barrett, H. Wohltjen, and A. Snow, *Nature* 301:694-695
- Electrodeposition of Tantalum Carbide Coatings from Molten Salts**, by K.H. Stern and S.G. Gadomski, *Journal of the Electrochemical Society* 130:300-305
- Excitation and Emission Spectra of the ${}^2A'' \longleftrightarrow {}^2E''$ System of the Gas-Phase Cyclopentadienyl Radical**, by H.H. Nelson, L. Pasternack, and J.R. McDonald, *Chemical Physics* 74:227-237
- Excited State Dynamics of NO₃**, by H.H. Nelson, L. Pasternack, and J.R. McDonald, *Journal of Chemical Physics* 79:4279-4284
- Fast Atom Bombardment: Evidence of Disproportionation and Recombination of a Synthetic Porphyrin in the Matrix**, by L. Kurlansik,* T.J. Williams,* J.E. Campana, B.N. Green,* L.W. Anderson,* and J.M. Strong,* *Biochemical and Biophysical Research Communications* 111:478-483
- Fast-Atom Molecular Secondary-Ion Mass Spectrometry**, by M.M. Ross, J.R. Wyatt, R.J. Colton, and J.E. Campana, *International Journal of Mass Spectrometry and Ion Processes* 54:237-247
- Fire Resistant Hydraulic Fluids**, J.B. Romans* and R.C. Little, *Fire Safety Journal* 5:115
- Fitting the Coulomb Potential Variationally in X α Molecular Calculations**, by B.I. Dunlap, *Journal of Chemical Physics* 78:3140-3142
- Gas-Phase Reactions of the Vinoxyl Radical with O₂ and NO**, by D. Gutman* and H.H. Nelson, *Journal of Physical Chemistry* 87:3902-3905
- Graphitized Carbon Fibers: A New Electrical Conductor with High Strength to Weight Properties**, by J.S. Murday and D.D. Dominguez, *Naval Research Reviews* 35:2-13
- Ionic Salt Limit in Graphite-fluoroarsenate Intercalation Compounds**, by J.W. Milliken and J.E. Fischer,* *Journal of Chemical Physics* 78:5800-5808
- Jet Fuel Freezing Point of Composition**, by T.L. Van Winkle and W.A. Affens, *Shale Oil Upgrading and Refining*, Butterworth Publishers, Boston, pp. 243-260
- Kinetics and Mechanism of the CH + N₂ Reaction. Temperature- and Pressure-Dependence Studies and Transition-State-Theory Analysis**, by M.R. Berman and M.C. Lin, *Journal of Physical Chemistry* 87:3933-3942
- Kinetics and Mechanisms of the Reactions of CH with CH₄, C₂H₆ and n-C₄H₁₀**, by M.R. Berman* and M.C. Lin, *Chemical Physics* 82:435-442
- Laser-Induced Excitation and Emission Spectra of NO₃**, by H.H. Nelson, L. Pasternack, and J.R. McDonald, *Journal of Physical Chemistry* 87:1286-1288
- Liquid Metal Substrate for Dynamic Secondary Ion Mass Spectrometry**, by M.M. Ross and R.J. Colton, *Analytical Chemistry* 55:1170-1171
- †Local-Density-Functional Approach to All-Trans-Polyacetylene**, by J.W. Mintmire and C.T. White, *Physical Review B* 28:3283-3290
- Mass Spectrometric Study of the Decomposition of CoSO₄ and CoSO₄ - Na₂S₄**, by C.M. Kramer and R.L. Jones, *Inorganica Chimica Acta* 76:L217-L218
- Mass Spectrometry of Secondary Ions: High Mass Molecular and Cluster Ions**, by R.J. Colton, *Proceedings of the Sixth International Conference on Ion Beam Analysis*, in Nuclear

- Instruments and Methods in Physics Research 218:276-286
- Mixed Mn, Na-Sulfate Reactions in Low Temperature Hot Corrosion**, by R.L. Jones, *Journal of the Electrochemical Society* 130: 273-279
- Modulation of the Electrical Conductance of Phthalocyanine Films by Circularly Polarized Light**, by T.W. Barrett, *Thin Solid Films* 102:231-244
- Molecular Level Fabrication Techniques and Molecular Electronic Devices**, by F.L. Carter, 1983 *International Symposium on Electron, Ion and Photon Beams in Journal of Vacuum Science and Technology B* 1:959-968
- Motions of o- and p-xylene in ZSM-5 Catalyst. Carbon-13 Nuclear Magnetic Resonance**, by J.B. Nagy,* E.G. Derouane,* H.A. Resing, and G.R. Miller,* *Journal of Physical Chemistry* 87:833-837
- NMR Spectroscopy of Synthetic Metals: Inter-calated Graphite**, by H.A. Rising, M.J. Moran,* G.R. Miller, L.G. Banks, C.F. Poranski, D.C. Weber, *Materials Research Society Symposia Proceedings*, Elsevier Publishing Co., New York, Vol. 20, pp. 355-361
- Observation of the Methyl Radical CH₃ in Irradiated, High-Purity Synthetic Fused Silica**, by E.J. Friebele and D.L. Griscom, *Journal of Non-Crystalline Solids* 57:167-175
- On the Temporal Increase of Tropospheric CH₄**, by D.H. Ehhalt,* R.J. Zander,* and R.A. Lamontagne, *Journal of Geophysical Research* 88:8442-8446
- pH Response of Platinum and Vitreous Carbon Electrodes Modified by Electropolymerized Films**, by C. Cheek,* C.P. Wales, and R.J. Nowak, *Analytical Chemistry* 55:380-381
- Preliminary Characterization of Electrodeposited W₂C Coatings for Wear Applications**, by K.H. Stern, I.L. Singer, C.C. Wu, and R.A. Jeffries,* *International Conference on Metallurgical Coatings*, in *Thin Solid Films* 108:9-17
- Production and Detection of Energetic Species by Laser Photolysis and Detection Techniques**, by J.R. McDonald, *Excimer Lasers-83*, American Institute of Physics, New York, AIP Conference Proceedings No. 100, pp. 307-311
- Proton Spin Relaxation and Molecular Motion in a Bulk Polycarbonate**, by A.J. Jones,* J.F. O'Gara,* P.T. Inglefield,* J.T. Bendler,* A.F. Yee,* and K.L. Ngai, *Macromolecules* 16:658-665
- Pyrolysis of Shale Oil, Crude and Vacuum Distillate Fractions**, by R.N. Hazlett and E.J. Beal, *Geochemistry and Chemistry of Oil Shales*, American Chemical Society, Washington, D.C., ACS Symposium Series 230, pp. 371-384
- Reactions of Nickel Atoms with Substituted Ethylenes**, by A.D. Berry, *Organometallics* 2:895-898
- Regularities and Irregularities in SIMS/FAB Spectra of Alkali Halides Analyzed via the Bond-Breaking Model**, by B.I. Dunlap, J.E. Campana, B.N. Green,* and R.H. Bateman,* *Journal of Vacuum Science and Technology A* 1:432-436
- Reissert Compounds and Their Open-Chain Analogs in Organic Synthesis**, by J.V. Cooney, *Journal of Heterocyclic Chemistry* 20: 823-838
- Reversible Optical Waveguide Sensor for Ammonia Vapors**, by J.F. Giuliani, H. Wohltjen, and N.L. Jarvis, *Optics Letters* 8:54-56
- Role of the Through-Space 2p-3p Overlap Effect in the Wittig Reaction**, by W.E. McEwen* and J.V. Cooney, *Journal of Organic Chemistry* 48:983-987
- Sampling Variability and Storage Stability of Volatile Organic Contaminants**, by H.G. Eaton, F.W. Williams, and D.E. Smith,* *Journal of Chromatographic Science* 21:77-84
- Secondary Ion Mass Spectrometry of Metal Halides. 3. Ionic Radii Effects in Alkali Halide Clusters**, by T.M. Barlak,* J.E. Campana, J.R. Wyatt, and R.J. Colton, *Journal of Physical Chemistry* 87:3441-3445
- Secondary Ion Mass Spectrometry of Metal Salts: Polyatomic Ion Emission**, by T.M. Barlak, J.E. Campana, J.R. Wyatt, B.I. Dunlap, and R.J. Colton, *International Journal of Mass Spectrometry and Ion Physics* 46:523-526
- Secondary Ion Mass Spectrometry of Organic Adsorbates on Carbon Particles and Liquid Metal Surfaces**, by M.M. Ross and R.J. Colton, 29th *National Symposium of the American Vacuum Society*, in *Journal of Vacuum Science and Technology A* 1:441-442
- Secondary Ion Mass Spectrometry of Polymers**, by J.E. Campana and S.L. Rose, *International Journal of Mass Spectrometry* 46:483-486
- Summary Abstract: Evidence for Core Hole Screening by 3d Electrons in Third Row Oxyanions**, by N.H. Turner and D.E. Ramaker, *Journal of Vacuum Science and*

- Technology A1:1229-1230**
- Surface Chemistry and Friction Behavior of Ti-Implanted 52100 Steel**, by I.L. Singer and R.A. Jeffries,* *29th National Symposium of the American Vacuum Society*, in *Journal of Vacuum Science and Technology A* 1:317-321
- Surface-Enhanced Raman Scattering from Vapor-Deposited Copper, Silver, and Gold. Excitation Profiles and Temperature Dependence**, by H.D. Ladouceur, D.E. Tevault, and R.R. Smardzewski, *Journal of Chemical Physics* 78:980-985
- Synchrotron Radiation X-ray Fluorescence Analysis**, by J.V. Gilfrich, E.F. Skelton, S.B. Qadri,* J.P. Kirkland,* and D.J. Nagel, *Analytical Chemistry* 55:187-190
- Temperature Effect on the Removal of Hydroxyl Radicals by a Polycrystalline Platinum Surface**, by G.T. Fujimoto, G.S. Selwyn, J.T. Deiser, and M.C. Lin, *Journal of Physical Chemistry* 87:1906-1910
- The SN_x Paste Electrode: Electrochemistry in Nonaqueous Media**, by R.J. Nowak, C.L. Joyal, and D.C. Weber, *Journal of Electroanalytical Chemistry* 143:413-417
- The Determination of the Oxidative Stability of Several Deuterated Lubricants by an Electronic Gas Sensor**, by H. Ravner and H. Wohltjen,* *37th Annual Meeting of the American Society of Lubrication Engineers*, in *Journal of the American Society of Lubrication Engineers* 39:701-705
- The Effect of Ammonia Ions on the Absorption and Fluorescence of an Oxazine Dye**, by J.F. Giuliani and T.W. Barrett, *Spectroscopy Letters* 16:555-563
- The Synthesis of Knorr's Pyrrole by Inverse Addition**, by J.V. Cooney, E.J. Beal, and R.N. Hazlett, *Organic Preparation and Procedures International* 15:292-295
- Theoretical Treatment of the Dielectric Response of All-Trans-Polyacetylene**, by J.W. Mintmire and C.T. White, *Physical Review B* 27:1447-1449
- Two Photon Resonance Enhanced Multiphoton Ionization Spectroscopy and State Assignments of the Methyl Radical**, by J.W. Hudgens, T.G. DiGiuseppe, and M.C. Lin, *Journal of Chemical Physics* 79:571-582
- Two-Dimensional Reorientation and Magnetic Resonance Line Shapes in Semioordered Solids**, by R.G. Kooser* and H.A. Resing, *Journal of Physical Chemistry* 87:2564-2574

Variational Fit to the Nonlocal Electron-Electron Exchange Potential: Is an Accurate N^3 Hartree-Fock Method Possible?, by B.I. Dunlap, *Physical Review Letters* 51:546-549

Water Permeation Through Elastomers and Plastics, by P.E. Cassidy,* T.M. Aminabhavi,* and C.M. Thompson, *Rubber Chemistry and Technology* 56:595-617

X α Approval for the Determination of Electronic and Geometric Structure of Polyacetylene and Other Chain Polymers, by J.W. Mintmire and C.T. White, *Physical Review Letters* 50:101-105

X α , Cr $_2$, and the Symmetry Dilemma, by B.I. Dunlap, *Physical Review A* 27:2217-2219

COMMUNICATIONS

A Distributed Reservation Scheme for Spread Spectrum Multiple Access Channels, by J.E. Wieselthier and A. Ephremides,* in *IEEE Global Telecommunications Conference, IEEE, New York, GLOBECOM '83 Conference Record, Vol. 2*, pp. 659-665

A Generalization of Isolated Word Recognition Using Vector Quantization, by D.K. Burton, J.E. Shore, and J.T. Buck, *Proceedings of IEEE International Conference on Acoustics, Speech, and Signal Processing, IEEE, New York*, pp. 1021-1024

Anomalous Union Bound Behavior for MFSK Signaling on Inverse Linear Channels, by P.J. Crepeau and D.N. McGregor, *IEEE Transactions on Communications* COM-31: 848-849

Discrete Utterance Speech Recognition Without Time Alignment, by J.E. Shore and D.K. Burton, *IEEE Transactions on Information Theory* IT-29: 473-491

Distributed Control of Broadcast Radio Networks with Changing Topologies, by D.J. Baker, in *IEEE INFOCOM '83, IEEE, New York*, pp. 49-55

Minimum Cross-Entropy Spectral Analysis of Multiple Signals, by R.W. Johnson, *IEEE Transactions on Acoustics, Speech, and Signal Processing* ASSP-31: 574-582

Performance of Alternative Adaptive Interference Canceller Configurations in a Shipboard Environment, by A.S. Eley, in *1983 IEEE Military Communication Conference Proceedings, IEEE, New York*, pp. 537-543

Performance of FH/MFSK with List Metric Detection Against Partial Based Noise and Random Tone Jamming, by M.A. Creighton,* P.J. Crepeau, and J.K. Omura,* in *MILCOM'83, 1983 IEEE Military Communications Conference*, IEEE, New York, Vol. 1, pp. 225-228

Speech Noise Reduction by Means of Multi-Signal Minimum-Cross-Entropy Spectral Analysis, by R. Johnson, J.E. Shore, J. Buck, and D. Burton, in *Proceedings of IEEE International Conference on Acoustics, Speech, and Signal Processing*, IEEE, New York, pp. 1129-1132

COMPUTER SCIENCE

Abstract Requirements Specification: A New Approach and Its Application, by C.L. Marquardt, M.E. Storm,* I. Schneider, and L. Esterowitz, *Journal of Applied Physics* 54:5645-5650

A Generalized Control Structure and Its Formal Definition, by D.L. Parnas, *Communications of the ACM* 26:572-581

A Simple Speckle Smoothing Algorithm for Synthetic Aperture Radar Images, by J.S. Lee, *IEEE Transactions on Systems, Man and Cybernetics* SMC-13:85-89

Digital Image Smoothing and the Sigma Filter, by J.S. Lee, *Computer Vision, Graphics, and Image Processing* 24:255-269

Executable Specifications for a Human-Computer Interface, by R.J.K. Jacob, *Conference on Human Factors in Computer Systems*, pp. 28-34

Formal Models for Computer Security, by C.E. Landwehr (translation into Japanese), *Shuppan Kyoritsu*, Tokyo, Japan, pp. 95-124

Investigating the Space of Chernoff Faces, by R.J.K. Jacob, *Recent Advances in Statistics: Papers in Honor of Herman Chernoff on His Sixtieth Birthday*, Academic Press, NY, pp. 449-468

Numerical Simulation for Droplet Combustion Using Lagrangian Hydrodynamics, by M.J. Fritts, D.E. Fyfe, and E.S. Oran, *Combustion Fundamentals Research*, NASA Conference Publication 2268, NTIS, Springfield, VA, pp. 7-12

On the Uses of Synchronization in Hard-Real-Time Systems, by G.R. Yoder, L.A. Cooley, and T.W. Crooker, *Corrosion Fatigue: Mechanics, Metallurgy, Electrochemistry and Engineering*, ASTM STP 801, American So-

ciety for Testing and Materials, Philadelphia, PA, pp. 159-174

Protecting Stored Data Remains a Serious Problem, by C. Landwehr, *Military Electronics/Countermeasures* 9:26-36

Real-Time Oceanographic Data Acquisition Systems Aboard Aircraft, by D. Steiger, *Proceedings 1983 Working Symposium on Oceanographic Data Systems*, IEEE Computer Society, Los Angeles, CA, pp. 27-29

Software Design for Image Information Systems, by S.K. Chang,* I. Jurkevich, A. Petty, and C.C. Yang, *IEEE EASCON'83, Technology Shaping the Future*, IEEE, New York, pp. 115-120

The Best Available Technologies for Computer Security, by C.E. Landwehr, *Computer* 16:86-100

Using Formal Specifications in the Design of a Human-Computer Interface, by R.J.K. Jacob, *Communications of the ACM* 26:259-264

COSMIC RAYS

Distributed Acceleration of Cosmic Rays, by R. Silberberg, C.H. Tsao, J.R. Letaw,* and M.M. Shapiro,* *Physical Review Letters* 51:1217-1220

Improvement of Calculations of Cross Sections and Cosmic-Ray Propagation, by R. Silberberg, C.H. Tsao, and J.R. Letaw,* in *Composition and Origin of Cosmic Rays*, D. Reidel Publishing Co., New York, pp. 321-336

Matrix Methods of Cosmic Ray Propagation, by J. Letaw,* C.H. Tsao, and R. Silberberg, in *Composition and Origin of Cosmic Rays*, D. Reidel Publishing Co., New York, pp. 337-342

Sources of Extragalactic Cosmic Rays: Photons and Neutrinos as Probes, by R. Silberberg and M.M. Shapiro,* in *Composition and Origin of Cosmic Rays*, D. Reidel Publishing Co., New York, pp. 231-244

Cosmic Rays from Active Galactic Nuclei and in Metagalactic Space, by M.M. Shapiro* and R. Silberberg, *Astrophysical Journal* 265:570-572

ELECTRONICS AND ELECTRICITY

A 16 GHz GaAs FET Frequency Divider, by C. Rauscher, *IEEE MTT-S International Microwave Symposium Digest*, IEEE, New York, pp. 349-351

Cylindrical-Rectangular Microstrip Antenna, by C.M. Krowne, *IEEE Transactions on Antennas and Propagation* AP-31:194-199

Degenerate Frequency Mixing in Saturable Amplifiers, by J. Reintjes, B.L. Wexler, N. Djeu, and J.L. Walsh, *Proceedings of the Conference on Optical Phase Conjugation and Instabilities*, in *Journal de Physique, Coloque Supplement 3*, tome 44, pp. 27-37

Dielectric and Width Effect on H-Plane and E-Plane Coupling Between Rectangular Microstrip Antenna, by C.M. Krowne, *IEEE Transactions on Antennas and Propagation* AP-31:39-47

Fast Turn-On Characteristics of Tungsten-Based Dispenser Cathodes Following Gas Exposures, by C.R.K. Marrian, G.A. Haas, and A. Shih, *3rd Tri-Services Cathode Workshop, Ft. Monmouth, New Jersey*, in *Applications of Surface Science* 16:73-92

†High-Frequency Doubler Operation of GaAs Field-Effect Transistors, by C. Rauscher, *IEEE Transactions on Microwave Theory and Techniques* MTT-31:462-473

High-Speed Microelectronics for Military Applications, by M.C. Peckerar and R.E. Neidert, *Proceedings of the IEEE* 71:657-666

Interatomic Analysis of the Oxidation of Thin Ba Films. II. Applications to Impregnated Cathodes, by G.A. Haas, A. Shih, and C.R.K. Marrian, *Applications of Surface Science* 16:139-162

Interatomic Auger Analysis of the Oxidation of Thin Ba Films. I. Characterization of the Low Energy Auger Spectrum, by G.A. Haas, C.R.K. Marrian, and A. Shih, *Applications of Surface Science* 16:125-138

Measurement of Directional Ocean Wave Spectra from a Moving Ship Platform, by D.L. Schuler, W.P. Eng, A.B. Reeves, and N.D. Smith,* in *1983 International Geoscience and Remote Sensing Symposium (IGARSS '83)*, IEEE, New York, Symposium Digest, Vol. 1. Remote Sensing: Extending Man's Horizon, pp. 8.1-8.3

Millimeter-Wave Phased Array Transmitters for ECM, by F. Peng, B. Chiang,* and B. Sheleg, *Microwave Journal* 26:81-89

The Modification of X and L Band Radar Signals by Monomolecular Sea Slicks, by H. Huhnerfuss,* W. Alpers,* A. Cross,* W.D. Garrett, W.C. Keller, P.A. Lange,* W.J. Plant, F. Schlude,* and D.L. Schuler, *Journal of Geophysical Research* 88:9817-9822

Preparation and Oxidation of a Thin Ba Film, by A. Shih, G.A. Haas, and C.R.K. Marrian, *Applications of Surface Science* 16:93-105

Reaction Products and Subsequent Thermal Decomposition of Ba Films Exposed to CO, CO₂, H₂O and O₂, by A. Shih, C.R.K. Marrian, and G.A. Haas, *Applications of Surface Science* 16:106-124

Secondary Emission Properties of Impregnated Tungsten Cathodes, by R.E. Thomas and C.D. Morrill,* *3rd Tri-Service Cathode Workshop, Ft. Monmouth, New Jersey*, in *Applications of Surface Science* 16:292-311

Slow Wave Propagation in Generalized Cylindrical Waveguides Loaded with a Semiconductor, by C.M. Krowne, in *1983 IEEE MTT-S International Microwave Symposium Digest*, IEEE, New York, pp. 402-404

†Surface Plasmon Studies of Oxidized Ba Films, by J.W. Gibson and R.E. Thomas, *Applications of Surface Science* 16:163-180

The Characterization of the Surfaces of Tungsten-Based Dispenser Cathodes, by C.R.K. Marrian, A. Shih, and G.A. Haas, *Applications of Surface Science* 16:1-24

INSTRUMENTATION

A Marine Gravity Measurement System for Fixed Wing Aircraft, by J.D. Clamons, J.M. Brozena, and L.J. Rosenblum, *1983 IEEE Proceedings of the Third Working Symposium in Oceanographic Data Systems*, IEEE Computer Society, Silver Spring, Maryland.

A Sensitive Fiber-Optic Gas Spectrophone, by D.H. Leslie, R.O. Miles, and A. Dandridge, *Fiber Optic and Laser Sensors*, SPIE, Bellingham, Washington, SPIE, Vol. 412, pp. 160-164

Automated Digital Benchtop Calibration System for Hydrophone Arrays, by L.D. Luker, J.F. Zalesak, C.K. Brown, and R.E. Scott, *Journal of the Acoustical Society of America* 73:1212-1216

Compensation of Linear Sources of Non-reciprocity in Sagnac Interferometers, by N.J. Frigo, *Fiber Optic and Laser Sensors*, SPIE, Bellingham, Washington, SPIE Vol. 412, pp. 268-271

Electron-Bombarded CCD Detectors for Ultraviolet Atmospheric Remote Sensing, by G.R. Carruthers and C.B. Opal, *AIAA 21st Aerospace Sciences Meeting*, AIAA-83-0106, AIAA, NY, pp. 1-7

Fiber-Optic Gyroscope with Polarization-Holding Fiber, by W.K. Burns, R.P. Moeller, C.A. Villarruel, and M. Abebe, *Optics Letters* 8:540-542

Picosecond Streak Camera Fluorometry: A Review, by A.J. Campillo and S.L. Shapiro,* *IEEE Journal of Quantum Electronics* QE-19:585-603

Solar Instruments on the P78-1 Spacecraft, by G.A. Doschek, *Recent Advances in the Understanding of Solar Flares*, in *Solar Physics* 86:9-17

Towed Thermistor System for Marine Research, by W.D. Morris, J.P. Dugan, B.S. Okawa, C.W. Martz, and E.E. Rudd, *1983 IEEE Proceedings of the Third Working Symposium on Oceanographic Data Systems*, IEEE Computer Society, Silver Spring, Maryland, pp. 147-153

LASER SCIENCES

A Unified Linear Formulation and the Operating Parameters of Cerenkov-Smith-Purcell, Bremsstrahlung and Compton Free Electron Lasers, by A. Gover* and P. Sprangle, *Free Electron Lasers*, Plenum Press, New York, pp. 1-89

Advanced Laser Technology and Applications, ed. by L. Esterowitz, SPIE, Bellingham, Washington, *Proceedings of SPIE*, Vol. 335, pp. 119

Amplification of a Diffraction-Limited Stokes Beam b: a Severely Distorted Pump, by R.S.F. Chang and N. Djeu, *Optics Letters* 8:139-141

Analysis of High-Efficiency Pulsed Harmonic Conversion, by R.C. Eckardt* and J. Reintjes, *Conference on Lasers and Electro-Optics*, Digest of Technical Papers, IEEE, New York, pp. 74-76

Analysis of Laser-Enhanced Adsorption/Desorption Processes on Semiconductor Surface Via Electronic Surface State Excitation, by W.C. Murphy,* A.C. Beri,* T.F. George,* and J.T. Lin, in *Laser Diagnostics and Photochemical Processing for Semiconductor Devices*, North-Holland, New York, pp. 273-282

Characteristics of Oblique Shock Waves Produced in an Expanding Laser Plasma, by T.N. Lee, *Physical Review A* 27:2082-2099

Characteristics of the Electron Beam Pumped Iodine Monofluoride Laser, by L.F. Champagne and J.E. Ehrlich,* *IEEE Journal of*

Quantum Electronics QE-19:129-131

Color-Center Laser Continuously Tunable from 1.67 to 2.46 μm , by I. Schneider and S.C. Moss,* *Optics Letters* 8:7-8

Demonstration of a Two-Stage Backward-Wave-Oscillator/Free-Electron-Laser, by Y. Carmel,* V.L. Granatstein, and A. Gover,* *Physical Review A* 27:2082-2099

Design and Operation of a Collective Millimeter-Wave Free Electron Laser, by R.H. Jackson,* S.H. Gold, R.K. Parker, H.P. Freund,* P.C. Efthimion,* V.L. Granatstein, M. Herndon, A.K. Kinkead, J.E. Kosakowski,* and T.J.T. Kwan, *IEEE Journal of Quantum Electronics* QE-19:346-356

Design Considerations for RF Pumping of Rare Gas Halide Lasers, by R. Waynant, C.P. Christensen,* and W.M. Bollen,* *Topical Meeting on Excimer Lasers*, IEEE, New York, Digest of Technical Papers, pp. MA4-1-MA4-5

Electron-Beam Pumped Kinetic Study of $\text{ArF}^*(B)$ State, by R.S.F. Chang, *Journal of Chemical Physics* 78:2210-2213

Evolution of Spontaneous and Coherent Radiation in the Free-Electron-Laser Oscillator, by P. Sprangle, C.M. Tang, and I. Bernstein,* *Physical Review A* 28:2300-2309

External Cavity Diode Laser Sensor, by R.O. Miles, A. Dandridge, A.B. Tveten, and T.G. Giallorenzi, *Fiber Optic and Laser Sensors*, SPIE, Bellingham, Washington, *SPIE* Vol. 412, pp. 28-36

Free Electron Laser with a Realizable Wiggler and Axial Guide Field, by H.P. Freund,* S. Johnston,* and P. Sprangle, in *Proceedings of the International Conference Lasers '82*, STS Press, McLean, Virginia, pp. 133-135

Further Studies of Large Aperture XeCl Discharge Laser Performance, by B.L. Wexler and R.L. Burnham, *Excimer Lasers-1983*, American Institute of Physics, New York, AIP Conference Proceedings No. 100, pp. 52-58

Further Studies of Large Aperture XeCl Laser Performance, by B.L. Wexler and R.L. Burnham, *Topical Meeting on Excimer Lasers*, IEEE, New York, Digest of Technical Papers, pp. MB3-1-MB3-2

Gain Mechanism in (AlGa)As Lasers: A Picosecond Approach, by A.P. DeFonzo, *Conference on Lasers and Electro-Optics*, IEEE, New York, Digest of Technical Papers, pp. 82-84

- High-Gain Millimeter and Submillimeter Free Electron Lasers**, by V.L. Granatstein, P. Sprangle, and R.K. Parker, in *Free Electron Lasers*, Plenum Publishing Co., New York, pp. 501-522
- High-Power, Submillimeter Free Electron Lasers Based on Intense Relativistic Electron Beams**, by V.L. Granatstein, R.K. Parker, and P. Sprangle, *Energy Storage, Compression, and Switching*, Plenum Publishing Co., New York, Vol. 2, pp. 139-147
- Initiation of a Pulsed-Beam Free-Electron-Laser Oscillator**, by P. Sprangle, C.M. Tang, and I.B. Bernstein,* *Physical Review Letters* 50:1775-1778
- Injection Locking of Multiple Laser Diodes**, by L. Goldberg, H.F. Taylor, and J.F. Weller, *Conference on Lasers and Electro-Optics*, IEEE, New York, Digest of Technical Papers, pp. 30-32
- Injection Locking to FM Sidebands of a Diode Laser**, by L. Goldberg, H.F. Taylor, and J.F. Weller, *1983 Optical Fiber Communication*, IEEE, New York, Digest of Technical Papers, p. 58
- Laser Light Backscattering Off an Electron Beam-Plasma System**, by H.H. Szu, *IEEE Journal of Quantum Electronics* QE-19:379-388
- Laser Oscillations at 3.5 μm from Fe^{2+} in n-InP:Fe**, by P.B. Klein, J.E. Furneaux, and R.L. Henry, *Applied Physics Letters* 42:638-640
- Lasers in Materials Processing**, ed. by E.A. Metzbowser, American Society for Metals, Metals Park, Ohio
- Long-Pulse, High-Current Free Electron Laser with No External Focussing**, by J.A. Pasour, R.F. Lucey,* and C.A. Kapetanakis, *Eighth International Conference on Infrared and Millimeter Waves*, IEEE, New York, Conference Digest
- Low Frequency Noise Properties of Stabilized GaAlAs Lasers**, by A. Dandridge, A.B. Tveten, and R.O. Miles, *Fiber Optic and Laser Sensors*, SPIE, Bellingham, Washington, SPIE Vol. 412, pp. 28-36
- Measured Gain for XUV Plasma Lasers at Varying Pump Intensities**, by R.H. Dixon, J.F. Seely, and R.C. Elton, *Applied Optics* 22:1309-1312
- Microwave Signal Generation with Injection-Locked Laser Diodes**, by L. Goldberg, H.F. Taylor, J.F. Weller, and D.M. Bloom,* *Electronics Letters* 19:491-493
- Mirrors That are Electron-Transparent for Use in Free-Electron Laser Oscillators**, by J.H. McAdoo* and V.L. Granatstein, *Optics Letters* 8:316-318
- Noise and Spectral Properties of GaAlAs Broadband Sources**, by A. Dandridge, R.P. Moeller, and W.K. Burns, *1983 Optical Fiber Communication*, IEEE, New York, Digest of Technical Papers, p. 72
- Noise and Spectral Properties of Semiconductor Lasers Operating at 1.3 μm** , by A. Dandridge, L. Goldberg, and R.O. Miles, *1983 Optical Fiber Communication*, IEEE, New York, Digest of Technical Papers, pp. 72-74
- Observation of an Energetic Neutral Flux from a Laser-Produced Plasma**, by R.H. Dixon, R.C. Elton, and J.F. Seely, *Optics Communications* 45:397-399
- Optical Injection Locking of an X-band FET Oscillator Using Coherent Mixing of GaAlAs Lasers**, by L. Goldberg, C. Rauscher, J.F. Weller, and H.F. Taylor, *Electronics Letters* 19:397-399
- Parameter Regimes for X-Ray Lasing in Plasmas**, by R.C. Elton, *Comments on Atomic and Molecular Physics* 13:59-67
- Photodynamics and Stability of Laser Active F_2^+ Centers**, by I. Schneider and C.R. Pollock,* *Journal of Applied Physics* 54:6193-6198
- Properties of Diode Lasers with Intensity Noise Control**, by A. Dandridge and A.B. Tveten, *Applied Optics* 22:310-312
- Study of Gain, Bandwidth, and Tunability of a Millimeter-Wave Free-Electron Laser Operating in the Collective Regime**, by S.H. Gold, W.M. Black,* H.P. Freund,* V.L. Granatstein, R.H. Jackson,* P.C. Efthimion,* and A.K. Kinkead, *Physics of Fluids* 26:2683-2688
- The Non-Linear Theory and Efficiency Enhancement of Free Electron Lasers**, by P. Sprangle, C.M. Tang,* and W.M. Manheimer, in *Energy Storage, Compression, and Switching*, Plenum Publishing Co., New York, Vol. 2, pp. 149-159
- The Non-Linear Theory of the Free Electron Laser with Transverse Dimensional Effect**, by P. Sprangle and C.M. Tang, in *Free Electron Lasers*, Plenum Publishing Co., New York, pp. 229-242
- Third Harmonic Conversion of XeF Laser Radiation—A Potential High Energy VUV Source**, by M. Diab, L.L. Tankersley, and 259

J. Reintjes, *Topical Meeting on Excimer Lasers*, IEEE, New York, Digest of Technical Papers, pp. TuA3-1-TuA3-4

Third-Harmonic Conversion of XeF Laser Radiation, by M. Dlabal, J. Reintjes, and L.L. Tankersley, *Topical Meeting on Excimer Lasers*, IEEE, New York, Digest of Technical Papers, pp. TuA3-1-TuA3-4

Three-Dimensional Theory of Free Electron Lasers with an Axial Guide Field, by H.P. Freund,* S. Johnston,* and P. Sprangle, *IEEE Journal of Quantum Electronics* QE-19:322-327

Three-Dimensional Theory of the Free-Electron Laser in the Collective Regime, by H.P. Freund* and A.K. Ganguly, *Physical Review A* 28:3438-3449

Unstable Electrostatic Beam Modes in Free-Electron-Laser Systems, by H.P. Freund* and P. Sprangle, *Physical Review A* 28:1835-1837

†Use of Induced Spatial Incoherence for Uniform Illumination of Laser Fusion Targets, by R.H. Lehmberg and S.P. Obenschain, *Optics Communications* 46:27-31

Use of XeCl Amplifiers for Degenerate Four-Wave Mixing, by B.L. Wexler, N. Djeu, and J. Reintjes, in *Excimer Lasers-1983*, American Institute of Physics, New York, AIP Conference Proceedings No. 100, pp. 165-171

XeCl Amplifier for Degenerate Four-Wave Mixing, by B.L. Wexler, J.F. Reintjes, and N. Djeu, *Topical Meeting on Excimer Lasers*, IEEE, New York, Digest of Technical Papers, pp. TuA4-1-TuA4-3

MATHEMATICS

An Approximation Theoretic Approach to Maximum Entropy Spectral Analysis, by C.L. Byrne* and R.M. Fitzgerald, *IEEE Transactions on Acoustics, Speech, and Signal Processing* ASSP-31:734-736

Comments on "Statistical Methods in Reliability", by H. Ascher, *Technometrics* 25:320-326

Cylindrical Bessel Functions for a Large Range of Complex Arguments, by J.P. Mason, *Computer Physics Communications* 30:1-11

Image Restoration and Resolution Enhancement, by C.L. Byrne, R.M. Fitzgerald, M.A. Fiddy,* T.J. Hall,* and A.M. Darling,* *Journal of the Optical Society of America* 73:1481-1487

Image Sampling and Interpolation, by W.H. Carter, in *Applications of Digital Image Processing*, SPIE, Bellingham, Washington, SPIE Vol. 38, p. 97

Limit of Continuous and Discrete Finite-Band Gerchberg Iterative Spectrum Extrapolation, by C.L. Byrne and D.M. Wells,* *Optics Letters* 8:526-527

Minimum Cross-Entropy Spectral Analysis and Classification—Introduction and Discussion of Possible Geophysical Applications, by J.E. Shore, *Proceedings of the IEEE 1983 3rd International Symposium on Computer Aided Seismic Analysis and Discrimination*, IEEE Computer Society Press, Los Angeles, California, pp. 57-59

Regression Analysis of Repairable Systems Reliability, by H. Ascher, in *Electronic Systems Effectiveness and Life Cycle Costing*, Springer-Verlag, New York, pp. 119-133

Solution to the Euler Equations of Motion by Pseudospectral Techniques, by L. Sakell, in *Scientific Computing*, North-Holland Publishing Co., New York, pp. 283-289

Some New Approaches to One and Two Dimensional Power Spectrum Estimation, by C.L. Byrne* and R.M. Fitzgerald, *Proceedings of ASSP Spectrum Estimation Workshop II*, IEEE, New York, pp. 202-204

The Effects of Artificial Viscosity on Time Integration Schemes for Nonlinear Partial Differential Equations, by G.A. Keramidas, in *Scientific Computing*, North-Holland Publishing Co., New York, pp. 193-198

MECHANICS

A Semi-Automated In-Plane Loader for Materials Testing, by P.W. Mast, L.A. Beaubien, M. Clifford,* D.R. Mulville,* S.A. Sutton,* R.W. Thomas, J. Tirosh,* and I. Wolock, *Experimental Mechanics* 23:236-241

Analysis of Stress Waves in Flawed Solids with a Multilaser Camera, by R.J. Sanford* and R.G. Hughes, *15th International Congress on High Speed Photography and Photonics*, SPIE, Bellingham, Washington, SPIE Vol. 348, pp. 575-584

Dynamic Young's Moduli of Some Commercially Available Polyurethanes, by R.N. Capps, *Journal of the Acoustical Society of America* 73:2000-2005

Fluid-Property Effects on Flow-Generated Waves on a Compliant Surface, by R.J. Hansen

and D.L. Hunston, *Journal of Fluid Mechanics* 133:161-177

Non-axisymmetric Instability of a Rotating Layer of Fluid, by Y.T. Fung, *Journal of Fluid Mechanics* 127:83-90

On the Dynamic Behavior of Wobblestone, by R.E. Lindberg and R.W. Longman,* *AAS/AIAA Astrodynamics Conference*, in *Acta Mechanica* 49:81-94

Rubber Modified Matrices, by R.Y. Ting, in *The Role of the Polymeric Matrix in the Processing and Structural Properties of Composite Materials*, Plenum Press, New York, pp. 171-188

The Effects of Yaw and Finite Length Upon the Vortex Wakes of Stationary and Vibrating Circular Cylinders, by S.E. Ramberg, *Journal of Fluid Mechanics* 128:81-107

Variational Formulation and Approximate Solutions of the Thermal Diffusion Equation, by G.A. Keramidas, *Numerical Methods in Heat Transfer*, John Wiley & Sons, New York, Vol. II, pp. 99-143

Visualization of Stress Waves in Flawed Solids, by R.J. Sanford and R.G. Hughes, *15th International Congress on High Speed Photography and Photonics*, SPIE, Bellingham, Washington, SPIE Vol. 248, pp. 575-584

METALLURGY

[†]A **Critical Analysis of Grain-Size and Yield-Strength Dependence on Near-Threshold Fatigue Crack Growth in Steels**, by G.R. Yoder, L.A. Cooley, and T.W. Crooker, *Fracture Mechanics: Fourteenth Symposium*, ASTM, Philadelphia, Pennsylvania, Vol. I. Theory and Analysis, ASTM STP 791, pp. 348-365

Correlation Between Microstructure and Coercivity of Amorphous $Fe_{0.82}B_{0.18,0.90}Tb_{0.05}La_{0.05}$ -Ribbons, by B.N. Das and N.C. Koon, *Metallurgical Transactions A - Physical Metallurgy and Materials Science* 14A:953-961

Corrosion Behavior of SiC/Al Metal Matrix Composites, by P.P. Trzaskoma, E. McCafferty, and C.R. Crowe,* *Journal of the Electrochemical Society* 130:1804-1809

Corrosion Fatigue: Mechanics, Metallurgy, Electrochemistry, and Engineering, ed. by T.W. Crooker and B.N. Leis,* ASTM, Philadelphia, Pennsylvania, ASTM Special Technical Publication 801, pp. 531

Creep Crack Growth Behavior of Several Structural Alloys, by K. Sadananda and P. Shahinian, *Metallurgical Transactions A* 14A:1467-1480

Design-, Operation-, and Inspection-Relevant Factors of Fatigue Crack Growth Rates for Pressure Vessel and Piping Steels, by W.H. Cullen and F.J. Loss, in *Fatigue: Environment and Temperature Effects*, 27th Sagamore Army Materials Research Conference, Plenum Press, New York, pp. 391-410

Detection of New ω Phase Morphologies in β -III Ti Using Transmission Electron Microscopy, by C.S. Pande and M. Fatemi, in *Proceedings of the 41st Annual Meeting of the Electron Microscopy Society of America*, San Francisco Press Inc., San Francisco, California, pp. 266-267

[†]**Detection of Several ω -Phase Morphologies in β -III Ti by Small-Angle Neutron Scattering and Transmission Microscopy**, by M. Fatemi, C.S. Pande, and H.R. Child,* *Philosophical Magazine A* 48:479-500

Effects of Microstructure and Frequency on Corrosion-Fatigue Crack Growth in Ti-8Al-1Mo-IV and Ti-6Al-4V, by G.R. Yoder, L.A. Cooley, and T.W. Crooker, in *Corrosion Fatigue: Mechanics, Metallurgy, Electrochemistry and Engineering*, ASTM, Philadelphia, Pennsylvania, ASTM STP 801, pp. 159-174

Environmental Influences on the Aqueous Fatigue Crack Growth Rates of HY-130 Steel, by C.T. Fujii and J.A. Smith, *Corrosion Fatigue: Mechanics, Metallurgy, Electrochemistry, and Engineering*, ASTM, Philadelphia, Pennsylvania, ASTM STP 801, pp. 390-402

Fatigue Crack Growth Theory and Experiment: A Comparative Analysis, by K. Sadananda, *Scripta Metallurgica* 17:1419-1424

Fatigue Testing in Natural and Marine Corrosion Environments Substitute Ocean Waters, by F.D. Bogar and T.W. Crooker, *Materials Performance* 22:37

Geometry Variations During Fatigue Growth of Surface Flaws, by M. Jolles and V. Tortorelli,* *Fracture Mechanics: Fourteenth Symposium*, ASTM, Philadelphia, Pennsylvania, Vol. I: Theory and Analysis, ASTM, STP 791, pp. I-297-I-307

Initiation of ZrC Dendritic Growth on the Surface of Spark Machined Zirconium, by J.D. Ayers, *Metallurgical Transactions A* 14A:5-10

- Laser Beam Welding at NIROP, a Navy Manufacturing Technology Program**, by E.A. Metzbower, R.A. Hella,* and G. Theodorski,* in *Lasers in Materials Processing*, American Society for Metals, Metals Park, Ohio, pp. 266-272
- Laser Beam Welding of Aluminum Alloy 5456**, by D.W. Moon and E.A. Metzbower, *Welding Journal* 62:53-s-58-s
- Mechanical Properties and Physical Metallurgy of HSLA Steel Laser Beam Weldments**, by P.E. Denney and E.A. Metzbower, in *International Conference on Technology and Applications of High Strength Low Alloy (HSLA) Steels*, American Society for Metals, Metals Park, Ohio, pp. 1-8
- Microstructures and Compositions of Oxide Films Formed on CoCrAlY and Y-Ion-Implanted CoCrAl Alloys**, by J.A. Sprague and G.R. Johnston,* in *Proceedings of the 41st Annual Meeting of the Electron Microscopy Society of America*, San Francisco Press, California, pp. 216-217
- Mismatch Stress Effects on Microstructure-Flow Size Dependence of K_{IC} and Strength of Metal Bonded Carbides**, by R.W. Rice, in *Science of Hard Materials*, Plenum Publishing Co., New York, pp. 631-648
- Plastic Flow Normalizing the Fatigue Crack Propagation Data of Several Steels**, by J.M. Krafft, *Fracture Mechanics: Fourteenth Symposium*, ASTM, Philadelphia, Pennsylvania, Vol. I: Theory and Analysis, ASTM, STP 791, pp. 1-380-1-405
- Significance of Nickel and Copper Content to Radiation Sensitivity and Postirradiation Heat Treatment Recovery of Reactor Vessel Steels**, by J.R. Hawthorne, *Effects of Radiation on Materials: Eleventh Conference*, ASTM, Philadelphia, Pennsylvania, ASTM STP 782, pp. 375-391
- Solidification Structure and Fatigue Crack Propagation in LB Welds**, by F.W. Fraser and E.A. Metzbower, in *Lasers in Materials Processing*, American Society for Metals, Metals Park, Ohio, pp. 196-207
- The Effect of Load Rates on Fatigue Crack Growth in Ti-8Al-1Mo-1V**, by G.R. Yoder, L.A. Cooley, and T.W. Crooker, *Engineering Fracture Mechanics* 17:185-188
- The Effects of Inconel 600 on the Toughness of HY-Steel Laser Welds**, by D.W. Moon and E.A. Metzbower, in *Lasers in Materials Processing*, American Society for Metals, Metals Park, Ohio, pp. 248-253
- The Effects of Ion Implantation on the Initial Stages of Hot Corrosion Attack of Cast Co-22Cr-11Al at 700°C**, by V. Provenzano, G.R. Johnston,* and J.A. Sprague, *International Conference on Metallurgical Coatings*, in *Thin Solid Films* 107:277-286
- Transmission Electron Microscopy of Rapidly Solidified Micron-Size Carbon Powders of Titanium and Zirconium**, by C.S. Pande and S. Smith,* *Proceedings of the 41st Annual Meeting of the Electron Microscopy Society of America*, San Francisco Press Inc., San Francisco, California, pp. 68-69
- Wear Testing Under High Load Conditions. The Effects of "Anti-Scuff" Additions to AISI 3135, 52100 and 9310 Introduced by Ion Implantation and Ion Beam Mixing**, by N.E.E. Hartley* and J.K. Hirvonen, *Ion Beam Modification of Materials International Conference*, in *Nuclear Instruments and Methods* 209/210:933-940

NUCLEAR SCIENCE

- Assuring Structural Integrity—the 1983 Post-SMIRT Seminars**, by L. Steele, *Nuclear Engineering International* 28:28-29
- Proton-Nucleus Total Inelastic Cross Sections: An Empirical Formula for $E > 10$ MeV**, by J.R. Letaw,* R. Silberberg, and C.H. Tsao, *Astrophysical Journal Supplement Series* 51:271-276
- Radiation Embrittlement and Surveillance of Nuclear Reactor Pressure Vessels: An International Study**, ed. by L.E. Steele, American Society for Testing and Materials, Philadelphia, Pennsylvania, ASTM STP 819
- Review and Analysis of Reactor Vessel Surveillance Programs**, by L.E. Steele, *Status of USA Nuclear Reactor Pressure Vessel Surveillance for Radiation Effects*, ASTM, Philadelphia, Pennsylvania, ASTM STP 784, pp. 227-272
- Simultaneous High Depth Resolution Profiling of Carbon and Oxygen**, by C.R. Gossett, *Proceedings of the Sixth Conference on Ion Beam Analysis*, in *Nuclear Instruments and Methods in Physics Research* 218:149-153
- Status of USA Nuclear Reactor Pressure Vessel Surveillance for Radiation Effects**, ed. by L.E. Steele, American Society for Testing and Materials, Philadelphia, Pennsylvania, ASTM STP 784,

The Bases for Surveillance Programs, by L.E. Steele, *Status of USA Nuclear Reactor Pressure Vessel Surveillance for Radiation Effects*, ASTM, Philadelphia, Pennsylvania, ASTM STP 784, pp. 1-14

OCEAN SCIENCE AND TECHNOLOGY

A Current-Induced Ekman Spiral in the St. Lawrence Estuary, by C.L. Trump, *Journal of Physical Oceanography* 13:1540-1543

Attenuation of Capillary and Gravity Waves at Sea by Monomolecular Organic Surface Films, by H. Huhnerfuss,* W. Alpers,* W.D. Garrett, P.A. Lange,* and S. Stolte,* *Journal of Geophysical Research* 88:9809-9816

†Azimuthal Structure of a Cyclonic Gulf Stream Ring, by R.P. Mied, G.J. Lindemann, and J.M. Bergin, *Journal of Geophysical Research* 88:2530-2546

Effects of Ship's Roll on the Quality of Precision CTD Data, by C.L. Trump, *Deep Sea Research* 30:1173-1183

Mid-Latitude Mesoscale Temperature Variability in Six Multiship XBT Surveys, by D.E. Harrison,* W.J. Emery,* J.P. Dugan, and B.C. Li, *Journal of Physical Oceanography* 13:648-662

NRL Remote Sensing Experiment, by G.R. Valenzuela, D.T. Chen, W.D. Garrett, and J.A.C. Kaiser, *EOS* 64:618-619

Parametric Dependence of Ocean Wave-Radar Modulation Transfer Functions, by W.J. Plant, W.C. Keller, and A. Cross,* *Journal of Geophysical Research* 88:9747-9756

Shallow Water Bottom Topography from Radar Imagery, by G.R. Valenzuela, D.T. Chen, W.D. Garrett, and J.A.C. Kaiser, *Nature* 303:687-689

Stability of Free Surface Ekman Layers, by G.F. Spooner, *Journal of Physical Oceanography* 13:663-677

Symposium on Wave Breaking, Turbulent Mixing and Radio Probing of the Ocean Surface, by G.R. Valenzuela, *Radio Science* 18:798

Temperature and Current Variability of a Gulf Stream Meander Observed off Onslow Bay, August 1977, by E.R. Levine* and J.M. Bergin, *Journal of Geophysical Research* 88:4663-4671

The Iceland Mantle Plume: Status of the Hypothesis After a Decade of New Work, by

P.R. Vogt, *Structure and Development of the Greenland-Scotland Ridge*, Plenum Publishing Corp., NY, pp. 191-213

The Two-Scale Radar Wave Probe and SAR Imagery of the Ocean, by W.J. Plant and W.C. Keller, *Journal of Geophysical Research* 88:9776-9784

OPTICAL SCIENCES

Absorption Spectrum of Sr I Between 1400 and 1900 Å, by C.M. Brown, M.S. Longmire,* and M.L. Ginter,* *Journal of the Optical Society of America* 73:985-993

Acousto-optic Phase Modulator for Single-Mode Fibres, by K. Nosu,* H.F. Taylor, S.C. Rashleigh, and J.F. Weller, *Electronics Letters* 19:606-607

Acousto-Optic Processors for Real-time Generations of Time-frequency Representations, by R.A. Athale, J.N. Lee, E.L. Robinson,* and H.H. Szu, *Optics Letters* 8:166-168

Acousto-optic Signal Processing. Theory and Implementation, ed. by N.J. Berg and J.N. Lee, *Marcel Dekker, Inc., New York*

An External Cavity Diode Laser Sensor, by R.O. Miles, A. Dandridge, A.B. Tveten, and T.G. Giallorenzi, *Journal of Lightwave Technology* LT-1:81-93

Bending Loss of Optical Fibers: Transduction Mechanism for Fiber-Optic Sensors, by N. Lagakos, D.S. Czaplak, J.H. Cole, J.A. Bucaro, and E.L. Green,* *Optical Fiber Communication*, IEEE, New York, Digest of Technical Papers, p. 40

Birefringence Correction for Single-Mode Fiber Couplers, by C.A. Villarruel, M. Abebe, and W.K. Burns, *Optical Fiber Communication*, IEEE, New York, Digest of Technical Papers, pp. 30-32

Comparison of Cutoff Wavelength Measurements for Single-Mode Waveguides, by C.C. Wang, C.A. Villarruel, and W.K. Burns, *Applied Optics* 22:985-990

Compensation Densities in n-Type $Hg_{1-x}Cd_xTe$ from Transport Properties of Optically Generated Free Carriers, by F.J. Bartoli, C.A. Hoffman, and J.R. Meyer, 1983 *U. S. Workshop on the Physics and Chemistry of Mercury Cadmium Telluride*, in *Journal of Vacuum Sciences and Technology* A1:1669-1671

- Coordinate Transformation from an Image Plane Directly to an Invariant Feature Surface**, by R.A. Messner and H.H. Szu, *IEEE Computer Society Conference on Computer Vision and Pattern Recognition*, IEEE Computer Society, Los Angeles, California, pp. 522-530
- Delayed Fragmentation of Acetonitrile upon Short-Pulse UV Irradiation: Possible Role of Long-Lived Superexcited Intermediates**, by B.B. Craig, W.L. Faust, and R.G. Weiss,* *Journal of Chemical Physics* 79:1286-1296
- Depolarization in a Single-Mode Optical Fiber**, by W.K. Burns, R.P. Moeller, and C.L. Chen,* *Journal of Lightwave Technology* LT-1:44-50
- Depolarized Broadband Source**, by R.P. Moeller and W.K. Burns, *Electronics Letters* 19:187-188
- Dynamic Thermal Response of Plastic-Jacketed Optical Fibers**, by G.S. Maurer and L. Schuetz, *1983 Optical Fiber Communication*, IEEE, New York, Digest of Technical Papers, p. 64
- Dynamic Thermal Response of Single-Mode Optical Fiber for Interferometric Sensors**, by L.S. Schuetz, J.H. Cole, J. Jarzynski, N. Lagakos, and J.A. Bucaro, *Applied Optics* 22:478-483
- Efficient Raman Downconversion in the Mid-Infrared**, by C.L. Marquardt, M.E. Storm, I. Schenider, S.C. Moses, and L. Esterowitz, *Conference on Lasers and Electro-Optics*, IEEE, New York, Digest of Technical Papers, pp. 234-236
- Electroluminescence**, by M.N. Kabler, in *Concise Encyclopedia of Solid State Physics*, Addison-Wesley Publishing Co., New York, pp. 66-68
- Fiber Optic Gradient-Field Magnetometer**, by K.P. Koo and G.H. Sigel, *1983 Optical Fiber Communication*, IEEE, New York, Digest of Technical Papers, pp. 36-38
- Fiber-Optic Gyroscopes with Broad-band Sources**, by W.K. Burns, C.L. Chen,* and R.P. Moeller, *Journal of Lightwave Technology* LT-1:98-105
- High Frequency Response of a Single Mode Fiber Optical Phase Modulator Utilizing a Piezoelectric Plastic Jacket**, by C.C. Ku,* R.P. De Paula,* J. Jarzynski, and J.A. Bucaro, *Fiber Optic and Laser Sensors*, SPIE, Bellingham, Washington, SPIE Vol. 412, pp. 178-184
- Infrared Transmitting Fluoride Glasses: Fibers**, by G.H. Sigel and D.C. Tran, *1983 Optical Fiber Communication*, IEEE, New York, Digest of Technical Papers, pp. 4-6
- Measurement of Fiber Birefringence by Wavelength Scanning: Effect of Dispersion**, by S.C. Rashleigh, *Optics Letters* 8:336-338
- Measurement of Polarization Mode Dispersion in High-Birefringence Fibers**, by W.K. Burns and R.P. Moeller, *Optics Letters* 8:195-197
- Measurement of Polarization-Mode Dispersion in High-Birefringence Fibers**, by W.K. Burns and R.P. Moeller, *1983 Optical Fiber Communication*, IEEE, New York, Digest of Technical Papers, p. 32
- Minionization of OH Absorption and Scattering Losses in Zirconium Fluoride Glasses**, by D.C. Tran, C.F. Fisher, K.L. Levin, and G.H. Sigel, *1983 Optical Fiber Communication*, IEEE, New York, Digest of Technical Papers, p. 6
- Numerical Parameter Study of Phase Conjugation in Stimulated Brillouin Scattering from an Optical Waveguide**, by R.H. Lehmberg, *Conference on Lasers and Electro-Optics*, IEEE, New York, Digest of Technical Papers, p. 158
- Numerical Study of Phase Conjugation in Stimulated Brillouin Scattering from an Optical Waveguide**, by R.H. Lehmberg, *Journal of the Optical Society of America* 73:558-566
- Optical Matrix Algebraic Processors: A Survey**, by R.A. Athale, *10th International Optical Computing Conference*, IEEE, New York, pp. 24-31
- Origins and Control of Polarization Effects in Single-Mode Fibers**, by S.C. Rashleigh, *Journal of Lightwave Technology* LT-1:312-331
- Performance Characteristics of a Passively Stabilized Fiber Interferometer Using a 3×3 Fiber Directional Coupler**, by K.P. Koo, A. Dandridge, and A.B. Tveten, *Optical Fibre Sensors*, IEEE, New York, IEEE Conference Publication Number 221, pp. 200-204
- Polarimetric Sensors: Exploiting the Axial Stress in High Birefringence Fibers**, by S.C. Rashleigh, *Optical Fibre Sensors*, IEEE, New York, IEEE Conference Publication Number 221, pp. 210-213
- Polarization Characteristics of LiNbO₃ Channel Waveguide Directional Couplers**, by C.H. Bulmer and W.K. Burns, *Journal of Lightwave Technology* LT-1:227

- Polarization Preserving Single-Mode-Fiber Coupler**, by C.A. Villarruel, M. Abebe, and W.K. Burns, *Electronics Letters* 19:17-18
- Power Spectrum of Birefringence Perturbations in the Single-Mode and Near-Multimode Regime** by S.C. Rashleigh, M.J. Marrone, and I.P. Kaminow,* *Optical Fiber Communication*, IEEE, New York, Digest of Technical Papers, pp. 32-34
- Preservation of Polarization in Single-Mode Fibers**, by S.C. Rashleigh and R.H. Stolen,* *Laser Focus* 19:155-161
- Pressure-Tolerant Fiber-Optic Feedthrough**, by C.A. Villarruel and A.S. Greenblatt,* *1983 Optical Fiber Communication*, IEEE, New York, Digest of Technical Papers, pp. 14-16
- Radiation Damage in Single-Mode Optical-Fiber Waveguides**, by E.J. Friebele, K.J. Long,* and M.E. Gingerich, *Applied Optics* 22:1754-1757
- Rayleigh Backscattering in a Fiber Gyroscope with Limited Coherence Sources**, by W.K. Burns and R.P. Moeller, *Journal of Lightwave Technology* LT-1:381-386
- Rayleigh Scattering in Fluoride Glass Optical Fibres**, by D.C. Tran, K.H. Levin, C.F. Fisher, M.J. Burk, and G.H. Sigel, *Electronics Letters* 19:165-166
- Signal Processing Using an Acousto-Optic Memory Device**, by J.N. Lee, in *Acousto-Optic Signal Processing: Theory and Implementation*, Marcel-Dekker, Inc., New York, pp. 203-224
- Statistical Radiometry**, by W.H. Carter, *Radio Science* 18:149-158
- Technology and Design Considerations for a Very-High-Speed Fiber-Optic Data Bus**, by H.F. Taylor, *IEEE Journal on Selected Areas in Communications* SAC-1:500-507
- Temperature Dependence of Stress Birefringence in an Elliptically Clad Fiber**, by S.C. Rashleigh and M.J. Marrone, *Optics Letters* 8:127-129
- The Field Distribution of a Focused Gaussian Beam Reflected at 45° from a Conducting Plane and Its Effects in Plasma-Ignition Experiments**, by W.H. Carter* and T.J. Wieting, *Journal of Applied Physics* 54:519-523
- The Naval Research Laboratory Materials Analysis Beam Line at the National Synchrotron Light Source**, by J.P. Kirkland,* D.J. Nagel, and P.L. Cowan,* *Proceedings of the International Conference on X-Ray and*

VUV Synchrotron Radiation Instrumentation, in *Nuclear Instruments and Methods* 208:49-54

- The Optical Kerr Effect in Fiber Gyroscopes: Effects of Nonmonochromatic Sources**, by N.J. Frigo, H.F. Taylor, L. Goldberg, J.F. Weller, and S.C. Rashleigh, *Optics Letters* 8:119-121

Trends in Optical Fiber Sensors, by J.A. Bucaro, T.G. Giallorenzi, J.H. Cole, G.H. Sigel, and A. Dandridge, *1983 Optical Fiber Communication*, IEEE, New York, Digest of Technical Papers, p. 36

Ultrasonic Fiber-Optic Sensor, by N. Lagakos, R.P. DePaula,* J.H. Cole, and J.A. Bucaro, *Conference on Lasers and Electro-Optics*, IEEE, New York, Digest of Technical Papers, pp. 212

PHYSICS

Effects of Compressibility on the Rayleigh-Taylor Instability, by I.B. Bernstein,* and D.L. Book, *Physics of Fluids* 26:453-458

Exact Solution of Coupled Equations and the Hyperspherical Formalism: Calculation of Expectation Values and Wavefunctions of Three Coulomb-Bound Particles, by M.I. Haftel and V.B. Mandelzweig,* *Annals of Physics* 150:48-91

Paley-Wiener Criterion for Relaxation Functions, by K.L. Ngai, A.K. Rajogopal,* R.W. Rendell, and S. Teitler, *Physical Review B* 28:6073-6075

Vorticity Generation by Asymmetric Energy Deposition in a Gaseous Medium, by J.M. Picone and J.P. Boris, *Physics of Fluids* 26:365-382

PLASMA PHYSICS

A Comparison of Ray Trajectories in Plasma Characterized by Cold and Warm Dielectric Tensors, by B. Hui, *IEEE Transactions on Plasma Science* PS-11:261-263

A Dynamic Model for the Auroral Field Line Plasma in the Presence of Field-Aligned Current, by H.G. Mitchell* and P.J. Palmadesso, *Journal of Geophysical Research* 88:2131-2139

Anode-Plasma Expansion in Pinch-Reflex Diodes, by D.G. Colombant and S.A. Goldstein,* *Physical Review Letters* 51:1562-1565

- Anomalous Resistivity Due to Low-Frequency Turbulence**, by A.L. Rowland* and P.J. Palmadesso, *Journal of Geophysical Research* 88:7997-8002
- A Note on Gyrotron Travelling Wave Amplifiers Using Rectangular Waveguides**, by Y.Y. Lau and L.R. Barnett, *IEEE Transactions on Electron Devices* ED-30:908-912
- Breakdown of the Atmosphere by Emission from a Millimeter-Wave Free-Electron Maser**, by S.H. Gold, W.M. Black, V.L. Granatstein, and A.K. Kinkead, *Applied Physics Letters* 43:922-924
- Computer Simulation of Multiple-Beam Final Focusing Systems for Heavy Ion Fusion**, by I. Haber, 1983 *Particle Accelerator Conference*, in *IEEE Transactions on Nuclear Science* NS-30:2616-2617
- Critical Elements of High Gain: An Update**, by S. Bodner, in *Laser Interactions and Related Plasma Phenomena*, Plenum Press, New York, Vol. 6, pp. 665-672
- Current Interruption in Inductive Storage Systems Using Inertial Current Source**, by I.M. Vitkovitsky, D. Conte, R.D. Ford, and W.H. Lupton, in *Energy Storage, Compression and Switching*, Plenum Publishing Co., New York, Vol. 2, pp. 953-971
- Current Status of Calculations and Measurements of Ion Stopping Power in ICF Plasmas**, by T.A. Mehlhorn,* E.J. Peek,* J. McGuire,* N. Olsen,* and F.C. Young, *Sandia National Laboratories Report* 83-1519, 26 pp.
- Dense Plasma Effects on K-Shell Dielectronic Satellite Lines**, by D. Duston, J.E. Rogerson, J. Davis, and M. Blaha,* *Physical Review A* 28:2968-2980
- Density and Temperature Profiles Within Laser-Produced Plasmas in the Classical-Transport Regime**, *Physics of Fluids* 26:3650-3659
- Drag Instability in the Modified Betatron**, by P. Sprangle and C.A. Kapetanakis, *Particle Accelerators* 14:15-28
- Drift-Resistive Interchange and Tearing Modes in Cylindrical Geometry**, by J.M. Finn,* W.M. Manheimer, and T.M. Antonsen,* *Physics of Fluids* 26:962-973
- Effect of an Electron Beam on the Current-Convective Instability**, by P.K. Chaturvedi* and S.L. Ossakow, *Journal of Geophysical Research* 88:4119-4121
- Effects of Ion-Acoustic Instability on Light Ion Beam Transport in Deuterium Channels**, by D.G. Colombant and W. Manheimer, *Physics of Fluids* 26:2704-2706
- Electron Cyclotron Resonance Heating of Weakly Relativistic Plasmas**, by K.R. Chu and B. Hui, *Physics of Fluids* 26:69-79
- Electron-Cyclotron Maser Instability Driven by Laser-Cone Distribution**, by Y.Y. Lau* and K.R. Chu, *Physical Review Letters* 50:243-246
- Electron-Ion Instabilities in a High-Current Modified Betatron**, by W.M. Manheimer, *Particle Accelerators* 13:209-230
- Enhanced X-Ray Gain in Neon-Like Ions by Direct Collisional Pumping with Suprathermal Electrons**, by J.P. Apruzese and J. Davis, *Physical Review A* 28:3686-3688
- Equilibrium of a High-Current Electron Ring in a Modified-Betatron Accelerator**, by C.A. Kapetanakis, P. Sprangle, D.P. Chernin,* S.J. Marsh,* and I. Haber, *Physics of Fluids* 26:1634-1648
- Erratum: Ballistic Pendula for Measuring the Momentum of a Laser-Produced Plasma [Rev. Sci. Instrum. 53, 1878-1881 (1982)]**, by J. Grun and B.H. Ripin, *Review of Scientific Instruments* 54:903
- Extreme Ultraviolet Emission from Gas Puff Plasmas**, by R.D. Bleach, P.G. Burkhalter, and D.J. Nagel, *Journal of Applied Physics* 54:1273-1277
- Finite-Width Currents, Magnetic Shear, and the Current-Driven Ion-Cyclotron Instability**, by P. Bakshi,* G. Ganguli,* and P. Palmadesso, *Physics of Fluids Letters* 26:1808-1811
- Generation of Lower Hybrid Waves by Inhomogeneous Electron Streams**, by M.J. Keskinen and J.D. Huba, *Journal of Geophysical Research* 88:3109-3115
- High-Power Microwave Energy Coupling to Nitrogen During Breakdown**, by W.M. Bollen,* C.L. Yee,* A.W. Ali, M.J. Nagurney,* and M.E. Read, *Journal of Applied Physics* 54:101-106
- Influence of Magnetic Shear on the Lower-Hybrid-Drift Instability in Finite β Plasmas**, by J.D. Huba and G. Ganguli,* *Physics of Fluids* 26:124-132
- Ionospheric Plasma Cloud Dynamics via Regularized Contour Dynamics. I. Stability and Nonlinear Evolution of One-Contour Models**, by E.A. Overman, N. Zabusky,* and S.L. Ossakow, *Physics of Fluids* 26:1139-1153

- Laboratory Simulations of Controlled Energetic Electron-Beam-Plasma Interactions in Space**, by E.P. Szuszcwicz, *AIAA Journal* 21:1374-1381
- Laser-Ablative Acceleration of Targets to near Inertial Fusion Conditions**, by B.H. Ripkin, S.E. Bodmer, P.G. Burkhalter, H. Green, H. Hellfeld, M.J. Herbot, R.H. Lemberg, C.K. Manda, E.A. McLean, S.L. Obenschain, J.A. Stamper, R.R. Whitlock, and F.C. Young, *Plasma Physics and Controlled Nuclear Fusion Research 1982*, International Atomic Energy Agency, Vienna, Vol. I, p. 139
- Light-Ion Inertial-Confinement Fusion Research at Naval Research Laboratory**, by G. Cooperstein, R.J. Barker,* D.G. Colombant, A. Drobot,* S.A. Goldstein,* R.A. Merger, D. Mosher, P.F. Ottinger,* F.L. Sandel,* S.J. Stephanakis, and F.C. Young, *Plasma Physics and Controlled Nuclear Fusion Research 1982*, International Atomic Energy Agency, Vienna, Vol. II, p. 361
- Linear Theory of the $E \times B$ Instability with an Inhomogeneous Electric Field**, by J.D. Huba, S.L. Ossakow, P. Satyanarayana,* and P.N. Guzdar, *Journal of Geophysical Research* 88:425-434
- Long-Wavelength Limit of the $E \times B$ Instability**, by J.D. Huba and S.T. Zalesak, *Journal of Geophysical Research* 88:10263-10265
- Microwave Air Breakdown Impulse**, by A.W. Ali, *Proceedings of the Second National Conference on High Power Microwave Technology*, Harry Diamond Laboratories, pp. 453-461
- Microwave-Energy Coupling in a Nitrogen-Breakdown Plasma**, by C.L. Yee,* A.W. Ali, and W.M. Bollen,* *Journal of Applied Physics* 54:1278-1283
- Nonlinear Evolution of Convecting Plasma Enhancements in the Auroral Ionosphere, Irregularities**, by M.J. Keskinen and S.L. Ossakow, *Journal of Geophysical Research* 88:474-482
- Numerical Simulation of the Axisymmetric Hollowing Instability of a Propagating Beam**, by G. Joyce and M. Lampe, *Physics of Fluids* 26:3377-3386
- Parametric Excitation and Suppression of Convective Plasma Instabilities in the High Latitude F Region Ionosphere**, by M.J. Keskinen, P.K. Chaturvedi,* and S.L. Ossakow, *Journal of Geophysical Research* 88:7239-7244
- Preliminary Design of the NRL Modified Betatron**, by J. Golden, J. Pasour, D.E. Pershing,* K. Smith,* F. Mako,* S. Slinker,* F. Mora,* N. Orrick, R. Altes,* A. Fliflet,* P. Champney,* and C.A. Kapetankos, 1983 *Particle Accelerator Conference*, in *IEEE Transactions on Nuclear Science NS-30*:2114-2116
- Production of Intense Light Ion Beams on a Multiterawatt Generator**, by J.H. Mainchem* and F.C. Young, *Journal of Applied Physics* 54:89-100
- Propagation of Intense Relativistic Electron Beams Through Drift Tubes with Perturbed Walls**, by M. Friedman, V. Serlin,* A. Drobot,* and L. Seftor,* *Physical Review Letters* 50:1922-1925
- Radiation Energetics of a Laser-Produced Plasma**, by D. Duston, R.W. Clark, J. Davis, and J.P. Apruzese, *Physical Review A* 27:1441-1460
- Rayleigh-Taylor Instability in an Inhomogeneous Ablatively Accelerated Fluid**, by D.G. Colombant and W.M. Manheimer, *Physics of Fluids* 26:3127-3130
- Realization of a Stable and Highly Efficient Gyrotron for Controlled Fusion Research**, by Y. Carmel,* K.R. Chu, A.K. Ganguly, D. Dialetis,* R. Seeley,* J.S. Levine, and V.L. Granatstein, *Physical Review Letters* 50:112-116
- Reply to the Comment by Sanmartin, Montanes, and Barrero**, by W. Manheimer, D.G. Colombant, and J.H. Gardner, *Physics of Fluids* 28:2755-2756
- Reply to the Comments of B. K. Shivamoggi**, by Y.Y. Lau and C.S. Liu,* *Physics of Fluids* 26:868
- Saturation of the Lower-hybrid-drift Instability by Mode Coupling**, by J.F. Drake,* P.N. Guzdar,* and J.D. Huba, *Physics of Fluids* 26:601-604
- Self-Consistent Theory of Equilibrium and Acceleration of a High-Current Electron Beam in a Modified Betatron**, by J.M. Finn* and W.M. Manheimer, *Particle Accelerators* 14:29-37
- Short Wavelength Laser Calculations for Electron Pumping in Neon-like Krypton (Kr XVII)**, by U. Feldman, A.K. Bhatia,* and S. Suckewer,* *Journal of Applied Physics* 54:2188-2197
- Short Wavelength Stabilization of the Gradient Drift Instability due to Velocity Shear**, by J.D. Huba and L.C. Lee,* *Geophysical* 267

Research Letters 10:357-360

Stabilization of the Lower-Hybrid-Drift Instability in Finite- β Plasmas, by J.F. Drake,* J.D. Huba, and N.T. Gladd,* *Physics of Fluids* 26:2247-2249

Stabilizing Effect of Gas Conductivity Evolution on the Resistive Sausage Mode of Propagating Beam, by M. Lampe and G. Joyce, *Physics of Fluids* 26:3371-3376

Stimulated Brillouin Backscattering in Long-Scale-Length Plasmas, by D.G. Colombant, W.M. Manheimer, and J.H. Gardner, *Physics of Fluids* 26:3148-3155

Studies of the Effects of a Long Pulse Electron Beam on the Autoaccelerator, by T.R. Lockner,* M. Friedman, P. Palmadesso, and B.R. Russe,* *Journal of Applied Physics* 54:6160-6174

Suprathermal Electron Tail Distributions in a Space-Simulation Beam-Plasma-Discharge, by E.P. Szuszcwicz, D.N. Walker, H.R. Anderson,* and D. Papadopoulos,* in *Active Experiments in Space*, ESTEC, Noordwijk, Netherlands, ESA Scientific and Technical Publications Branch, p. 189

Tapered Interaction Gyro-TWA Experiments, by L.R. Barnett,* Y.Y. Lau,* D. Dialetis,* and K.R. Chu, *Proceedings of the IEEE International Electron Device Meeting (IEDM 83)*, IEEE, New York, pp. 280-283

The Morphology of a Multi-Bubble System in the Ionosphere, by J. Chen,* P. Satyanarayana,* and S.L. Ossakow, *Journal of Geophysical Research* 88:5528-5536

Uniform Ablative Acceleration of Targets by Laser Irradiation at 10^{14} W/cm², by S.O. Obenschain, R.R. Whitlock, E.A. McLean, B.H. Ripin, P.H. Price,* D.H. Phillion,* E.M. Campbell, M.D. Rosen, and I.M. Auerbach, *Physical Review Letters* 50:44-48

Vacuum Inductive Store/Pulse Compression Experiments on a High Power Accelerator Using Plasma Opening Switches, by R.A. Meger, R.J. Comisso,* G. Cooperstein, S.A. Goldstein,* *Applied Physics Letters* 42:943-945

Vibrational Relaxation and Dissociation in Air, by A.W. Ali and S. Slinker, *XVIIth Interna-*

tional Conference on Phenomena in Ionized Gases, Dusseldorf, Germany, Vol. 4, pp. 596-597

RADAR

A Comparison of Noncoherent and Coherent MTI Improvement Factors, by F.F. Kretschmer, F.C. Len, and B.L. Lewis, *IEEE Transactions on Aerospace and Electronic Systems* AES-19:398-404

A "Superresolution" Target Tracking Concept, by W.F. Gabriel, *1983 International Symposium Digest Antennas and Propagation*, IEEE, New York, pp. 195-198

Error Tolerance, Gain and Beamwidth of a Low Sidelobe Phased Array, by J.K. Hsiao, *1983 International Symposium Digest Antennas and Propagation*, IEEE, New York, pp. 377-380

Errors of Numerical Integration by Use of Table Look-Up, by J.K. Hsiao, *1983 International Symposium Digest Antennas and Propagation*, IEEE, New York, pp. 224-227

Improved Three Subaperture Method for Elevation Angle Estimation, by W.B. Gordon, *IEEE Transactions on Aerospace and Electronic Systems* AES-19:114-122

Ionospheric Irregularities and Their Potential Impact on Synthetic Aperture Radars, by E.P. Szuszcwicz, P. Rodriguez, M. Singh,* and S. Mango, *Radio Science* 18:765-774

RADIATION TECHNOLOGY

2 MeV Electron Irradiation Effects in (Hg,Cd)Te CCDS, by J.R. Waterman and J.M. Killiany, *IEEE Transactions on Nuclear Science* NS-30:4209-4215

A Simple, Inexpensive Device for Ion-Bombardment Cleaning of Samples in Ultrahigh Vacuum, by V.M. Bermudez and R.E. Thomas, *Journal of Vacuum Science and Technology* A1:1557-1558

Alpha-Particle Induced Switching in Josephson Tunnel Junctions, by R. Magno, R. Shelby,* M. Nisenhoff, A.B. Campbell, and J. Kidd, *Applied Superconductivity Conference*, in *IEEE Transactions on Magnetics* MAG-19:1286-1290

An MOS Dosimeter for Use in Space, by L.S. August, R.R. Circle,* J.C. Ritter, and J.S.

Tobin,* 1982 Nuclear Science Symposium, in *IEEE Transactions on Nuclear Science* NS-30:508

Applications of a Microbeam to the Problem of Soft Upsets in Integrated Circuit Memories, by A.R. Knudson and A.B. Campbell, 1982 IEEE Conference on the Application of Accelerators in Research and Industry, in *IEEE Transactions on Nuclear Science* NS-30:1232-1235

†**Dose Dependence of Single Event Upset Rate in MOS dRAMS**, by A.R. Knudson, A.B. Campbell, and E.C. Hammond,* 1983 Annual Conference on Nuclear and Space Radiation Effects, in *IEEE Transactions on Nuclear Science* NS-30:4508-4513

ESR Studies of Damage Processes in X-Irradiated High Purity α -SiO₂:OH and Characterization of the Formyl Radical Effect, by D.L. Griscom, M. Stapelbroek,* and E.J. Friebele, *Journal of Chemical Physics* 78:1638-1651

Exothermic Reactions in TATB Initiated by an Electron Beam, by A. Stolovy, E.C. Jones, J.B. Aviles, A.I. Namenson, and W.A. Fraser, *Journal of Chemical Physics* 78:229-235

Improved System for Energy-Dispersive X-ray Diffraction with Synchrotron Radiation, by E.F. Skelton, S.B. Qadri,* A.W. Webb, C.W. Lee,* and J.P. Kirkland,* *Review of Scientific Instruments* 54:403-409

Investigation of Soft Upsets in Integrated Circuit Memories and Charge Collection in Semiconductor Test Structures by the Use of an Ion Microbeam, by A.R. Knudson and A.B. Campbell, *Proceedings of the Sixth International Conference on Ion Beam Analysis in Nuclear Instruments and Methods in Physics Research* 218:625-631

Microprocessor-Controlled Radiation Testing Circuit Design, by T.S. Lim,* R.L. Martin,* and D.O. Patterson, *IEEE SOUTHEASTCON '83*, IEEE, New York, pp. 13-17

Modeling Total Dose Radiation Effects in Narrow Channel Devices, by M.C. Peckerar, D.B. Brown, H.C. Lin,* and D.I. Ma,* *SIAM/IEEE Conference on Numerical Simulation of VLSI Devices*, in *IEEE Transactions on Electron Devices* ED-30:1159-1164

Radiation Effects in N-Channel MNOS CCDs at Low Temperature, by N.S. Saks and J.M. Modolo, *IEEE Transactions on Nuclear Science* NS-30:4197-4204

Radiation Effects on the Electrical Properties of Solid Insulation, by F.J. Campbell, *Engineering Dielectrics. Vol. IIA. Electrical Properties of Solid Insulating Materials: Molecular Structure and Electrical Behavior*, American Society for Testing and Materials, Philadelphia, Pennsylvania, ASTM STP 783, pp. 619-662

Radiation Induced Soft Foils in Space Electronics, by E.L. Peterson, 1982 *IEEE Conference on the Application of Accelerators in Research and Industry*, in *IEEE Transactions on Nuclear Science* NS-30:1638-1641

Recovery of Damages in Rad-Hard MAS Devices during and after Irradiation by Electrons, Protons, Alphas, and Gamma Rays, by G.J. Brucker,* O. Van Grenten,* E.G. Stassinopoulos,* P. Shapiro, L.S. August, and T.M. Jorden,* 1983 *Annual Conference on Nuclear and Space Radiation Effects*, in *IEEE Transaction on Nuclear Science* NS-30:4157-4161

Suggested Single Event Upset Figure of Merit, by E.L. Petersen, J.B. Langworthy, and S.E. Diehl,* 1983 *Annual Conference on Nuclear and Space Radiation Effects*, in *IEEE Transactions on Nuclear Science* NS-30:4533-4539

X-Ray Fluorescence Analysis Using Synchrotron Radiation, by J.V. Gilfrich, E.F. Skelton, D.J. Nagel, and A.W. Webb, *Advances in X-Ray Analysis* 26: 313-323

SOLID STATE

A Model for the Dielectric Response of Na β -Alumina at Intermediate Temperatures, by U. Strom and K.L. Ngai, *Proceedings of the International Conference on Solid State Ionics*, in: *Solid State Ionics*, 9&10:283-286

Ab Initio Cluster Calculations of the Electronic Structure of Crystalline BeF₂, by K.L. Bedford, *Solid State Communications* 45:487-490

Abrasion Resistance Microhardness and Microstructures of Single-Phase Niobium Nitride Films, by I.L. Singer, R.N. Bolster, S.A. Wolf, and E.F. Skelton, *International Conference on Metallurgical Coatings*, in *Thin Solid Films* 107:207-215

Amorphous Thin Film Diffusion Barriers on GaAs and InP, by W.T. Anderson, A. Christou, and J.E. Davey, *Interfaces & Contacts, Materials Research Society Symposia Proceedings*, Vol. 18, North Holland, New

- York, pp. 57-67 and in: *Thin Solid Films* 104:57-67
- Au-Mg Improved Ohmic Contacts to p-GaAs**, by N.A. Papanicolaou and A. Christou, *Electronics Letters* 19:418-419
- Auger and Electron Energy-Loss Study of the Al/SiC Interface**, by V.M. Bermudez, *Applied Physics Letters* 42:70-72
- Auger and Electron Energy-Loss Study of the Pd/SiC Interface and Its Dependence on Oxidation**, by V.M. Bermudez, *Applications of Surface Science* 17:12-22
- Bonding and Equation of State for MgO**, by L.L. Boyer, *Physical Review B* 27:1271-1275
- Boron And Hydrogen Bonding in B-Doped a-Si:H - An NMR Study**, by W.E. Carlos, S.G. Greenbaum, and P.C. Taylor, Proceedings of the 16th International Conference on the Physics of Semiconductors, in: *Physica* 117&118B+C:886-888
- Characterization of Magnetic/Dielectric Materials at Millimeter-Wave Frequencies**, by F.J. Rachford and D.W. Forester, 1983 International Magnetism Conference, INTERMAG, in: *IEEE Transactions on Magnetism* MAG-19:1883-1888
- Complex Defects in GaAs and GaP**, by P.J. Lin-Chung, *Materials Research Society Symposium Proceedings* 14:267-270
- Computer Study of Self Sputtering of Cu and Ni at 90 KeV**, by M. Rosen, G.P. Mueller, and W.A. Fraser, *Nuclear Instruments and Methods* 209/210:63-33
- Correlated DLTS and EPR Measurements of Defects in As-Grown and Electron Irradiated p-Type GaP**, by P.M. Mooney,* T.A. Kennedy, and M.B. Small,* Proceedings of the 12th International Conference on Defects in Semiconductors, in *Physica* 116B+C:431-435
- Damaged-Induced Isolation in n-Type InP by Light-Ion Implantation**, by P.E. Thompson, S.C. Binari, and H.B. Dietrich, *Solid State Electronics* 26:805-810
- Defect Processes in Thin Films of Metal Oxides**, by R.H. Bassel and I. Manning, *Ion Implantation for Materials Processing*, Noyes Data Corporation, Park Ridge, NJ, pp. 230-231
- Density-Functional Theory of Excitation Spectra of Semiconductors: Application to Si**, by C.S. Wang* and W.E. Pickett, *Physical Review Letters* 51:597-600
- Dielectric Response of Na β -Alumina: Evidence for a "Glass Transistor"**, by K.L. Ngai and U. Strom, *Physical Review B* 27:6031-6036
- Direct Electromagnetic Generation of High Frequency Acoustic Waves in Semiconductor Superlattices**, by J.J. Quinn,* U. Strom, and L.L. Chang,* *Solid State Communications* 45:111-112
- Disorder Phenomena in β -Alumina**, by U. Strom, *Solid State Ionics* 8:255-279
- Dispersion Behavior of Modes in Partially Open Microstrip on a Semiconductor Layered Substrate**, by C.M. Krowne, 1983 International Symposium Digest Antennas and Propagation, IEEE, New York, pp. 660-663
- Dispersion in Slow Wave Two-Layered Semiconductor Loaded Parallel-Plate Waveguide**, by C.M. Krowne, 1983 International Symposium Digest Antennas and Propagation, IEEE, NY, pp. 656-659
- Dissipation and Dynamic Nonlinear Behavior in the Quantum Hall Regime**, by M.E. Cage,* R.F. Dziuba,* B.F. Field,* E.R. Williams,* S.M. Girvin,* A.C. Gassard,* D.C. Tsui,* and R.J. Wagner, *Physical Review Letters* 51:1374-1377
- Dynamic Dielectric Response of Electron-Hole and Electron-Electron Interactions**, by J.R. Meyer and F.J. Bartoli, *Physical Review B* 28:915-926
- Dynamic Dielectric Response to Carrier-Carrier Interactions in Narrow-Gap Semiconductors**, by J.R. Meyer and F.J. Bartoli, 1983 U.S. Workshop on the Physics and Chemistry Of Mercury Cadmium Telluride, in: *Journal of Vacuum Science and Technology* A1:1752-7155
- Effects of Thermal Annealing on the Refractive Index of Amorphous Silicon Produced by Ion Implantation**, by J.E. Fredrickson,* C.N. Waddell,* W.G. Spitzer,* and G.K. Hubler, *Ion Implantation for Materials Processing*, Noyes Data Corporation, Park Ridge, New Jersey, pp. 219-229
- Electric Field Induced Effects at the Si-SiO₂ Interface: Theory and Experiment**, by M.G. Ancona, *Journal of Applied Physics* 54:5231-5239
- Electrical and Structural Characterization of Implantation Doped Silicon by Infrared Reflection**, by G.K. Hubler, P.R. Malmberg, C.N. Waddell,* W.G. Spitzer,* and J.E. Fredrickson,* *Ion Implantation for Materials Processing*, Noyes Data Corporation, Park

- Ridge, New Jersey, pp. 195-218
- Electron Mobility in Low-Temperature $\text{Hg}_{1-x}\text{Cd}_x\text{Te}$ Under High-Intensity CO_2 Laser Excitation**, by F.J. Bartoli, J.R. Meyer, C.A. Hoffman, and R.E. Allen, *Physical Review B* 27:2248-2263
- Electron Power Loss in the (100)n Channel of a Si Metal-Oxide-Semiconductor Field-Effect Transistor. I. Intrasubband Phonon Scattering**, by C.M. Krowne, *Journal of Applied Physics* 54:2441-2454
- Electron Power Loss in the (100)n Channel of a Si Metal-Oxide-Semiconductor Field-Effect Transistor. II. Intersubband Scattering**, by C.M. Krowne, *Journal of Applied Physics* 54:2455-2467
- Electron-Hole Liquid Condensation: Systematics and Scaling Relations**, by T.L. Reinecke, A. Forchel,* H. Schweizer,* B. Laurich,* R. Hangleiter,* J. Wagner,* and W. Schmid,* Proceedings of the 16th International Conference on the Physics of Semiconductors, in: *Physica* 117&118B+C:315-317
- Electron-Impurity Scattering Rates of Dilute Alloys of Cu as Measured by Surface-State Resonances**, by A.J. Baratta,* A.C. Ehrlich, *Physical Review B* 28:4136-4142
- Electronic Spin of the Ga Vacancy in GaP**, by T.A. Kennedy, N.D. Wilsey, J.J. Krebs, G.H. Stauss, *Physical Review Letters* 50:1281-1284
- Electronic Structure, Superconductivity, and Magnetism in the C15 Compounds ZrV_2 , ZrFe_2 and ZrCo_2** , by B.M. Klein, W.E. Pickett, D.A. Papaconstantopoulos, L.L. Boyer, *Physical Review B* 27:6721-6731
- Ellipsometric Investigation of the Silicon/ZnO Interface**, by E.D. Palik, V.M. Bermudez, Ellipsometry and Other Optical Methods for Surface and Thin Film Analysis, in: *Journal de Physique Colloque* C10:C10-179-C10-182
- Evidence for Associated Deep Donor-Acceptor Pair Recombination EL2 Emission Band in GaAs**, by B.V. Shanabrook, P.B. Klein, S.G. Bishop, Proceedings of the 16th International Conference on the Physics of Semiconductors, in: *Physica* 117&118B+C:173-175
- Far-Infrared Conductivity and Anomalous Below-Gap Absorption in Superconducting Granular NbN**, by D.R. Karecki,* G.L. Carr,* S. Perkowitz,* D.U. Gubser, and S.A. Wolf, *Physical Review B* 27:5460-5466
- Far-Infrared Shifted Cyclotron Resonance in a Charge-Density-Wave System, NbSe_3** , by R.J. Wagner and N.P. Ong,* *Solid State Communications* 46:491-495
- Faraday Rotation and Ellipticity in Electron Inversion Layers of Si MOS Structures**, by H. Piller* and R.J. Wagner, *Application of High Magnetic Fields in Semiconductor Physics, Lecture Notes in Physics*, vol. 177, Springer-Verlag, New York, pp. 199-202
- Fermi Surface Properties of CeSn_3 and Related Compounds**, by W.R. Johnson,* G.W. Crabtree, A.S. Edelstein,* and O.D. McMasters, *Journal of Magnetism and Magnetic Materials* 31-34:377-382
- Fully Macroscopic Description of Electrical Conduction in Metal-Insulator-Semiconductor Structures**, by M.G. Ancona and H.F. Tiersten,* *Physical Review B* 27:7018-7045
- Growth of Epitaxial Fe on GaAs by Metalorganic CVD**, by R. Kaplan, *Journal of Vacuum Science and Technology* A1:551-553
- High Efficiency Mid-IR Generation by Raman Downconversion in Liquid Nitrogen**, by C.L. Marquardt, M.E. Storm,* I. Schneider, and L. Esterowitz, *Journal of Applied Physics* 54:5645-5650
- High Pressure Structural Phase Transition in AgGaTe_2** , by S.B. Qadri,* Z. Rek,* A.W. Webb, E.F. Skelton, and S.A. Wolf, *Journal of Applied Physics* 54:6897-6899
- High Pressure Studies of Ge Using Synchrotron Radiation**, by S.B. Qadri,* E.F. Skelton, and A.W. Webb, *Journal of Applied Physics* 54:3609-3611
- High Quality Niobium Nitride-Niobium Josephson Tunnel Junctions**, by E.J. Cukauskas, M. Nisenhoff, D.W. Jillie,* H. Kroger,* and L.N. Smith,* *IEEE Transactions on Magnetics* MAG-19:831-834
- High-Resolution Magneto-Optical Studies of Free and Bound Holes in p-Type InSb**, by C.L. Littler,* D.G. Seiler,* R. Kaplan, and R.J. Wagner, *Physical Review B* 27:7473-7488
- Intrinsic Infrared Absorption of Halide Glasses**, by H.B. Rosenstock* and L.L. Boyer, *Glass Technology* 24:168-169
- LEED and AES Studies of the Initial Growth of Ge on GaAs(100)**, by B.J. Mrstik, *Surface Science* 124:253-266
- Low-Temperature Nuclear Spin Relaxation in β -Aluminas**, by S.G. Greenbaum and U. Strom, *Solid State Communications* 46:437-440

- Materials Modification by Ion Implantation**, by J.K. Hirvonen and C.R. Clayton,* *Surface Modification and Alloying of Laser, Ion, and Electron Beams*, Plenum Press, New York, Chapter 12, pp. 323-383
- Microwave Dielectric Echoes in Na β -Alumina**, by M. von Schickfus* and U. Strom, *Physical Review B* 28:1068-1075
- Migration Current and Implant Densities in Steady-State Ion Implantation**, by I. Manning, *Ion Implantation for Materials Processing*, Noyes Data Corporation, Park Ridge, New Jersey, pp. 95-106
- New Semiempirical Construction of the Slater-Koster Parameters for Group-IV Semiconductors**, by Y. Li* and P.J. Lin-Chung, *Physical Review B* 27:3465-3470
- NMR Studies of Fluoride and Fast Ion Conducting Glasses**, by K.L. Ngai, A.K. Rajagopal,* and R.W. Randall,* *Journal of Non-Crystalline Solids* 56:27-32
- NMR Studies of Hydrogen Diffusion in Palladium and β -LaNi₅ Hydrides**, by K.L. Ngai, A.K. Rajagopal,* and R.W. Rendall,* *Electronic Structure and Properties of Hydrogen in Metals*, Plenum Press, New York, pp. 473-478
- Nonexponential Decay in Relaxation Phenomena**, by A.K. Rajagopal,* K.L. Ngai, R.W. Rendell, and S. Teitler, Symposium on Random Walks, in *Journal of Statistical Physics* 30:285-292
- Observation of a Structural Phase Transition in TbPO₄ Via Induced Infrared Activity**, by G.A. Prinz and J.F.L. Lewis, *Journal of Magnetism and Magnetic Materials* 39:285-289
- On the Electronic Structure of CeN and CeAl₂**, by W.E. Pickett and B.M. Klein, 16th Rare Earth Research Conference, in: *Journal of the Less-Common Metals* 93:219-225
- Optically and X-Ray Induced Paramagnetism in Amorphous Phosphorus**, by B.C. Shanabrook and P.C. Taylor, *Physical Review B* 28:1239-1243
- Pairs of Intrinsic Defects in III-V Semiconductors: Electronic States and Interaction Energies**, by T.L. Reinecke, Proceedings of the 16th International Conference on the Physics of Semiconductors in: *Physica* 117&118B+C:194-196
- Photoenhanced Oxidation of Gallium Arsenide**, by V.M. Bermudez, *Journal of Applied Physics* 54:6795-6798
- Photoluminescence and Photoluminescence Excitation Spectroscopy of the EL2 Emission Band in GaAs**, by B.V. Shanabrook, P.B. Klein, E.M. Swiggard, and S.G. Bishop, *Journal of Applied Physics* 54:336-340
- Photoluminescence Excitation Spectroscopy of Fe-Doped GaP**, by B.V. Shanabrook, P.B. Klein, and S.G. Bishop, Proceedings of the 16th International Conference on Defects in Semiconductors, in: *Physica* 116B+C:444-448
- Present and Projected Status of GaAs Materials Technology**, by E.M. Swiggard, Proceedings of the IEEE Gallium Arsenide Integrated Circuit Symposium - GaAsIC, IEEE, New York, pp. 26-29
- Pressure Effects in HfTe₅ and ZrTe₅**, by W.A. Fuller, S.A. Wolf, T.J. Wieting, R.C. La Coe,* P.M. Chaikin,* and C.Y. Huang,* *Journal de Physique Colloque C3* 44:C3-1709-C3-1712
- Pressure-Induced Disproportionation in CuBr**, by E.F. Skelton, S.B. Qadri,* A.W. Webb, R.G. Ingalls,* and J.M. Tranquada,* *Physics Letters* 94A:441-443
- Properties of a New Molybdenum Nitrogen Phase**, by W.W. Fuller, S.A. Wolf, D.U. Gubser, E.F. Skelton, and T.L. Francavilla, *Journal of Vacuum Science and Technology* A1:517-519
- Properties of Amorphous Silicon Produced by Ion Implantation: Thermal Annealing**, by W.G. Spitzer,* G.K. Hubler, and T.A. Kennedy, *Nuclear Instruments and Methods* 209/210:309-312
- Properties of Ferrimagnetic Echoes in Yttrium Iron Garnet Cylinders**, by F. Bucholtz and D.C. Webb, *Journal of Applied Physics* 54:5331-5338
- Raman Scattering in Highly Disordered Amorphous Phosphorus**, by R.J. Pomian,* J.S. Lannin,* and B.V. Shanabrook, *Physical Review B* 27:4887-4894
- Rigorous Channeling Stability Theorems**, by A.W. Saenz, *Physics Letters* 93A:337-340
- Self-Consistent Augmented-Plane-Wave Band-Structure Calculations of Si and Ge with Overlapping Spheres**, by D.A. Papaconstantopoulos, *Physical Review B* 27:2569-2572
- Shear Force Effects on Sidewall Penetration of Extended Dislocations in Phosphorus Implanted Emitters**, by W.F. Tseng and G.E. Davis, *Materials Research Society Symposium Proceedings* 14:389-394
- SiH and SiOH Electromodulation at Si-SiO₂ In-**

- interfaces in a Multiple Internal Reflectance Configuration, by A. Stella,* L. Miglio,* E.D. Palik, R.T. Holm, and H.L. Hughes, Proceedings of the 16th International Conference on the Physics of Semiconductors, in: *Physica* 117&118B+C-Part II:777-778
- Solid Phase Epitaxial Regrowth of Amorphous Silicon on Molecular Beam Epitaxial Silicon/Si Layers**, by A. Christou, B.R. Wilkins, and J.E. Davey, *Applied Physics Letters* 42:1021-1023
- Spin Dependent Formation and Decay of the Triplet Antisite Centre in GaP**, by N. Kiloran,* B.C. Cavenett,* M. Godlewski,* T.A. Kennedy, and N.D. Wilsey, Proceedings of the 12th International Conference on Defects in Semiconductors, in: *Physica* 113B+C:425-430
- Spin Dynamics of HoAl₂**, by J.J. Rhyne* and N.C. Koon, *Journal of Magnetism and Magnetic Materials* 31-34:608-610
- Spinwave Resonance in MBE Grown Iron Films**, by C. Vittoria, J.J. Krebs, and G.A. Prinz, *Journal of Magnetism and Magnetic Materials* 37:6111-6115
- Sputtering from Binary Alloys - A Technique for Evaluating Change in Surface Binding Energy**, by G.W. Reynolds,* R.G. Allas, J.M. Lambert,* and P.A. Treado,* 1982 IEEE Conference on the Application of Accelerators in Research and Industry, in *IEEE Transactions on Nuclear Science* NS-30:1749-1751
- Stable Tantalum Silicide Schottky Barrier or n-Type Gallium Arsenide Evaluated at Elevated Temperatures**, by W.F. Tseng and A. Christou, *Electronics Letters* 19:330-332
- Study of the Magnetic Superconductor, Y₉Co₇, at High Pressure and High Magnetic Field**, by C.Y. Huang,* C.E. Olsen,* W.W. Fuller, J. Huang,* and S.A. Wolf, *Solid State Communications* 45:795-797
- Study of Ion-Implantation Damage in GaAs:Be and InP:Be Using Raman Scattering**, by C.S. Rama Rao, S. Sundaram,* R.L. Schmidt, and J. Comas, *Journal of Applied Physics* 54:1808-1815
- The Effects of Methane in the Deposition of Superconducting Niobium Nitride Thin Film at Ambient Substrate Temperature**, by E.J. Cukauskas, *Journal of Applied Physics* 54:1013-1017
- The Effects of Transient Radiation on GaAs Schottky Diode FET Logic Circuits**, by E.R. Walton,* W.T. Anderson, R. Zucca,* and J.K. Nottoff,* 1983 Annual Conference on Nuclear and Space Radiation Effects, in *IEEE Transactions on Nuclear Science* NS-30:4178-4182
- Theoretical Studies of Dilute Hydrogen Impurities in Palladium**, by B.M. Klein and W.E. Pickett, *The Electronic Structure and Properties of Hydrogen in Metals*, Plenum Press, New York, pp. 277-282
- Theoretical Study of Native Defects in III-V Semiconductors**, by P.J. Lin-Chung and T.L. Reinecke, *Physical Review B* 27:1101-1114
- Theoretical Study of Optical Absorption in Hydrogenated Amorphous Silicon**, by W.E. Pickett, D.A. Papaconstantopoulos, and E.N. Economu,* *Physical Review B* 28:2232-2234
- Thermal Expansion and Magnetostriction of Mixed Valence and Kondo Systems**, by A.S. Edelstein and N.C. Koon, *Solid State Communications* 48:269-272
- Thermal Expansion and Zero-Point Displacement in Isotopic Lithium Hydride**, by A.R. Ruffa, *Physical Review B* 27:1321-1325
- Transient Luminescence, Transport and Photoconductivity in Chalcogenide Glasses**, by K.L. Ngai, *Polarons and Excitons*, Plenum Press, New York, pp. 210-245
- Transient Radiation Effects at X-Band in GaAs FETs**, by W.T. Anderson and S.C. Binari, 1983 Annual Conference on Nuclear & Space Radiation Effects, in: *IEEE Transactions on Nuclear Science* NS-30:4205-4208
- U.S. Navy Programme in Small Cryocoolers**, by M. Nisenhoff and E.A. Edelsack,* Second Biennial Conference on Refrigeration for Cryogenic Sensors and Electronic Systems, *Cryogenics* 23:357-366
- Vacuum Methods for Layer Deposition and Application to Device Structures**, by A. Christou, *Technology of Stratified Media*, SPIE, Bellingham, Washington, SPIE Vol. 387, pp. 80-88
- Work Function Measurements and Their Relation to Modern Surface Analysis Technique**, by G.A. Haas, R.E. Thomas, A. Shih, and C.R.K. Marrian, *Surface Imaging and Analysis with High Spatial Resolution in Ultramicroscopy* 11:199-206
- X-Ray Spectral Line Coincidences Between Fluorine K- and Transition Metal L-Series Lines**, by P.G. Burkhalter, G. Charatis,* and P.D. Rockett,* *Journal of Applied Physics* 54:6138-6149

SPACE SCIENCE AND TECHNOLOGY

- 31.4-GHz Flux Density Measurements of a Complete Sample of Sources from the 5-GHz S5 Survey**, by B.J. Geldzahler and H. Kuhr,* *Astronomical Journal* 88:1126-1132
- 3C395—A Quasar with Asymmetrical Radio Structure**, by K.J. Johnston, J.H. Spencer, A. Witzel,* and E.B. Fomalont,* *Astrophysical Journal* 265:L43-L47
- A Comparison of High-Energy Events in the Quiet Sun with Solar Flares**, by G.E. Brueckner, *Recent Advances in the Understanding of Solar Flares*, in *Solar Physics* 86:259-265
- A Quantitative Study of Magnetic Flux Transport on the Sun**, by N.R. Sheeley, J.P. Boris, T.R. Young, C.R. DeVore,* and K.L. Harvey,* *Solar and Magnetic Fields: Origins and Coronal Effects*, IAU Symposium No. 102, pp. 273-278
- A Survey of HEAO 1 of Clusters of Galaxies. III. The Complete Abell Catalog**, by M.W. Johnson,* R.G. Cruddace, M.P. Ulmer,* M.P. Kowalski,* and K.S. Wood, *Astrophysical Journal* 266:425-445
- Analysis and Numerical Simulation of the Effect of Ion Pederson Mobility on Ionospheric Barium Clouds**, by S.T. Zalesak, J.A. Fedder, and S.L. Ossakow, *Journal of Geophysical Research* 88:8003-8012
- Associations Between Coronal Mass Ejections and Soft X-ray Events**, by N.R. Sheeley, R.A. Howard, M.J. Koomen,* and D.J. Michels, *Astrophysical Journal* 272:249-254
- Atomic Oxygen Emissions Observed from Pioneer Venus**, by R.R. Meier, D.E. Anderson, and A.I.F. Stewart,* *Geophysical Research Letters* 10:214-217
- Chromospheric Jets; Possible Extreme-Ultraviolet Observations of Spicules**, by K.P. Dere, J.D.F. Bartoe, and G.E. Brueckner, *Astrophysical Journal* 267:L65-L68
- Circumstellar Envelope Structure of Late-Type Stars**, by P.F. Bowers,* K.J. Johnston, and J.H. Spencer, *Astrophysical Journal* 274:733-754
- Cosmic Ray Transport in the Atmosphere: Dose and LET-Distributions in Materials**, by C.H. Tsao, R. Silberberg, J.H. Adams, and J.R. Letaw,* *1983 Annual Conference on Nuclear and Space Radiation Effects*, in *IEEE Transactions on Nuclear Science* NS-30:4398-4404
- Determination of Atmospheric Composition and Temperature from the U.V. Airglow**, by R.R. Meier and D.E. Anderson, *Planetary and Space Sciences* 31:967-976
- Direct Measurements of the Gradual Extreme Ultraviolet Emission from Large Solar Flares**, by D.M. Horan, R.W. Kreplin, K.P. Dere, *Solar Physics* 85:303-312
- Dynamics and Spectroscopy of Asymmetrically Heated Coronal Loops**, by J.T. Mariska and J.P. Boris, *Astrophysical Journal* 267:409-420
- Extrapolation of Space-Simulation Beam-Plasma Investigations to Shuttle-Borne Applications**, by E.P. Szuszczewicz, *AIAA Journal* 21:1674-1678
- Far-Infrared and Submillimeter Observations of Stellar Radiative and Wind Heating in S140 IRS**, by P.R. Schwartz, H.A. Thronson, Jr.,* C.J. Lada,* H.A. Smith, W. Glacurim,* D.A. Harper,* and S.H. Knowles, *Astrophysical Journal* 271:625-631
- Far-Infrared Observations of the Type 1 Seyfert Galaxy NGC 4051**, by H.A. Smith, H.A. Thronson, Jr.,* D.A. Harper,* J. Smith,* C.J. Lada,* W. Glacurim,* and R.F. Loewenstein,* *Astrophysical Journal* 274:571-576
- Formation and Photochemistry of Methylamine in Jupiter's Atmosphere**, by J.A. Kaye and D.F. Strobel, *Icarus* 55:399-419
- Gamma Rays and Neutrinos as Complementary Probes in Astrophysics**, by M.M. Shapiro* and R. Silberberg, *Proceedings of the XVIII General Assembly of the IAU*, in *Space Science Reviews* 36:51-56
- H0323+022: A Puzzling High-Latitude X-Ray/Optical/Radio Source**, by R. Doxsey,* H. Bradt,* J. McClintock,* L. Petro,* R. Remillard,* G. Ricker,* D. Schwartz,* and K. Wood, *Astrophysical Journal* 264:243-247
- H0547-14: X-Ray Flux from a Weak Gamma-Ray Burst**, by C. Armbruster, K.S. Wood, J.F. Meikens, D.J. Yentis, H.W. Smathers, Jr., E.T. Byram, T.A. Chubb, and T.H. Friedman, *Astrophysical Journal* 269:779-790
- HCN Formation on Jupiter: The Coupled Photochemistry of Ammonia and Acetylene**, by J.A. Kaye and D.F. Strobel, *Icarus* 54:417-433
- High Density Gas Associated with "Molecular Jets": NGC 1333 and NGC 2071**, by P.R. Schwartz, J.A. Waak, and H.A. Smith, *Astrophysical Journal* 267:L109-L114
- High Resolution Telescope and Spectrograph**

- Observations of Solar Fin Structure in the 1600 Å Region**, by J.W. Cook, G.E. Brueckner, J.D.F. Bartoe, *Astrophysical Journal* 270:L89-L93
- High-Sensitivity Observations of HD 44179: The Red Rectangle**, by B.J. Geldzahler, N.L. Cohen,* *Publications of the Astronomical Society of the Pacific* 95:489-490
- Implications of the Ratio ($61 \leq Z \leq 75$)/($76 \leq Z \leq 83$) on the Origin and Propagation of the Ultra-Heavy Cosmic Rays**, by R. Silberberg, C.H. Tsao, J.H. Adams, and J.R. Letaw,* *Proceedings of the 18th International Cosmic Ray Conference, Vol. 2, p. 325*
- Intensity and Extinction Irregularities in the H₂ Emission from Orion**, by H.A. Smith, H.P. Larson,* M.A. Feierberg, and U. Fink, *Astronomical Journal* 88:469-475
- LET-Distributions and Radiation Doses Due to Cosmic Rays**, by R. Silberberg, C.H. Tsao, J.H. Adams, and J.R. Letaw,* *1983 Annual Conference on Nuclear and Space Radiation Effects*, in IEEE Transactions on Nuclear Science NS-30:4398-4404
- Limits to the Rate of Component Separation in Scorpius X-1**, by E.B. Fomalont,* B.J. Geldzahler, R.M. Hjellming,* and C.M. Wade,* *Astrophysical Journal* 275:802-807
- Lines of Fe XII Sensitive to Coronal Electron Density**, by U. Feldman, L. Cohen,* and G.A. Doschek, *Astrophysical Journal* 273:822-828
- Luminous Molecular Hydrogen Emission in the Galaxy System NGC 3690-IC 694**, by J. Fischer, M. Simon,* J. Benson,* and P.M. Solomon,* *Astrophysical Journal* 273:L27-L30
- Mass and Energy Balance in the 1973 August 9 Flare**, by K.P. Dere and J.W. Cook, *Astronomy and Astrophysics* 124:181-187
- Microwave Spectroscopy of H₂O in the Stratosphere and Mesosphere**, by P.R. Schwartz, C.L. Croskey,* R.M. Bevilacqua, and J.J. Olivero, *Nature* 305:294-295
- Models for Cosmic Ray Propagation at Energies $10^8 - 10^{14}$ eV**, by R. Silberberg, C.H. Tsao, M.M.* Shapiro, and J.R.* Letaw, *Proceedings of the 18th International Cosmic Ray Conference, Vol. 2, p. 179*
- Multiple Fluorescent Scattering of N₂ Ultra-violet Emissions in the Atmospheres of the Earth and Titan**, by R.R. Conway, *Journal of Geophysical Research* 88:4784-4792
- Numerical Simulations of Loops Heated to Solar Flare Temperatures: I. X-Ray and UV Spectroscopy**, by G.A. Doschek, C.C. Cheng, E.S. Oran, J.P. Boris, and J.T. Mariska, *Astrophysical Journal* 265:1103-1119
- Numerical Simulations of Solar Flare Temperatures. I. Gasdynamics**, by C.C. Cheng, E.S. Oran, G.A. Doschek, J.P. Boris, and J.T. Mariska, *Astrophysical Journal* 265:1090-1102
- †Observations of High-Energy Jets in the Corona Above the Quiet Sun, the Heating of the Corona, and the Acceleration of the Solar Wind**, by G.E. Brueckner, J.D.F. Bartoe, *Astrophysical Journal* 272:329-348
- On the N₂ Lyman-Birge-Hopfield Band Nightglow**, by R.R. Meier and R.R. Conway, *Journal of Geophysical Research* 88:4929-4934
- On the Unresolved Fine Structures of the Solar Atmosphere in the $3 \times 10^4 - 2 \times 10^5$ Temperature Region**, by U. Feldman, *Astrophysical Journal* 275:367-373
- Optical and Radio Structure of the Quasar PkS 0812+02**, by S. Wyckoff,* K. Johnston, F. Ghigo,* L. Rudnick,* P. Wehinger,* and A. Boksenberg,* *Astrophysical Journal* 265:43-50
- Phosphine Photochemistry in Saturn's Atmosphere**, by J.A. Kaye* and D.F. Strobel, *Geophysical Research Letters* 10:957-960
- Photochemistry of the Reducing Atmospheres of Jupiter, Saturn and Titan**, by D.F. Strobel, *International Reviews in Physical Chemistry* 3:145-176
- Propagation and Origin of Energetic Cosmic Rays, $10^{14} - 10^{19}$ eV**, by J.R. Letaw,* R. Silberberg, C.H. Tsao, and M.M. Shapiro,* *Proceedings of the 18th International Cosmic Ray Conference, Vol. 2, p. 283*
- Propagation of Cosmic Rays in the Atmosphere and Energy Deposition in Detectors**, by R. Silberberg, C.H. Tsao, J.H. Adams, J.R. Letaw,* *Proceedings of the 18th International Cosmic Ray Conference, Vol. 5, p. 380*
- Radiation Doses and Biological Effects of Cosmic Rays**, by R. Silberberg, C.H. Tsao, J.H. Adams, J.R. Letaw, *Proceedings of the 18th International Cosmic Ray Conference, Vol. 2, p. 398*
- Radiation Transport Effects on the OI 1356-Å Limb Intensity Profile in the Dayglow**, by D.J. Strickland* and D.E. Anderson, *Journal of Geophysical Research* 88:9260-9264
- Radio Frequency Observations of Galactic X-Ray Sources**, by B.J. Geldzahler, *Astrophysical Journal* 264:L49-L53
- Real-Time—In-Situ—Targeting of Geoplasma** 275

Domains for Purposes of Chemical Injection and Artificial Triggering of Equatorial Spread-F, by E.P. Szuszczewicz, D.W. Walker, J.C. Holmes, R.S. Narcisi,* J. Buchan,* B. Reinisch,* L. Kegley, and M. Swenney, *Active Experiments in Space*, ESA SP-195, pp. 265-269

Si III Line Ratios in the Sun, by P.L. Dufton,* A. Hibbert,* A.E. Kingston,* and G.A. Doschek, *Astrophysical Journal* 274:420-428

Solar Flare X-Ray Spectra from the P78-1 Spacecraft, by G.A. Doschek, *Recent Advances in the Understanding of Solar Flares*, in *Solar Physics* 86:49-58

Solar Radiometry: Spectral Irradiance Measurements, by G.E. Brueckner, *Advances in Space Research* 2:177-183

Solrad 11 Observations of the Far-Ultraviolet Background, by C.S. Weller, *Astrophysical Journal* 268:899-904

Superluminal Motion in the Quasar 3C 345, by S.C. Unwin,* M.H. Cohen,* T.J. Pearson,* G.A. Seielstad,* R.S. Simon, R.P. Linfield,* and R.C. Walker,* *Astrophysical Journal* 271:536-550

The Arc Second Radio Structure of 12 BL Lacertae Objects, by J.S. Ulvestad,* K.J. Johnston, and K.W. Weiler,* *Astrophysical Journal* 266:18-27

The Brighter 94 Micron Sources Observed by the Far-Infrared Sky Survey Experiment, by S.D. Price,* K. Shivanandan, T.L. Murdock, and P.F. Bowers, *Astrophysical Journal* 275:125-129

The Distribution of 6 Centimeter H₂CO in Orion Molecular Cloud 1, by K.J. Johnston, P. Palmer,* T.L. Wilson,* and J.H. Bieging, *Astrophysical Journal* 271:L89-L93

The Gas Density and Distribution Within 2 Parsecs of the Galactic Center, by R.L. Brown* and K.J. Johnston, *Astrophysical Journal* 268:L85-L88

The He D₃ as a Diagnostic for the Hard and Soft X-Rays from Solar Flares, by U. Feldman, M. Liggett,* H. Zirin,* *Astrophysical Journal* 271:832-846

The HI Content of Envelopes Around Evolved Stars, by G.R. Knapp* and P.F. Bowers, *Astrophysical Journal* 266:701-702

The S201 Far-Ultraviolet Imaging Survey I. Two Fields at High Galactic Latitude, by G.R. Carruthers and T. Page,* *Astrophysical Journal* 53:623-642

276 **The 1982 September Radio Outburst of Cygnus**

X-3: Evidence for Emission Expanding at $\geq 0.38c$, by B.J. Geldzahler, K.J. Johnston, J.H. Spencer, W.J. Klepczynski,* F.J. Jos-ties,* P.E. Angerhofer,* D.R. Florikowski,* D.D. McCarthy,* D.N. Matsakis,* and R.M. Hjellming,* *Astrophysical Journal (Letters)* 273:265-269

The Troposphere-Stratosphere Radiation Field at Twilight: A Spherical Model, by D.E. Anderson, *Planetary and Space Science* 31:1517-1523

The Variability of Single Event Upset Rates in the Natural Environment, by J.H. Adams, *1983 Annual Conference on Nuclear and Space Radiation Effects*, in *IEEE Transactions on Nuclear Science* NS-30:4475-4480

The Variation of Response with Registration Temperature in Solid State Nuclear Track Detectors and its Implications for Cosmic Ray Composition Studies, by J.H. Adams, A. Thompson,* D. O'Sullivan,* and L.P. Beahm, *Proceedings of the 18th International Cosmic Ray Conference*, Vol. 8, p. 127

Total and Partial Inelastic Cross Sections of Proton-Nucleus Reactions, by R. Silberberg, C.H. Tsao, and J.R. Letaw,* *Proceedings of the 18th International Cosmic Ray Conference*, Vol. 2, p. 194

Type I Noise Storms and the Structure of the Extreme Ultraviolet Corona, by G.E. Brueckner, *Solar Physics* 85:243-265

VLA Observations of the $^2\pi_{3/2}$ J = 3/2 OH Masers Associated with Orion A, by S.S. Hansen* and K.J. Johnston, *Astrophysical Journal* 267:625-629

VLA Positions of OH/IR Stars, by P.F. Bowers and T. deJong,* *Astronomical Journal* 88: 655-657

STRUCTURE RESEARCH

A New Role for L-Ascorbic Acid: Michael Donor to α , β -Unsaturated Carbonyl Compounds, by G. Fodor,* R. Arnold,* T. Mohocsi,* I. Karle, and J. Flippen-Anderson, *Tetrahedron* 39:2137-2145

A Simple Rule for Finding and Distinguishing Triplet Phase Invariants with Values near 0 or π with Isomorphous Replacement Data, by J. Karle, *Acta Crystallographica* A39:800-805

Cooperative Programming in Crystallography, by R.A. Alden, G. Bricogne,* S.T. Freer,* S.R. Hall,* W.A. Henderson, P.B. Machin,*

- R.J. Nunn,* A.J. Olson,* G.N. Reike,* S. Sheriff, J.M. Stewart,* J. Sygusib,* L. Ten Eyck,* and K.D. Watenpugh,* *Computers and Chemistry* 7:137-148
- † **Crystal Structure of 2-Bromo-2-Nitroadamantane (I) $C_{10}H_{14}BrNO_2$, and 2,2-Dinitroadamantane (II) $C_{10}H_{14}N_2O_4$** , by C. George and R. Gilardi, *Acta Crystallographica* C39:1674-1676
- Crystal Structure of Leucine-Enkephalin**, by A. Camerman,* D. Mastropaolo,* I. Karle, J. Karle, and N. Camerman,* *Nature* 306:447-450
- Crystal Structures, Molecular Conformations, Infrared Spectra and ^{13}C NMR Spectra of Methylproline Peptides in the Solid State**, by J.L. Flippen-Anderson, R. Gilardi, I.L. Karle, M.H. Frey,* S.J. Opella,* L.M. Gierash,* M. Goodman,* V. Madison,* and N.G. Delaney,* *Journal of the American Chemical Society* 105:6609-6614
- Diffraction Evidence for Distorted Graphite-Like Ribbons in an Activated Carbon of Very Large Surface Area**, by J.H. Konnert and P. D'Antonio, *Carbon* 21:193-196
- Estimation of Protein Secondary Structure from the Laser Raman Amide I Spectrum**, by R.W. Williams, *Journal of Molecular Biology* 166:581-603
- Hierarchical Symmetry in Annelid Hemoglobins**, by W.A. Hendrickson, in *Invertebrate Oxygen Binding Proteins*, Harwood Academic Publishers, London, Life Chemistry Reports, Suppl. 1, pp. 167-185
- Isolation and Identification of Novel Lactones from Male Mexican Fruit Flies**, by J.B. Stokes,* E.C. Uekel,* J.D. Warthen,* M. Jacobson,* J.L. Flippen-Anderson, R. Gilardi, L.M. Spishakoff,* and K. Wilgar,* *Journal of Agricultural and Food Chemistry* 31:1162-1167
- Lawrence Olin Brockway**, by J. Karle and L.S. Bartell,* in *Crystallography in North America*, American Crystallographic Assoc., New York, pp. 116-119
- Multiple-Scattering Effects in EXAFS Spectroscopy of Oxygen-Bridged Iron Complexes. Possibility of Angle Determination by EXAFS Analysis**, by M.S. Co,* W.A. Hendrickson, K.O. Hodgson,* and S. Doniach,* *Journal of the American Chemical Society* 105:1144-1150
- Purification of Synthetic Warburganal Intermediates by Open Column and High Performance Liquid Chromatography**, by J.D. Warthen,* R.M. Waters,* J.L. Flippen-Anderson, and R. Gilardi, *Chromatographia* 17:623
- Recollections and Reflections**, by I.L. Karle and J. Karle, in *Crystallography in North America*, American Crystallographic Assoc., New York, pp. 277-283
- Structure of the Active Center of Hemerythrins**, by S. Sheriff, W.A. Hendrickson, and J.L. Smith, in *Invertebrate Oxygen Binding Proteins*, Howard Academic Publishers, London, Life Chemistry Reports, Suppl. 1, pp. 305-308
- Structure of Trimeric Haemerythrin**, by J.L. Smith, W.A. Hendrickson, and A.W. Addison,* *Nature* 303:86-88
- Tetramethoprim and Pentamethoprim Synthesis, Antibacterial Properties and X-Ray Structures**, A. Brossi, P.N. Sharma, K. Takahashi, J.F. Chiang, I. Karle, and G. Seibert, *Helvetica Chimica Acta* 66:795-800
- The Molecular Structure of Mesitylene as Determined by Electron Diffraction**, by A. Almenningen,* I. Hargittai,* S. Samdal,* J. Brunvoll,* A. Domenicano,* and A. Lowrey, *Journal of Molecular Structure* 96:373-377
- The Structure of Trisdiphenylthiophosphinoyl Methanide, A Mesomerically Stabilized Carbanion**, by S.O. Grim,* R.D. Gilardi, and S.A. Sangokoya,* *Angewandte Chemie, International Edition in English* 22:254-255
- [Leu⁵]Enkephalin Four Cocrystallizing Conformers with Extended Backbones that Form an Antiparallel β -Sheet**, by I.L. Karle, J. Karle, D. Mastropaolo,* A. Camerman,* and N. Camerman,* *Acta Crystallographica* 339:625-637

FORMAL REPORTS

ACOUSTICS

- 8677 **Low-Frequency Acoustic Source Levels of Large Merchant Ships**, by E.B. Wright and J. Cybulski
- 8685 **Three-Dimensional Parabolic-Equation-Based Estimation of the Ocean Acoustic Field**, by J.S. Perkins, R.N. Baer, L.F. Roche,* and L.B. Palmer*
- 8695 **Transverse Horizontal Coherence and Low-Frequency Array Gain Limits in the Deep Ocean**, by L.B. Palmer, D.M. Dundore, B.B. Adams, and J.J. McCoy
- 8729 **Performance Characteristics of Passive Coherence Estimators**, by A.A. Gerlach
- 8730 **Ray Theory vs the Parabolic Equation in a Long-Range Ducted Environment**, by A. Tolstoy, E.R. Franchi, and K.R. Nicolas
- 8741 **Optimum Depth of Propagation in Shallow Water**, by D.A. Gershfeld and F. Ingenito

ARTIFICIAL INTELLIGENCE

- 8768 **Responding to a Call for Fire**, by H. Hamburger and J.R. Slagle
- 8769 **Decision Support System for Fire Support Command and Control**, by J.R. Slagle, M.W. Gaynor,* and H. Hamburger*

ATMOSPHERIC SCIENCES

- 8703 **Measurements of Atmospheric Aerosols: Experimental Methods and Results of Measurements off the East Coast of the United States**, by W.A. Hoppel, J.W. Fitzgerald, and R.E. Larson
- 8738 **A New Data Base of Supercooled Cloud Variables for Altitudes up to 10,000 Feet AGL and the Implications for Low Altitude Aircraft Icing**, by R.K. Jeck
- 8746 **Computer-Model Results for the Beach-Escarpment-Induced Distortion of On-Shore Wind Flow at the Northwest Point of San Nicholas Island, California**, by J.L. Walmsley* and T.V. Blanc

BIOSCIENCES

- 8688 **Exposure of Creosote-Naive and Creosote-Conditioned *Limnoria tripunctata* (Menzies) to Untreated and Creosote-Treated Wood**, by K.K. Parrish, W.R. Barger, and J.D. Bultman
- 8759 **Use of Fraunhofer Lines to Detect Remotely Bioluminescence in Daylight**, by R.V. Lynch, W.R. Hemphill, and A.F. Theisen*
- 8772 **Stimulation of Bioluminescence in Dinoflagellates by Controlled Pressure Changes**, by T.Q. Donaldson, S.P. Tucker,* and R.V. Lynch

CHEMISTRY

- 8656 **Submarine Hull Insulation Fire Test I—1 June 1981**, by J.I. Alexander, H.W. Carhart, H.G. Eaton, S. Kaska, C.R. Kaplan, S.R. Lustig, R. Matuszko, R.S. Sheinson, J.P. Stone, T.T. Street, P.A. Tatem, T.M. White, F.W. Williams, and H.J. St. Aubin
- 8662 **Submarine Hull Insulation Fire Test II—1 July 1981**, by J.I. Alexander, D.J. Bogan, H.W. Carhart, H.G. Eaton, C.R. Kaplan, S. Kaska, S.R. Lustig, R. Matuszko, R.S. Sheinson, J.P. Stone, T.T. Street, P.A. Tatem, T.M. White, F.W. Williams, and H.J. St. Aubin
- 8672 **Submarine Hull Insulation Fire Test III—17 September 1981**, by J.I. Alexander, D.J. Bogan, H.W. Carhart, H.G. Eaton, C.R. Kaplan, R.S. Sheinson, J.P. Stone, T.T. Street, P.A. Tatem, T.M. White, F.W. Williams, and H.J. St. Aubin
- 8673 **Fuel Sediment Analysis by ESCA**, by M. Wechter and R.N. Hazlett
- 8692 **A Statistical Examination of the Effect of Composition on the Freezing Points of Hydrocarbon Mixtures**, by W.A. Affens, R.N. Hazlett, and D.E. Smith*
- †8727 **Submarine Hull Insulation Fire Test IV—7 December 1981**, by J.I. Alexander, D.J. Bogan, H.W. Carhart, H.G. Eaton, C.R. Kaplan, R.S. Sheinson, T.T. Street, P.A. Tatem, and F.W. Williams

- 8779 **High-Temperature Deuterated Lubricants: Additives, Mechanisms, and Methods**, by J.E. Campana

COMMUNICATIONS

- +8637 **Preliminary System Concept for an HF Intra-Task Force Communication Network**, by J.W. Wieselthier, D.J. Baker, A. Ephremides, and D.N. McGregor
- 8676 **Controlled Test Procedures for Using Intervocalic Consonants to Assess Speech Intelligibility: A Feasibility Study**, by A. Schmidt-Nielsen
- 8686 **A Wideband HF Receiving Subsystem**, by J.B. Wood
- 8701 **Performance of Alternative Adaptive Interference Canceler Configurations in a Shipboard Environment**, by A.S. Eley
- 8704 **Which is the Better Entropy Expression for Speech Processing: $-S \log S$ or $\log S$** , by J.E. Shore
- 8710 **Adaptive Feedforward Linear Wideband HF Power Bank**, by D.C. Andrews, E.E. Barr, T.E. Oliver,* and B.S. Abrams*
- 8716 **800-b/s LPC Rate Converter**, by L.J. Fransen
- 8748 **Noun Phrase Compression in Navy Messages**, by C.L. Heitmeyer

COMPUTER SCIENCE

- 8667 **Algorithms for Single-Signal and Multisignal Minimum-Cross-Entropy Spectrum Analysis**, by R.W. Johnson
- 8679 **A Methodology for Collecting Valid Software Engineering Data**, by V.R. Basili* and D.M. Weiss
- 8734 **Interface Specifications for the SCR(A-7E) Application Data Type Module**, by P.C. Clements, S.R. Faulk, and D.L. Parnas
- 8755 **Automated Acceptance Test Procedures for Wideband Microwave Synthesized Signal Generator Testing**, by J.J. O'Neill and T.H. Gattis
- 8780 **Accuracy of Software Development Activity Data: The Software Cost Reduction Project**, by L.J. Chmura and A.F. Norcio*
- 8705 **A FORTRAN Subroutine to Evaluate Spherical Bessel Functions of the First, Second, and Third Kinds for Complex Arguments**, by J.P. Mason

MATHEMATICS

- 8417 **A General Model for the Contact Correlation Problem**, by I.R. Goodman
- 8687 **Cylindrical Bessel Functions for a Large Range of Complex Arguments**, by J.P. Mason
- 8707 **On a Relation Between Maximum-Likelihood Classification and Minimum-Cross-Entropy Classification**, by J.E. Shore
- 8731 **Multisignal Minimum-Cross-Entropy Spectrum Analysis with Weighted Priors**, by R.W. Johnson and J.E. Shore

METALLURGY

- 8646 **Laser Welding of Mild Steel at NIROP**, Minneapolis, by E.A. Metzbowser

OCEAN SCIENCE AND TECHNOLOGY

- 8659 **Plans for a Remote Sensing Experiment in the Nantucket Shoals (SEBEX) (December 1, 1980)**, by G.R. Valenzuela and D.T. Chen

RADAR

- 8492 **Coupled Amplifier Module Feed Networks for Phased Array Antennas**, by R.A. Steinberg
- 8658 **Bicollimated Near-Field Gregorian Reflector Antenna**, by J.B.L. Rao
- 8661 **A Two-Priority Frame-Synchronization Algorithm**, by J.O. Coleman
- 8669 **A New Technique for Reducing Radar Response to Signals Entering Antenna Sidelobes**, by B.L. Lewis and J.B. Evins
- 8671 **Parametric Study of a Nonsuppressing CFAR Detector**, by J.D. Wilson
- 8678 **Invariant Clustering Using Scattering Matrices**, by G.V. Trunk
- 8681 **Parameter Estimation and Target Detection in a Distributed-Clutter Environment**, by F.C. Lin, B.L. Lewis, and F.F. Kretschmer
- 8693 **Doppler Processing of Radar Clutter Echoes with Limited Range Extents**, by B. Cantrell

- 8694 **Aperture Efficiency Considerations in the Convolution Synthesis of Symmetrical Hexagonal Arrays**, by J.P. Shelton and S.R. Laxpati*
- 8698 **Survey of Radar ADT**, by G.V. Trunk
- 8700 **A Matched Filter Doppler Processor for Airborne Radar**, by H.A. Andrews and S.L. Sheller
- 8709 **Microcomputer Aided Tracking (MCAT)**, by A.B. Mays, D.C. Cross, and J.L. Walters
- 8713 **Performance Analysis of a Three-Dimensional Microwave Lens in a Cylindrical Array Scanning Application**, by H.P. Coleman and J.P. Shelton
- 8728 **Range Resolution of Targets**, by G.V. Trunk
- 8740 **A FORTRAN Computer Program to Compute the Radiation Pattern of an Array-Fed Paraboloid Reflector**, by J.K. Hsiao
- 8744 **A New Derivation for the Rough Surface Reflection Coefficient and for the Distribution of Sea Wave Elevations**, by A.R. Miller, R.M. Brown, and E. Vegh

RADIATION

- 8761 **Dependence of Thermoluminescence Output on Temperature During Irradiation for Several Thermoluminescence Phosphors**, by K.J. King and T.L. Johnson

SPACE SCIENCE AND TECHNOLOGY

- 8653 **The Solar Spectrum 3069 Å-2095 Å From the Echelle Spectrograph Flown in 1961 and 1964. An Extension of Rowland's Preliminary Table of Solar Spectrum Wavelengths**, by C.E. Moore, R. Tousey, and C.M. Brown
- †8675 **Actuator-Placement Considerations for the Control of Large Space Structures**, by R.E. Lindberg
- 8778 **Frequency Stability Analysis of GPS NAVSTARs 3 and 4 Rubidium Clocks and the NAVSTARs 5 and 6 Cesium Clocks**, by T.B. McCaskill, J.A. Buisson, and S.B. Stebbins

PATENTS

- 4,356,296—**Fluorinated Diacrylic Esters and Polymers Therefrom**, October 26 to James R. Griffith and Jacques G. O'Rear
- 4,357,180—**Annealing of Ion-Implanted GaAs and InP Semiconductors**, November 2 to Bela Molnar
- 4,357,608—**Scanning Radar System**, November 2 to Bernard L. Lewis
- 4,359,411—**Flexible Semiconductive Polymers**, November 16 to Oh-Kil Kim and Robert B. Fox
- 4,359,735—**Multi-Sampling-Channel Pulse Compressor**, November 16 to Bernard L. Lewis and Frank F. Kretschmer, Jr.
- 4,359,736—**Frequency-Phase Coding Device**, November 16 to Bernard L. Lewis
- 4,359,738—**Clutter and Multipath Suppressing Sidelobe Canceller Antenna System**, No-

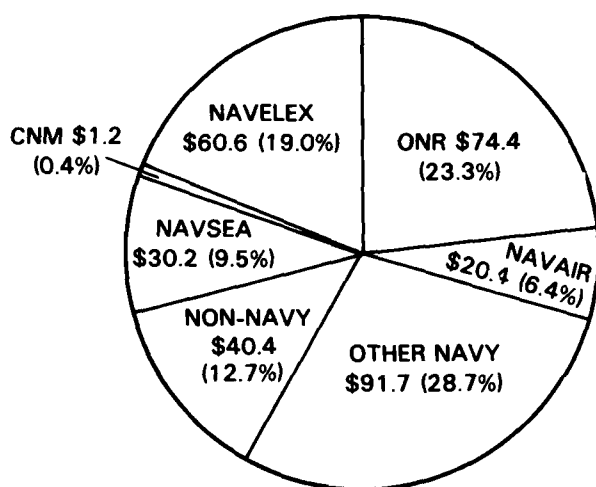
- vember 16 to Bernard L. Lewis
- 4,360,182—**High-Agility Reflector Support and Drive System**, November 23 to James W. Titus
- 4,360,924—**Laser Bottlenecking Technique**, November 23 to J. Gary Eden
- 4,361,879—**Ferrofluid Transducer**, November 30 to Peter S. Dubbelday and Robert W. Timme
- 4,362,932—**Wide Band Data Processing Technique**, December 7 to Bernard L. Lewis
- 4,362,968—**Slow-Wave Wideband Cyclotron Amplifier**, December 7 to Kwo R. Chu, Philip A. Sprangle, and Victor L. Granatstein
- 4,363,114—**Low Noise Remote Optical Fiber Sound Detector**, December 7 to Joseph A. Bucaro, James H. Cole, and Henry D. Dardy
- 4,364,048—**Interleaved Sweep Radar Display for Improved Target Detection**, December 14 to

- William M. Waters, and George J. Linde
 4,368,479—**Silicon Barrier Josephson Junction Configuration**, January 11 to Kenneth L. Davis
 4,368,987—**Conjugate-Phase, Remote-Clock Synchronizer**, January 18 to William M. Waters
 4,370,621—**High Efficiency Gyrotron Oscillator and Amplifier**, January 25 to Phillip A. Sprangle, Robert A. Smith, and Kwo R. Chu
 4,371,809—**Integral-Shadow-Grid Controlled-Porosity Dispenser Cathode**, February 1 to Richard E. Thomas, George A. Hass, and Richard F. Greene
 4,371,838—**Optical Fiber Waveguide for Measuring Magnetic Fields**, February 1 to David L. Griscom
 4,371,874—**Chaff Dipole Elements and Method of Packaging**, February 1 to Richard L. Bloom
 4,372,642—**Multiple Thin Film Adsorption of Reflected Substrate Modes in Waveguide System**, February 8 to Arnold H. Singer and Ronald T. Holm
 4,373,190—**Efficient, Precompression, Bandwidth-Tolerant Digital Pulse Expander-Compressor**, February 8 to Bernard L. Lewis and Frank K. Kretschmer
 4,374,048—**Electrically Conductive Polymeric Compositions**, February 15 to Oh-Kil Kim and Robert B. Fox
 4,374,665—**Magnetostrictive Devices**, February 22 to Norman C. Koon
 4,374,781—**Alkylated Phosphazene Oligomers and Method of Preparation**, February 22 to Harry H. Allock and Paul J. Harris
 4,375,334—**Nephelometer**, March 1 to Hermann E. Gerber
 4,375,372—**Use of Cubic Rare Earth-Iron Laves Phase Intermetallic Compounds as Magnetostrictive Transducer Materials**, March 1 to Norman C. Koon, and Albert I. Schindler
 4,375,429—**Photodichroic Crystals**, March 1 to Irwin Schneider, William C. Collins, Oscar Imber, and Philipp H. Klein
 4,376,248—**Fiber Optical Magnetic Field Sensor Using Magnetostrictive Material**, March 8 to Thomas G. Giallorenzi and George H. Sigel
 4,376,917—**Solid-State Cyclotron Maser**, March 15 to Achintya K. Ganguly, Kenneth L. Davis, and Kwo R. Chu
 4,378,497—**Optical Fiber Magnetic Field Sensor with Thermal and Acoustic Isolation**, March 29 to Thomas G. Giallorenzi
 4,379,295—**Low Sidelobe Pulse Compressor**, April 5 to Bernard L. Lewis and Frank F. Kretschmer
 4,379,979—**Controlled Porosity Sheet for Thermionic Dispenser Cathode and Method of Manufacture**, April 12 to Richard E. Thomas and Richard F. Greene
 4,379,994—**Feed-Forward Amplifier**, April 12 to Ronald M. Bauman
 4,381,148—**Power Meter For High Energy Lasers**, April 26 to Peter B. Ulrich, Gary I. Trusty, and Daniel H. Leslie
 4,384,291—**Efficient Low-Sidelobe Pulse Compression**, May 17 to Bernard L. Lewis and Frank F. Kretschmer, Jr.
 4,387,010—**Method of Separating ^{15}N from Natural Abundance NO** , June 7 to Jimmie R. McDonald and Andrew P. Baronavski
 4,387,353—**Active Waveguide Coupler for Surface Acoustic Waves**, June 7 to Thomas G. Giallorenzi and Joseph F. Weller
 4,389,590—**System for Vectoring Waveforms Using Spatial Dispersion**, June 21 to Robert R. Whitlock
 4,389,618—**Adaptive Feed-Forward System**, June 21 to Ronald M. Bauman
 4,390,881—**Real-Data Digital-Real-Weight Canceller**, June 28 to Bernard L. Lewis and Frank F. Kretschmer, Jr.
 4,394,624—**Channelized Feed-Forward System**, July 19 to Ronald M. Bauman
 4,395,095—**Optical System for Infrared Tracking**, July 26 to Richard F. Horton
 4,396,867—**Inductive Intense Beam Source**, August 2 to Peter J. Turchi and Ihor M. Vitkovitsky
 4,399,011—**Separation of Hydrogen Isotopes**, August 16 to David S. Y. Hsu and Thomas J. Manuccia, Jr.
 4,402,770—**Hard Magnetic Alloys of a Transition Metal and Lanthanide**, September 6 to Norman C. Koon
 4,404,562—**Low Sidelobe Linear FM Chirp**, September 13 to Frank F. Kretschmer, Jr. and Bernard L. Lewis
 4,405,198—**Extended Fiber Optic Sensor Using Birefringent Fibers**, September 20 to Henry F. Taylor
 4,405,237—**Coherent Anti-Stokes Raman Device**, September 20 to Thomas J. Manuccia and John F. Reintjes
 4,406,763—**Separation of Carbon Isotopes**, September 27 to David S. Y. Hsu and Thomas J. Manuccia

NRL FUNDING PROFILE

SOURCES OF R&D FUNDS (IN MILLIONS)

**FY 1983
ACTUAL \$318.9**



ONR - OFFICE OF NAVAL RESEARCH
 NAVEX - NAVAL ELECTRONIC SYSTEMS COMMAND
 NAVSEAS - NAVAL SEA SYSTEMS COMMAND
 CNM - CHIEF OF NAVAL MATERIAL
 NAVAIR - NAVAL AIR SYSTEMS COMMAND

R&D FUNDS BY TYPE (IN MILLIONS)

TYPE OR PURPOSE OF FUNDS	FY 83	
	ACTUAL	PERCENT
6.1 RESEARCH	\$ 64.1	20.1
6.2 EXPLORATORY DEVELOPMENT	63.3	19.9
6.3 ADVANCED DEVELOPMENT	17.5	5.5
6.4 ENGINEERING DEVELOPMENT	27.1	8.5
6.5 MANAGEMENT & SUPPORT	7.2	2.3
6.6 OPERATIONAL SYSTEMS DEVEL.	78.6	24.6
SUBTOTAL	257.8	80.9
OTHER PROCUREMENT, NAVY	8.3	2.6
OPERATIONS & MAINTENANCE, NAVY	8.7	2.7
OTHER	44.1	13.8
TOTAL	318.9	100.0

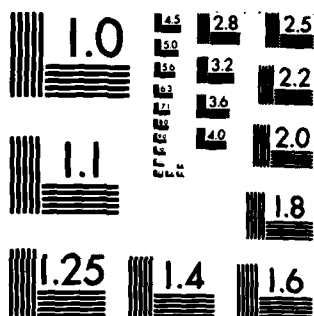
AD-A150 650 NAVAL RESEARCH LABORATORY 1983 REVIEW(U) NAVAL RESEARCH 4/4
LAB WASHINGTON DC 1983

UNCLASSIFIED

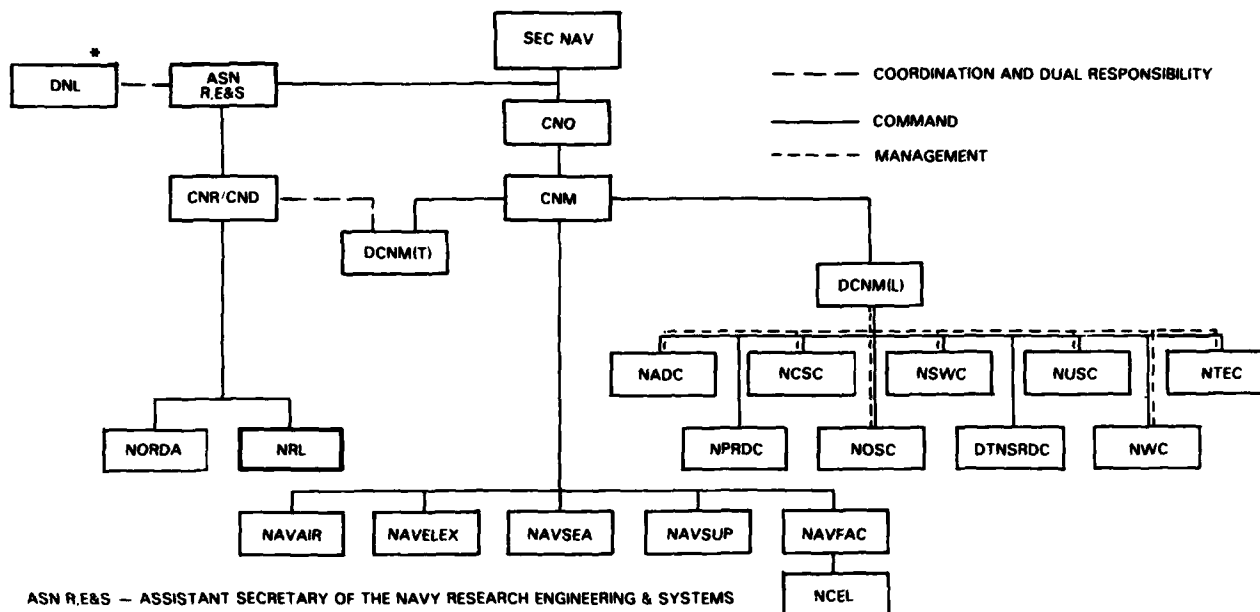
F/G 5/1

NL

END
FILMED
DTIC



MICROCOPY RESOLUTION TEST CHART
NATIONAL BUREAU OF STANDARDS-1963-A



ASN R.E.S. — ASSISTANT SECRETARY OF THE NAVY RESEARCH ENGINEERING & SYSTEMS

DNL — DIRECTOR OF NAVY LABORATORIES

CNR/CND — CHIEF OF NAVAL RESEARCH/CHIEF OF NAVAL DEVELOPMENT

DCNM(T) — DEPUTY CHIEF OF NAVAL MATERIAL (TECHNOLOGY)

NORDA — NAVY OCEAN RESEARCH & DEVELOPMENT ACTIVITY

DCNM(L) — DEPUTY CHIEF OF NAVAL MATERIAL (LABORATORIES)

NADC — NAVAL AIR DEVELOPMENT CENTER

NCSC — NAVAL COASTAL SYSTEMS CENTER

NSWC — NAVAL SURFACE WEAPONS CENTER

NUSC — NAVAL UNDERWATER SYSTEMS CENTER

NPRDC — NAVY PERSONNEL RESEARCH & DEVELOPMENT CENTER

NOSC — NAVAL OCEAN SYSTEMS CENTER

DTNSRDC — DAVID TAYLOR NAVAL SHIP RESEARCH & DEVELOPMENT CENTER

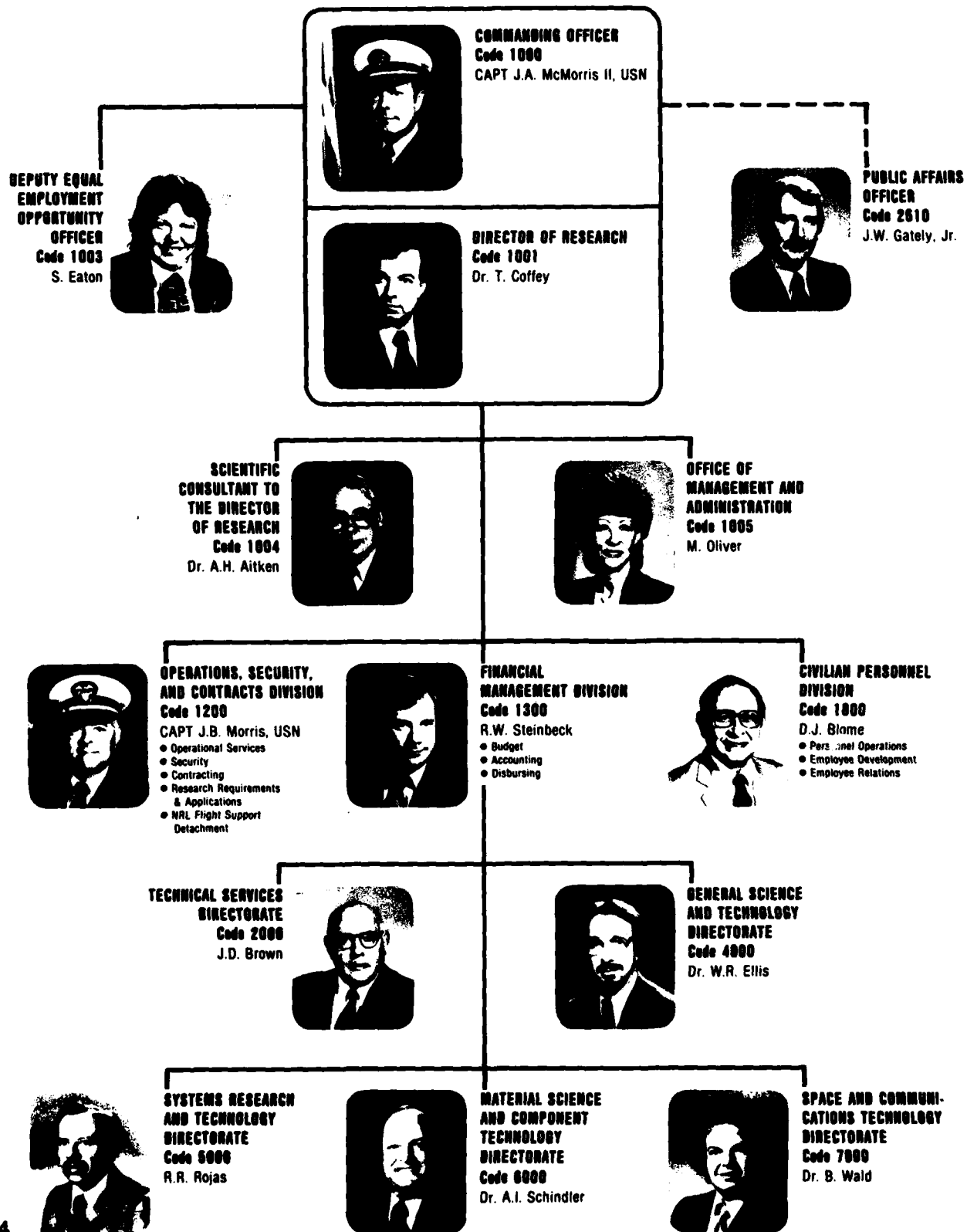
NWC — NAVAL WEAPONS CENTER

NTEC — NAVAL TRAINING EQUIPMENT CENTER

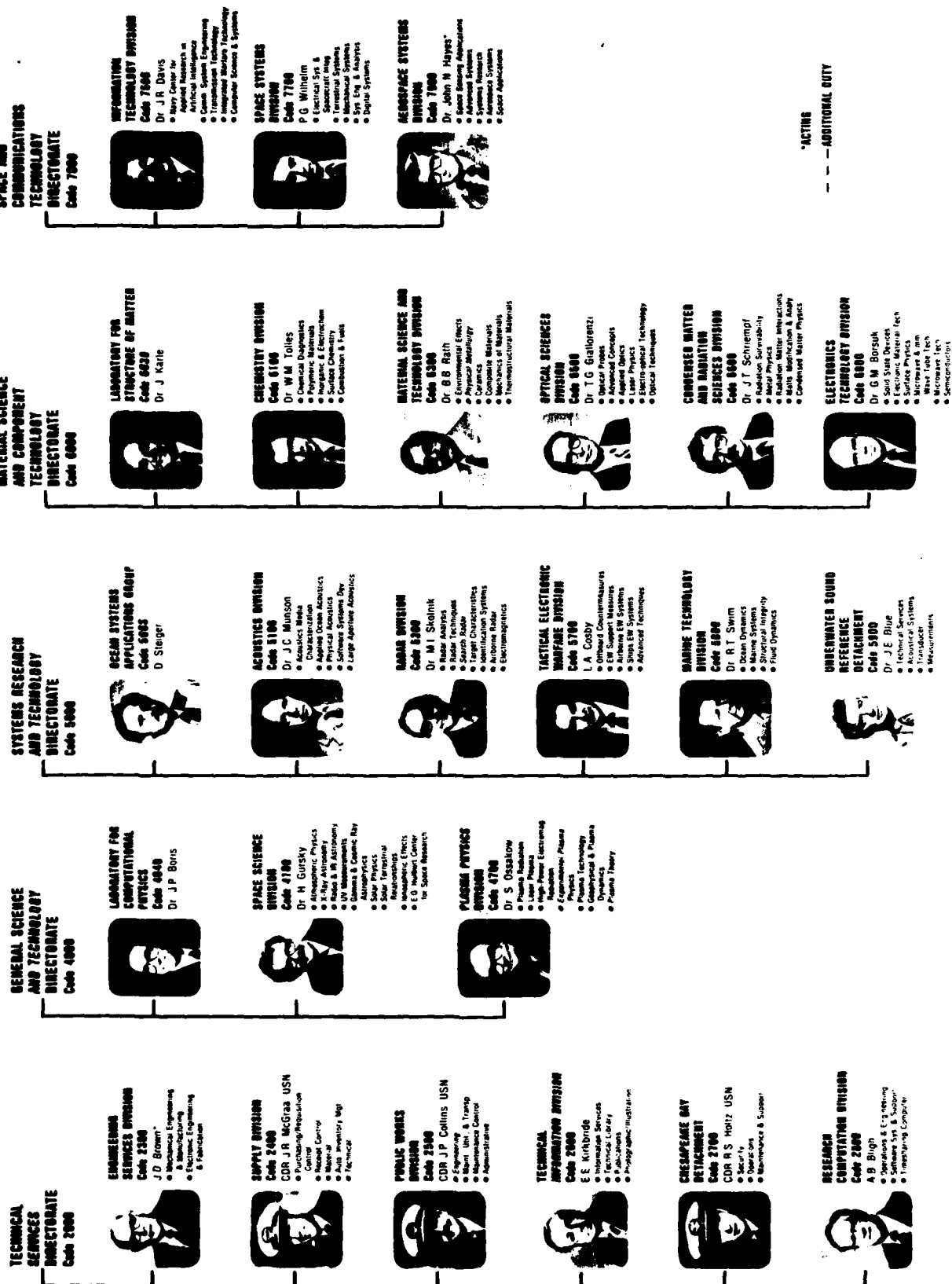
NCEL — NAVAL CIVIL ENGINEERING LABORATORY

* also serves as DCNM(L)

ORGANIZATIONAL CHART DECEMBER 1983



ORGANIZATIONAL CHART (Continued)



*ACTIVE
-- -- ADDITIONAL DUTY

Code	Office	Key Personnel	Extension*
------	--------	---------------	------------

EXECUTIVE DIRECTORATE

1000	Commanding Officer	CAPT J.A. McMorris II, USN	73403
1001	Director of Research	Dr. T. Coffey	73301
1003	DEEO Officer	Ms. S.A. Eaton	72486
1004	Scientific Consultant to the Dir. of Res.	Dr. A.H. Aitken	73724
1005	Head, Office of Management and Admin.	Ms. M. Oliver	73086
2610	Public Affairs Officer	Mr. J.W. Gately, Jr.	72541
1200	Chief Staff Officer	CAPT J.B. Morris, USN	73621
1220	Head, Security Branch	Mr. M.B. Ferguson	73048
1300	Comptroller	Mr. R.W. Steinbeck	73405
1800	Head, Civ. Pers. Div.	Mr. D.J. Blome	73421
1810	Personnel Operations	Mr. D.J. Blome	73421

TECHNICAL SERVICES DIRECTORATE

2000	Assoc. Dir. Res. for Tech. Services	Mr. J.D. Brown	72879
2004	Patent Counsel	Dr. W.T. Ellis	73428
2010	Safety Officer	Mr. H.C. Kennedy, Jr.	72249
2020	Head, Administrative Services Office	Mrs. L.V. Dabney	73858
2300	Engineering Services Officer	Mr. J.D. Brown**†	72879
2400	Supply Officer	CDR J.R. McGraa	73446
2500	Public Works Officer	CDR J.P. Collins, USN	73371
2600	Head, Tech. Info. Div.	Mr. E.E. Kirkbride	73388
2700	Chesapeake Bay Detachment Officer	CDR R.S. Holtz, USN	301-257-4002
2800	Head, Research Computation Division	Mr. A.B. Bligh	72751

GENERAL SCIENCE AND TECHNOLOGY DIRECTORATE

4000	Assoc. Dir. Res. for General Sci. & Tech.	Dr. W.R. Ellis	73324
4040	Head, Lab. for Computational Physics	Dr. J.P. Boris	73055
4100	Supt., Space Science Div.	Dr. H. Gursky	76343
4700	Supt., Plasma Physics Div.	Dr. S. Ossakow	72723

SYSTEMS RESEARCH AND TECHNOLOGY DIRECTORATE

5000	Assoc. Dir. Res. for Systems Res. & Tech.	Mr. R.R. Rojas	73294
5100	Supt., Acoustics Div.	Dr. J.C. Munson	73482
5300	Supt., Radar Div.	Dr. M.I. Skolnik	72936
5700	Supt., Tactical Elec. Warfare Div.	Mr. L.A. Cosby	76278
5800	Supt., Marine Technology Div.	Dr. R.T. Swim	73314
5900	Supt., Underwater Sound Reference Det.	Dr. J.E. Blue	305-859-5120

MATERIAL SCIENCE AND COMPONENT TECHNOLOGY DIRECTORATE

6000	Assoc. Dir. Res. for Material Science & Component Tech.	Dr. A.I. Schindler	73566
6030	Head, Lab. for Structure of Matter	Dr. J. Karle	72665
6070	Head, Health Physics Staff	Mr. J.N. Stone	72232
6100	Supt., Chemistry Div.	Dr. W.M. Tolles	73026
6300	Supt., Mat. Sci. & Tech. Div.	Dr. B.B. Rath	72926
6500	Supt., Optical Sciences Div.	Dr. T.G. Giallorenzi	73171
6600	Supt., Condensed Matter & Radiation Sciences Div.	Dr. J.T. Schriempf	72931
6800	Supt., Electronics Tech. Div.	Dr. G.M. Borsuk	73525

SPACE AND COMMUNICATIONS TECHNOLOGY DIRECTORATE

7000	Assoc. Dir. Res. for Space & Comm. Tech.	Dr. B. Wald	72964
7500	Supt., Information Technology Div.	Dr. J.R. Davis	72903
7700	Supt., Space Systems Div.	Mr. P.G. Wilhelm	76547
7900	Supt., Aerospace Systems Div.	Dr. V.E. Noble	73468

*Direct-in-Dialing (202) 76-; AUTOVON 29-

**Acting

†Additional duty

NRL REVIEW STAFF

The *NRL Review* is a result of the collaboration of the scientific, engineering, and support staff with the Technical Information Division (TID). In addition to the scientists and engineers who provided material for the *Review*, the following have also contributed to its publication.

Senior Science Editor: Jack Kaiser

Associate Science Editors: Mark Herbst, *General Science and Technology*
Felix Rosenthal, *Systems Research and Technology*
Richard Nekritz, *Material Science and Component Technology*
Paul Crepeau, *Space and Communications Technology*

Senior TID Editor: Kathleen Parrish

Head, Technical Information Division: Earle E. Kirkbride

Covers and color page design: T. Phillips

Chapter title pages: B. Zevgolts, T. Phillips

Mission page: T. Phillips, B. Zevgolts

Dedication page: R. Baturin, B. Zevgolts

"NRL" and "Programs for Professional Development": K. Parrish and J. Kaiser

"Papers, Reports, and Patents": M. Long

"Special Awards and Recognition": M. Long, P. Creech

Photographic production: A. MacDonald, W. Nafey, D. Boyd,
J. Marshall, W. Fuller, M. Savell

Computerized composition production: D. Wilbanks, J. Kogok,
B. Zevgolts

Editorial assistance: I. Barron, R. Baturin, P. Creech, G. Harrison-Rashin,
M. Long, D. Nelson

Computerized composition assistance: M. Bray, C. Cain, A. Cook, D. Martin,
J. Mickelinc, K. Morin, P. Newman, C. Sims, C. Ward

Graphic services assistance: J. Milligan, L. Jackson, L. Musselman

Production coordination: M. Peevy, T. Calderwood, S. Smith

Valuable assistance in other matters was given by G. Blakes, D. DeYoung, B. Duffield, T. Elam, R. Fluornoy,
W. Fox, L. Greenway, D. Haffer, J. Hays, B. McMorrow,
D. Nolan, C. Pasquini, E. Pickenpugh, R. Reed, B. Shea

EMPLOYMENT OPPORTUNITIES FOR ENTRY-LEVEL AND EXPERIENCED PERSONNEL

This Review illustrates some of the exciting science and engineering carried out at NRL as well as the potential for new personnel.

The Naval Research Laboratory offers a wide variety of challenging positions that involve the full range of work from basic and applied research to equipment development. The nature of the research and development conducted at NRL requires professionals with experience. Typically, there is a continuing need for electronics, mechanical aerospace, ceramic, and materials engineers; metallurgists with bachelor's and/or advanced degrees; and physical and computer scientists with Ph.D. degrees. Opportunities exist in the areas described below.

Ceramic and Materials Scientists/Engineers. These employees work on the mechanical properties, coating and materials processing, and materials research.

Electronics Engineers. These engineers work in the following areas: communication satellite design, analog and digital signal processing, information processing, strategic and tactical communication systems design, instrumentation, microcomputer design, satellite attitude-control systems, image processing, IR sensors, focal plane arrays, radar, inverse scattering phenomena, statistical communication theory, electro-optics, hardware/software interfacing, artificial intelligence, electromagnetic (EM) scattering, digital electronics, fiber optics, optical information processing, semiconductor device processing, microwave tubes, threat systems analysis, electroacoustic optics, RF measurement design, EM propagation, EM theory, HF radar propagation analysis, electronic warfare simulation, pulsed power technology, vacuum electronics, microwave technologies, networking techniques, speech processing, Navy C³I, electronic countermeasure systems design, spacecraft attitude controls, and orbitology.

Mechanical and Aerospace Engineers. These employees may be assigned to satellite thermal design, structural design, propulsion, experimental fluid mechanics, experimental structural mechanics, solid mechanics, elastic/plastic fracture mechanics, materials characterization of composites, finite-element methods, nondes-

tructive elevation, characterization of fracture resistance of structural alloys, and combustion.

Computer Science Graduates. Employees in this field are involved with artificial intelligence, software engineering, software systems specifications, computer design/architecture, systems analysis, and command information systems.

Chemists. Chemists are recruited to work in the areas of inorganic and organometallic synthesis, solution kinetics and mechanisms, surface analysis, organic chemistry, combustion, colloid/surface chemistry, fire suppression, and nuclear decay.

Physicists. Physics graduates may concentrate on such fields as electromagnetics, image processing, inverse scattering phenomena, acoustics, inversion theory, mathematical modeling of scattering processors, radar system development, electro-optics, focal plane arrays, signal processing, plasma physics, astrophysics, semiconductor technology, relativistic electronics, beam/wave interactions, low-temperature physics, superconductivity, physical/chemical vapor disposition of thin and thick coatings, wave propagation, ionospheric physics, computational hydrodynamics, computational atomic physics, and supersonic, gas-dynamic numerical modeling.

FOR FOREIGN NATIONALS

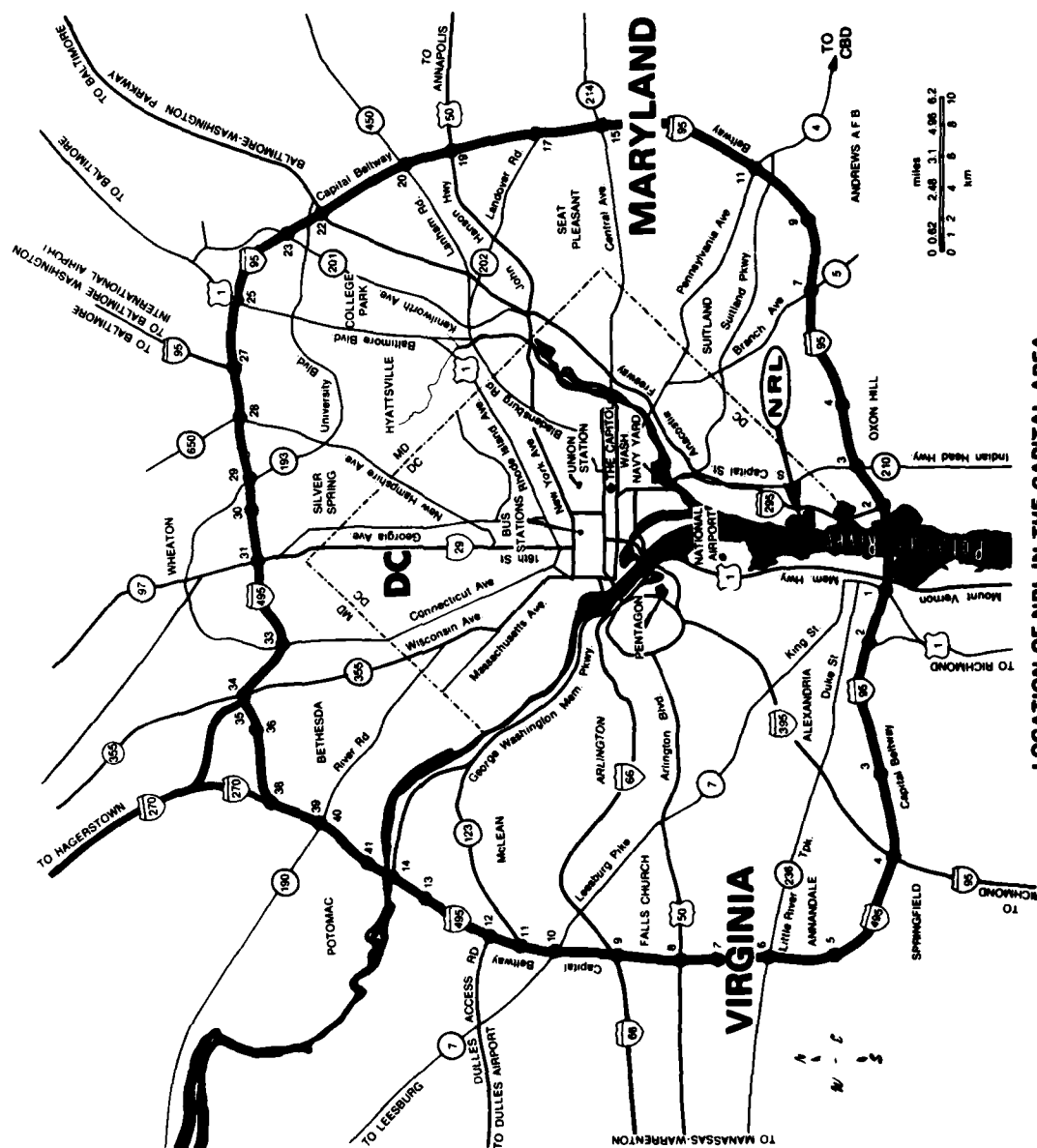
U.S. citizenship is required for employment with NRL.

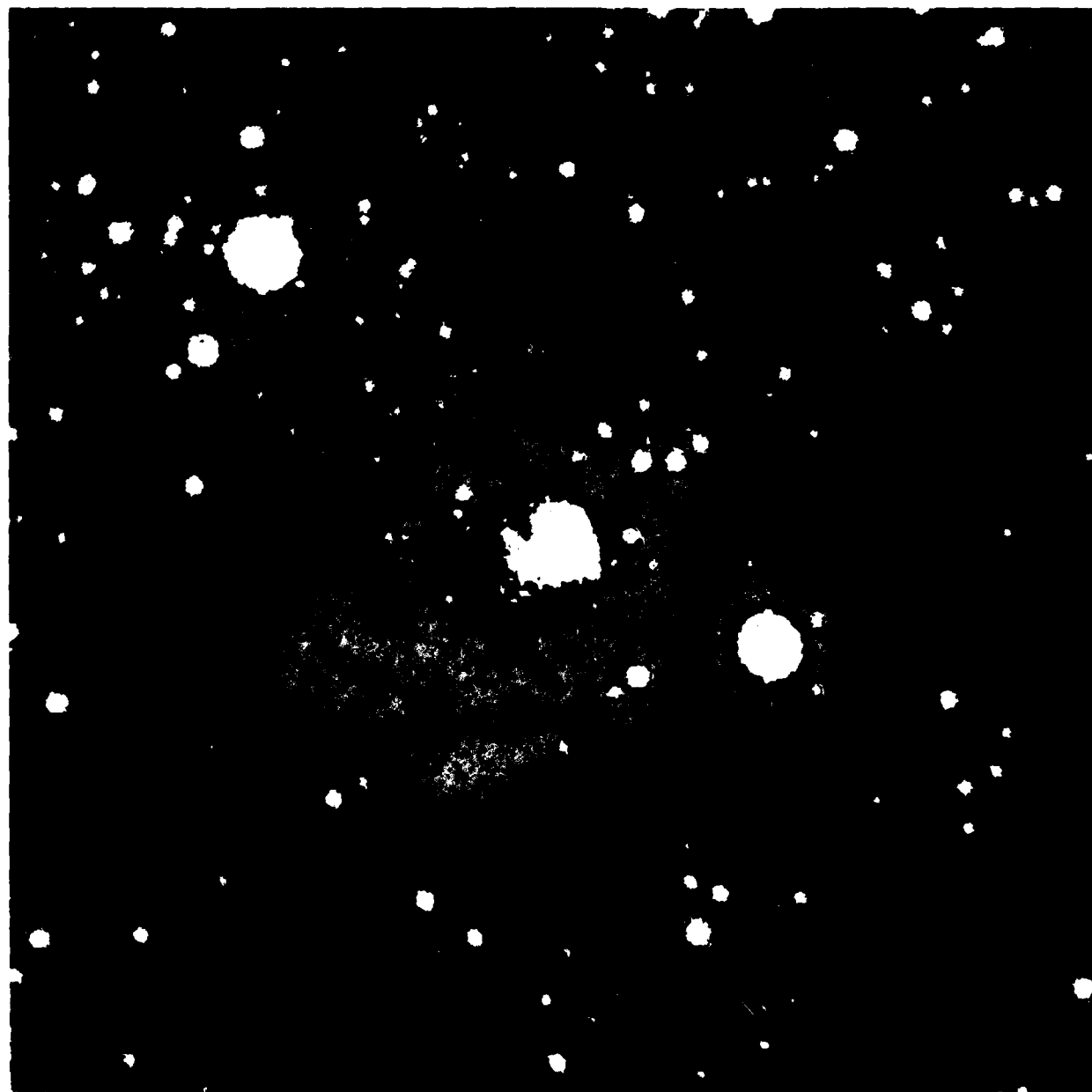
APPLICATION AND INFORMATION

Interested applicants should submit a résumé or a Federal Employment Application Form (OPM 1282), which can be obtained from local officers of the Office of Personnel Management and Personnel Offices of Federal agencies, to the address below.

Direct Inquiries to:

Naval Research Laboratory
Civilian Personnel Division, Code 83 1813 RV
Attn: Marguerite Luck
Washington, D.C. 20375-5000
202-767-3030





END

FILMED

4-85

DTIC